Hydrodynamics and Mass Transfer Processes associated with the absorption of oxygen in liquid films flowing across a rotating disc

by

S.T. Lim, B.Sc.

Thesis submitted for the degree of Doctor of Philosophy in the Faculty of Engineering of the University of Newcastle upon Tyne

Department of Chemical Engineering
University of Newcastle upon Tyne

October 1980

TO MY PARENTS

ACKNOWLEDGEMENTS

The author wishes to extend his gratitude to his supervisor, Mr. J.E. Porter, for his guidance, constructive criticism and enlightening and interesting discussion throughout this research project.

The author also wishes to thank the following:

To Professor F. Goodridge in whose laboratory the research was carried out and The Robert Wood Fellowship for providing the necessary financial support.

To Mr. E.T. Horsley, for his excellent work in the construction of the experimental apparatus, and all the technical staff under him, especially Mr. D. Burman and Mr. R. Randles, for their advice and assistance during the construction of the photographic Flash Synchronizer and the photographs respectively.

Finally, thank is also extend to his colleagues for making this research period a memorable one and to Mr. T.K. Tan and his beloved wife (God Parents) for their encouragement and understanding during his studies ('A' Level) in Penang.

ABSTRACT

This study is concerned with mass transfer to a liquid film as it flows across the surface of a rotating disc, and in particular with the absorption of oxygen into films of water. The primary aim of the study was the measurement of the distribution of oxygen concentration across the disc radius, for a wide range of liquid flowrates, rotational speeds, and the comparison of these distributions with those resulting from a range of theoretical models of this process.

These comparisons, and the observation that with flow and rotary speeds of practical interest, the liquid films invariably exhibit characteristic surface waves indicate the importance of this hydrodynamic condition with respect to the mass transfer process.

The main dimensionless variables which are influential in describing flow on the disc have been identified, and used in the formulation of satisfactory mass transfer design equation.

A note on the layout of this Thesis

The study reported here is divided into two sections, the first dealing with some aspects of the hydrodynamic behaviour of liquid films flowing radially across the surface of a rotating disc, the second with the absorption of oxygen into such films. A number of earlier, detailed studies of the time averaged behaviour of such flows have proved successful in producing accurate correlations between experimental conditions such as disc speed, liquid flow and appropriate rheological characteristics and radial distributions of film thickness and average film velocity. However it was apparent in preliminary studies that the finer hydrodynamic detail of such flows, particularly the surface waves associated with the flow of mobile liquids, and their influence on actual area available for mass transfer and internal film mixing required special attention. Since hydrodynamics and mass transfer studies on rotating surfaces present special problems in experimentation, the two aspects of the problem were studied separately and it was considered quite appropriate that this approach should be reflected in the layout of this thesis.

CONTENTS

HYDRODYNAMIC

INTRODUCTION

AND

LITERATURE SURVEY

ON

HYDRODYNAMICS

1. INTRODUCTION

The theory and practice of heat and mass transfer have been subject to intensive study for the last few decades. The reasons for this are economic; heat and mass transfer are the bases of some of the most important industrial processes. Among these are the gas absorption and desorption, distillation and water cooling. Any improvement which is effected in these processes, either from greater understanding of their principles or empirical development of new technique, has been, and will continue to be, of great economic value.

In the processes mentioned it is desired to transfer material from one phase to another. The two phases may or may not be of the same physical state. Transfer may take place between a liquid and a gas, a liquid and a liquid, and all other combinations. The material transferred may be a component of two mixtures each of which comprises one of the phases or it may be the whole of one phase.

The gas-liquid system is industrially the most important. There is a variety of situations in which transport of mass occurs in gas-liquid interface which is either expanding or contracting. The simultaneous heat and mass transfer which occurs during the bubble growth period on the plate of distillation column or in a nucleate boiling apparatus, the absorption of gases into a liquid film while it spreads over a solid object and the absorption of gases into expanding or contracting liquid jets or sheets provide a few examples of this phenomenon.

The absorption of oxygen into thin liquid films under the action of centrifugal force form the gas-liquid system considered in this work.

Most of the theoretical and experimental research on the flow of a liquid in thin films deals with films formed under

the action of gravity on stationary, inclined and vertical planes. Such films are of interest because a thin film presents a very large transfer surface for a given volume of through-put. Very little information on films produced by centrifugal forces on rotating surfaces is available. Centrifugal forces can be much larger than gravity. The films on rotating discs can thus be made thinner more rapidly and the size of the equipment for a given through put can be made smaller than in the case of a film developing on stationary planes. This makes it attractive for certain applications. It is therefore considered desirable to have liquid films generated on rotating discs.

The importance of thin liquid films lies in the fact that the internal resistance to heat and mass transfer is minimised by the presence of a wave motion which is the characteristic of these films, and in that they present a very large transfer area per unit volume of through put.

The solution to the mass transfer problem does, necessarily, depend on the prior knowledge of the hydrodynamics of the situation. Unfortunately, a comprehensive analysis of the complex surface motion has not yet proved possible, and hence, mass and heat transfer coefficients cannot be calculated without recourse to empirical work.

It has been shown experimentally by many research investigators (1,2) that the rates of heat and mass transfer to falling films are consistently higher than those predicted using the assumptions that the film is waveless and laminar, and the turbulence created by the interfacial waves, is known to be mainly responsible for this increase (2,3,4). It has also been suggested (2,5,6) that the interfacial area may be considerably extended by the presence of the waves, but it is difficult to proportion the relative magnitudes of the effects due to interfacial turbulence and interfacial area increase resulting from these waves.

This work has been planned and carried out to investigate the hydrodynamics and mass transfer characteristics of thin liquid films formed on the rotating surface independently, with the influence of the former being properly taken into account in the treatment of the latter.

The main parameters characterising the flow process of the liquid film on a rotating disc are film thickness, surface velocity, velocity profile and surface waves. Thus, in validating any hydrodynamics model, measurements must be made upon the gross results of these phenomena. In the case of mass transfer rate between two phases the concentration profiles across the disc with flow rates and rotational speeds were measured.

Beek and Kramers(7) pointed out the stretching of the interface creates a normal velocity component to the interface which makes mathematical treatment of the problem complex. This situation has arisen repeatedly in the study of mass transfer considered by a number of researchers (7,8). Beek and Kramersconsidered mass transfer with a change in interfacial area and distinguished between a 'crude model' and 'approximate model'. Venkataraman(61) applied these two models, using gas absorption of carbon dioxide into non-wavy water films on a rotating disc of diameter 12.8 cm and shown that the 'crude model' predicted mass transfer rates up to 23% lower than the measured values, while the 'approximate model' predicted values up to 7% higher. When the latter model was modified to take into account the effect of inertial and Coriolis forces on the flow, this agreed with the measured values. However, this was carried out at limited range of flow rates of 1.2 to 18 cm^3/s and disc speeds of 400 to 800 rpm, from which it appears that laminar flow prevailed within this range of values. It is therefore decided to investigate with wider ranges of flow rates (14.5 to 60.5 cm^3s), disc speeds (230 to 1110 rpm) and different radial positions across the 36 cm diameter disc, so as to indicate and determine completely the type of flow prevailing within the

liquid film on a spinning disc and to ascertain when other phenomena such as rippling flow becomes important. The relative importance of wave motion in increasing interfacial surface areas and inducing mixing within the film, was considered. The influence of the distributor, ie entrance effects, the effects of interfacial induced by the adjacent gas phase were considered and subjected to experimental investigation.

Since this study was concerned with a physical absorption process the oxygen water system was chosen as the most convenient one for the purpose. Reliable diffusivity data for the absorption of oxygen into water are available in the literature, together with information indicating the effects of surfactant materials.

Following the independent studies of hydrodynamics and mass transfer, this thesis has been orgainsed so that the earlier chapters deal with the flow problem while the later ones deal with the study of mass transfer.

2. LITERATURE REVIEW

HYDRODYNAMICS

2.1 ASSOCIATE FIELDS (FALLING FILMS)

When a liquid flows as a thin film over a vertical or inclines surface, waves develop and it has been shown that enhanced rates of heat and mass transfer are associated with the onset of rippling flow (1,9). In certain cases these changes are phenomenal (1,10,11). A twenty fold increase in the rate of absorption of carbon dioxide, for instance, has been noticed (10). Therefore, the understanding of the mechanics of film flow is important in those cases of heat and mass transfer which involve two-phase flow, such as the flow in the film reactors, vertical condensers, packed towers, water tube boilers and so on. But due to the absence of fundamental information concerning the hydrodynamics of the liquid film, except a very low Reynolds number, much experimental data has been recorded in an attempt to understand the film flow mechanism. The presence of these ripples has caused the mass and heat analyses in industrial equipment, in general, therefore rested on empirical methods.

(A) Film Thickness

Hopf (12) in 1910 initiated the film thickness measurement on the flow of liquid films down solid surfaces, and since that time, many investigators (see Table 1) have reported on measurements of liquid film thickness at various values of Reynolds numbers. Experimental methods used have been either direct methods in which the surface is touched by a micrometer screw and by some type of probe, usually attached to the micrometer screw, or indirect methods. The indirect methods are:-

(1) Weighing the liquid which drains from the plate, by Warden (13) and Fallah et al (14).

(2) Shadow photographs by Brauer (15).
(3) Weighing the hold-up as the tower is in operation by Kamei and Oishi (16).
(4) Light absorption by Stainthorp and Batt (17) and Stainthorp and Allen (18).
(5) Photographic method by Muenz and Marchello (19).
(6) X-Ray method by Solesio (20).
(7) Electircal conductivity technique by Telles and Duckler (21).
(8) Radioactive material by Jackson (4).

Criticism of each method has been given in Table 1.

Nusselt (22) has presented an analysis of the flow of liquids down inclined plates, and he has derived the expression $\delta=(3\nu Q/g)^{1/3}$ (see Appendix A) for the thickness of the flowing film in the laminar region, making the assumption that there were no ripples on the film and that there was no surface shear. Early workers (12,23) have concluded that the results of film thickness measurements agreed well with the Nusselt film thickness. Fulford (24) collected data for a wide variety of liquids, varying from very mobile hydrocarbon oil to glycerol, for film flow on vertical walls and at slopes down to about 1 degree to the horizontal. These values of the film thickness were recalculated and plotted as dimensionless thickness parameter δ^+ against Re_1 and compared with equation A14 (Nusselt) and A15 (Kapitza) (see Appendix A). It appears that, in the laminar region, the values fell near the line given by equation A14 for the most part. Above the values of Re_1 from 300 to 400, the experimental values deviated systematically from this line. In the laminar region, even when waves were present at the gas liquid boundary, the δ^+ values appeared to agree better with equation A14 for a smooth film than with the predictions of the Kapitza theory of wavy flow A15. However, more recent film thickness measurements in the laminar wavy regime obtained by improved technique (5,24,28) have shown that there are appreciable reductions in the mean film thickness in the wavy flow regime for both vertical and sloped surfaces, as predicted by the Kapitza theory.

TABLE 1: FILM THICKNESS MEASUREMENT TECHNIQUES

TECHNIQUE	COMMENT	REFERENCE
(1) Weighing of liquid drains	Simple but special precautions have to be taken on the design of distributor to avoid erroneously high drainage quantity.	Warden (13) Fallah (14)
(2) Shadow photographs	Very complicated, suitable for film thickness measurements only.	Brauer (15)
(3) Weighing the hold-up	Simple but not accurate.	Kamei and Oishi (16)
(4) Light absorption	Accurate and suitable dye may have to be added to give output sensitivity.	Stainthorp and Batt (17) Stainthorp and Allen (18)
(5) Photographic method	Complicated and accurate.	Muenz and Marchello (19) Clegg (37)
(6) X-Ray	Complicated and expensive.	Solesio (20)
(7) Electrical conductivity	Electrolyte needed.	Telles and Duckler (21)
(8) Radioactive	Complicated and expensive.	Jackson (4)
(9) Capacitive	Accurate and simple.	Bell (26) Ali (27)

(B) The Interfacial Structure

Numerous experiments in the past have shown that in flow down a wall the stream is noticeably agitated by waves, even in the absence of air flow, except at very low flow rates. The apparent absence of waves at low Reynolds numbers on thin films has led several investigators to assume that, for the flow down a vertical plane, there exists a critical value of Reynolds number (Re_i) below which uniform laminar flow is entirely stable. That is, the flow is in a condition where small disturbances of every kind are suppressed. Numerous estimates of the critical Re_i have been stated. Binnie Re_i = 4.4 (29), Friedman and Miller Re_i = 0.25 (30), Grimley Re_i = 6.2 (31), Kirkbride Re_i = 2.0 (28). On the theoretical side the work of Kapitza (32) led to an estimate of 5.8 for the critical value and that of Yih (33) gave about 1.5. Jackson (4), Grimley (31) and Clegg (25) have also proposed empirical correlations to determine the value of critical Reynolds number Re_i. Benjamin argued that a critical Reynolds number in the usual sense does not exist for the particular case of uniform flow down a vertical plane. In other words, for all finite Re there is a class of wave-like disturbances which undergo unbounded amplification according to a linearised theory, and that the presence or absence of surface tension does not alter this general conclusion.

When the value of Re_i has been exceeded experimentally in the investigations, the wave motion set in, but the waves do not appear at the edge of the distributor. There is always a distance below the distributor when the wave motion is said to start, ie the line of wave inception. Most investigators observed that the distance of the line of wave inception below the distributor increases as the flow rate increases, except that Allen (3) has shown that the reverse trend is observed at very low flow rates.

Since waves motion is encountered frequently in industrial process equipment, this led to the recognition of the need for

quantitative film rippling studies. Greenberg (34) used the light absorption technique to obtain the wave profile, where a light beam passed through the dyed liquid flowing film such that the amount of the light transmitted depends on the thickness of the film. Allen (3) modified the light absorption technique by incorporating a second light spot and photocell 1.6 cm below the main system and by comparison of the two traces which were displayed on a double beam oscilloscope he has been able to determine the wave velocity. Stainthorp and Wild (35) have modified the light absorption technique using two beams of light in order to monitor both the local film thickness variations with time, and wave velocity. Hewitt et al (36) have also modified the light absorption method by directing a beam of ultraviolet light onto the film into which fluorescent dye has been dissolved. The visible component of the generated light was separated from the ultraviolet light by the use of a spectroscope, and the light passing from this instrument was directed into a photosensitive cell. The method was developed in order to avoid refraction at the surface of the waves. Detailed descriptions and other light absorption techniques are given in (37). Black (38) has objected to the light absorption technique on the grounds that the refraction of light at the surface of the film may cause some errors but Clegg (37) mentioned most workers using this technique have designed their optical system in such a way that this effect is minimised.

Duckler and Bergelin (6), Portalski (5) and Shirotsuka et al (39) have used the capacitance technique to monitor the variation in the instantaneous film thickness where a capacitive circuit is created between the probe and the metal plate. The probes used by the above workers are 3.17 mm, 2 mm and 0.3 mm in diameter respectively. The author's opinion is that this technique will not be able to produce a better wave profile than the light absorption technique. Since the diameter of the probes used were of very small diameter, the

separation between the probe and the plate must also be small for measurable capacitances to exist. This technique therefore will not be suitable.

(C) Velocity Distribution

Velocity profiles within laminar liquid films in uniform flow under gravity have been predicted by Nusselt (22). For the turbulent region Duckler (40) assumed the applicability of the universal velocity profile, ie a unique dimensionless correlation of velocity profile data using the parameters u^+ and y^+ (see Appendix B). Experimental verification has been complicated by the very small film thicknesses usually involved. The first attempt to do this was made by Grimley (31) who used an ultra-microscope technique on a vertical film in laminar flow. This work was followed much later by Wilkes and Nedderman (41), who used a stereoscopic method in conjunction with suspended air bubbles to determine velocity profiles at a Reynolds number in the region of four. In this way, at very small distances downstream and in the absence of surface ripples, they obtained results which are in agreement with the Nusselt equation. At approximately the same time Tracey and Lester (42) confirmed the validity of the use of the universal velocity profile in turbulence region by means of a pitot tranverse in a film inclined at a shallow angle. Atkinson and Caruthers (43), using the hot-wire technique, also confirmed the correlation by the Nusselt equation in laminar flow and that for the turbulent region ,by using the universal velocity profile.

The major difficulty of measuring velocity distributions within the falling liquid films arises from the fact that the thickness of falling films normally encountered are of the order of one millimetre or less. Common velocity measurement techniques snch as the pitot tube, hot-wire anemometers, etc, as mentioned above, will inevitably disturb the films, if not destroy them. The stereoscopic technique described by Wilkes and Nedderman (41) is tedious and cannot be conveniently applied to fluctuating flow such as wavy falling liquid films. A

considerable amount of data is required for statistical analysis.

Popovich and Hummel (44) developed a photochromic dye-tracer technique which is capable of measuring velocity distributions in a liquid stream without disturbing the liquid. This technique is based on the tautomeric shift of 2 - (2, 4 - dinitro - benzyl) - pyridine in an organic solvent, such as ethyl alcohol, under ultraviolet irradiation.

(D) Interfacial Area

Experimentally it has been observed by many investigators that if a liquid film flows down a vertical plate its free surface is disturbed by wave motion and ripples. This wave motion and ripples intensify heat and mass transfer. Stirba and Hurt (2) and Emmert and Pigford (1) have obtained mass transfer results which show a large increase in the rate of transfer of Co_2 into water, due to rippling.

Wave motion and ripples probably caused the increase in the rates of heat and mass transfer in two ways: (a) by an increase in the interfacial area of the film, and (b) by mixing in the liquid film. To approportion the relative magnitudes of these two effects on heat and mass transfer resulting from the waves, it is necessary to know the increase in interfacial area or the degree of mixing in the film. Unfortunately the problem of evaluation of the degree of mixing in the film is a very difficult one. Hence, many workers have diverted to investigate the increase in the interfacial area rather than film mixing.

Brauer (15) was the first one who measured the surface wave profile of a liquid film formed on a 45 mm rod. He photographed the liquid film and measured the length of the profile along the liquid surface from an enlarged photograph. This method is open to objection, as mentioned by Clegg (37), because the actual profile of the waves is not seen, since the troughs of the waves will be masked by the peaks or

troughs of the waves in front or behind those being examined (unless the wave profile is symmetrical around the rod). It is also difficult to measure the length of the wave profile when the amplitude of the waves is very small. Brauer obtained the surface area increase from 0.5% to 3.0% for Reynolds number varied between 25 to 1675. Before Brauer, early estimation by visual observation on the increase in interfacial area was judged by Stirba and Hurt (2). They considered the increase in interfacial area was probably less than 50%. Jepsen (45) used the capacitometer to measure the wave profile of falling film formed on a wetted wall inclined at $9^{o}44'$ to the horizontal. He obtained the percentage increases in interfacial area between 1.4% to 2.3% for Reynold numbers from 183 to 458.

Light absorption technique has been used by Allen (3) to estimate the increase in interfacial area due to rippling for iso-propyl alcohol at Re = 25.5. He obtained a 0.06% increase in interfacial area. At the same Reynolds number he calculated a 5% increase based on the equation of Portalski (see Appendix D) In Allen's technique, he came across the difficulty of converting the amplitude - time profiles obtained by sampling at fixed points to amplitude - distance profiles, this was because of the varying velocity of the waves. He therefore formed a correction for this by measuring the wave lengths on the time axis of the profiles, converting to seconds and then multiplying by the wave velocity. Such correction can only be made (as mentioned by Clegg) provided that the waves did not change shape as they moved down the column.

Shirotsuka et al (39) used the electrical capacitance probe to obtain the wave profiles on liquid film with and without air flow. The probe diameter used was 0.3 mm (an improved version of Duckler and Bergelin (6)). Since the probe diameter was small, there is a limit for such application as mentioned earlier by the author. They concluded that the increase in interfacial area was less than 0.2% for water at Re of 163 under conditions of high velocity air flow, and showed an increase of as little as 0.03% for water at same Re with no air flow.

An increase in interfacial area due to rippling when a film was flowing over rough surfaces was measured by Vouyoucalos (46). Lycopodium powder was sprinkled onto the surface of the film and several photographs were taken with the aid of a short duration flash. The length of the resulting surface profile was measured using a curvometer and it was concluded that the increase in interfacial area was 8% for water.

Portalski (5) has made a theoretical and practical determination of the increase in interfacial area due to periodic wave motion. He used the wave profile due to Kapitza (32) and substituted it into the standard calculus expression to obtain the length of a line, and thus obtained an expression for the increase in interfacial area. The theoretical results calculated at medium flow rate are very much too high as compared with most experimental results. The possible reason is the theoretical expression for the wave length, which is only accurate at very low Reynolds numbers, and gives wave lengths which are much too short at higher flow rates. Second reason is that the actual surface profiles are much more irregular than those predicted by the Kapitza analysis. Portalski used a capacitance probe method to obtain the wave profiles and used an ordinary opisometer to measure the increase in length. He obtained 3.3% increase in interfacial area at Re_1 of 3.0 for 82% glycerine solution using his equation, and by using optisometer measurement he obtained 2.5% experimentally. Allen (3) has raised the objection (as mentioned in (37)) that the profiles do not appear to have been calibrated, and he pointed out unless the original waves were amplified to the same extent in both axes, then an error will have occurred in the measurement of the practical values.

Clegg (37) has developed two new techniques for the study of the inception and growth of waves on falling liquid film. The first technique involved the instantaneous sampling of the varying film thickness at fixed points at the wetted

wall using a light absorption method where all the information from the digitised sampling unit was automatically recorded on punched computer tape and subsequently processed in a computer. Second method was by photographic means, where wave motion on dyed liquid films were taken, and using microdensitometry to produce profiles of the developing waves. His results obtained include measurements of the wave growth rates, the variations of the maximum wave height, mean film thickness, residual film thickness in the area of wave inception and the interfacial area increase due to wave motion. He argued that the interfacial area increase given by Portalski's equation is too high for medium liquid flow rate. This was mainly due to the theoretical wave length used in the formulation of the Portalski equation (5), which was too small in comparison with the experimental one. Many workers (3,5,24) have shown that the practical and theoretical values of λ, the wave length of the regular wave motion differs by about an order of magnitude at the higher flow rates. From this it can be seen (5) that an error of a factor of 10 in λ would produce an error of a factor of 100 in the percentage increase in interfacial area. Clegg from his experimental results obtained a correlation for the interfacial area increase for water on wetted wall as:

$$\Delta S\% = 0.008\ Re^{2/3} \qquad (1)$$

which in fact is insignificant, producing no effect in mass and heat transfer operations.

(E) Effect of Surface Tension on Waves

Whitaker (47) studied the role of surface tension, surface viscosity and surface elasticity in stabilising falling liquid films at low Reynolds numbers. Surface tension and surface viscosity were found to decrease the growth rates of an infinitesimal disturbance, but are not capable of stabilising the film. Surface elasticity gives rise to a critical Reynolds number, below which the flow is stable to

all disturbances. Levich (48) has confirmed the importance of surface elasticity in suppressing wave formation. Benjamin (49) results also strongly suggest that surface elasticity is generally the essential mechanism in the observed stabilising effect of surface-active agents and that films flowing down vertical walls are always unstable in the absence of contamination.

Holfam et al (50) have found that the wave inception distance and the equilibrium wave amplitude, in the wavy laminar flow regime on the vertical plate, decrease as the surface tension number increases for a given Reynolds number, This is contradictory to the linear stability analyses which predict that the wave inception length should increase as surface tension number (N_σ) increase. The author explained that the wave inception distance appears to decrease as $N_\sigma$increases for a fixed Re. This may be due to an increase in the initial wave growth rate as $N_\sigma$increases.

2.2 REGIME TRANSITIONS

Ripples are observed on falling liquid films above a certain value of Re_l as given by several investigators (5,10,11). It is therefore possible to identify several regimes of film flow. Thus, Brauer (51) gives the following regimes as:

$Re_l < 4$: Smooth and laminar film

$4 < Re_l < 10$: Undulation across the film

$10 < Re_l < 20$: Sinusoidal waves gradually replaced by regular waves

$Re_l > 20$: Random waves

Brauer states that the transition boundaries for fluids other than water as functions of a parameter K, defined as:

$$K = \frac{\rho \sigma}{g \mu^4} \qquad (2)$$

and the first transition marking the end of the smooth laminar film is:

$$Re_l = 0.306\ K^{0.1} \qquad (3)$$

The rippling transition is agreed by numerous investigators (41,52) but the turbulent transition (Re_l above 400) is a little less uncertain as compared with equation B8 and B17 (see Appendix B).

2.3 FILM BREAKDOWN

A number of models have been presented by numerous investigators to account for the breakdown of a vertical laminar liquid film under isothermal conditions as well as the mechanism of film rupture produced by gas absorption or temperature gradients in the liquid.

Hartley and Murgatroyd (53) have considered two criteria for dry-patch production under laminar flow and shear induced laminar/turbulent flow at the free liquid interface. The two criteria were:

(A) A force-balance of the surface tension and the stagnation pressure of the fluid at the upstream point of a dry patch.

(B) Minimum total energy (kinetic and surface tension energy) in a laterally unrestrained liquid film.

By employing the velocity profiles of the Nusselt model, and the Universal Velocity Profile model, several analytical equations predicting the onset of film breakdown were obtained. However, only the Nusselt model results agreed with the experimental data, for which the results were given as:

$$\text{For Criterion A} \quad \delta_c = 1.72 \left(\frac{\sigma}{\rho}(1-\cos\alpha)\right)^{1/5} \left(\frac{\nu}{g}\right)^{2/5} \quad (4.1)$$

$$\text{and} \quad Q_{1c} = 1.69 \left(\frac{\sigma}{\rho}(1-\cos\alpha)\right)^{3/5} \left(\frac{\nu}{g}\right)^{1/5} \quad (4.2)$$

$$\text{For Criterion B} \quad \delta_c = 1.34 \left(\frac{\sigma}{\rho}\right)^{1/5} \left(\frac{\nu}{g}\right)^{2/5} \quad (5.1)$$

$$\text{and} \quad Q_{1c} = 0.803 \left(\frac{\sigma}{\rho}\right)^{3/5} \left(\frac{\nu}{g}\right)^{1/5} \quad (5.2)$$

where δ_c is the film thickness at breakdown and Q_{1c} the minimum wetting rate.

Iijima and Kuzuoka (54) presented their minimum wetting data under isothermal conditions for systems methanol-water and glycerol-water, which representing a viscosity varied from 1 to 12 centipoise and surface tension from 76 to 26 dynes/cm. From the experimental data, they obtained empirical equation given as:

$$\frac{\delta \rho^2}{\mu^4} = 0.11 \log_e\left(\frac{\sigma}{7.0}\right) \qquad (6)$$

where δ is the film thickness obtained from Nusselt model.

Hobler and Czajka (55) obtained the minimum wetting rates for water and glycerol-water mixtures over a number of inclined planes of stainless steel, aluminium, copper and glass and presented the correlation as:

$$\frac{4\,\Gamma}{\mu} = 0.615\ We_z^{0.974}\ (1-\cos\theta)^{0.6} \qquad (7)$$

for $1.3 < 4\,\Gamma/\mu < 1000$

where We_z = Weber number

The difference between the experimental procedures in the above two cases was that, in the former case, the minimum wetting rates were measured, when the liquid flow rates were reduced and a dry-parch was formed, whilst in the second case this was determined when liquid just fully covered a previously dry surface

Bond and Donald (56) studied the absorption of ammonia from an ammonia-air gas stream into water using a wetted wall column. They measured the minimum wetting rate required to maintain a complete film on the wall surface for different gas concentrations and various inlet liquid temperatures. Experimental data showed that the minimum wetting rate was increased progressively as the inlet ammonia concentration increased, and was decreased as the temperature of the inlet liquid was increased. The minimum wetting rate was increased

by an increase in the ammonia concentration in the inlet gas, but was decreased when the temperature of the liquid was increased due to the heat of solution being partially offset by the cooling effect of evaporation from the liquid surface. Bond and Donald explained the minimum wetting rate was caused by the difference in the surface tension between the trough and the crest of the ripples on the column.

Norman and Binns (57) measured the minimum wetting rates for the distillation of mixtures of methanol with water in a wetted-rod column. The values were found to depend on the liquid surface tension, σ, and on the change in surface tension, $\Delta\sigma$, due to mass transfer from the vapour to the liquid. They noted that when the transfer results in an increase in the surface tension of the liquid, the film is very stable, whereas a reduction in surface tension renders the film unstable and causes a considerable increase in the minimum wetting rate. The results were correlated by the equation:

$$\frac{3q\,\mu}{\rho g} = 1.26 \times 10^{-6} - 1.76 \times 10^{-6}\ \sigma\ \Delta\sigma \qquad (8)$$

A model is also presented by Ponter et al (58) to account for breakdown of a vertical laminar liquid film exposed to a soluble contercurrent gas stream (ethanol-water) on vertical copper, stainless steel, perspex and carbon surfaces. The conditions under which a stable dry-patch is first formed can be predicted by equation:

$$\frac{\Gamma}{\mu} = 1.12\ (1-\cos\theta)^{0.6}\ \left(\frac{\rho\gamma_e^3}{\mu g}\right)^{0.2} \qquad (9)$$

Film breakdown caused by temperature gradients has also been investigated (54,55).

2.4 RADIAL FLOW AND FILM THICKNESS ON A STATIONARY DISC

The hydrodynamics of a radial outflow of a viscous liquid, moving in the form of a thin, continuous, laminar film over the surface of a stationary disc has been studied by Tyabin and Glinkin (59) and Watson (60). They made several assumptions, as follows:

(A) The friction of the liquid film on the surrounding gaseous atmosphere is negligible, and

(B) the thickness of the film is considerably less than the radius of the stream considered.

Watson studied the boundary layer equation:

$$V_r \frac{\partial V_r}{\partial r} + V_y \frac{\partial V_r}{\partial y} = \nu \frac{\partial V_r}{\partial y} \qquad (10)$$

and

$$\frac{\partial}{\partial r} (rV_r) + \frac{\partial}{\partial y} (rV_y) = 0 \qquad (11)$$

with the boundary conditions

at the wall $y = 0 \quad V_r = 0 \quad V_y = 0$ (12.1)

at the free surface $y = \delta \quad \frac{\partial V_r}{\partial y} = 0$ (12.2)

Watson obtained the minimum film thickness as:

$$\delta_c = 2.31 \left(\frac{r_i^4 \nu}{Q} \right)^{1/3} \qquad (13)$$

and the radius at which the minimum thickness occurs as

$$r_c = 0.3155 \left(\frac{Q r_i^2}{\nu} \right)^{1/3} \qquad (14)$$

Glinkin and Tyabin also considered the boundary layer equations above and, assuming the surface radial velocity was a function of r only, they showed that the thickness at any radius was given by:

$$\delta = \frac{\delta_i r_i}{r} + \frac{5\pi\nu}{3Q'}\left(r^2 - \frac{r_i^3}{r}\right) \qquad (15)$$

where r_i is the radius of the distributor and δ_i is the film thickness at the entry of the disc (distributor gap).

Analysis of the above equation shows that the thickness of the film decreases continuously with increase in the radius, according to a curvilinear law, until a certain critical radius after which it begins to increase and the radius at which the critical minimum thickness occurs is:

$$r_c = \left(\frac{3Q\,\delta_i r_i}{10\,\pi\nu} - \frac{r_i^3}{2}\right)^{1/3} \qquad (16)$$

if r_i is small

$$r_c = 0.46\left(\frac{Qr_i\,\delta_i}{\nu}\right)^{1/3} \qquad (17)$$

substituting r_c into the equation (15), the minimum film thickness is given as:

$$\delta_c = 3.28\left(\frac{\delta_i^2 r_i^2}{Q}\right)^{1/3} - 11.38\left(\frac{r_i^8\,\nu^4}{Q^4\,\delta_i}\right)^{1/3} \qquad (18)$$

From the above analyses, it was noticed that the two analyses result in similar expression on the controlling parameters if $r_i = \delta_i$. The author opinion that this is only true when the distributor used is very small.

2.5 ROTATING DISC

GENERAL

When a liquid is introduced at the centre of a rotating disc, it spreads across the disc with centrifugal force of rw^2. Considering the forces acting on a whole element of liquid extending from the surface of the disc to the free surface of the liquid, the product of the mass of the element and its acceleration can be equated with the balance of centrifugal and viscous retarding force (61)

$$\rho \frac{\partial(V_r)}{\partial t} = \rho w^2 r + \frac{\partial \tau}{\partial y} \qquad (19)$$

In addition to these forces, in the case of liquid of low viscosity another force becomes important as a result of the increased radial velocity compared to the circumferential velocity of the disc. This force, termed Coriolis force, acts normal to the radius and in a direction opposite to that of rotation. Due to this, the tangential velocity of the liquid is less than that of the disc. This phenomena has been termed as the 'slip' of liquid over the surface of the disc.

Earlier workers (62,63) have used this principle (rotating disc) in the design of atomisation and spray drying equipment in which the liquid film, after accelerating across the disc, is discharged into a gaseous atmosphere where it disintegrates into a fine spray. Similar work has been carried out by Hinze and Milburn (64) with rotating cones.

Rotating discs and cones have been used to improve heat transfer during evaporation, condensation and heat exchange operations. This method is particularly important for heat sensitive products because of the relatively low residence time, compared with the conventional shell and tube devices. The low residence time means that a higher processing temperature can be employed since the product of increasing decomposition rate (due to the higher temperature) and shorter time at the higher

temperature will still be less overall than for conventional devices. A higher processing temperature has an additional advantage in that the ratio (death rate of thermophilic bacteria/decomposition rate of material) increases five fold for every $10^{o}C$ rise in processing temperature (Bell (26)). Thus, Viter et al (65), in a pilot plant trial of a rotating conical heat exchanger used in concentrating an alcoholic extract of digitalis, found that degradation of the glucosides present fell by 25% compared with a conventional evaporator's product.

Theoretical and experimental studies of rotating evaporation and condensation equipment have been made by Hickman(66), Rees (67), Nandapurkar and Beatty (68), and Sparrow and Gregg (69,70).

Venkataraman (61) has investigated both experimentally and theoretically the fluid dynamics and mass transfer to the liquid film. He considered this as a model for a study of mass transfer to an expanding interface.

Espig and Hoyle (72) used the micrometer technique to study the effect of the formation of waves in thin liquid film on film thickness. They found that film thickness is greater than that predicted by theory and they were able to correlate their results with the flow Reynolds number. The author's opinion that the above technique is open to error due to surface tension effect and the maximum film thickness being measured (ie the trough of the waves were measured). Numerous other workers (see Section 2.14) have also developed different techniques for the measurements of film thickness formed across the disc, varying flow rates and rotational speed.

Dixon et al (73) carried out some interesting experiments tracing the path taken by the liquid which was fed in the centre of the spinning disc. They observed the single drop of dyed liquid supplied to the centre of the disc which was being covered with white paper. The path taken from the centre of the

disc to the outer edge was found to be a logarithmic spiral. The drops were subjected to two main forces, the first being the centrifugal forces acting radially outwards and the second which corresponded to Coriolis acceleration acting at right angles to the radius and in a direction opposite to that of rotation. The result was a tangent to the spiral at that point making a constant angle with the radius which could be represented by the equation:

$$p = r \sin \alpha \qquad (20)$$

where p is the length of perpendicular from the origin to the tangent to the spiral, r is the radius vector of the spiral and α is the angle made by the intersection of the radius vector and the tangent to the spiral.

They concluded that the path taken by a drop was increased by (i) an increase in the angular velocity of the disc, (ii) an increase in the surface tension of the drop, and (iii) a decrease in the viscosity of the drop, and that, for the case of water, it never reached the angular velocity of the disc and for a significant proportion of the angular velocity to be taken up by the water, the disc had to be fairly large.

3. THEORETICAL DEVELOPMENTS

3.1 CENTRIFUGAL MODEL

Emslie et al (74) and several investigators (61,89) have developed theoretical equations to describe the flow of a Newtonian fluid on a rotating disc. With the assumption that gravitational forces are negligible compared to centrifugal forces, there is no 'slip' on the disc and that only the centrifugal force and viscous drag are considered with all other terms being ignored (see Appendix C), that:

$$\nu \frac{d^2 v_r}{dy^2} = -w^2 r \qquad (21)$$

The physical interpretation of the model is that of the fluid rotating everywhere at the same rate as the disc, moving out over the disc purely radially with the driving centrifugal force balanced by the fluid's viscous drag.

By integrating equation (21) subjected to the boundary conditions

$$y = 0 \quad V_r = 0 \quad \text{at the disc surface} \qquad (22.1)$$

$$y = \quad \frac{\partial V_r}{\partial y} = 0 \quad \text{at the free surface} \qquad (22.2)$$

The radial velocity is given by

$$V_r = \frac{w^2 r}{\nu} \left(\delta y - y^2/2 \right) \qquad (23)$$

The average velocity, $\bar{V}_r$, is given by

$$\bar{V}_r = \frac{1}{\delta} \int_0^{\delta} V_r \, dy = \frac{w^2 r \delta^2}{3 \nu} \qquad (24)$$

After substituting for V_r from equation (23), equating to the flow rate per unit area available for flow gives the film thickness in terms of the system parameters.

$$\bar{v}_r = \frac{w^2 r \delta^2}{3\nu} = \frac{Q}{2\pi r \delta} \qquad (25.1)$$

or $$\delta = \left(\frac{3}{2\pi}\frac{Q\nu}{w^2 r^2}\right)^{1/3} \qquad (25.2)$$

Venkataraman (61) has developed two dimensionless groups Re and Ta and equation (25.2) can be rewritten as

$$\frac{\delta}{r} = \left(\frac{3}{2}\right)^{1/3}\left(\frac{Q\nu}{w^2 r^5}\right)^{1/3}$$

$$= \left(\frac{3}{2}\right)^{1/3}\left(\frac{Re}{Ta^2}\right)^{1/3} \qquad (26)$$

where $Re = \frac{Q}{r\nu}$ $\quad Ta = \frac{w r^2}{\nu}$

The group Re, containing the flow rate, is a form of Reynolds number for the flow and the group Ta, containing the rotational speed, is the Taylor number applicable to the flow. It should be notices that for a given flow rate and rotational speed, Re decreases and Ta increases with increasing radius. Hence, equation (26) can be rewritten as

$$\frac{\delta}{r} Re = \left(\frac{3}{2}\right)^{1/3}\left(\frac{Re^2}{Ta}\right)^{2/3} \qquad (27)$$

$$\text{or } \frac{\delta}{r}(Ta)^{1/2} = \left(\frac{3}{2}\right)^{1/3}\left(\frac{Re^2}{Ta}\right)^{1/6} \qquad (28)$$

The mean residence of the film on the disc may be obtained by substituting (equation (25.2)) into the average velocity, which gives

$$\bar{V}_r = \left(\frac{w^2 Q^2}{12\pi^2\nu}\right)^{1/3} r^{-1/3} \qquad (29)$$

noting $\bar{V}r = \frac{dr}{dt}$ over the depth at that radius, then integrating

$$\frac{dr}{dt} = \left(\frac{Q^2 w^2}{12\pi^2\nu}\right)^{1/3} r^{-1/3} \qquad (30)$$

subject to $\quad t = 0 \quad r = r_i \qquad (31.1)$

$$t = t_r \quad r = r_e \qquad (31.2)$$

gives $$t_r = \frac{3}{4}\left(12\pi^2\right)^{1/3}\left(\frac{\nu(r_e^4 - r_i^4)}{w^2 Q^2}\right)^{1/3} \qquad (32)$$

$$\text{or} \qquad wt_r = \frac{3}{4}\left(12\pi^2\right)^{1/3}\left(\frac{Ta}{Re^2}\right)_o^{1/3}\left(1-\left(\frac{r_i}{r_e}\right)^4\right)^{1/3} \qquad (33)$$

where $\left(\frac{Ta}{Re^2}\right)_o$ is computed at the outer radius.

Fraidenraich (75) divided the flow of thin film on the disc into three regions:

(1) The central region (extends from the centre up to r_c) - where the viscous forces are much larger than the centrifugal forces and the radial component of the initial forces.

(2) The intermediate region - where the inertial and convective forces are equally important.

(3) The external region (from a radius r_e up to infinity) - where the flow is mainly determined by the interplay of viscous and centrifugal forces.

The central region leads to boundary layer problem and film thickness varies as r^2 and the radial velocity as r^{-3}

under the condition that $\dfrac{w^2 r^2 \delta^3}{Q} \ll 1$

or equivalent $\dfrac{Re^2}{Ta} \gg 0.49 \qquad (34)$

$$\delta = \frac{0.62\,\nu r^2}{Q}, \qquad r_c = \left(\frac{Q}{(w\,\nu)^{\frac{1}{2}}}\right)^{1/2}$$

For the external region, using a power series expansion, the film thickness obtained decreases as $r^{-\frac{2}{3}}$ and the radial velocity as $r^{-\frac{1}{3}}$

under the condition that $\dfrac{Q\,\delta}{r^2\nu} \ll 1$

or equivalent $\dfrac{Re^2}{Ta} \ll \dfrac{1}{\sqrt{3}} \qquad (35)$

$$\delta = \left(\frac{3Q\,\nu}{w^2 r^2}\right)^{1/3}, \qquad r_e = \left(\frac{Q}{w\nu^{\frac{1}{2}}}\right)^{1/2}$$

or $\dfrac{\delta}{r} = 3^{1/3}\left(\dfrac{Re}{Ta^2}\right)^{1/3}$ (compared Eq 26) $\qquad (36)$

The intermediate region was only a patching solution, joining the solutions of the two limiting cases considered above. The maximum film thickness was given as

$$\delta_{max} = 0.66 \left(\frac{\nu}{w}\right)^{1/2} \tag{37}$$

with the radial velocity assumed to vary smoothly between the central and external region.

Activos et al (76) and Zinnatullin (77,78) have derived an expression for film thickness on a rotating disc, for a non-Newtonian power law fluid.

Commencing with a shear stress equation of the type

$$\tau = K \left(\frac{dV_r}{dy}\right)^n \tag{38.1}$$

the centrifugal model may be written as

$$\frac{K}{\rho} \frac{d}{dy} \left(\frac{dV_r}{dy}\right)^n = -w^2 r \tag{38.2}$$

with the boundary conditions of equation (22.1) and 22.2). The radial velocity is given as

$$V_r = \frac{n}{n+1} \left(\frac{\rho}{K} w^2 r\right)^{1/n} \left(\delta^{1+n/n} - (\delta - y)^{1+n/n} \right) \tag{39}$$

Integrating again with respect to y and dividing by δ gives $\bar{V}_r$. Equating $\bar{V}_r$ to the flowrate divided by flow area gives an expression similar to equation (25.2)

$$\delta = \left(\frac{1+2n}{2\pi n}\right)^{n/1+2n} \left(\frac{Q}{r} \left(\frac{K}{\rho}\right)^{1/n} \left(\frac{1}{w^2 r}\right)^{1/n}\right)^{n/1+2n} \tag{40.1}$$

$$\text{or } \frac{\delta}{r} = \left(\frac{1+2n}{2\pi n}\right)^{n/1+2n} \left(\frac{Q}{r^{1+3n/n}} \left(\frac{K}{\rho}\right)^{1/n} \left(\frac{1}{w^2 r}\right)^{1/n}\right)^{n/1+2n} \tag{40.2}$$

Note equation (26) and (40.2) are similar if $k = \mu$ and $n = 1$. Tyabin et al (79) have derived similar equations for a visco-plastic medium which exhibits a critical yield stress. The equations for film thickness, once the material has yielded, are essentially unchanged.

Uklisty et al (80) studied film thickness of non-Newtonian liquid by using the electric contact probe technique on a disc of diameter of 25 cm (other parameters see Table 2) and deduced from Zinnatullin (77) the film thickness as

$$\delta = \left(\frac{q}{2\pi B r^{1+n/n}} \right)^{n/2n+1} \qquad (41)$$

where

$$B = \frac{n}{2n+1} \, 0.88^{n+1/2n} \left(\frac{\rho}{K} \right)^{1/n} w^{2/n} \qquad (42)$$

and

$$q = \frac{Q}{2\pi r} \qquad (43)$$

Kostromin et al (81) investigated the thickness of the film of a quasiviscous fluid on a 14 cm diameter disc (other parameters see Table 2). They expressed the viscosity properties of the fluid by an arbitrary rheological law and obtained a complicated correlation between film thickness, flow rate and other parameters. Electrical conductivity technique was used to determine the film thicknesses on the disc. The average divergence of the theoretical and experimental values of the film thickness was given less than 10%.

Yurchenko et al (82) have considered the centrifugal model in which two immiscible liquids are flowing out over the disc in two layers, one on the other. The results reduce to equation 23-25 for the limiting case as the upper layer tends to zero flow rate.

TABLE 2: SUMMARY OF PREVIOUS WORK

INVESTIGATOR	SPEED rpm	FLOW cm /s	DISC DIAMETER cm	REYNOLD	TAYLOR x 10^{-3}	FLUID	INLET TYPE	METHOD	REF
Espig and Hoyle	100-2000	0.6-24	19	10-1180	15-540	Water	1	2	(74)
Gazley and Charwat Charwat et al	60-1080	0.3-13	14	6-1800	7-650	Water	1	3	(95)
Venkataraman	300-1500	1.2-18	12.7	0-300	30-190	Water	1	1	(61)
Clare and Jeffs	0-3000	12-163	10.1	150-4200	30-200	Water cacl2	2	4	(90)
Matsumoto et al	200-900	5-30	12.7	2-108	17-200	Water	2	2	(85)
Vachagin and Nicholaev	0-2500	2.4-24	7.2	50-320	48-326	Water	1	5	(83)
Bell	40-910	8.3-750	44	30-5000	10-5000	Water	2	6	(26)
Zinnatullin	430-1150	0.2-40	6.5	-	-	Water 2%PAC	1	2	(78)
Zinnatullin et al	400-1200	0.2-40	6.5	-	-	Water 2.5%CMC	1	5	(77)
Watts	500-1500	60-180	30	20-3000	1-5000	Various	1	5	(89)
Uklistyi	300-1060	5.2-21	25	-	-	2-3.9% CMC	2	2	(80)
Kastromin	1000-2860	6.3-31	14	-	-	10-22% gelatin	2	7	(81)
Ali	300-1600	12-277	30	1340	1900	Various	2	6	(27)

INLET 1

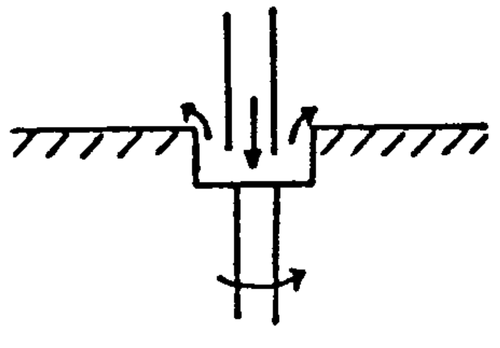

INLET 2

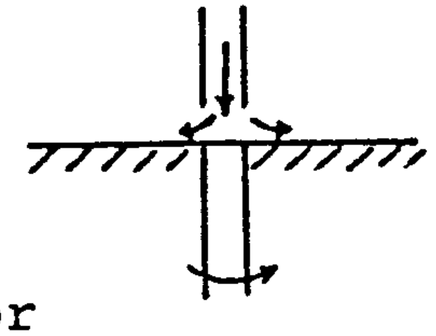

Distributor

METHOD

(1) Micrometer
(2) Micrometer and Elect
(3) Photodensimetric
(4) Elect Resistance
(5) Average Velocity
(6) Capacitative Technique
(7) Conductivity

3.2 CORIOLIS MODEL

Dixon et al (73) showed that, low viscosity liquid drop such as water, it will never reached the angular velocity of the disc and for a significant proportion of the angular velocity to be taken up by the water, the disc had to be fairly large. This was due to Coriolis force, which will be circumferential in direction and opposite to the direction of rotation. This led to the consideration of this additional force to the centrifugal model on thin liquid film flow on rotating disc.

The appropriate equations for solution (see Appendix C) are

$$\nu \frac{\partial^2 V_r}{\partial y^2} = - \frac{V_\theta^2}{r} \qquad (46.1)$$

$$\nu \frac{\partial^2 V_\theta}{\partial y^2} = \frac{V_\theta V_r}{r} + V_r \frac{\partial V_\theta}{\partial r} \qquad (46.2)$$

after neglecting lower order magnitude terms and substituting $V_\theta = rw$ into equations (46.1) and (46.2) gives

$$\nu \frac{\partial^2 V_r}{\partial y^2} = -w^2 r \qquad (47.1)$$

$$\nu \frac{\partial^2 V_\theta}{\partial y^2} = 2wV_r \qquad (47.2)$$

Emslie et al (74) show that equation set (47) will be equal to the centrifugal model if

$$w^2 r >> 2wV_r$$

using the results for V_r and δ from the centrifugal model then the critirionfor neglecting the Coriolis acceleration was

$$\frac{Q^2}{\nu w r^4} << 1 \qquad (48)$$

Notice that the group $Q^2/\nu w r^4$ can be written as Re^2/Ta. Hence the limitations of the centrifugal model are controlled by the magnitude of the group Re^2/Ta. It is apparent that no matter

how small the values of Re^2/Ta, any finite value whatsoever implies that equation (47.2) cannot be strictly taken as zero. However, for sufficiently small values of Re^2/Ta, the solution of equation set (47) should closely approximate that of centrifugal model. Therefore theoretical estimation of the centrifugal model can be justified from equation (47.1).

Vachagin and Nikolaev (83), after obtaining a solution to equation set and assuming that V_θ and V_r were given by equations of the form wr(f) when f was function of y alone, then the end result of their analysis is

$$\frac{\sinh (2A) - \sin (2A)}{\cosh (2A) + \cos (2A)} = \frac{2}{\pi} \left(\frac{Re^2}{Ta} \right) \qquad (49)$$

Where $A = \frac{\delta}{r} Ta^{\frac{1}{2}}$ and the above equation (49) shows A implicity as a function of Re^2/Ta. They compared the results of this expansion with the centrifugal model and concluded that the models were nearly identical if

$$\frac{\delta}{r} (Ta)^{1/2} < 0.5 \qquad (50)$$

or equivalently $\frac{Re^2}{Ta} < 0.512$

Zinnatulin et al (78) in their expansion of equation set (47) for non-Newtonian fluids again compared the theoretical solution against that of the centrifugal model and concluded that they were nearly identical if

$$\frac{2}{\pi} \frac{Re}{Ta} \frac{r}{\delta} < 0.01 \qquad (51)$$

or equivalently $\frac{Re^2}{Ta} < 1.85 \times 10^{-6}$

Rauscher et al (84) obtain two criteria from their expansion of the simplified three-dimensional Navier-Stokes equation (see later). Firstly, equating the magnitudes of centrifugal and coriolis forces. Secondly, by considering the additional terms introduced into the expansion for δ, then for the centrifugal model to fit

$$\frac{\delta}{r} << 1$$

Matsumota et al (85,86) considered the polynomical expansion of the equations equivalent to VanKataraman's equations for a disc in an infinite medium and concluded that the centrifugal model was found if

$$\frac{\delta}{r} (Ta)^{1/2} < 1 \qquad (52)$$

or equivalently $\frac{Re^2}{Ta} < 1.447$

An approximate solution to equation set (47) has been obtained by Bell (26). By differentiating equation (47.2) twice with respect to y, then substituting for V_r' from equation (47.1) gives V_r and V_θ. However, one of the boundary conditions used was in error (y = o, $V_r = V_\theta$ = o should be y = o V_r = o V_θ = rw). Hence the equation set (47) was rederived and gives

$$\frac{\partial^4 V_\theta}{\partial y^4} = -\frac{2w^3 r}{\nu^2} \qquad (53)$$

Integrating four times

$$V_\theta = \frac{1}{12} \frac{w^3 r}{\nu^2} y^4 + \frac{A}{6} y^3 + \frac{B}{2} y^2 + C y + D \qquad (54)$$

where A, B, C and D are functions of w, ν, r only. Forming $\frac{\partial^2 V_\theta}{\partial y^2}$ and using equation (47.2) gives

$$V_r = - \frac{w^2 r}{2\nu} y^2 + \frac{A\nu}{2w} y + \frac{B\nu}{2w} \qquad (55)$$

Using boundary conditions

$$y = 0 \qquad V_r = 0 \qquad V = rw \qquad (56.1)$$

$$y = \delta \qquad \frac{dV_r}{dy} = \frac{dV_\theta}{dy} = 0 \qquad (56.2)$$

gives the constants

$$A = \frac{2w^3 r\delta}{\nu^2} \qquad B = 0 \qquad C = -\frac{2}{3} \frac{w^3 r\delta^3}{\nu^2} \qquad D = rw$$

giving the final distribution as

$$V_r = \frac{w^2 r}{\nu} \left(\delta y - \frac{y^2}{2} \right) \tag{57.1}$$

and

$$V_\theta = \frac{w^3 r}{3\nu^2} \left(\delta y^3 - 2\delta^3 y - \frac{1}{4} y^4 \right) + rw \tag{57.2}$$

Rauscher et al (84) considered the same equations (Appendix C) neglecting the normal velocity and its derivatives. A polynomial expansion was undertaken, subject to the boundary conditions of no solid surface velocity and zero free surface interfacial drag. Surface curvature and tension were considered as boundary conditions. The resulting expansions are infinite, but the first significant terms of the expansion are

$$V_r = \frac{w^2 r}{\nu} \left(\delta y - \frac{\delta^2}{2} \right) \tag{58.1}$$

$$V_\theta = \frac{w^3 r}{\nu^2} \left(-\frac{2}{3}\delta^3 y + \frac{1}{3}\delta y^3 - \frac{y^4}{12} \right) \tag{58.2}$$

$$V_y = \frac{w^2}{\nu} \left(\frac{y^3}{3} - \frac{2}{3}\delta y^2 \right) \tag{58.3}$$

The difference in equation (57.2) and (58.2) was due to the boundary condition considered.

3.3 GENERAL MODELS

Marshall et al (87) in their investigation of several methods of atomising liquids, derived an equation for laminar flow on a smooth disc which can be shown as

$$V_r \frac{dV_r}{dr} + \frac{12\pi^2 \mu r^2 V_r^3}{Q^2 \rho} - rw^2 = 0 \qquad (59)$$

However, they did not experimentally verify the equation put forward.

Clare (88) gives the theoretical treatment of a laminar film flow on rotating disc as

$$V_r \frac{dV_r}{dr} - K^2 rw^2 + \frac{12\pi^2 \mu r^2 V_r^3 \rho}{Q^2} = 0 \qquad (60)$$

where k is the drag factor and Q = weight rate of flow of liquid. Clare claimed that the acceleration term can simply be omitted. He then showed that the solution thus obtained is a reasonable approximation over a useful range of values of the parameter. The equation (60) presented is seen to be identical to that of Marshall et al (87) except for the drag factor term (method of derivation was not given).

Watts (89) derived an equation similar to equation (59) by considering 'momentum flow rate' at a given radius, by defining

$$M = \int_0^{\delta} \rho V_r^2 \, dy \qquad (61)$$

and centrifugal force - Viscouse drag = Mass X acceleration

$$\text{or} \qquad \delta\rho w^2 r - \mu \left(\frac{dV_r}{dy} \right)_{y=0} = \delta\rho \frac{dV_r}{dt} \qquad (62)$$

and equating the left-hand side of equation 62 to the radial rate of change of momentum, dM/dr, then by using the centrifugal model velocity profile Watts obtained the relationship

$$\frac{d\delta}{dr} = -\frac{\delta}{r} - \frac{10\pi^2 r^3 \delta^3 w^2}{3Q^2} + \frac{5\pi r\nu}{Q} \qquad (64)$$

but $$\frac{dV_r}{dr} = \frac{d}{dr}\left(\frac{Q}{2\pi r\delta}\right) = \frac{Q}{2\pi}\frac{d}{dr}\left(\frac{1}{r\delta}\right)$$

$$= \frac{Q}{2\pi}\left(-\frac{1}{\delta r^2} - \frac{1}{r\delta^2}\frac{d\delta}{dr}\right) \qquad (65)$$

which gives $$\frac{dV_r}{dr} = \frac{5}{6}\left(\frac{w^2 r}{V_r} - \frac{12\pi^2 \mu r^2 V_r^2}{\rho Q^2}\right) \qquad (66)$$

note, equation (59) and (66) are similar except the factor 5/6.

Venkataraman (61) considered a force balance on an annular element of liquid of thickness δ on the disc which takes into effect of Coriolis and inertial forces. The circumferential velocity profile at any radius on the disc was assumed to be represented by a polynomial which was chosen to satisfy the boundary conditions in the circumferential direction.

$$y = 0 \qquad V_\theta = rw \qquad (67.1)$$

$$y = \delta \qquad V_\theta = V_{\theta s} \qquad \frac{dV_\theta}{dy} = 0 \qquad (67.2)$$

and obtained the equations as

$$V_r \frac{dV_r}{dr} + \frac{12\pi^2 \nu r^2 V_r^3}{Q^2} - \frac{V_\theta^2}{r} = 0 \qquad (68.1)$$

$$V_r \frac{dV_\theta}{dr}(1 - V_r) + 2V_\theta V_r - \frac{12\pi^2 \nu r^2 V_r^2}{Q^2}(wr - V_\theta) = 0 \qquad (68.2)$$

Equation set (68) was solved numerically by Venkataraman and he concluded that the effects of inertial and Coriolis are effective only at a small distance from the distributor.

3.4 TURBULENT FLOW

Clare and Jeffs (90) derived equations to describe the flow of thin liquid film on the rotating disc. They obtained for a laminar flow

$$V_r \frac{dV_r}{dr} - K^2 r w^2 + \frac{12\pi^2 \mu \rho r^2 V_r^3}{Q^2} = 0 \qquad (69)$$

and for turbulent flow

$$V_r \frac{dV_r}{dr} - K^2 r w^2 + \frac{\pi \rho f r V_r^3}{Q} = 0 \qquad (70)$$

where K is a drag factor, Q = weight rate of flow of liquid, f = friction factor. They claimed that if the initial acceleration term of equation (69) is ignored, that is, the differential term is omitted, centrifugal film thickness δ similar to equation (25.2) is obtained and for the turbulent flow as

$$\frac{\delta}{r} = \left(\frac{f}{16\pi^3} \frac{Q^2}{w^2 r^6} \right)^{1/3} \qquad (71)$$

Jones (91) followed Clare and Jeffs's work by ignoring the differential term and she was able to show that for the majority of flow conditions studied by Clare and Jeffs, the inlet inertia should not play a significant part.

Marshall et al (87,87a) also proposed an equation for the flow of liquid film on rotating disc, involving friction factor (as in equation (71)) which is equivalent to that of Fanning friction factor for full tube flow. The proposed equation is

$$V_r \frac{dV_r}{dr} + \left(\frac{fr}{2Q} \right) V_r^3 - w^2 r = 0 \qquad (72)$$

For laminar flow $f = \frac{24\pi^2 \nu r}{Q}$ with the assumption that semi-parabolic model for velocity profile applies.

For turbulent flow f = (viscous drag)/ρV_r^2

Venkataraman (61) employed Sleicher's (92) equation for the eddy viscosity

$$\frac{\varepsilon}{\nu} = by^{+2} \qquad b = 0.091 \qquad (73)$$

Where y^+ is a dimensionless group used in the universal velocity profile analysis, equation

he assumed that $$\frac{dv_r^+}{dy^+} = \left(1 - \frac{y^+}{\delta^+}\right) / \left(1 + \frac{\varepsilon}{\nu}\right) \qquad (74)$$

and obtained $$v_r^+ = \frac{1}{b} \arctan by^+ - \frac{1}{2b^2\delta^+} \ln (1+b^2y^{+2}) \qquad (76)$$

second integration gives

$$Re = \frac{2}{b^2}\left((x - \frac{1}{x})\arctan x + 1 - \ln (1+x^2)\right)$$

where

$$x = b\delta^+$$

Davies (93) has used Sleicher's equation for single phase flow on plane film flow and obtained numerical results close to Lilleleht's data (see 93) for horizontal air/water film flow. He concluded that Sleicher's expression is strictly applicable for $\delta^+ << 30$ (ie before the turbulent region in the universal velocity profile).

Watts (89) employed Reichard's (see 89) expression for eddy diffusivity and obtained

$$\frac{\varepsilon}{\nu} = K\left(y^+ - \beta\tanh\left(\frac{y^+}{\beta}\right)\right) \qquad (77)$$

where k and β are constants. Venkataraman and Watts's expression has shown that their film thicknesses for turbulent flow are greater than those of the laminar model.

3.5 EXPERIMENTAL RESULTS

(A) Film Thickness

Espig (72) used a micrometer pointer with electrical surface contact indication for measurements of film thicknesses of water flow on a rotating disc. He obtained a correlation $(\frac{\delta}{r}(Ta)^{\frac{2}{3}})$ Vs Re, which is produced as an extension of film flow on a vertical plate with the gravity term replaced by rw^2. His experimental results showed considerable scatter about the above correlation.

Vankataraman (61) used micrometer pointer and capacitive techniques for measuring film thickness on a rotating disc, but the latter technique was inadequate to obtain reproducible results. Thus, the technique finally employed was the micrometer probe technique, similar to that of Espig (72). Bell (26) explained the difficulty found by Venkataraman in applying the capacitive technique was probably due to the fact that the probe head and the connections from the probe to the capacitometer were not shielded from stray fields and fringing effects. The data collected by Venkataraman showed good agreement to the centrifugal model (see fig 3).

Matsumoto et al (85) used the similar method as Espig and Venkataraman on a 12 cm diameter disc rotating at speeds up to 90C rpm. The viscosity of the fluids investigated varied from 9.6 cs to 58.3 cs. The results obtained are in good agreement with the centrifugal model (see fig 3.1).

Clare and Jeffs (90) and Clare and Ashwood (94) employed electrical measurement of the resistance of the flowing film to infer film thickness. They came across several difficulties in creating the annular ring electrodes, maintaining electrical insulation between the rings and the remainder of the flow circuit and the interpretation of the operative radii of the measurement taken. They compared their results to the simple theories

of laminar and turbulent flow (90) and concluded that their results were in good agreement with the centrifugal model if Re was less than a critical value. The critical value given was in the range between 1600 to 5480. No reasonable explanation was given for the variation found. (fig. 3.2)

Gazley and Charwat (95) and Charwat (96) used the light absorption technique to study the flow of water and water/surfactant mixtures on a rotating glass disc. They showed that the film thicknesses for both liquids were indistinguishable; the same but with less scatter about the correlation groups $(\frac{\delta}{r})$ against (Re/Ta^2) for the water surfactant system, compared to water. They also noted that the surface disturbances were considerably reduced for the water/surfactant system. (fig. 3.3,3.4)

Vachagin and Nikolaev (83) employed high speed photographic technique, where poppy grains were mixed with the fluid and photographs were taken. The average radial velocity at a given radius was thus found, from which the radial distribution of thickness may be calculated. Data obtained was close in agreement to the theoretical model. (fig. 3.5)

Watts (89) used the same technique as Vachagin and Nikolaev with carbon black particles instead of poppy grains in the castor oil films and neutrally buoyant oil droplets in water and water/glycerol films. The results are poorly correlated for water but for liquids of higher viscosity the results were in reasonable agreement with the centrifugal model. Watts suggested the discrepancy between experimental and centrifugal model results seems to be more attributable to the technique used than to anomolous behaviour of the fluid. (fig. 3.6,3.7,3.8)

Bell (26) employed the capacitive technique to study the film flow of water over a disc of diameter at a maximum speed of 1000 rpm. The data were in good agreement with centrifugal model except for $\frac{Re^2}{Ta} > 1$ when the critical centrifugal model is no longer applicable (see Section 3.2). He concluded that the

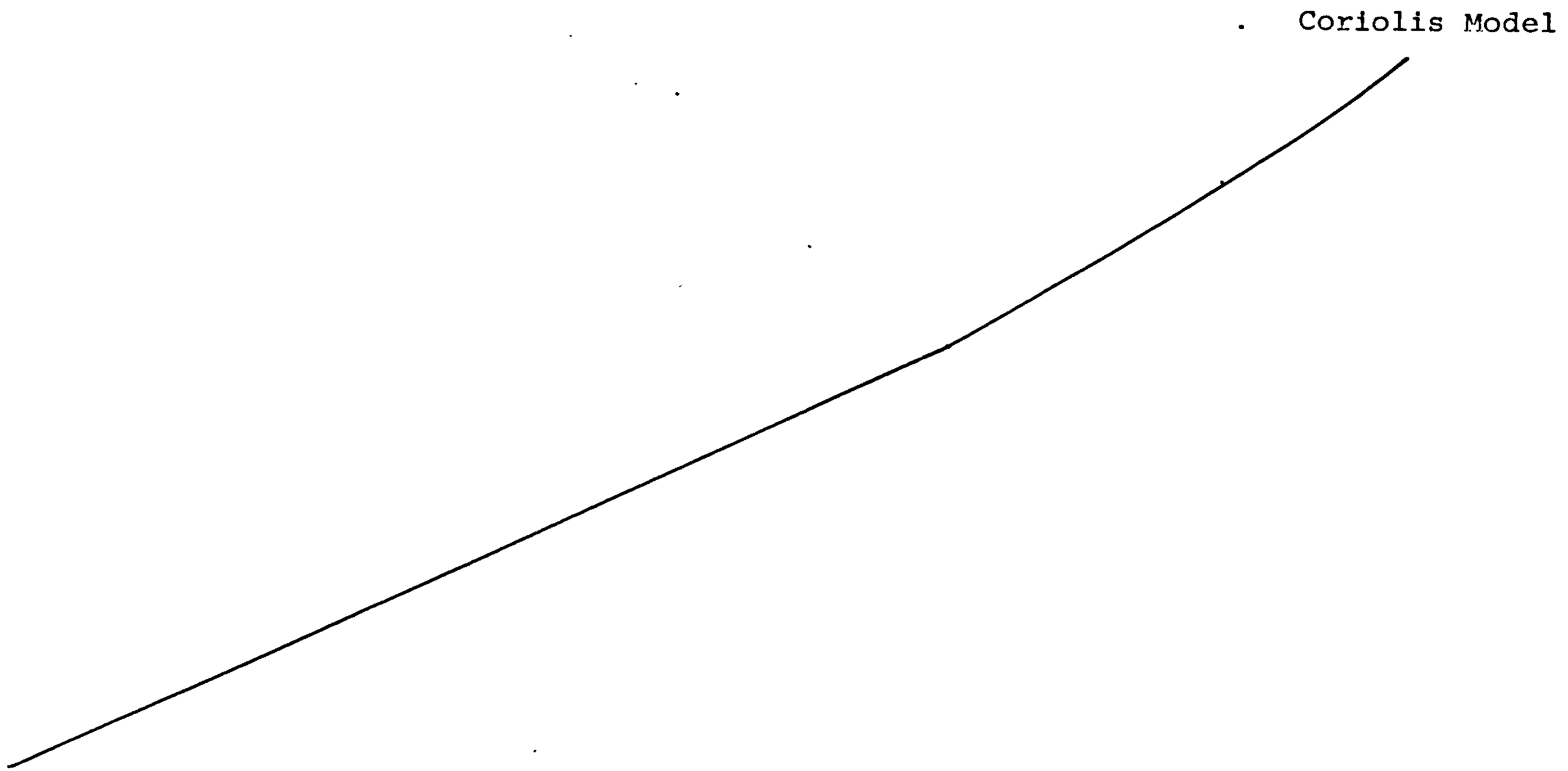
Coriolis Model

Eq 27

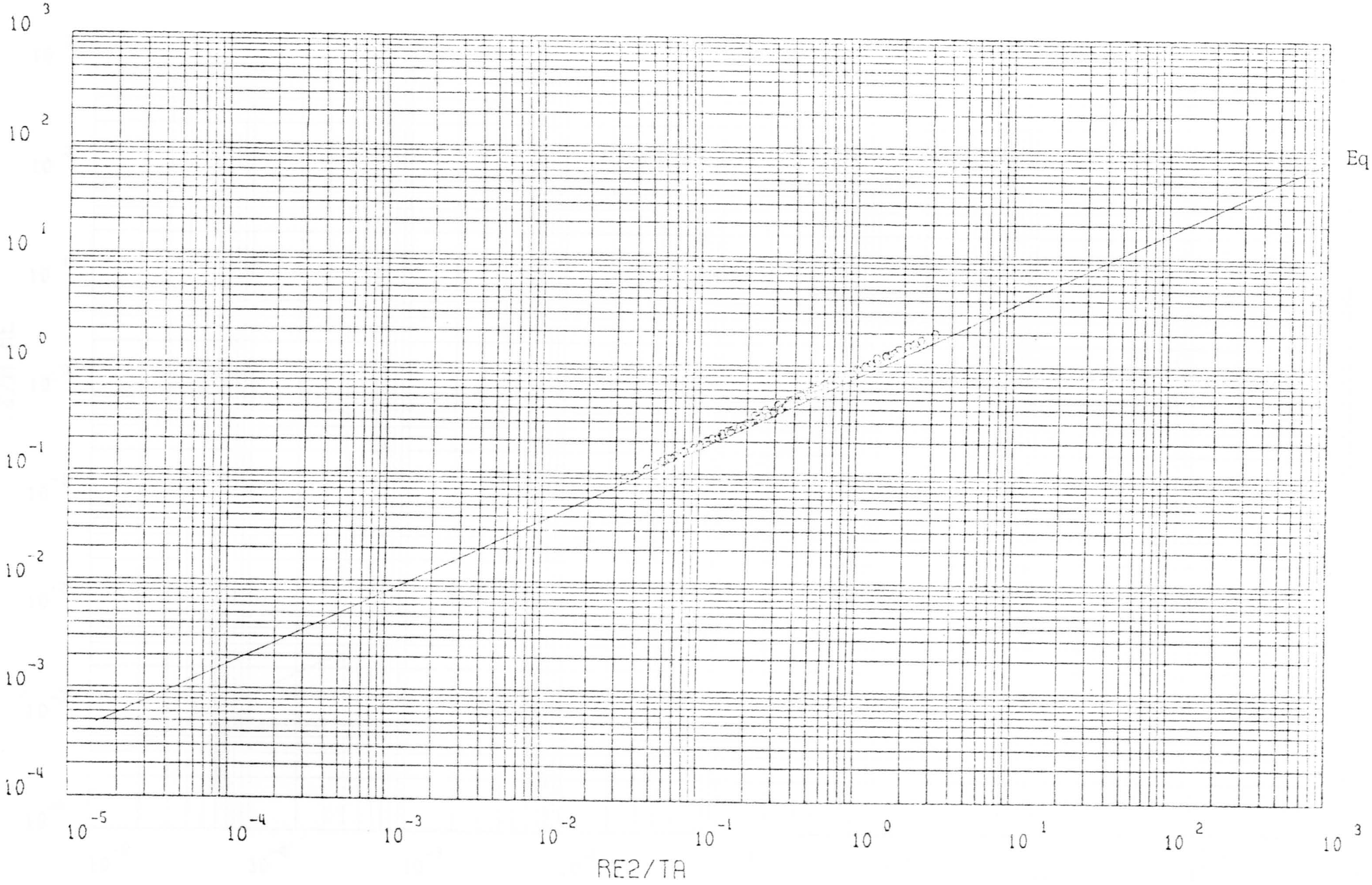

FIGURE 3.0 VENKATARAMAN'S DATA (27)

10^{3}
10^{2}
10^{1}
10^{0}
10^{-1}
10^{-2}
10^{-3}
10^{-4}

δ/R RE

. Coriolis Model

Eq 27

10^{-5} 10^{-4} 10^{-3} 10^{-2} 10^{-1} 10^{0} 10^{1} 10^{2} 10^{3}

RE2/TA

FIGURE 3.0 VENKATARAMAN'S DATA (27)

Eq 27

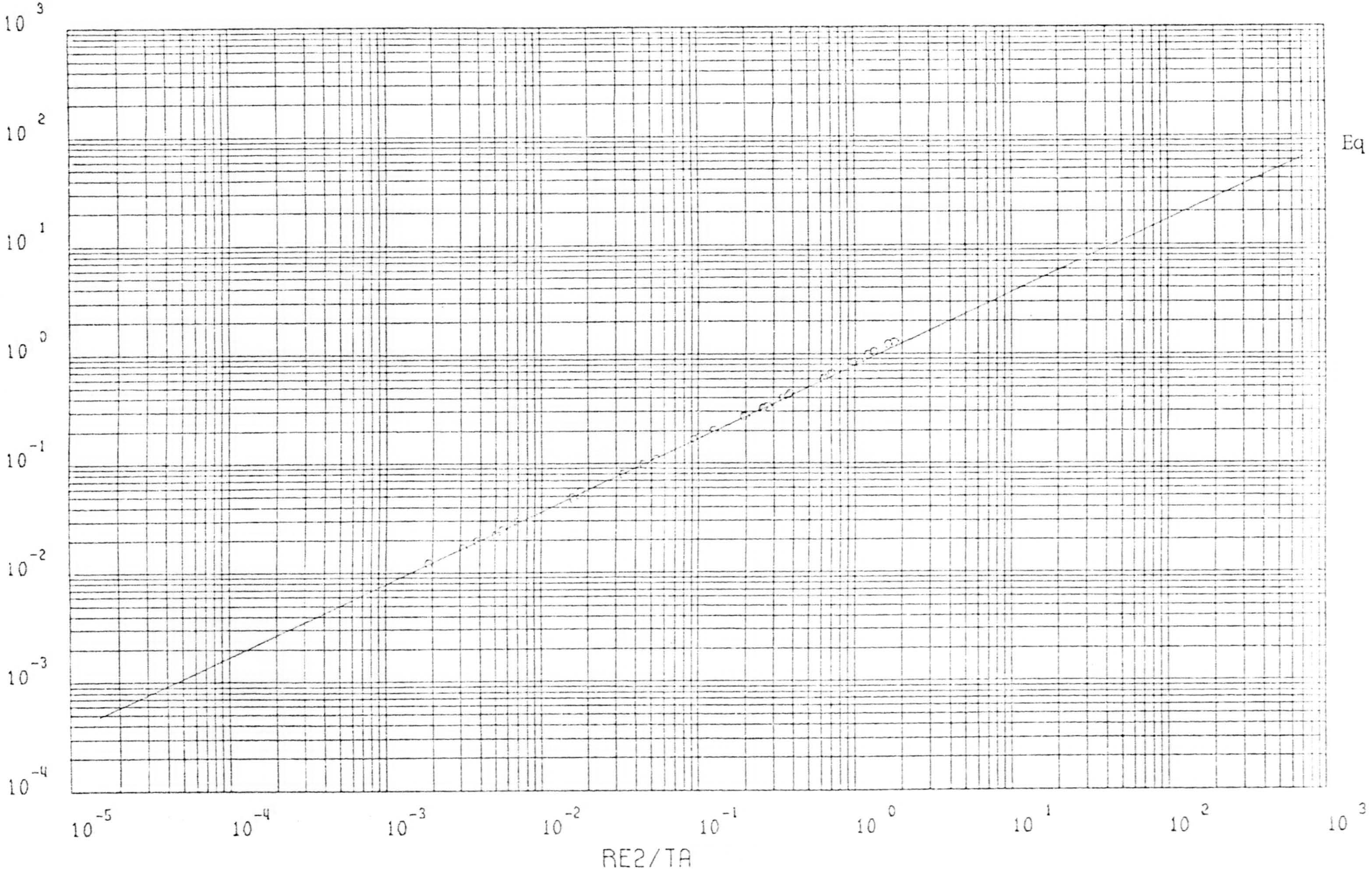

FIGURE 3.1 DATA OF MATSUMOTO et al (27)

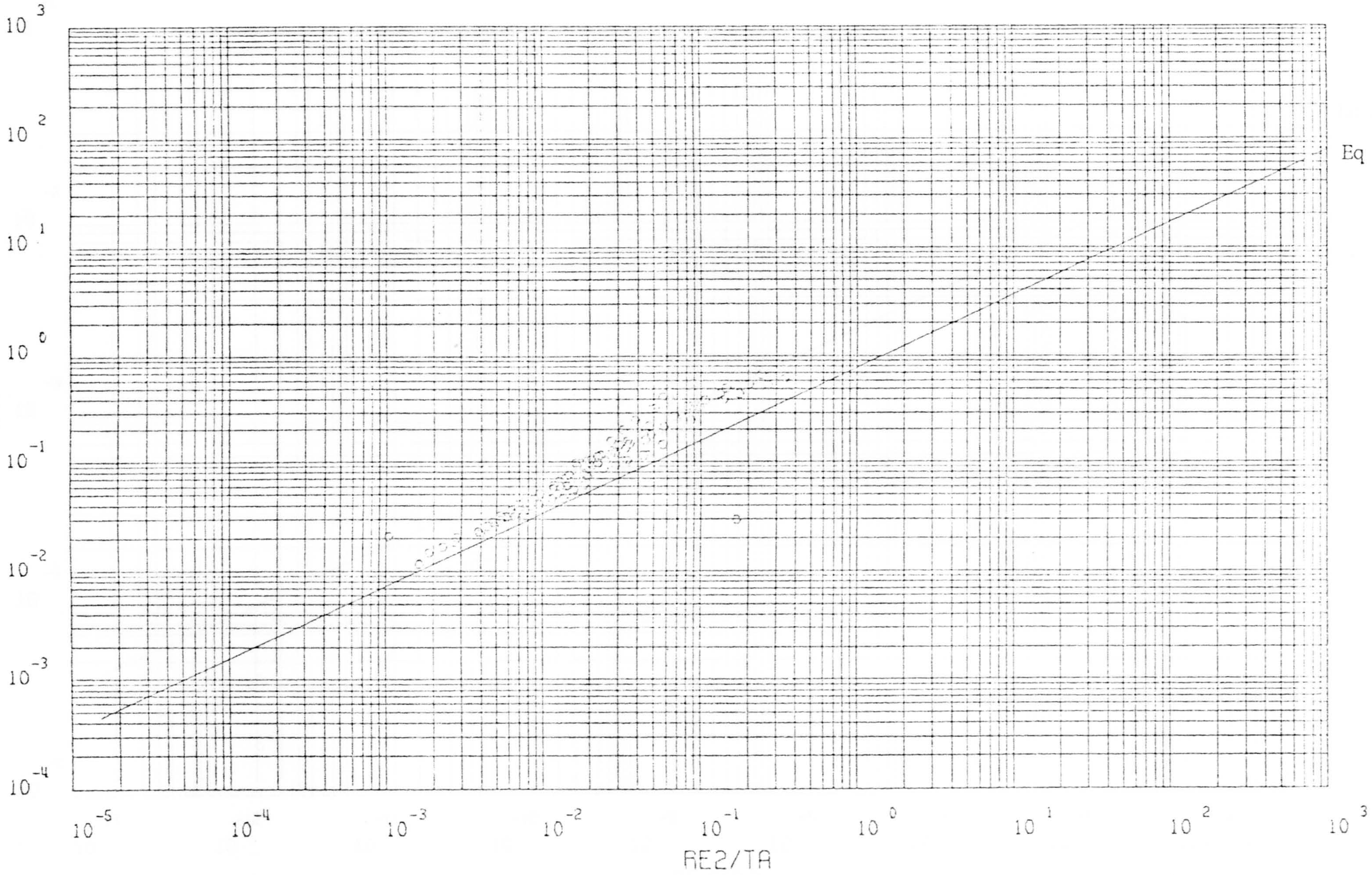

Eq 27

FIGURE 3.2 THE DATA OF CLARE AND JEFFS (27)

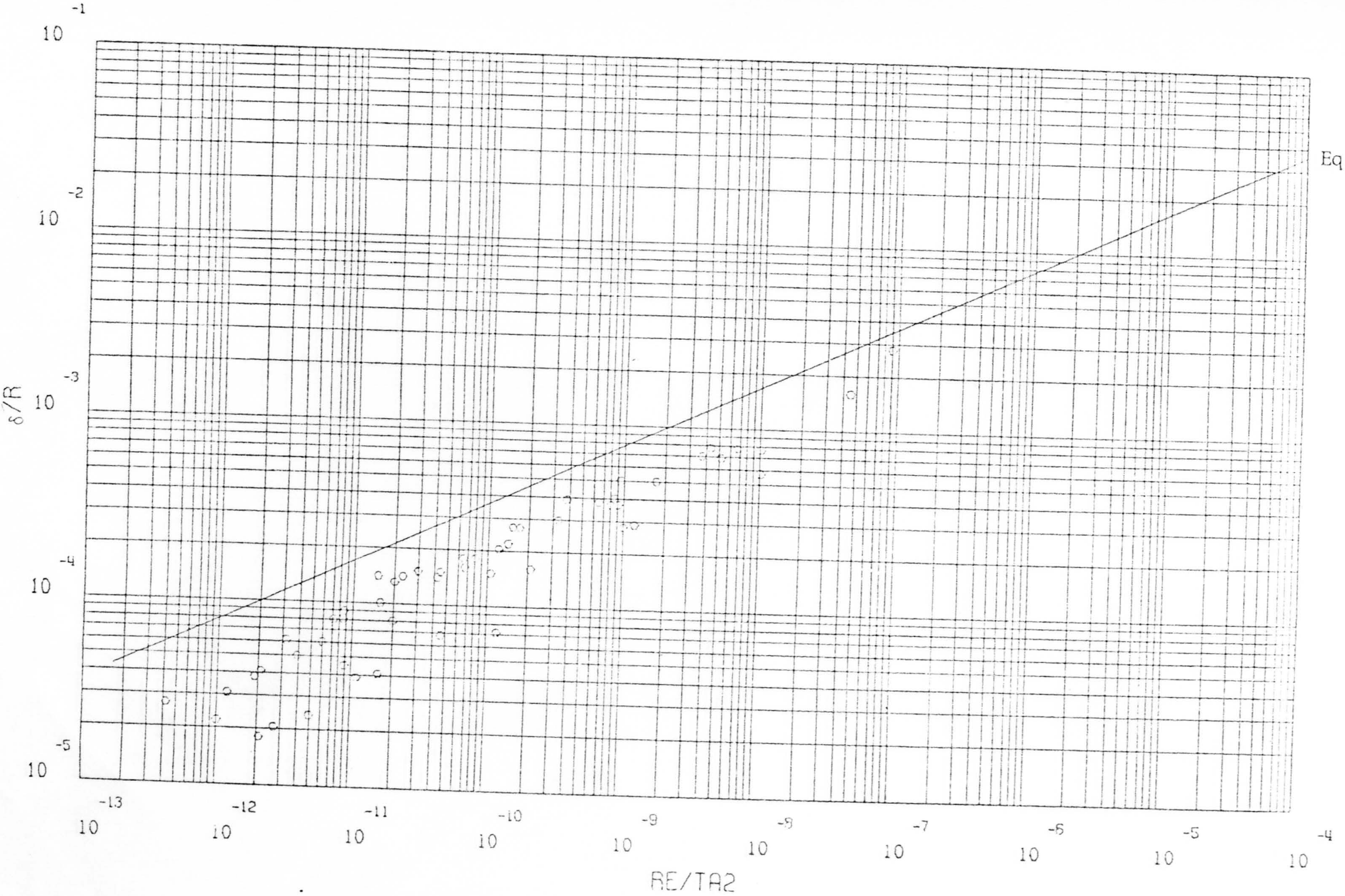

FIGURE 3.3 WATER DATA OF CHARWAT et al (27)

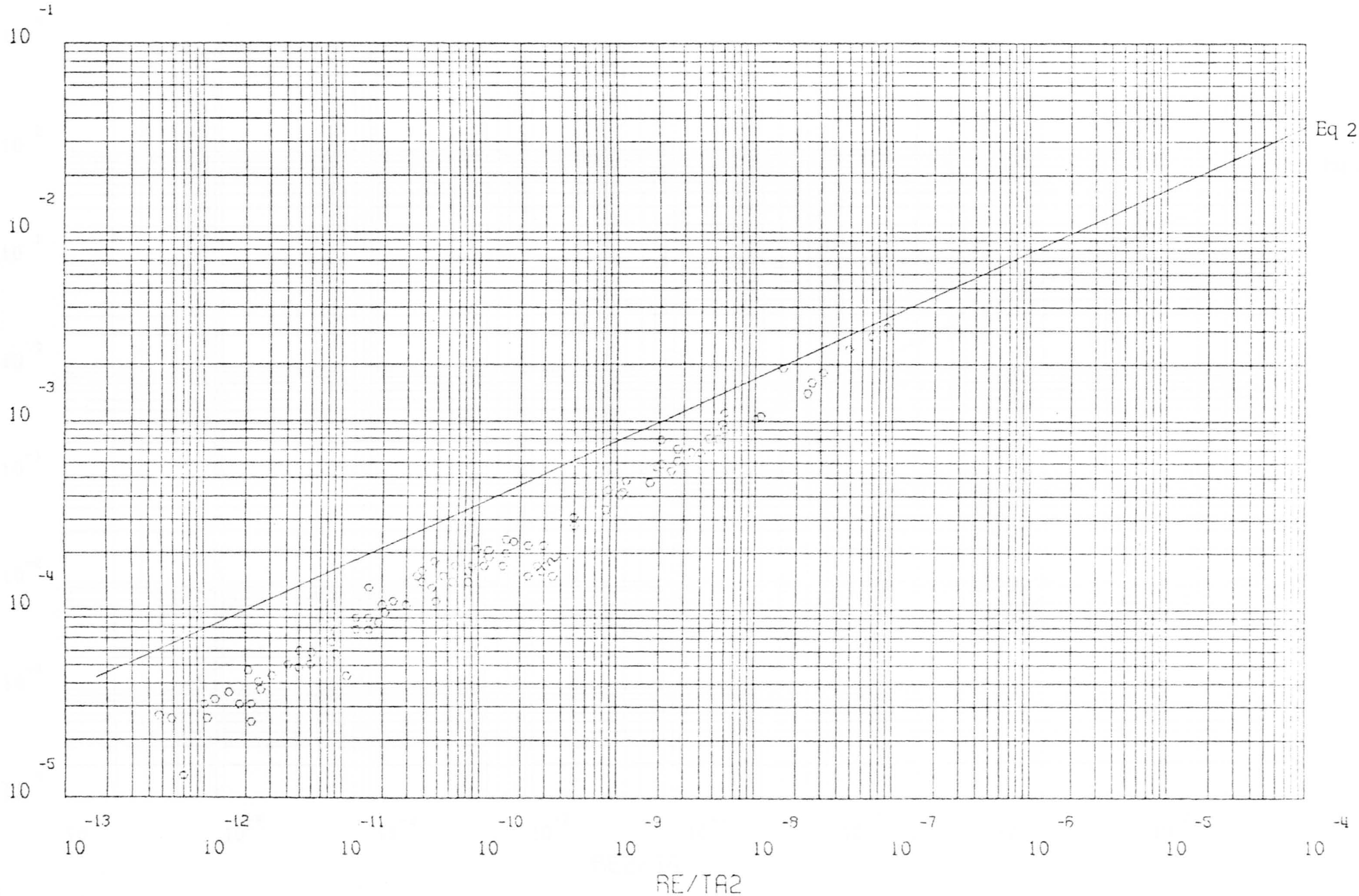

FIGURE 3.4 WATER/SURFACTANT DATA OF CHARWAT et al (27)

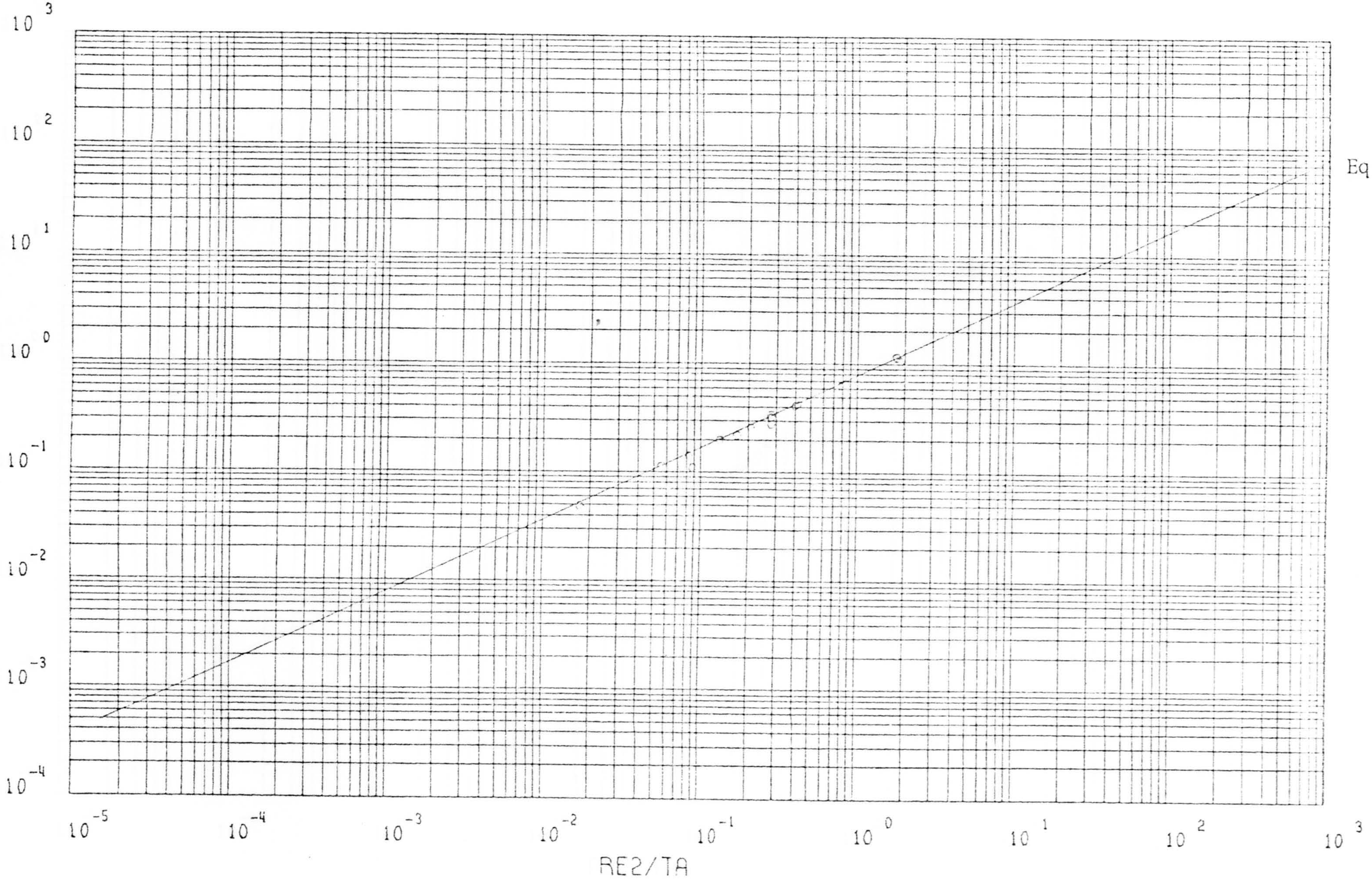

Eq 27

FIGURE 3.5 DATA OF VACHAGIN AND NIKOLAEV (27)

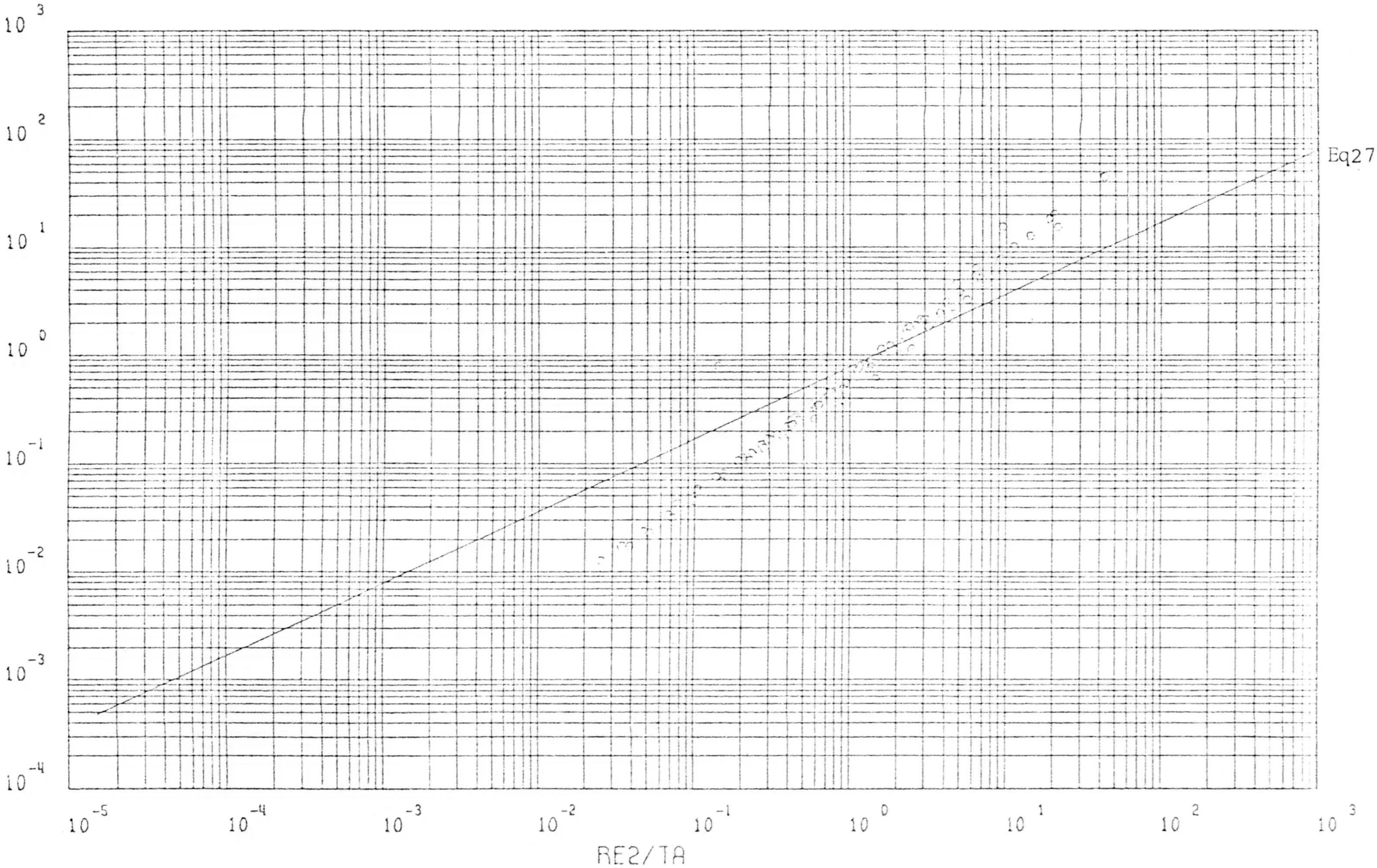

FIGURE3.6 WATTS WATER DATA (27)

Eq 27

δ/R RE

10^{3} 10^{2} 10^{1} 10^{0} 10^{-1} 10^{-2} 10^{-3} 10^{-4}

10^{-5} 10^{-4} 10^{-3} 10^{-2} 10^{-1} 10^{0} 10^{1} 10^{2} 10^{3}

RE2/TA

FIGURE 3.7 WATTS GLYCEROL/WATER DATA (27)

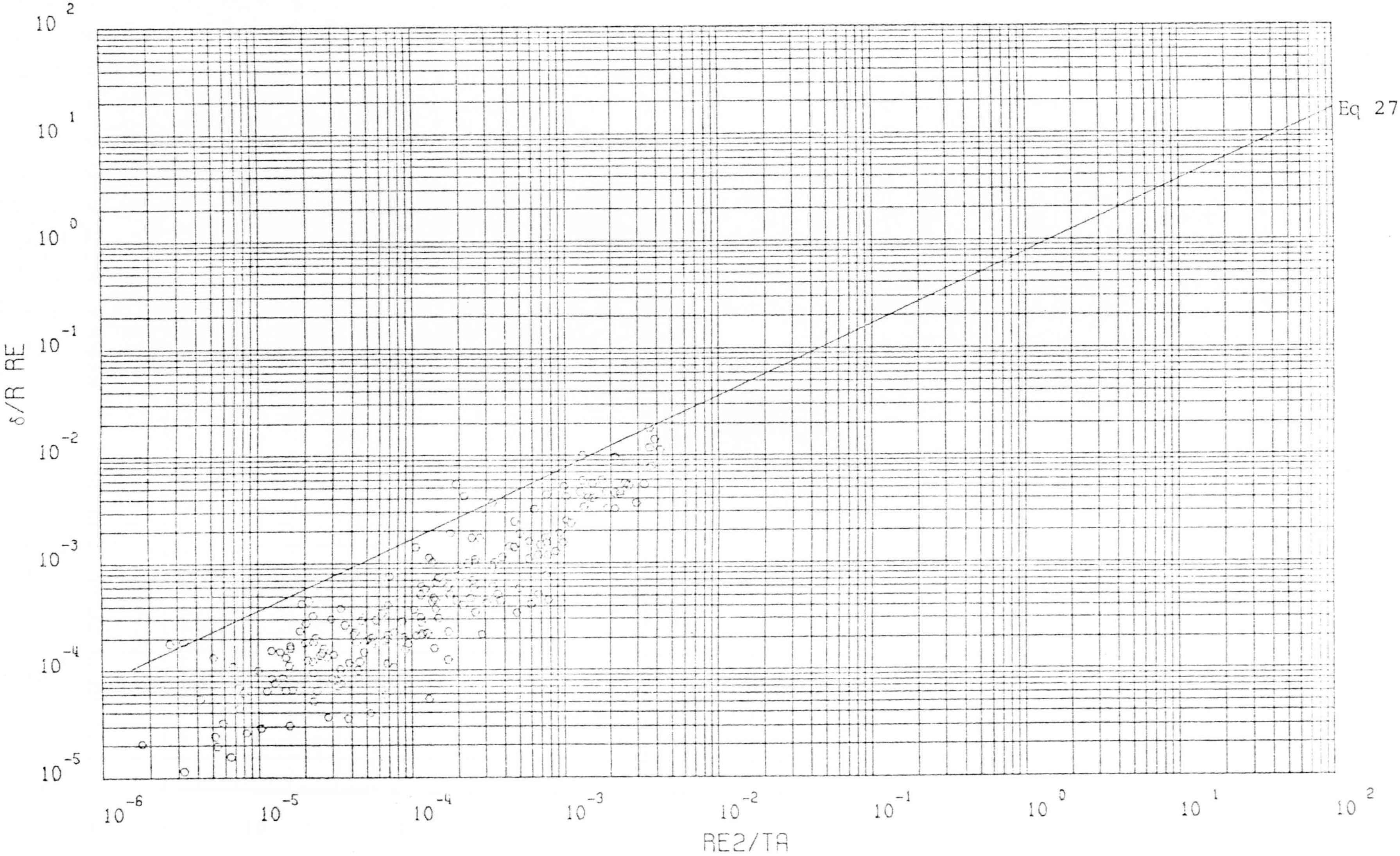

FIGURE 3.8 WATTS CASTROL OIL DATA (27)

Eq 27

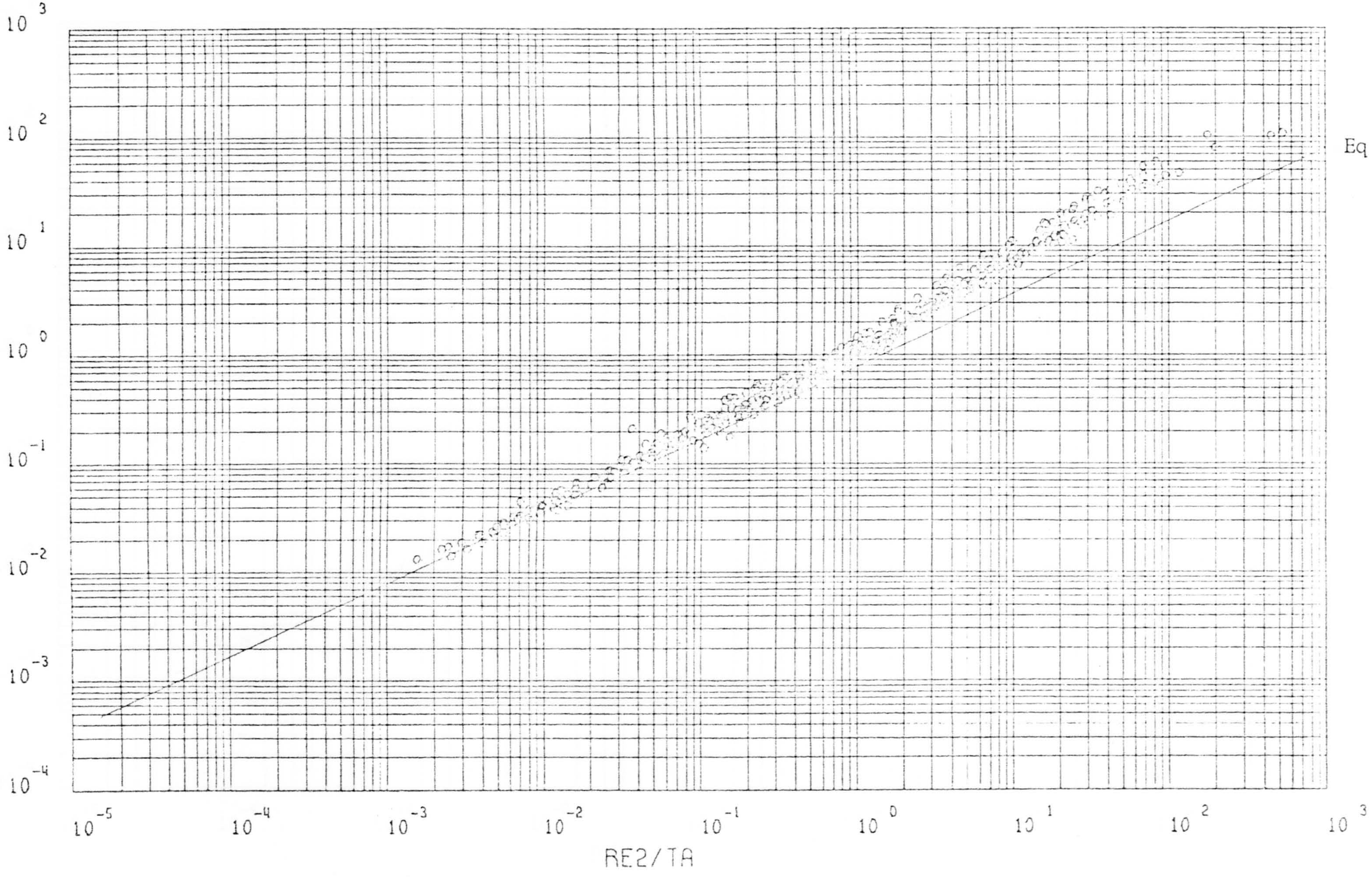

FIGURE 3.9 BELL'S DATA (27)

Eq 27

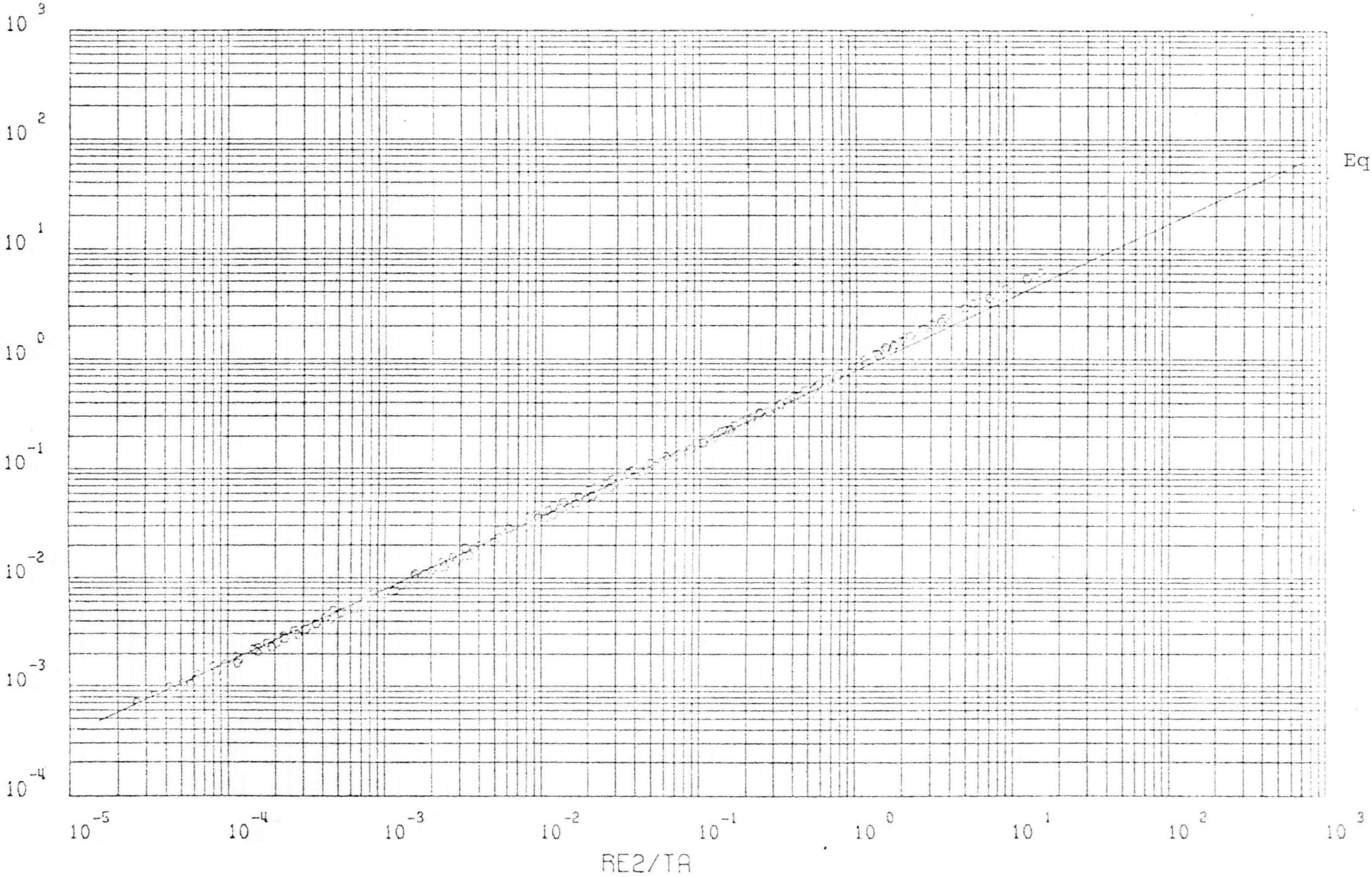

FIG 3.10 EXPERIMENTAL FILM THICKNESS RESULTS FOR OIL (27) DOUBLE PROBE

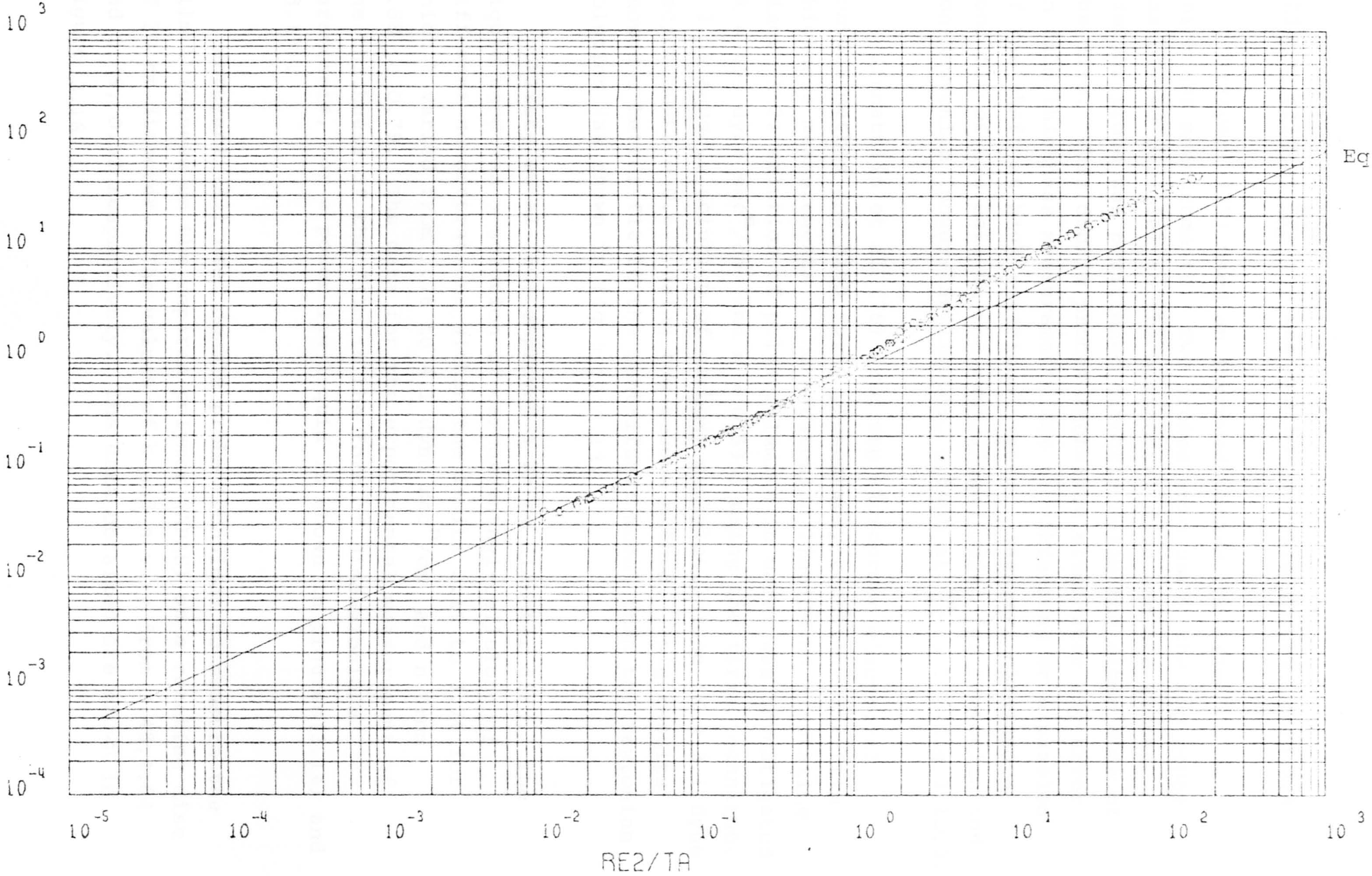

Eq 27

FIG 3.11 EXPERIMENTAL FILM THICKNESS RESULTS FOR WATER (27) DOUBLE PROBE

thicker film at $\frac{Re^2}{Ta} > 1$ was due to oriolis forces. (fig 3.9)

Jazayeri (27) used an improved method for film thickness measurements. Two probes were used, the top probe was placed parallel to the horizontal disc and the second similar probe was positioned directly below the other side of the disc. This double probes technique eliminates any error in film thickness measurements due to vibrations or expansion of the shaft at high rotational speed. Jazayeri obtained a good fit of his data to the centrifugal model for Newtonian and non-Newtonian (power-law)liquids, except at $\frac{Re^2}{Ta} > 1$. (fig 3.10,3.11)

Zinnatulin et al (78) used the microprobe electrical contact method and high speed photography technique for film thickness measurements of non-Newtonian liquids on a rotating disc. A 2% solution of polyacrylamide in water was investigated (k = 455 dyne sec^n/cm and n = 0.535) using the first technique. A 2.5% aqueous solution of carboxy methylcellulose (K = 3.1 dyne sec/cm and n = 0.67) using the second method. Thie results showed a better fit to the centrifugal model than the Newtonian solution (as shown in fig 3.12,3.13)

Uklisty et al (80) employed a 25 cm diameter disc. The liquid used was a solution of carboxymethyl-cellulose of different concentrations within the limits 2.1% to 3.7% for which k varied from 1.76 to 4.1 dyne sec^n/cm and n from 0.88 to 0.79. The data for the experimental measurement of the thickness of the film in the form of dimensionless parameters, for a power law liquid is shown in figures(3.14) and (3.15).

Jazayeri (27) used double probe technique to measure the film thickness on the separan polymer (APAS) on a rotating disc of 30 cm diameter. The values of k and n vary from 3.48,4.84 and 0.46, 0.52 respectively. The data obtained are shown in figure 3.16

POWER LAW CORRELATION

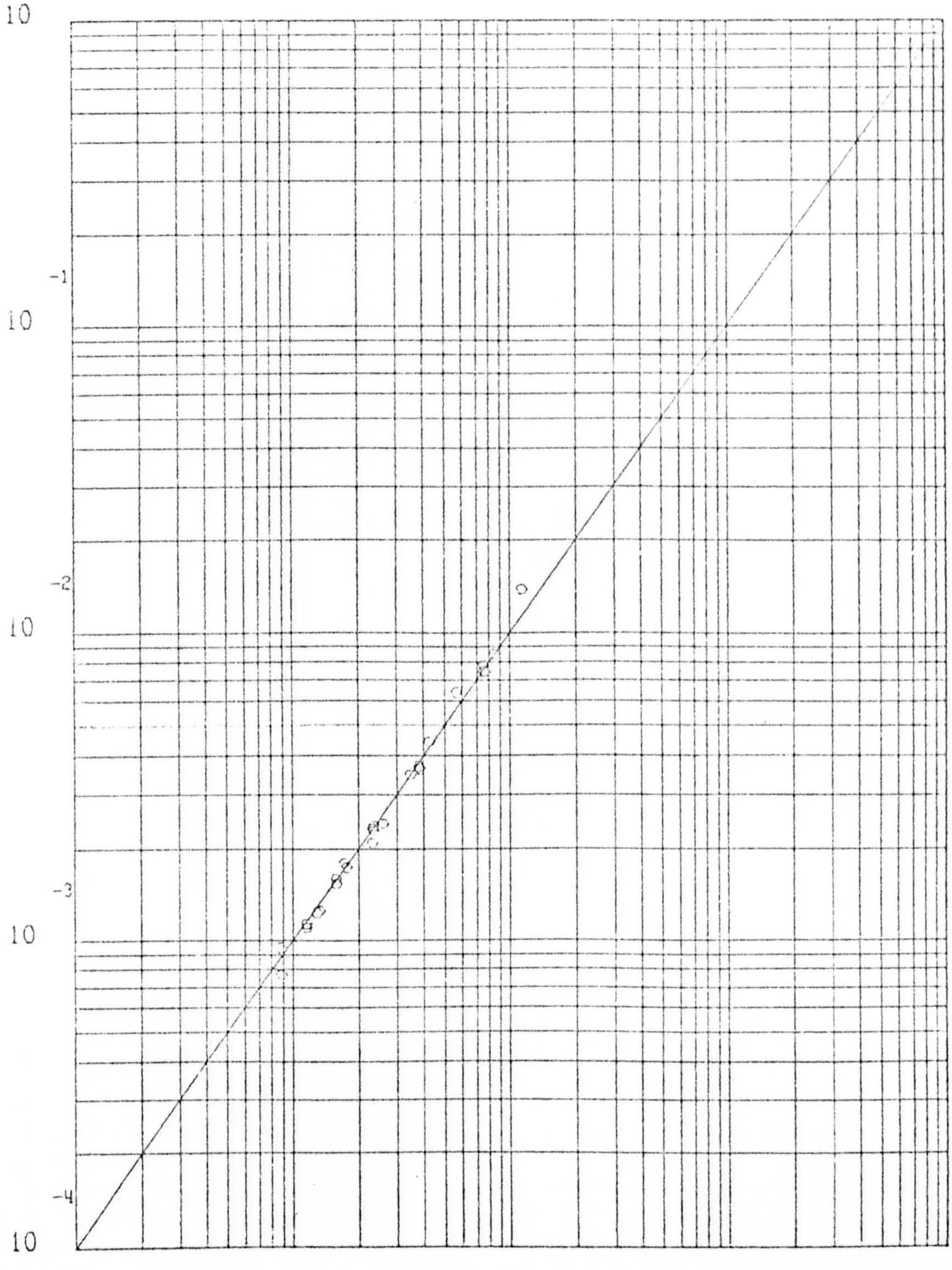

$$\left(\left(\frac{2n+1}{2\pi n} \right)^n \frac{KQ^n}{\rho\, \omega^2 r^{3n+2}} \right)^{\frac{1}{2n+1}}$$

Eq 40.2

FIG 3.12 THE DATA OF ZINNATULLIN ET AL(27) n = 0.535

POWER LAW CORRELATION

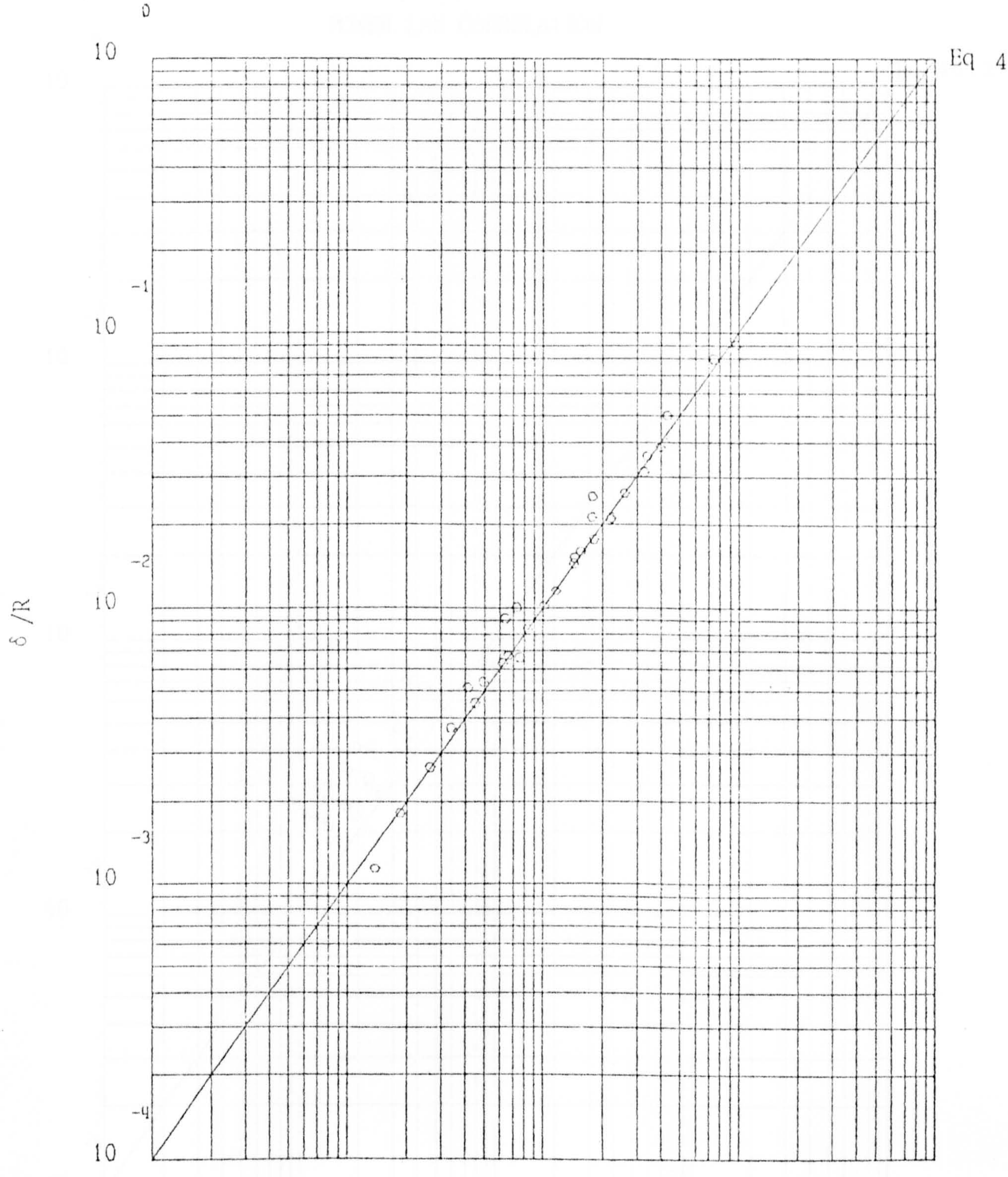

FIG 3.13 THE DATA OF ZINNATULLIN ET AL[27] n = 0.67

POWER LAW CORRELATION

Eq 40.2

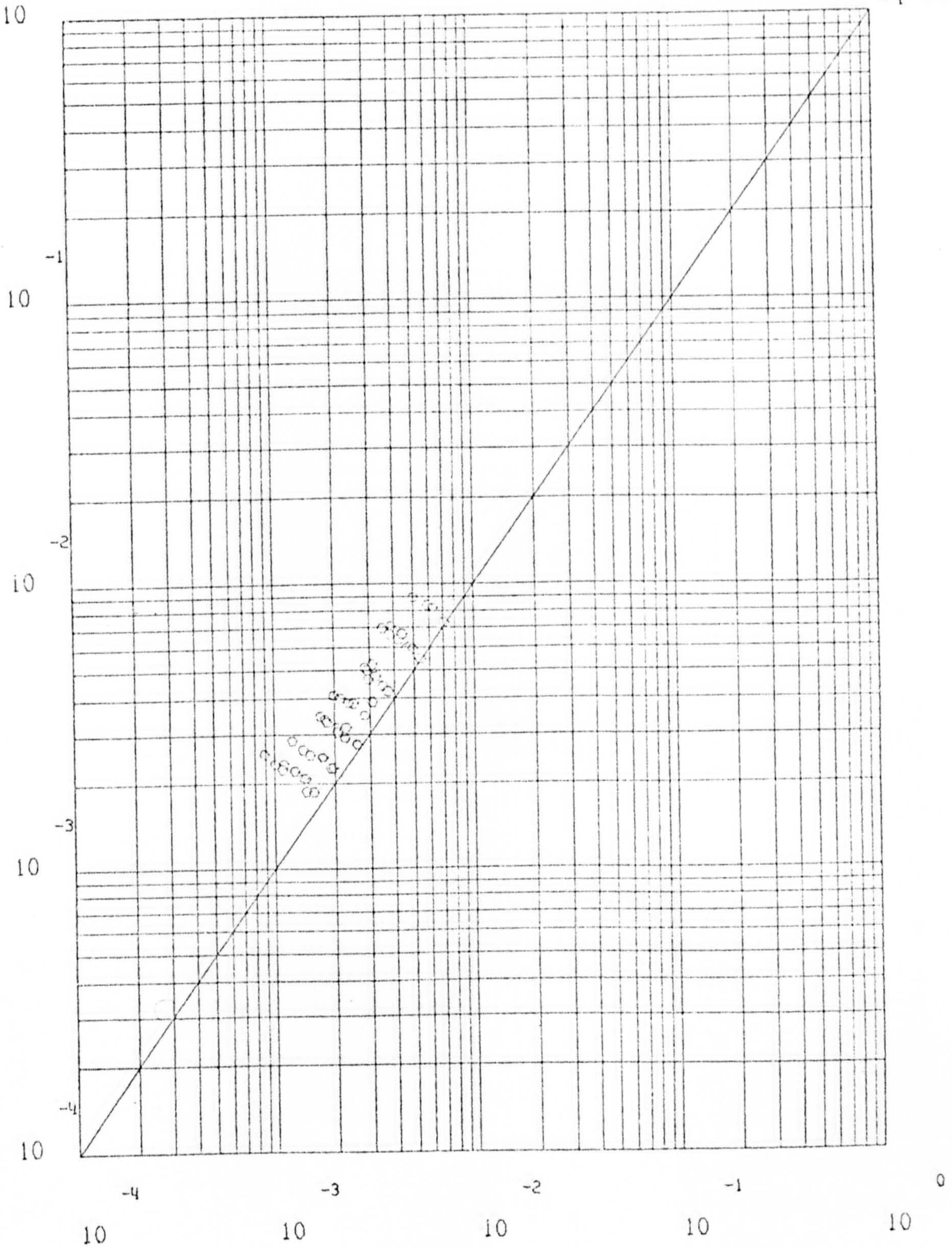

$$\left(\left(\frac{2n+1}{2\pi n} \right) \frac{KQ^n}{\rho \omega^2 r^{3n+2}} \right)^{\frac{1}{2n+1}}$$

FIGURE 3.14 THE DATA OF UKLISTY et al(27)n = 0.79

POWER LAW CORRELATION

Eq 40.2

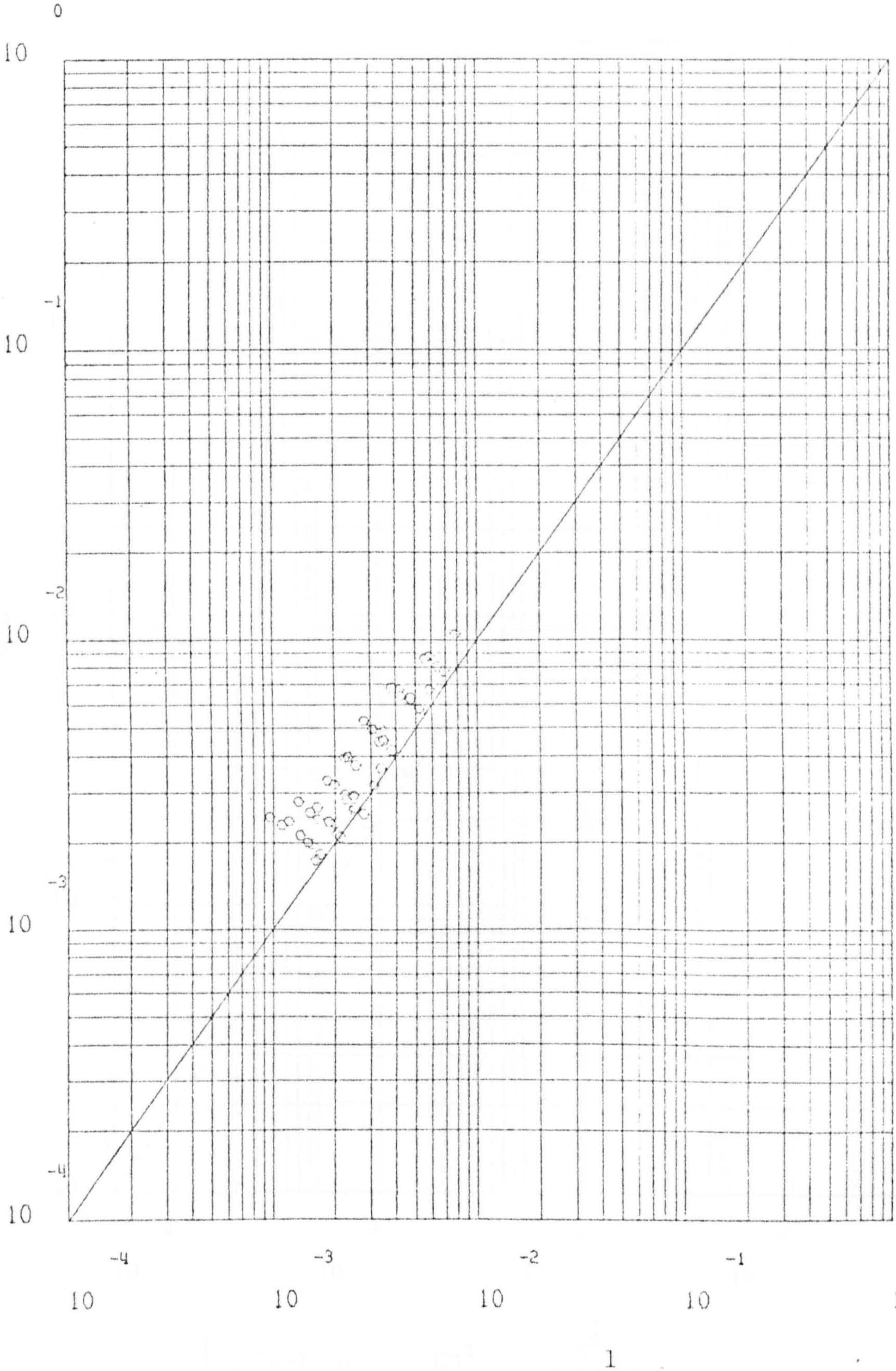

$$\left(\left(\frac{2n+1}{2\pi n} \right) \frac{KQ^n}{\rho \omega^2 r^{3n+2}} \right)^{\frac{1}{2n+1}}$$

FIGURE 3.15 THE DATA OF UKLISTY et al(27) n = 0.88

POWER LAW CORRELATION

Eq 40.2

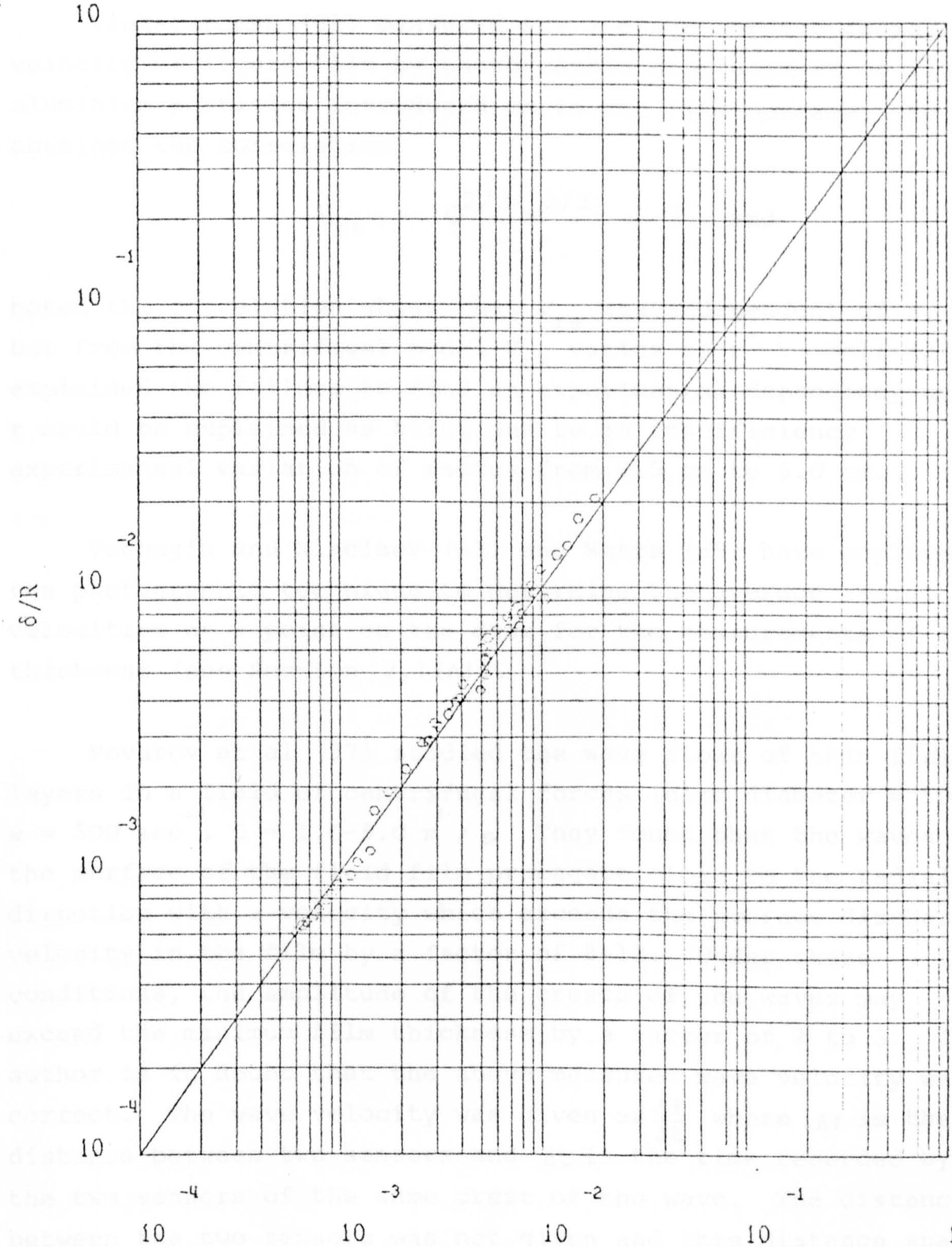

FIG 3.15 EXPERIMENTAL FILM THICKNESS RESULTS FOR SEPARAN/WATER SOLUTION (27)

(B) Velocity Measurement

Venkataraman (61) measured the average surface radial velocity of liquid film by photographic displacement of fine aluminium particles introduced on to the film surface. He obtained the correlation

$$V_{rs} \propto Q^{2/3} w^{2/3} \quad \text{and}$$

noted the correlation shows that V_{rs} was independent of r, but from the centrifugal model V_{rs} varies as $r^{-\frac{1}{3}}$. Bell (26) explained the failure to find an experimental dependency upon r could be explained as being due to an insufficiency experimental variation of radius from 2.5 cm to 5.0 cm.

Vachagin and Nikolaev (83) and Watts (89) have employed the photographic technique to determine the average radial velocities at a point on the disc for the measurements of film thickness (see Section 2.1(A)).

Povarov et al (97) studied the wave flows of thin fluid layers in a field of centrifugal forces (disc diameter = 50 cm, $w = 500\ sec^{-1}$, $Q = 1.0\text{-}5.0\ m^3/s$. They found that the waves on the surface of the fluid film propagate close to the radial direction with a velocity which exceeds the average discharge velocity in the film by a factor of 8-12. Under these conditions, the amplitude of the crests of the waves may exceed the minimum film thickness by a factor of 2 to 3. The author is in doubt that the above measured wave velocity was correct. The wave velocity was given as $\frac{\Delta \ell}{\Delta t}$ where $\Delta \ell$ is the distance between two sensors and Δt is the time recorded by the two sensors of the same crest of the wave. The distance between the two sensors was not given and this distance apart if greater than the minimum wave length of the wave would definitely give error in the above measurement.

Kamiya and Kayano (98) used photographic technique and obtained a correlation for experimental surface radial velocity as

$$V_{r,exp} = 0.47 \left(\frac{Q^2 w^2}{\nu r} \right)^{1/3} \quad (78)$$

which indicates values about two times larger than the mean velocity of the radial direction obtained theoretically from the balance between centrifugal force and frictional force given as

$$V_r = \left(\frac{Q^2 w^2}{12\pi^2 \nu r} \right)^{1/3} \quad (79)$$

Waves

Charwat et al (96) carried out qualitative observations of waves formation on rotating disc (o < Q < 8 cc/:, o < N < 720 rpm). They noted three distinct flow regimes in the 'laminar' flow region.

(A) A smooth undisturbed flow
(B) Concentric ring waves which move outward and decay at outer radius
(C) Spiral waves which tend to decay at large radii, but usually break up into very rough and random pattern of disconnected wedge-like wavelets.

They found that for water at a fixed speed, increasing flow rate gradually caused the smooth film to form concentric waves and at higher flow rates, spiral waves formed at greater radii. At a fixed flow rate increasing the rotating speed gradually damped any concentric waves present, formed a smooth film and finally caused spiral waves to form.

De Graaf (99) in his experiments was unable to obtain a completely smooth film for water on a rotating disc but finding instead that at low speeds and flow rates the film tended to break down into rivulets.

(C) Film Breakdown

Butuzov and Rifert (100) observed an incomplete film at

a flow rate of less than 4 cm^3/s in the speed range 95 rpm < w < 290 rpm. Clare and Jeffs (90) noted a broken film for Q < 10 cm^3/s at a speed of 3000 rpm and small radii an increment of 3 cc/s was sufficient to reform a complete film at that radius. Charwat et al (96) used the We group for film breakdown correlation

$$We = \frac{V_r}{\left(\frac{\sigma}{\rho\delta}\right)^{1/2}}$$

Bell (26) used the model of Hartley and Murgatroyd (53) for planar film breakdown for the case of rotating film breakdown. The criterion for a continuous film are given as

$$Q_c > 5.5 \left(\frac{\nu r^4}{w^2}\right)^{1/5} \left(\frac{\sigma}{\rho}\right)^{3/5} \qquad (80)$$

and

$$Q_c > 10.63 \left(\frac{\nu r^4}{w^2}\right)^{1/5} \left(\frac{\sigma(1 - \cos\alpha)}{\rho}\right)^{1/5} \qquad (81)$$

(C) <u>Inertial Effect</u>

Venkataraman (61), assuming angular symmetry, no slip (ie no velocity gradient in the circumferential direction) in the liquid film, gave the equation of motion in the radial direction including the inertial term as

$$\nu \frac{d^2V_r}{dy^2} + V_r \frac{dV_r}{dr} = -w^2 r \qquad (82.1)$$

and obtained

$$V_r \frac{dV_r}{dr} + \frac{12\pi^2 \mu r^2 V_r^3}{Q^2 \rho} - rw^2 = 0 \qquad (82.2)$$

Venkataraman solved equation (82.2) numerically and noted that for the range of variables in the experiment the inertial forces were important only in very small region in the centre of the disc, negligible in proportion to the total area of the disc. Venkataraman also noted that for any one speed of the disc the increase in the liquid flow rate increases the zone of acceleration of liquid film, and hence the zone of influence of inertial force. An identical effect arises when the liquid flow rate is kept constant and the speed of the disc is increased.

Bell (26) investigated the effect of distributor gap on liquid film flow using equation (82.1) and boundary condition

$$y = 0 \quad V_r = 0 \tag{83.1}$$

$$y = \delta \quad \frac{dV_r}{dy} = 0 \tag{83.2}$$

$$r = r_i \quad V_r = \frac{Q}{2\pi r_i G} \quad \text{Where G = distributor gap} \tag{83.3}$$

non-dimensionalising is performed using

$$r^* = \frac{r}{r_i} \qquad y^* = \frac{Y}{\delta} \qquad \text{and} \qquad V_r^* = \frac{V_r Gr}{Q} \tag{84}$$

Equation (82.1) becomes

$$\left(\frac{Re}{Ta^2} \left(\frac{r}{\delta} \right)^2 \frac{r^*}{A} \right) \frac{\partial^2 V_r^*}{\partial y^{*2}} + \left(\frac{Re}{Ta} \frac{r^*}{A} \right) r^* V_r^* \frac{\partial V_r^*}{\partial r} = -1 \tag{85}$$

where A is the apsect ratio $\left(\equiv \frac{G}{r_i} \right)$

Bell noted that the non-linearity (in the second group of equation (85)) makes this a difficult equation to solve. The groups that define the action of inertia upon the fluid are $\frac{Re}{Ta}$ and r*/A.

Bell experimentally pointed out that the entry conditions appear to have no effect upon the flow if

$$\frac{Re}{Ta} \frac{r^*}{A} = \frac{Q}{W^2 r G} << 1.5 \tag{85a}$$

(E) Interfacial Drag

Charwat et al (96) investigated the addition of interfacial shear to the centrifugal model, using Schlicting (100b) air/solid surface drag given by

$$\tau = \mu_a (0.51\ rw) \left(\frac{w}{\nu_a} \right)^{1/3} \tag{86}$$

and assuming that the air/water interface drag could be represented

by the classical drag of an air flow induced by a rotating disc, and that the air/water interface was stationary, Charwat et al deduced the expressions

$$V_{rs} = \frac{w^2 r^2}{2\nu} + \delta\left(\frac{\mu_a}{\mu_l}\right)(0.51\ rw)\left(\frac{w}{\nu_a}\right)^{1/2} \qquad (87)$$

$$\text{and}\ \frac{\delta}{r} = \left(\frac{3}{2\pi}\right)^{1/3}\left(\frac{Re}{Ta^2}\right)^{1/3} - 0.255\left(\frac{\rho_a}{\rho_l}\right)\left(\frac{1}{Ta}\right)^{1/2} + O\left(\frac{\mu_a}{\mu_l}\right)^2 \qquad (88)$$

From equation (88) it can be noted that the effect of induced air flow is to create thinner film.

(F) Coriolis Effect

Charwat et al (96) carried out a simple experiment to check the relative ratio of Vrs to $V_{\theta s}$. Dipping a pointer to the free surface of the flow film a wake is developed. The angle of the wake to the radial direction at that point is given by them as

$$\tan\Phi = \left.\frac{V_\theta}{V_r}\right|_s \qquad (89)$$

They used the expressions V_θ and V_r given by Rauscher (equation set 58) and obtained

$$\frac{V_\theta}{V_r} = \left(\frac{1}{3}\right)^{1/3}\left(\frac{Re^2}{Ta}\right)^{1/3}\left(\frac{A-2-A^3/4}{1-A/2}\right) \qquad (90)$$

which gives

$$\Phi = \tan^{-1}\left(c.\left(\frac{Re^2}{Ta}\right)^{1/3}\right) \qquad \text{and} \qquad (91)$$

Noted the constant c varies with $A(=\frac{y}{\delta})$ giving c = 1.733 for A = 1 (ie free surface), c = 1.647 for A = 0.5 and c = 1.387 for A = o. Thus the variation is not major although the angle of the wake will depend upon the depth of the pointer penetrating the film.

Their results found to be reasonable agreement with equation (91).

Bell (26) carried out a similar experiment and found that the correlation fitted well for $\frac{Re^2}{Ta}$ 10, appropriate to the centrifugal model, and above this value effective Coriolis forces come into consideration.

(G) Turbulence

Clare and Jeffs (90) concluded that the controlling parameter for turbulent flow is the group Re, for laminar flow Re 2000-6000. Yurchenko et al (82), however, showed that the group (Re.Ta) controlled the onset of interfacial mixing of a two layer film, and this mixing marked the onset of turbulence. The critical value given was

$$(Re.Ta) = 3 \times 10^8 \qquad (92)$$

Bell (26) collected film thickness data in the range 2.6×10^8 to 2.4×10^9 for (Re Ta) values, and compared these with the centrifugal model. Thus any evidence of turbulence as controlled by parameter (Re Ta) should be visible. As reported earlier, Vankataraman (61) and Watts (89) gave expressions for turbulence film thickness to be greater than that of centrifugal model. Bell reported that the points are distributed fairly evenly over the full range of $\frac{Re^2}{Ta}$ with many consistent with the centrifugal model line when the Coriolis influence is negligible. Bell concluded that there is no evidence of any 'turbulent' film thickneing up to (Re Ta) = 2.4×10^9 and Yurchenko's criterion is strictly applicable to interfacial agitation.

4. EXPERIMENTAL FACILITY

GENERAL

The work described in this thesis consists primarily of two parts, hydrodynamic studies and mass transfer studies; similarly the equipment designed may be viewed to serve these two investigations. At the design stage, hydrodynamic equipment had to be sized and chosen with reference to the ultimate mass transfer investigation (without any fundamental changes in flow conditions). However, to maintain the division of these two studies in this work, it has been organised so that only design directly applicable to the hydrodynamic study has been considered first with the mass transfer design being considered later.

4.1 HYDRODYNAMIC EQUIPMENT DESIGN

General Consideration

The main aim of this experimental investigation is to collect experimental information to enable a comparison to be made between various hydrodynamic models developed, and the experimental data. Thus, measurements are required of the film thickness, velocity profile and surface velocity with varying radius rotational speed, flow rate and fluid physical properties of the liquid. However, at the beginning, it was decided that direct measurement of a velocity profile within the film is extremely difficult and was beyond the present experimental capabilities and an indirect method (based for example upon residence time techniques by Asbjornsen (100a)) would require considerable development. It was decided, therefore, to conduct a thorough investigation of film thickness variation, and to collect some indicative data of other phenomena such as amplitude, wave length and the increase in the surface area due to surface waves.

Film thickness measurement has been carried out by Bell (26) using the single probe capacitive method (where a capacitive

circuit is created between a single probe and a parallel metal plate, the rotating disc) to measure the gap between the probe and a dry and wet rotating disc. Since the measurement of film thickness on the disc is down to less then 100 μm, any vibration or movement of the disc or expansion of the shaft due to high rotational speed will affect the sensor output. To avoid such problems, a two probe technique was investigated Jazayeri (27). In this arrangement one probe is mounted above the disc, with it axis normal to the disc. A second probe is mounted below the disc with its axis in line with that of the upper probe.

The present technique selected was the microdensiometer method, similar to that used by Clegg (37) on falling liquid film, where selected concentration of dyed liquid films were taken by photographic means and using microdensitometry to produce profiles of the surface waves. This method is capable of giving point measurement and enables a comparison to be made with Jazayeri's mean film thickness. This technique also permits a determination of the surface area increase due to the presence of waves (this has not been carried out by any previous investigator for flow on rotating surfaces).

The selection of this microdensoimetric film thickness technique demanded that the rotating plate be polished and that the photographic plate taken must be of the same section of the rotating disc in order to ensure the similar reflections on the plate for the same dye concentration. Several dye concentrations were tested the best being a concentration of 0.5 g/l of Nigrosine technical water soluble dye, this was chosen for the present experiment. To satisfy the above condition, a triggering unit was buit . The principle of the triggering unit is described more fully in Section 4.4.2 and the circuit design in figure 4.5.

4.2 MECHANICAL DESIGN

(A) Rotating Disc

The choice of material for the disc was governed by machinability of the surface to a high degree of smoothness, wettability and corrosion resistance to water. Aluminium was chosen as the material of construction for the disc due to its lightness, corrosion resistance to water and its amenability to a fine surface finishing.

The rotating disc used in this work is shown in section in figure 4.1 (photograph A) it forms part of the rotating equipment. It is 36 cm in diameter with an effective flow area from 2.25 cm to 18 cm radius. A disc of this diameter was chosen to avoid the difficulties encountered in the design of a large balanced disc. On the other hand a small diameter disc could involve the entrance effect playing an important role in the fluid dynamics of the liquid film on the disc. The smooth surface was brought to a mirror-like finish by using progressively finer grades of emery paper and finally,polished with jeweller's rouge on the buffing wheel. The mirror-like finish proved particularly helpful for taking good photographs of the even reflections on the disc surface which provide the measurement of the film thickness and the surface area increase due to the surface waves. At a distance of 72 mm from the centre of the aluminium disc, six equi-spaced holes of 8 mm diameter were drilled and counter-sunk to allow the bolt heads to lie flush with the surface of the disc. A central hole of 30 mm diameter was drilled through the disc.

An aluminium adaptor attached to the top of a taper-lock bush was used to fix the aluminium disc to the rotating system. The adaptor had six equi-spaced holes, of 8 mm diameter, on a 72 mm radius. The centre of the adaptor was drilled and tapped with 6 mm diameter holes to accept the liquid distributor from above. A centrally raised collar of diameter 30 mm was provided.

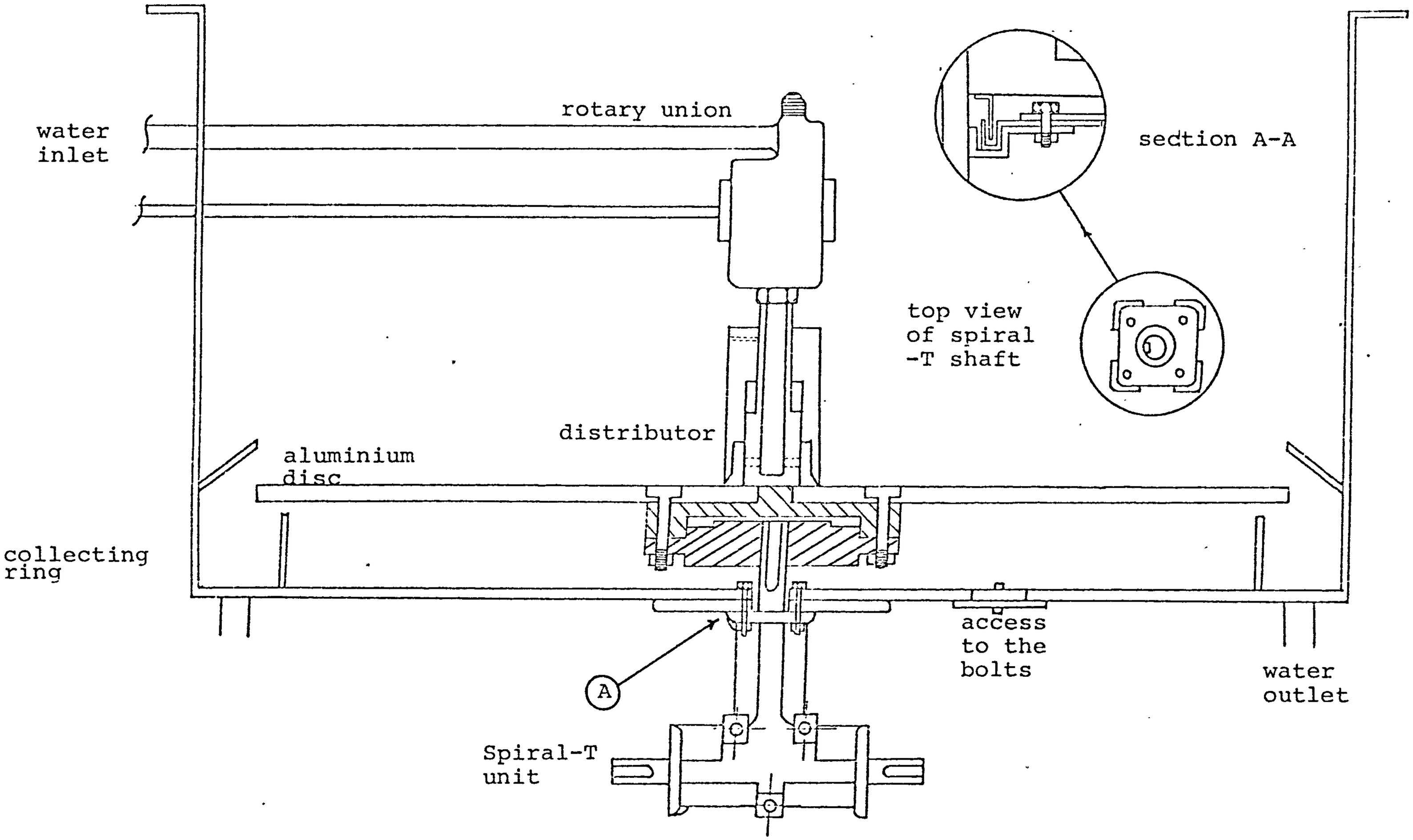

FIGURE 4.1 ROTATING DISC ASSEMBLY

ROTATING DISC
UNIT

DATA LOGGER

STROBOSCOPE

PHOTOGRAPH A

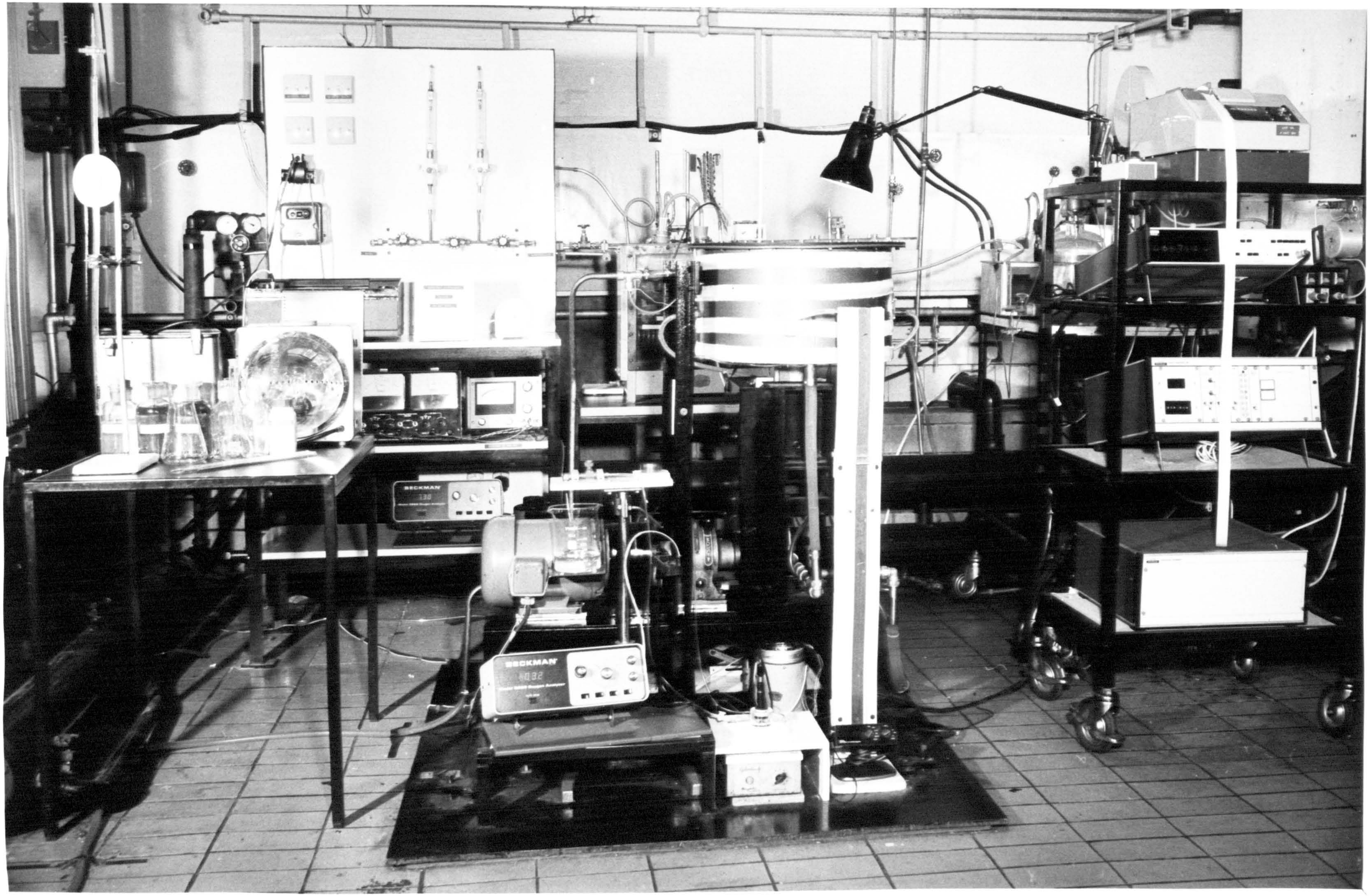
BECKMAN
130
BECKMAN
4032

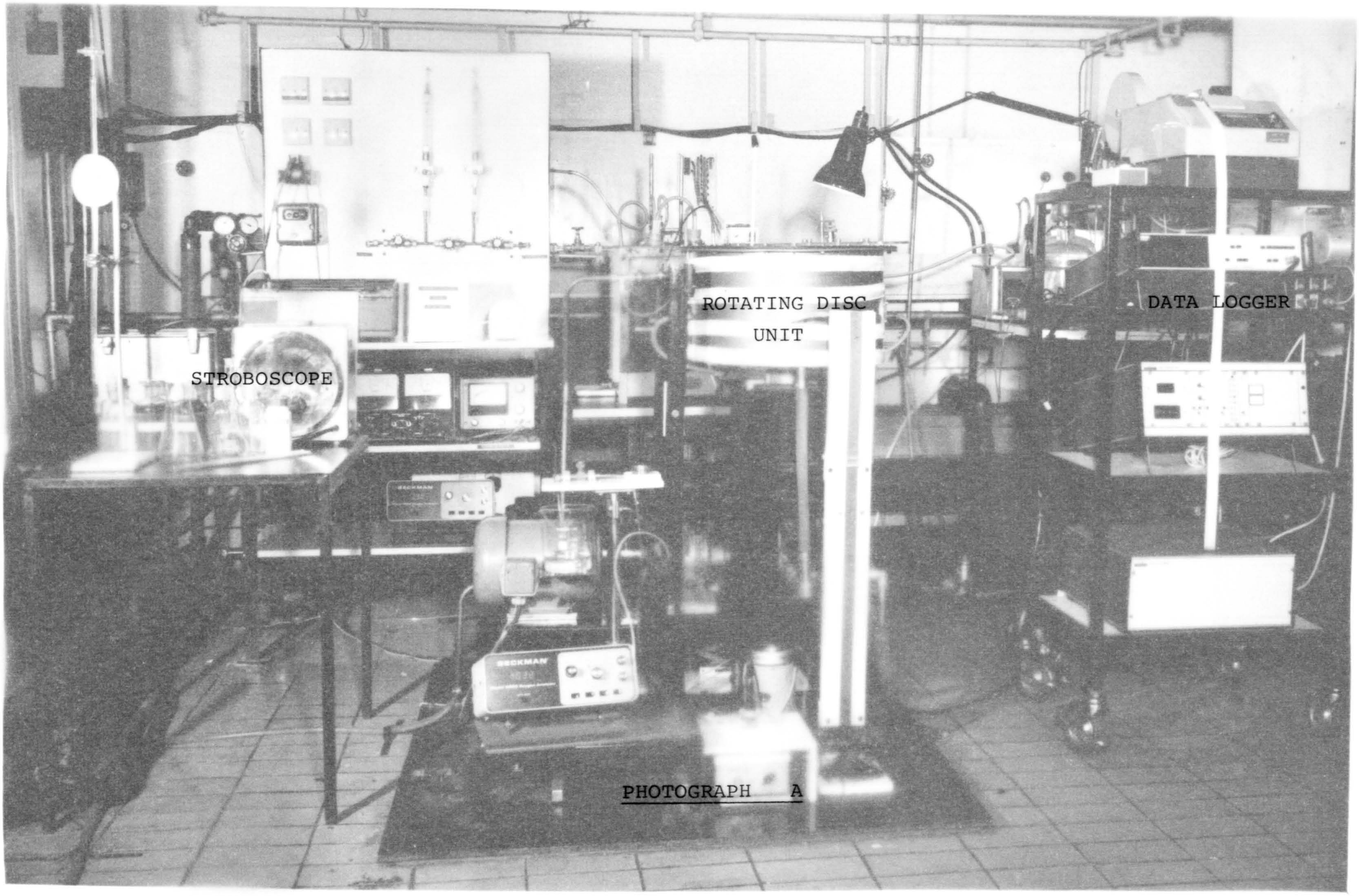

PHOTOGRAPH A

The aluminium disc was bolted to the adaptor and the table-lock bush using the six holes with the bolt heads going just below the surface of the disc. The central hole of the disc was pushed fitted on to the raised central collar of the adaptor to provide a continuous surface to the centre of the disc. The six exposed slots of the bolt heads were coated with a thin layer of silicon rubber and a layer of resin (David's Isopon) to produce a flush surface. The set fillings were smooth finished with fine sand papers. A thin plastic gasket was used in between the disc and the adaptor to prevent any water seeping through the central hole into the rotating unit. A cork gasket of 1/16" thickness was used between the aluminium adaptor and the table-lock bush.

(B) Liquid Feed Distributor

The design of the liquid feed distributor at the centre of the disc was governed by two main factors:

(1) To introduce the liquid at the rotational speed before being spread onto the disc. This minimised the inertial and coriolis effects.
(2) It was necessary to distribute the liquid uniformly on the surface of the disc without the impinging or jetting of the liquid on the rotating disc.

The liquid distributor was made of two parts, the inner section and the outer section, as shown in figure 4.2 (photograph B). At the base of the inner section was a spigot screw of 6 mm diameter which secured the inner section onto the raised central collar of the aluminium adaptor. The base diameter of this inner piece was designed to cover the area around the push fit of the aluminium disc onto the adaptor. To prevent seepage of liquid between the push fit, silicon rubber was spread around this area before the inner distributor was tightened to the adaptor. A central core of 16 mm diameter , and depth of 60 mm was machined with the upper

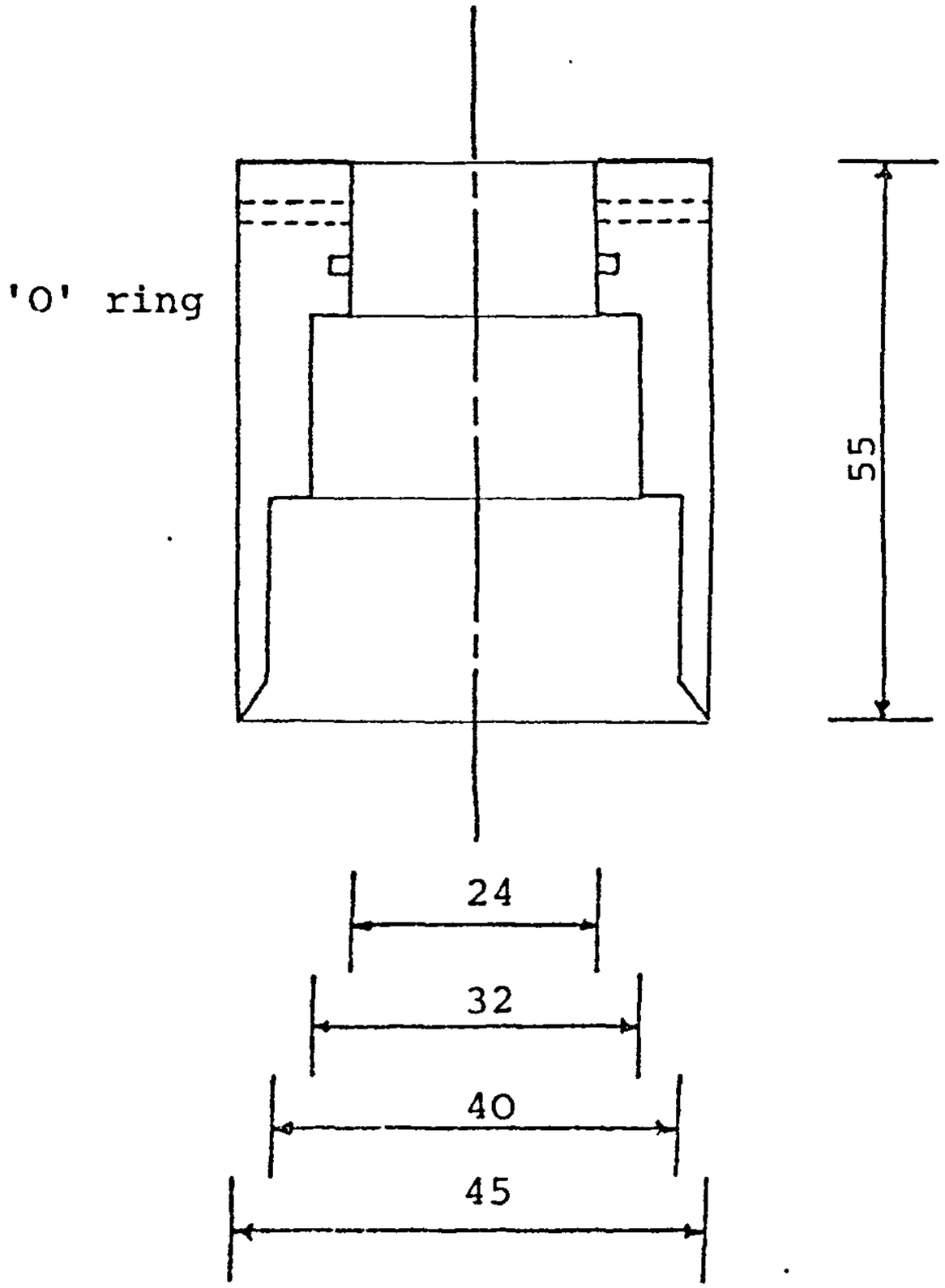

INNER SECTION

MATERIAL: BRASS

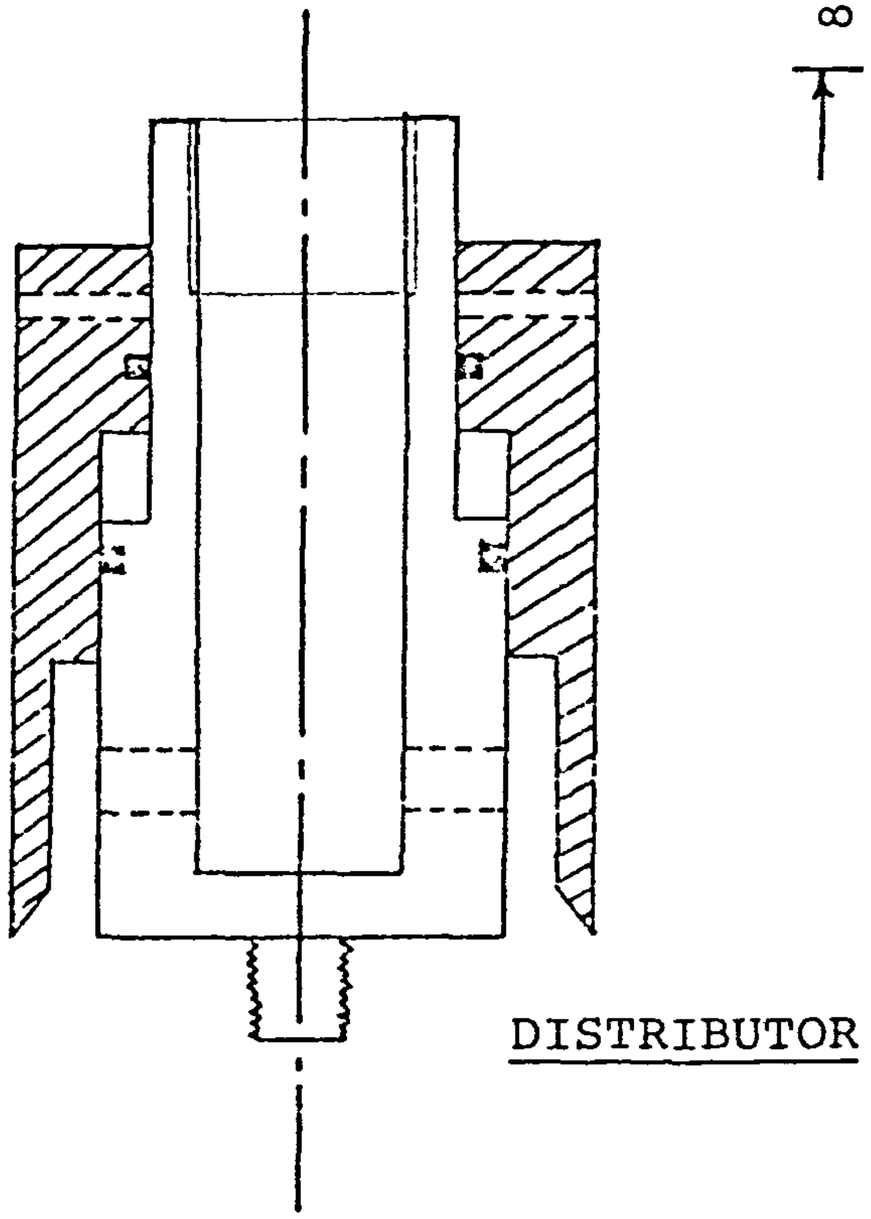

DISTRIBUTOR

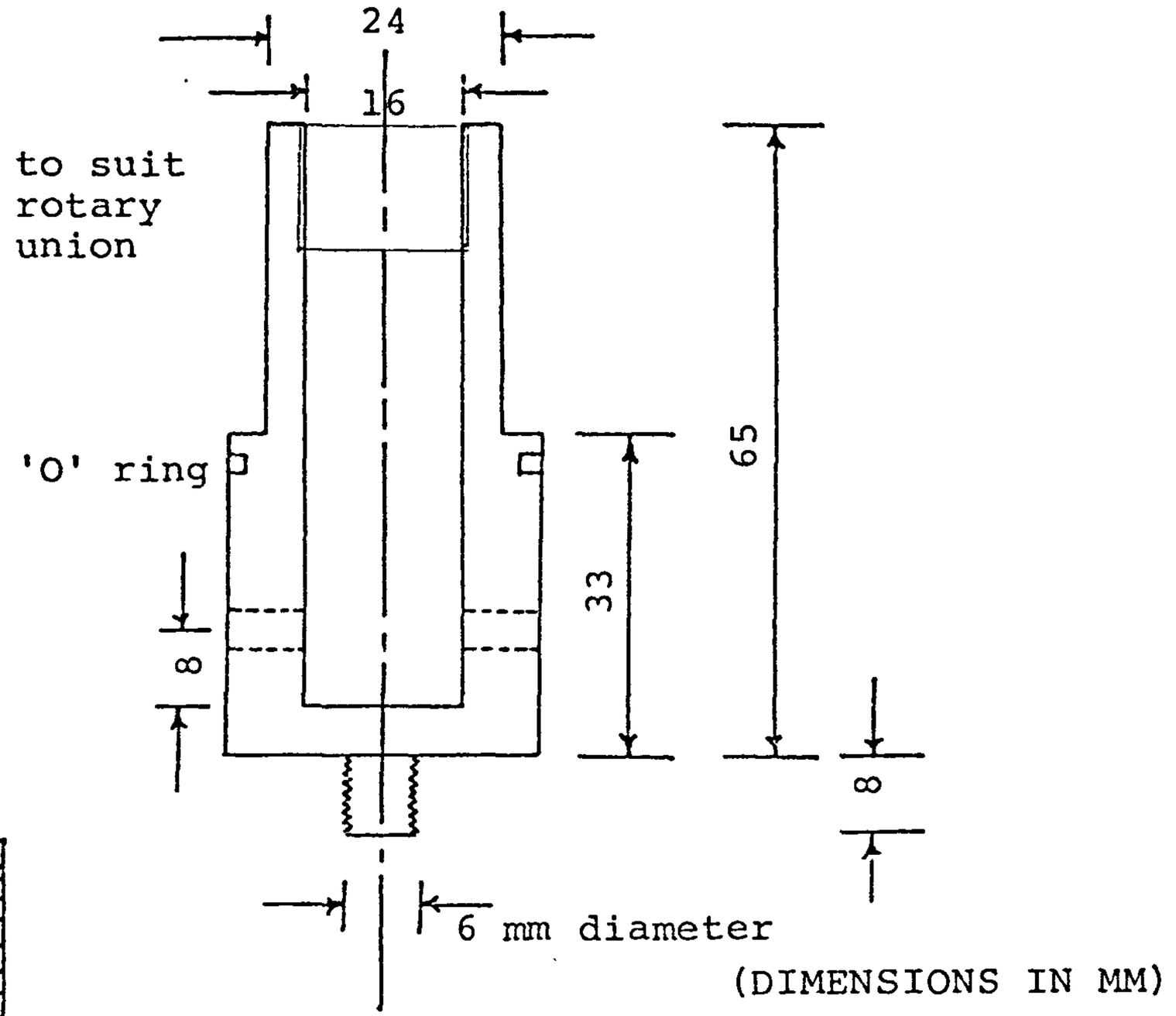

(DIMENSIONS IN MM)

OUTER SECTION

MATERIAL: BRASS

FIGURE 4.2 DISTRIBUTOR DESIGN

DISTRIBUTOR

ROTARY UNION

PHOTOGRAPH B

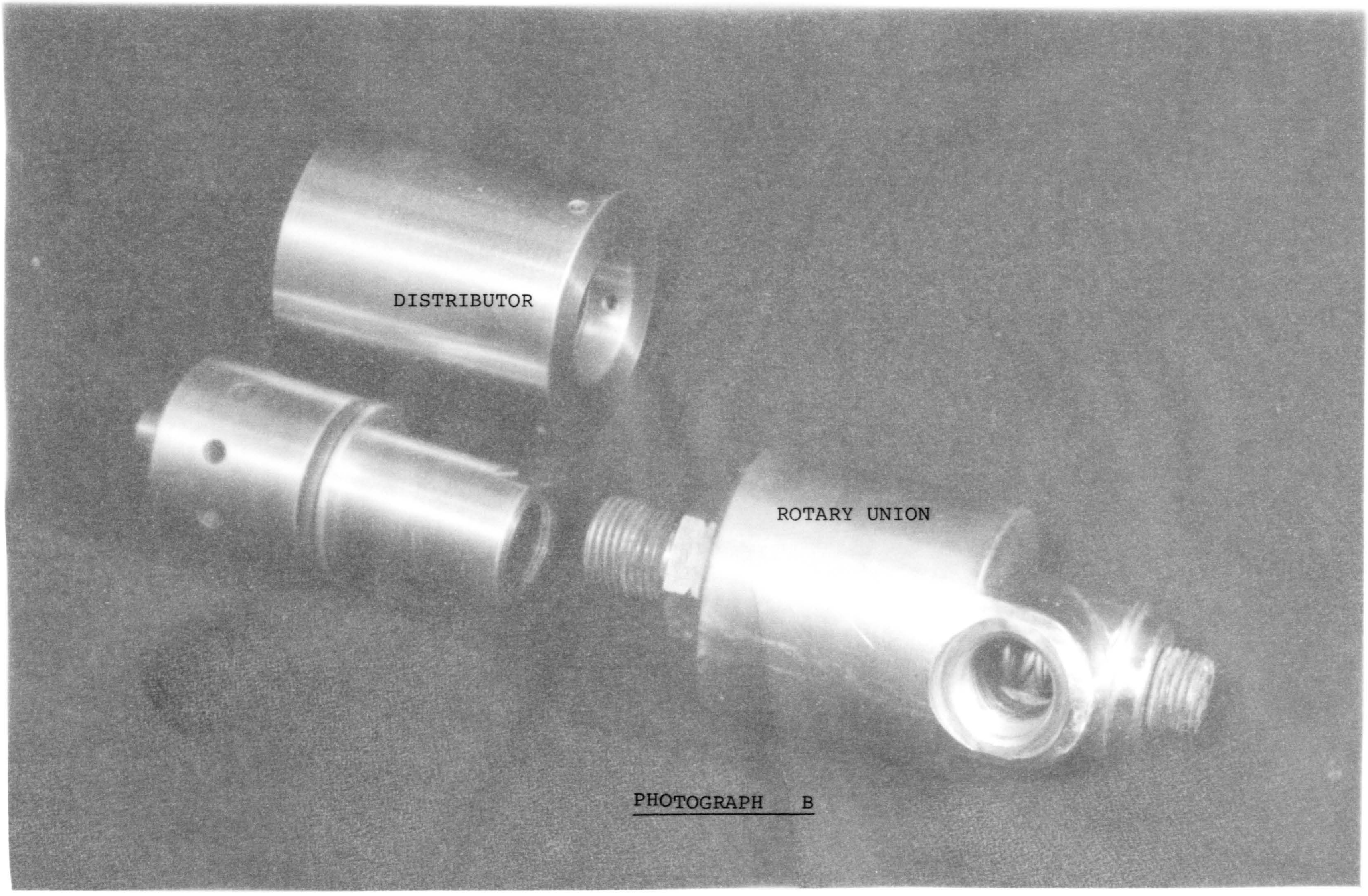

PHOTOGRAPH B

portion internally threaded to accept the rotary union. At a height of 8 mm above the base of the inner core, eight holes of 4 mm diameter were drilled equally spaced to provide even distribution of the feed liquid. Two 'O' ring seals were incorporated between the joint of inner and outer sections to prevent liquid gaining access to the top of the outer section of the distributor. The interior of the outer section of the distributor was smooth finished with a knife edge of an angle 53 degree as shown in the figure 4.2. The distributor gap (the gap between the disc surface and the body edge) can be adjusted and set by sliding the outer section of the distributor. Three 4BF grub screws were used to hold the outer section to the inner section of the distributor.

The rotary union used (55-003 model) was provided by Deublin Company Manufacturing. It was carefully tightened to the inner section of the distributor and tested on the lathe, to ensure that the two pieces were running true and no serious vibration occurred when the disc was rotating at high speed. The rotary union was held in position by an aluminium block which fitted the outer diameter of the rotary union, and was secured to the main framework by two aluminium rods.

The screw threads on the rotating assembly are all locked by set screws and are all designed so that with the designed sense of rotation (clockwise looking vertically downward) all screws are tightened by inertia loads in deceleration.

(C) Structural Support for the Rotating Disc Assembly

The detailed design of the structural support for the rotating disc assembly is shown schematically in figure 4.3.

The supporting structure was made of 2" x 2" angle bar with dimension of 91.0 cm long x 30.0 cm wide x 31.0 cm high to form the base structure. A ¼" thick mild steel plate

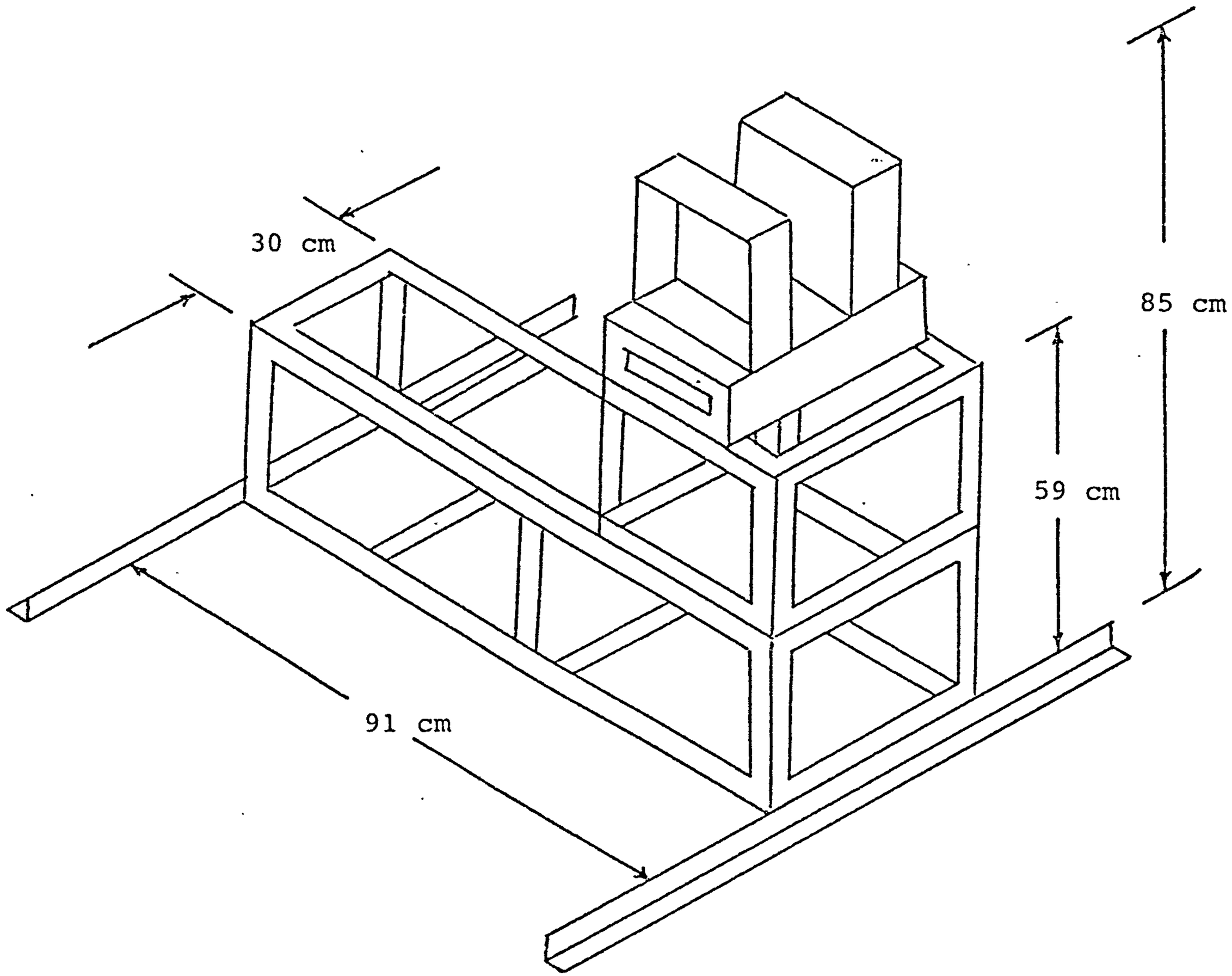

FIGURE 4.3 STRUCTURAL SUPPORT FOR THE ROTATING DISC ASSEMBLY

was welded to support the motor, variable gear box and coupling on one side and the housing for the spiral - T gear unit on the other side. The base of this supporting structure was stabilised by two pieces of 2" x 2" angle bar welded across the ends of the framework. Four bolts were provided at the corners to level the framework.

The motor used for driving the disc was mounted on the mild steel plate. The base of the motor was supported on a shim steel to level it with the height of the variable gear box. The motor shaft was coupled to the gear box through a variable clutch coupling to avoid initial speed of the motor on the rotary assembly.

The housing for the spiral - T gear unit was raised to a suitable height for the convenience of later experiments on mass transfer investigation. The raised platform, made of 1½" x 1½" angle bar with dimension of 25.0 cm long x 30.0 cm wide x 28.0 cm high was welded to the base structure. The housing consists of two vertical ½" thick mild steel plates, measuring 18 cm x 18 cm, which were machined and fixed with position locating dowels. The machined faces of the spiral - T gear box were held and bolted to the steel plate. The other sides of the mild steel plates were welded to four 18 cm long x 18 cm wide x 1 cm thick mild steel plates to enable the whole housing unit to be bolted on to a 30.0 cm long x 16 cm wide mild steel channel,which in turn was welded to the raised platform.

The corrosion of the mild steel plates and the angle bar are delayed by coating with black protective paint. The entire framework was supported on a ½" thick rubber pad to evenly distribute the load over the laboratory floor and to insulate the apparatus from the stray mechanical vibrations.

(D) <u>The Drive</u>

A 3 phase 1.5 Hp motor, capable of maximum speed of 1400 rpm, was used in this study. A variable gear box with accurate

control at any speed coupled to the motor shaft through a variable clutch coupling. The disc was driven by the motor connected by a 'V' bolt, SPZ 1010 Fenner Alpha 400, on pulleys, (No Fenner 160 SPZ). The pulley's diameter ratio for the motor and the spiral - T shaft was 1:2. This enabled the minimum rotational speed of 230 rpm on the disc to a maximum speed of 1120 rpm. The whole pulleys and belt unit was enclosed with a protective guard.

(E) Collecting Ring

In the mass transfer experiment succeeding the hydrodynamic study, the liquid film is exposed to the gas of interest (21% oxygen) and the mass rate is measured. At this design stage certain consideration has to be taken into account such as to eliminate the interfacial resistance, where the gas must be kept and saturated at the same temperature as the liquid. Hence, it was considered essential to isolate the absorption chamber from the outside air.

Since the mass transfer tests were to be made in the same set-up, it became necessary to develop a suitable liquid collecting arrangement to keep the flow conditions identical for the hydrodynamic and mass transfer studies.

The absorption chamber consists of the brass base plate 3mm thick with central hole of 7.45 cm diameter and four equi-spaced, 11 mm diameter holes at radius 5.375 cm from the centre. These holes were located similarly to those of spiral - T unit and seal plate, which enabled the three units to be held together. Two holes of 20 mm diameter were drilled 180^{o} apart, at a distance of 25 mm from the rim of the base plate. 1" Copper outlet tubes were soft soldered into place to provide the liquid outlet to the drain. Two annulus rings of brass, height 51 mm and 26 cm (1.5 mm thick) soft soldered at distance 50 mm apart from the rim respectively to form an annular collecting ring for the liquid thrown off from the

disc. The outer ring forms the major part of the absorption chamber with height 34 mm above the top of the rotating union. A flange of width 1¼" and ⅛" thickness was soldered to the top of the outer ring, with 24 equally spaced holes to suit the O BA bolts. A further two strips of brass, forming a plane cylinder of 2 cm high was welded on top of the other strip to form a cone of 45° angle to the plane cylinder. This cylinder was a push fit to the outer collecting ring and held in position by three pegs, soft soldered around the outer collecting ring at a height 36 mm from the base plate.

(F) Seal Plate

This plate isolates the absorption chamber from the outside air (Photograph C). A central hole of 29 mm diameter was drilled and an annular drain was machined at radius 16.5 mm and 22.5 mm from the centre of the plate. Silicon fluid (DC 200/1000 cs - a product of DOW Corning Limited) was used as a gas-tight seal. A circular cylinder of 2 mm thick and 13 mm high bolted to the bottom of the table-lock bush and dip into the drain to form the isolation. Four holes of 11 mm diameter were drilled at radius 53.75 mm (similar to the collecting ring and spiral - T unit) from the centre of the 14.5 cm diameter plate.

Silicon liquid seal was used because of its low volatility and hence reduced the chance of contaminating the gas atmosphere within the absorption chamber.

(G) Disc Assembly

The seal plate was centrally placed onto the spiral - T gear unit and the trough or the drain was filled half full with silicon oil seal. The collecting ring with the four 11 mm diameter holes was located in line with the seal plate and bolted together onto the spiral -T unit. The taper-lock bush carrying the annular cylinder was dipped several times into

DISC

PHOTOGRAPH C

SEAL PLATE

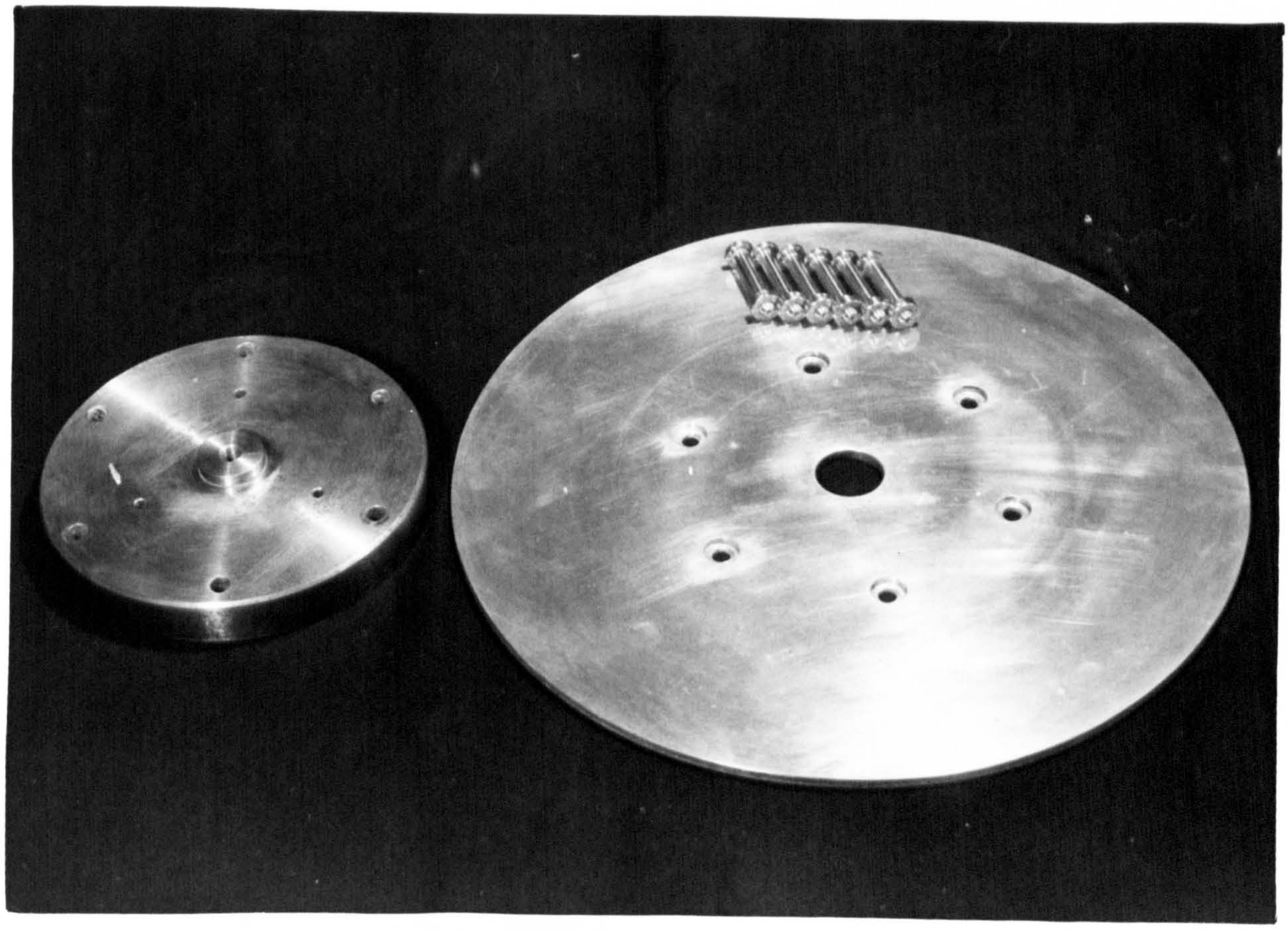

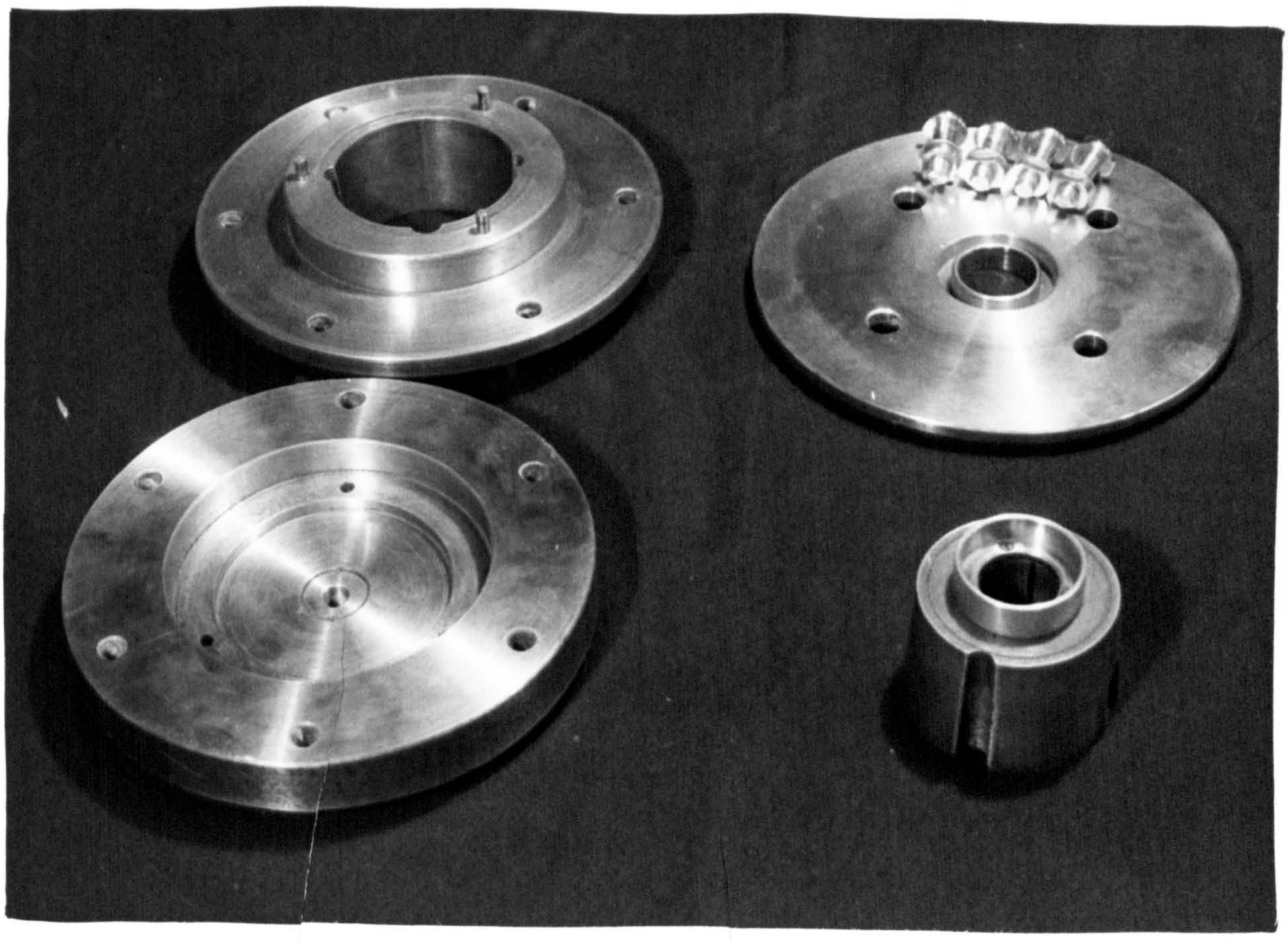

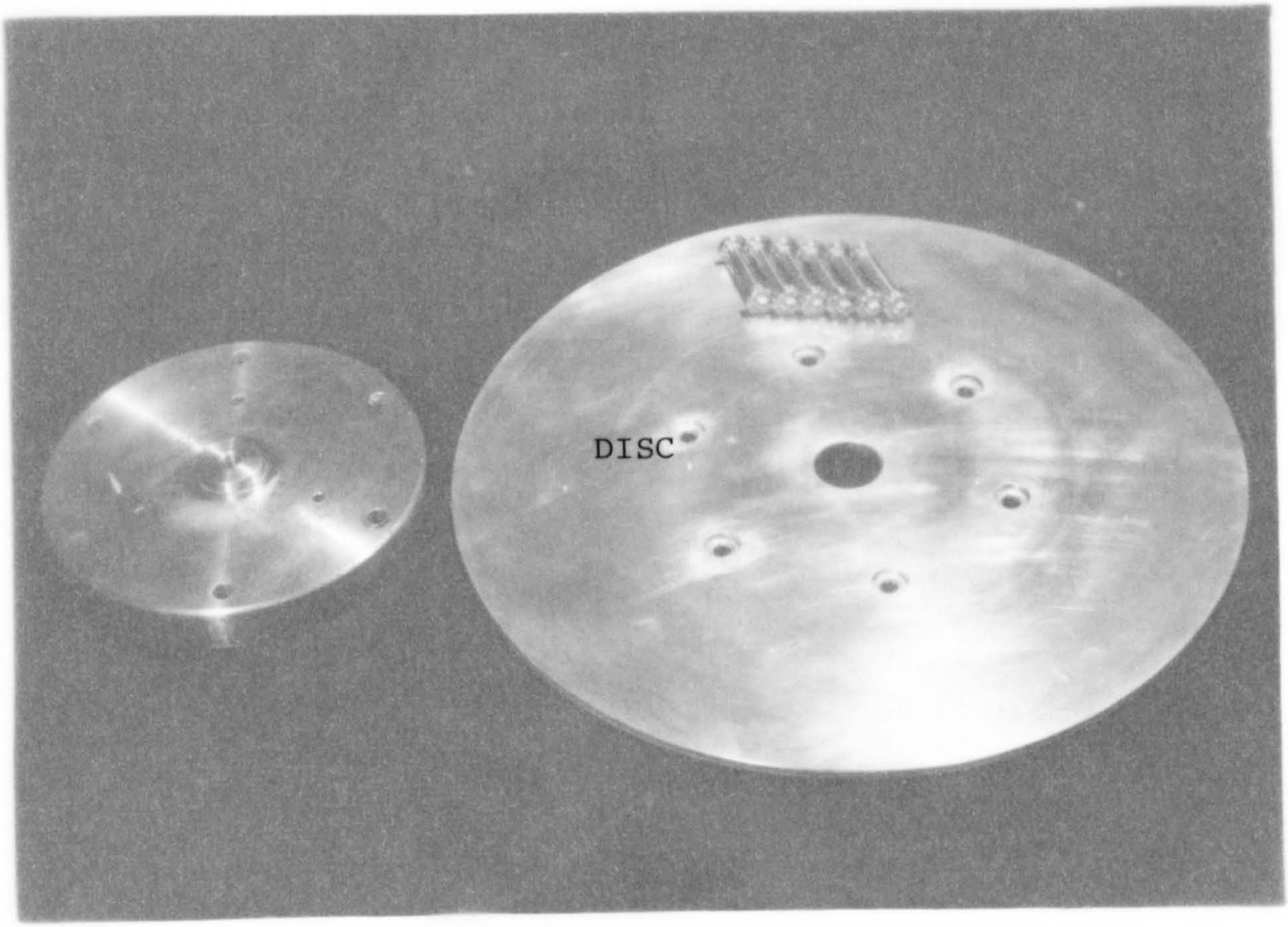

PHOTOGRAPH C

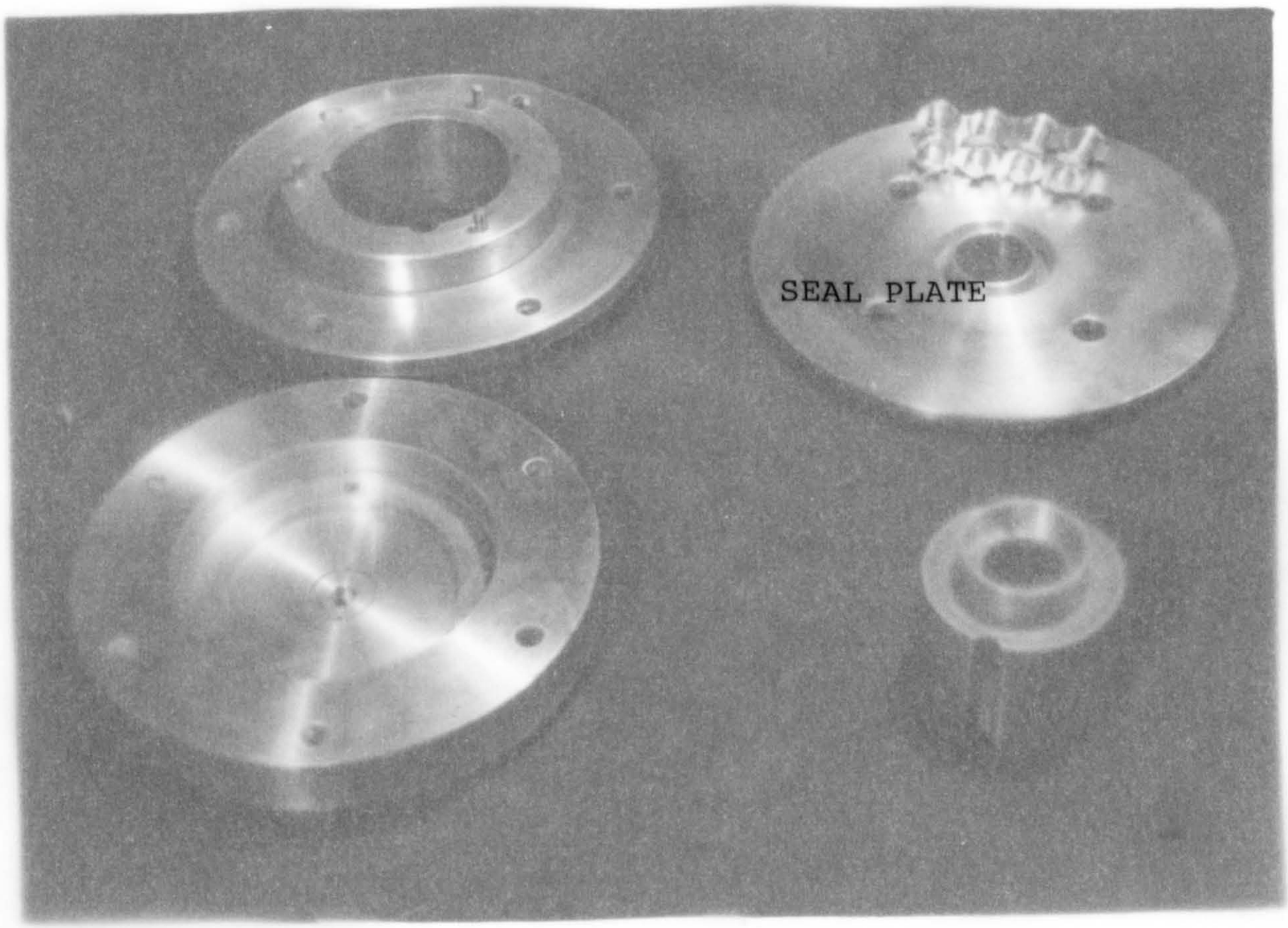

the silicon liquid seal. This determined the height of the taper-lock bush to be fitted onto the uppermost shaft and prevented any overflow of seal liquid at high rotational speed. The seal completely isolated the gas atmosphere in the absorption chamber below the disc and the shaft.

The aluminium adaptor with a $\frac{1}{8}$" thick cork gasket was seated onto the taper-lock bush and the aluminium disc was a push fit on to the raised collar of the adaptor with a thin layer of plastic gasket in between to prevent any seepage of liquid. The disc was securely fitted onto the adaptor and the taper-lock bush with six bolts. The bolt heads were countersunk into the disc to form a continuous surface. As it was essential for the disc to be carefully balanced for accurate measurement of the thickness of the liquid film, the six bolts were tightened carefully and the variation of flatness of the disc was continuously checked down to 0.001" at the rim. The exposed slot screw was coated with a thin layer of silicon rubber before resin was applied to form a smooth surface. Silicon rubber was also applied around the area of push fit, to ensure no liquid could gain access into the adaptor. The distributor and the rotary union were being stabilised with two aluminium rods secured to the main framework through the absorption chamber. The tolerances given for the fit of the distributor were as low as are normally used for spindles of lathes (approximately of the order of 0.002") where very true running is needed.

(H) Fluid Circuit

The liquid circuit is shown diagrammatically in figure 4.4 (Photograph D). Liquid under test is held in two 0.2273 $m^3 \times 10^3$ tanks (50 gallon). An immersion heater of 3.0 kW (240v) output together with thermostat was fitted to each tank to maintain temperature of $25^{o}c$. When tank 1 is in use valve V_1 to the pump P1 and through the recycle 1" copper tubing line controlled by valve V_2. Pump P1 is a single phase, 0.5 Hp

FLUID CIRCUIT

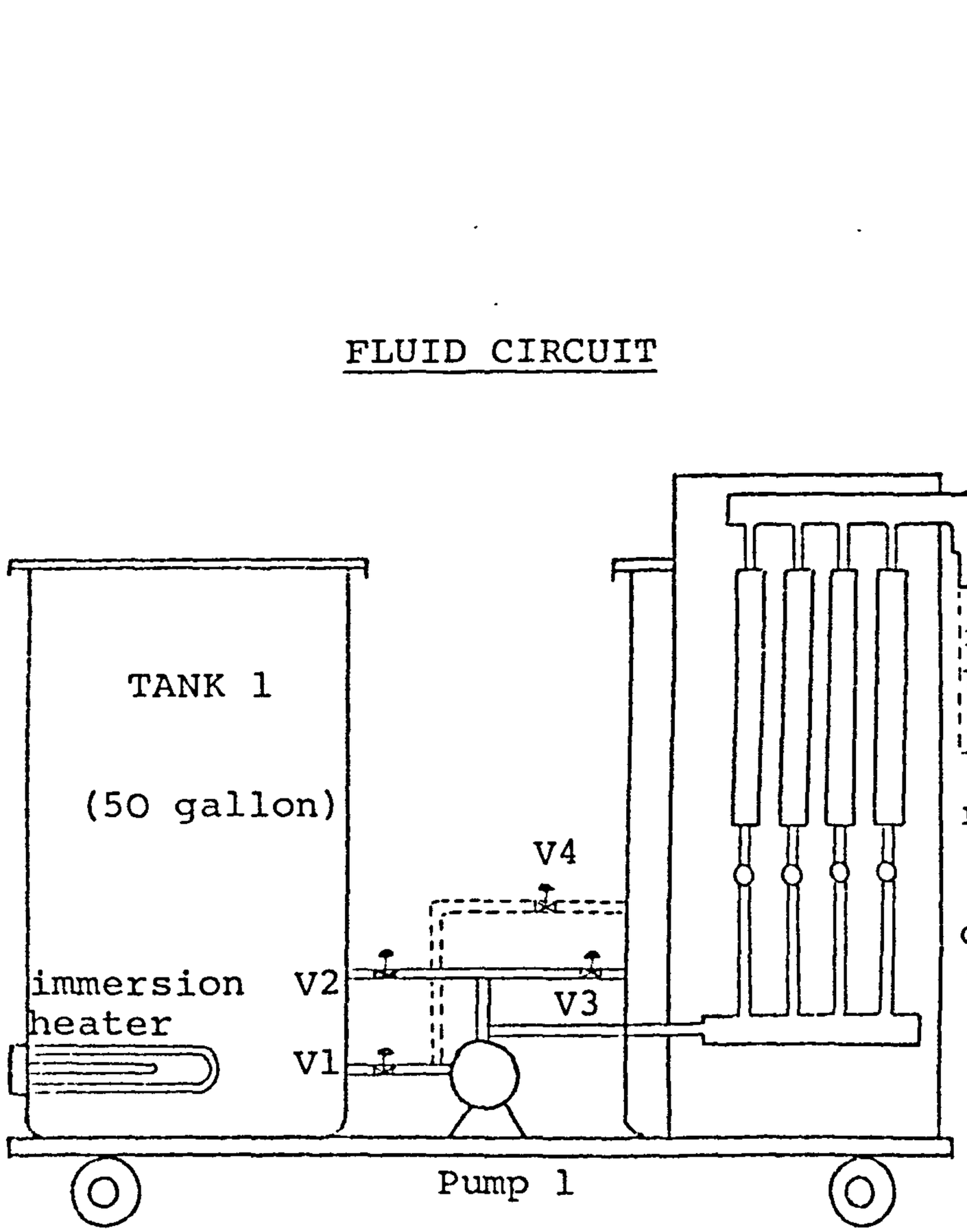

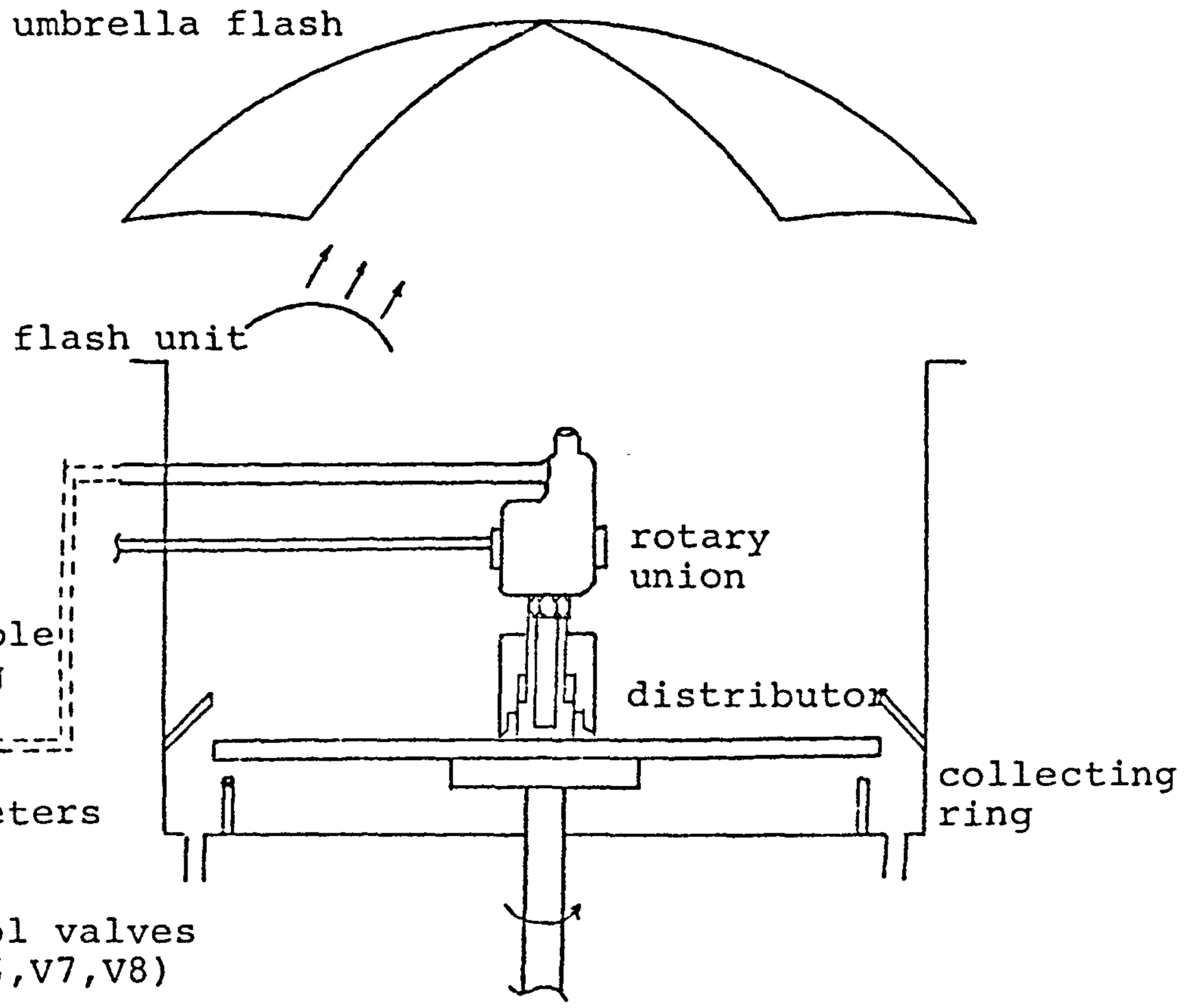

ROTATING DISC UNIT

FIGURE 4.4 FLUID CIRCUIT AND ROTATING DISC UNIT

NITROGEN

ROTAMETERS

TANK 1

TANK 2

OXYGEN
METER

PHOTOGRAPH D

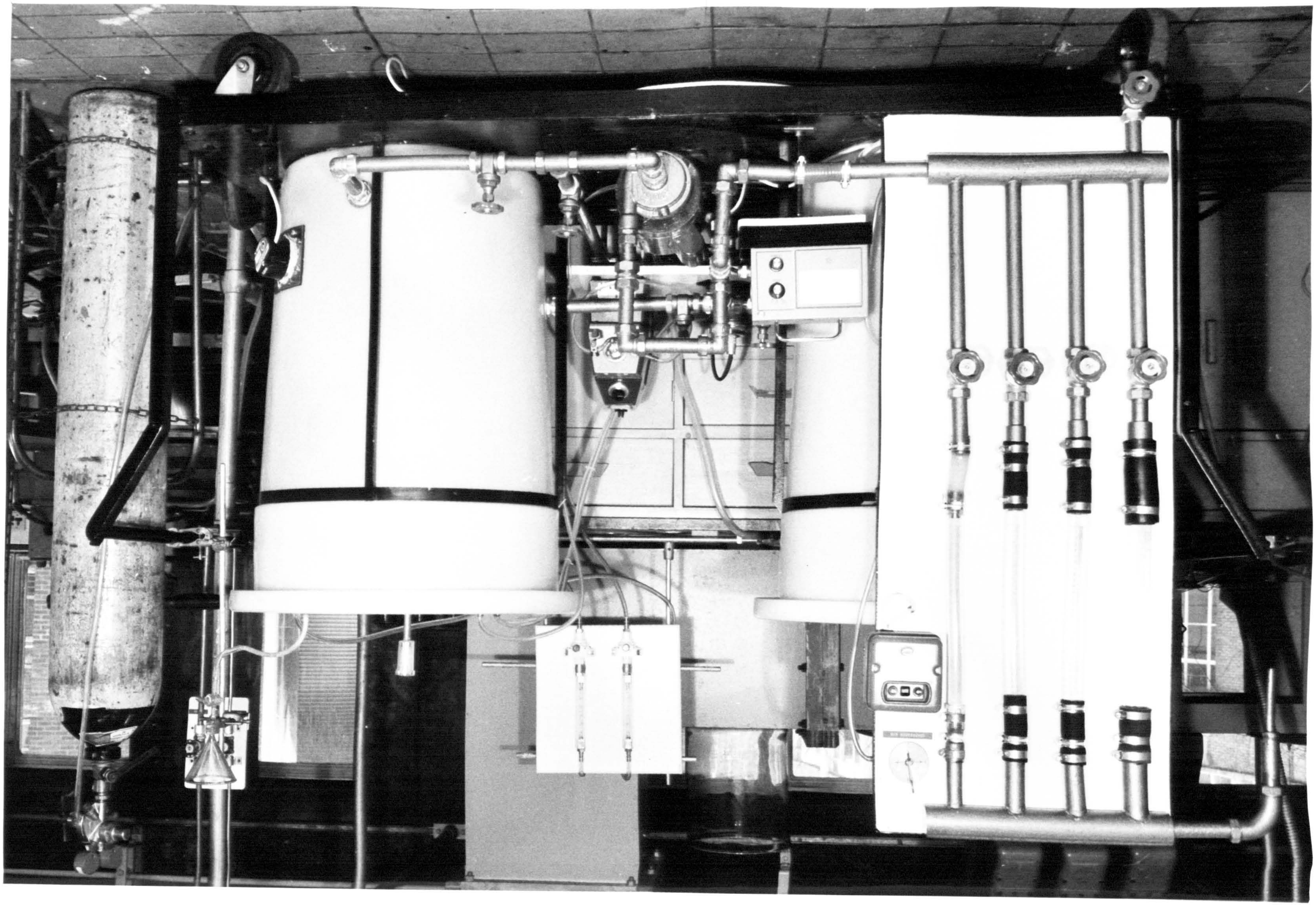

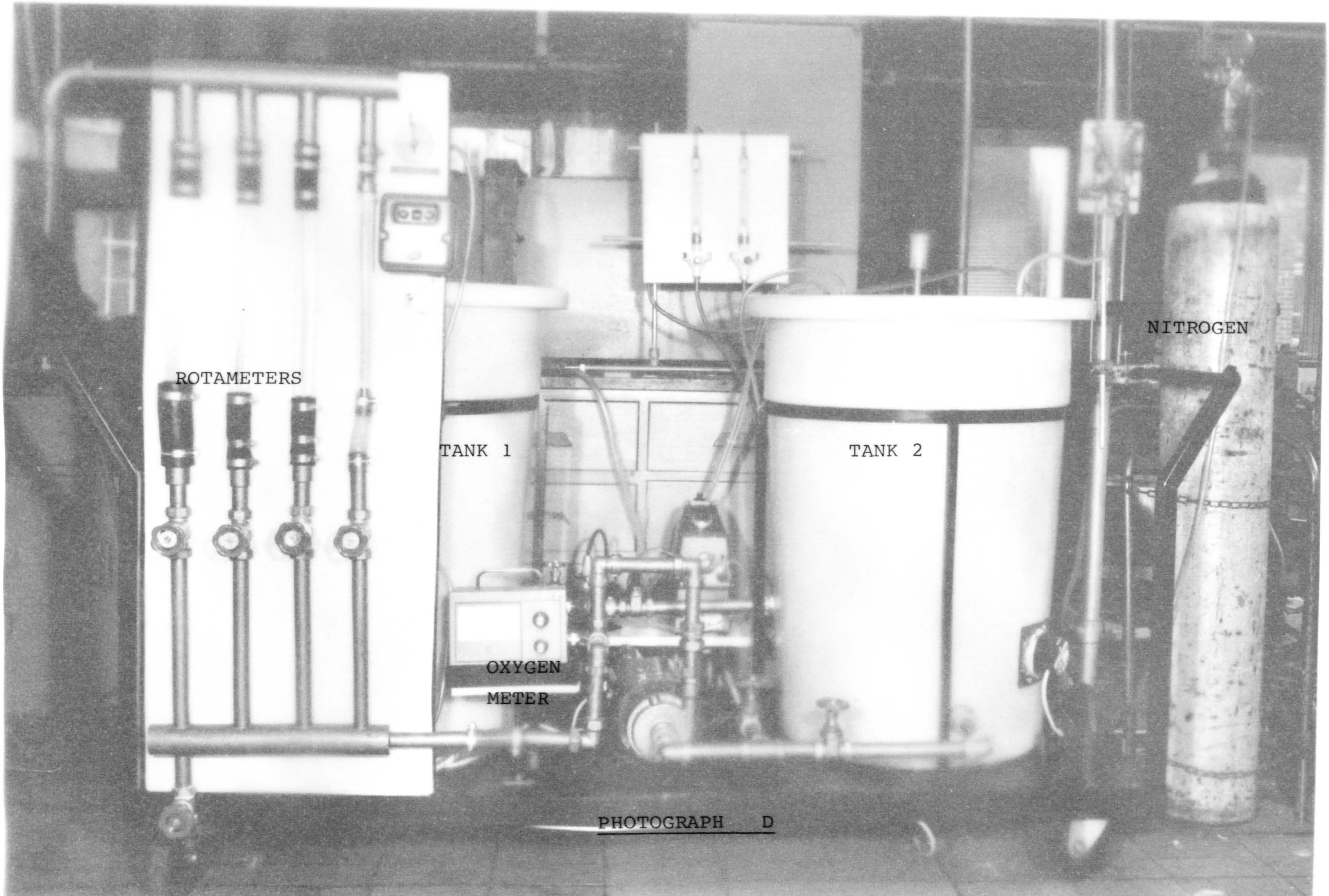

PHOTOGRAPH D

electric motor, with maximum rating of 1000 gallon/hour. This pump was chosen due to its ability to pump the maximum flowrate required in the present tests. Pump p1 passes liquid through a manifold before entering to any of a bank of four rotameters connected in parallel. Each rotameter is proceeded by fine control valves, V_5, V_6, V_7 and V_8. The rotameters (from Rotameter Company Limited) are types Metric 14, Metric 18E and Metric 24P, allowing smooth and overlapping delivery rates from $14 \times 10^{-6} m^3/s$ to $100 \times 10^{-5} m^3/s$. During high flow rate, the by-pass valve V_2 was closed to permit maximum possible flowrate through the rotameters.

From the rotameter fluid is fed via ½" diameter pvc tubing to a rotary union and the distributor. The outer section of the distributor was adjusted to produce a uniform film of liquid at the lowest flow rate (14.5 cc/s) and highest speed (1120 rpm) investigated in this study.

Liquid collected in the collecting ring leaves through two 20 mm diameter hole at the collector base plate as described in Section 4.2. The two streams are brought together by elbow joint of 1" copper tubing. The used liquid is discarded to prevent any accumulation of impurities into the tanks.

(I) Rotational Speed Measurement

A tachogenerator was used for the rotational speed measurements. An adaptor was designed to accept the end of the 1" diameter shaft of the spiral - T gear unit and the tachogenerator end, the tachogenerator being stabilised with an arm rod threaded and a lock nut secured to the spiral - T unit. The output of the tachogenerator was logged on paper tape by the Department's data logging system, Solartron-Schlumberger analogue scanner, data transfer unit and digital volt meter A211. This equipment is visible on the right of

Photograph 1. The data output given by the manufacturers (Muirheads Limited) being linear at 3 volts per 1000 rpm.

4.3 EXPERIMENTAL

CALIBRATION

(A) Rotameters

The rotameters used in this experimental programme are shown in Photograph D. In order to calibrate these rotameters (Metric 14, Metric 18E and Metric 24P), a special calibration rig was constructed. This rig consists of a tank (30 gallon) placed on top of a load cell (serial number 686 - AB Bofors, Electronics Dividson, 3-69020 Bofors, Sweden) mounted on a movable trolley. Recommended input voltage ranges from 15 to 18v were applied from a power stabilised source to the load cell. The rated output was 2.236 mv/v input for 500 kg of liquid.

Pump P1 was switched on and the valves V_3 and V_4 (see fig 4.4) were closed to isolate tank 2 from the system. The by-pass valve V2 was fully open and the rest of the control valves (V_5, V_6, V_7 and V_8) to the rotameters were shut. The temperature of the water was raised to 25^{o}c with the 3 kW immersion heater. The supply water was adjusted until it became steady,and then filling of the tank was started. While the filling operation was being performed, visual checks confirmed that the rotameter reading remained steady . The output from the load cell was recorded on Telsec recorder (Type X) and the volumetric flow rate was calculated from the chart recorder The results were put through a curve-fitting program available in the University's IBM computer. These calibration curves are shown in Appendix E for the Metric 14, Metric 18E and Metric 24P rotameters respectively.

(B) Thermocouple Calibration

A standard copper-constantan thermocouple wire (36 SWG by Saxonia Company Limited) was used for measurement of the water

inlet temperature and the air temperature in the absorption chamber. The junction was made with soft solder and each thermocouple was constructed with its own ice point junction. The junctions were shielded by glass envelopes, 10 cm long by 3 mm diameter. The calibration was done with temperatures varied from 5^{o}c to 95^{o}c and checked against a mercury and glass thermometer (0.5^{o}c). The output of the thermocouples was registered on the portable digital voltmeter. This was repeated with hot air and the accuracy was found to be high (Appendix E).

(C) Tachogenerator Calibration

A tachogenerator fitted to the shaft of the spiral - T gear unit was used for rotational speed measurement. The output from the device was given linear at 3 volts per 1000 rpm by manufacturers (Muirhead Limited). The tachogenerator was recalibrated on a Chesterfield lathe in the Department's workshop, and checked against a hand-held Smiths Industries Limited tacho, up to 3000 rpm. The polynomial regression curve-fit for these results are shown in Appendix E.

4.4 EXPERIMENTAL RUN

(A) Preliminary Run

The aim of these runs was to find the concentration of dye (nigrosine technical soluble dye) at which the best illumination on the photographic plate would be obtained; for the measurement of the instantaneous film thickness, and hence surface area increase, by a microdensometric technique.

This experimental technique is only capable of giving reliable results if certain precautions are observed.

(1) Observations (on the photographic plate) must be restricted to a given position on the rotating disc, to give a similar reflective area for all the experimental runs.

(2) The twin flash unit (Ernest Turner high speed flash) must be positioned such that the curvature of the surface (waves) does not cause an excessive loss or gain by refraction or reflection at the surface. The refraction effect was minimised by using a white umbrella reflector which reflected light evenly onto the liquid surface. The reflection effect can be eliminated if condition (1) is satisfied.

(3) The light source for the microdensometer must be a single point source such that the 'blending' of waves does not occur. In practice a balance must be obtained between source size and equipment sensitivity.

Condition (1) was satisfied by the design of the single shot photographic flash synchroniser (detail see Section 4.4.2) The umbrella reflector and twin flash unit positions were tried out with water until a best illumination on the photographic plate was obtained.

Water in the 50 gallon tank was heated up to 25°c and maintained at that temperature with a thermostat. A known weight of dye was dissolved in a separate container before it was added to the tank. The dyed liquid in the tank was recycled to ensure adequate mixing for at least half an hour. Meanwhile the motor which drives the disc and the twin flash unit was switched on and warmed up for at least 15 minutes before the experimental run. The positioning of the flash, umbrella reflector and camera were carefully chosen and marked. The liquid was then introduced onto the disc through lengths of flexible ½" tubing installed in the line between the rotameters and the inlet of the rotary union. When the liquid flows were steady through visual observation on the disc, the surface of the film was photographed using an Asahi pentax, 35 mm single lens reflex camera.

In these experimental runs, various concentrations of nigrosine dye (0.05 to 1.5 g/l), in tap water were used. A concentration of 0.5 g/l solution of nigrosine dye in water was found to give the best illumination on the negative at all flow rates and speeds at which measurements of thickness and surface area increase were desired. The final position of the flash, umbrella reflector and camera was noted for later experimental runs.

(B) Calibration of Microdensometer

Six stationary films of different thickness were photographed over an area of interest on the disc, with the positioning of the flash units and camera as in the preliminary run. The differences in thickness for each film across the disc were measured with a thin stainless needle mounted on a micrometer head. As the micrometer head was turned, the needle travelled downward until it just met and touched its image in the interface. The thickness relative to the surface of the disc was read from the micrometer. A total of six readings across the disc were taken for each film thickness.

The photographic plate or negative placed on the microdensometer reader gave an output relative to the thickness of the film, when scanned through the regions of interest (ie calibrated region). These data were recorded on paper tape and later processed by a Cromenco micro-computer to give the relationship between the voltage output and the six known thicknesses of the liquid films on a radius of the disc. This was repeated for the other stationary films of different thicknesses. The results were put through a polynomial curve fitting programme to obtain the six calibration curves across the disc.

4.4.1 PROCEDURE

Prior to the experimental runs, tank 1 was washed and rinsed with tap water. Liquid, with a dye concentration of 0.5 g/l, was then heated up to 25^{o}C. Meanwhile the disc was polished with Dura wool, cleaned with soap solution and polished dry with tissue. This distributor gap was adjusted to 0.03" (in accordance with Bell's (gap-thickness correlation) which ensured that liquid entered the disc smoothly. The flow rates and rotational speeds chosen in this experimental study varied from 14.5 to 60.5 cc/s and 230 to 1120 rpm respectively.

The disc was brought up to the speed at which the run was to be conducted and the spiral - T unit was allowed to reach a steady working temperature. This operation required about 30 minutes to perform. The rotameter setting was adjusted and the equipment allowed to come to thermal equilibrium and photographs were taken. To prevent any impurities accumulating the dyed water was not recycled after traversing the disc.

The developed films (negatives) were cut into strips, two negatives long, and analysed under the microfiche reader. The smallest distinct wave length was noted. The original slit source light in the microdensometer was redesigned into a small single dot source light to ensure that when the negative was being scanned through the microdensometer, the smallest whole wave length could be included. However, this introduces conflicting requirements, a small dot source produced accurate results but too small a photocell voltage output and vice versa. The size of the dot source was chosen in this study with measurable electrical signal coming from the photocell to the data logger unit. The amount of light transmitted to the photocell depends on the height of the film, and the sensitivity can be adjusted by putting a different dye concentration in the liquid (this latter case has been observed from the preliminary runs).

Two sets of separate experimental runs were carried out (i) film thickness measurements, and (ii) surface area increase due to waves. In the case of film thickness measurements only the regions surrounding the calibrated points were taken. This provides a quick comparison of film thickness with the theoretical models and an estimate of the accuracy of this technique. In the second case,where surface area is of interest, the minimum distinct wave length was determined from all the runs (negatives). It was found to be about 2mm. Thus, the increment of distance across the disc while scanning through the negative was set to be 0.23 mm; which roughly gives about eight readings per minimum wave length.

Data tapes were used to provide the 'official' results of the experiments. However, whilst conducting the runs note was taken of the approximate average voltages visible on the voltmeter. These, and the approximate system parameters, were used to calculate the approximate film thicknesses. These results were plotted immediately on a large scale graph to check the regions to which results were applicable , and where further results were required. This technique ensured an even distribution of the parameters studied.

4.4.2 ONE-SHOT PHOTOGRAPHIC FLASH SYNCHRONISER

Purpose of the Device

To synchronise the Ernest Turner high speed twin flash unit with a given position of the rotating disc and to allow only one flash at this position and to latch off for subsequent revolutions of the disc.

Principle of Operation

An infra-red reflective opto-switch detects a reflective strip on the rotating shaft of the disc drive unit. When the reflective strip passes the opto-switch the input to the first comparator is driven low causing its output to go high (figure 4.5).

This low-to-high output transition is coupled via a capacitor charger. This causes the dual line relay to energise momentarily, its contact triggering the flash unit.

Simultaneously, the comparator output transistor drives the second comparator output low, holding down the input to the first comparator, so that the reflective switch is disabled. This ensures that the flash unit cannot be retriggered on subsequent revolution of the rotating disc.

Two methods of resetting the unit are provided. The first is a manually operated push button on the side of the case. When this is depressed the output of the first comparator is grounded, which both resets the second comparator, which'enables'the opto-switch by removing the latched input to the first comparator, and discharges the transistor coupling capacitor through the diode connected between the transistor base and ground. While the button is held in, the unit is disabled since the output of the first comparator is held low, but is ready to operate as soon as the button is released.

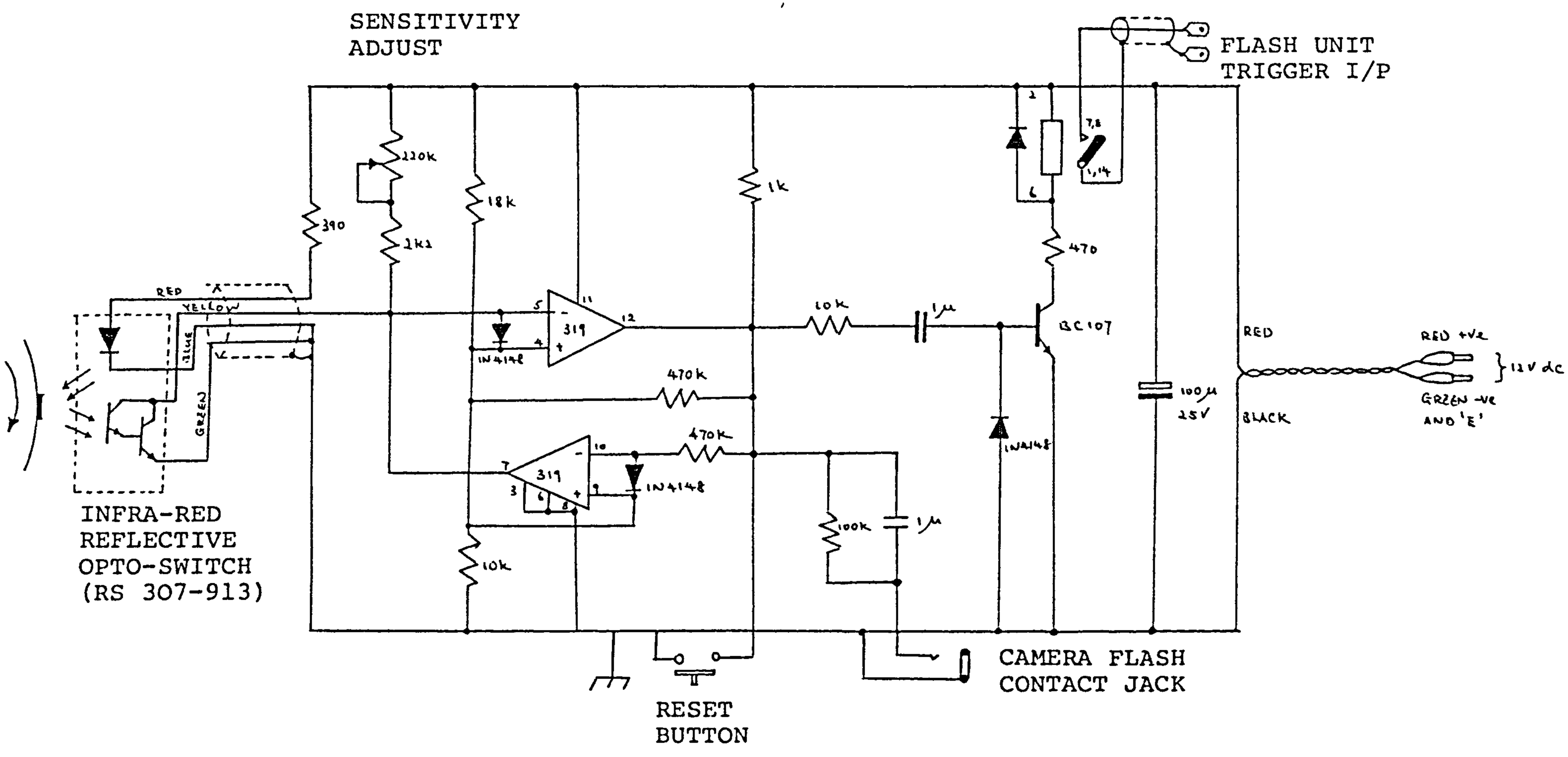

FIGURE 4.5 CIRCUIT DIAGRAM FOR THE ONE-SHOT PHOTOGRAPHIC FLASH SYNCHRONISER

The second method of resetting makes use of the camera's flash contact. When the camera shutter opens and the contact closes, the output of the first comparator is brought low through the coupling capacitor in series with the jack socket, thus resetting the system in a similar manner to that provided by the push button. The capacitor is necessary as a direct connection to the flash contact of the camera would disable the unit, as holding in the reset push button, so that no flash would occur until after the camera shutter had closed. The look resistor ensures that the capacitor does not remain charged after the unit has triggered while the camera contact is closed.

This method of resetting was provided so that the exposure time could be kept to a minimum in order to reduce ghosting of the photograph by the ambient light, the maximum time required being not greater than the time required for one revolution of the disc. Since the synchronising unit is reset after the camera shutter opens, the shutter must remain open until the reflective strip passes the opto-switch.

When the disc is rotating at 240 rpm the maximum time required to ensure that the flash occurs while the shutter is open is ¼ second. At higher speeds of the disc, correspondingly higher shutter speeds can be used. Appreciably longer exposure times are required to ensure reliable synchronisation when using the manual reset button.

5 RESULTS AND DISCUSSION

Reference to Figures 5.1 to 5.6 which show the crest of waves observed across the disc at different flow rates and rotational speeds. There are three regions which may be distinguished.

(A) A waveless region which extends from the edge of distributor to the line of inception.
(B) A short zone of fairly regular waves
(C) Randomly disturbed waves

Figures 5.1 to 5.6 are condensed into Figure 5.7 and the significance of the diagram can be understood if one considers the action of increasing rotational disc speed at particular flow rate of 30 cc/s. At low rotational disc speed, a small central area of disc is covered with smooth film. If the disc speed increases to say 30 rad/s, then the intersection of Q/w on figure intersects on the line 4 cm. That is the smooth film now covers an area up to 4 cm from the edge of the distributor. At a larger radius, 2 to 3 cm from the distance of wave inception, regular waves are observed and this occurred only at low rotational speed and flow rate. The remainder of the area is covered with random waves. These similar observations were noted by Bell (26), however, the smooth film regions were very much larger than the present observations. This may be due to the inlet system used for introducing the liquid onto the disc, as well as the distributor gap and technique of measuring the wave inception.

Increasing the flow rate from 10 cc/s at a speed of say 40 rad/s shows the following series of events. At a flow rate of 10 cc/s the film is smooth up to a radius of about 2 cm from the edge of the distributor. At a flow of 25 cc/s the smooth film extends radius between 3 cm but less than 4 cm. Increasing the flow rate further, say 50 cc/s, gives signs of jetting from the inlet causing the smooth film to occupy a smaller area. These signs of jetting at high flow rate are presumably due to imperfections in the inlet design.

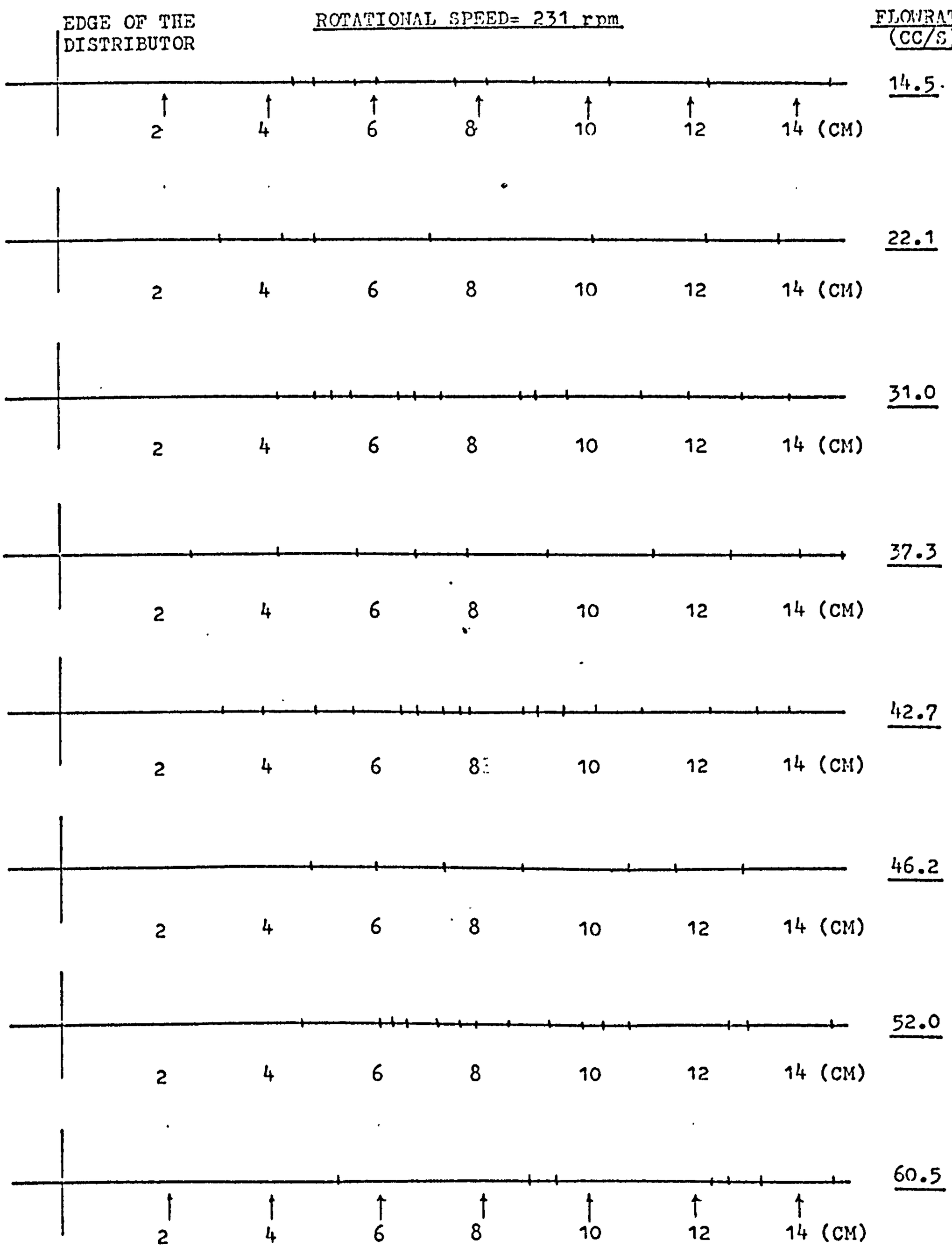

FIGURE 5.1 PEAK OF WAVES OBSERVED ACROSS THE DISC

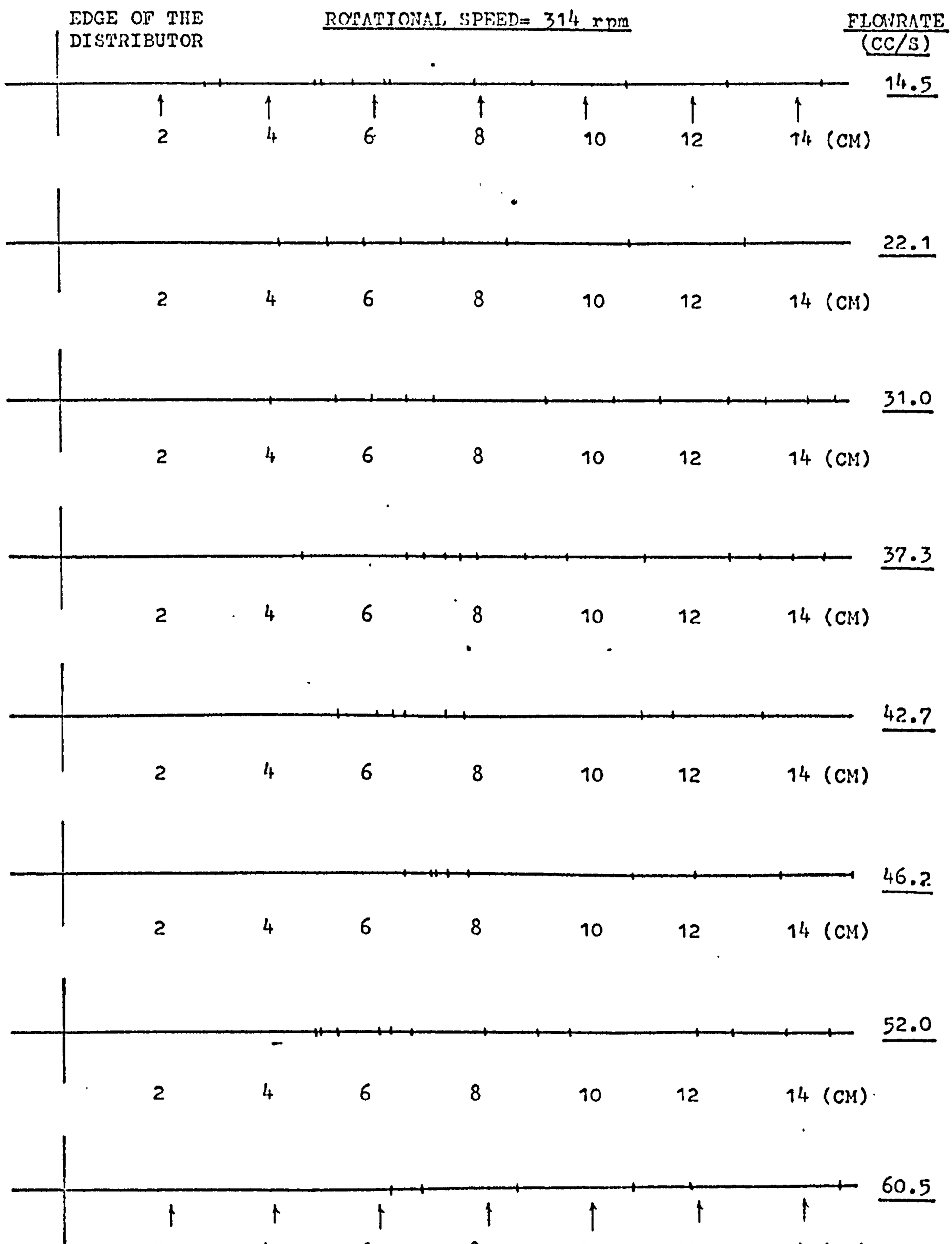

FIGURE 5.2 PEAK OF WAVES OBSERVED ACROSS THE DISC

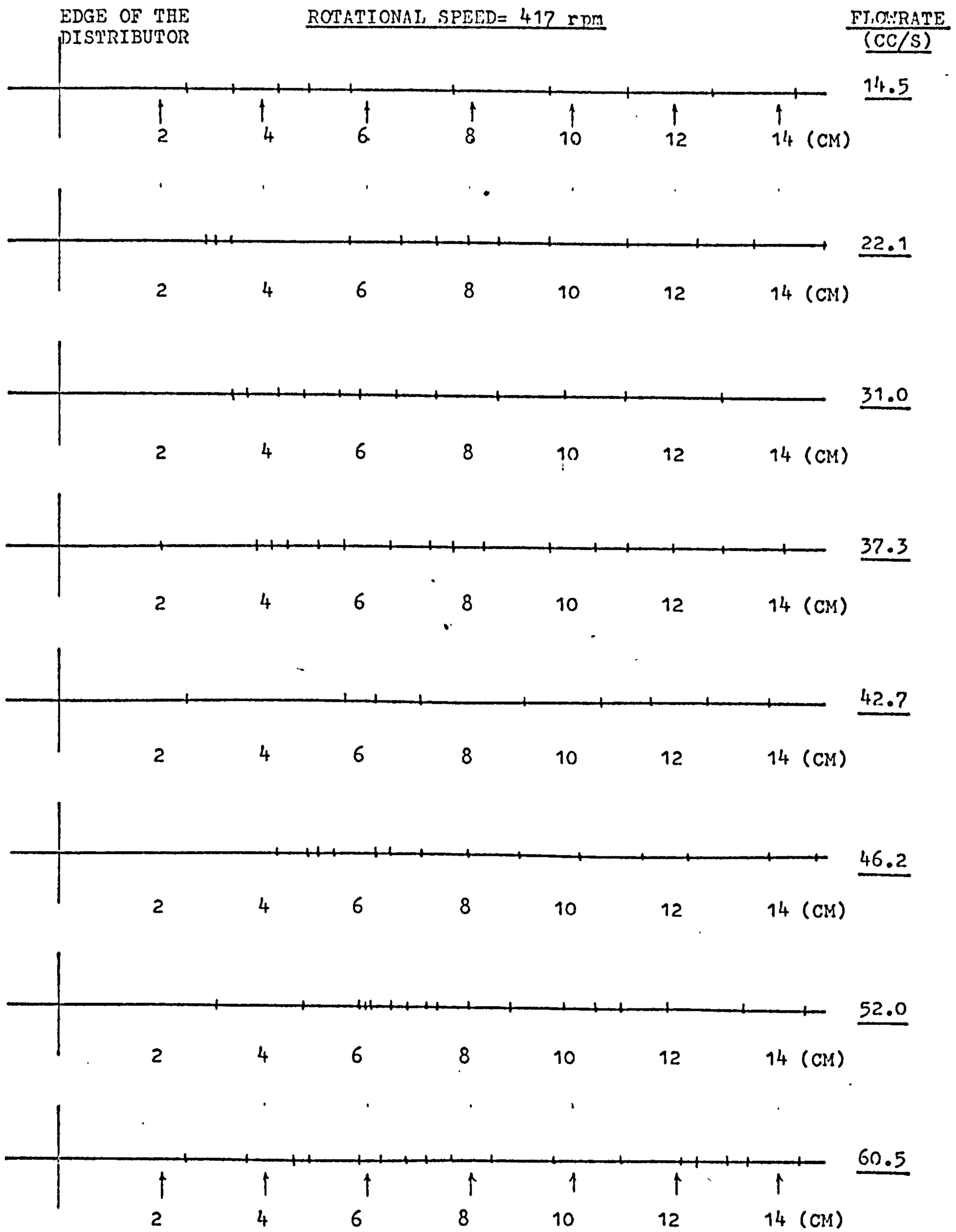

FIGURE 5.3 PEAK OF WAVES OBSERVED ACROSS THE DISC

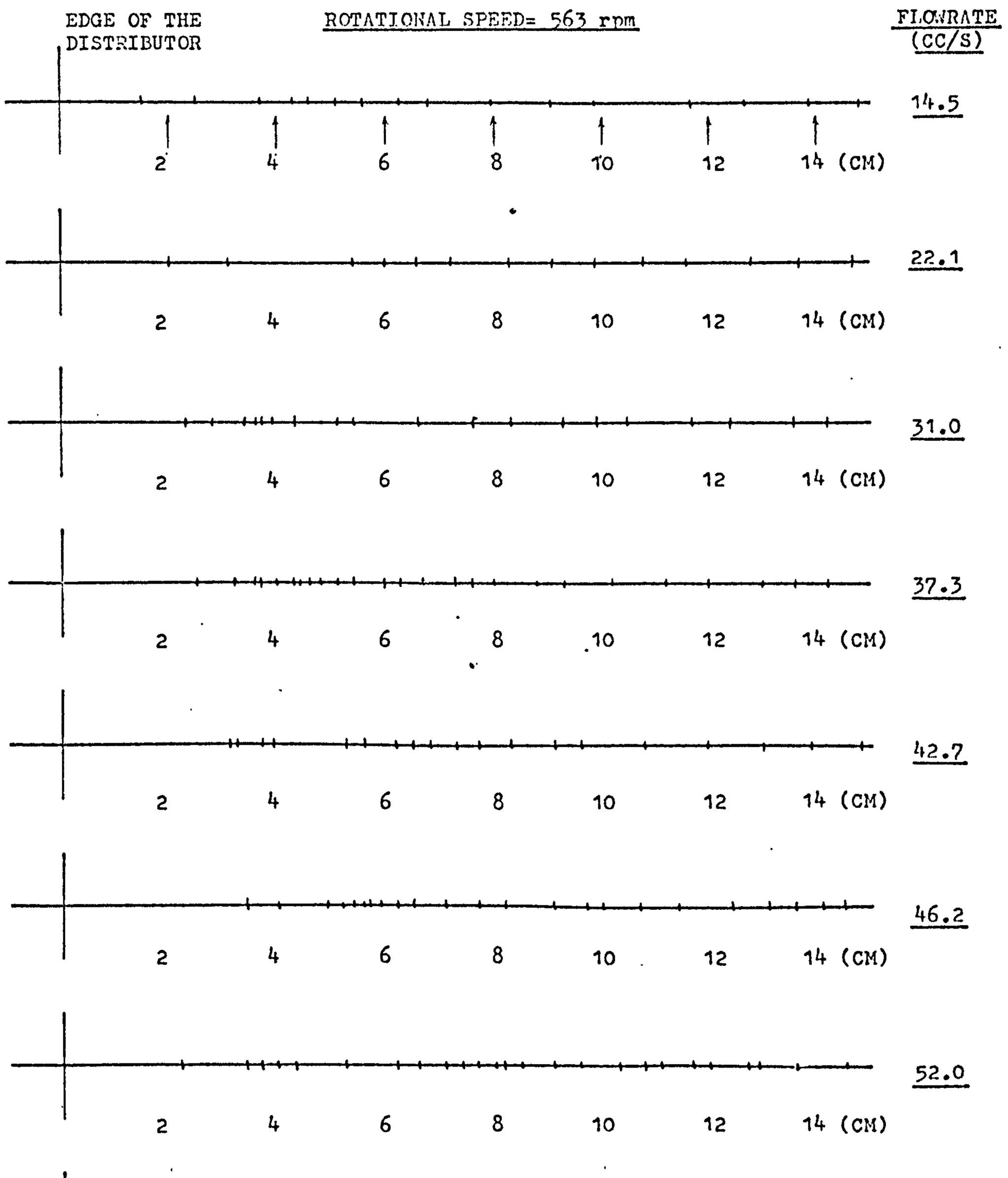

FIGURE 5.4 PEAK OF WAVES OBSERVED ACROSS THE DISC

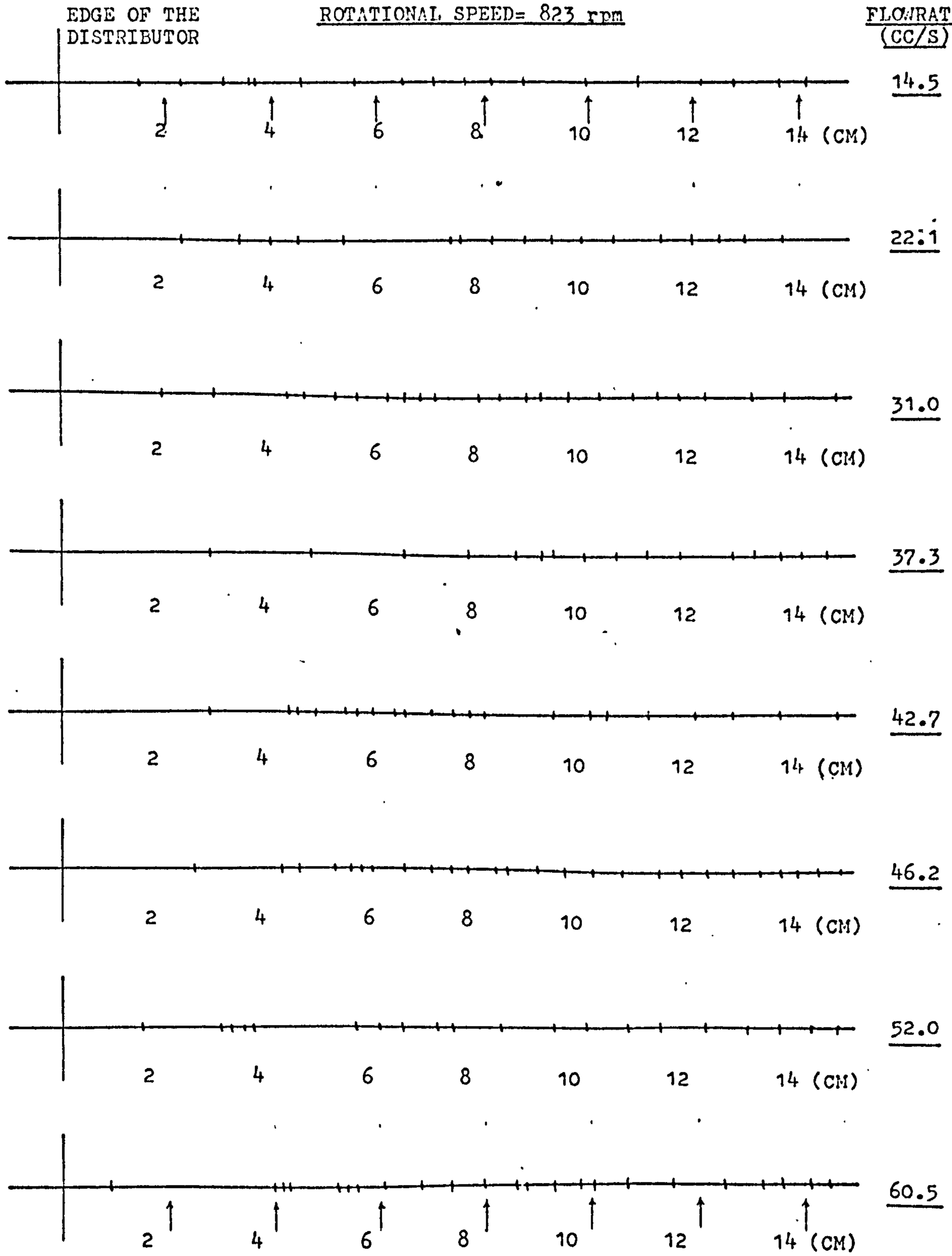

FIGURE 5.5 PEAK OF WAVES OBSERVED ACROSS THE DISC

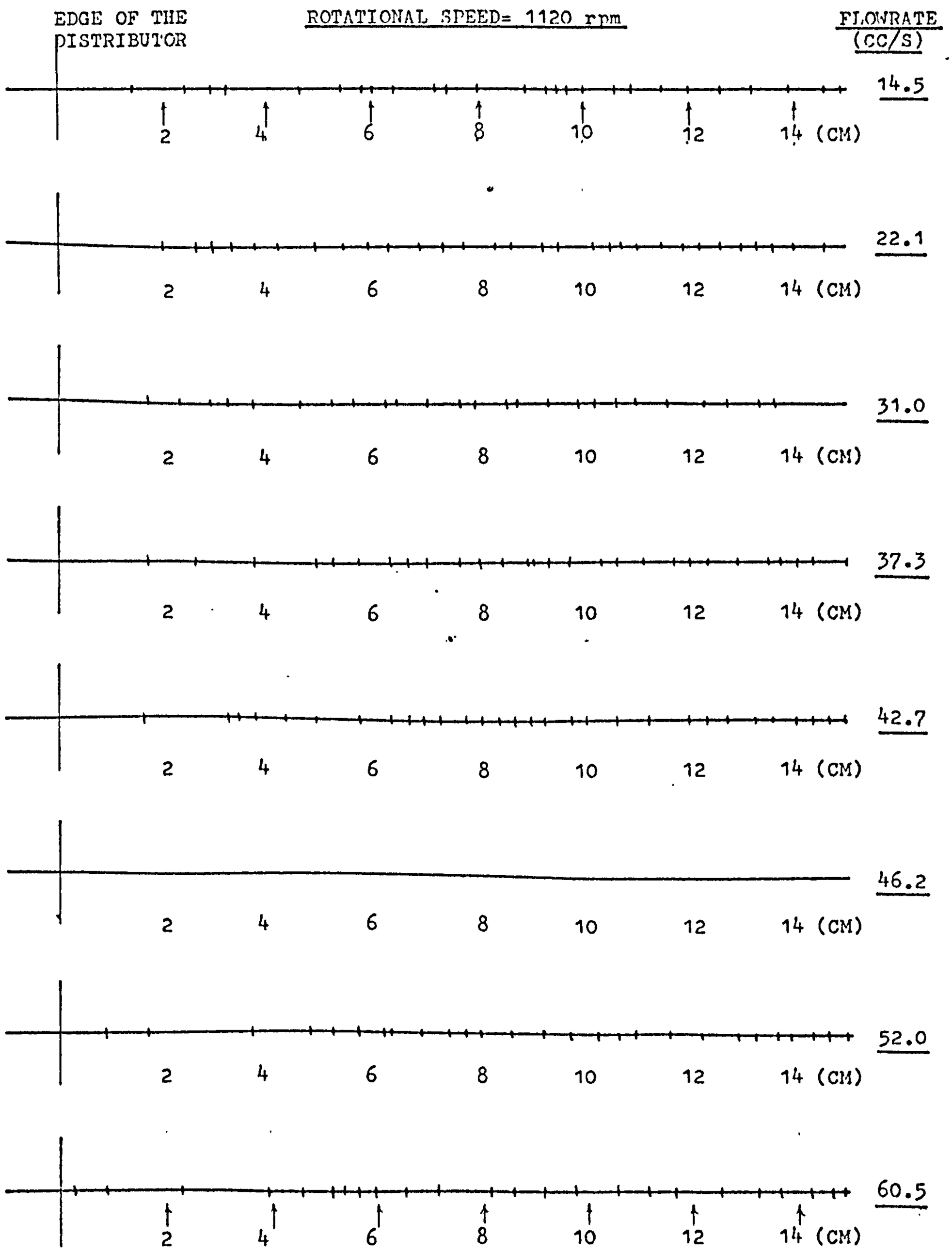

FIGURE 5.6 PEAK OF WAVES. OBSERVED ACROSS THE DISC

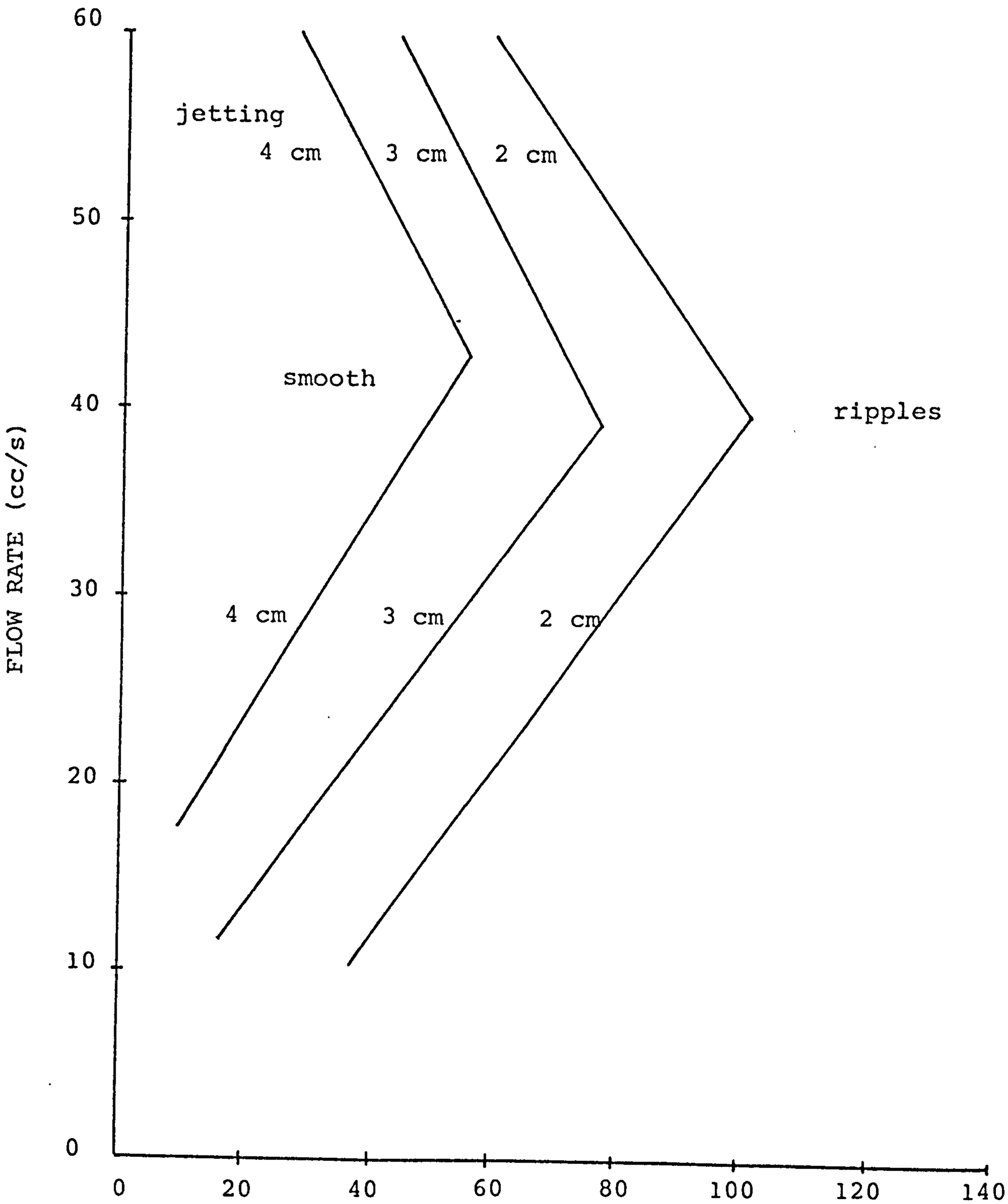

FIGURE 5.7 FLOW REGIMES

5.1 FILM THICKNESS

There are all together 282 measurements of film thickness which were made for varying system parameters. ($14.5 < Q < 60.5$ cc/s, $6 < r < 18$ cm, $24.24 < w < 118$ rad/s) give values of $80 < Re < 1030$ and $8 \times 10^4 < Ta < 4 \times 10^6$. These measurements were at radii at which film thickness was not influenced by the inlet conditions, namely distributor gap and initial liquid velocity, using equation 85a (Bell (26)).

All the raw data are stored in computer tape as official data, and the computed dimensionless group as shown in Tables G1 to G11 (Appendix G).

The data are presented graphically in Figures 5.8, 5.9 and 5.10, and correlated in terms of $(\frac{\delta}{r}, \frac{Re}{Ta^2})$, $(\frac{\delta}{r}Re, \frac{Re^2}{Ta})$, $(\frac{\delta}{r}(Ta)^{\frac{1}{2}}, \frac{Re^2}{Ta})$ respectively.

It will be noted that Figure 5.9 shows the best correlation and shows that the centrifugal model relationship

$$\frac{\delta}{r}Re = (\frac{3}{2\pi})^{\frac{1}{3}} \ (\frac{Re}{Ta})^{\frac{2}{3}}$$

is obeyed up to values of $\frac{Re^2}{Ta}$ of about 3. This should be compared with Section 3.2 and Figure 5.8 (Bell's model), which shows that deviation occurs above $\frac{Re^2}{Ta} = 1$, where the Coriolis model fits the data to a remarkable degree. It can be concluded, therefore, the analytical prediction of Coriolis influence for $\frac{Re^2}{Ta}$ greater than about one is correct, or providing $\frac{Re^2}{Ta}$ is much less than unity the centrifugal model will apply.

The scatter of Figure 5.10 is more apparent than real since the ordinate is scaled some 3 times larger than in the other two figures. Figure 5.10 shows that a slight advantage may be had in correlating the data in terms of $\frac{\delta}{r}(Ta)^{\frac{1}{2}}$ rather than $\frac{\delta}{r}(Re)$ in that numerical spread of the data is distinguishly shown.

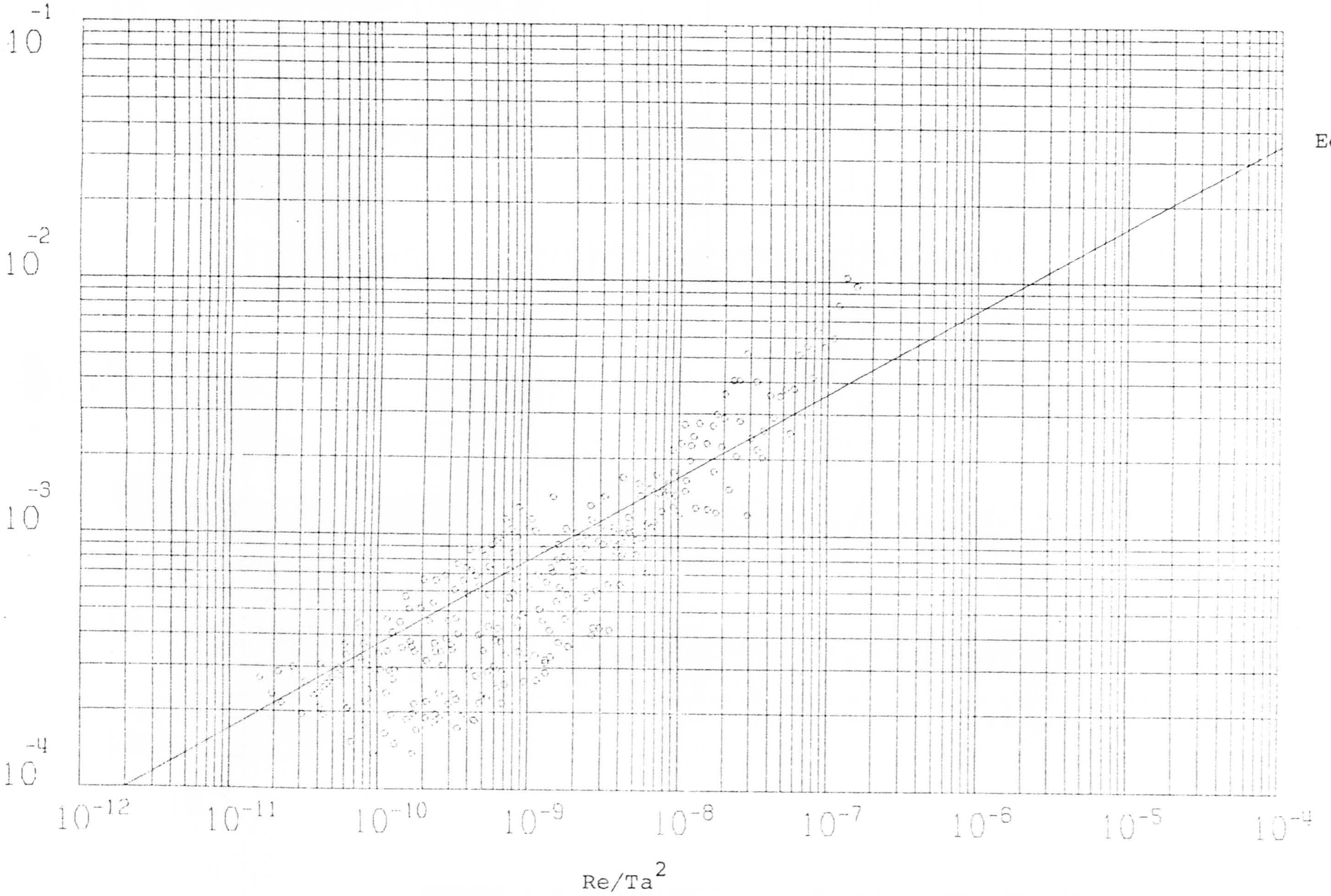

Eq 26

FIGURE 5.8 EXPERIMENTAL FILM THICKNESS RESULTS

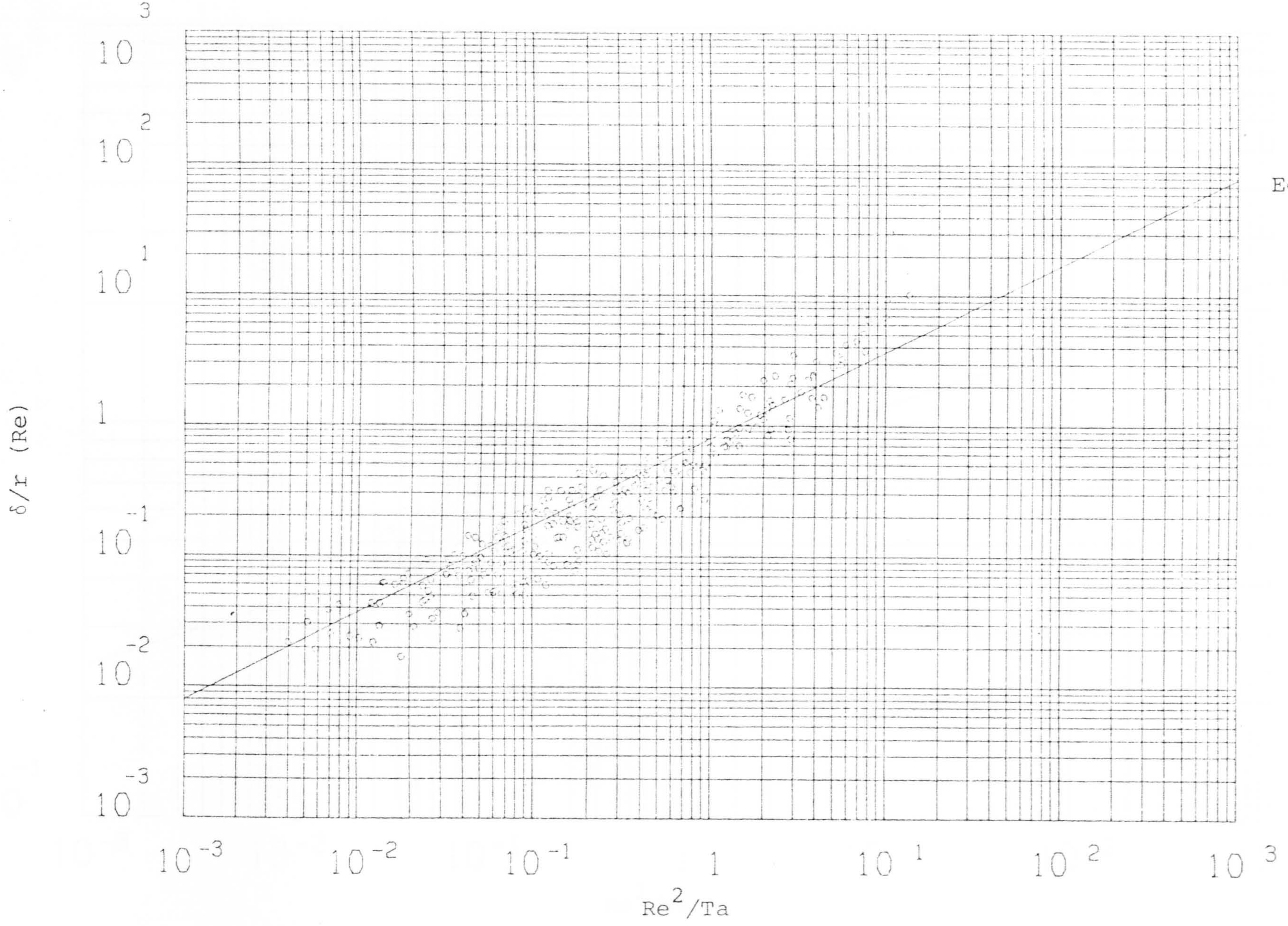

Eq 27

FIGURE 5.9 EXPERIMENTAL FILM THICKNESS RESULTS

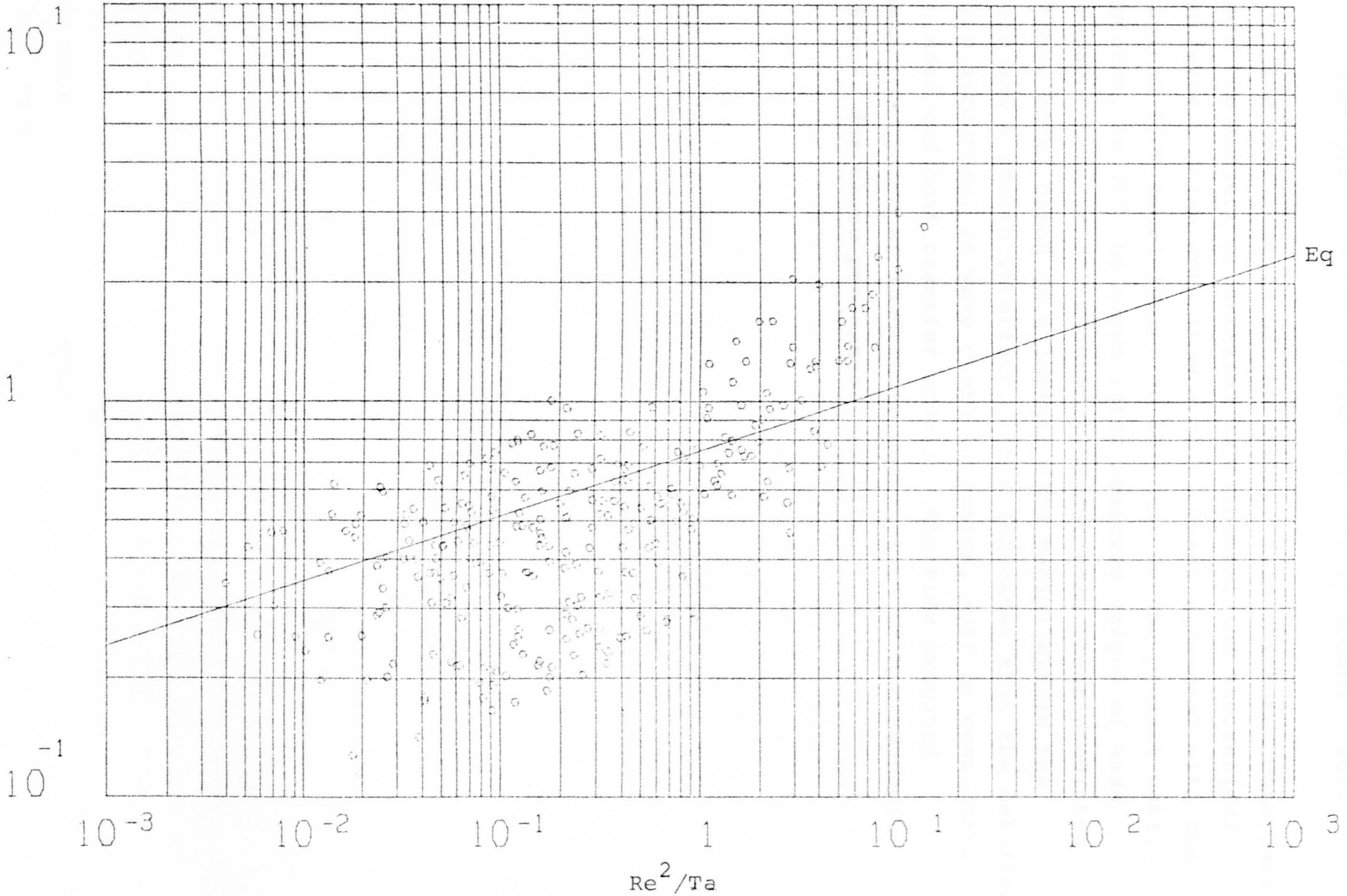

FIGURE 5.10 EXPERIMENTAL FILM THICKNESS RESULTS

The spread in the figures was mainly around ±35%.

The measurements of the average film thickness data have been the subject of detailed experimental and theoretical analysis. These data show a much closer agreement with the laminar flow model (Equation 27) than do the present data. However, as will be shown later measured values of mass transfer rate are considerably higher than those predicted from a model based on a laminar flow regime within the film and a smooth interface. This indicates that the detailed flow structure, ie wave characteristics, must be considered in mass and heat transfer models, the time averaged behaviour being an inadequate description of hydrodynamic effects for these processes.

5.2 WAVE INCEPTION

In observing the flow of liquid in undulatory film flow on a rotating disc, it was noted that a smooth entrance region existed near the edge of the distributor. It started at the edge of the distributor and extended a finite distance across the disc to the point at which waves appeared on the film surface. This distance, from the edge of the distributor to the point at which waves were first perceptible on the surface of the film is called 'the length of wave inception'. 'The length of wave inception' was determined from visual and photographic observations of the wavy film flow. It was observed that the onset of wavy flow did not take place gradually but rather it occurred very sharply and distinctively and in general the region of wave inception is characterised by a comparatively orderly wave motion at low flow rate and rotational speed of the disc. At high flow rate and rotational speed, the regular wave motion is very short-lived and it breaks up quickly into random rippling. For constant distributor gap, 'the length of wave inception' determined for water was given in Table G17 and has a dimensionless correlation given as (see Figure 5.11)

$$R^* = 576.10\ Re_o^{0.07}\ Ta_o^{-0.66}$$

where $$R^* = \frac{\text{inception}}{r_o},\quad Re_o = \frac{Q}{r_o \nu},\quad Ta_o = \frac{Wr_o^2}{\nu}$$

It can be seen that as the flow rate increased, the length of wave inception progressed further across the disc, evidently because the liquid was accelerating in that region. Such behaviour has also been reported by Stainthorp and Allen (18), Jackson (4) and Tailby and Portalski (100c) for the flow of Newtonian liquids down a vertical tube and plate. However, at high rotational speed, the length of wave inception decreased due mainly to the high centrifugal forces which are more dominant than the effect of flow increase, as shown from the dimensionless correlation.

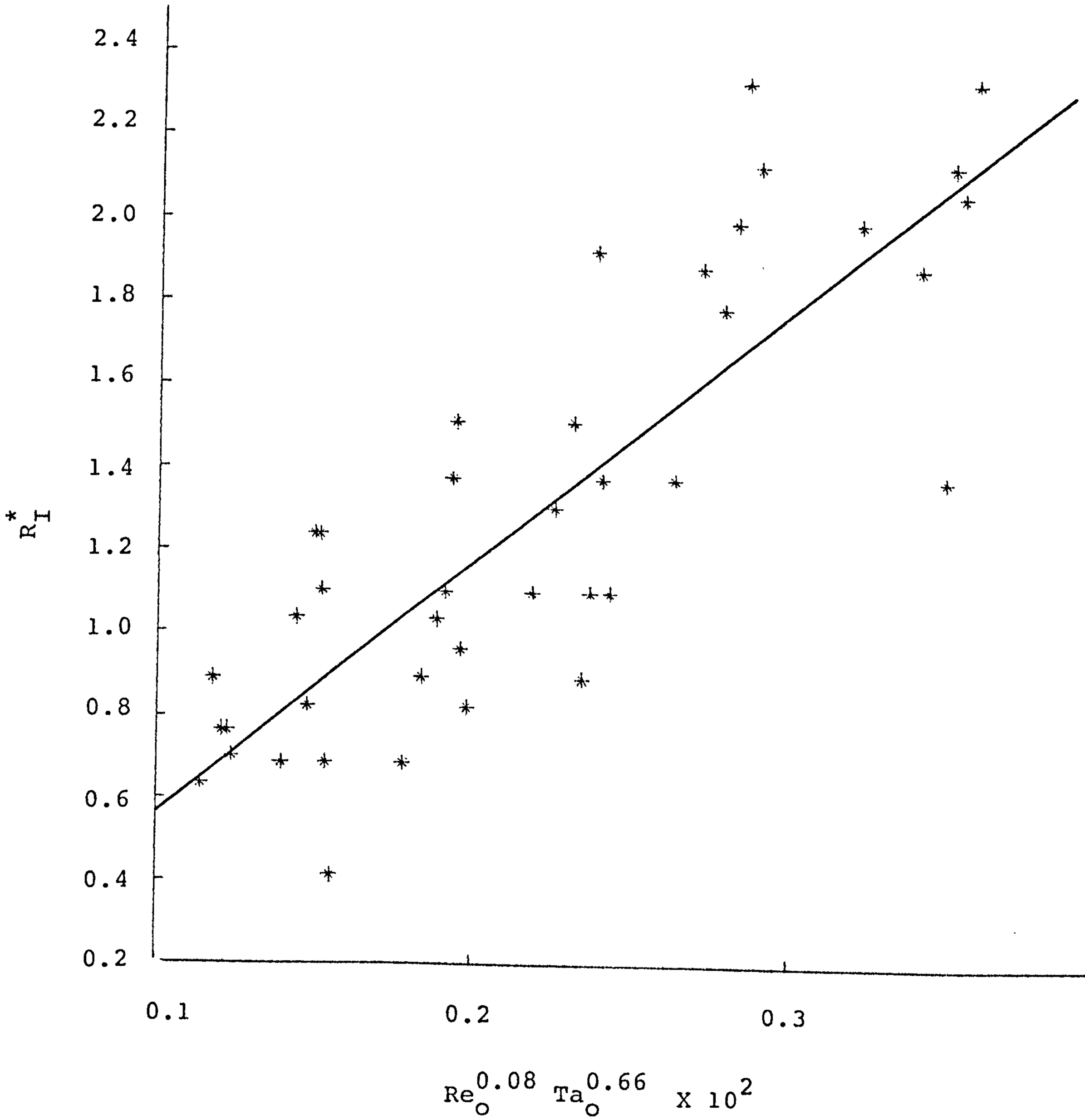

FIGURE 5.11 WAVE INCEPTION CORRELATION

5.3 WAVE AMPLITUDE

The surface profiles of thin liquid films formed on a rotating disc are recorded in Figures 5.14-5.25, (using the microdensometric technique). This showed that when ripples first formed on the surface of a thin liquid film, they were of a fairly uniform frequency and amplitude. As the liquid flow rate and rotational speed were increased, the frequency and amplitude of the waves became irregular. It was noted that at any one position across the disc, the measured amplitude increases with flow rate and decreases with increased rotational speed. With particular flow rate and rotational speed, the wave amplitude approaches a constant amplitude further across the disc. These measurements were given in Table G18 and correlated into dimensionless group given as (Figure 5.12)

$$A^* = Re^{0.06} \quad Ta^{-0.59} \times 0.604$$

where $A^* = \frac{A}{r_o}$, $Re = \frac{Q}{r\nu}$, $Ta = \frac{wr^2}{\nu}$

The observed trend of the wave amplitude was expected in the right direction with the system variables. However, there is so far no theoretical expression obtained for wavy flow on rotating disc. Therefore, comparisons were made with that of Portalski's equation for falling liquid film to predict the wave amplitude of a two-dimensional wavy flow.

$$\text{wave amplitude for falling film} = 1.339 \left(\frac{\nu Q}{g}\right)^{\frac{1}{3}}$$

$$\text{wave amplitude for rotating disc} = 1.339 \left(\frac{\nu Q}{rw^2}\right)^{\frac{1}{3}}$$

The expected difference between the calculated values and the results obtained in this work can be seen in Table 5.1.

The calculated values were very much higher than experimental values. Although the experimentally determined results were small, it may nevertheless be of interest to modify the Portalski equation to predict the amplitude of wave which is found in practice on rotating disc.

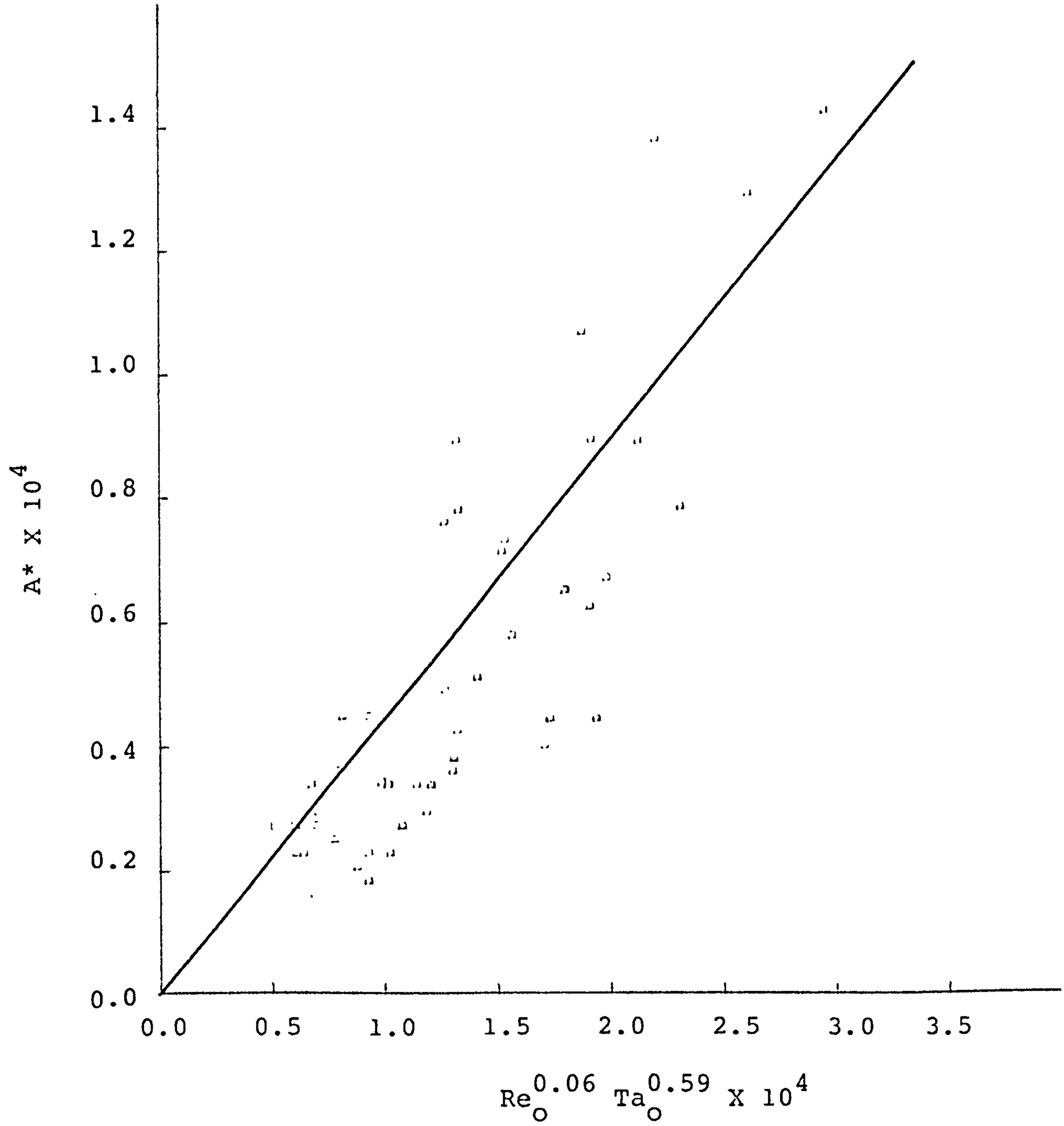

FIGURE 5.12 WAVE AMPLITUDE CORRELATION

5.4 WAVELENGTH

The wavelengths of symmetric, regular waves occurring at the point of wave inception were measured as a function of liquid flow rate and rotational speed. It is evident, indeed that only at the line of wave inception, the waves remain stable (low flow rate) with a constant wavelength and practically lose their regularity some distance further from the line of wave inception . (see Photographs R1,R2,R3). By visual observations using a stroboflash under all flow conditions of the liquid films, it was ascertained that, except for very low flow rates and rotational speeds or at the line of wave inception of wave motion, no single stroboscopic frequency could be found to give an absolutely 'stationary' picture of the rippled film formed across the disc. It was in this region directly below the line of wave inception that all wavelength measurements were made.

Since there are no theoretical expressions generally applicable for predicting the wavelength (as in wave amplitude) of liquid films on a rotating disc, Portalski's equation (Appendix D) for conditions of pseudo-laminar flow where the wave motion is two-dimensional was used for the comparison. In which the gravitational force was substituted with the centrifugal force

ie $\lambda = 7.2 \left(\frac{\nu \delta}{Qg}\right)^{\frac{1}{2}}$ $\lambda = 7.2 \left(\frac{\nu \delta_o}{Qr_o w^2}\right)^{\frac{1}{2}}$

However, it must be borne in mind that the flow-pattern predicted by Portalski's equation is only observed and valid under very restricted conditions of flow in the region where waves are just beginning to develop for falling liquid film.

The experimental results (Table G19 and Figure 5.13) show clearly that the measured wavelengths were larger than the predicted. This may be explained by a general observation that in many film flows,the waves show great tendency to coalesce into groups with the result that the wavelength of the

N = 824 rpm Q = 14.5 cc/s

N = 231 rpm Q = 14.5 cc/s

PHOTOGRAPH R1

N = 1120 rpm Q = 14.5 cc/s

N = 417 rpm Q = 14.5 cc/s

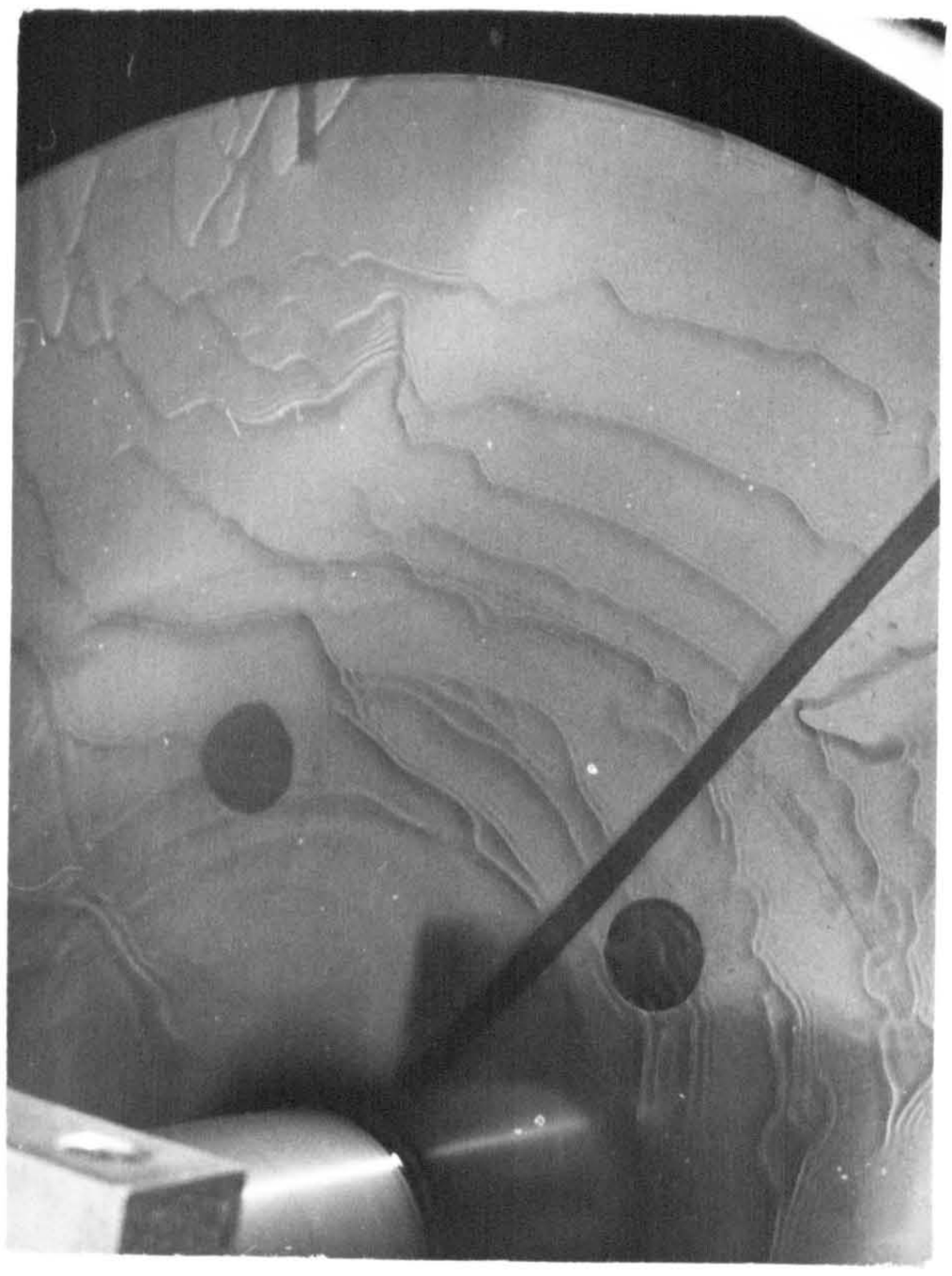

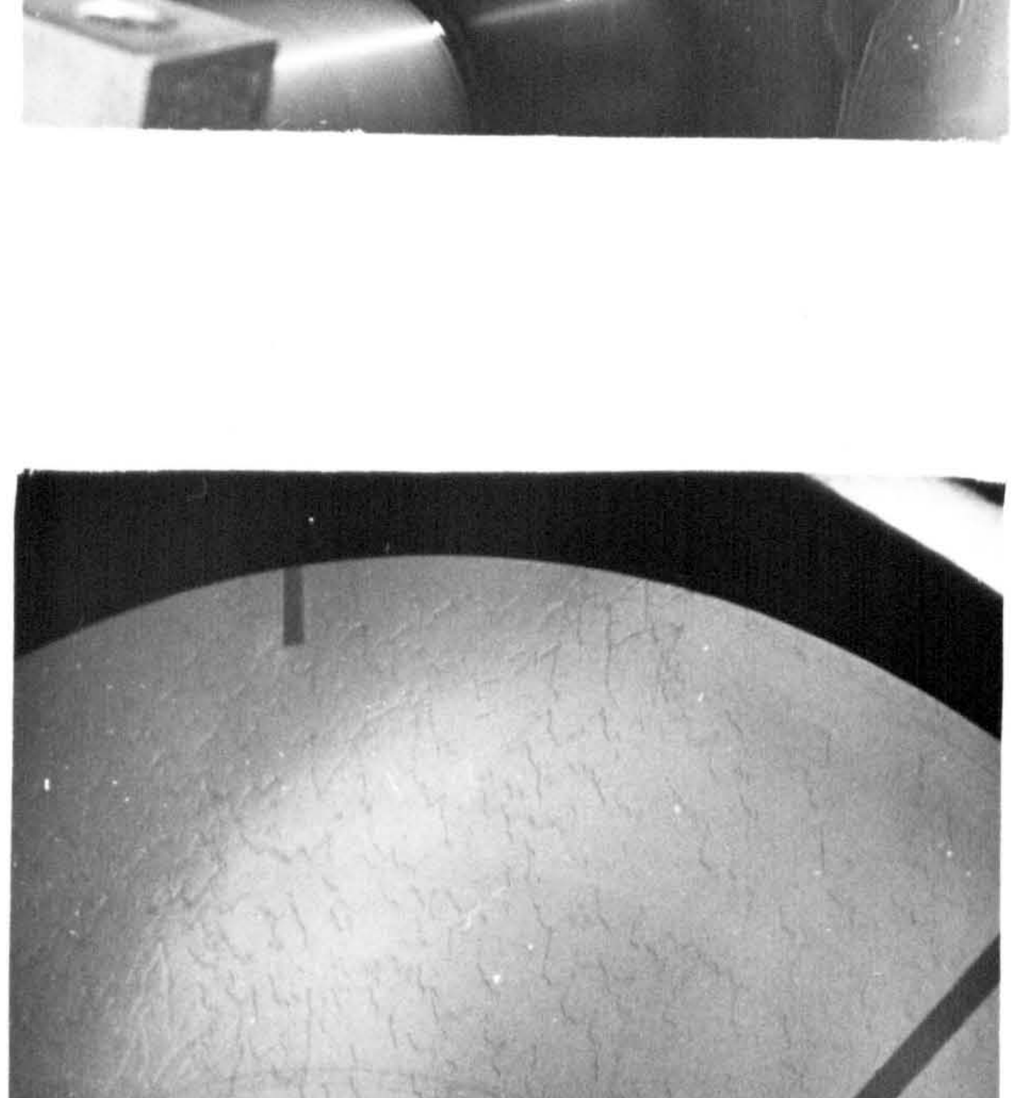

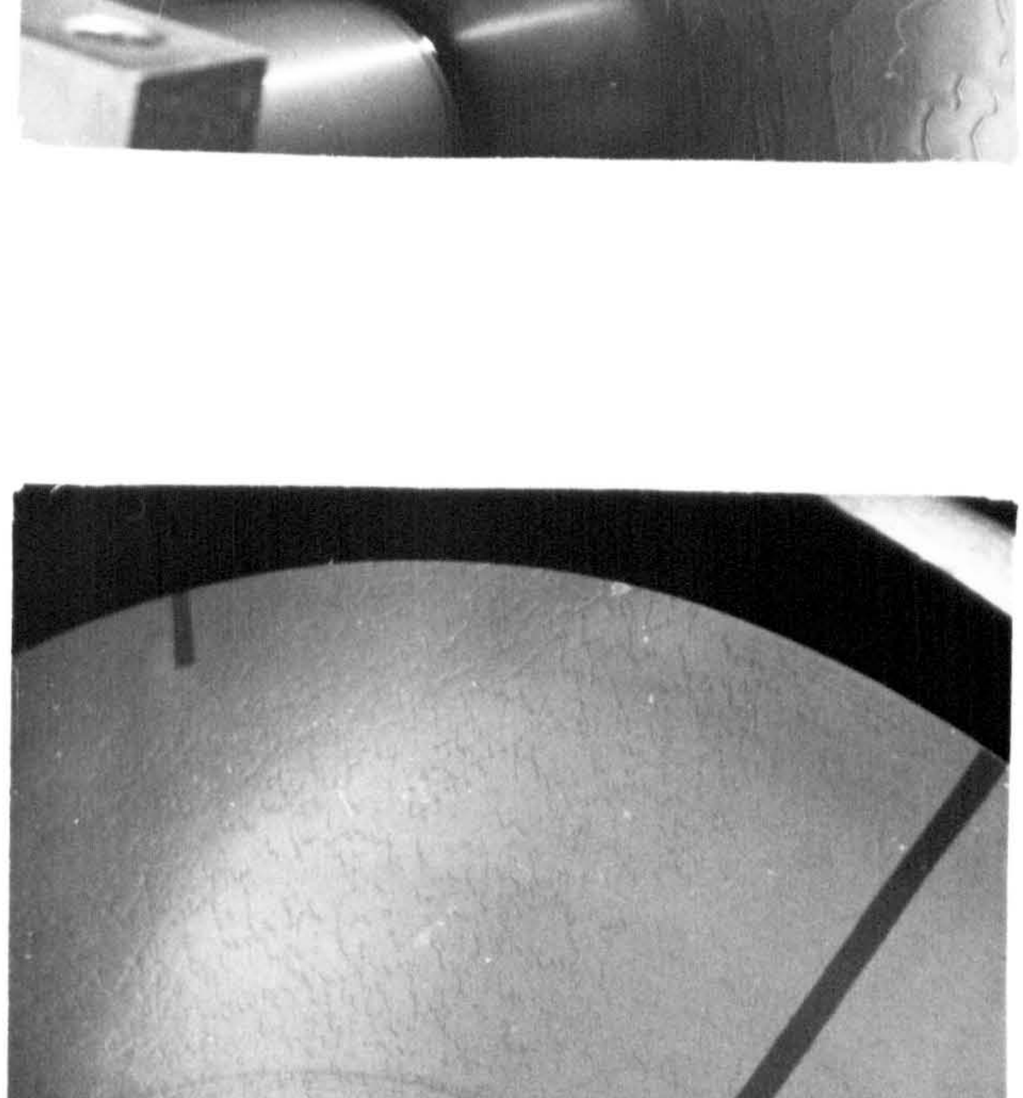

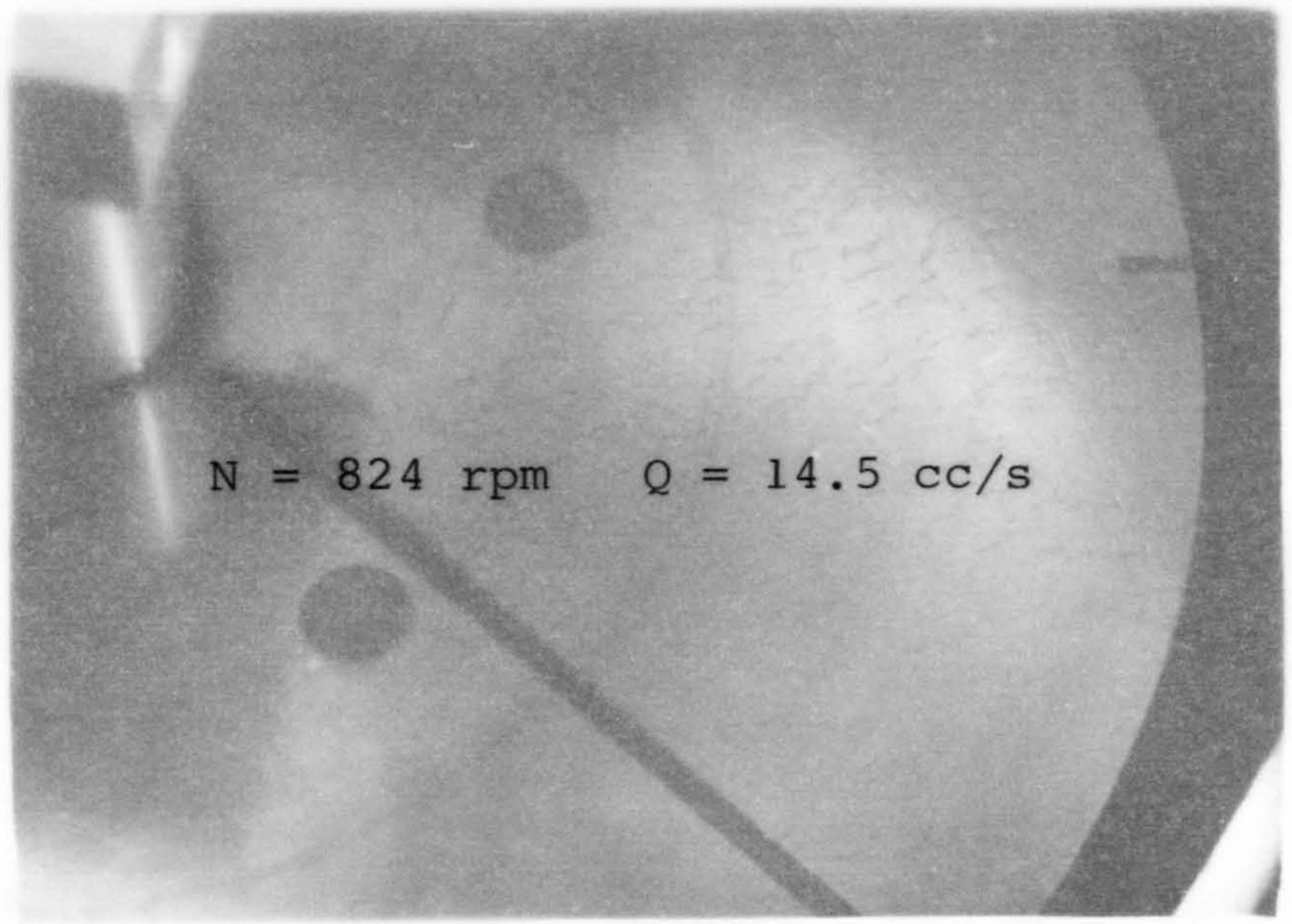

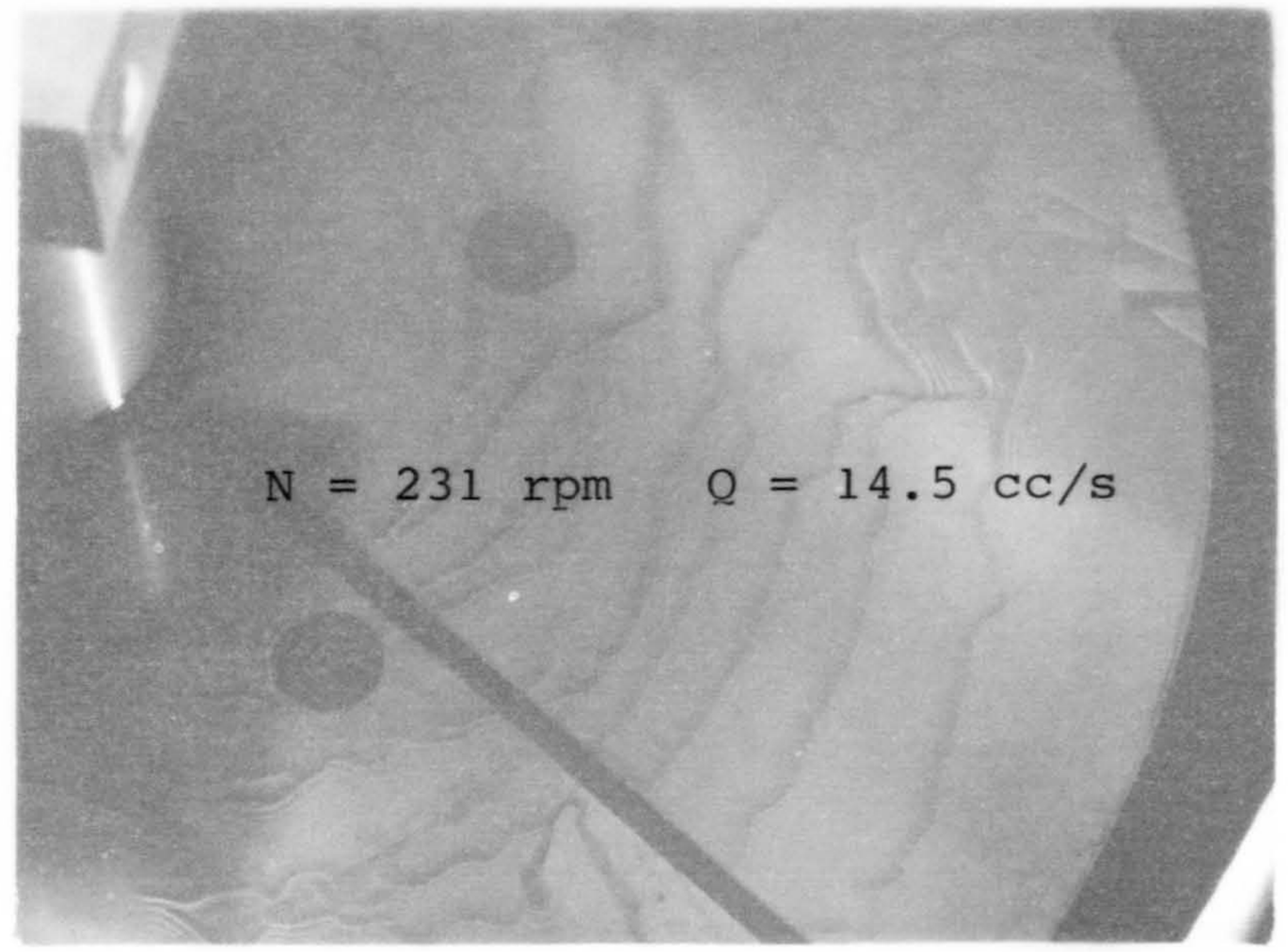

PHOTOGRAPH R1

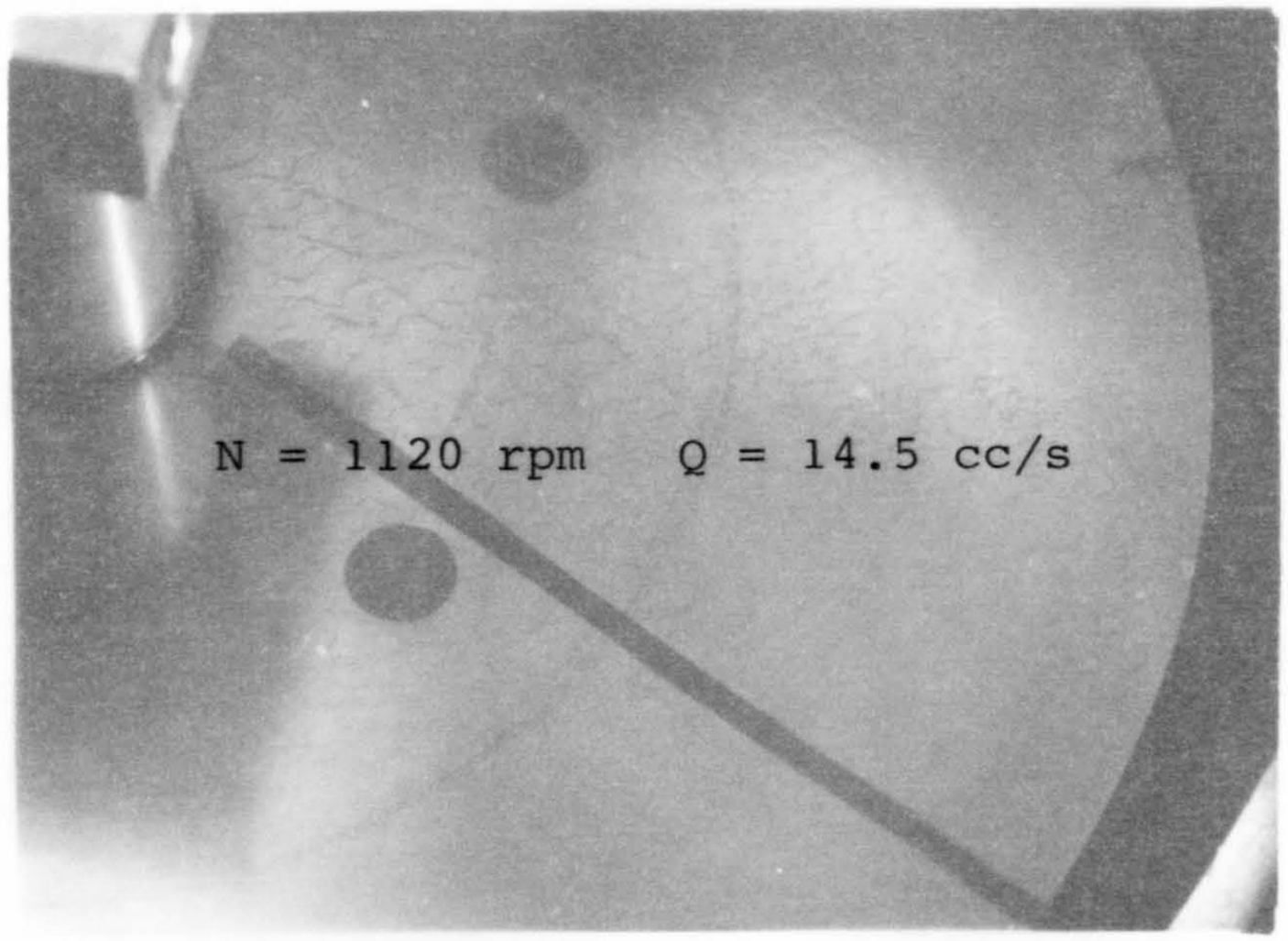

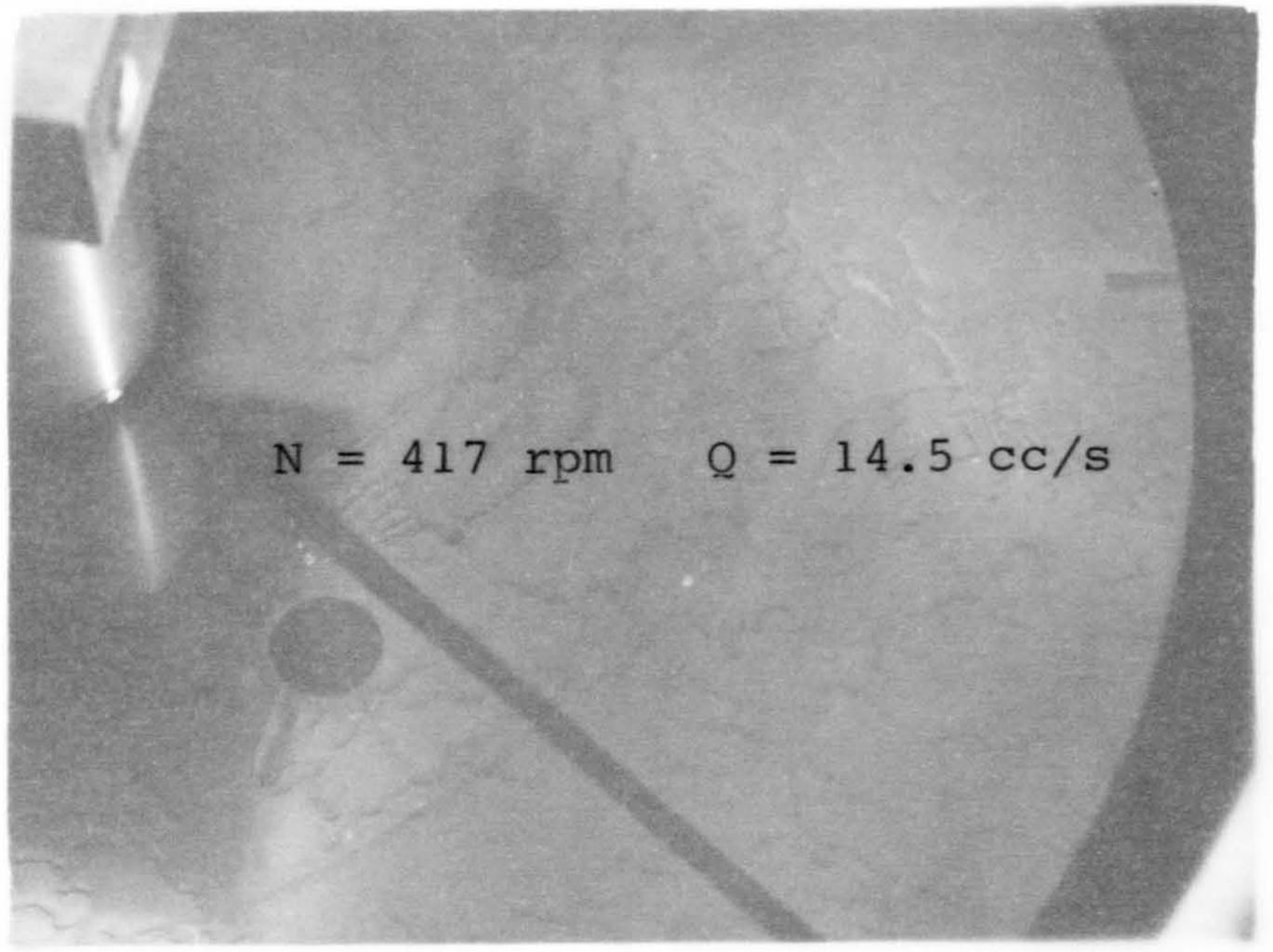

N = 824 rpm Q = 31.0 cc/s

N = 231 rpm Q = 31.0 cc/s

PHOTOGRAPH R2

N = 1120 rpm Q = 31.0 cc/s

N = 417 rpm Q = 31.0 cc/s

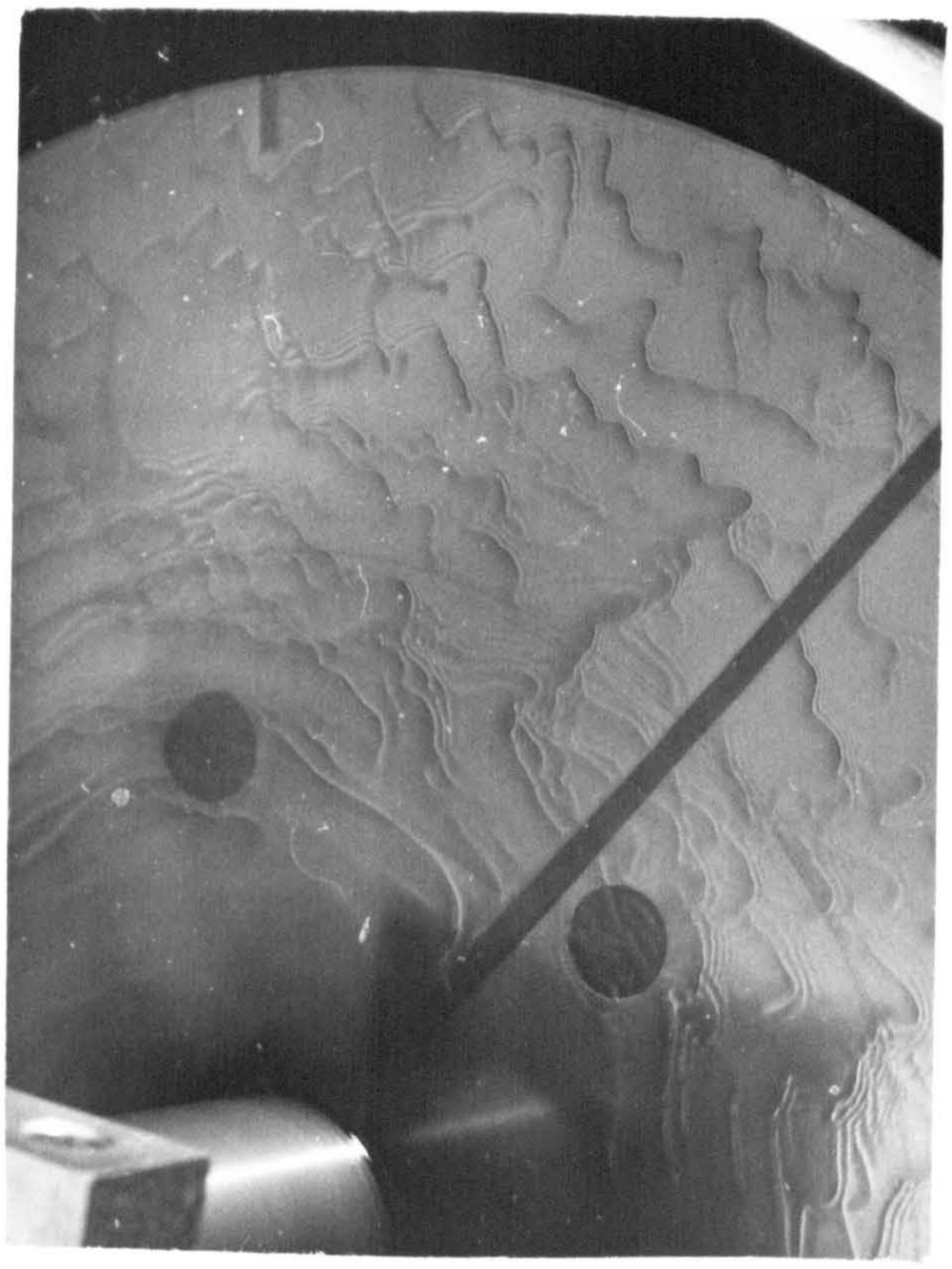

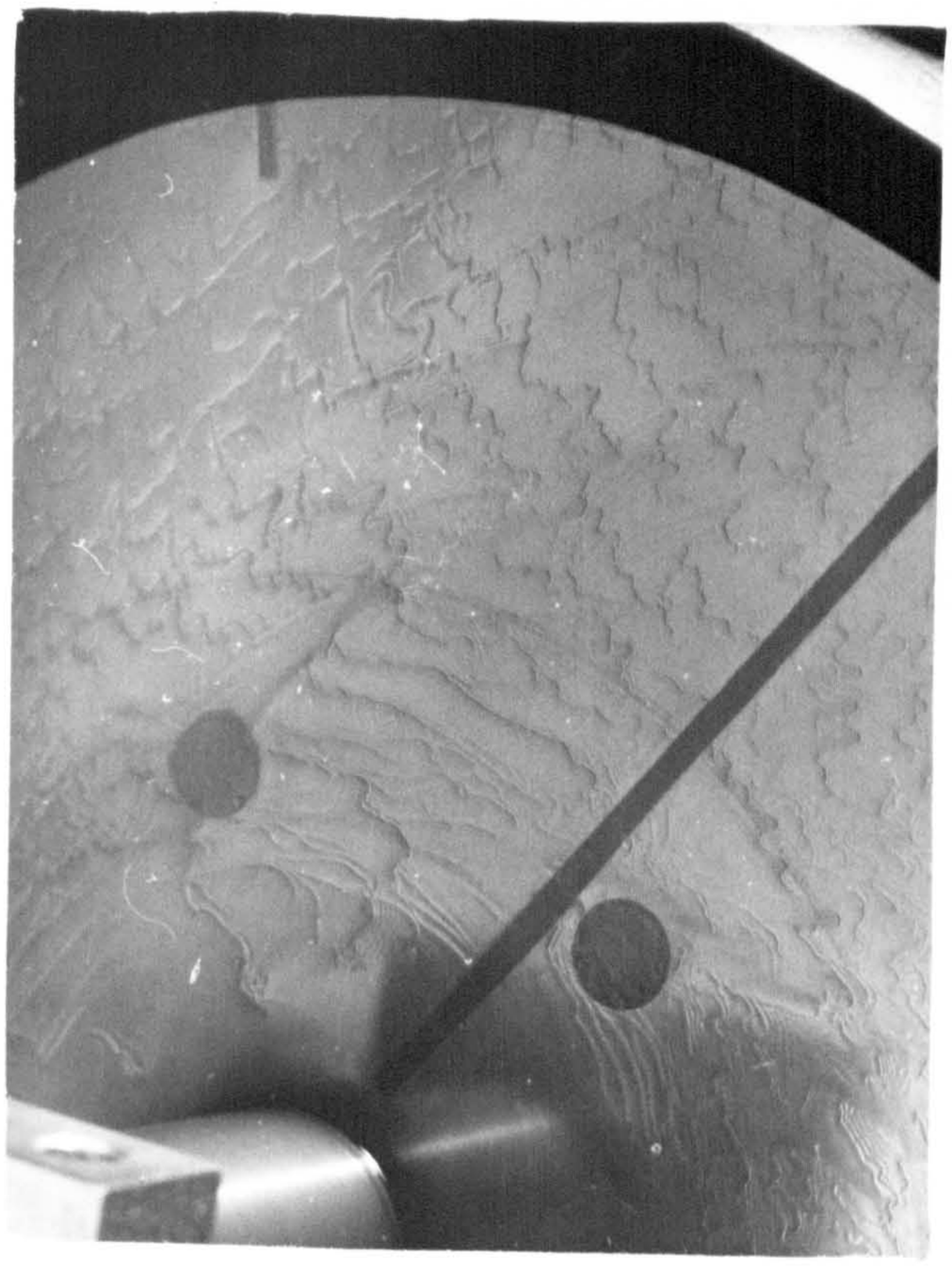

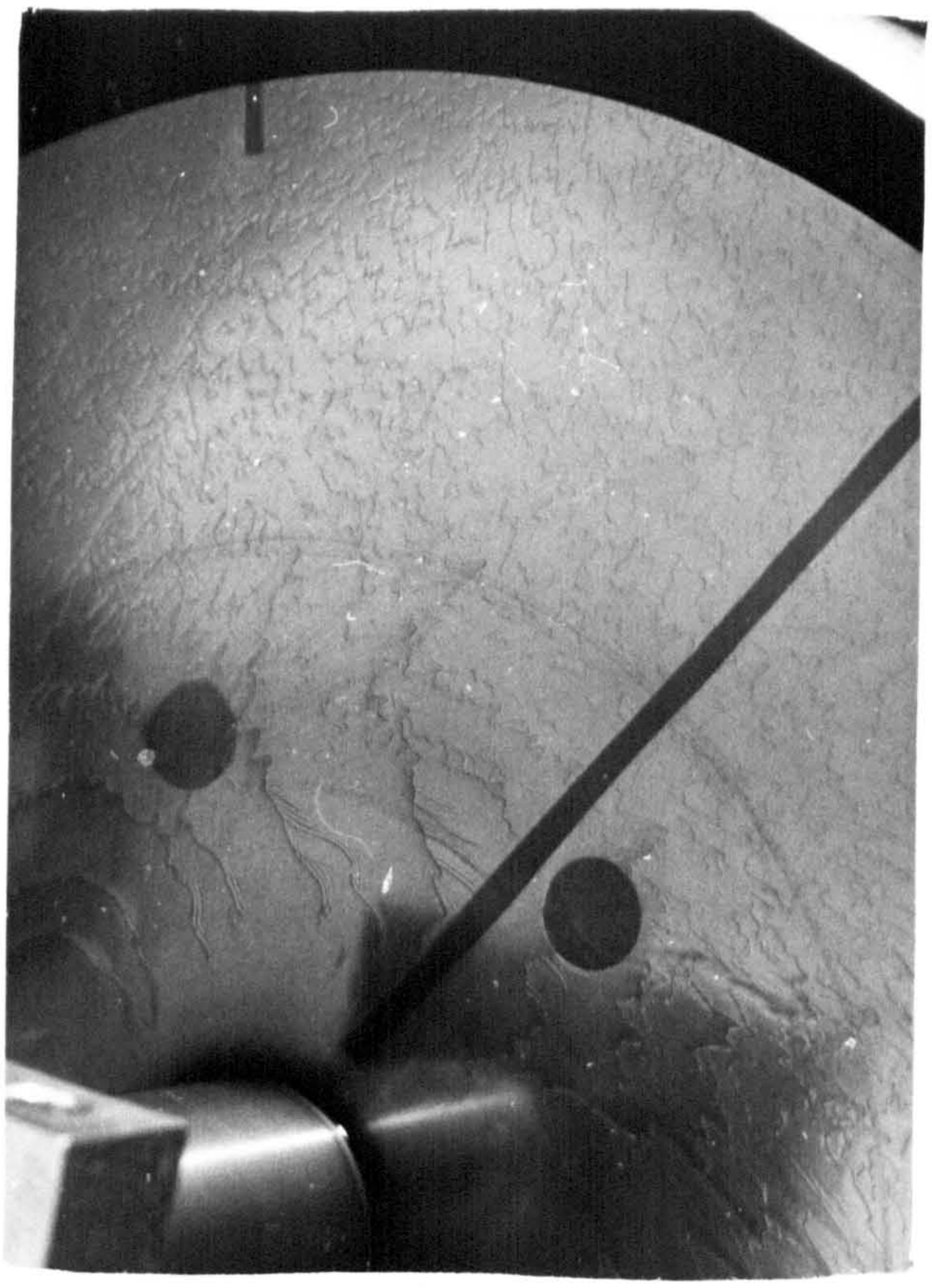

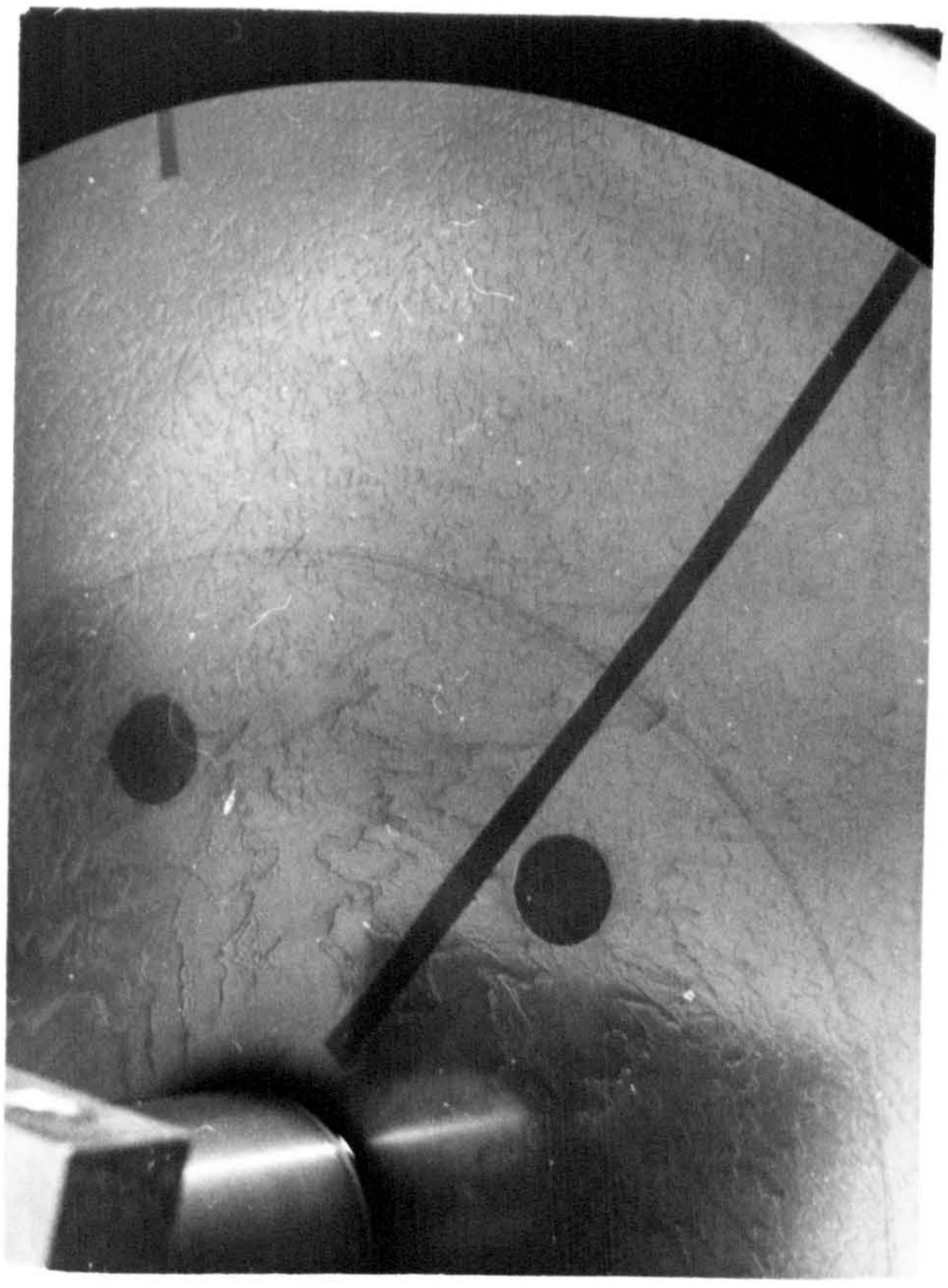

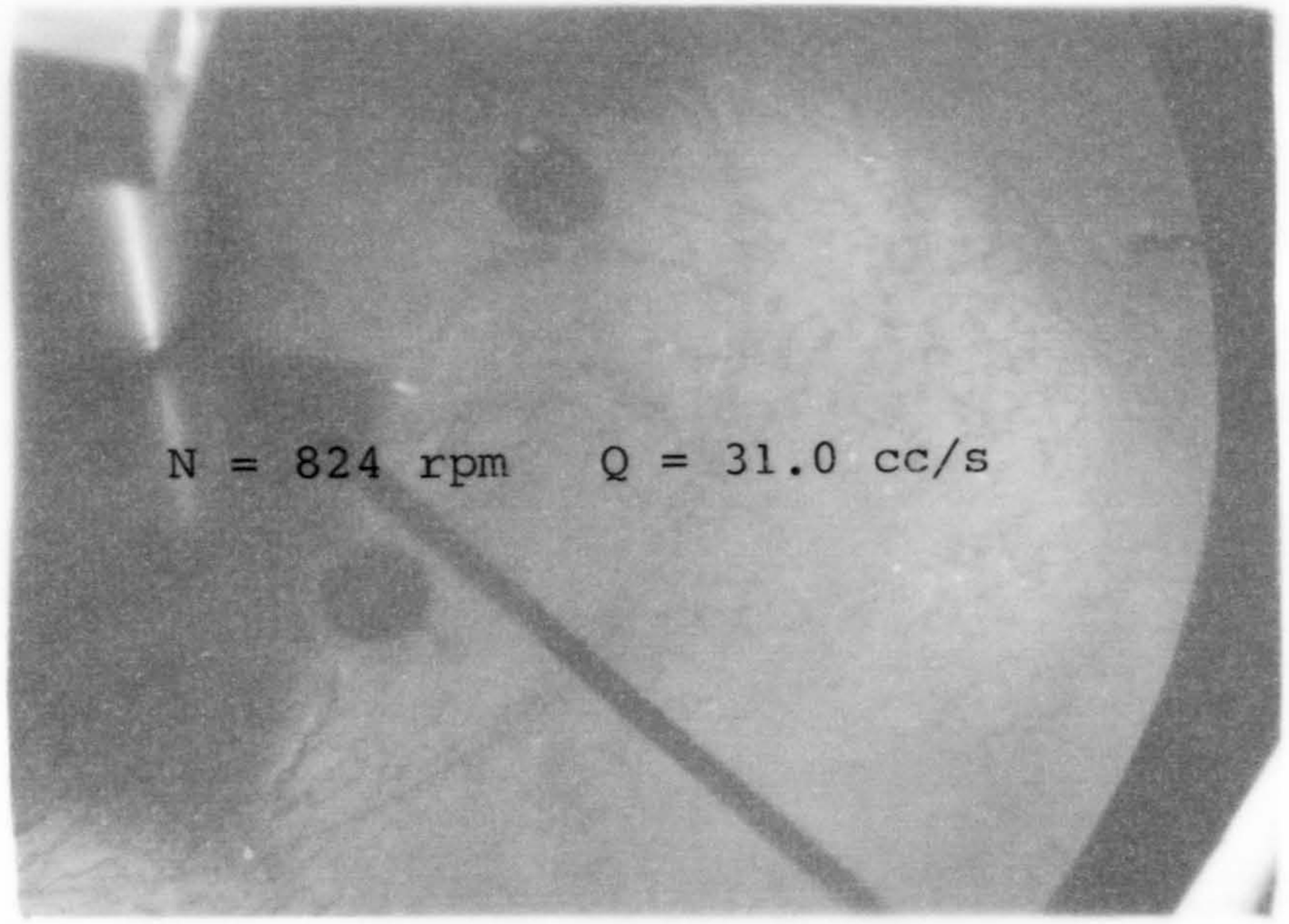

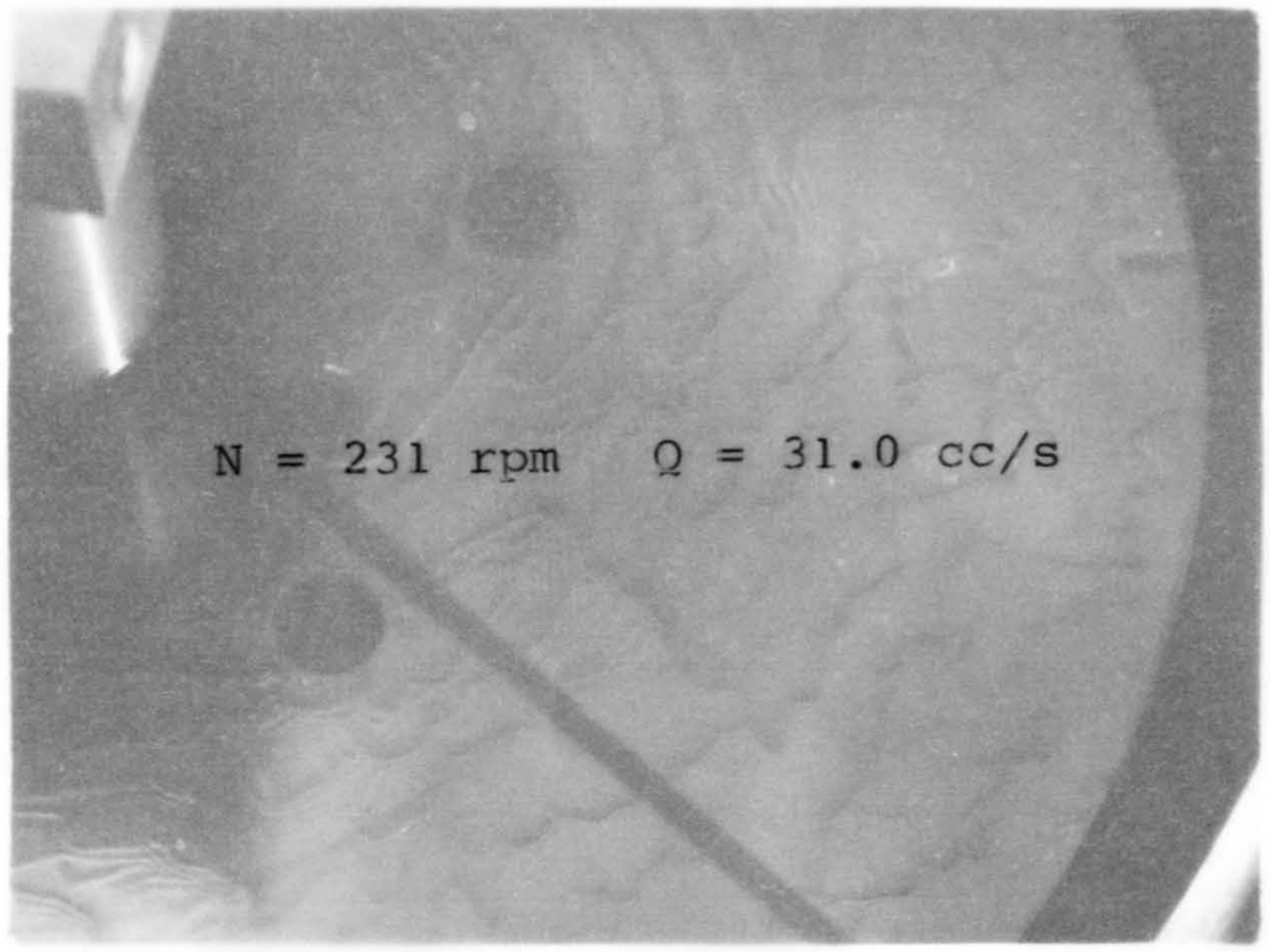

PHOTOGRAPH R2

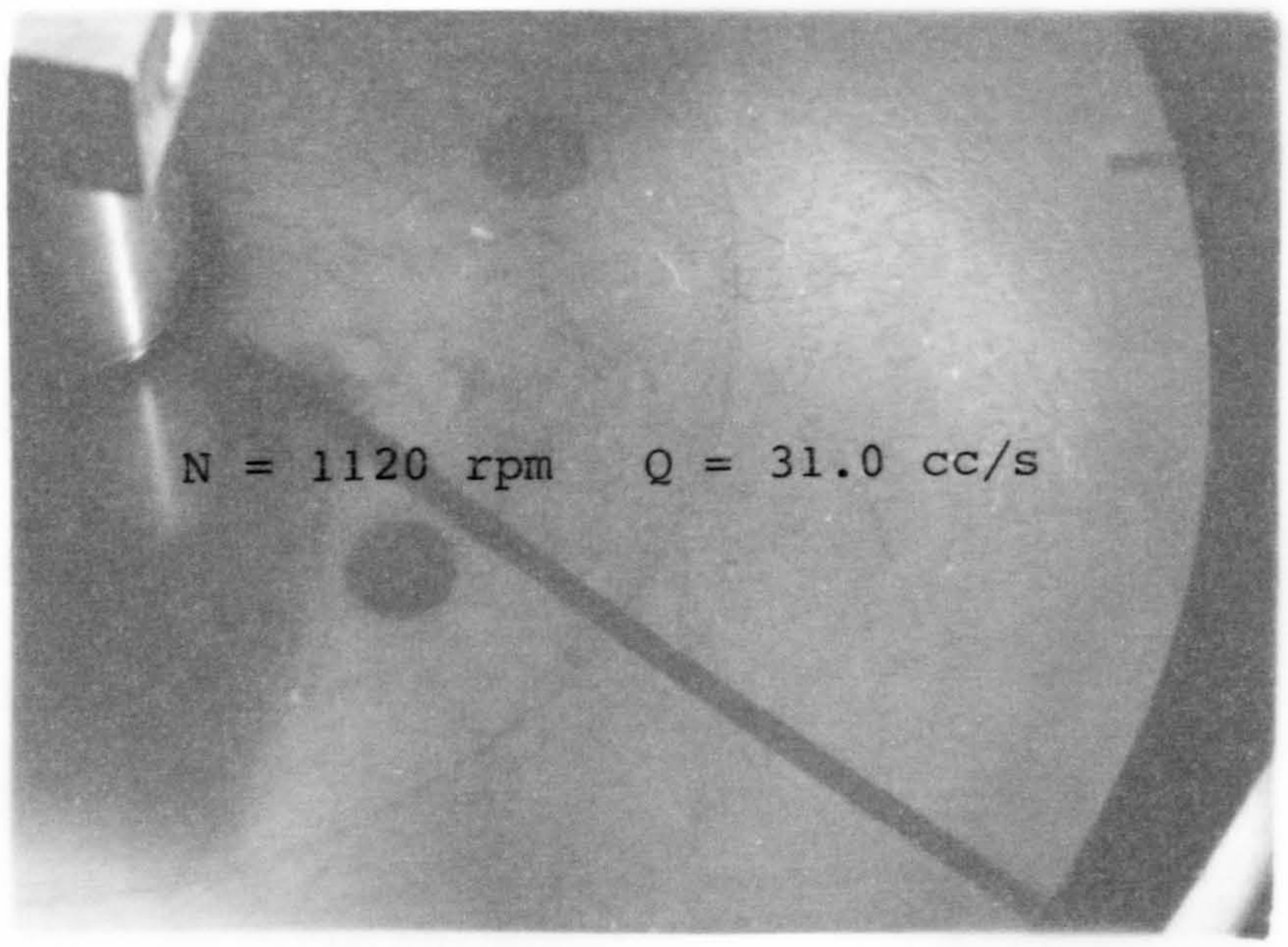

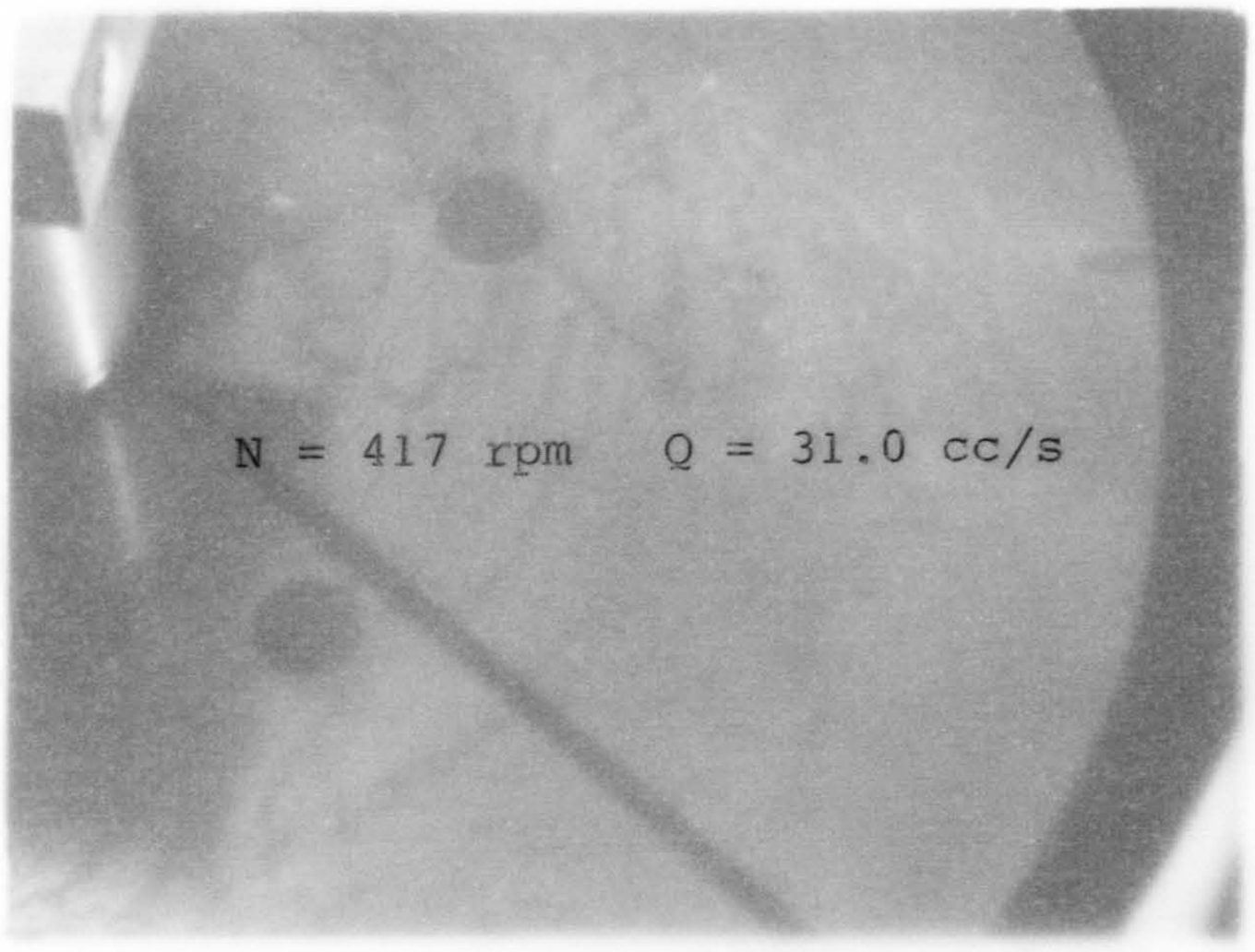

N = 824 rpm Q = 52.0 cc/s

N = 231 rpm Q = 52.0 cc/s

PHOTOGRAPH R3

N = 1120 rpm Q = 52.0 cc/s

N = 417 rpm Q = 52.0 cc/s

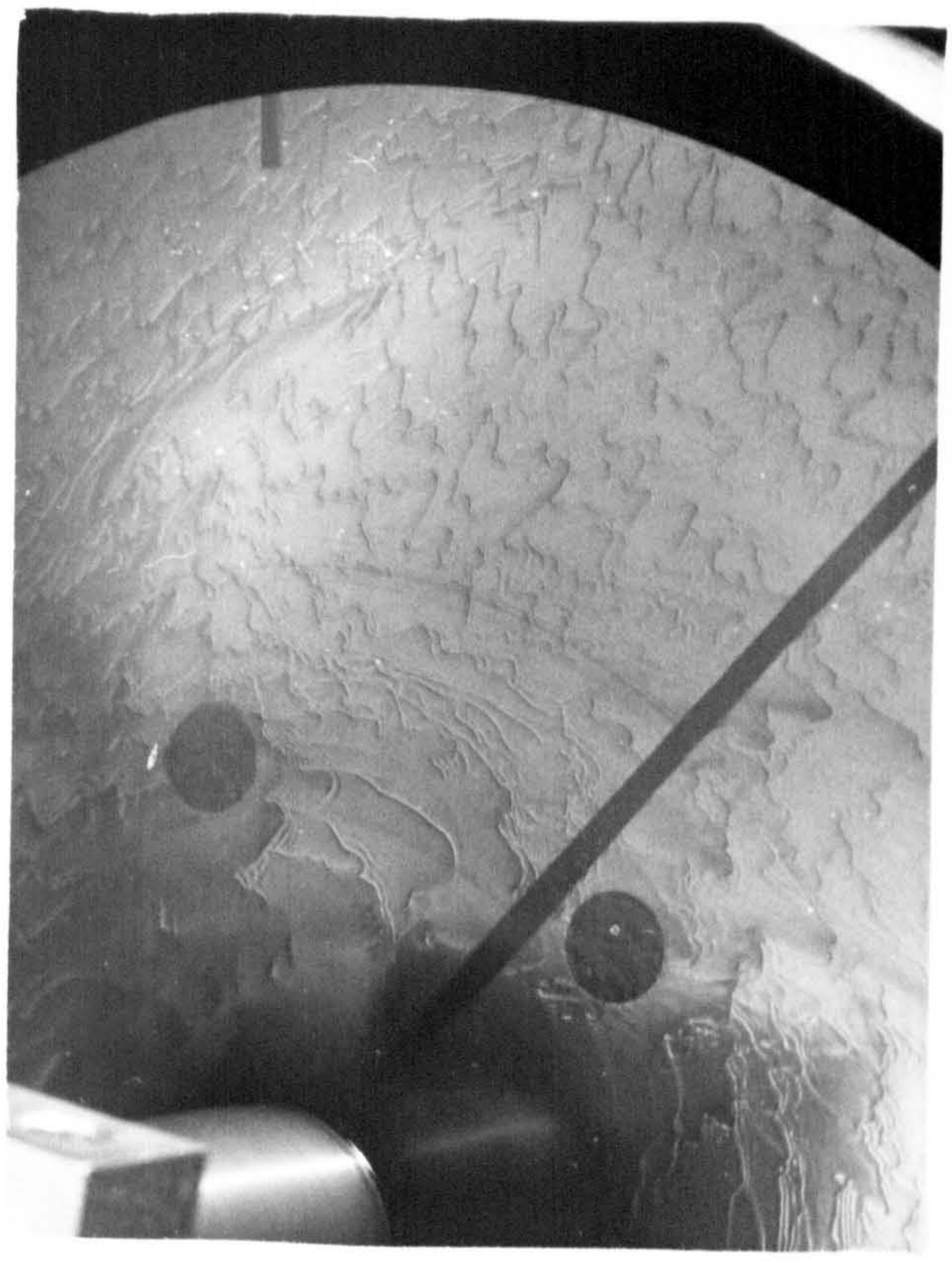

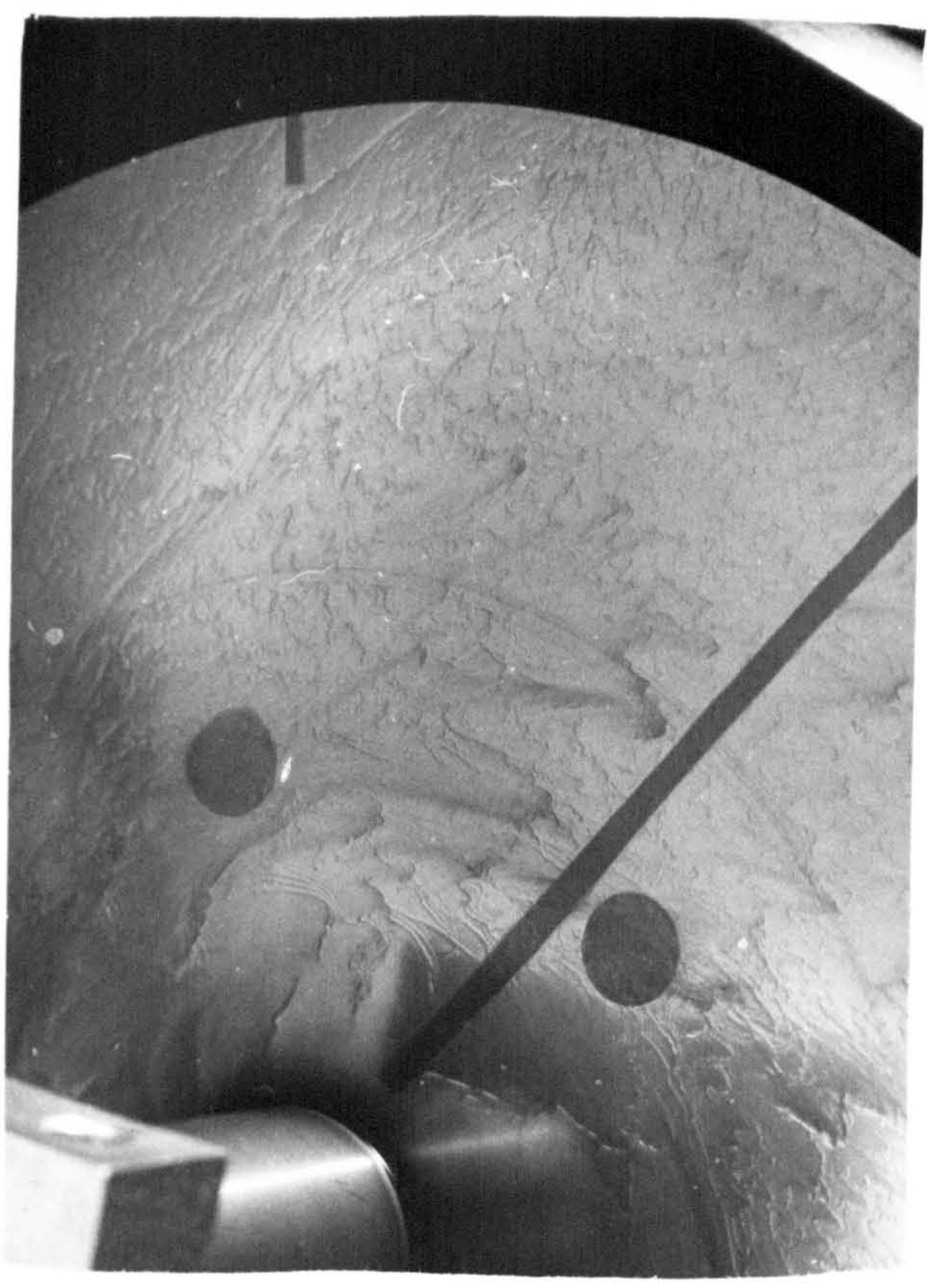

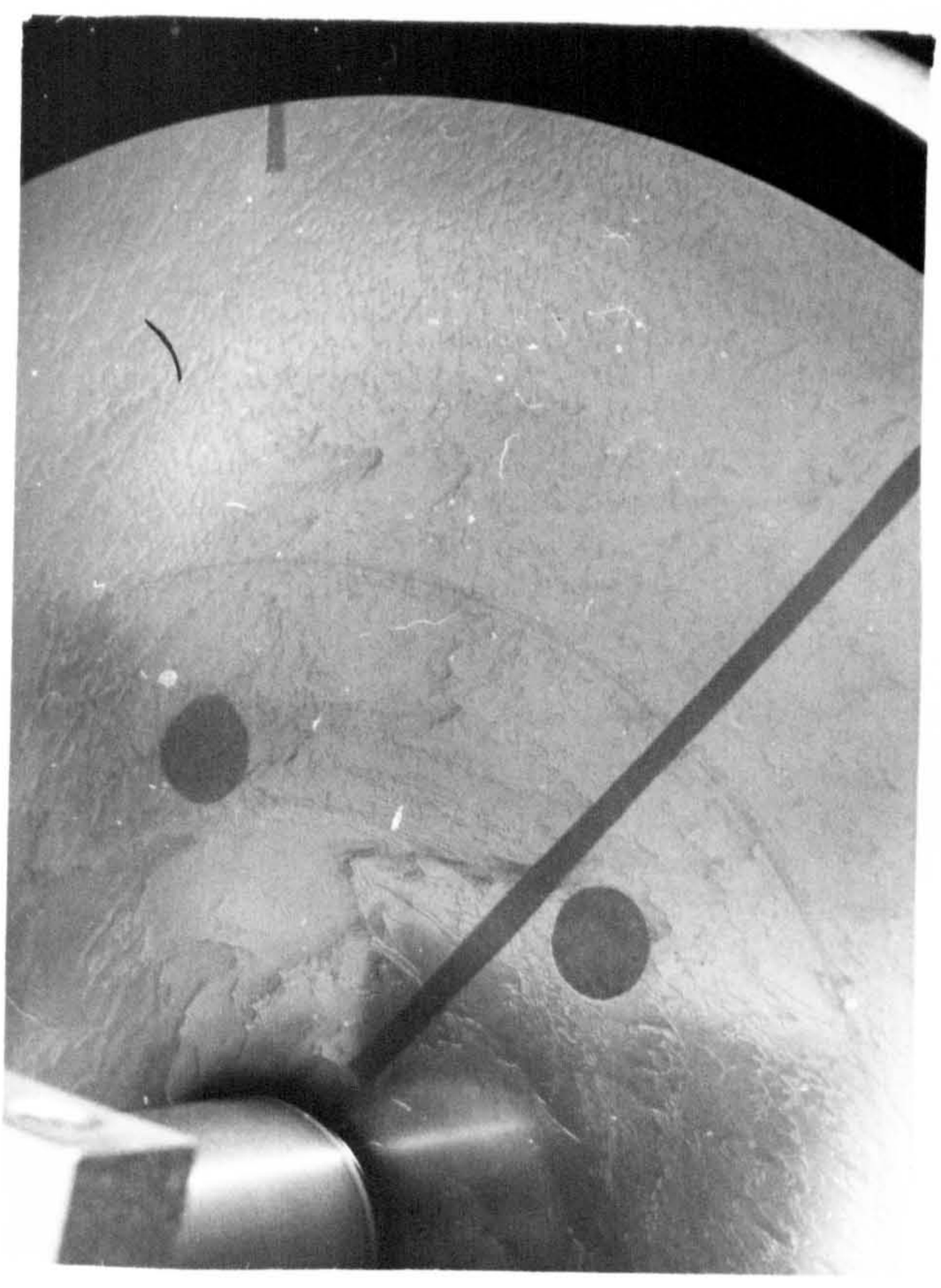

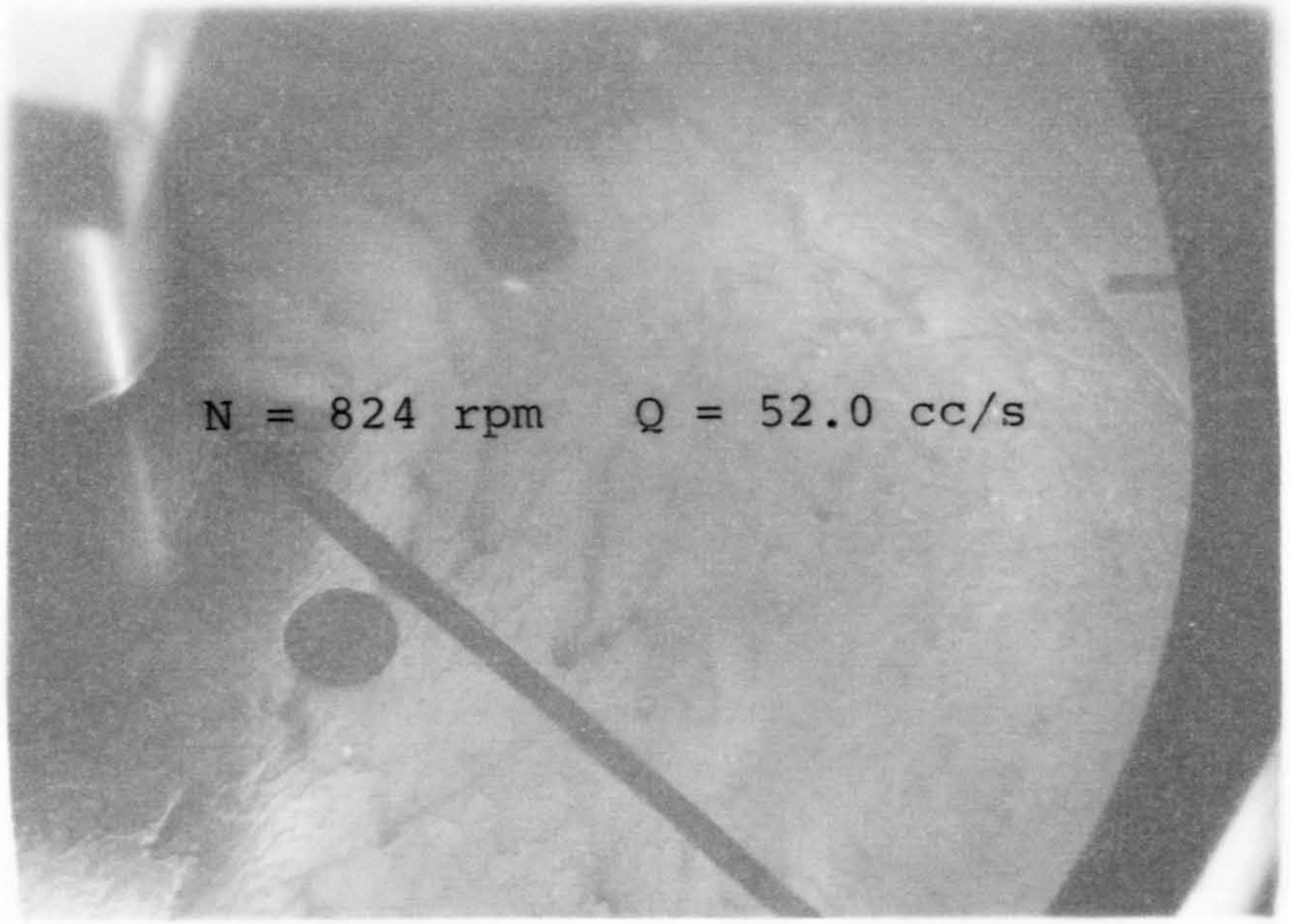

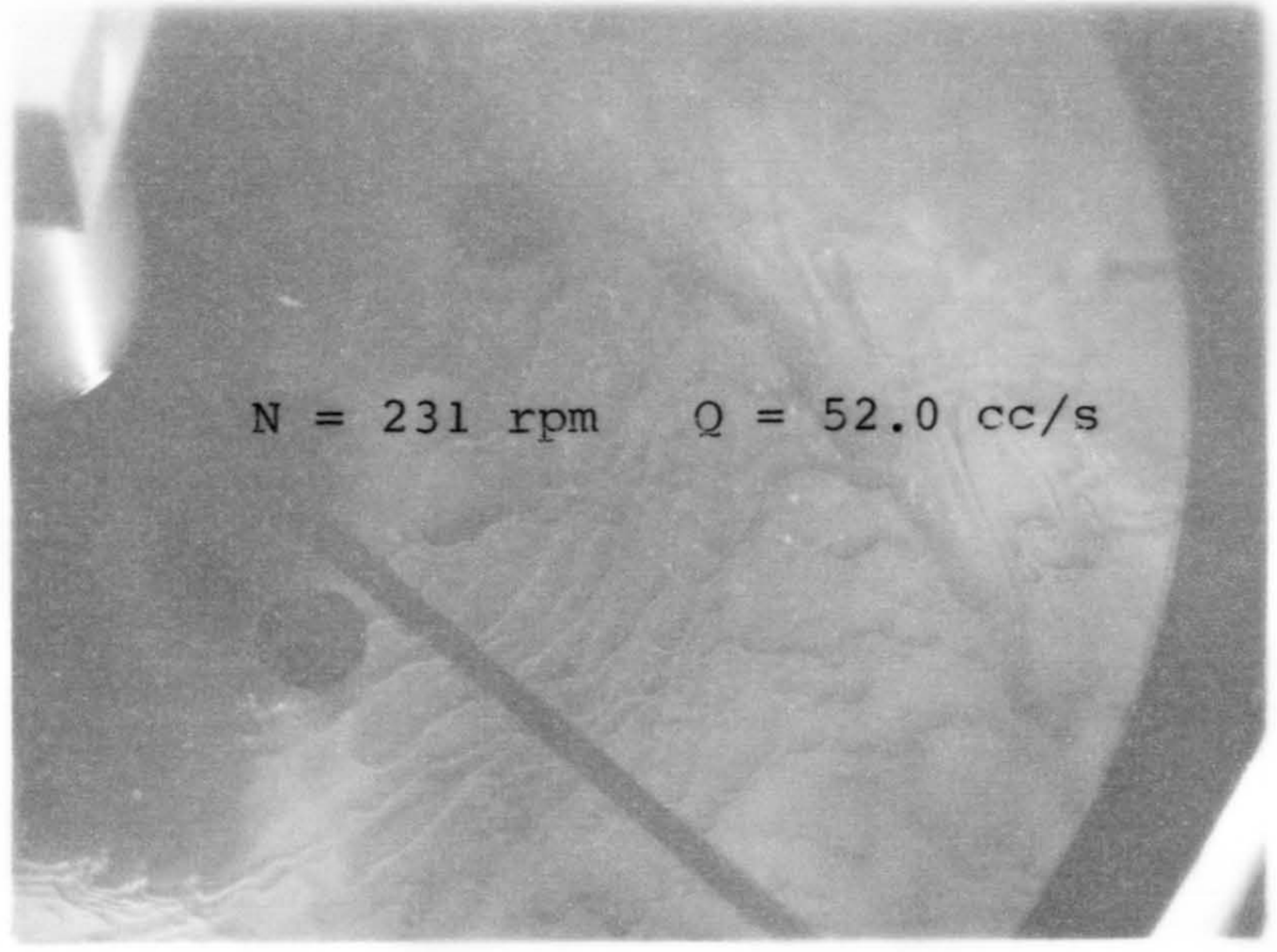

PHOTOGRAPH R3

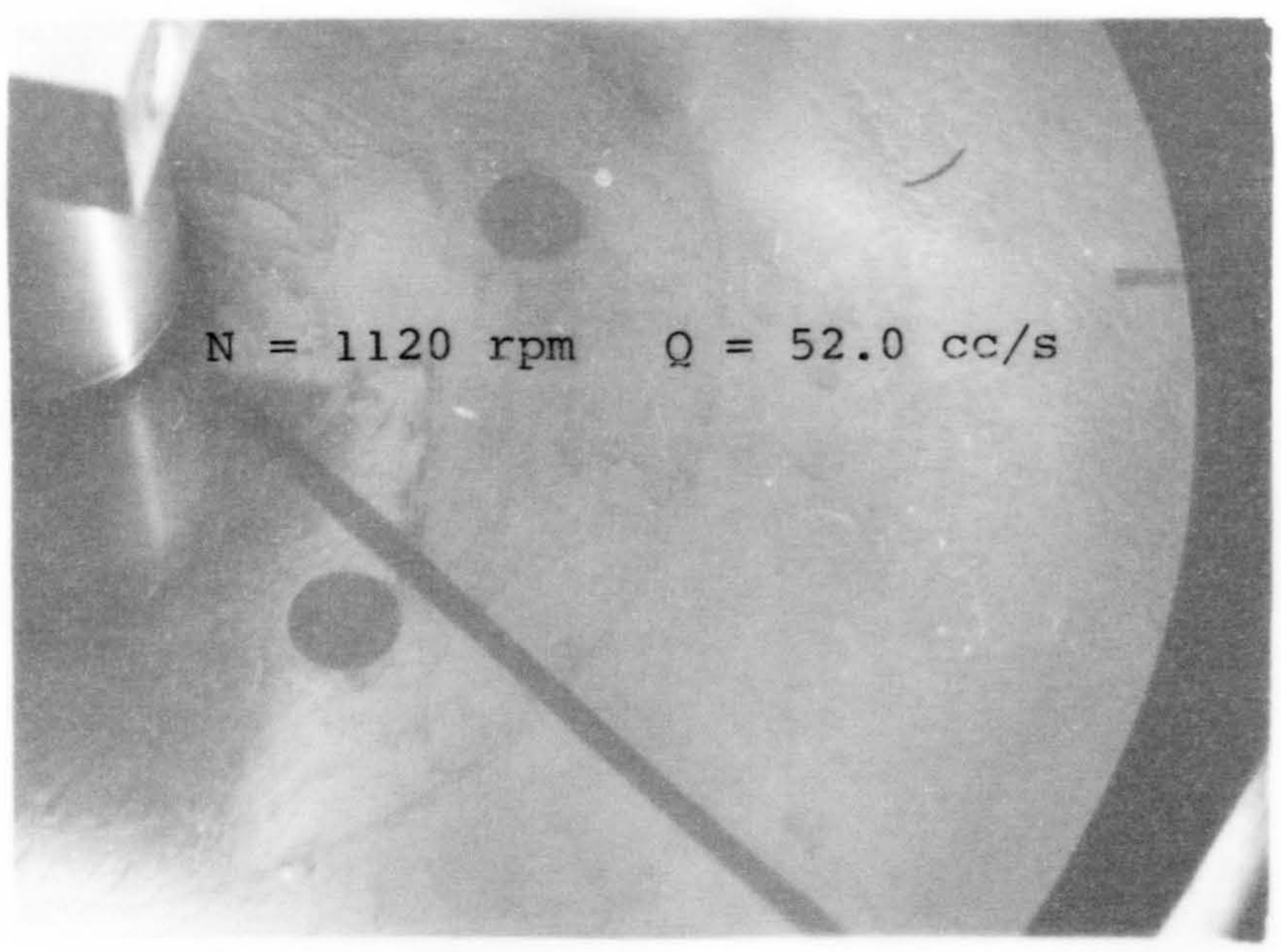

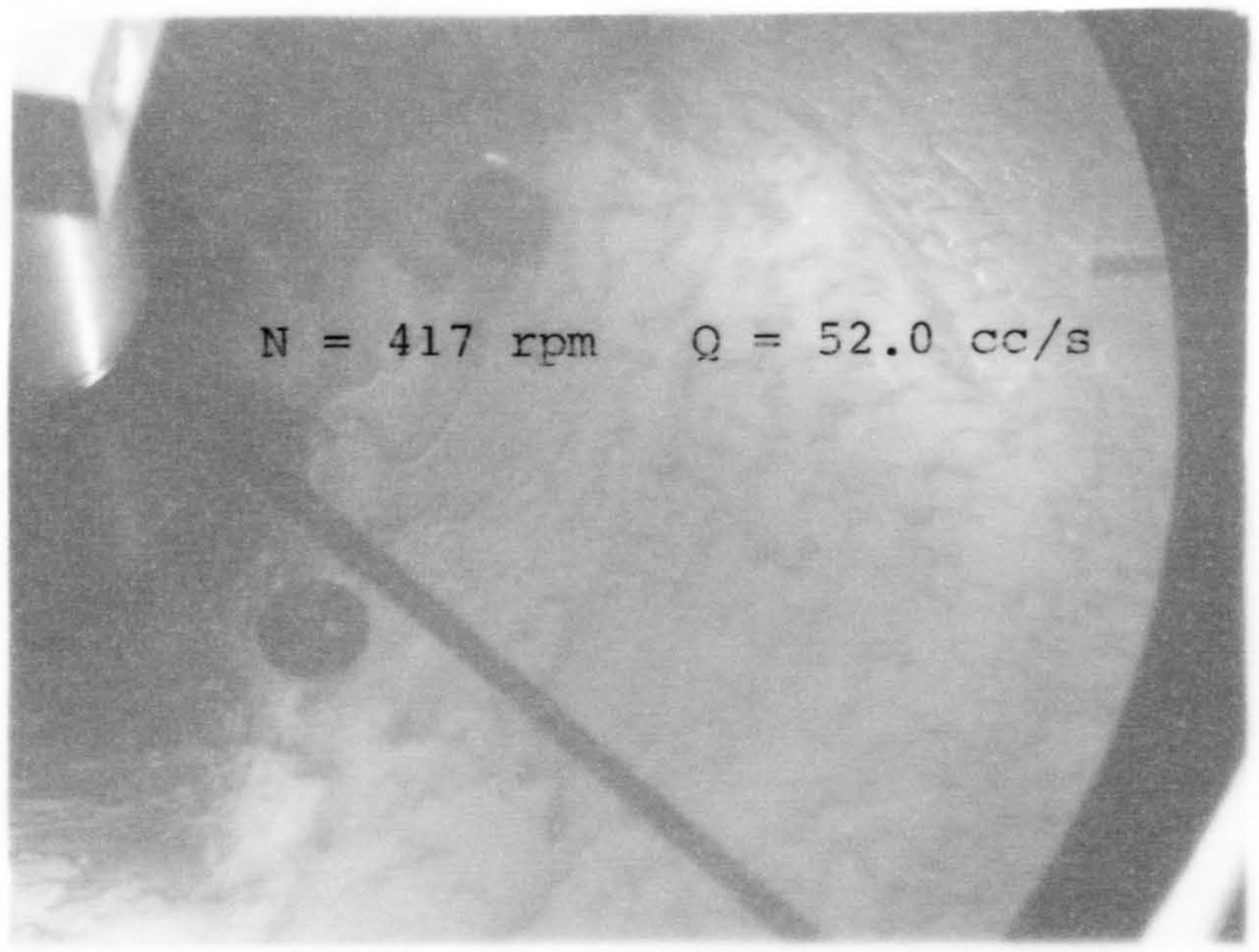

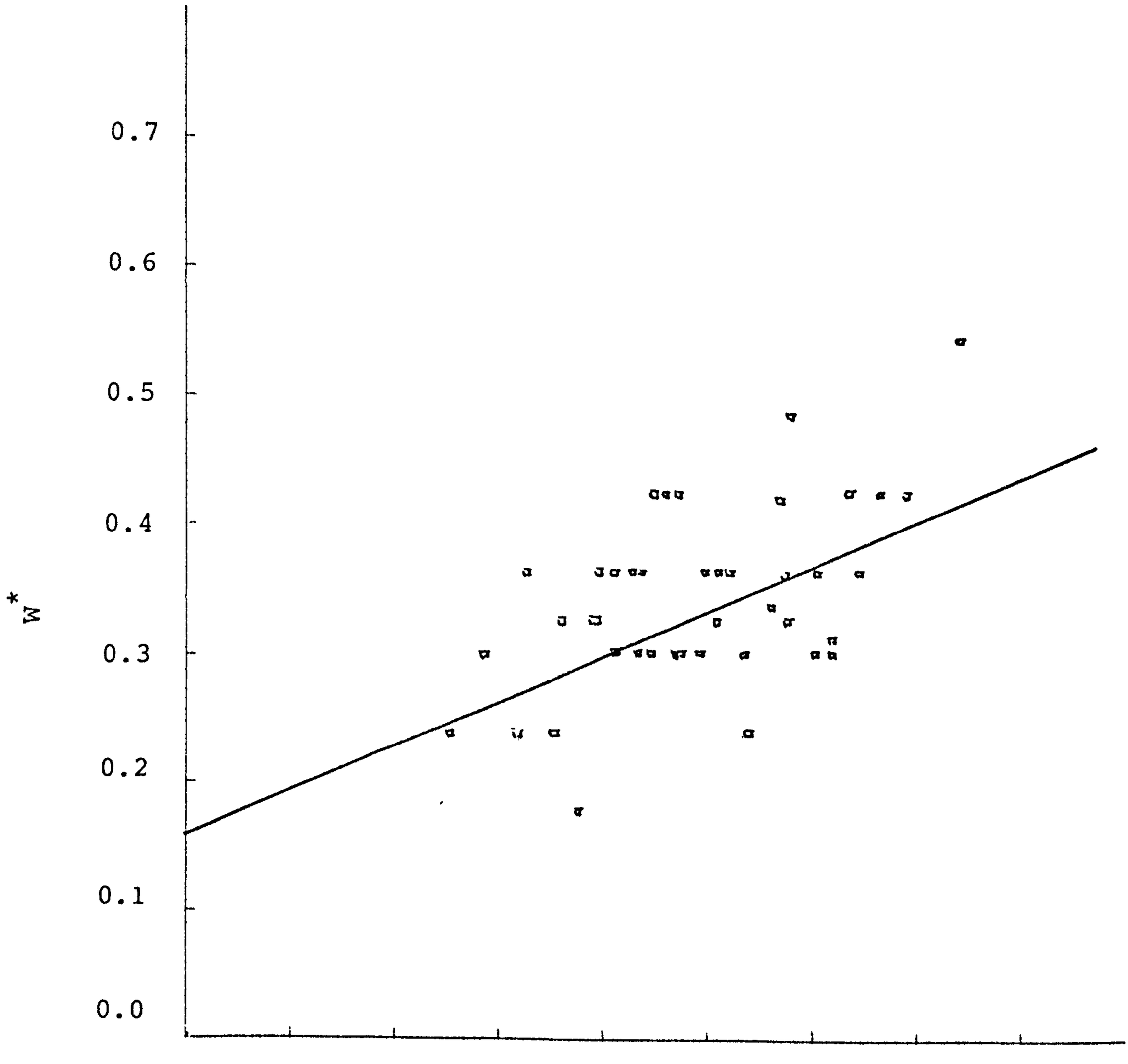

FIGURE 5.13 WAVELENGTH CORRELATION

predominant waves are slightly larger than those established by the theoretical analysis. In addition, the surface elasticity may help to explain the discrepancy between the theory and the experimental data. That is, surface elastic effects inhibit the formation of waves thus delaying their appearance. The occurrence of this phenomenon would also yield the experimental wavelengths larger than predicted theoretically.

5.5 SURFACE AREA

This part of work was carried out in order to find the variation of the interfacial area in the presence of waves. It was noted visually and photographically in previous sections that regular waves followed only a few centimetres of travel, and become remarkably random on the interface after a further short distance. Therefore, it is vitally important to measure the extent by which the surface is increased by the presence of waves and to provide an explanation for the existence of the ripples on the surface of the thin films. This measurement could also be used to proportion the relative magnitudes of the effects on the mass transfer rate of internal film mixing and interfacial area increase resulting from the ripples (see Part II of this thesis).

So far there is no work which has been done in the investigation of interfacial area increase due to waves on a rotating disc. A microdensometric technique was employed in this work to measure the surface wave profile and hence compared with the theoretical model (smooth film) as shown in Figures 5.14-5.25. A departmental micro-computer was used to determine the percent surface area increase due to the wave profile compared with the mean thickness across the disc was given in Table G19 a,b.

A theoretical expression using Portalski's equation (Appendix D) to predict the increase in surface area for falling film was also put forward for comparison. The fractional surface area increase given by Portalski's equation is, after simplification

$$\Delta s = (1.44\ \frac{Ao}{\lambda})^2$$

where $$Ao = 1.339\ (\frac{\nu Q}{r w^2})^{\frac{1}{3}} \qquad \lambda = 7.2\ (\frac{\nu \delta_o}{Q r_o w^2})^{\frac{1}{2}}$$

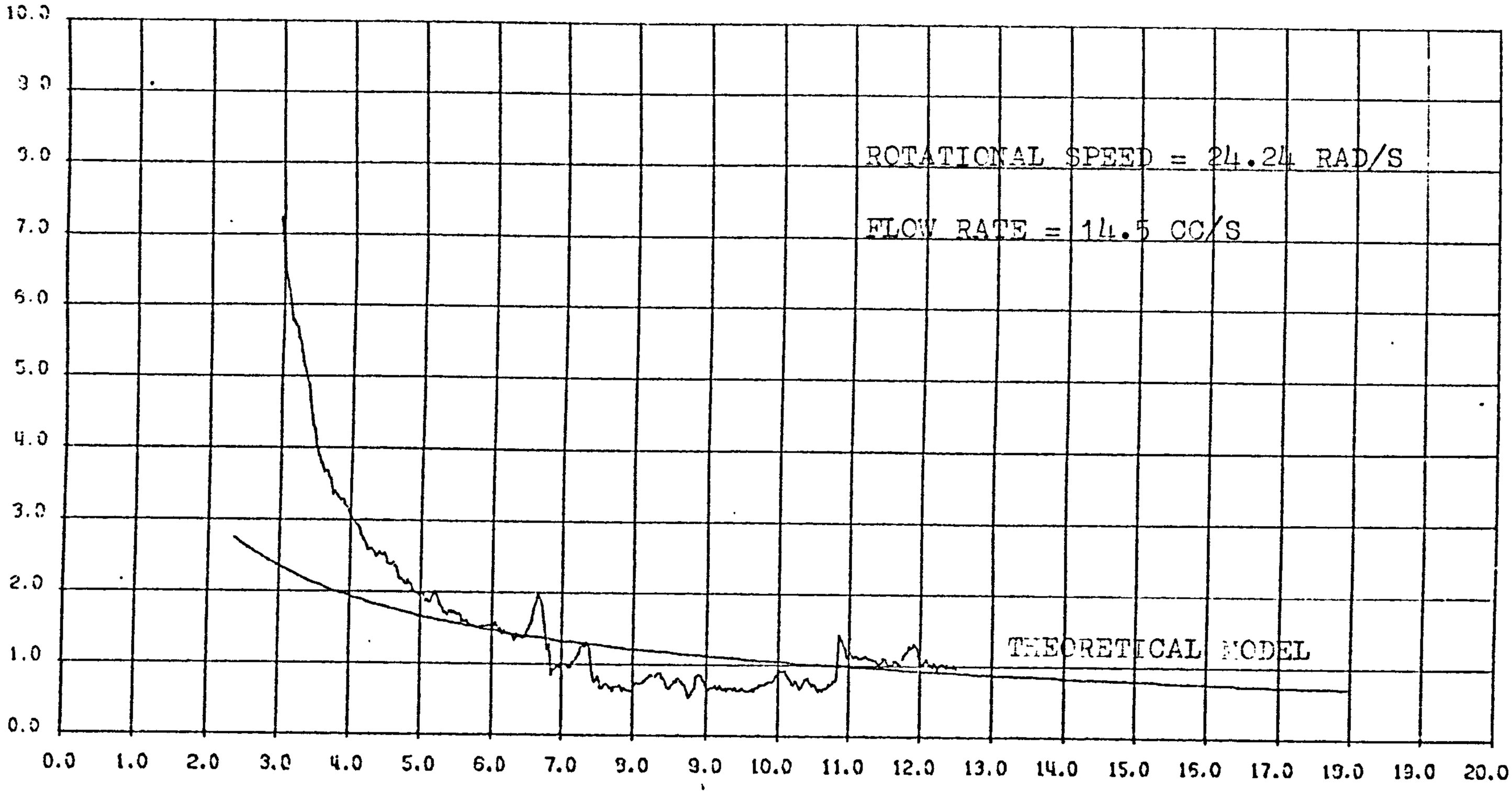

FIGURE 5.14 SURFACE WAVE PROFILE ACROSS THE DISC

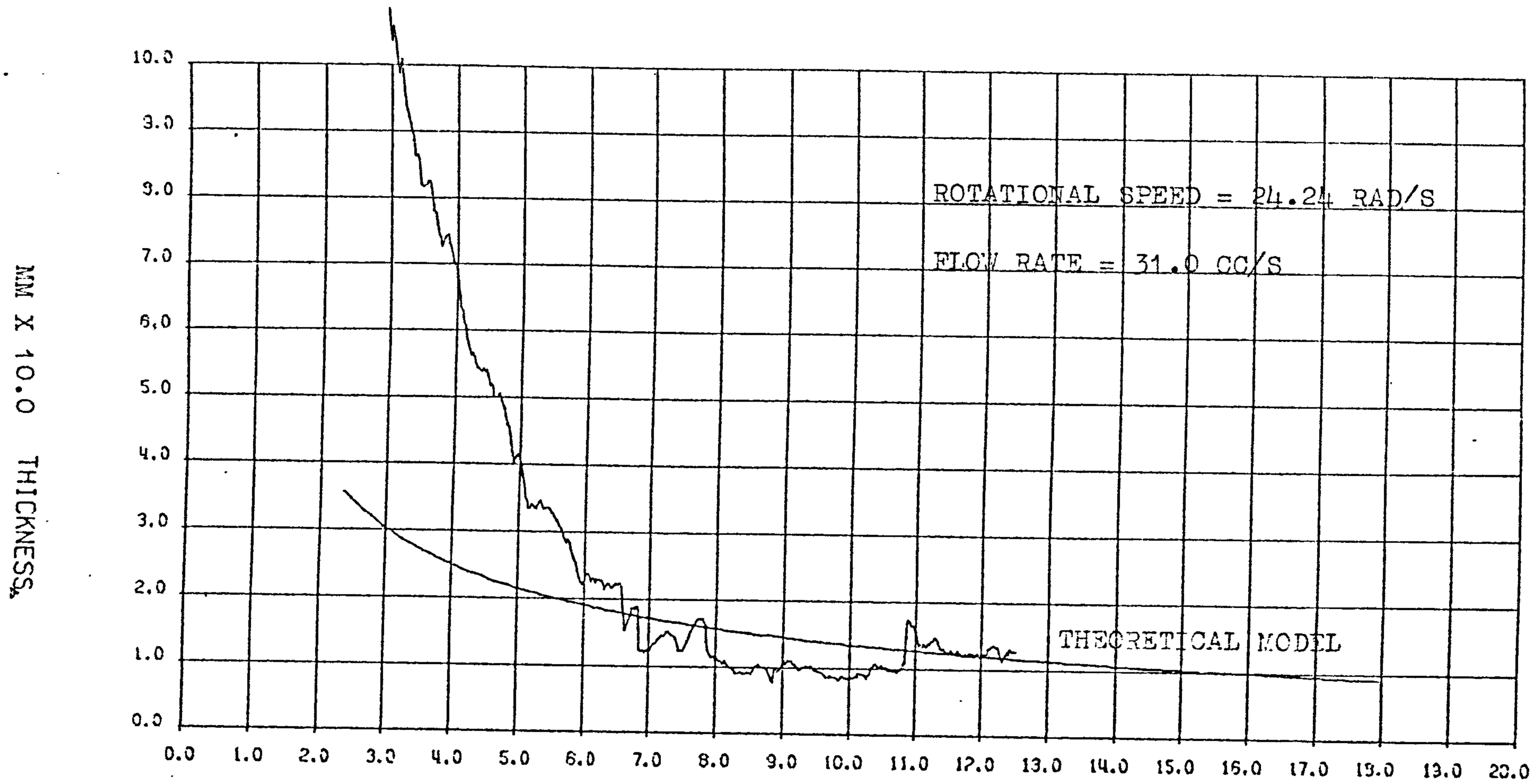

FIGURE 5.15 SURFACE WAVE PROFILE ACROSS THE DISC

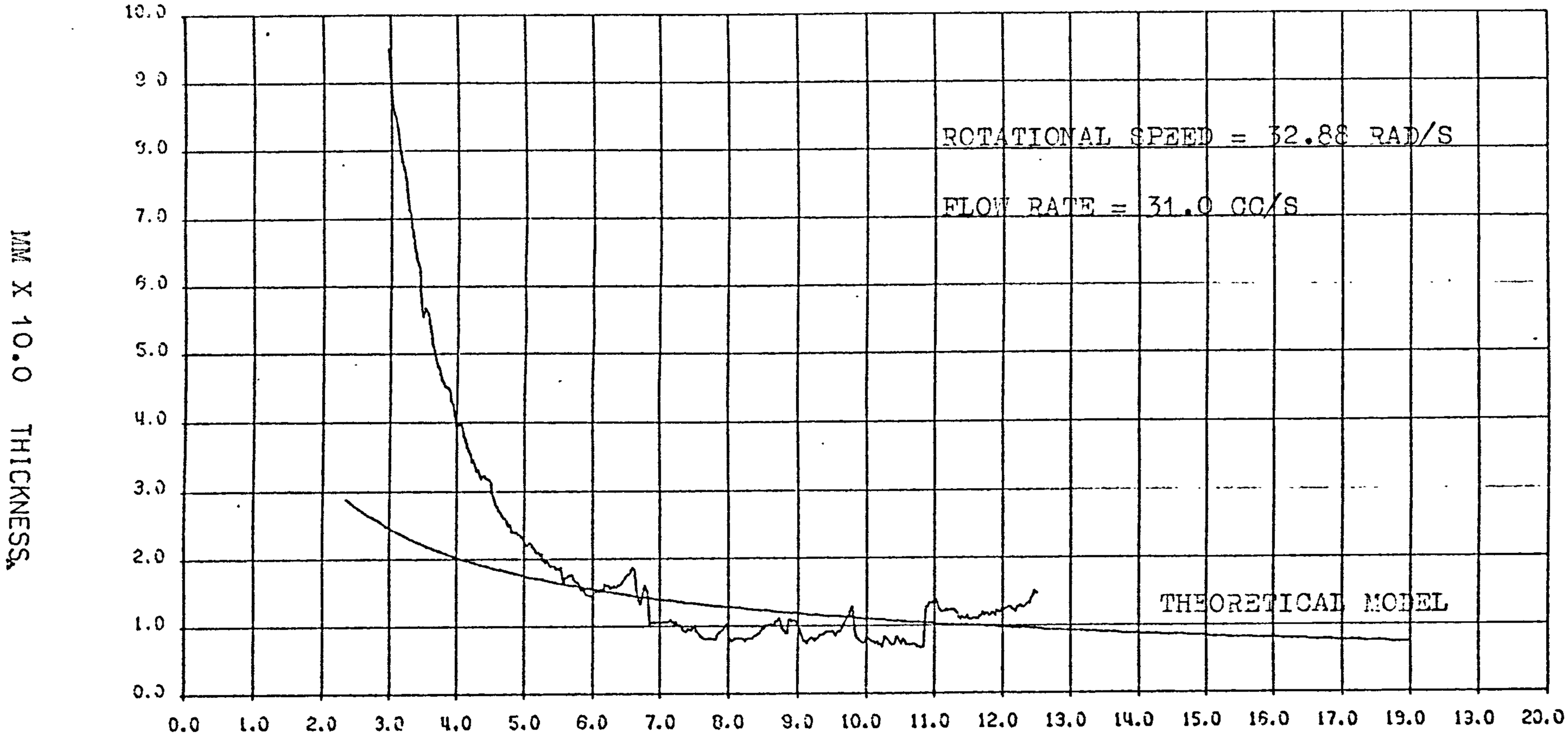

FIGURE 5.16 SURFACE WAVE PROFILE ACROSS THE DISC

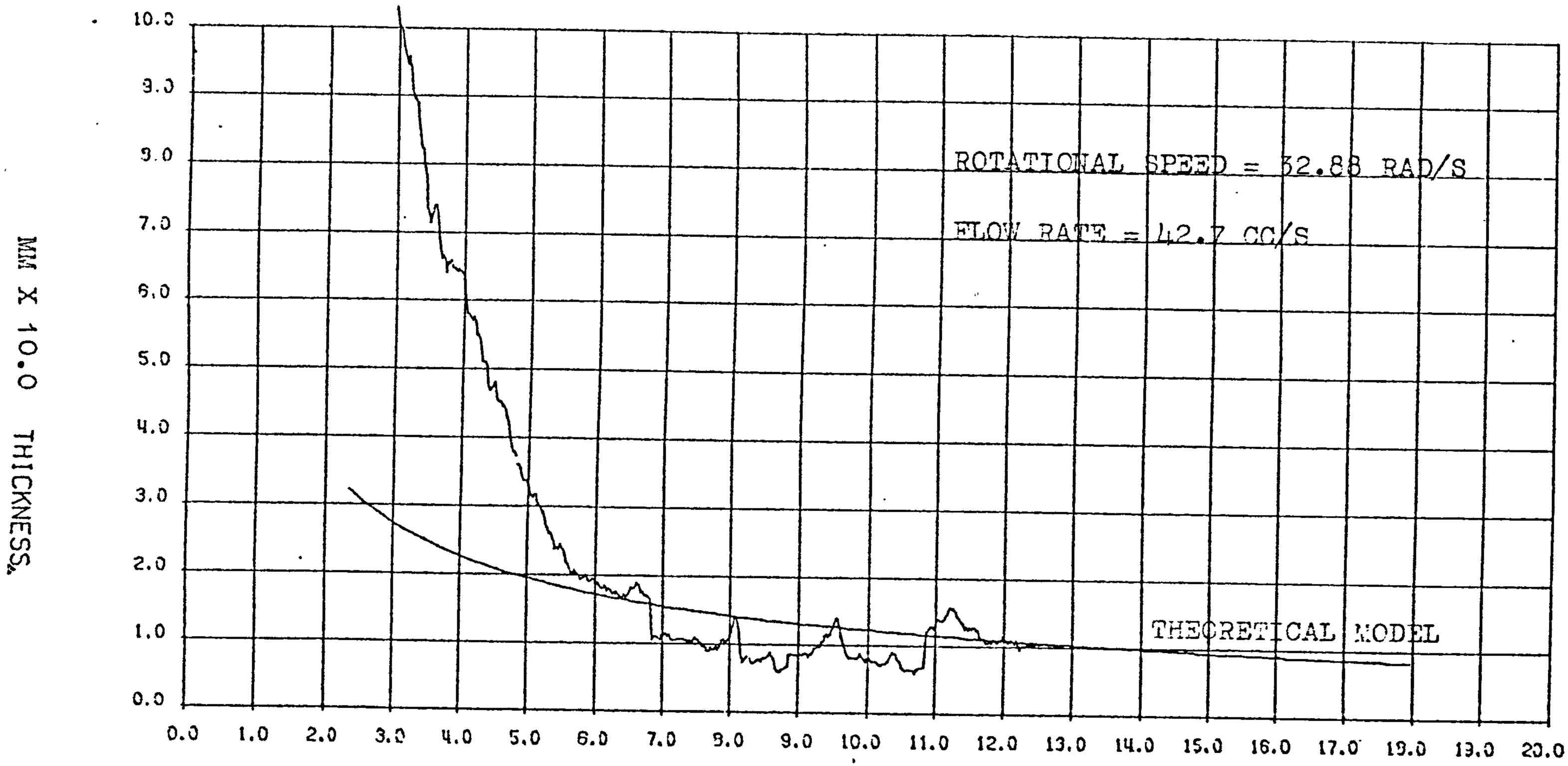

FIGURE 5.17 SURFACE WAVE PROFILE ACROSS THE DISC

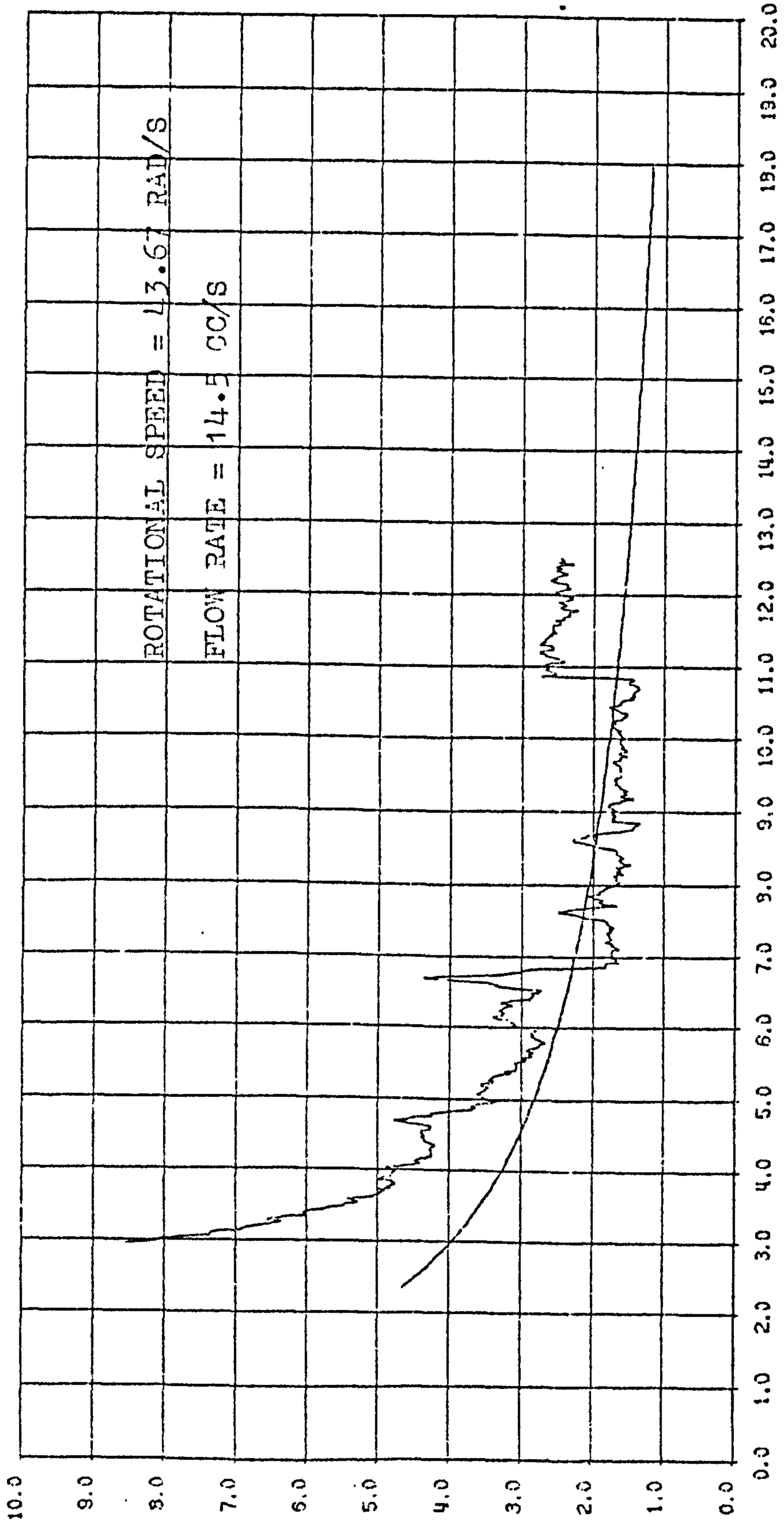

FIGURE 5.18 SURFACE WAVE PROFILE ACROSS THE DISC

MM X 25.0 THICKNESS

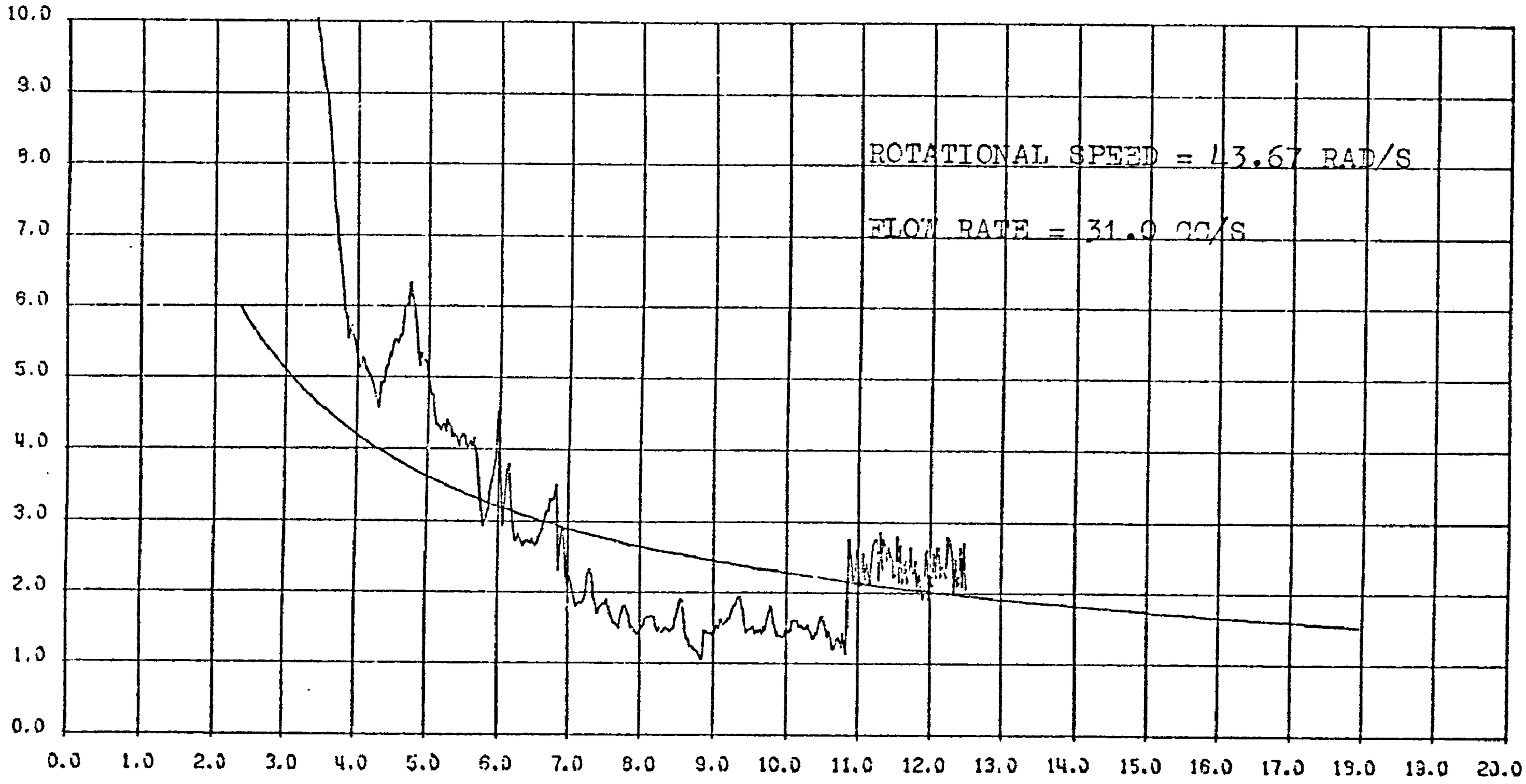

FIGURE 5.19 SURFACE WAVE PROFILE ACROSS THE DISC

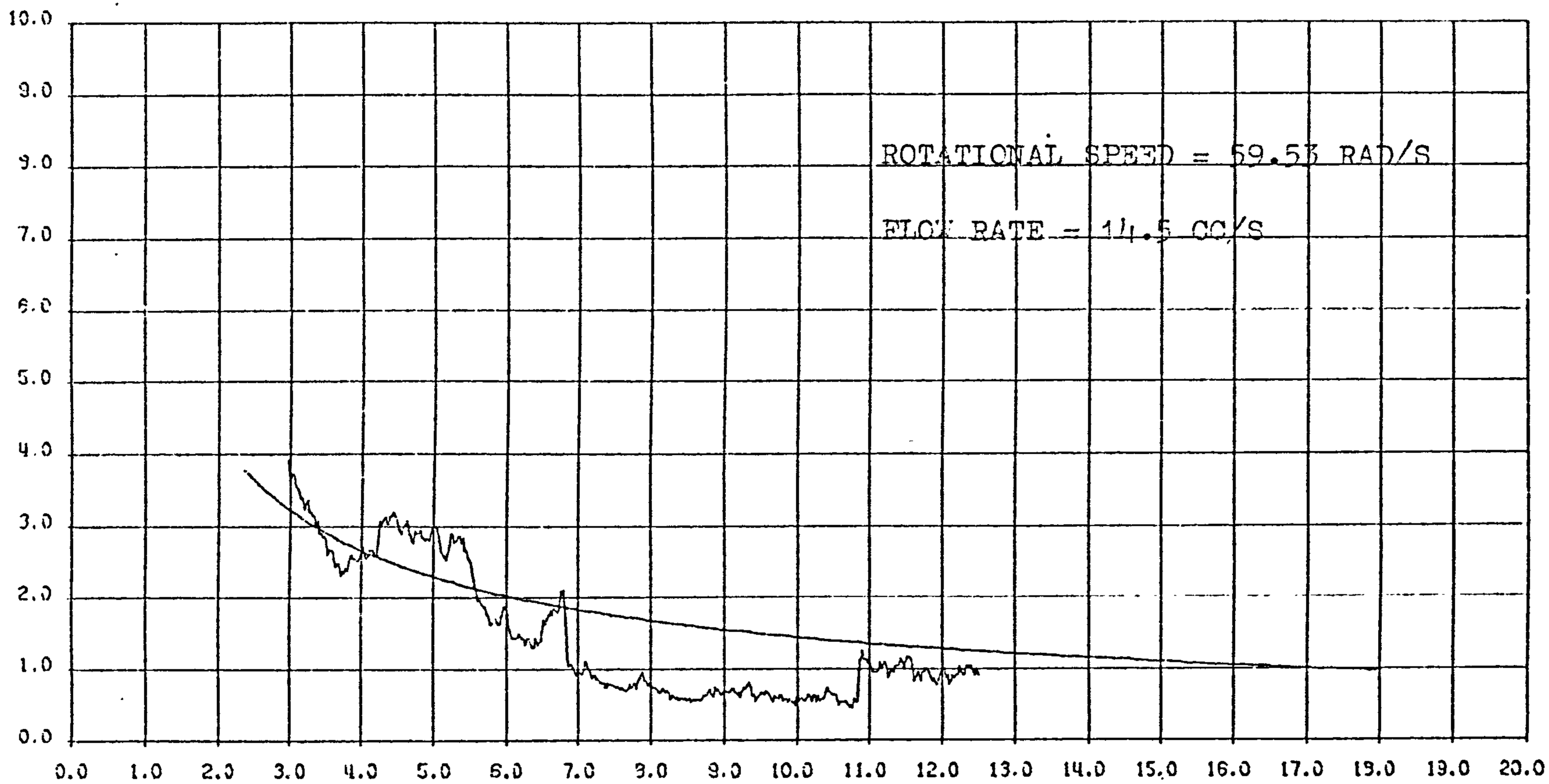

FIGURE 5.20 SURFACE WAVE PROFILE ACROSS THE DISC

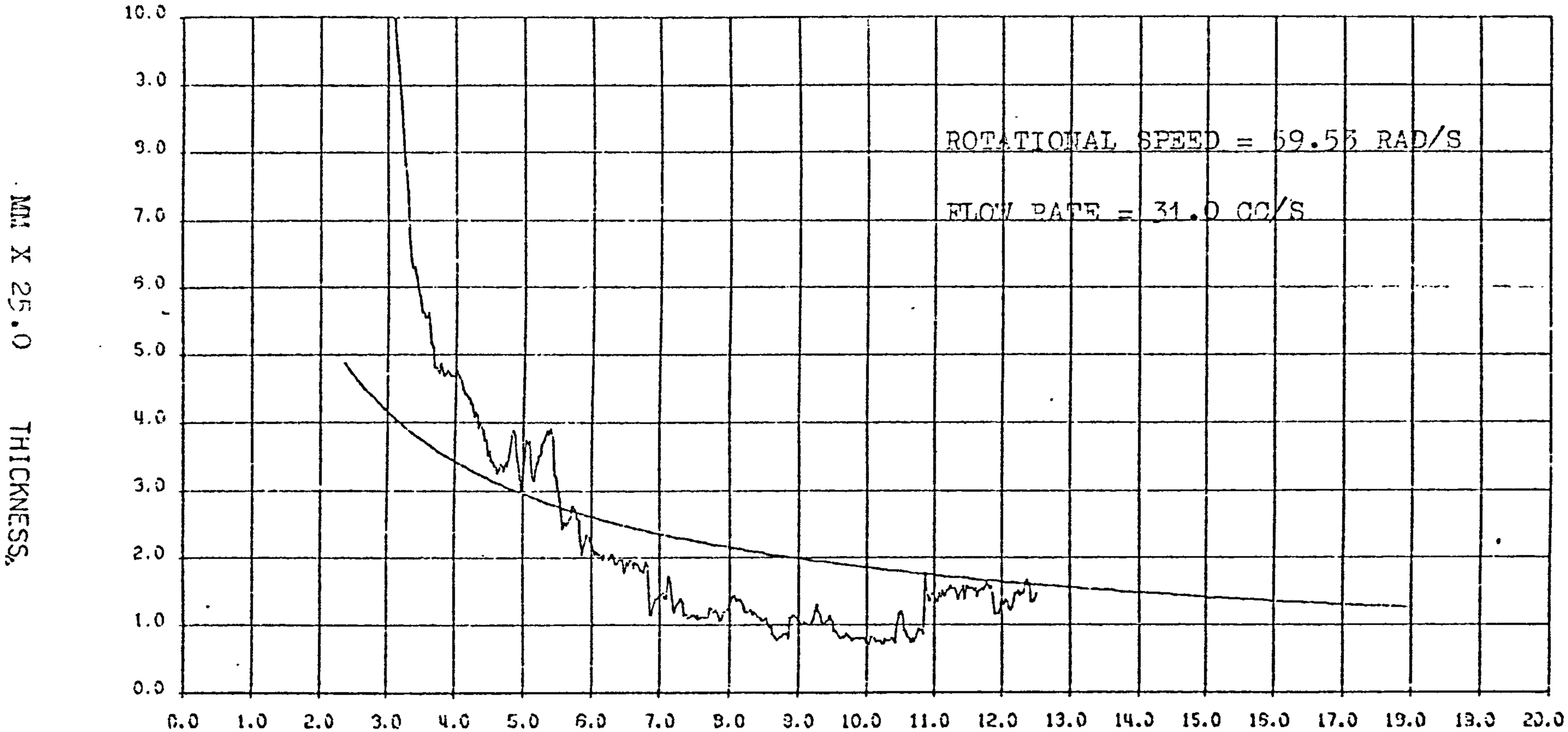

FIGURE 5.21 SURFACE WAVE PROFILE ACROSS THE DISC

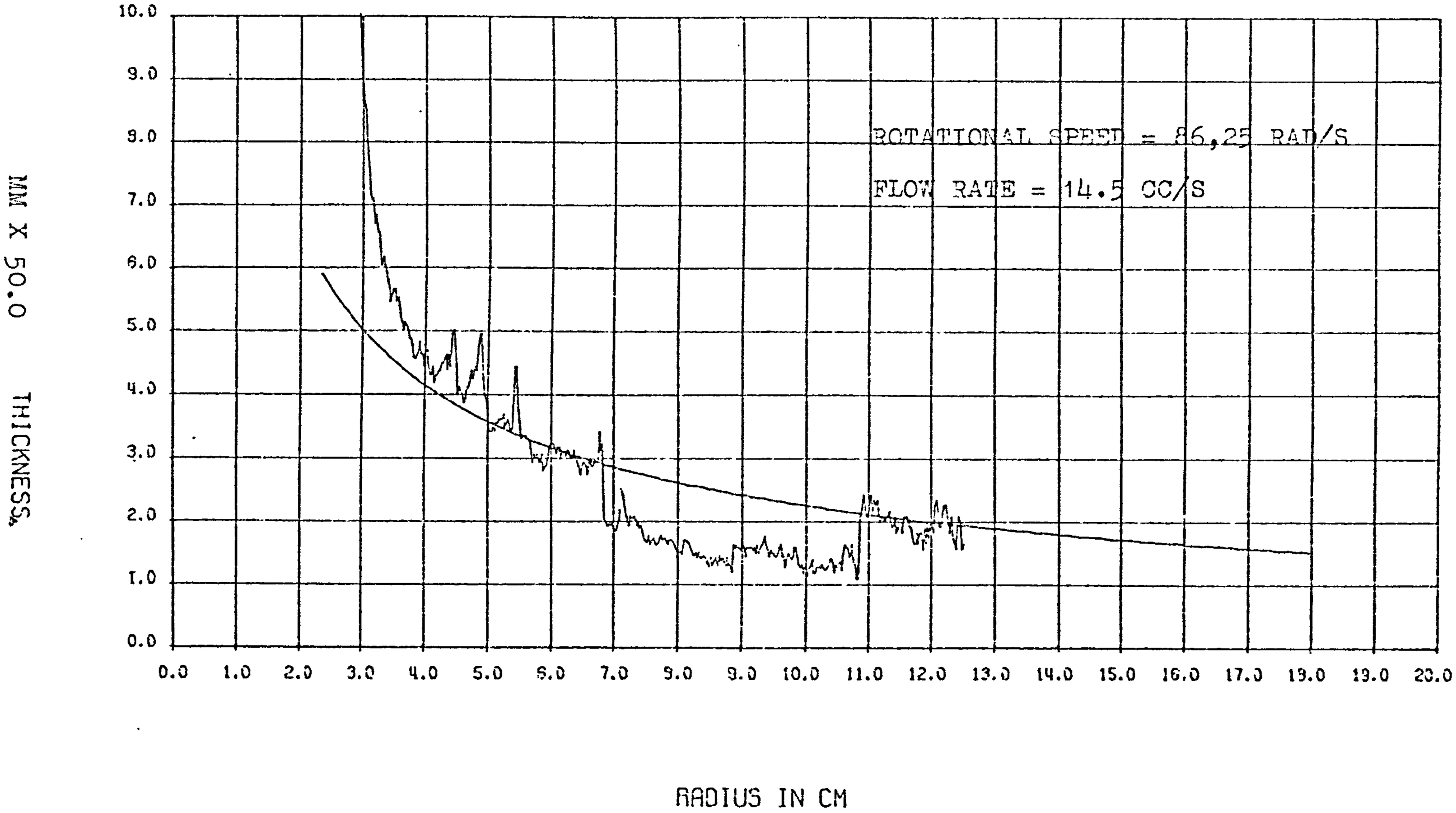

FIGURE 5.22 SURFACE WAVE PROFILE ACROSS THE DISC

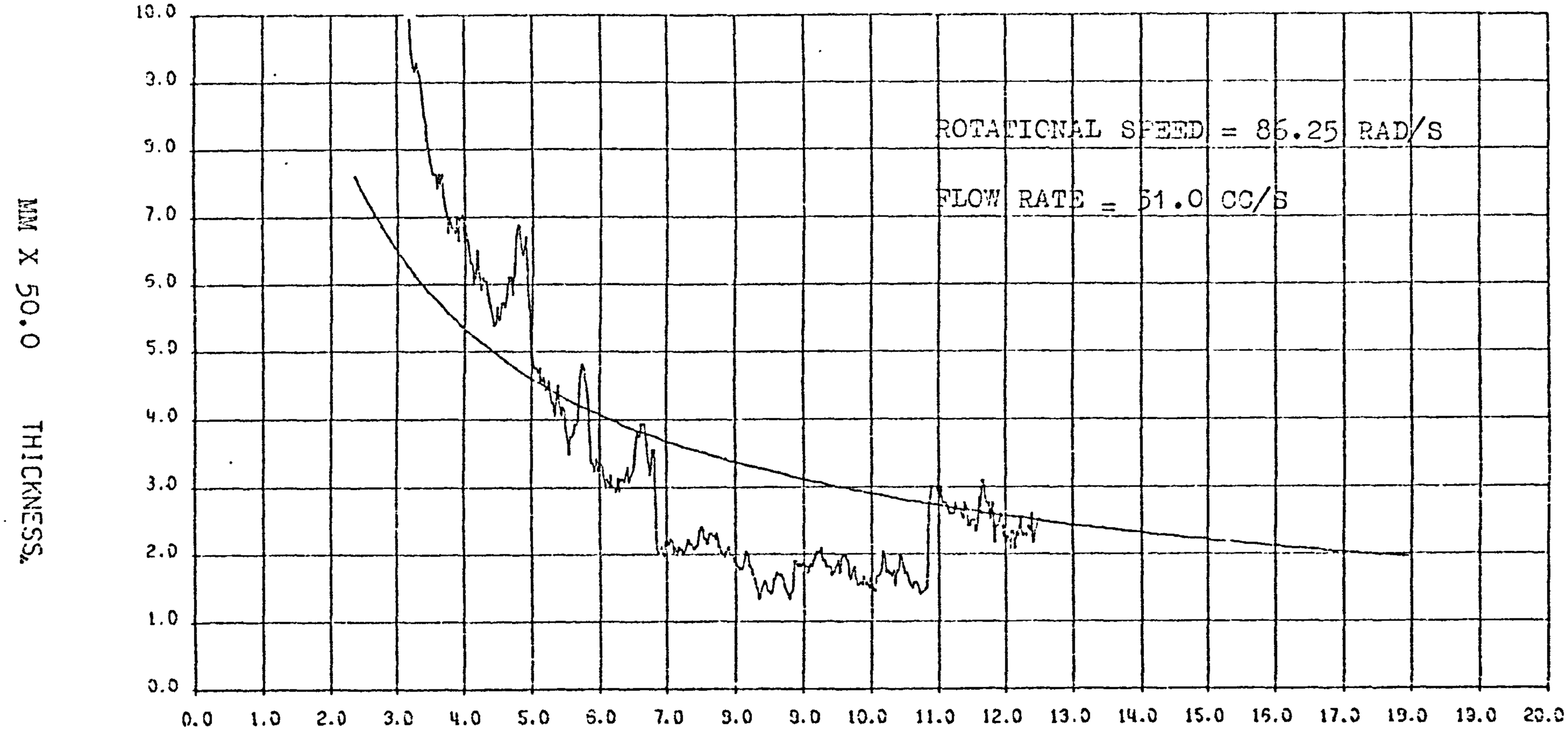

FIGURE 5.23 SURFACE WAVE PROFILE ACROSS THE DISC

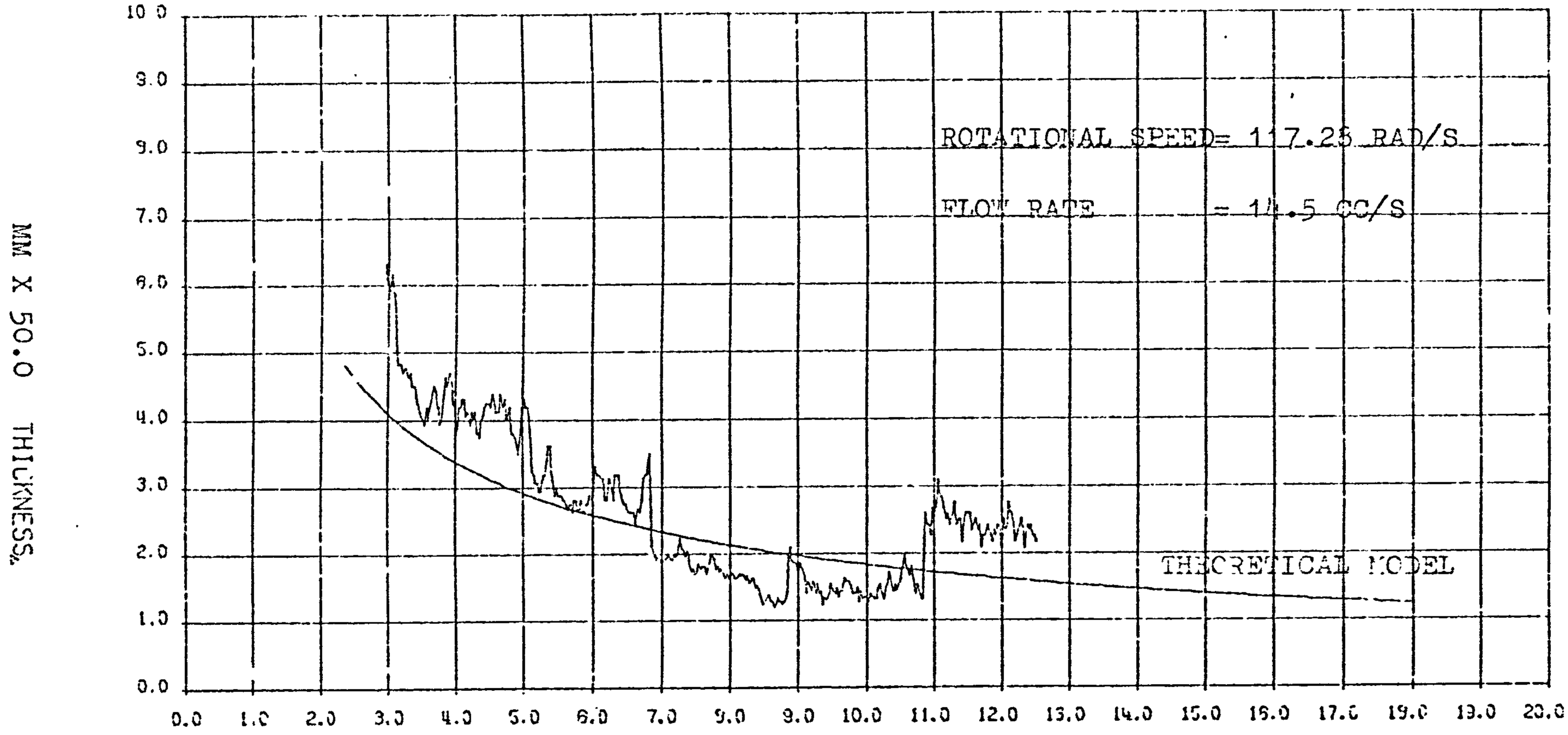

FIGURE 5.24 SURFACE WAVE PROFILE ACROSS THE DISC

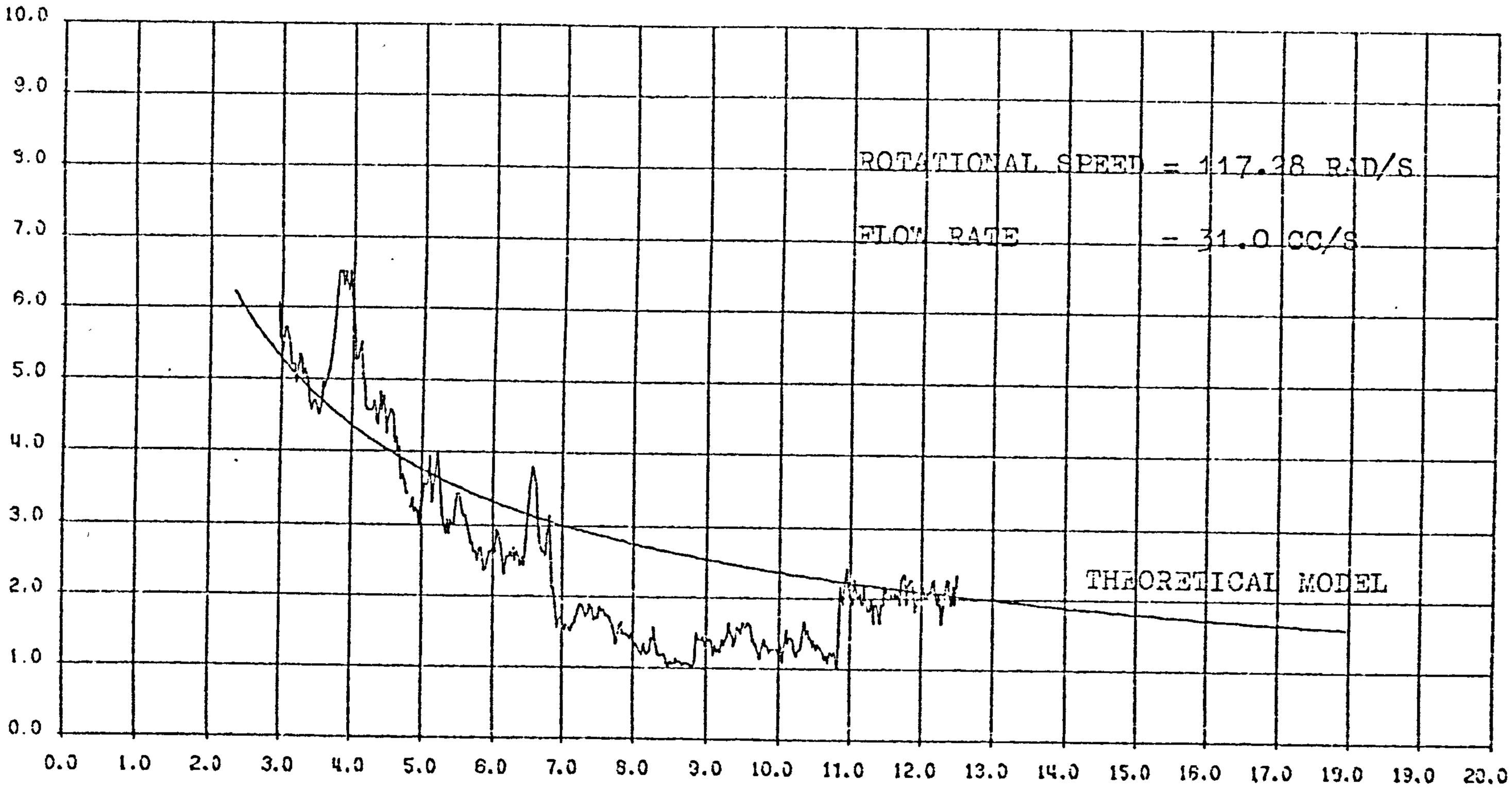

FIGURE 5.25 SURFACE WAVE PROFILE ACROSS THE DISC

TABLE 5.1 MINIMUM AND MAXIMUM WAVELENGTH AND AMPLITUDE

	MINIMUM (m)	MAXIMUM (m)
wavelength at inception (substituted Portalski's equation)	0.144E-02	0.145E-01
experimental wavelength	0.600E-02	0.935E-02
wave amplitude (substituted Portalski's equation)	0.240E-04	0.162E-03
experimental amplitude	0.247E-05	0.267E-04

The experimentally determined results show that the increase in interfacial area is small (see Data Table G19a,b) compared with that of Portalski's equation applied to rotating disc range from 0.1247% to 21.176% (within the system varaiable).

The minimum and maximum theoretical values of amplitude and wavelength within the system variables were given in Table 5.1 respectively. It was noted that the experimentally amplitude was several times smaller than the theoretical amplitude and that of wavelength was many times smaller than the theoretically determined values. From the above relationship it can be seen that the error in wavelength would give rise to a much larger error in Δs, and this is the most obvious reason for the discrepancy between the experimental and predicted results of Δs.

The practical correlations of wave amplitude and wavelength were used in the new correlation for the determination of Δs for water given as

$$\Delta s = 1.1958 \times 10^{-3} \, Re^{0.05} \, Ta^{-0.33 \times 10^{-2}}$$

6. CONCLUSIONS

1) The film thickness for values of $\frac{Re^2}{Ta} < 1$ is given as

$$\frac{\delta}{r}(Re) = 0.488 \left(\frac{Re^2}{Ta}\right)^{0.58} \quad \text{standard deviation=0.18}$$

compared with the simple centrifugal model

$$\frac{\delta}{r}(Re) = 0.782 \left(\frac{Re^2}{Ta}\right)^{0.67} \quad \text{(Equation 27)}$$

2) Other phenomena of wave characteristics are given as

A) $R_I^* = 576.1\ Re_o^{0.08}\ Ta_o^{-0.66}$ standard deviation= 0.11

where R_I^* is the dimensionless length of wave inception

B) wavelength at wave inception

$$W^* = 0.312\ Re_o^{0.18}\ Ta_o^{-0.12} \quad \text{standard deviation=0.08}$$

C) wave amplitude

$$A^* = 0.604\ Re^{0.06}\ Ta^{-0.59} \quad \text{standard deviation=0.15}$$

D) surface area increase was found to be negligle to have any significant effect on mass transfer.

$$\Delta s = 1.20 \times 10^{-3}\ Re^{0.05}\ Ta^{-0.33E-02}$$

standard deviation=0.03

7. RECOMMENDATIONS FOR FUTURE WORK

Hydrodynamics Studies

(1) The initial experimental work on wavy flow should be extended and augmented by analysis. The effects of surfactants (different surface tension and viscosity, which have important implication in the commercial processing of industrial liquids should be investigated.)

(2) Techniques for the measurement of surface velocity of the liquid film should be developed.

(3) The effect of roughened surfaces on the characteristics of liquid films formed on a rotating disc should be investigated.

(4) Further work on establishing the validity bounds of various models should be undertaken. Several brief reviews show that interfacial drag, for example, is usually negligible. However, the presence of other surfaces in a multi-disc unit may lead to appreciable drag. Therefore, effect of a shroud, with and without induced air flow, should be investigated.

LITERATURE SURVEY

ON

MASS TRANSFER

8. INTRODUCTION

It has been realised for some time that the ripples formed on a falling film cause some forms of mixing which must be responsible for enhanced rates of mass transfer. This led several investigators (139,140,141) to use the Kapitza theory of wave motion to indicate the increase in the transfer rates. However; whilst the theory does predict an increase relative to the flat film behaviour, observed increases are still two to three fold larger than predicted values. This is not entirely surprising since the observed values are based on the overall measurements which have been made when the flow pattern is not the simple wave-motion as assumed in the above theory. Stainthorp and Allen (18) have shown that the flow-pattern predicted by Kapitza is only observed under very restricted conditions of flow and in the region where waves are just beginning to develop. Further, Stainthorp and Wild (35) observed under typical experimental conditions of film flow on a vertical tube, the wave motion changes very rapidly from near periodic at the commencement to large solitary waves with which are associated a number of ripples. No analysis of this flow pattern has yet appeared but it may well involve mixing within the waves which caused considerable increase in mass transfer rates.

So far there is no work which has been done on mass transfer into rippling films formed on a rotating disc. It is clearly necessary to obtain some information about local transfer coefficients under rippling conditions but this implies the measurement of local concentrations in a stream of varying thickness and requires the measurements to be made in a film which is less than 100 micrometres thick without disturbing the flow. Different measuring techniques have been investigated; however, in the present investigation samples were taken with the scoop technique (Section 10.2.3) where little interference occurred on the liquid film (see future work for measurements without disturbing the flow).

Experimental data were collected at different radii with vary -ing flow rates and rotational speeds and finally correlated into an empirical correlation.

Owing to the lack of knowledge as to what is taking place in the liquid phase near the phase boundary, this work was undertaken only to study the physical system, without reaction, since an understanding of the mechanism of liquid-phase mass transfer is essential for the development and application of any fundamental theory for the combined diffusion case.

Basic mass transfer theories are collected in Section 9.1 of the literature survey, in order to understand the early proposed theories. In Section 9.2 the effect of surface tension and pressure on the mass transfer coefficient is dealt with. Sections 9.3 and 9.4 deal with the associated field of mass transfer into thin falling films with laminar, wavy, and turbulent flow and the Marangoni effect. Section 9.5 and 9.6 deal with mass transfer in infinte medium and with mass transfer in non-ripple film formed on rotating disc. Section 9.7 deals with different methods for the measurements of dissolved oxygen in water. Section 9.8 deals with the effects of surface active agents on the diffusivity.

9. LITERATURE SURVEY

9.1 BASIC MASS TRANSFER THEORY

In the study of interfacial mass transfer, three basic concepts form the basis of physical absorption theory. They are the film theory (101,102), the penetration theory (103) and surface renewal theory (104). The two film-model, propounded by Whitman, suggests that the resistance to transfer in each phase could be regarded as lying in a thin film close to the interface. The transfer across these films is regarded as a steady state process of molecular diffusion. The turbulence in the bulk fluid is considered to die out at the interface of the films. Higbie, in his penetration model, assumes that the eddies in the fluid bring an element of fluid to the interface where it is exposed to the second phase for a definite interval of time, after which the surface element is mixed with the bulk again. Thus, fluid whose initial composition corresponds with that of the bulk fluid remote from the interface is suddenly exposed to the second phase. It is assumed that equilibrium is immediately attained by the surface layers and that a process of unsteady state molecular diffusion then occurs and that the element is remixed after a fixed interval of time. Danwokwerts suggested that each element of surface would not be exposed for the same time, but that a random distribution of ages would exist. He assumed that the probability of any element of surface becoming destroyed and mixed with the bulk of the liquid was independent of the age of the element.

Toor and Marchello (105) proposed a film-renewal model which incorporates some of the principles of both the two-film theory and the penetration theory. This model suggests that the total resistance to transfer lies within a laminar film at the interface, as in the two-film theory, but the mass transfer is regarded as an unsteady state process. It is assumed that fresh surface is formed at intervals from fluid which is

brought from the bulk of the fluid to the interface by the action of the eddy currents. Mass transfer then takes place in the penetration theory, with the exception that the resistance is confined to the finite film, and material which traverses the film is immediately completely mixed with the bulk of the fluid. For short times of exposure, when none of the diffusing material has reached the far side of the layer, the process is identical to that postulated in the penetration theory. For prolonged periods of exposure when a steady concentration gradient has developed, conditions are similar to those considered in the two-film theory.

In the absorption of gas into a liquid, the mixing that takes place may be either molecular diffusion, in which case for unsteady state absorption, Fick's second law applies

$$\frac{\partial C}{\partial t} = D\nabla^2 C \qquad (93)$$

or by eddy diffusion in turbulent flow which can be approached by either phenomenological reasoning which defines a Prandtl length of mixing, or by a statistical theory based on the random behaviour of eddies in a turbulent field (106).

The driving force causing diffusion is the concentration gradient through the gas film, interface, and liquid film, and for a gradient ΔC, the basic mass transfer equation can be written as (107)

$$\frac{\partial m}{\partial t} = KA\Delta C \qquad (94)$$

The overall resistance to mass transfer from the gas to the liquid phase can be written as the sum

$$\frac{1}{K_L} = \frac{1}{Hk_g} + \frac{1}{k_L}$$

Where K_L is the overall mass transfer coefficient; $\frac{1}{K_L}$ is the overall resistance; $\frac{1}{k_g}$ is the gas phase resistance; $\frac{1}{k_L}$ is the

liquid phase resistance and H is the Henry Law constant. For low solubility of gases in water $\frac{1}{Hk_g}$ is negligible in comparison to $\frac{1}{k_L}$, and K_L is nearly equal to the liquid side mass transfer coefficient, k_L. Therefore, the overall rate of mass transfer from the gas phase to the liquid phase can be written as:

$$\frac{\partial m}{\partial t} = V \frac{\partial C}{\partial t} = k_L A \left(C^* - C_b \right) V$$

or

$$\frac{\partial C}{\partial t} = k_L a \left(C^* - C_b \right) = - D \left(\frac{\partial C}{\partial x} \right)_{x=0} a \quad (95)$$

where a is the interfacial area per unit volume, D is the diffusivity of the gas in the liquid, $(\frac{\partial C}{\partial x})_{x=o}$ is the concentration gradient of the solute, and C* and C_b are the saturation and bulk concentrations of solute, in mass per volume units.

The solubility of the solute in the liquid, C* , depends upon temperature, the partial pressure of the gas above the liquid, and the dissolved salt concentration in the liquid (108). Both k_L and a depend on the fluid dynamics obtained in the gas-liquid contacting apparatus and upon the physical properties of the solvent and solute.

Whitman's film theory (101,102) assumes a stationary film of thickness δ exists at the mass transfer interface. A material balance of gas in a differential element from x = o to x = δ yields Fick's second law, assuming uni-directional mass transfer at steady state

$$D \frac{\partial^2 C}{\partial x^2} = 0 \quad (96)$$

boundary conditions

$$\begin{aligned} x &= o & C &= C^* \\ x &= \delta & C &= C_b \end{aligned} \quad (97)$$

Integration yields

since $$-D\left(\frac{\partial C}{\partial x}\right)_{x=o} = k_L\,(C^*-C_b)$$

$$= -D\,\frac{(C^*-C_b)}{-\delta}$$

$$= \frac{D}{\delta}\,(C^*-C_b) \qquad (98)$$

then Whitman's film theory defines the mass transfer coefficient as

$$k_L = \frac{D}{\delta}$$

Similarly, starting with Fick's second law, Higbie's penetration theory (103) under restrictive boundary condition yields

$$\frac{C - C_b}{C^* - C} = \operatorname{erfc}\left(\frac{x}{2\sqrt{Dt^*}}\right)$$

In this case, steady-state condition is not attained since the surface is constantly being renewed by other liquid elements. t* is the residence time of a liquid element which is assumed to be constant. This leads to the mass transfer coefficient of:

$$k_L = 2\sqrt{\frac{D}{\pi t^*}} \qquad (99)$$

Danckwerts's surface renewal model (104), assumes that liquid element is not exposed for a constant time. This assumption leads to a value of

$$k_L = \sqrt{Ds} \qquad (100)$$

where s is the rate of surface renewal and 1/s is the average life of surface elements.

Toor and Marchello (105), used the mass transfer equation

$$\frac{\partial C}{\partial t} = D\frac{\partial^2 C}{\partial x^2} \qquad (101)$$

with boundary conditions

$$\begin{aligned} t &= o \quad & C &= C_L \\ x &= o \quad & C &= C_i \\ x &= L \quad & C &= C_L \end{aligned} \tag{102}$$

where C_i and C_L are assumed independent of time, t, and L is a distance below the interface where the concentration remains constant at C_L, the bulk concentration.

At short times, that is t is small, the solution is given as:

$$N = - D \left(\frac{\partial C}{\partial x} \right)_{x=0}$$

$$= \left(C_i - C_L \right) \sqrt{\left(\frac{D}{\pi t}\right)} \left(1 + 2 \sum_{n=1}^{\infty} \exp \left(- \frac{n^2 L^2}{Dt} \right) \right) \tag{103}$$

and for long times

$$N = \left(C_i - C_L \right) \frac{D}{L} \left(1 + 2 \sum_{n=1}^{\infty} \exp \left(- \frac{n^2 \pi^2 Dt}{L^2} \right) \right) \tag{104}$$

For short time of exposure, when none of diffusing material has reached the far side of the layer, equation (103) approaches that postulated in the penetration theory. For longer periods of exposure when a steady concentration gradient has developed, equation (104) is similar to the two film theory.

Kishinevskii (109) has developed a model for mass transfer across an interface in which he considers that molecular diffusion is assumed to play no part, where fresh material is continuously brought to the interface as a result of turbulence within the fluid and that, after exposure to the second phase, the fluid element attains equilibrium with it and then becomes mixed again with the bulk of the phase. He describes the mass transfer coefficients as

$$K_L = \sqrt{\left(\frac{4 D_T}{\pi \Delta T}\right)} \tag{105}$$

where D_T is the effective diffusion coefficient and ΔT is the contact time. He solves

$$\frac{\partial C}{\partial T} = (D_{mol} + D_{turb}) \frac{\partial^2 C}{\partial Y^2} + \frac{\partial C}{\partial Y} \frac{\partial D_{turb}}{\partial Y} \qquad (106)$$

with boundary conditions

$$\begin{array}{llll} C = C^* & \text{at} & y = o & T > o \\ C = o & \text{at} & y = \infty & T > o \\ C = o & \text{at} & y \quad o & T = o \end{array} \qquad (107)$$

Many other models have been proposed, such as Harriott's random eddy model (110) consisting of a random distribution of distances and contact times of eddies arriving at or near the interface. For constant distance and time, he arrives

$$\frac{KH}{D} = \frac{1.13H}{\sqrt{Dt}} \qquad (108)$$

and for constant distance and variable time

$$\frac{KH}{D} = \frac{1.0H}{\sqrt{Dt}} \qquad (109)$$

Fortescue and Pearson (111) describe an eddy model which they represent as a series of roll cells with a characteristic length scale, ℓ . The mean mass transfer coefficient is defined as

$$K_{rc} = - \frac{D}{\ell} \int_0^{\ell} \left(\frac{\partial C}{\partial y} \right)_{y=0} dx \qquad (110)$$

where y is the distance below the interface and x a horizontal distance.

Other models include that of Ruckenstein (112), which modified Danckwerts' theory of surface renewal, assuming a hydrodynamic microstructure in each liquid element, with a velocity component along the interface dependent only upon x and t and not on y, the distance from the interface.

Ruckenstein also developed a roll cell model in which an element has both a translatory and circulatory motion.

9.2 THE EFFECT OF SURFACE TENSION ON MASS TRANSFER COEFFICIENT

A number of authors (113,114) have shown experimentally that the solubility of such gases as H_2, N_2, O_2 and etc in various liquid is decreased as the surface tension of the solvent increases. The first theoretical analysis of the dependence between surface tension and gas solubility was given in the work of B.G. Ziokind and Ya.S. Kazarnovskii (114). Starting from this work, and taking into consideration the Maxwell-Boltzmann distribution theorem, Uhlig (115) produced a formula describing the relation between the solubility coefficient, the surface tension, the radius of the gas molecules being absorbed, and the energy of interaction E between the molecules of the gas being dissolved and of the solvent.Ziokind Shows that in the cases of gas absorption where there is a powerful interaction between the molecules being absorbed and those of the solvent, such as solvation or a more complete chemical reaction, the change of surface tension in itself cannot have any marked effect on the solubility of the gas.

Levich (116) shows that as long as the conditions for stability of the surface are observed, the change in its dimensions due to capillarity can be neglected. Thus, in the case of water absorption of SO_2, NH_3 and Co_2 in the presence of surface active materials, the surface tension as such does not have a significant effect either on the film coefficient of the rate of absorption or on the driving force. The basic reason for the change in the absorption rate must therefore lie in the effects of the addition of surface active material.

Ternovskaya and Belopol'skii (117) investigated the absorption rate of SO_2 by water in the presence of surface active agents (sul'fanol, merzolyat and nekal) and they concluded that the decrease in the rate of absorption of SO_2 by water in the presence of surface active material cannot be due to the decrease caused in the surface tension of the

absorbent. Long before reaching the inactive part of the surface tension isotherm, the rate of absorption ceased to depend on the concentration of the surface active material. Therefore, the reason for the change in the absorption rate must be due to the formation of an absorbed layer, which changes the hydrodynamic conditions of transfer of the gas being absorbed in the flowing liquid film. Davies et al (118) found that hydrodynamics resistance rather than mono-layer resistances are predominant.

Kamei and Oishi (16) concluded that surface tension had no effect on mass transfer coefficient, however, the surface tension varied only 9% in their temperature range so that such a conclusion was hardly warranted. Won et al (119) investigated the effect of surface tension on mass transfer coefficient with 100% variation in surface tension. They found that the coefficient increases with surface tension, which is in apparent contradiction to the Levich theory (if the common assumption of a one half power dependence on molecular diffusivity for the mass transfer coefficient is accepted). Therefore a possible conclusion is that either the dependence of surface tension predicted by Levich is incorrect, or $K_L \alpha D^{\frac{1}{2}}$ does not hold for low surface tension liquids.

Gamenson et al (120) carried out experiments on the rate of absorption of oxygen from the air by water flowing in an open channel. They found that the addition of commercial detergents decreased the rate of absorption, the decrease increasing with concentration of detergent. Downing et al (121) studied the rate of absorption of oxygen into water agitated in various ways. They found that the mass transfer coefficient fell steeply up to a detergent concentration of about 0.5 ppm but that further addition of detergent caused little reduction.

Lamont and Scott (122) claim that surface tension is an insignificant parameter in mass transfer in turbulent flows.

9.2.1 DEPENDENCE OF PRESSURE ON MASS TRANSFER COEFFICIENT

Yoshida and Arakawa (123) have studied the pressure dependence of liquid phase mass transfer coefficient and they found there was a declining dependence of the transfer rate on the pressure as the pressure was increased from one to two atmospheres and they postulated that oxygen transfer occurred by an absorptive and adsorptive mechanism operating simultaneously, Phillips (124) used the similar relation as above and found that the mass transfer rates increased with pressure. He explains when the partial pressure of oxygen is changed by changing the total pressure in the system, the absorptive component of transfer will be affected directly, but the adsorptive component of transfer will remain constant, since the amount of transferring gas absorbed on the surface of the liquid is not affected by changing the total pressure. However, if the partial pressure of oxygen was increased by increasing the mole fraction of oxygen in the gas, the absorptive and adsorptive components of transfer are affected equally

$$OTR = K_L A \left(C^* - C_L \right) + 9.7 \times 10^{-7} A_f Y \qquad (111)$$

where OTR is the overall transfer rate and Y is the mole fraction of oxygen in gas phase.

9.3 ASSOCIATED FIELDS

MASS TRANSFER INTO FALLING LIQUID FILMS

9.3.1 LAMINAR FILMS

It has been observed experimentally by many investigators (1,2) that if a liquid film flows down a vertical plate, its free surface is nearly always disturbed by wave motion and ripples. Investigators found that mass transfer rates were many fold greater than could have been predicted on the basis of the true molecular diffusion in a perfect laminar liquid film.

Portalski (5) explained the increase in the mass transfer rate is probably due to a combination of two effects: the vigorous bulk mixing due to rippling, and the increase in the interfacial area caused by the wave motion and ripples.

The second effect has been investigated quantitatively (see section on hydrodynamics) and its contribution was insignificant to account for the large increase in the rate of absorption mentioned above. It follows, therefore, that the first effect in the enhanced bulk mixing due to wave motion and rippling is the major factor in the rate increase in absorption process.

The problem of the appearance of wave motion has been investigated by Benjamin(49) and Yih (33) using the instability theory, as well as experimentally by (22,30,31). The conclusion arrived at by the instability theory was that laminar motion is unstable for any value of Reynolds number, but experimentally led to the conclusion that there exists a critical value of Reynolds number for the transition from laminary to wave motion (detail see Part 1 of the thesis).

Goodridge and Gartside (125) investigated the mass transfer into near-horizontal liquid films of inclination

less than 20 minutes. They claimed that ripple free films are produced with Reynolds numbers (Re*) to 900 and this technique provides a means of determining liquid diffusivities of sparingly soluble gases to a greater accuracy than has been reported in the literature.

Lynn et al (126) studied the absorption of SO_2 by water and other aqueous solutions using relatively long wetted-wall column (12 to 22 cm) with no gas phase resistance. The results of the investigation show that in the presence of small concentrations of a surface active material (Teepol) the rate of absorption is very well predicted by the penetration theory and that the hydrolysis reaction of the system SO_2-H_2O is very rapid relative to the contact times involved, so that absorption of SO_2 by water may be considered as physical absorption.

The absorption rate per unit area is given as

$$\Phi = 2 (C^* - C_o)(\frac{3D}{2\pi})^{1/2}(\frac{g}{3\nu})^{1/6}\Gamma^{1/6} h_e^{-1/2} \qquad (112)$$

Kamei and Oishi (16) showed that the falling liquid film at low value of Reynolds number is not in a perfect laminar state except at very small value of Reynolds number, but it has a pseudo-laminar flow in which ripples appear on the surface of the liquid film. With the transition of the flow from perfect laminar to pseudo-laminar the true molecular diffusion is present no longer, but the turbulent diffusion reveals itself gradually under such conditions the actual diffusion coefficient is not D_L (molecular diffusion), but $D_L = D_L + D_L'$ (D_L' is a coefficient of eddy diffusion dependent on the state of flow only).

D_L' is larger than D_L about 6 to 12 times at $Re_l = 2000$
D_L' is larger than D_L about 50 to 60 times at $Re_l = 10{,}000$

The absorption parameter of pure Co_2 into water film was given as

$$\tau_m = 1.92 g^{1/3} \bar{D}_L \ell (\frac{\mu_L}{\rho_L})^{-1.67} Re_l^{-1.33} \qquad (113)$$

In the case of countercurrent flow of gas, Kamei and Oishi found theoretically the film thickness increases and the mass rate τ_m decreases as given respectively as

$$\frac{B}{B_o} = 1 + \frac{\tau_s}{2\rho B_o g} \qquad (114)$$

and

$$\tau_m = \frac{8}{3}\frac{1}{Re_l}\frac{\rho D}{\mu}\frac{\ell}{B_o}\left(1 - \frac{\tau_s}{\rho B_o g}\right) \qquad (115)$$

But experimental results showed that at low Re_l (100-700) and different Re_g, the mass rate increases this is contrary to the above mentioned theory. Kamei and Oishi explained that when the liquid film is disturbed, $\bar{D}_L$ becomes greater than the case of the stagnant gas due to the gas flow, τ_m increases in spite of the variations of film thickness of shear stress.

Hatta (127) considered theoretically the case of diffusion into a liquid film on a flat surface. The assumption made was that there is no velocity gradient with the film. This condition is approached if the depth of penetration of the absorbed material in the film is small compared with the film thickness.

Hatta found that

$$\frac{C_2 - C_1}{C^* - C_1} = 1 - \frac{8}{\pi^2}\left(e^{-p} + \frac{e^{-9p}}{9} + \frac{e^{-25p}}{25} + ...\right) \qquad (116)$$

where $p = Y\pi^2 a \frac{Dx}{Q'}\left(\frac{a\rho g \sin\phi}{3\mu Q'}\right)^{1/3}$ and Y lies between 1/4 to 3/8

Sherwood and Pigford (68) have shown for falling film

$$p = \frac{\pi^2}{4}\left(\frac{Dt}{b^2}\right)$$

Sherwood and Pigford (128) collected many data, Emmert and Pigford (1), Vivan and Peaceman (129), Kamei and Oishi (16) and Grimley (31), and it is found that at large Reynolds numbers there is a wide deviation between the experimental

results and the calculated results. Brauer (9) has shown that the actual results may be as much as three times higher than those predicted by the above theory.

Fulford (130) explained this increased rate of mass transfer is due to the mixing action of the ripples at the free surface, and not to an increase of the interfacial area due to the ripples, as sometimes assumed, since Bruaer (51) has shown that this increase in interfacial area does not exceed about 3%.

Oliver and Atherinos (131) investigated the mass transfer to liquid films on an inclined plane. For gas liquid mass transfer system assuming the flow is steady-state, mass transfer only into the liquid and that the velocity distribution is parabolic, the mass transfer equation takes the form

$$V_s \left(2\left(\frac{y}{b}\right) - \left(\frac{y}{b}\right)^2 \right) \frac{\partial C}{\partial X} = D\frac{\partial^2 C}{\partial y^2} \qquad (117)$$

For short contact times, in which the penetration of the gas molecules into the film is small, it may be assumed that the film travels at the surface velocity, in this case, equation reduces to

$$V_s \frac{\partial C}{\partial X} = D\frac{\partial^2 C}{\partial y^2} \qquad (118)$$

with boundary conditions

$$\begin{aligned} C &= C_o \quad \text{at} \quad x = o \\ C &= C_i \quad \text{at} \quad y = \delta \\ \frac{dC}{dy} &= o \quad \text{at} \quad y = o \end{aligned} \qquad (119)$$

This equation is solved by Pigford (152) giving the ratio of $\frac{C_2 - C_1}{C^* - C_1}$ in terms of the parameter equation.

On substitution of the film Reynolds number, the kinematic viscosity of the liquid and the angle of inclination of the plane, the mass transfer coefficient for short contact time

is obtained as

$$K_L = 1.08 \left(\frac{D}{L} \right)^{1/2} \left(\nu g \sin\theta \right)^{1/6} Re_l^{1/3} \qquad (120)$$

A solution has also been obtained by Pigford for long contact times

$$K_L = 2.36 D \left(g \sin\theta \right)^{1/3} \nu^{-2/3} Re_l^{-1/3} \qquad (121)$$

Oliver and Atherinos's results showed that the mass transfer coefficients increased with increased angle of inclination. The greatest deviation from smooth film theory occurred in the case of the vertical plate, where the mass transfer increase of 250%. For 45^{o} inclination showed 160% increase and $7^{o}30'$ inclination 90% increase. Oliver and Atherinos explained the increase of mass due to the onset of rippling at lower Reynolds number as the slope increases and that wave velocity increases and wave length decreases as the slope becomes steeper.

Rotem and Neilson (133) obtained the concentration of solute in a film flowing down an inclined plane by solving the complete diffusion equation including the diffusion effect in the direction of flow. The problem of diffusion transfer to a liquid film had been considered by Vyazvov as long ago as 1940. However, in that study the axial diffusion was neglected. The complicated correlation (detail see original article) showed the influence of axial conduction is particularly notable near the start of the mass transfer surface, but the approach taken above is no longer admissable when surface rippling ensues.

Murty and Sarma (134) studied analytically the absorption rates of a gas into an accelerating, non-Newtonian wave free laminar falling liquid film flowing along an inclined wall for the developing region. Murty and Sarma observed that in the case of dilatant fluids, the concentrate profile falls above the characteristic of the Newtonian fluids, whereas for

pseudoplatic, the concentration profile lies below. In other words, for given system conditions and given location, the concentration at a particular point in the liquid film increases with the flow behaviour index 'n'. It was also noted that the Sherwood number decreases along the flow direction and tends to asymptotic values at distances far away from the exit of the slit. As can be anticipated, the Sherwood number Sh, is high when the concentration gradient is very steep, ie as 'n' increases, the Sherwood number decreases or, in other words, the rate of absorption decresseswith the increase in 'n'.

9.3.2 WAVY FLOW

Muenz and Marchello (135) investigated the influence of small surface waves mechanically generated at the liquid surface on mass transfer from pure gases into water. Muenz and Marchello expressed their experimental results in terms of an effective diffusivity which they found to vary as the 7/6 power of the molecular diffusivity and the 1/3 power of the frequency. Control experiments with non waved surfaces were also conducted and the marked increases in mass transfer over that predicted by mass diffusion for no-wave control runs are attributed to natural convection motions.

Natural convection motion may occur by either or both of two mechanisms. The first is the bouyant effect which occurs when fluid density is changed due to mass or heat transfer. A second possible mechanism is surface motion arising from Marangoni instability. This motion is caused by perturbations in surface concentrations which in turn cause changes in surface tension and result in force in balances at the surface (136).

The Grashof Number is generally used to characterise the influence of natural convection in a system (78)

$$N_{Gr} = \frac{g\rho^2 \nu a^3 \Delta Z}{\mu^2} \qquad (122)$$

Where negative values of N_{Gr} indicate a decrease of surface tension as concentration increases with the reverse effect for a positive value - oxygen has a negative value.

Goren et al (137) investigated the effect of standing waves of controlled amplitude and frequency on the steady state rate of mass transfer through thin horizontal film. They found that the increase in the steady state mass transfer rate to go as the square of the wave amplitude.

Rice (138) developed a new theory to predict mass transfer at an interface undergoing stationary oscillations. The theory describes mass transfer when a slightly soluble gas is dissolving in a dynamic liquid interface. It is shown that mass transfer under these conditions is a function of the square of wave amplitude, and depends, in a complex way, on a characteristic Smith and Reynolds number. The latter quantities are defined in terms of the characteristic wave length and frequency of the system periodicity. Using the Kapitza hydrodynamic parameters, the mass transfer theory is compared with data from a wetted wall column. The equation obtained was

$$\frac{K_L^*}{K_L} = 1 + 0.0018\ N_{ref}^{7/4}\ N_x^{1/4} \qquad (123)$$

where the dimensionless group N_{Ref} is the wetted perimeter flow Reynolds number defined as

$$N_{ref} = \frac{4Q_f}{\nu}$$

and the group N_x represents surface tension-viscosity effects

$$N_x = \nu^4 g \left(\frac{\rho}{\sigma}\right)^3 \qquad (124)$$

Rice noted that the theory tends to over predict the effect of enhanced mass transfer owing to ripples when the per cent of non-rippling flow was taken into account. Using the Kapitza hydrodynamics, the mass transfer theory appears to be accurate up to a flow Reynolds number of around 900.

Howard and Lightfoot (139) developed a method for predicting rates of gas absorption into laminar rippling films in terms of the surface velocities. The description can be used with any of the presently known hydrodynamic models of rippling films, provided they satisfy two relatively non-restrictive conditions: (i) the ripples are of a two dimensional nature, being of constant thickness in

the direction normal to their direction of propagation, and having no velocity components in this transverse direction, and (ii) the ripples propagate at constant celerity and with constant shape.

The equation given as

$$K_x = CV_o\frac{\sigma}{\pi}^{\frac{1}{2}} \left(\sqrt{\left(\frac{D}{LV_o}\right)} \right) \Lambda \qquad (125)$$

where Λ due to the effect of wave (detail see original article)

Ruckenstein and Berbente (140) explained the differing effects of wave motion on heat and mass transfer, using the velocity distribution expressions suggested by Kapitza. The equation of convective diffusion for a liquid film flowing down a vertical plate is of the form

$$\frac{\partial C}{\partial t} + V_x\frac{\partial C}{\partial X} + V_y\frac{\partial c}{\partial y} = D\frac{\partial^2 C}{\partial y^2} \qquad (126)$$

using Kapitza expression

$$h = \bar{h} \left(1 + \sin kz \right) \qquad (127)$$

$$V_x =$$

and

$$3\bar{V} \left(1 + (\beta-1)\alpha\sin kz - (\beta-1)\alpha^2\sin^2 kz \right) \left(\frac{Y}{h} - \frac{Y^2}{2h^2} \right) \qquad (128)$$

Where α is the dimensionless ratio of wave amplitude, k = wave number and β = propogation velocity/mean velocity since the diffusion coefficient is small, the penetration depth due to diffusion is small too. Hence the concentration varies appreciably only in the immediate vicinity of the interface. For this reason, Ruckenstein and Berbente solved the convective diffusion equation using the velocity components expression valid in the region of interest, ie for small value of y. Therefore, V_x and V_y are expanded into power series, neglecting terms of higher than first order in Y.

Finally obtained the average coefficient of amplification as

$$\bar{\Psi} = \frac{1}{2\pi} \int_0^{2\pi} \Psi \, d(kz) \tag{129}$$

where $\Psi^2 = \frac{KX(2/3\beta - z)^2}{\phi(\theta) - I(z)}$

$K = 0.95 \left(\frac{g\rho\theta}{\sigma\nu}\right)^{1/2}$ $\alpha = 0.46$ and $\beta = 2.4$ from Kapitza

Ruckenstein and Berbente concluded that the use of the velocity distribution obtained by Kapitza leads to the conclusion that the average amplification factor $\bar{\Psi}$ equals approximately 1.3 after a few cm only and that this limiting value is independent of flow rate. This conclusion was in disagreement with (Emmert, Kamei and Brauer), which show that initially $\bar{\Psi}$ grows rapidly with the flow rate, approaching a limiting value of approximately equal to 2. However, it is interesting to note that the empirical correction of Kapitza's velocity distribution improves the results, since this correction produces a rapid growth of $\bar{\Psi}$ with increasing flow rate, up to values comparable with the experiemental ones.

Kapitza's (32) theory predicts a strong dependence of the wave length on velocity, while experiment shows it to be practically independent on velocity; it predicts also a constant value for the ratio between the wave velocity and the average liquid velocity, while experiment shows a decrease with the increase of the average velocity of the liquid.

Hence, Kapitza's velocity distribution must be refined in order to lead to results satisfactorily as to the prediction of the rate of mass transfer. For the time being, there is no other way seemingly possible by which theoretical information on mass transfer in wave motion is obtainable. Ruckenstein and Berbente used the theoretical expression on periodic waves by Kapitza to enable them to obtain complete quantitative information related to the coefficient of mass transfer.

Javdani (141) presented the amplification in mass transfer due to the presence of the waves as a function of wave parameters, namely wave length, wave velocity and wave amplitude and hydrodynamic conditions in the films. A major difficulty in testing the theory is lack of experimental results under controlled hydrodynamic conditions, the wave characteristics, especially amplitude, will vary along the film and with time. For this reason interpretation of the effect of waves on mass transfer can be made only when equilibrium wave properties are maintained along the entire surface of the film. Javdani therefore considered with mass transfer to waves of constant amplitude at low Reynolds number, the resulting analysis give

$$\frac{Sh}{Sh_{smooth}} = 1 + 0.2216En^{1/2} - 0.0208\ (En^{\frac{1}{2}})^2 + 0.00692\ (En^{\frac{1}{2}})^3 + \ldots.$$

For $(En^{\frac{1}{2}}) < 1.26$ (130)

where $Sh_{smooth} = (2/\sqrt{\pi})n^{-\frac{1}{2}}$ is the Sherwood number predicted by penetration theory for smooth films.

$$E = 0.15\,\varepsilon \qquad \varepsilon = \tfrac{1}{2}\alpha^2 A^2\ (C_r - \frac{3}{2})\ PeRe$$

$$\alpha = \text{wave number} = \frac{2\pi\bar{u}}{\lambda}$$

$$A = \text{equilibrium amplitude}$$

$$C_r = \text{wave velocity}$$

$$n = \frac{DL}{\bar{h}^2 Us}$$

Javdani noted that the above theory is valid at short contact times where the eddy diffusivity can be replaced by its linear approximation and when the assumptions behind the penetration model become justified otherwise the approximation will overestimate the effect of the waves in enhancing the rate of mass transfer. Also since the results of linear hydrodynamic

stability for very small wave numbers have been used the theory is limited to mass transfer into thin films with two dimensional wave of long wave length, at sufficient low Reynolds number.

The dependence of the enhancement in the mass transfer coefficient on a single dimensionless group has been predicted by Ruckenstein and Berbente (142). The dimensionless group derived by them consists of parameters which can be reduced to a combination of Reynolds and Weber number only. Javdani stated that the adequacy of this parameter to describe mass transfer behaviour is questionable because the existence of diffusivity in the convective diffusion equation should introduce the Peclet number. Also the penetration type solution should introduce another dimensionless group, ie the contact time 'n'. Moreover, unlike the result presented in Javdani, the result given by Ruckenstein and Berbente, Howard and Lightfoot (139) does not show the explicit dependence of the amplification in the mass transfer coefficient on individual wave parameters. In conclusion, Javdani's theory developed through the assumption of existing fluctuations in concentration indicates that there is a direct relation between enhancement in the rate of mass transfer and hydrodynamic conditions in the film. This relation explicitly includes the effect of wave characteristics such as wave length, wave velocity and wave amplitude. The theory presented can therefore predict, without the help of any adjustable parameter, the amplification in mass transfer rate at low Reynolds number and small contact time.

9.3.3 TURBULENT FLOW

Brotz (143) carried out experimental work on the absorption of Co_2 by water films, and of methane by pentadecane, and found that the experimental results agreed well with the prediction of his mass transfer coefficient equation for rippled film or turbulent film written as

$$K_L = \left((g\nu)^{1/3} \frac{D}{Z} \right)^{1/2} f(Re_f) \qquad (131)$$

where
$$f(Re_f) = 1.15Re_f^{0.33} \quad \text{for } Re_f < 300$$
$$f(Re_f) = 0.07Re_f^{0.83} \quad \text{for } 590 < Re_f < 300$$
$$f(Re_f) = 0.19Re_f^{0.67} \quad \text{for } Re_f > 590$$

Brauer (51) gives a survey of the large range of values given for the critical Reynolds number ranging from 290 (100d) to 590 (143), above which the bulk of the film no longer remains in laminar motion.

Brauer (9,51) proposed a new model for mass transfer to flowing liquid film and gives the equation for mass transfer coefficient as

$$K_L = \frac{D}{V} \left(\frac{g^2}{\nu} \right)^{1/3} F(Re_f) \qquad (132)$$

where

$$F(Re_f) = 2.02Re_f^{1/3} \quad \text{for } Re_u < Re_f < Re_c$$
$$F(Re_f) = 3.61Re_f^{1/5} \quad \text{for } Re_c < Re_f < Re_k$$
$$F(Re_f) = 0.22Re_f^{2/3} \quad \text{for } Re_f > Re_k$$

$$Re_u = 1.35K^{1/10} \qquad Re_c = 0.018K^{1/3} \qquad Re_K = 35.0K^{1/10}$$

where $k_L = \nu\sigma^3/g^2\mu^4$ and v' is the velocity at the edge of the laminar sublayer and it has been found indirectly, using the mass transfer data of Kamei and Oishi (16), as 0.066m/sec

$$k_L = \frac{D\tau}{\mu v'},$$

Brumfield et al (144) applied the film hydrodynamics determined by Telles and Duckler, together with a turbulent mass transfer model and an empirical estimate for the macroscale, and provided a coherent description of a mass transfer mechanism which was found to be in agreement with overall mass-transfer measurements. The model considered the turbulent falling films consist of two distinct flow substructures: a laminar base film flowing next to the wall and turbulent wave which slide at much higher velocities on the top of this base film. These waves have an extremely large base to height ratio, move independently of each other, and may better be envisioned as solitary segments of thicker turbulent. Brumfield considered two limiting cases of no mixing and complete mixing between the base film and waves and noted that the no mixing calculations seem to agree better. The calculations show that the mass transfer coefficient for the waves are of the order of five times that for the base film. With no mixing, the bulk concentration in the wave increases much more rapidly down the column than that in the film. This was explained, for the no mixing extreme, the calculated values of k_L showed some sensitivity to diffusivity and the distant of the macroscale and less sensitivity is observed for the complete mixing case.

Stirba and Hurt (2) used Pigford and Johnstone's solution to solve the apparent diffusivity for carbon dioxide absorption into turbulent falling liquid film. The results showed that at Re*= 5000, The apparent diffusivity is about 10 times the molecular diffusivity. It is apparent from the results that one is dealing with turbulent flow and that as far as mass transfer is concerned turbulence appears to persist through the flowing layer.

Pigford and Johnstone solution given as

$$\frac{C_2 - C_i}{C_1 - C_i} = 0.786\, e^{-5.12n} + 0.100\, e^{-39.3n} + \ldots\ldots \qquad (134)$$

where $$n = \frac{DL}{B^2 V_m}$$

for low values of n the series may be expressed as

$$\frac{C_2 - C_i}{C_1 - C_i} = 1 - \frac{3}{\sqrt{\pi}} \sqrt{n} \qquad (135)$$

Banerjee, Scott and Rhodes (145) developed a model to relate the mass transfer rate to the rate of viscous dissipation in the turbulent flow near the surface and the liquid phase mass transfer coefficient is then related to the average wave length, amplitude and speed of the surface disturbances.

Using the root mean square vorticity near the surface and applying a theory proposed by Philips (146), the viscous dissipation near the surface has been found as a function of wave length, amplitude and velocity.

$$K_L = \sqrt{D} \left(\frac{\varepsilon}{\nu} \right)^{1/4} \qquad (136)$$

where ε is the viscous dissipation of energy which may be calculated from the exact relation (Batcheler, 1953) as

$$\varepsilon = - w^2 \nu \qquad (137)$$

and applying Philips's theory can be written as

$$\varepsilon \approx a^4 k^4 c^2 \qquad (138)$$

and $$K_L = (Da^2 K^3 C)^{1/2} \qquad (139)$$

using $a = 6.0 \times 10^{-4} N_{Re*}^{\frac{2}{5}}$ and $c = 9.64 \times 10^{-2} N_{Re*}^{\frac{16}{15}}$ from Fulford

finally $$K_L = 2.93 \times 10^{-3} \sqrt{D} N_{Re*}^{0.933} \qquad (140)$$

The above equation is applied to turbulent falling film in the absence of gas flow when a sparingly soluble gas is being absorbed.

Lamourelle and Sandall (147) carried out experimentally the gas absorption into a turbulent liquid flowing down a wetted-wall column and interpreted their results in terms of an eddy diffusivity model and indicated that the eddy diffusivity increases as the square of the distance from the interface.

Lamourelle and Sandall derived from the diffusion equation for diffusion in fully developed, two-dimensional flow in terms of an eddy diffusivity as

$$u\frac{\partial C}{\partial X} = \frac{\partial}{\partial y}\left(\left(D + \varepsilon_D \right) \frac{\partial C}{\partial y} \right) \qquad (141)$$

With the assumptions that the axial transport is negligible and there is no diffusion-induced velocity and the eddy diffusivity is assumed to decrease continuously from a high value in the bulk liquid to zero at the gas-liquid interface due to the action of surface tension.

Boundary conditions of interest are

$$\begin{aligned} y = o \qquad & C = C_s \\ y = \delta \qquad & \frac{\partial C}{\partial y} = o \end{aligned} \qquad (142)$$

sufficiently far downstream the concentration profile become fully developed and may be expressed as

$$\frac{\partial}{\partial X}\left(\frac{C_s - C}{C_s - C_b} \right) = 0 \qquad (143)$$

and the mass transfer coefficient is defined by

$$N_A = K_L \left(C_s - C_b \right) \qquad (144)$$

substituting equation 143 and 144 and expressing the concentration in dimensionless form results in

$$\frac{\partial}{\partial y}\left(D + \varepsilon_D \right) \frac{\partial C}{\partial y} \Big) + \frac{K_L u \bar{C}}{q} = 0 \qquad (145)$$

Integrated twice, applying the boundary conditions, and the resulting expression for $\bar{c}$ may be substituted into the equation of the bulk concentration to give a complicated expression for k_L (see original article).

Since D is very small and goes to zero at the surface it is assumed, therefore, that only the first term in the expansion for the eddy diffusivity needs to be retained for k_L

ie $$K_L = \int_0^{\alpha} \frac{1}{D + ay^n} \, dy$$ This was

integrated to give $$K_L = \frac{n}{\pi} a^{1/n} D^{1-1/n} \sin \frac{\pi}{n} \qquad (146)$$

Where a is a function of Re and k_L may be written as

$$K_L = \alpha Re^{\beta} D^{\gamma} \qquad (147)$$

From experimental data, the constants were determined by a least squares linear regression analysis and give

$$K_L = 0.481 \, Re^{0.837} D^{0.537} \qquad (148)$$

Lamourelle and Sandall noted that for the case of transport near a free surface, Levich (48) and Davies (148) gave the eddy diffusivity varies as the square of the distance from the free surface and for the transport between a solid wall and turbulent liquid. Elrod (149) and Tien and Wasan (150) have shown that the eddy diffusivity must vary with distance from the wall raised to an exponent of number not less than 3.

King (151) studied the mass transfer processes to and from a free gas-liquid interface involving concepts of surface renewals and of a damped eddy diffusivity profile in the vicinity of the surface.

For large surface age and sufficient large n value, steady state mass transfer will occur, in which k_L is independent of t, which is obtained similar to equation 146.

Using the correlation of Calderbank and Moo-Young relating the rate of energy dissipation to turbulent mass transfer coefficients at fixed surfaces (ie n = 4) and applied to falling film King obtained

$$a = \left(0.24 \left(\frac{g^4 \rho^5}{\mu^5} \right)^{1/12} \left(\frac{4\Gamma}{\mu} \right)^{1/6} \right)^4 \qquad (149)$$

It is the author's opinion that the above correlation will over estimate the mass transfer coefficient on falling film. The value of n used for fixed surface is not applicable to the gas liquid interface, where n was found to be 2 by Lamourelle (147), Levich (48) and Davies (148).

Banerjee, Rhodes and Scott (152) proposed a model for the absorption process which takes into account eddies formed within the film by passages of waves. Applying Harriott's random eddy modification of the penetration theory, together with an approach suggested by Levich for calculating the distance to which the eddies approach the surface enabling the liquid phase mass transfer coefficient to be predicted from a knowledge of the wave length, wave frequencies and liquid flow rates. Thus, this method proposed makes it unnecessary to know the velocity profile within the film.

Levich has deduced from dimensional considerations the distance to which a turbulent eddy approached the free liquid interface.

$$H = \left(\frac{\sigma \nu}{\rho V_o^3} \right)^{1/2}$$

where Vo is the characterising velocity

The velocity within the part of the eddy closest to the liquid surface may be assumed to be the same velocity as that of the wave. Therefore, the eddies come to within average distances from the surface can be written as

$$\bar{H} = \left(\frac{\sigma \nu}{\rho u_w^3} \right)^{1/2} \qquad (150)$$

and application of Harriott's random eddy model to obtain k_L as

$$\frac{K_L \bar{H}}{D} = 0.7 \left(\frac{H}{\sqrt{Dt}} \right)^{3/4} \qquad (151)$$

where $$t = \frac{\lambda}{\bar{u}_w - \bar{u}_s}$$

using Stainthorp and Allen $U_w = 2.95\ N_{Re}^{\frac{1}{2}}$ cm/sec to obtain H and using $\lambda = 1.0$ cm and average values of wave and surface velocity to find t.

Prasher and Fricke (153) proposed a model which is expressed in terms of eddy diffusivity to liquid-phase controlled mass transfer in falling films. The eddy diffusivity used in the model is empirically related to the hydrodynamics in thin films in such a way that the eddy diffusivity is affected by both surface tension and viscosity of the liquid.

At steady state diffusion equation for the solute gas is given by

$$\frac{\partial}{\partial y} \left(\left(D + a y^n \right) \frac{\partial C}{\partial y} \right) = 0 \qquad (152)$$

and boundary conditions

$$\begin{aligned} C &= C_s \quad \text{at} \quad y = o \\ C &= C_b \quad \text{at} \quad y = \lambda \end{aligned} \qquad (153)$$

and finally obtained

$$K_L = \frac{n}{\pi} \sin \left(\frac{\pi}{n} \right) a^{1/n} D^{1-1/n} \quad \text{(similar to equation 146)}$$

for values of n ranges from 2 to 4, but data of Emmert and Pigford (1), Kamei and Oishi (16) and Lamourelle (147) seem to fix n = 2.

Considering all the terms effecting the eddy diffusivity which may be written as

$$D_E = \text{constant } f\ (\sigma,\rho,\nu,\delta,\varepsilon,g\ )y^2 \tag{154}$$

$$a = \text{constant } f\ (\ \sigma,\rho,\nu,\delta,\varepsilon,g\ )$$

where
$$= c\,\frac{\rho}{\sigma}\left(\frac{\delta^3\varepsilon^3}{g\ \nu}\right)^{\frac{1}{2}} \tag{155}$$

Using the film thickness for turbulent film given by Brauer (51) to obtain the energy of dissipation

$$\delta = (400)^{-1/5}\left(\frac{3\nu^2}{g}\right)^{1/3}\left(\frac{Re}{4}\right)^{8/15} \tag{156}$$

$$V_m = (400)^{1/5}\left(\frac{g\nu}{3}\right)^{1/3}\left(\frac{Re}{4}\right)^{7/15} \tag{157}$$

and
$$\varepsilon = gV_m \tag{158}$$
$$= 400^{1/5}\left(\frac{g^4\nu}{3}\right)^{1/3}\left(\frac{Re}{4}\right)^{7/15}$$

whence
$$K_L = \frac{2}{\pi}\,a^{1/2}D^{1/2} \qquad \text{for} \quad n = 2$$
$$= C^{1/2}\,\frac{2}{\pi}\,\frac{\rho^{\frac{1}{2}}}{\sigma^{\frac{1}{2}}}\left(\frac{\delta^3\ \varepsilon^3}{g\ \nu}\right)^{1/4} D^{1/2} \tag{159}$$

compared with Kamie and Oishi, Emmert and Pigford and Lamourelle data, Prasher and Fricke obtained

$$K_L = \frac{0.0108}{\pi}\left(\frac{\rho}{\sigma}\right)^{\frac{1}{2}}\left(\frac{\delta^3\ \varepsilon^3}{g\ \nu}\right)^{\frac{1}{4}}D^{\frac{1}{2}} \tag{160}$$

Jepsen et al (45) used interferometer technique to measure the concentration profiles of Co_2 diffusion into thin water films with waves flowing down an inclined plate of 9 degrees 44 minutes to the horizontal. Jepsen noted a marked increase in the central region of the film, with the diffusivity tending toward the molecular diffusivity tending toward the molecular diffusivity at the boundaries of the film. The effect of the wave was to compress and expand the profile as the surface of the film changed, but indicated no direct effect as the variation of eddy diffusivity normal to the liquid surface. Jepsen proposed an explanation for the large increase in eddy diffusivity due to the presence of a surface layer where eddy diffusivity approaches zero and the rate of mass transfer is

controlled only by molecular diffusivity. In extremely turbulent systems, this layer would be very small, while in the flow regime where waves form but are well behaved, the layer would be much thicker.

Davies and Warner (154) studied the absorption of Co_2 into water flowing over a smooth and rough plate. They noted that the transfer rate in large scale roughness can be up to 3.5 times greater than into water over a smooth plate. The gas absorption is greater when the roughness is of a form which induces 'wake-interference' oscillations in the flowing water.

Using Levich's theoretical approach (which relates the damping of turbulence eddies at a free surface to the mass transfer rates). The mass transfer coefficient may be written as

$$K_L = 0.35 D^{1/2} b^{3/4} g^{3/4} (\sin\theta)^{3/4} \rho^{1/2} \nu^{-1/2} \qquad (161)$$

The results at $Re_l = 700$, $\theta = 24^{o}56'$ and $\frac{\ell}{e} = 6.7$ gives k_L for Co_2 is 3.5×10^{-2} cm/s compared with 1.0×10^{-2} cm/s for a smooth plate under these conditions. The calculated value from equation (161) for turbulent flow is 0.3×10^{-2} cm/s. Davies and Warner explained the discrepancy may be partly the result of error in the numerical coefficients of the theoretical equation, but is due principally to waves on the smooth and the rough plates increasing k_L being too simple to represent the complicated flow. Davies's (155) recent visual observation noted that the local eddy velocity could be four times the characteristic velocity and therefore the results expected to be about factor of 8 increase for the case of rough plate.

Henstock and Hanratty (156) proposed an absorption process which is controlled by eddies whose length and velocity are characterised by bulk turbulent properties and that in a region

of thickness δ close to the interface the turbulence is damped by viscosity. They also noted that the rate of absorption by a liquid film can be greatly increased by causing the gas to flow concurrently.

The result found for falling film compared with other experimental results give

$$ShSc^{-1/2} = 0.0077m^{+3/2} \qquad (162)$$

where $m^+ = \frac{mV^*}{\nu_L} = ((0.707Re^{1/2})^5 + (0.0610Re^{0.9})^5)^{0.2}$

where $V^* = \sqrt{\frac{\tau}{\rho_L}}$

For sheared liquid

$$m^+ = ((0.707Re^{1/2})^{2.5} + (0.0379Re^{0.9})^{2.5})^{0.5} \qquad (163)$$

and the effect of gas flow can be better taken into account by the relation

$$ShSc^{-1/2} = 0.0077m^{+3/2} \left(1 + 1.8\exp(-30F) \right) \qquad (164)$$

where $F = \frac{\nu}{Re_G^{0.9}} \frac{\nu_L}{\nu_G} \sqrt{\frac{\rho_L}{\rho_G}}$

According to the equation, the influence of an increasing gas velocity at a fixed liquid flow rate would appear as a decrease in the thickness of the liquid layer and a proportionate increase in k_L.

Chung and Mills (157) studied the effect of liquid viscosity and interfacial shear on the liquid side mass transfer coefficient for turbulent falling films. Experiments were carried out with the absorption of carbon dioxide into a liquid film formed on the inside of a 2.05 cm ID, 1.98 m long vertical tube. Chung and Mills concluded that for absorption from a stagnant gas into distilled water at 25°C, the mass transfer coefficients obtained were

$$K_L \quad 1.22\times10^{-6}\ Re^{0.67} \tag{165}$$

The mass transfer coefficient for seven other test liquids (Ethylene glycol-water mixtures) could be given as

$$\frac{K_L}{(\nu g)^{1/3}} = Re_L^n\ Sc^{-1/2} f(\nu(g\rho^3/\sigma^3)^{1/4}) \tag{166}$$

where the Reynolds number exponent n increased with viscosity was correlated as

$$n = 2.08\ Sc^{0.095}(\nu(g\rho^3/\sigma^3)^{1/4})^{0.277}$$

The Reynolds number for transition from wavy laminar to turbulent flow was given from 1000 to 1200. The co-current gas flow interfacial shear resulted in a marked increase in k_L but with counter-current gas flow at low velocities k_L decreased with increasing gas velocity.

Koziol et al (158) studied mass transfer in the liquid phase for carbon-dioxide absorption in water flowing in the form of a thin film on the external surface of vertical steel pipes. The correlation equations were given for three different regions as

(1) pseudolaminar flow ($170 < Re_z < 355$)

$$Sh_z = 1.668\ Re_z^{0.39} Sc^{0.5} \left(\frac{\theta_z}{h}\right)^{0.5} \tag{167}$$

(2) flow with a transitional character ($355 < Re_z < 1080$)

$$Sh_z = 3.882\ Re_z^{0.24} Sc^{0.5} \left(\frac{\theta_z}{h}\right)^{0.5}$$

(3) Reynolds number values $1080 < Re_z < 2513$

$$Sh_z = 8.923\times10^{-4}\ Re_z^{0.71} Sc^{0.5}$$

where $\theta_z = \left(\frac{\eta^2}{g\rho^2}\right)^{1/3}$ (the equivalent linear dimension)

η = dynamic viscositic $\quad Re_z = \frac{4\Gamma}{\eta}$

h = height of the pipe $\quad Sh = \frac{K_L \theta_z}{D}$

Koziol et al noted that the most powerful effect of the Reynolds number on the value of mass transfer coefficients is observed in the turbulent region, and the weakest in the transitional region. The experimental data are close to those obtained by Kamie and Oishi (16) but are higher than those theoretical results of Brauer (9) and Lamourelle and Sandall (147).

9.3.4 MARANGONI EFFECT

Ruckenstein (159) considered quantitatively the changes in the velocity distribution and the mass transfer due to tangential stresses (Marangoni effect). He noted that for $\frac{d\sigma}{dz} > o$, the interfacial velocity increases, and so does the mass transfer coefficient and for $\frac{d\sigma}{dz} < o$, the velocity at the interface and the mass transfer coefficient decrease.

From the equation of motion down the plane, the flow rate of liquid per unit wetted perimeter is given by

$$\Gamma = \int_0^{\delta} U \, dy = \frac{g\delta^3}{3\nu} + \frac{\delta^2}{2\mu} \frac{d\sigma}{dz} \qquad (170)$$

and Ruckenstein noted that for the same flow rate, the thickness δ is smaller in the case $\frac{d\sigma}{dz} > o$ and greater in the case $\frac{d\sigma}{dz}$ o than the value corresponding to $\frac{d\sigma}{dz} = o$. When compared with $\frac{d\sigma}{dz} = o$, the potential energy of the film is smaller when $\frac{d\sigma}{dz} > o$ and larger when $\frac{d\sigma}{dz} < o$. Positive values of $\frac{d\sigma}{dz}$ therefore lead to stabilization of the laminar motion, and negative values to destabilization. Therefore, it is expected that positive values of $\frac{d\sigma}{dz}$ will inhibit the formation of wavy flow, while negative values will promote this change. Ruckenstein obtained the mass transfer coefficient in a flow film as

$$K_L = \left(\frac{D}{\pi z} \left(\frac{g\delta^2}{2\nu} + \frac{\delta}{\mu} \frac{d\sigma}{dz} \right) \right)^{1/2} - \frac{V}{2} \qquad (171)$$

when Γ is small enough, V_δ is so small that equation above becomes

$$K_L = \left(\frac{D}{\pi z} \left(\frac{g\delta^2}{2\nu} + \frac{\delta}{\mu} \frac{d\sigma}{dz} \right) \right)^{1/2} \qquad (172)$$

in this case the surface tension affects mass transfer only through the term $\frac{d\sigma}{dz}$.

When Γ is sufficiently large $\frac{g\delta^2}{2\nu} >> \frac{\delta}{\mu} \frac{d\sigma}{dz}$ and the effect of $\frac{d\sigma}{dz}$ on the transfer coefficient can be neglected. The above equation, however, is not applicable at Re > 30 when the film motion becomes wavy.

Smigelschi et al (160) studied the rate of carbon dioxide absorption in water, under the influence of artificially produced Marangoni effect, where the radial surface movements were generated by dissolving continuously in its middle, liquids which lowered the surface tension of water. A theoretical approach using the experimentally determined surface velocity profiles to calculate the mass transfer coefficients in the liquid phase which are in good agreements with the experimental data.

The average mass transfer coefficient obtained may be written as

$$K_L = \frac{4}{R^2 - r_s^2}\left(\frac{aD}{\pi(3+m)}\left(R^{3+m} - r_s^{3+m}\right)\right)^{1/2} \qquad (173)$$

where $u = ar^m$ from experimental results.

9.4 INFINITE MEDIUM

Kreith et al (161) considered an experimental analogy approach to heat transfer by measuring the sublimation rate of napthalene coated discs rotating in an infinite environment under laminar and turbulent conditions. For laminar flow the original analysis of Wagner (162) on heat transfer from a rotating disc to ambient air was used and was characterised by

$$Sh = \frac{K_c r}{D} = C\ (Ta)^{0.5} \qquad (174)$$

where $c = f\ (Sc)$

and given as

Sc	0.74	1.0	2.5	5.0	7.5	10.0
c	0.33	0.39	0.60	0.80	1.0	1.1

Experimental results for $Sc = 2.4$ gives close agreement with the equation up to $Ta = 2 \times 10^5$.

An analogy technique was used for heat, mass and momentum transfer for turbulent flow and using a three layer model, laminar sublayer, transition and turbulent flow and obtained the expression as

$$Sh = \frac{Ta Sc \beta_m \sqrt{C_{or}/2}}{5\beta_m Sc + 5\ln(5\beta_m Sc + 1) + 2/C - 14}$$

where β_m = ratio of eddy diffusivities of mass and momentum
C_{or} = local drag coefficient at r

The effect of placing a stationary surface at various distances parallel to the rotating disc surface was also investigated experimentally in the laminar flow regime at rotational speeds of 1000 and 2000 rpm. The test results showed that the presence of a shrouding surface decrease the

rate of mass transfer. At a clearance to diameter ratio of 0.25 the mass transfer for the shrouded disc was only about 10% less than that for a comparable free disc, but drops to 80% of the free disc mass transfer rate at a clearance ratio of 0.05. As the clearance is further decreased the mass transfer rate decreases rapidly. The effect on the mass transfer rate of the disc was also investigated. It was found that for a given clearance ratio and speed, the rate of mass transfer was larger with the 8-in stationary surface (same diameter with the rotating disc), than with a large stationary surface. Kreith et al also carried out similar experiment with stationary disc having a 1" diameter hole at the centre. From the inspection of the data they found that even at clearance ratios as small as 0.02 the rate of mass transfer in the radial outflow system is equal to that for a free disc. At 2000 rpm and clearance ratios between 0.01 and 0.02 the Sherwood number in the radial outflow system with naturally induced flow was found to be actually larger than the corresponding Sherwood number for a free disc.

Kreith et al (163) further investigated the mass transfer from a partially enclosed rotating disc with forced source flow at a Sc = 2.4 in the range of Ta_r from zero to 4×10^4, mass flow Taylor numbers from 5×10^3 to 1×10^5, and spacing ratios from 0.06 to 0.3 and obtained the expression as

$$Sh = \left(\frac{z}{2r}\right)^{0.55}\left(1.36 + 1.29\times10^{-5}Ta_r + 3.57\times10^{-10}Ta_r - 3.51\times10^{-15}Ta_r + 1.84\times10^{-20}Ta_r^4\right) Ta_m^{(0.83-1.2\times10^{-4}Ta_r)} \quad (176)$$

where $Ta_r = wr_o/\nu$

$Ta_m = m/2\pi z\mu$

They concluded that the transition from laminar to turbulent flow on a partially enclosed rotating disc occurs at a lower local rotational Taylor number than on a disc rotating in an infinite environment; the transition Taylor number was further

reduced by the super-position of free-induction source flow. The flow over the entire surface of a partially enclosed rotating disc with forced source flow was turbulent at mass flow Taylor number (Ta_m) above 5×10^3. In the turbulent flow regime the mass transfer characteristics of a partially enclosed rotating disc with free-induction source flow are similar to those with forced source flow if the mass Taylor numbers are identical and free-induction source flow increases the rate of mass transfer over that obtainable without induction only at small spacing ratios.

Tien and Campbell (164) studied the mass transfer from isothermal rotating naphthalene - coated cones (vertex angles varied from 60^o to 180^o) in a similar manner to Kreith et al. For laminar flow region and sc = 2.4 they obtained

$$Sh = 0.625\, Ta^{\frac{1}{2}} \qquad (177)$$

which is in good agreement with Kreith's data. They noted that the laminar/turbulent transition occurred in the range $2.0 \times 10^5 < Ta < 2.5 \times 10^5$ and their experimental turbulent data compared favourably with the anology proposed by Kreith. For 60^o cone the Sherwood numbers in the range $1.0 \times 10^5 < Ta < 4 \times 10^5$ were found to be larger and they explained probably due to the early flow transition at $Ta = 1 \times 10^5$. This early transition gives a larger portion of the surface covered by turbulent flow and consequently a higher mass transfer coefficient. At high Taylor numbers the increased portion, due to early transition, as compared to the portion covered by turbulent flow becomes small and the increase of mass transfer coefficient is small at higher Taylor numbers.

Federov et al (165) also consider the heat/mass transfer analogy for naphthalene evaporating from a rotating disc for Taylor numbers up to 1×10^6. They found the transition regime between $Ta = 1.4 \times 10^5$ and 2.0×10^5 which was comparatively lower than that given by Tien and Campbell. The difference was

explained due to the surface temperature of naphthalene being 2-4^{o}C higher than the surrounding, which was not taken into account in Tien and Campbell data. From the experimental data the relationship given

For laminar region $\bar{Sh} = 0.348\ (Ta)^{0.5}$ (178)

For turbulent region $\bar{Sh} = 0.0207\ (Ta)^{0.8}$ (179)

Mishra and Singh (166) present a comprehensive review of previous experimental work in heat and mass transfer from a rotating disc. The results of these investigators were re-examined and, together with their own data, correlating expressions were proposed for laminar and turbulent flow mass transfer from rotating disc.

For laminar flow region ($Ta < 3 \times 10^{5}$) which was valid for all Schmidt number

$$\bar{Sh} = \frac{0.62Sc}{0.5657+Sc^{2/3}}\ Ta^{1/2} \quad (180)$$

and for high Sc, the data agree well with

$$\bar{Sh} = 0.62\ Sc^{1/3}Ta^{1/2} \quad (181)$$

For turbulent region ($Ta > 5 \times 10^{5}$) and ($0.72 < Sc < 3869\,8$) a Prandtl analogy was derived by considering eddy penetration of viscous and diffusion sublayers and the correlation was given as

$$\bar{Sh} = Sc^{1/3}(317.16+0.00838Ta^{0.9}(1-(2.6x10^{5}/Ta)^{1.4})) \quad (182)$$

Mishra and Singh (167) also considered the mass transfer from rotating disc to non-Newtonian fluids at high Schmidt number and the correlation given as

$$\bar{Sh} = 0.62Sc^{1/3}Ta^{1/2}\frac{A_n}{A_1} \quad (183)$$

where $A_n = \frac{1}{0.893}\left(\frac{6n+6}{5n+7}\right)\left(\frac{3+n}{6n+6}\right)^{1/3}(a)^{\frac{n+1}{6}}$

A_1 is the value of An for n = 1

and a is defined from the approximate linear velocity profile which is the dimensionless radial velocity gradient at the disc surface.

n	0.2	0.5	1.0	1.5
An	0.7223	0.6812	0.6179	0.5533

Shulman et al (168) studied analytically a boundary-value problem on convective mass transfer of a disc rotating in non-linear pure viscous fluid with the power-law rheological equation of state. Experimental data obtained using electrochemical method were in good agreement with the analytical expression given as

$$\bar{Sh} = \frac{\phi(n)}{0.89} Sc^{1/3} Ta^{1/3} \left(\frac{n+2}{n+1}\right) \left(1-\left(\frac{R_o}{r}\right)^{\frac{5n+7}{2(n+1)}}\right)^{-1/3} \qquad (184)$$

R_o is the radius of 'lacquered' disc section

$\phi(n) = \left(\frac{5n+7}{18n+18}a\right)$ 'a' is the dimensionless gradient of radial velocity at the disc surface

Hansford and Litt (169) studied both theoretically and experimentally on the solid-liquid mass transfer from a rotating disc to non-Newtonian solutions. An expression for the mass transfer has been derived in terms of the system parameters and the power-law constants of the liquid.

$$\bar{Sh} = \frac{\phi(n)}{0.89} Sc^{1/3} Ta^{\frac{(n+2)}{3(n+1)}} \qquad (185)$$

where $\phi(n) = \left(\frac{6n+6}{5n+7}\right)\left(\frac{a}{3}\right)^{1/3}$

$$a' = a\left(1 + \frac{(1-n)}{2(1+n)}\right)$$

where $Sc = \frac{NW^{n-1}}{D}$ $Ta = \frac{W^{2-n} r^2}{N}$ $N = \frac{K}{\rho}$

They noted that at high rotational speeds the slope of the experimental mass transfer curve is predicted by the theory. At lower rotational speeds, secondary flows were observed about the rotating disc producing anomalous mass transfer effects corresponding to the speeds at which the changes in the type of flow occurred.

9.5 MASS TRANSFER TO RADIALLY MOVING FILM

Sovova and Prochazka (170) proposed a novel method of measurement of diffusivities of gases in liquids by measuring the rate of absorption of a gas into a laminar film of liquid flowing radially over the surface of a horizontal disc.

At steady state and using the distribution of concentration of gas dissolved in liquid described by the differntial equation

$$\frac{1}{r}\frac{\partial(rVC)}{\partial r} = D\frac{\partial^2 C}{\partial y} \qquad (186)$$

with boundary conditions

$$\begin{array}{lll} y \to o & r = r_2 & C = C_p \\ y = o & r \propto r_2 & C = C^+ \\ y \to \infty & r \propto r_2 & C = C_p \end{array} \qquad (187)$$

and assuming small penetration depth, the parabolic velocity profile (verified by photochromic technique) may be linearised with the result

$$V = -\frac{3Qy}{rh^2\pi} \qquad (188)$$

since the analytical solution to the equation obtained by substituting the parabolic velocity profile into equation is not known.

Solution to equation(186)then takes the form

$$\bar{C} = 1 - \frac{1}{\Gamma(4/3)} \int_0^{\eta} e^{-\eta^3} d\eta \qquad (189)$$

where $\bar{C} = \frac{(C - C_p)}{(C^+ - C_p)}$; $\eta = (\frac{2Q}{3\pi h^2 Dx})^{1/3} y$; $x = r_2^2 - r_1^2$

and the rate of absorption is given by

$$N = KA(C^+ - C_p)$$

$$= \frac{C^+ - C_p}{\Gamma(4/3)} \left(\frac{3\pi D\ (r_2^2 - r_1^2)}{2hQ_1}\right)^{2/3} Q_1 \qquad (190)$$

where $Q_1 = 2\pi f(1.70x10^{-2}f^{0.08} - 0.137 - 0.0151)$ and f is the speed of revolution of impeller

A solution to this problem has also been published by Merson and Quinn (171) but the results were 10 to 30% higher.

Sovova and Prochazka (170) noted a standard deviation of 3.5 to 4.3% for their individual measurements mainly due to the error of chemical analysis. The molecular diffusivity found for Co_2 was in good agreement with literature. They suggested that this could be due to interfacial turbulence caused by the Marangoni effect. The author suggests that the discrepancy could very well be due to the assumption of an unstretched interface in the above derivation (see section mentioned by Venkataraman).

9.6 MASS TRANSFER TO THIN LIQUID FILM ON ROTATING DISC

Venkataraman (61) studied the mass transfer of Co_2 into thin smooth liquid film (surfactant added) formed on rotating disc and proposed several models to compare with the experimental results.

(A) 'Crude Model'

This model assumed that a surface element is not stretched or contracted as it grows older. The rate of mass transfer by non-steady diffusion from a surface element dA, with an age t, and saturated concentration at interface c_i into the water with zero concentration is given by

$$d\phi = C_i\sqrt{\frac{D}{\pi t}}\ dA(t)$$

Total mass transfer is shown to be

$$\phi = C_i\sqrt{\frac{D}{\pi}}\int_0^{t_e} t^{-1/2}\ \frac{dA}{dt}.dt \qquad (191)$$

Where t_e is the maximum age of the disappearing surface element.

Equation (191) can be integrated when A(t) is known. For a liquid film in laminar flow on the disc

$$\frac{dA}{dt} = 2\pi r V_{rs} \qquad (192)$$

where V_{rs} is the surface velocity of the film. From equations

$$V_{rs} = \frac{rw^2\delta^2}{2\nu} \quad \text{and} \quad \delta = \left(\frac{3\nu Q}{2\pi r^2 w^2}\right)^{1/3}$$

$$V_{rs} = Br^{-1/3} \quad \text{where} \quad B = 0.306\ \frac{w^{2/3}Q^{2/3}}{\nu^{2/3}}$$

$$\text{thus} \quad V_{rs} = \frac{dr}{dt} = Br^{-1/3}$$

The age of any surface element at radius r_1 is obtained as

$$t = \int_{r_o}^{r_1} \frac{dr}{Br^{-1/3}}$$

$$= \frac{3}{4} B \left(r_1^{4/3} - r_o^{4/3} \right) \qquad (193)$$

where r_o is the radius of the distributor

Substituting, $\frac{dA}{dt}$, t and dt into equation

$$\phi = 4C_i \sqrt{\frac{\pi DB}{3}} \int_r^{r_1} \frac{r}{\sqrt{r^{4/3} - r_o^{4/3}}} dr$$

$$= 6C_i \sqrt{\frac{\pi DB}{3}} \left(\frac{r_1^{2/3}}{2} \sqrt{r_1^{4/3} - r_o^{4/3}} + \frac{r_o^{4/3}}{2} \ln\left(r_1^{2/3} + \sqrt{r_1^{4/3} - r_o^{4/3}}\right) - \frac{r_o^{4/3}}{2} \ln r_o^{2/3} \right)$$

(B) 'Approximate' Model

This model takes into consideration of normal velocity V_z as the surface element changes while aging. Close to the interface the normal velocity is taken as proportional to z, the distance measured from interface

$$V_z = \left. \frac{\partial V_z}{\partial Z} \right|_{z=o} Z \qquad (195)$$

Restricting the analysis to depths of penetration such that equation (195) holds, then from the continuity equation,

$$\left. \frac{\partial V_z}{\partial Z} \right|_{z=0} = -\alpha(t) \qquad \text{ie function of surface age}$$

The diffusion equation, taking into account the convective mass transport normal to interface is

$$D \frac{\partial^2 C}{\partial Z} + \alpha(t) Z \frac{\partial C}{\partial Z} = \frac{\partial C}{\partial t} \qquad (196)$$

This equation was solved by Beek and Kramers (7) with boundary conditions

$C = o$	at	$z > o$	and	$t = o$
$C = o$	at	$z = \infty$	and	$t > o$ (197)
$C = C_i$	at	$z = o$	and	$t > o$

By method of moments, the mass transfer rate is given by

$$\phi = 2C_i\sqrt{\frac{D}{\pi}}\left(\int_0^{t_e}\left(\frac{dA}{dt}\right)^2 dt\right)^{1/2}$$

similar $\frac{dA}{dt} = 2\pi r V_{rs}$

$= 2\pi B r^{2/3}$ where $B = 0.306\frac{w^{2/3}Q^{2/3}}{\nu^{1/3}}$

and $\phi = 4C_i\sqrt{\pi DB}\left(\int_{r_c}^{r_1} r^{5/3}\, dr\right)^{1/2}$

$= 4C_i\sqrt{\pi DB}\left(\frac{3}{8}\left(r_1^{8/3} - r^{8/3}\right)\right)^{1/2}$ (198)

(C) Mass Transfer to the Liquid Film on a Spinning Disc (small depth of penetration)

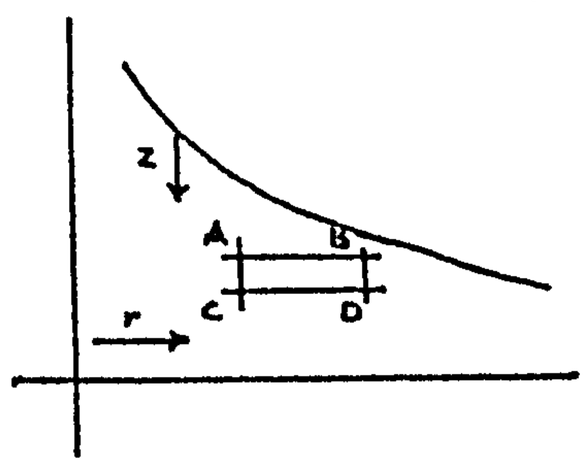

Under steady-state condition, the amount of solute within the element is constant and a mass balance exists between the diffusion across the streamline AB and convection across the vertical lines AC. Assuming no convection across streamlines and the diffusion in the direction of r.

The material balance in the element ABCD is given by

$$2\pi r V_r\left(\frac{\partial C}{\partial r}\right) dr\, dz = 2\pi r D\left(\frac{\partial^2 C}{\partial z^2}\right) dr\, dz$$

$$\text{ie} \quad V_r\left(\frac{\partial C}{\partial r}\right) = D\left(\frac{\partial^2 C}{\partial z^2}\right) \qquad (199)$$

Where y_1 is in dimensionless distance normal to the interface,

$$Y_1 = \frac{z}{\delta}$$

Hence equation (199) becomes

$$\delta^2 V_r\left(\frac{\partial C}{\partial r}\right) = D\left(\frac{\partial^2 C}{\partial y_1^2}\right) \qquad (200)$$

From equation

$$V_r = \frac{rw^2}{\nu} (\delta^2 - \frac{z}{2}^2)$$

and $$V_{rs} = V_r \,_{z=\delta} = \frac{rw^2\delta^2}{2\nu}$$

Thus $$V_r = V_{rs}(2(\frac{z}{\delta}) - (\frac{z}{\delta})^2) \qquad (201)$$

However, since z is taken as the distance from interface in the equations for mass transfer, z is replaced by $(\delta-z)$ in equation (201).

This gives $$V_r = V_{rs}(1 - y_i^2)$$

and $$\delta^2 V_{rs}(1-y_i^2)(\frac{\partial C}{\partial r}) = D(\frac{\partial^2 C}{\partial y_i})$$

By defining $$\frac{d\psi}{dr} = \frac{1}{\delta^2 V_{rs}} \qquad (202)$$

then $$(1-y_i^2)(\frac{\partial C}{\partial \psi}) = D(\frac{\partial^2 C}{\partial y_i^2})_{\psi} \qquad (203)$$

with boundary conditions

$$\begin{aligned} C &= C_i \quad \text{at} \quad y_i = o \\ \frac{dC}{dy} &= o \quad \text{at} \quad y_i = 1 \\ C &= o \quad \text{at} \quad r = r_o \end{aligned} \qquad (204)$$

For small depth of penetration of diffusing molecules, the y term is neglected and the equation is solved by Pigford (132)

$$\frac{C}{C_i} = \text{erfc}\, \frac{y_i}{2\sqrt{D\psi}}$$

therefore $$-D\frac{\partial C}{\partial y_i}_{y_i=0} = C_i\sqrt{\frac{D}{\pi\psi}} \qquad (205)$$

The rate of absorption is

$$\phi = -\int_{r_i}^{r_1} 2\pi r\, D(\frac{\partial C}{\partial z})_{z=0} dr$$

Using equation (202) and arbitrarily fixing a value $\psi = o$ at $r = r_o$ and ψ corresponding to r_1,

$$\phi = 2\pi rD \int_0^{\psi} - \delta V_{rs} \left(\frac{\partial C}{\partial y_i}\right)_{y_i=0} d\psi \qquad (206)$$

But $V_{rs} = \frac{rw^2\delta^2}{2\nu}$ and $Q = \frac{2\pi r^2 w^2 \delta^3}{3\nu}$

therefore $$\delta V_{rs} = \frac{3Q}{4\pi r}$$

substitute in equation (206)

$$\phi = \frac{3QD}{2}\int_0^{\psi} -\frac{\partial C}{\partial y_i}_{y_i=0} d\psi \qquad (207)$$

substituting equation (206) into equation (207)

$$\phi = 3QC_i\sqrt{\frac{D\psi}{\pi}} \qquad (208)$$

From equation (202)

$$\frac{d\psi}{dr} = \frac{1}{\delta^2 V_{rs}}$$

$$\int_0^{\psi} d\psi = \int_{r_i}^{r_1} \frac{dr}{\delta^2 V_{rs}}$$

$$\psi = \frac{3\nu}{4w^2}\left(\frac{2\pi w^2}{3Q\nu}\right)^{4/3}\left(r_1^{8/3} - r^{8/3}\right)$$

$$\phi = C_i\left(\frac{27}{4}\frac{D}{\pi}\frac{Q^{2/3}w^{2/3}}{\nu^{1/3}}\left(\frac{2\pi}{3}\right)^{4/3}\left(r_1^{8/3} - r_i^{8/3}\right)\right)^{1/2} \qquad (209)$$

(D) Mass Transfer with Greater Depth of Penetration

From equation (203)

$$(1-y_i^2)\left(\frac{\partial C}{\partial \psi}\right)_{y_i=0} = D\left(\frac{\partial^2 C}{\partial y_i^2}\right)_{\psi} \qquad (210)$$

and boundary conditions

$$\begin{aligned} C &= C_i \quad \text{at} \quad y_i = o \\ \frac{dC}{dy} &= o \quad \text{at} \quad y_i = 1 \\ C &= o \quad \text{at} \quad r = r_o \end{aligned} \qquad (211)$$

The above equation has been solved by Pigford (132) and gives

$$\phi = QC_i(1-0.7857\exp(-5.121p)+0.1001\exp(-39.31p)+$$

$$0.036\exp(-105.6p)+0.0181\exp(-207.7p)+....) \qquad (212)$$

where $p = D\psi_1$ and ψ_1 is similar to equation (208a)

(E) Mass Transfer included the Cumulative Effect of Inertial and Coriolis Forces on Flow

The mass transfer rate, for small depth of penetration given as

$$\phi = 3QC_i\sqrt{\frac{D\psi}{\pi}} \qquad (213)$$

and $$\int_0^{\psi} d\psi = \int_{r_o}^{r_1} \frac{dr}{h^2 V_{rs}}$$

in this model, which included the inertial and coriolis forces, the average radial velocity has to be taken which is $\frac{2}{3}$ of the surface velocity if the parabolic radial velocity profile is assumed

ie $$\int_0^{\psi} d\psi = \int_{r_o}^{r_1} \frac{2}{3\delta^2 V_{rav}} dr \qquad (214)$$

using the relation

$$Q = 2\pi r V_{rav}\delta$$

eliminating δ from equation (214)

$$\int_0^{\psi} d\psi = \psi = \frac{8\pi^2}{3Q^2}\int_{r_o}^{r_1} r^2 V_{rav}\, dr \qquad (215)$$

substituting ψ in equation (213) to obtain the mass transfer rate into the liquid film.

Venkataraman noted the crude model predicted mass transfer rates up to 23% lower than the measured values, while the more rigorous model predicted values up to 7% higher. However, when the latter model was modified to take account of the inertial and Coriolis on the flow, the agreement between the theory and measured values was within the experimental error.

9.7 DETERMINATION OF DISSOLVED OXYGEN

9.7.1 INTRODUCTION

The determination of dissolved oxygen in water has been studied by numerous workers over many years, and an extensive literature on the subject now exists. The various methods of estimation of dissolved oxygen differ widely in their emphasis on such features as sensitivity, specificity for oxygen, rapidity and simplicity of operation. For example, some methods are intended for the accurate determination of relatively high concentrations of oxygen in impure water, while other methods are more suited to the determination of micro quantities of oxygen in high-purity water. A number of techniques are designed for routine use by comparatively unskilled operators, but in other methods, considerable manual dexterity must be acquired if the best possible precision is to be considered.

The diverse methods may be classified into chemical and physical types. The majority of the chemical methods are based on the Winkler reaction, in which dissolved oxygen reacts with freshly precipitated manganous hydroxide to form an oxidised compound that is estimated indirectly by procedures discussed later. The physical methods include those based directly on gasometric, galvanic, polarographic, colorimetric and thermal conductivity principles.

The standard laboratory technique for oxygen determination by the Winkler method, does not lend itself easily to automatic, continuous monitoring. For many years a great deal of attention has been paid to the problem and earlier systems were based on the gasometric method, in which the dissolved gas is extracted from the water and analysed in the gaseous phase for oxygen or the bare electrode sensor such as thallium or rotating platinum. The former is at present unsuitable for use with water containing less than about 0.3 mg/l by weight of dissolved oxygen, but is particularly important because it is the only absolute or primary reference method available for proving the accuracy of

other procedures, physical or chemical. The latter suffered, in the main, from the poisoning and other interferences from constituents in the sample. However, recent years have seen the development of the use of membrane-covered sensors. There are two principal types of membrane-covered sensors, the galvanic and polarographic. These electrodes are unaffected by strong wastes which interfere with the iodometric method or its modifications, coloured solutions or liquors which contain readily oxidizable substances. Though most of the physical methods listed above have been developed to the stage of continuous recording, all the instrumental responses must be calibrated at some time by a proven method, usually chemical (172).

9.7.2 PRINCIPLES OF THE METHODS

(A) Winkler Method

The Winkler method with its modifications (173) is widely used for the determination of dissolved oxygen in water and sewage, and is generally accepted as a standard method. Manganous sulphate is reacted with oxygen in the sample to give manganic hydroxide. Upon acidification of the manganic hydroxide in the presence of an alkaline iodide solution some of the iodine is liberated as free iodine in the following reaction.

$$2Mn(OH)_2 + O_2 \xrightarrow{KOH} Mn_2O_2(OH)_2$$

$$Mn_2O_2(OH)_2 + 2KI + 2H_2SO_4 \longrightarrow 2MnSO_4 + 2H_2O + 2KOH + I_2$$

The amount of iodine released is equivalent to the oxygen originally present in solution. The free iodine is measured by titrating the sample with 0.25N sodium thiosulphate solution using starch as an indicator. Since the Winkler method is an indirect iodometric method, reagent may be used in excess. This makes the preparation of samples for analysis easy and eliminates the need for highly standardised reagents. Titration of the iodine is, however, time consuming and a tedious part of the analysis.

(B) Colorimetric Method (174)

Colorimetric methods of analysis can be and have been used to simplify dissolved oxygen determinations. Several colorimetric modifications of the Winkler method have been proposed that depend upon visual comparison of the colour produced in the samples with prepared standards (175). Brigg et al (176) described equipment for making continuous dissolved oxygen determinations in stream water. The operation is based on the use of Winkler reagents. The intensity of the colour of the iodine solutions, and, therefore, the concentration of dissolved oxygen, are measured with a spectrophotometer.

For the spectrophotometer calibration, it was first necessary to determine experimentally the wavelength of the light to be used in the calibration. This was accomplished by plotting a spectrophotometric graph of per cent transmittance versus wavelength for several known concentrations of iodine in distilled water. The iodine solutions were prepared by the Winkler method and were analysed by titration with 0.25N sodium thiosulphate solution. A portion of each iodine solution was analysed in the spectrophotometer to determine per cent transmittance at the various wavelengths.

The spectrophotometer will be calibrated at a suitable wavelength. Ordinarily, it is preferable that calibrations be made at wavelengths where absorption is a maximum. A steeply rising or falling section of the curve should be avoided because a small error in the setting of the wavelength could produce a large error in per cent transmittance.

Iodine solutions used in the instrument calibration were also prepared by the Winkler method using distilled water. The per cent transmittance of each sample was plotted against the dissolved oxygen in the sample as measured by titration. The iodine solution was found to behave according to the Lambert-Beer Law (177). Therefore, it would have been necessary to establish only one point to draw the calibration curve. Several points will be determined, in order to eliminate errors in titration.

(C) Thermal Conductivity Method (178)

This method is based on the difference in electrical and thermal conductivity between platinum spirals in contact with pure hydrogen and with a mixture of hydrogen and oxygen. Hydrogen is generated by electrolysis and divided into two streams, one of which passes directly over two heated platinum spirals while the other is passed through the feed water to sweep out dissolved oxygen passing over the other two heated

platinum spirals of a wheatsone bridge. If one pair of spirals is exposed to pure hydrogen and the other pair to a mixture of hydrogen and oxygen in the contact chamber, the temperatures of the two pairs of spiral will differ and a deflection of the galvanometer will be caused which is proportional to the amount of oxygen in the mixture. The galvanometer scale can therefore be calibrated to read directly the dissolved oxygen content of the feed water.

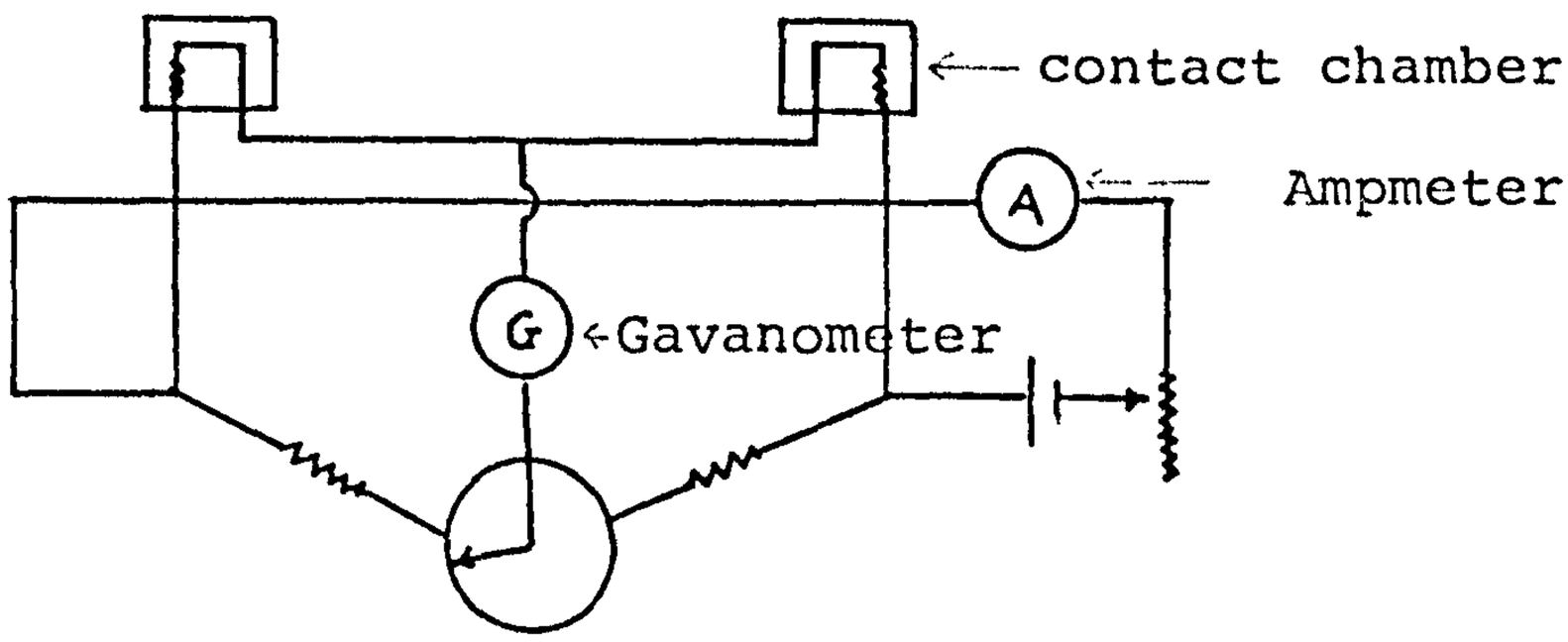

circuit to show the thermal conductivity method

(D) Membrane Electrode Method

Even though various modifications of the iodometric methods have been developed to eliminate or minimise the effects of interferences the method is still inapplicable in a variety of industrial and domestic wastewaters. Moreover, the iodometric method is not ideally suited for field testing and cannot be adapted easily for continuous monitoring purposes or for dissolved oxygen determinations in situ. With the membrane covered electrode systems these problems are minimised or eliminated.

Membrane electrodes of the polarographic as well as the galvanic type have been used for dissolved oxygen (DO) measurements in lakes and reservoirs, for stream survey and control industrial effluents, for continuous monitoring of DO in activated sludge units, and in estuarine and oceangraphic studies. Being completely submersible, membrane electrodes

are well suited for analysis in situ. Thier portability and ease of operation and maintenance render them particularly convenient for field applications. In laboratory investigations, membrane electrodes have been used for continuous DO analysis in bacterial cultures, including the BOD test.

Oxygen-sensitive membrane electrodes of the polarographic as well as the galvanic are basically composed of two metal electrodes of different electropositivity which are immersed in an electrolyte and contain within a fixed cell volume by a semi-permeable membrane. The hydrophobic membrane allows oxygen to permeate into the cell. The basic difference between the galvanic and the polarographic system is that in the former the electrode reaction is spontaneous, while in the latter an external source of applied voltage is needed to polarise the indicator electrode. The applied potential or a potential generated by the electrodes causes metal ions to enter the solution at the anode and electrons to flow from anode to cathode.

$$M \longrightarrow M^{++} + 2e^{-}$$

Oxygen is then reduced at the cathode

$$\frac{1}{2}O_2 + H_2O + 2e^{-} \longrightarrow 2OH^{-}$$

The resulting hydroxyl ions react with the metal ions at the anode,

$$\frac{1}{2}O_2 + H_2O + M^{++} \longrightarrow M(OH)_2$$

The steady state diffusion current produced is proportional to the partial pressure of the oxygen in the sample at a constant temperature.

Membrane electrodes are commercially available in some variety. In all these instruments, the 'diffusion current' is

linearly proportional to the concentration of molecular oxygen in the test solution. The current can be converted easily to concentration units (eg mg/l) by a number of calibration procedures.

Membrane electrodes exhibit a relatively high temperature coefficient, which is largely due to changes in the membrane permeability. The effect of temperature on the electrode sensitivity, ϕ(amp/mg/l), can be expressed by the following simplified relationship (179)

$$\log \phi = 0.43\ mt + b$$

where t is the temperature in degree centigrade, m is a constant which depends on the membrane material, and b is a constant which largely depends on the membrane thickness. It is apparent that if ϕ and m are determined for one temperature, it is possible to calculate the sensitivity at any desired temperature, as follows:

$$\log \phi = \log \phi_o + 0.43\ m(t - t_o)$$

Temperature compensation can be made automatically also, by using thermistors in the electrode circuit. However, thermistors may not compensate fully over a wide temperature range. For certain applications where high accuracy is required, it is recommended that calibrated nomographic charts be used to correct for temperature effect. If the dissolved oxygen membrane electrode is used in large changes of the salt content of the test solution, then a correction should be made for the effect of salting-out on electrode sensitivity (27). The electrode sensitivity varies with the salt concentration according to the following relationship

$$\log \phi_s = 0.43\ M_s c_s + \log \phi_o$$

where ϕ_s and ϕ_o are the sensitivities in the salt solution and

distilled water respectively, c_s is the salt concentration, and m_s is a constant (salt-out coefficient). If ϕ_o and m_s are determined, it is then possible to calculate the sensitivity for any value of c_s.

The sensitivity of the membrane electrodes is dependent on the membrane, in terms of both material and thickness. Several membrane materials have been tested by the group at Beckman Instruments Inc (180) saran, mylar, teflon, pvly vinyl chloride, natural rubber, silicon rubber and polyethylene. Polyethylene gave the best performance characteristics but for some situations and for corrosive gases, teflon has distinct advantages. Teflon is approximately 2.5 times as permeable as polyethylene for a given thickness and thus permits detection of lower concentrations of gas. The sensitivity of the electrode appears to be inversely proportional to the thickness of the membrane; the response time is shorter with thinner membrane. Physical strength appears to be the limiting factor with respect to how thin the membrane can be. Muller (181) has shown and obtained a quantitative expression for the marked dependence of 'diffusion current' on the velocity of flow of the solution past the electrodes.

9.8 DIFFUSION COEFFICIENT

The variations in the values of the diffusion coefficient of oxygen reported in the literature are sufficiently wide to give one a great deal of freedom in making a choice of a value to use. Thus the theoretical mass transfer rate will depend on the particular values chosen for the diffusivity. The value taken for this work is that recommended by Cullen and Davidson (182) as being the most reliable and show agreement among different experimental technique.

There are several expressions available for predicting diffusion rates in liquids successfully in a variety of systems. However, certain limitations still exist, for example none of the expressions is capable of predicting diffusivities for all the systems involving a liquid solvent. This may be due to the fact that variations in intermolecular force fields were not taken into consideration. The widely used Wilkes and Chang equation is not accurate when the solvent is a viscous liquid (183) or when the solute is a small molecule (185). While the Gainer-Metzner equation appeals to work for cases in which the solvent is viscous, it is not applicable when the diffusing species is a gas. Akgerman and Gainer (186) have proposed a correlation for diffusion coefficient using absolute rate theory. They claimed that their expression would be able to account for intermolecular forces and gives better than all other correlations. More recently, Scridhar and Potter (187) used the concept of Hilderbrand (188) and Dullien (189) equations to form a simple expression which can predict gas liquid - liquid diffusivities with confidence. All the correlations are shown in Table 9A

For Wilke and Chang

D_{AB} = mass diffusivity μ_B = viscosity

T = absolute temp in K

M_B = is the molecular wt of solvent

V_b = is the molal volume of solute at normal boiling pt in cm /g mole (25.6 for O)

ϕ_B = 'association' parameter for solvent B

TABLE : 9A DIFFISION COEFFICIENT CORRELATIONS

Author	Expression D_{AB}	Comment	Calculated D at 25°C O_2-H_2O
Wilke and Chang (184)	$= \frac{7.4\times10^{-8}(\phi_B M_B)^{1/2}}{V_b^{0.6}} \times \frac{T}{\mu_B}$	Not accurate when solvent is viscous liquid	1.8 (at 20°C)
Gainer and Metzner (183)	(see equation below)	Not applicable when the diffusing species is a gas	Nil
Akgerman and Gainer (186)	$= \frac{KT}{\varepsilon_A \mu_B} (\frac{N}{V_B})^{1/3} \exp(\frac{E_{\mu,B} - E_{D,AB}}{RT})$	Not very suitable for liquid-liquid system	2.4
Sridhar and Potter (187)	$= 0.088 (\frac{V_B^{*4/3}}{N^{2/3}}) (\frac{KT}{\mu V_B}) (\frac{1}{V_A^{*2/3}})$	Suitable for both gas-liquid and liquid-	2.4

$$D_{AB} = \frac{KT}{\varepsilon_A \mu_B} (\frac{N}{V_B})^{1/3} (\frac{M_B}{M_A})^{1/2} \exp(\frac{E_{\mu,B} - E_{D,AB}}{RT})$$

For Gainer and Metzner

D_{AB} = diffusivity of particle A through liquid B
K = Boltzmann's constant
T = Absolute temp
ε = Parameter describing the geometrical configuration of the diffusing molecule and its neighbours
μ_B = Viscosity of the solvent
N = Avogadro's number
V_B = Molar volume of solvent B
$E_{\mu,B}$ = Energy to overcome viscosity energy barrier
$E_{D,AB}$ = Activation energy for the diffusion process
R = Universal gas constant

Different experimental techniques have been used to determine the molecular diffusivities of oxygen in water. Davidson and Cullen (182) used a sphere to determine molecular diffusivities which is equivalent to using a short wetted wall column. Laminar liquid jet hydrodynamics has been used by Duda and Vrentas (190). Their results also show that there is no conclusive evidence that demonstrates the existence of a significant interfacial resistance in uncontaminated laminar jet experiments as shown in that of Chang and Toor (191) and Baird and Davidson (192). Wise and Houghton (193) and Krieger et al (194) using a new technique for determining diffusion coefficient of dissolved gases in liquids by measuring the rate of collapse of bubbles, ie by following the bubbles diameter as a function of time, the diffusivity was obtained from the initial linear slope of a plot of bubble diameter square versus time (knowing the saturation solubility of the gas in the liquid). Fernell and Himmelblau (195) have claimed that no solubility data were required to determine the diffusion coefficient in their work using the laminar dispersion in a capillary. Recently, a new method (170) of measurement of diffusivities of gases in liquids has been proposed consisting of measuring the rate of absorption of a gas into a laminar film of liquid flowing radially over the surface of a horizontal disc. Other techniques have been summarised in

(190). The values obtained for the diffusivities of oxygen in water by the above mentioned techniques are shown in Table 9B

TABLE :9B EXPERIMENTAL VALUES OF DIFFUSION COEFFICIENT OF O_2 AT 25^0C

Author	Method	Diffusion Coefficient at 25^oC cm^2/s
Davidson and Cullen (182)	Sphere	2.45×10^{-5}
Duda and Vrentas (190)	Laminar liquid jet	2.07×10^{-5}
Wise and Houghton (193)	Rate of collapse of bubble	2.6×10^{-5}
Fernell and Himmelblau (195)	Laminar dispersion in a capillary	2.2×10^{-5}
Krieger et al (194)	Rate of collapse of bubble	3.49×10^{-5} (29.6 0.2^oC)
Vivian and King (196)	Diaphragm cell technique	2.41×10^{-5}

9.8.1 THE EFFECT OF SOLUTE ON DIFFUSION COEFFICIENT

Onda et al (197) study on the effect of solute concentration on the diffusivity of Co_2 - water system. They reported that the diffusion coefficient of carbon dioxide was decreased about 30% when the initial concentration of carbon dioxide was increased from 0 to 60% of the equilibrium value. But most experimental research has been assuming that the diffusion coefficient is independent of the concentration of the solute gas in the solvent.

Consider the four equations below

Gordon (198) $$D = D_1\left(1 + \frac{\partial \ln f_1}{\partial \ln f_2}\left(\frac{\eta_1}{\eta_2}\right)\right) \quad (216)$$

Erying et al (199) $$D = D_1\left(1 + \frac{\partial \ln \gamma_1}{\partial \ln x_1}\right) \quad (217)$$

Darken (200) $$D = \left(x_1 D_1 + x_2 D_2\right)\left(1 + \frac{\partial \ln \gamma_1}{\partial \ln x_1}\right) \quad 218)$$

Hartley and Crank (201) $$= KT\left(\frac{x_1}{\sigma_2 \eta} + \frac{x_2}{\sigma_2 \eta}\right)\left(1 + \frac{\partial \ln \gamma_1}{\partial \ln x_1}\right) \quad (219)$$

These equations above are the same as shown in (202). Consider for example, Gordon's equation. Since the concentration of the dissolved gas in the liquid phase is very low under the normal conditions, the viscosity of the solution should be essentially the same as that of the pure solvent.

Equation (216) becomes

$$D = D_1^{o}\left(1 + \frac{\partial \ln f_1}{\partial \ln f_2}\right) \quad (220)$$

In a very dilute solution $\left(\frac{\partial \ln f_1}{\partial \ln f_2}\right) \simeq o$, therefore, Gordon's theory predicts that the diffusion coefficient of carbon dioxide in water does not vary significantly with concentration since the above four equations are alike, would lead to the same conclusion. Hence, for all practical purposes, the diffusion coefficient of a gas in dilute solution can be taken as constant.

Tang and Himmelblau (202) studied the diffusion of Co_2 in water at 25^{o}C in a liquid jet as the function of solute concentration and they found that the smallest value of diffusion coefficient obtained at an initial feed concentration of about 60% of the saturated solubility of Co_2 was only about 3% lower than the average value of diffusion coefficient determined with zero initial feed concentration. This conclusion differs significantly from that of Onda et al (197) where as mentioned, a 30% drop in diffusion coefficient was observed. The difference of 30% in Onda results may be due to the measured c_i value because diffusion coefficient (D) changes twice for one error in concentration measurement.

9.8.2 THE EFFECT OF ELECTROLYTE ON DIFFUSION COEFFICIENT

The effect of electrolyte on diffusion coefficient has been studied by Gubbins (203) using Eyring rate theory and Podolsky theory and obtained

$$\frac{D}{D_o} = 1 - \frac{Ax}{(1-x) + (V_1+V_2)x}$$

where they found D/D_o varies approximately linearly with electrolyte concentration and that the change in D/D_o produced by a given electrolyte is little affected by temperature or solute for the solutes studied.

V. Linek et al (204) studied the influence of molecular diffusion on mass transfer in a mechanically agitated gas-liquid contactor. They found that the value of m from the relation $K_L \sim D^m$ is not influenced significantly by either the impeller speed or the gas supply to the contactor. The values of exponent m increases with an increasing concentration from average value of 0.46 obtained for water, up to about 0.67.

Iraj and Turner (205) used a laminar jet instrument to measure the molecular diffusivities of oxygen. For polymeric solutions, they found that the diffusivities are a function of concentration and type of polymer used. The molecular diffusivities were shown to be decreased for all polymeric solutions except for 1000 mg/l solution of ET-597.

Other workers such as Davidson and Cullen (182) have found that the addition of solute always reduces the saturation of a gas, such as the polymeric solution in equilibrium with air is lower than the saturation value for distilled water in equilibrium with air.

Goffi (206) found that the oxygen mass transfer coefficient decreased with increasing electrolytic concentration for a given inorganic salt and increasing valency of the cationic species.

In particular it was shown that the cationic valency increased from one (Na^{+}) to three (A^{+3}) for a given salt concentration there was a substantial decrease in $K_L a$.

Goffi explained the reduction in the oxygen mass transfer coefficient ($K_L a$) was attributed to ion-solvent interaction which enhanced the structural orientation of the water molecules. Since the oxygen was in the non-reactive environment and because the oxygen molecule is non-polar, the presence of ionic species did not affect the oxygen transfer directly. However, by enhancing the water structure through the electrostatic fields which the ions establish in solution, the diffusion of oxygen was retarded.

The reduction of $K_L a$ with increased structural enhancement of the electrolytic solutions was shown by the dependence of the overall $K_L a$ on the three independent variables: viscosity, the energy of hydration and the McCall-Douglass parameters (explained later). These three variables are related to the ionic entropy of solution. Since the ionic entropy of solution is a measure of the order-disorder resulting from the presence of the ionic species in the solution, the results show the increase in the resistance to oxygen mass transfer was highly dependent on the structuring of the water molecules in the vicinity of the ions. Further evidence of the importance of the structural change brought about by ionic species in the solution was also shown by (206), the decrease of $K_L a$ with increasing ionic strength. The ionic strength is the electrostatic contribution to the activity coefficient and is a measure of ion-solvent interactions. Therefore, as the ionic strength increased, indicating a more highly structured solution, the resistance to oxygen mass transfer increased. The relationship between $K_L a$ and the ionic strength was not surprising as the solubility of the gaseous component, which is dependent on the structural configuration of the liquid phase, has also been shown to decrease with increasing ionic strength.

Therefore, Goffi has concluded that the bulk structural enhancement of the water molecules, which is brought about by the presence of the inorganic electrolytes and magnified at the liquid surface, was the reason for the increase in the resistance to oxygen mass transfer.

The McCall-Douglass Parameter (206)

McCall and Douglass (207) have introduced a parameter which is concentration dependent for comparing the effects of various electrolytes on the self-diffusion of water, the water self-diffusion parameter. This parameter defined as 'the relative change of di fusion coefficient of water between zero and one molar', and is represented mathematically as $\Delta_1 = \frac{D_1 - D_o}{D_o}$. The decreasing value of water self diffusion parameter is a result of a decrease in the water self diffusion coefficient in electrolytic solutions. Wang (208) and Devell (209) have attributed the reduction in the water self-diffusion coefficient in electrolytic solutions to an increased structural enhancement of the water molecules. McCall and Douglass (207) have shown that the water self-diffusion parameter is linearly related to the ionic entropy of solution, which contributes to the order-disorder concept of Wang and Devell. Therefore, as the water molecules become more structured in the ion co-spheres the ionic entropy of the solution decreases, as do the water self diffusion parameter and the transfer of oxygen.

The increased resistance to oxygen transfer is not a direct result of the electrostatic fields of the ions on the oxygen molecules, as the oxygen molecules are non-polar. Long and McDevitt (210) studied the solubility of non-electrolytes in electrolytic solutions and found that the solubility of the non-polar molecules was strongly dependent on the properties of the electrolytic solution rather than on the interaction of the non-polar molecules with the solution.

The results of Long and McDevitt (1952) suggest that a possible explanation for the decrease in the rate of oxygen

transfer with increasing structural enhancement in the liquid phase is a result of a reduction in the number of interstitial sites capable of harbouring an oxygen molecule. This in turn would increase the diffusional path of non-polar molecules.

Hydration Considerations (206)

The increased obstruction to the movement of the non polar molecules, which may be considered to be the primary factor reducing the diffusion of the oxygen, is a direct result of the hydration of the ionic species. The hydration energies for the individual ions, as reported by Bernal and Fowler (211) were combined to give the energy of hydration per ion-pair of the inorganic electrolytes. This energy and the concentration of the corresponding salts were then multiplied to give the energy of hydration of the component ions per unit volume of the solution. As the energy of hydration per unit volume increase, the resistance to oxygen transfer increases. Essentially, a greater quantity of the free water molecules are influenced as the salt concentration increases. The increased structural enhancement results in an increase in the fluid viscosity and a decrease in the diffusion of oxygen. Therefore, the energy of hydration per unit volume of solution can be considered a very important and basic quantity which throws light upon the magnitude of ion-water interactions and the structural changes occurring in the solution.

Ionic Entropy (206)

The viscosity, water self-diffusion parameter and the energy of hydration are all related to the ionic entropy of solution. Gurney (212) has shown that the viscosity, diffusion coefficient and ionic entropy are lineary related. The energy of hydration is related to the entropy of solution (Gurney, 1953) and McCall and Douglass (207) have shown the existence of a linear relationship between the ionic entropy of solution and the water self-diffusion parameter. The correlation of the above independent variables with the ionic entropy of solution

and the water self-diffusion parameter. The correlation of the above independent variables with the ionic entropy of solution shows further the dependence of the volumetric mass transfer coefficient on ion-solvent interaction. For the cation of importance, the entropy of solution is in the order $Na^{+} > Mg^{+2} > A^{+3}$ (213). This again shows that the greater the structural enhancing ability of the particular ions, the greater the increase in the resistance to oxygen mass transfer.

10 MASS TRANSFER EQUIPMENT

10.1 GENERAL

A study of mass transfer in the liquid films flowing across the rotating disc was carried out using the apparatus described earlier. In this case the disc was enclosed in an absorption chamber in order that the liquid films could be exposed to saturated air, at atmospheric pressure. Several techniques were devised, to enable measurements of oxygen concentration, as a function of radial positions, to be made. The pickup probe (to be described later) was eventually chosen since this produced the minimum level of disturbance in the region up to the probe. This devise was also suitable for operation over the range of flowrates and disc speeds used in this series of experiments.

The basic consideration in the design of the disc and the absorption chamber are similar to those of the hydrodynamic studies. The description of the techniques and auxillary equipment used for the measurement of the mass transfer rate are outlined below. Finally, details of a typical mass transfer experimental run are given.

The flow sheet of the equipment is shown in Figure 4.4 and the arrangement of the equipment for the study of mass transfer is given schematically in Figure 10.1.

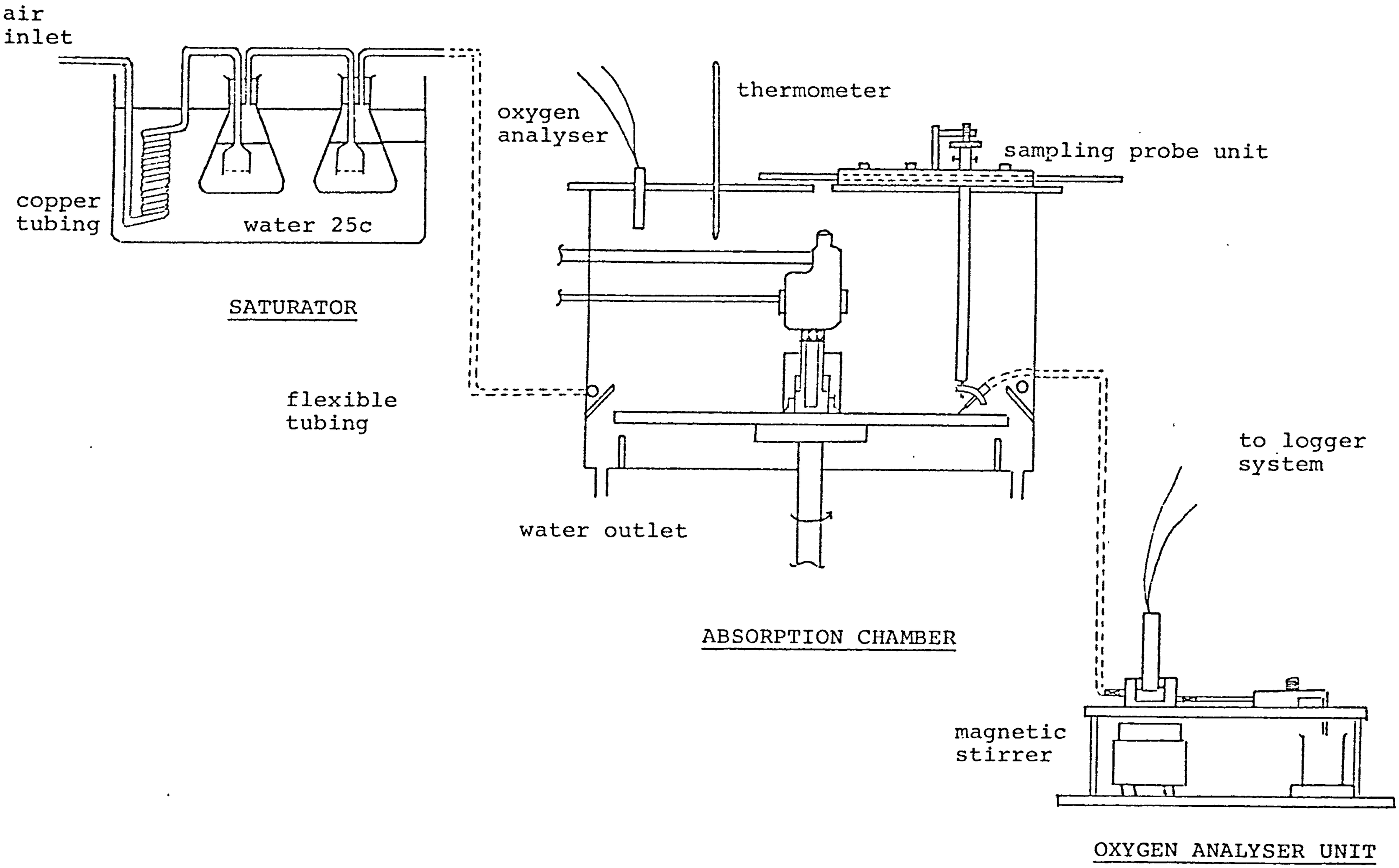

FIGURE 10.1 SCHEMATIC DIAGRAM OF ABSORPTION UNIT

10.2 DESIGN CONSIDERATION

Several important factors were taken in the design of the mass transfer system:

(A) The sampling probe was designed with several factors in mind. The vertical movement, the angle of the pick up probe made with the disc about a fix point, rotational movement in order to orientate the probe in the direction of the liquid film and the radial movement across the disc.

(B) The absorption chamber enclosing the spinning disc must be perfectly gas-tight to prevent inaccuracies in the measurement of absorption rate due to the unsaturated air coming into contact with the saturated air in the absorption chamber. The absorption chamber initially was designed with the intention of increasing the percentage of oxygen in the chamber. Therefore, a perfectly gas-tight chamber was essential in order to prevent gas leak or counter-diffusion of gas inside with that of air outside.

(C) The geometry of the absorption chamber and the situation of the purge gas inlet and outlet lines were to be such that efficient and complete purging was possible.

In addition to these essential requirements, it was considered desirable to have the chamber lid made of transparent material to enable the visual observation of the water film while absorption was taking place. A slide-window on the absorption chamber was also provided for the observation of the sampling probe in contact with the disc surface. Furthermore, it was considered ideal to have the sampling probe easily dismantled and the chamber lid removable to allow quick changes of the probe as shown in photographs E and F and the cleaning of the disc surface.

10.2.1 The Chamber Lid

The chamber lid of diameter 53.5 cm was trapanned out from a 1/8" thick high impact plastic (Davic - ICI Plastic Division). Two similar lids were required to hold the weight of the sampling probe secured onto the slider housing as shown in Photograph E. 24 Equally spaced holes of 3/16" diameter were drilled to enable the lids to be bolted to the flange of the absorption chamber with an annular 1/18" thick cord gasket in between. Five holes were drilled on the lid to form the outlet for the purge gas. Four of these holes with diameter 5/8" were located as near to the side wall of the absorption chamber as possible and the fifth one at the centre of the lid with 1¼" diameter hole. During experimental run, the centre hole was kept open and the rest of the four holes were closed by rubber bungs. Two of the rubber bungs were drilled and fitted with oxygen sensor and a glass thermometer, which measured the oxygen concentration and served to indicate the temperature in the absorption chamber respectively.

PHOTOGRAPH E

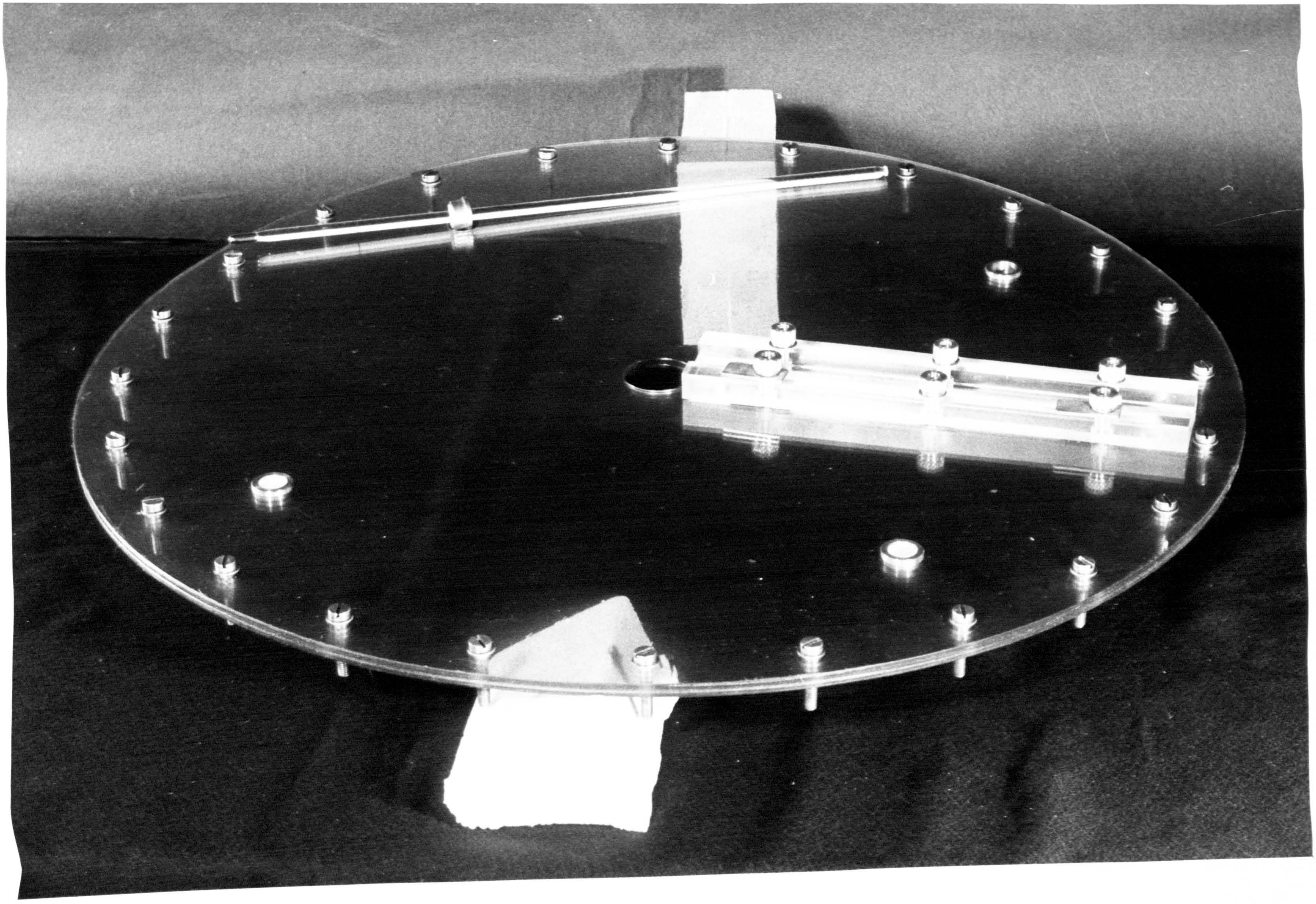

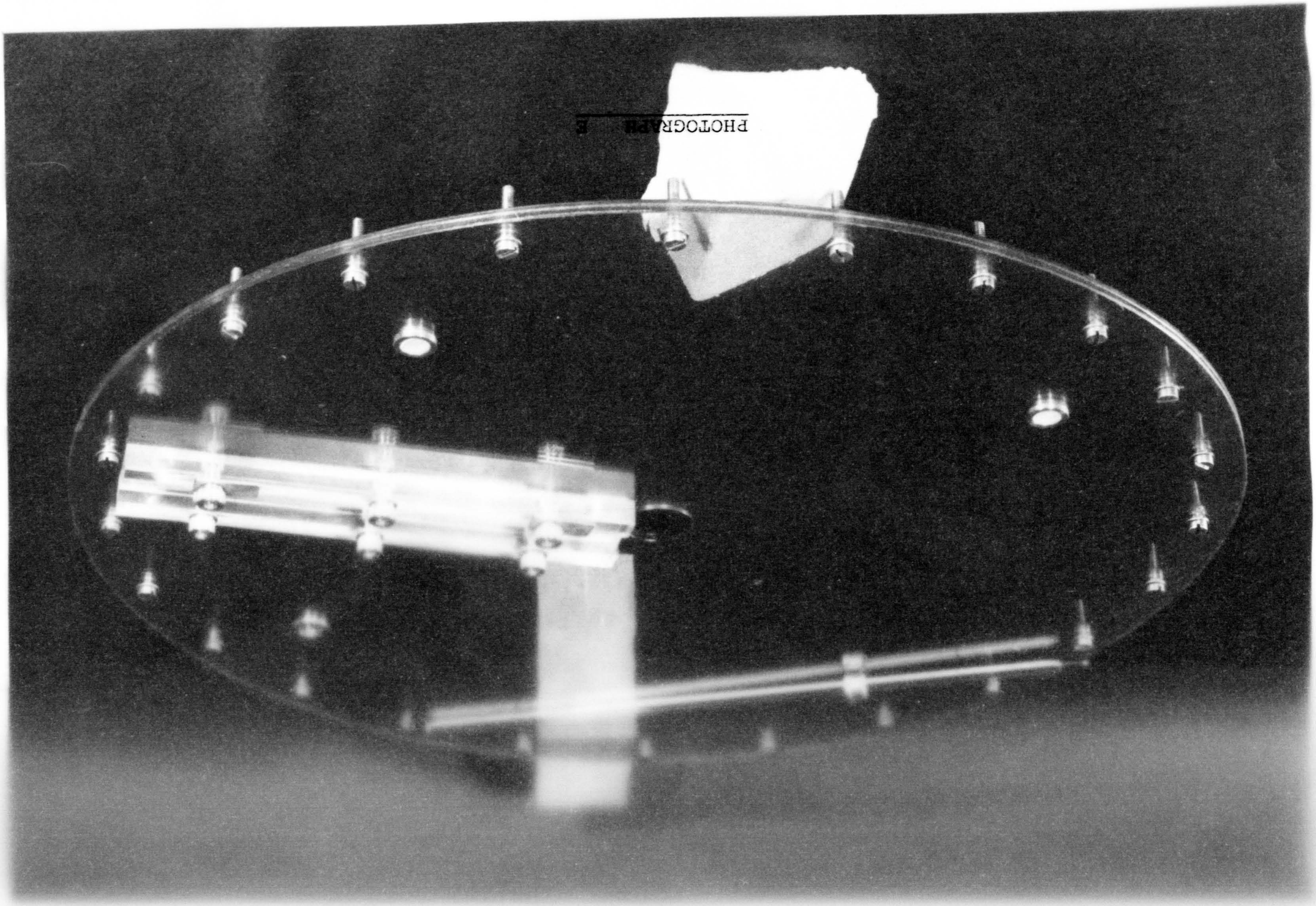
PHOTOGRAPH

10.2.2 Saturator and Inlet Air Supply to Absorption Chamber

The compressed air supply from the main line was regulated down to 5 psi before it was passed through a coil of copper tubing immersed in a constant temperature tank maintained at 25°C. This air supply was saturated with water by bubbles using a sintered glass disc in glass tubing dipping in two half-filled 1 litre conical flasks kept at 25°C, before entering the absorption chamber, minimising the gas phase resistance to the mass transfer. Since water evaporation or condensation was eliminated by presaturation, the observed change in the dissolved gas concentration was due to absorption alone.

This presaturated air was introduced into the absorption chamber through two ¼" diameter tubing bent in the form of circular arch. The centre of each arch was drilled and welded to a threaded inlet tubing. This enabled the copper tubing to be bolted onto the wall of the absorption chamber. Four 1/8" daimeter holes were drilled equally spaced around the arch, with all the holes facing 45° upward. Thus the saturated air was introduced into the absorption chamber at eight different points, equidistant from the centre of the disc. This ensured a complete mixing in the gas phase in the absorption chamber.

10.2.3 Sampling Probe

The complete design of the sampling probe is shown in Figures 10.2, 10.3, 10.4 and Photographs F, G , H. It was designed with few considerations as mentioned earlier.

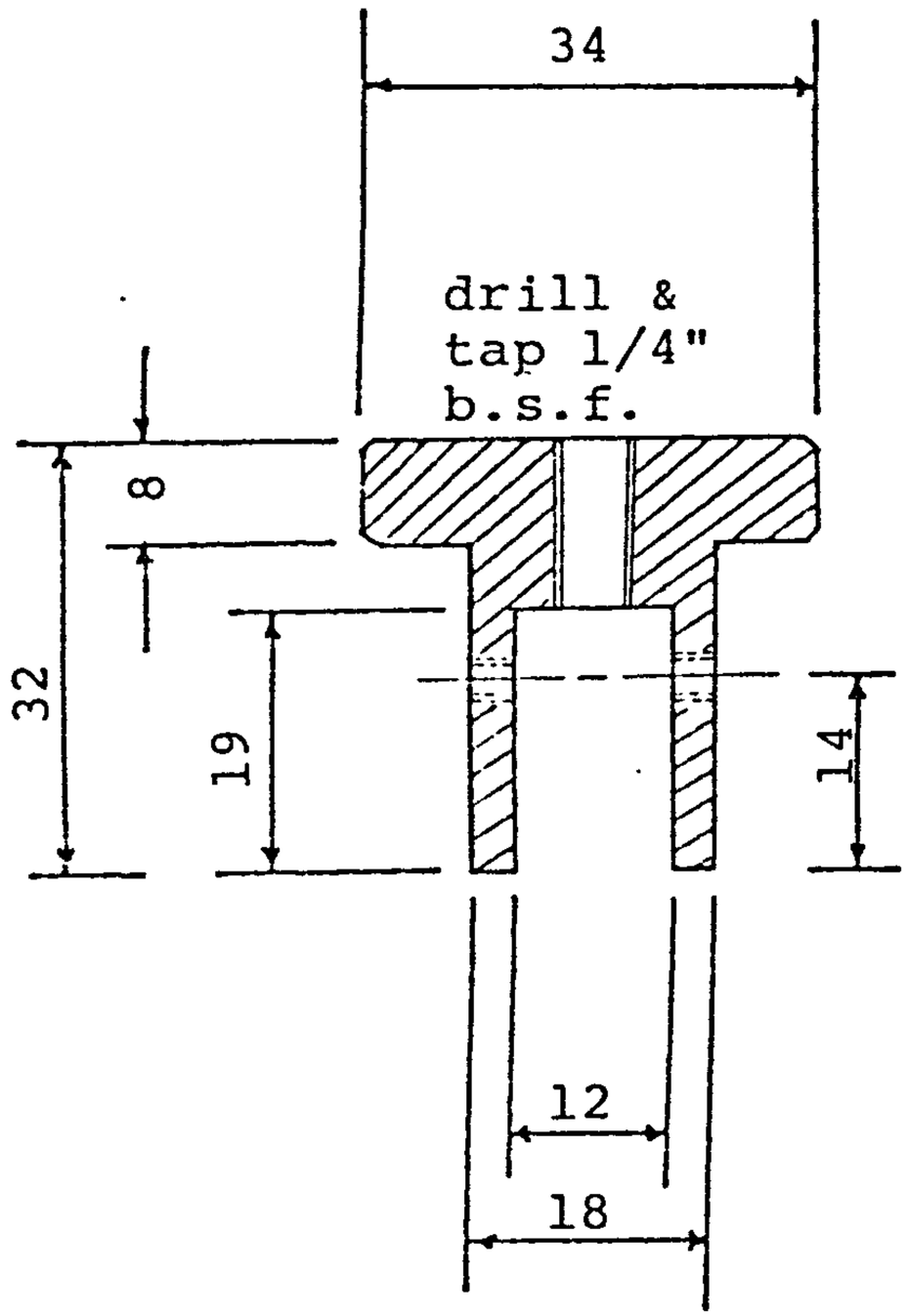

(DIMENSIONS IN MM)

CONTROL WHEEL

MATERIAL: BRASS

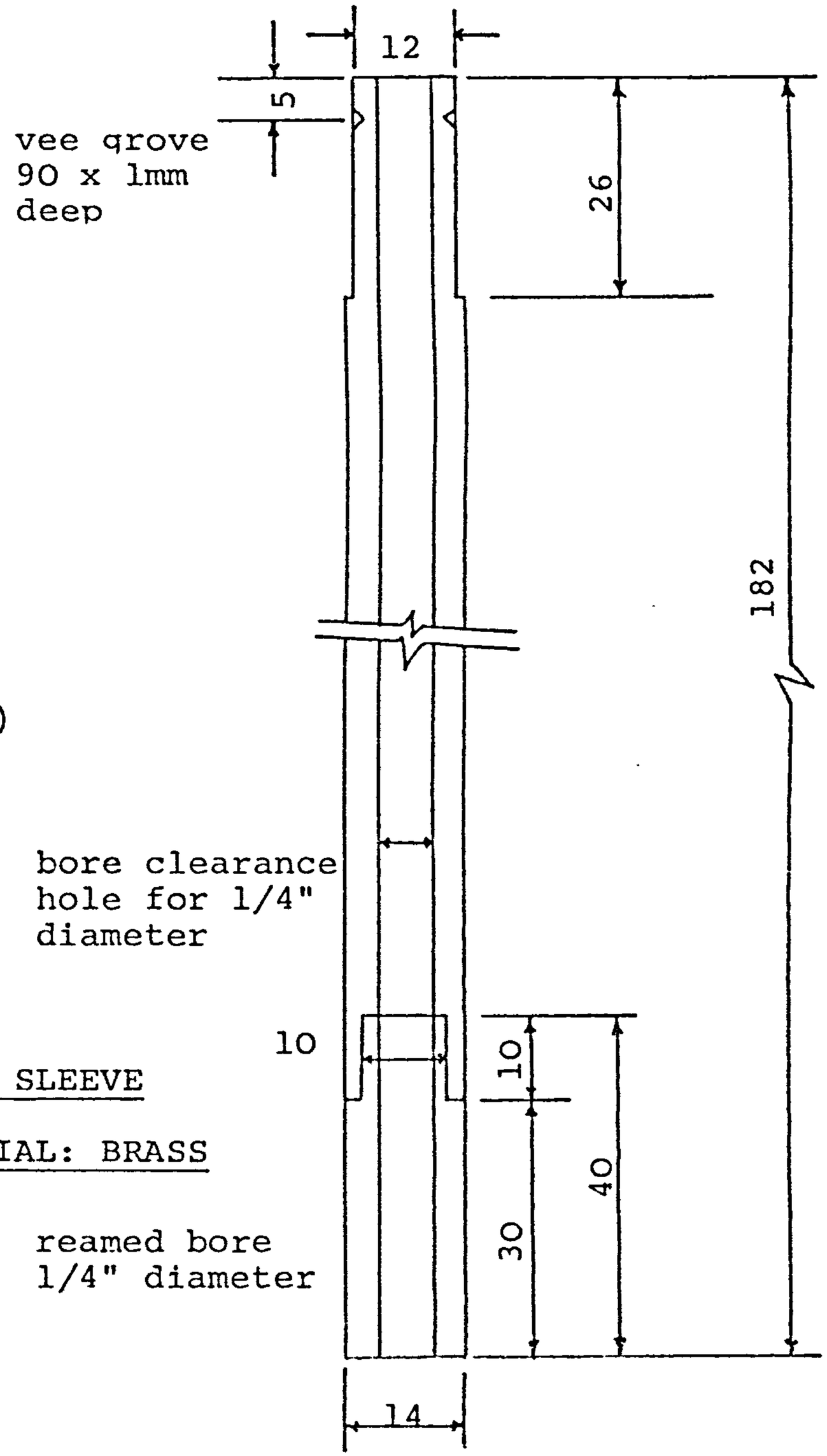

GUIDE SLEEVE

MATERIAL: BRASS

FIGURE 10.2 SAMPLING PROBE

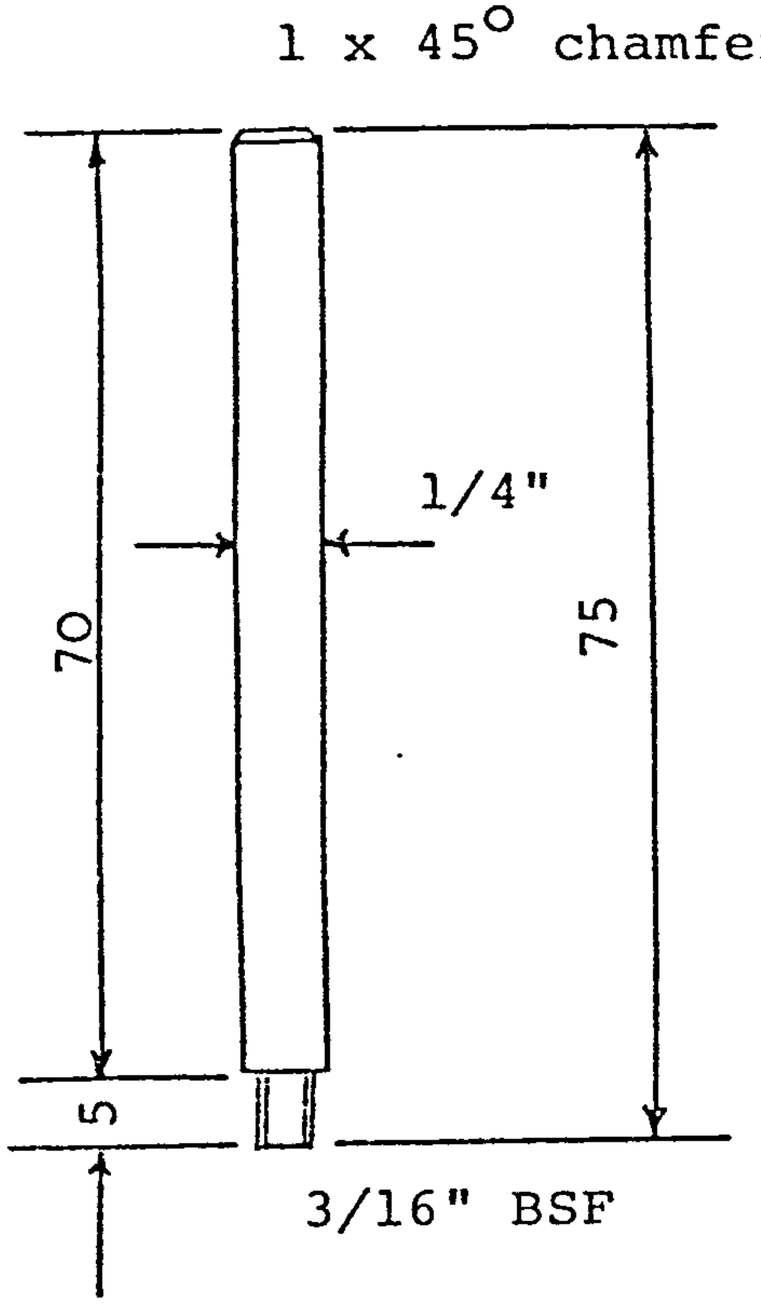

GUIDE ROD

MATERIAL: STAINLESS STEEL

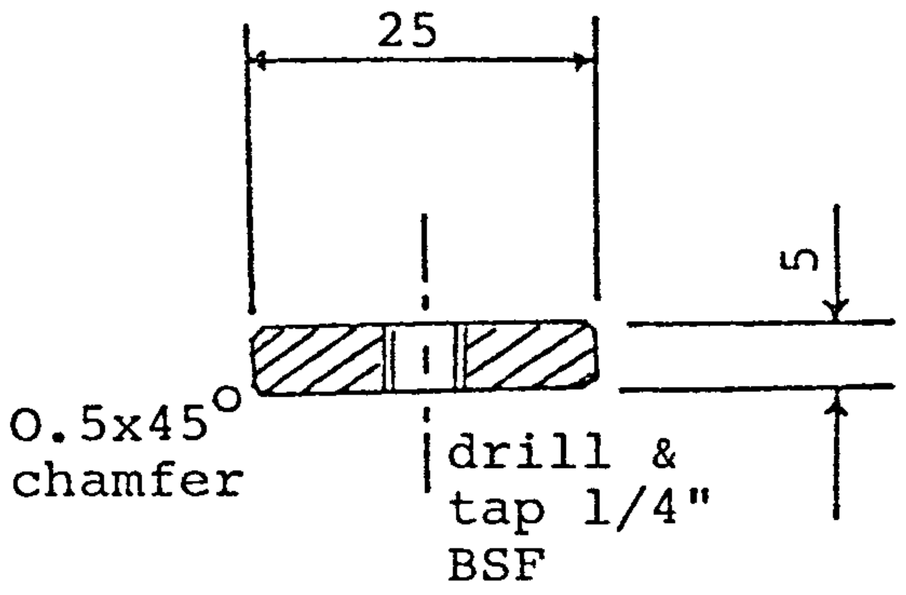

LOCK NUT

MATERIAL: BRASS

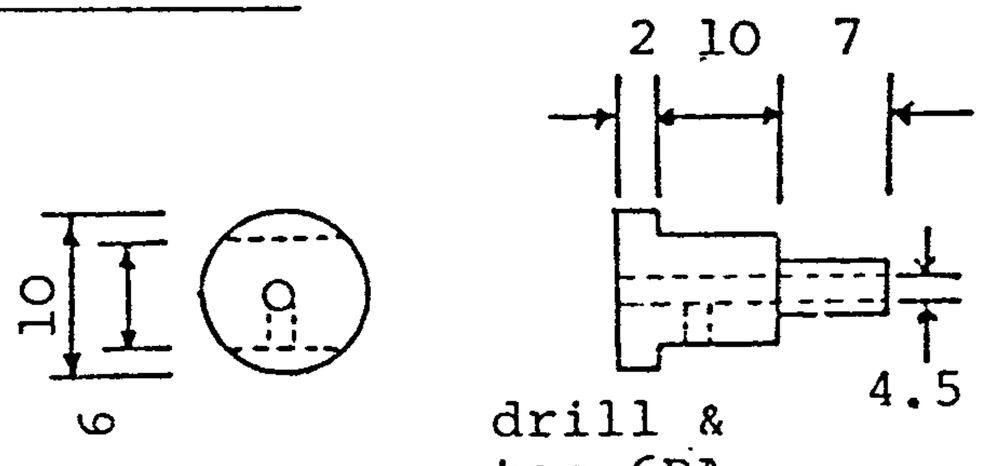

PROBE HOLDERS

MATERIAL: BRASS

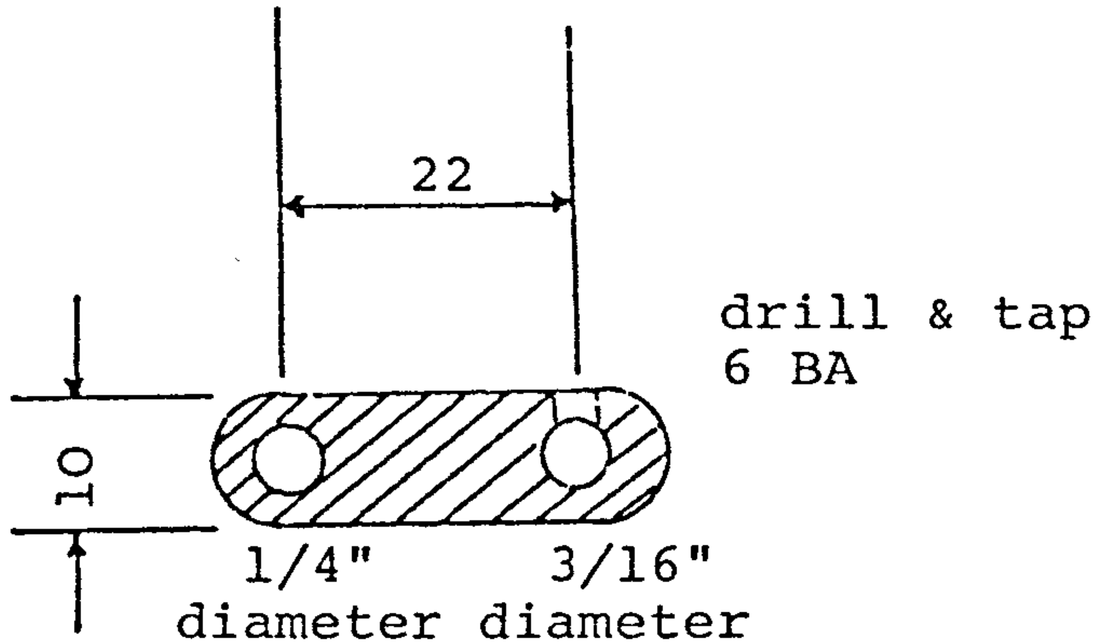

GUIDE LINE

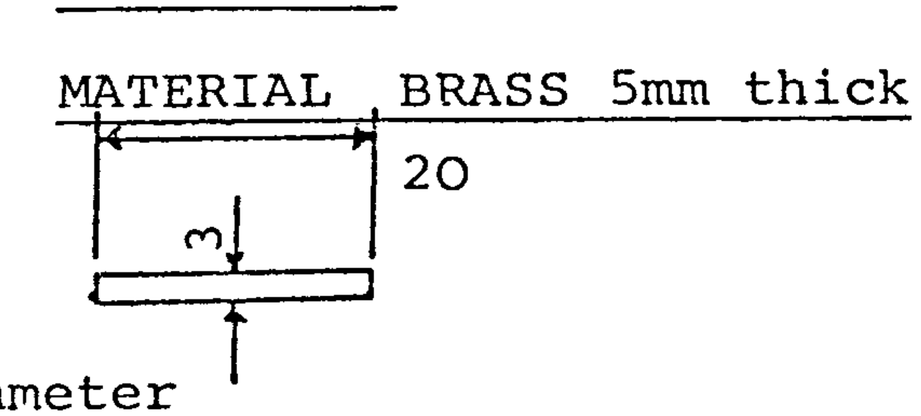

PROBE TUBE

MATERIAL: STAINLESS STEEL

(Dimensions in mm)

FIGURE 10.3 SAMPLING PROBE

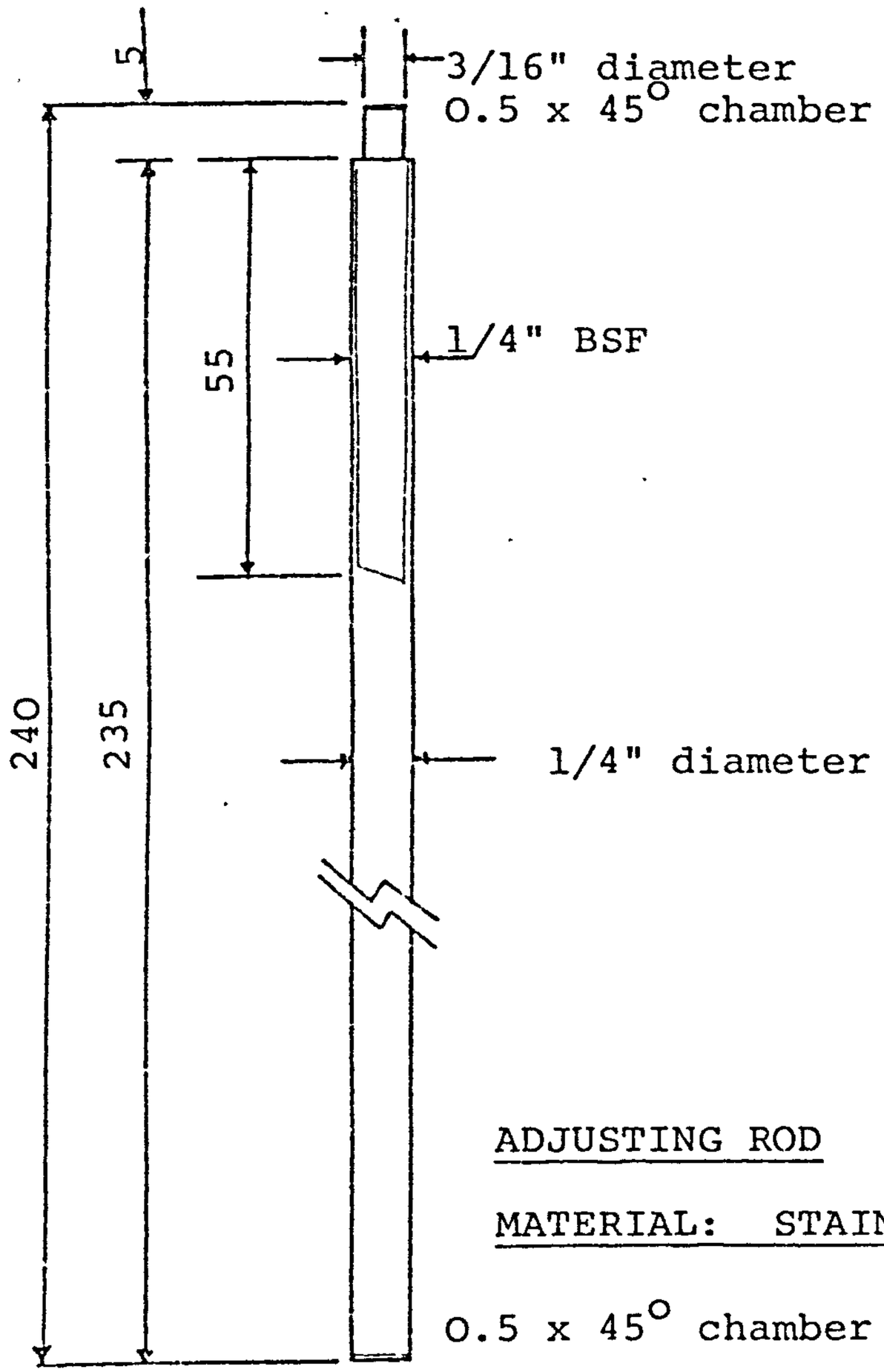

ADJUSTING ROD

MATERIAL: STAINLESS STEEL

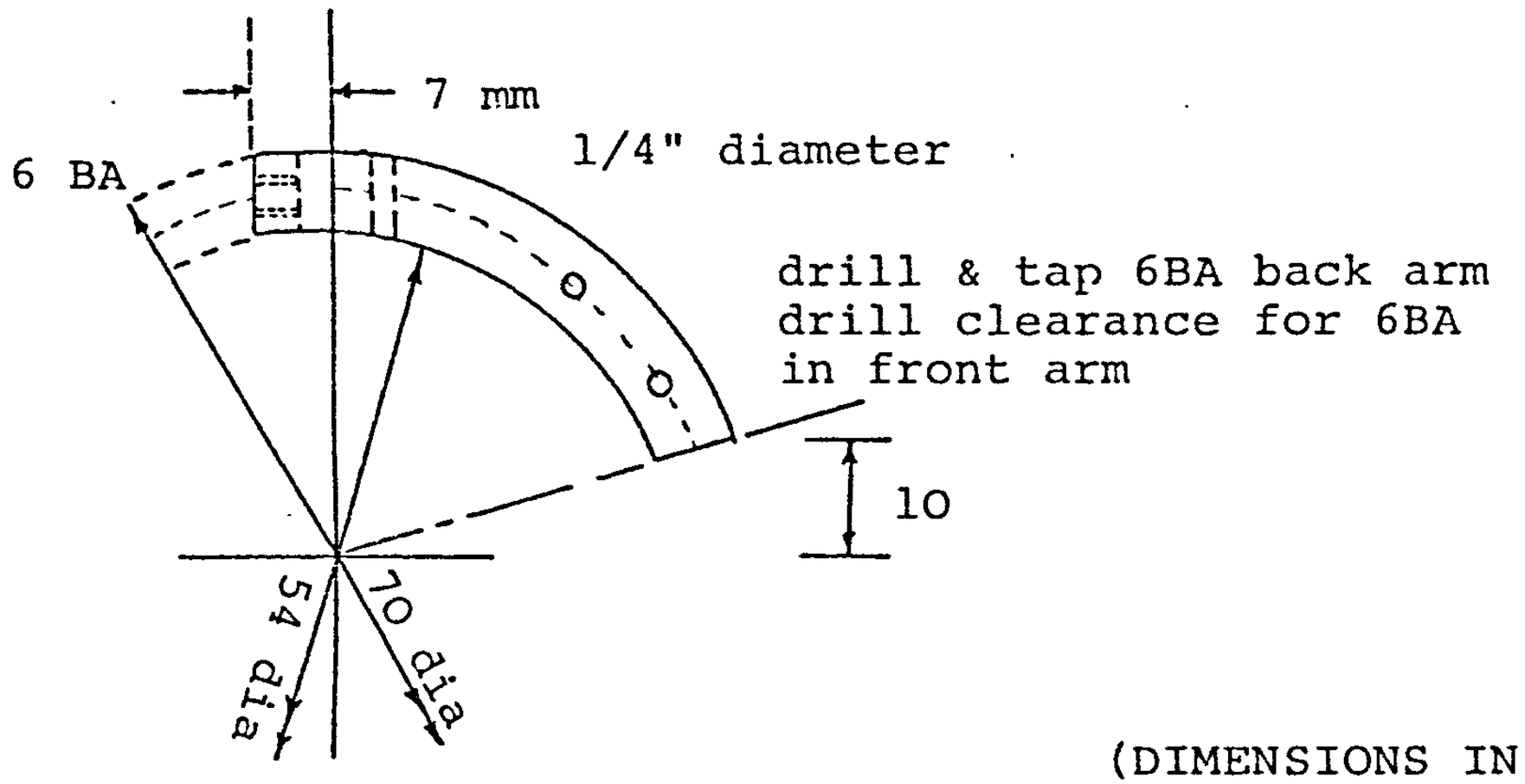

(DIMENSIONS IN MM)

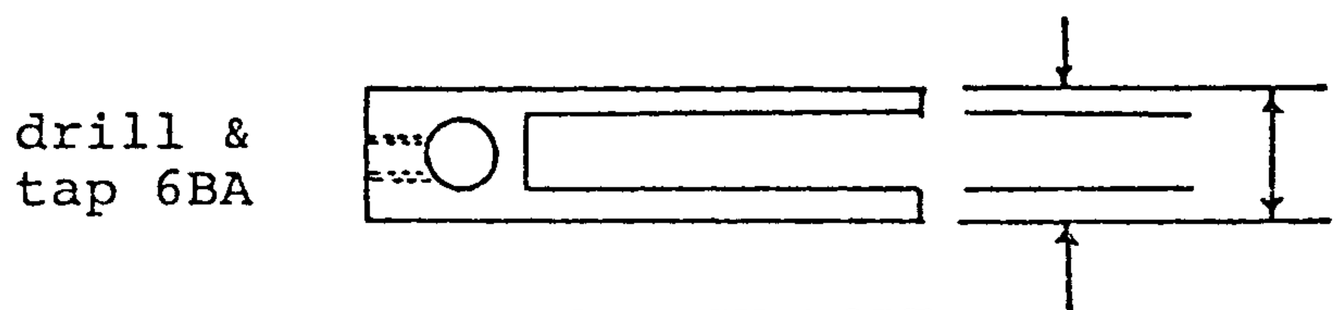

PROBE SUPPORT

MATERIAL: BRASS

FIGURE 10.4 SAMPLING PROBE

PHOTOGRAPH F

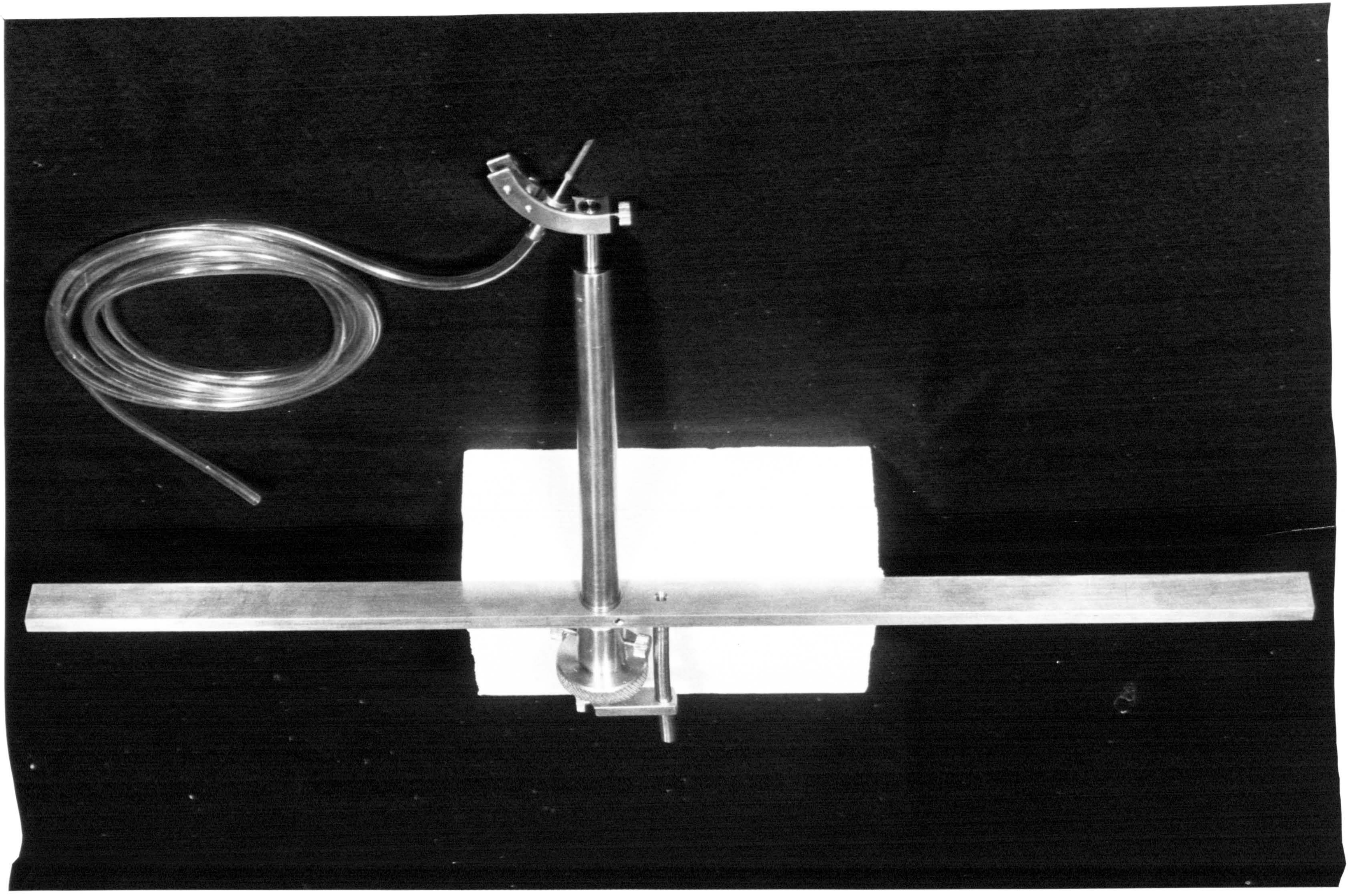

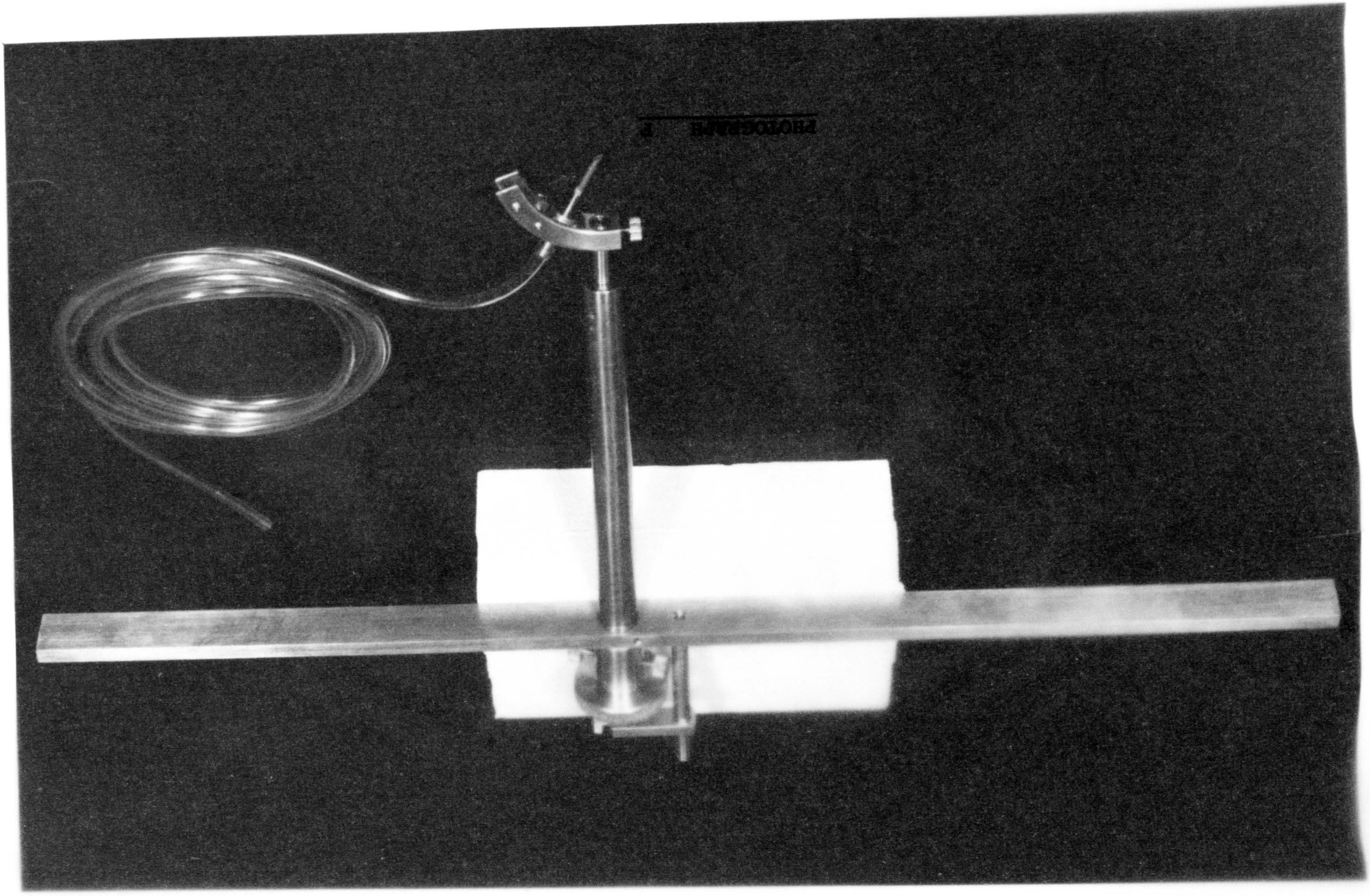
PHOTOGRAPH

PHOTOGRAPH G

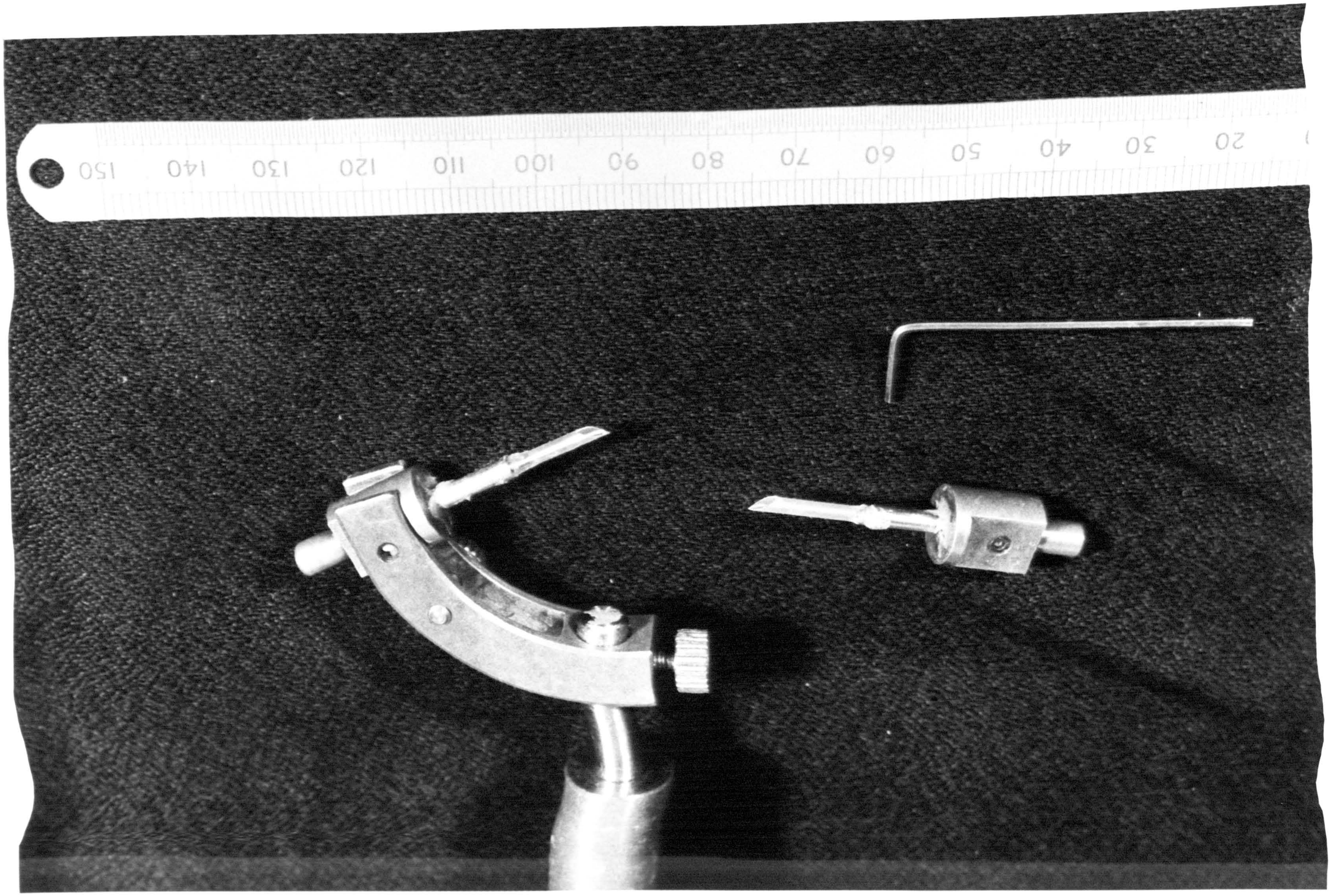

PHOTOGRAPH E

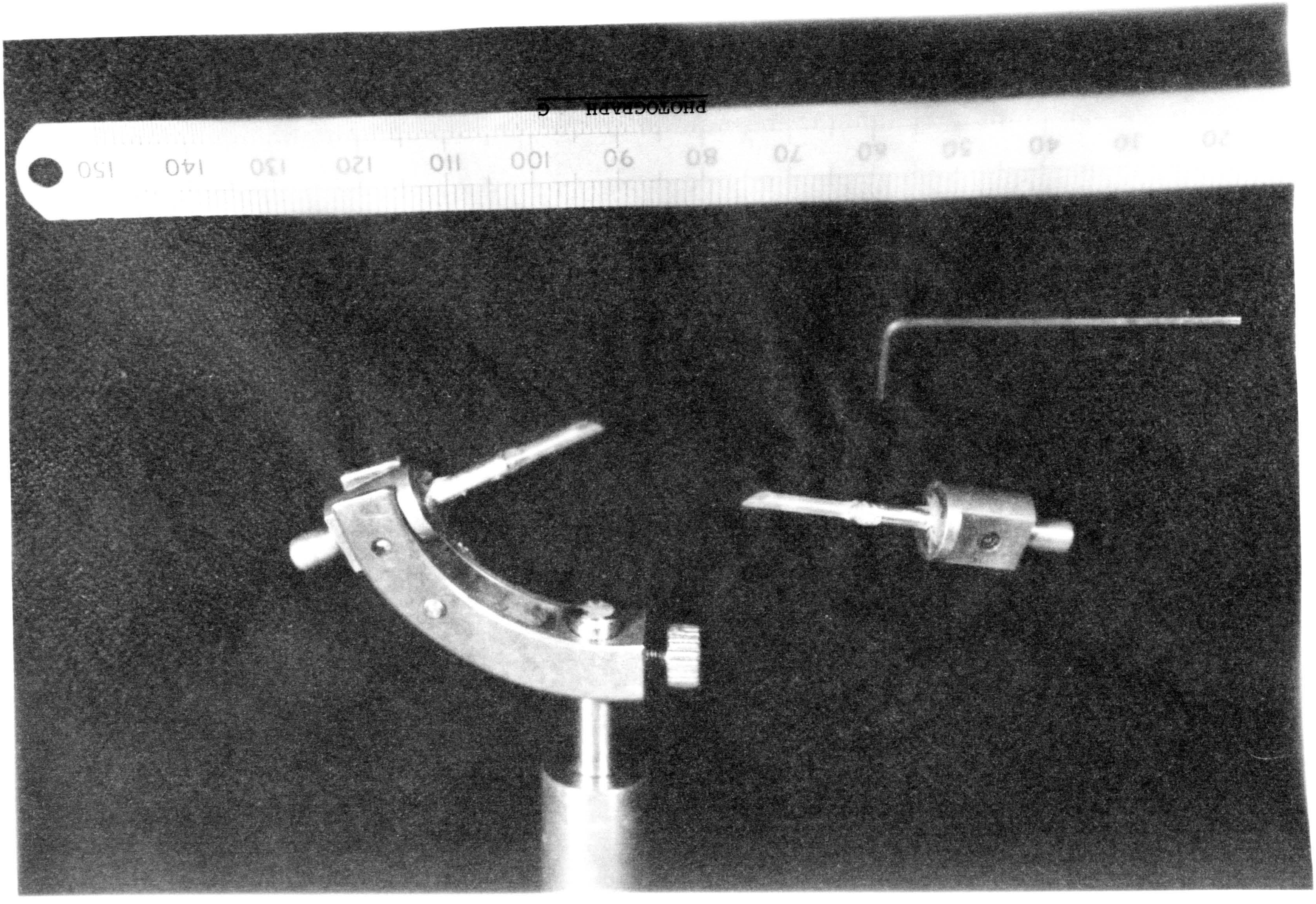

PHOTOGRAPH H

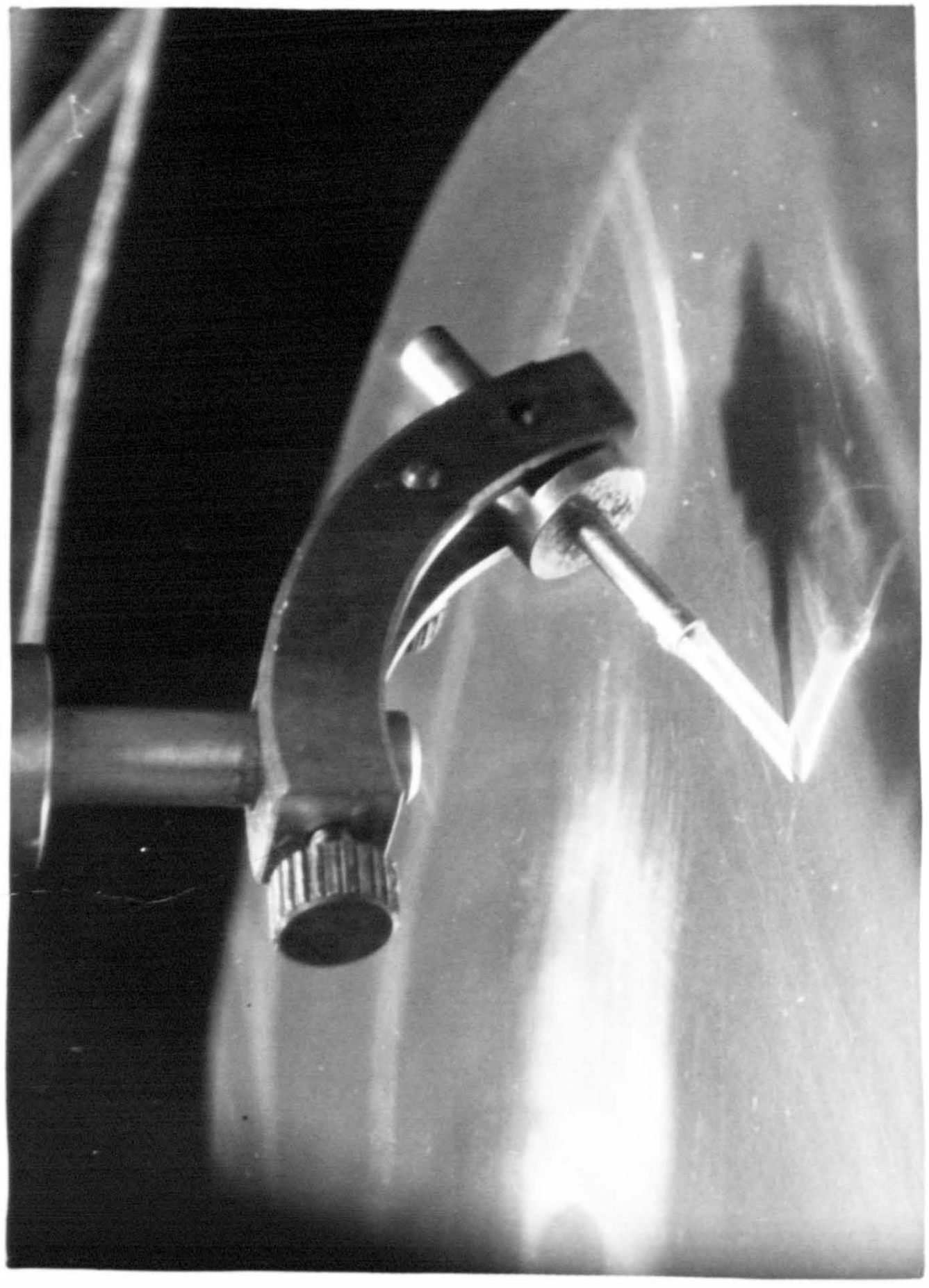

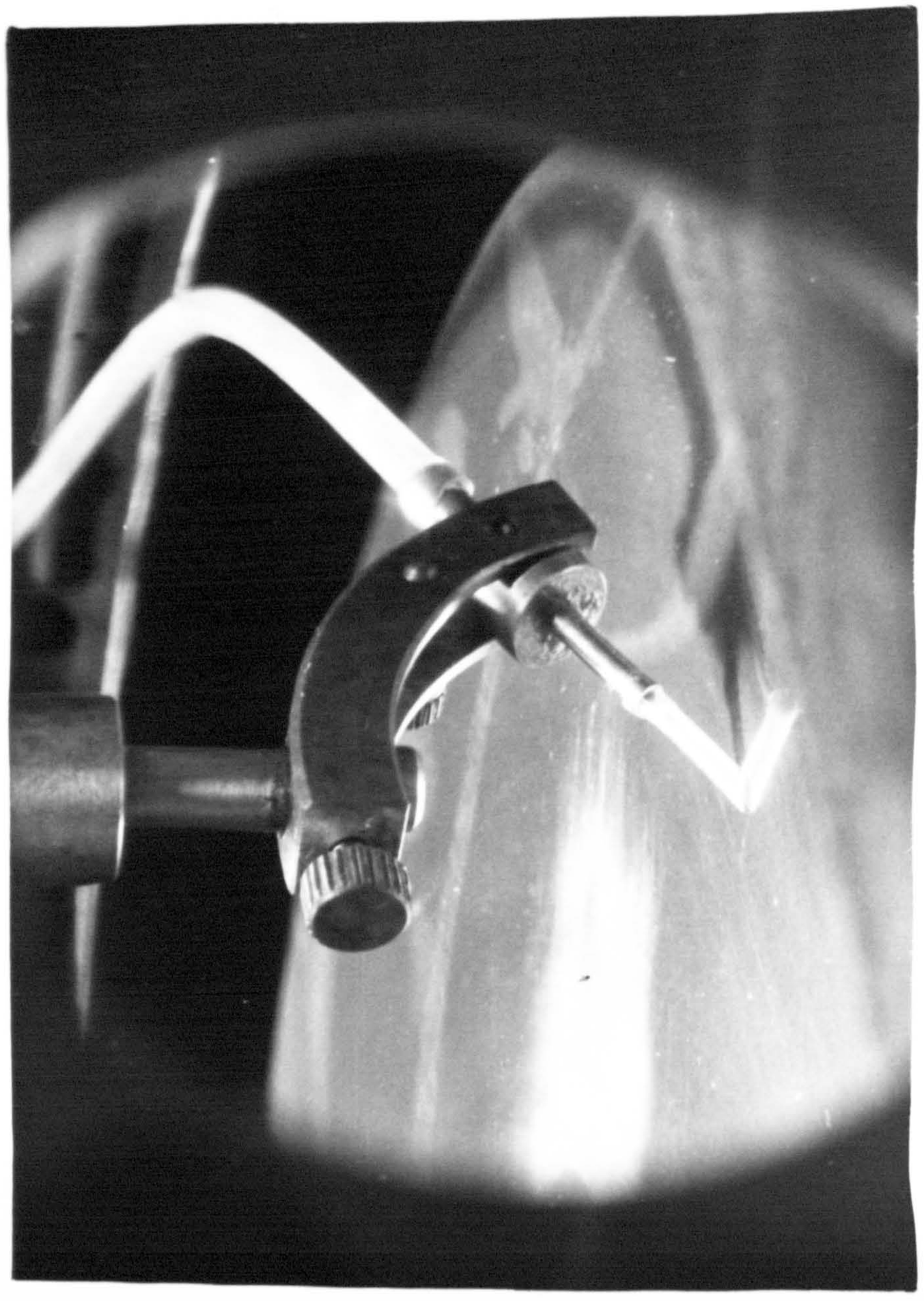

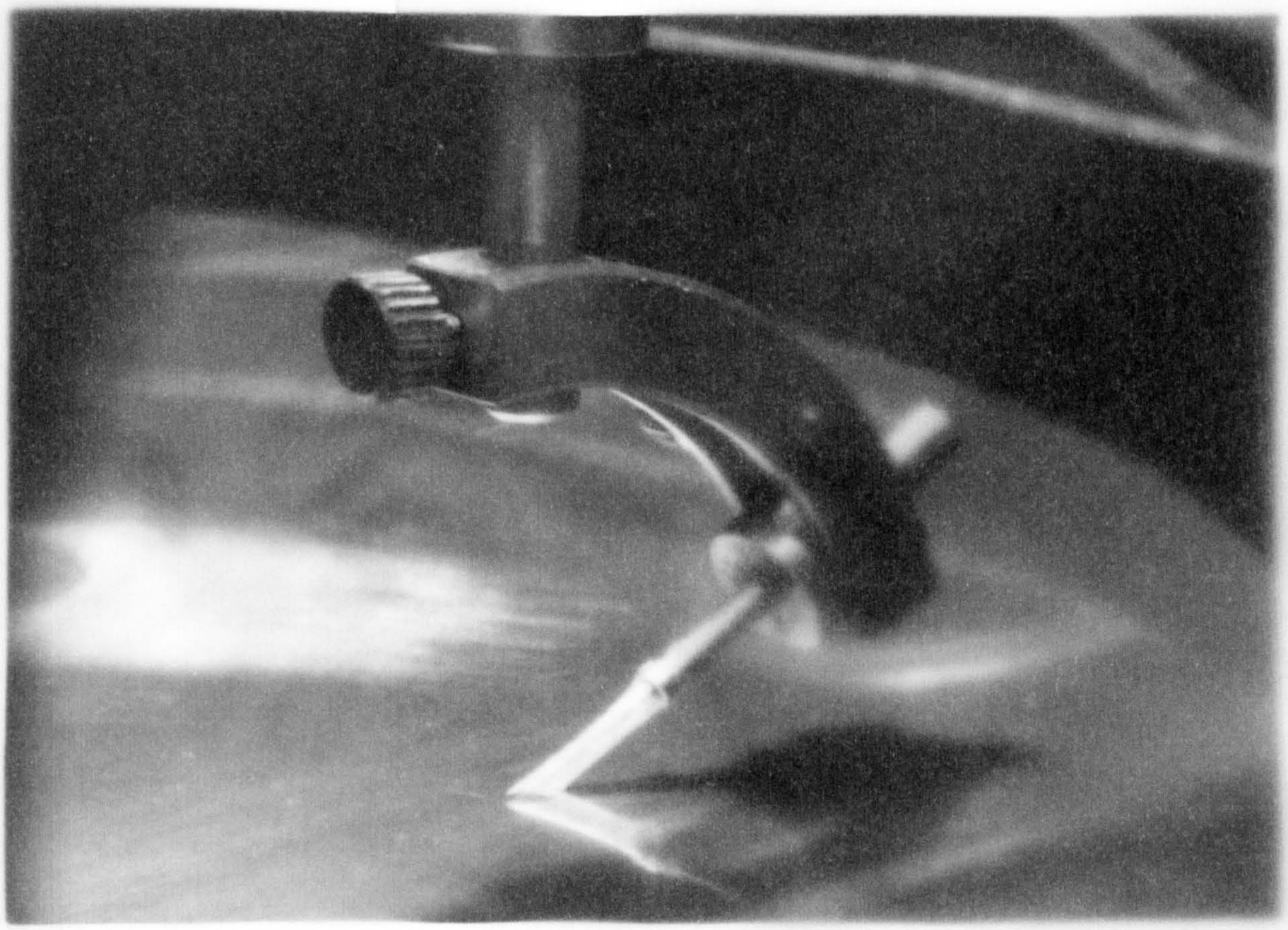

PHOTOGRAPH H

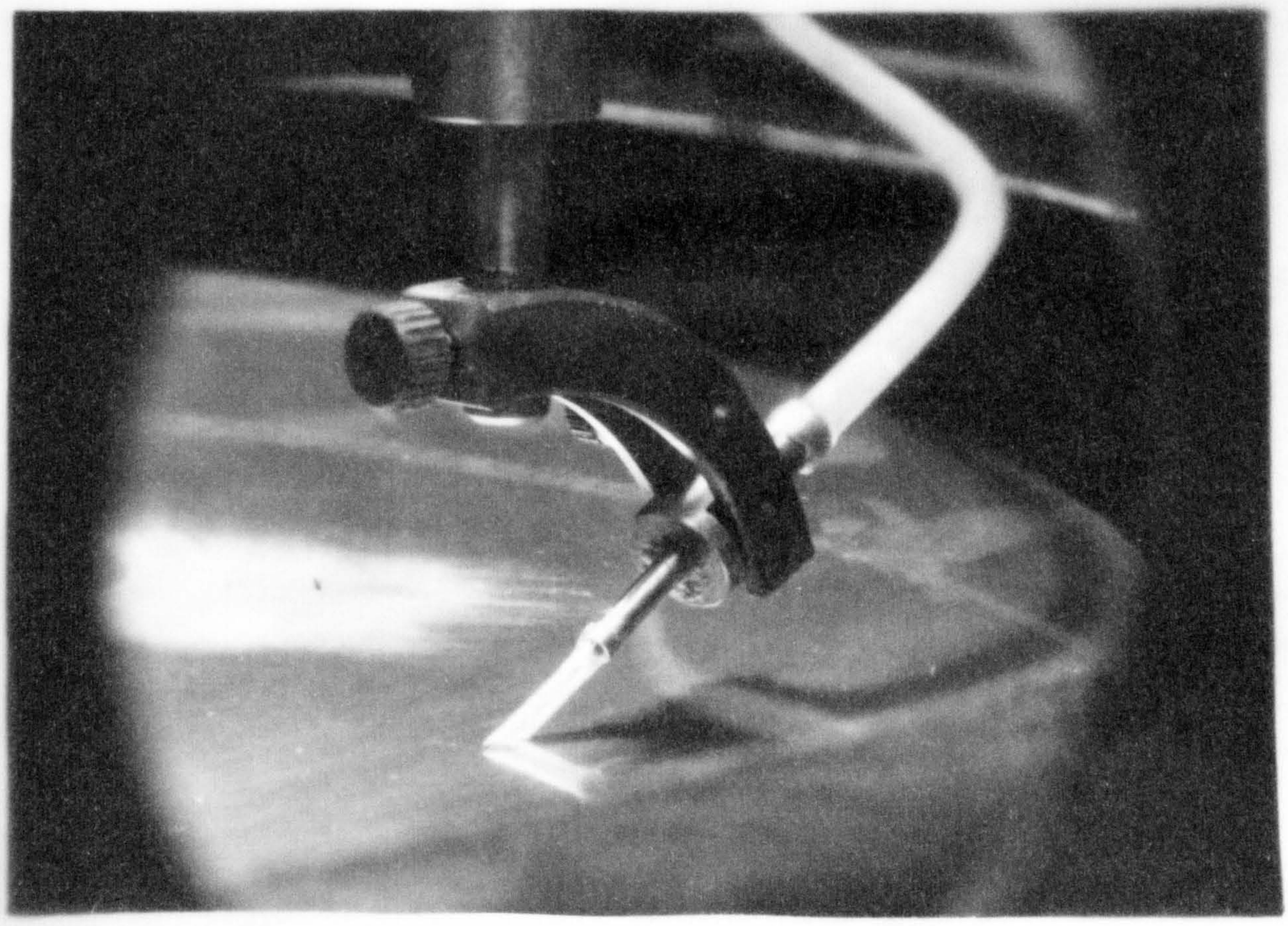

10.2.4 Oxygen Analyser

The oxygen analysers used in this study to determine the dissolved oxygen in the inlet and outlet solution are the Beckman model 0260 oxygen analyser. This analyser, which polarographically measured the partial pressure of oxygen and provides a voltage output with adjustable span from 0 to 100 millivolts for monitoring oxygen measurements. The sensor responds to the oxygen partial pressure by producing a signal that is amplified for readout on the meter and an output to the data logger unit. This analyser also has an auto read (automatic read) function that indicates when a stable reading is obtained.

In operation, when the sensor is placed in the sample, oxygen from the sample diffuses through the membrane, which separates the sample from the internal polargraphic cell. Diffused oxygen is reduced electrochemically in the cell, resulting in current flow proportional to the partial pressure of oxygen in the sample. The sensor, by its nature, consumes a small amount of oxygen in normal operation. Therefore, oxygen sample in the vicinity of the sensor tip must be replenished continuously to avoid inaccurate sensor response. When the sensor is first placed in the sample, the sample should be stirred to ensure proper equilibration between the sample and sensor. To satisfy the above mentioned requirements, a flow cell was designed to accept the sensor and a small magnetic follower in it to obtain a constant speed of liquid around the sensor (see Photograph I). The inlet and outlet of the flow cell are connected to two plastic (3 mm ID) stop cock to retain the sample of liquid. Since the electrical output is proportional to the partial pressure of oxygen in the sample, a point value is sufficient for the calibration line. The residual current observed in the oxygen-free medium can be suppressed by adjusting the zero control on the analyser.

OXYGEN ELECTRODE

CONTROL VALVE

STIRRER

PHOTOGRAPH I

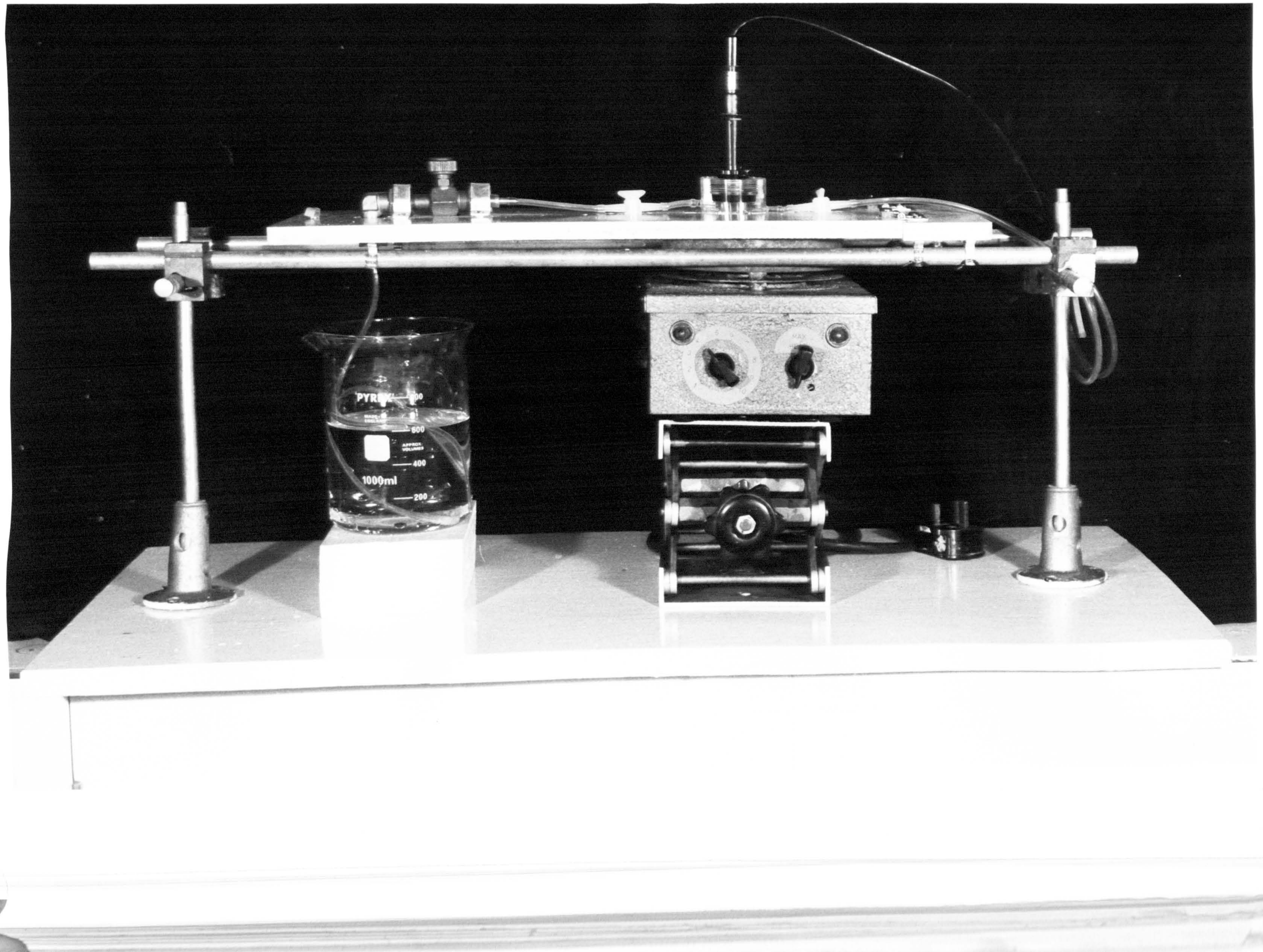
1000ml
600
400
200

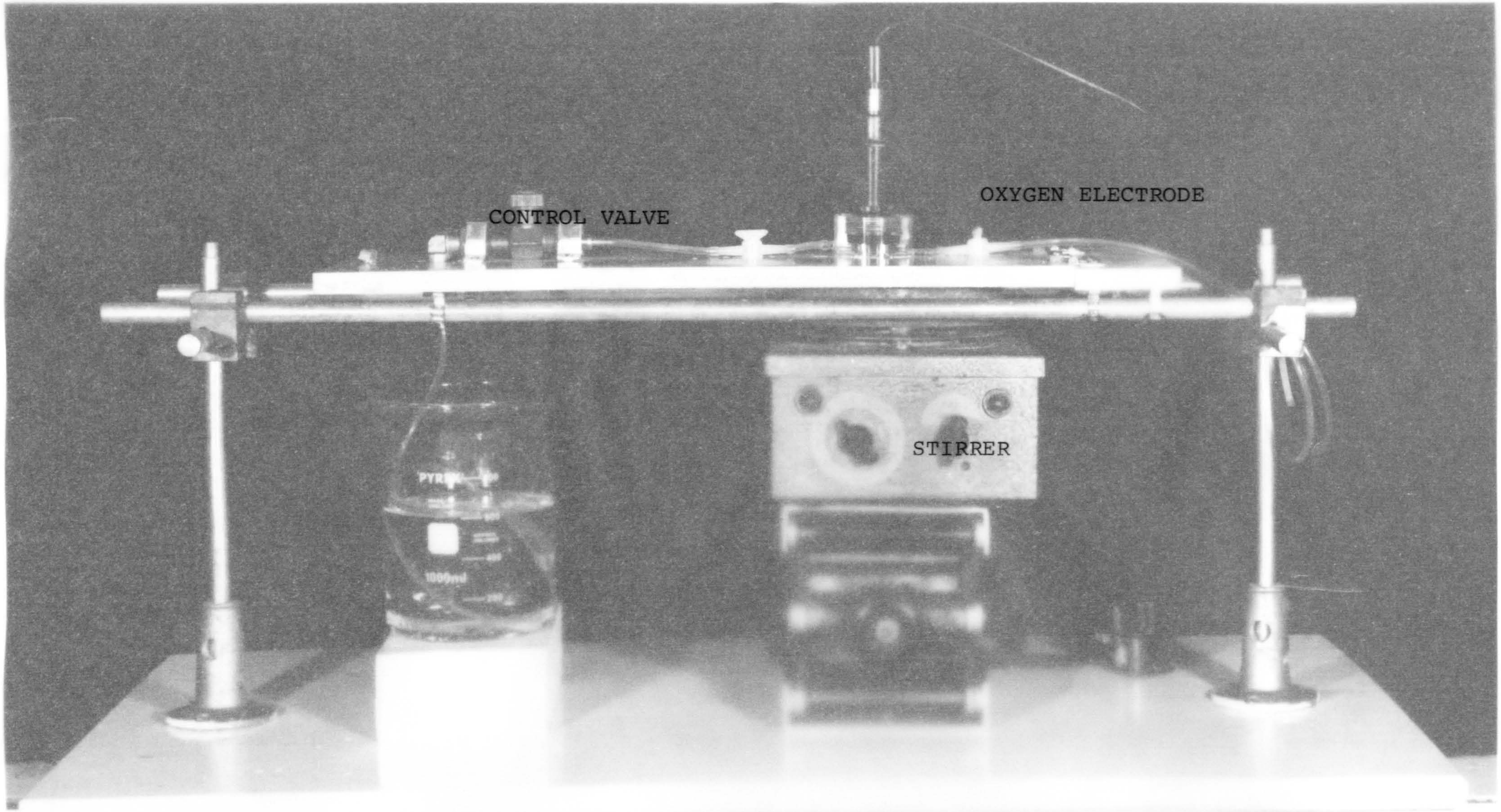

PHOTOGRAPH I

E/lO Oxygen Module and Electrode 21

The oxygen electrode 21 was inserted through a rubber bung and fitted onto one of the four corner holes on the chamber lid. This electrode measured the oxygen concentration in the gas phase to indicate whether any inert gas was being built up while the absorption run was being carried out. The principle of this analyser is similar to that of Beckman 0260 type. The output from the analyser was used to drive a potentiometric recorder for monitoring oxygen measurements in the absorption chamber.

10.2.5 Deoxygenation of Test Water

There are several ways in which deoxygenation of the water can be carried out. Since oxygen is only physically absorbed in the water, it can be removed by forcing nitrogen into the water which replaces the oxygen molecules. An alternative method involves adding an oxidising material which reacts with the oxygen in the water.

The oxygen level in the 50 gallon tank was reduced to near zero in this work by the addition of technical grade sodium sulphite (Na_2SO_3) and a cobalt salt acting as a catalyst. This reaction stoichiometrically requires 7.9 mg/l of sodium sulphite per mg/l of dissolved oxygen. Concentration of cobalt ion added as catalyst should be a minimum of 0.5 mg/l and should not exceed 1.5 mg/l. At this range of concentration the cobalt ion catalyses the reaction of sodium sulphite with dissolved oxygen, but does not interfere with the Winkler dissolved oxygen determination. Sodium sulphite requirements are based on the mean system saturation and the amount of excess chemical to be used. Normally 1.25 times the stoichiometric requirement is used, although tests have been conducted using from 95 to 200% of the stiochiometric. In this study, only the stiochiometric amount of sodium sulphite was added in each run, in order to avoid the complication introduced on the diffusion coefficient and mass transfer coefficient by the addition of salt as explained in Sections 9.5.1 and 9.5.2.

The temperature of the water in the 50 gallon tank was raised up to 25^{o}C with 3 kW immersion heater. Cobalt chloride was added in the form of cobalt chloride hexahydrate ($CoCl_2\ 6H_2O$) to achieve a Co^{+2} ion concentration of 0.5 mg/l. The stoichiometric amount of sodium sulphite was added to react with the dissolved oxygen and the resulting sulphate remain as inert dissolved material which does not take part in any further reactions. A peristaltic pump was used to obtain a continuous sampling from the tank with an oxygen analyser inserted in the line, to determine the oxygen concentration in the tank after the

stiochiometric amount of sodium sulphite has been added. Nitrogen was then introduced through two sintered metal cylinders (1" diameter x 12" long) immersed at the bottom of the tank for 1 hour to near complete deoxygenation of the test water.

10.3 PRELIMINARY RUN

The aim of this experimental run was to determine the angle of the sampling tube made with the surface of the rotating disc, at which continuous air free liquid samples, with minimum disturbance to the liquid film, can be obtained.

The sampling tube was chosen after trying a number of tube sizes and materials. A 1.9 mm diameter special Polyethelene tubing proved to be most satisfactory. This sampling tube was secured to a glass holder which served, at the same time, for measurement of the angle of the tube with the disc surface. The inlet end of the sampling tube was cut to an angle (varied from 30-70^{o}) and the cut faced into the film flow of the liquid. The cut, angled tubes were adjusted to make varying angles with the disc. This was to determine the angle at which the flow was disturbed least, and air-free samples were obtained. These angles were measured with a protractor lowered near to the glass holder and duplicated later for the mass transfer studies.

10.4 EXPERIMENTAL RUN

Tap water in the 50 gallon tank was adjusted to 25^{o}C by a 3 kW immersion heater and maintained within ± 0.5^{o}C of the desired value by a thermostat. Pump P1 was switched on to obtain circulation in the tank. In a mean time, a stiochiometric amount of technical sodium sulphite and cobalt chloride were prepared.

Dissolved cobalt chloride was added to the tank and followed a few minutes later by the sodium sulphite solution. Continuous liquid samples were withdrawn from the tank by a peristaltic pump to a pre-calibrated oxygen analyser in the line. The analogue output from the oxygen analyser shows the dissolved oxygen concentration in the tank. To ensure near complete deoxygenation of the water, nitrogen was introduced into the tank through two metal sintered cylinders (1" diameter x 12" long) immersed at the bottom of the tank for at least 60 minutes. The tank was covered with only a single outlet vent. During the experimental run, a continuous blanket of nitrogen was introduced above the liquid phase and the outlet vent was connected to an air-lock, which facilitated the tank being maintained at a pressure very close to atmospheric pressure.

The main air supply to the saturator was regulated down to 5 psi and stabilised with two flowstats before the gas rotameters. The volumetric flowrate was adjusted and kept at 10 litres/min and maintain at the same temperature as the liquid film to prevent the vaporization of the liquid film into the gas phase in the absorption chamber. This minimised the gas phase resistance in the mass transfer studies. Pre-saturated air in the absorption chamber was maintained at the desired temperature of 25 ^{o}C. By preventing heat loss through the brass absorption chamber to the surroundings,the chamber was surrounded with several heating coils controlled with a voltage regulator.

Calibration of the inlet and outlet oxygen analysers was carried out while the above procedures were in progress.

A constant temperature bath, kept at 25^{o}C, was saturated with air (21% oxygen) and another separate 5 litre container was depleted of oxygen (similar conditions to that of tank 1). Transparent flexible polyethene tubing (1/8" diameter) was connected to the flow cell a few feet below the two containers. By natural siphoning, samples of liquid can be drawn from the containers respectively to the flow cell. The flow cell with inlet and outlet valves rests on the top of a magnetic stirrer as shown in Photograph I. This ensured a constant volume of sample being retained and kept at a similar condition, that is the same stirrer speed. Initially, problems arose with bubbles being trapped in the flow cell, which introduced error. These were difficult to remove. To eliminate such a problem the flow cell was redesigned with the outlet valve higher than that of the inlet and the whole platform was hinged, enabling it to move 140^{o} anticlockwise.

For calibration of the electrode, the flow cell was flushed with deoxygenated water for a few minutes with the fine control valve totally open. A sample was taken by closing the inlet and outlet valves of the flow cell. When the analyser meter showed a steady reading, the zero control was adjusted till the digital output on the meter was reading zero. This was repeated to ensure a correct zero setting. The output from the meter was logged on paper tape by the Department's data logging system. Similar runs were carried out for the saturated liquid and the meter reading was adjusted to the desired reading corresponding to the pre-determined oxygen concentration in the liquid.

The duplicated angle and the cut front of the sampling tube for a particular run was set to the probe holder. All joints were sealed with vacuum seal. The sampling tube connected to the oxygen analyser via a probe holder by means of intramedic polyethylene tubing which allowed visual observation of the liquid sample. Before the experimental run, the polyethylene tubing and the flow cell were filled with deoxygenated water for the siphoning purposes. Thus, carefully

applying suction to the sampling tube, it was possible to draw continuous air free samples from the disc. The liquid sampling rate was controlled by a fine valve located on the discharge side of the flow cell.

Normally during a run the speed of the disc was maintained at a constant value while the flow rate was varied over a desired range. This was due to the fact that once the flow rate was changed to a new value, it reached this new value almost instantaneously, whereas the speed of the disc tended to increase slowly before reaching a new steady value. Thus, in the course of a run during which the speed of the disc was kept constant, the water flow rate was varied from minimum to maximum range (60.5 cc/s).

When the absorption chamber was completely filled with saturated air (at 25 $\pm 1^{o}C$) and maintained at a steady reading as indicated by the E1/O oxygen analyser on a telsec recorder, the run commenced.

The motor driving the disc was switched on and the speed of the disc was measured with a tachogenerator indicated on a digital volt meter. When the speed reached a desired steady value, the water flow on the disc was started and maintained at a particular rate. The temperature throughout the system of gas and liquid phase was kept at 25 $\pm 1^{o}C$.

The cut front of the sampling tube was lowered and oriented in such a direction of the liquid film (as pre-described in Section 10.3) that provided a minimum disturbance and continuous air free samples to be obtained in the polyethylene tubing. Samples were taken into the flow cell when a completely bubble-free flow was maintained in the line. When the oxygen meter showed a steady reading, all the required data were recorded on the data logger system. For different values of the variables, the liquid feed rate, radius across the disc and the rotational speed of the disc, an identical procedure was carried out.

From time to time, and at the end of the run, the original calibrations of the oxygen analysers were rechecked. This was done to make sure that there was no drift in the readings of the meters. The oxygen concentration in the absorption chamber was also checked frequently on the telsec recorder. This would determine any build up of inert gas in the absorption chamber.

At the end of the run, the water flow onto the disc and the air supply to the absorption chamber were stopped. The disc was left running for a while to expel any liquid in the distributor.

11 RESULTS AND DISCUSSION

Some three hundred measurements of mass transfer were made and the results of these experiments are presented in tabular form in Appendix G. In all cases oxygen was absorbed from air to water films flowing across the disc, the absorption chamber containing the air was maintained at $25 \pm 1^{o}C$ and atmospheric pressure in all experiments. The range of system parameters investigated is given below.

Flow rate	14.5	< Q <	60.5	cc/s
Rotational speed	24.2	< W <	117.3	rad/s
	230	< N <	1120	rpm
Radial position	60	< r <	180	mm

The experimental runs were generally accompanied by slight variations of temperature ($\pm 1^{o}C$), and therefore absorption rates were corrected to the reference temperature of $25^{o}C$. These small corrections were based on the models for absorption presented in section 9.6 which indicate that the mass transfer rate is proportional to the saturation concentration C*, diffusivity of oxygen in water D, and the kinematic viscosity of the liquid ν, in the following manner,

$$\text{Mass transfer rate} \sim C^{*}\, D^{1/2}\, \nu^{-1/6}$$

The maximum value of the correction required for the specified temperature variation was found to be ±1.5 %.

The basic experimental data for mass transfer into a liquid film as it flows across the radius of the disc are show in Figures 11.1 to 11.6 inclusive. Each of these graphs shows the effect of liquid film flowrate (in the range 14.5 to 60.5 cc/s) on the rate of oxygen absorption into the liquid at a particular disc speed. In all cases the

line denoted by (2) represents mass transfer occuring between the nozzle and the edge of the disc, whilst the line (3) shows mass transfer occuring between the nozzle and the collecting ring. Therefore (3) includes mass transfer into the liquid in film flow on the disc, plus mass transfer in the spray between the edge of the disc and the collecting ring. The graphs also include a line representing one of the theoretical models, Equation 194 (page 124) the so called 'crude' model. The scatter in these data for mass transfer on the disc (2) at low rotational speeds, Figures 11.1 and 11.2, reflects the diffuculty in achieving the efficient collection of samples with the pickup probe. Under these conditions the liquid velocity at the probe inlet was usually insufficient to induce an adequate, steady flow through the measuring section. In all experiments it was necessary to use the syphoning effect to produce this flow; however at low disc speeds (<400 rpm) this presented a difficult problem, since the flow was controlled manually using needle valves. The measurement of liquid samples taken from the collecting ring did not present any such problems, since the sampling probe was completely submerged in a low velocity stream under all operating conditions.

Returning to the detailed discussion of Figures 11.1 to 11.6, these graphs exhibit a number of interesting characteristics. Figure 11.1 shows that at the lowest disc speed and flowrate used in these experiments the mass transfer to the spray at the edge of the disc represents a significant contribution to the total oxygen transfer to the liquid. At rotary speeds up to about 600 rpm the contribution to mass transfer provided by the spray increases with increasing flowrate. At rotary speeds in excess of 600 rpm the mass transfer across the disc surface becomes progressively dominating, until at the maximum disc speed of 1110 rpm (Figure 11.6) the liquid is virtually saturated when it

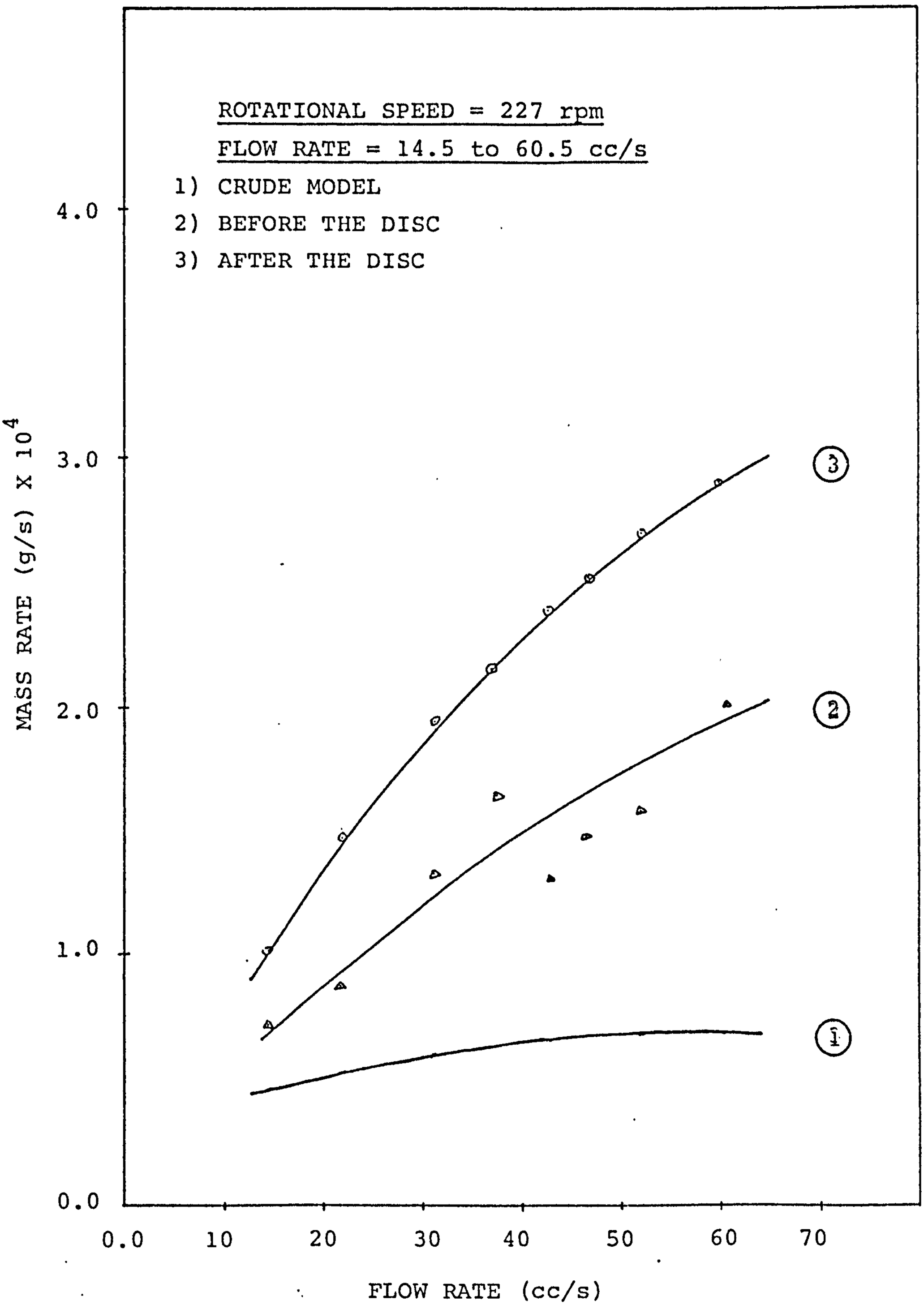

FIGURE 11.1 MASS TRANSFER RATE BEFORE AND AFTER THE DISC

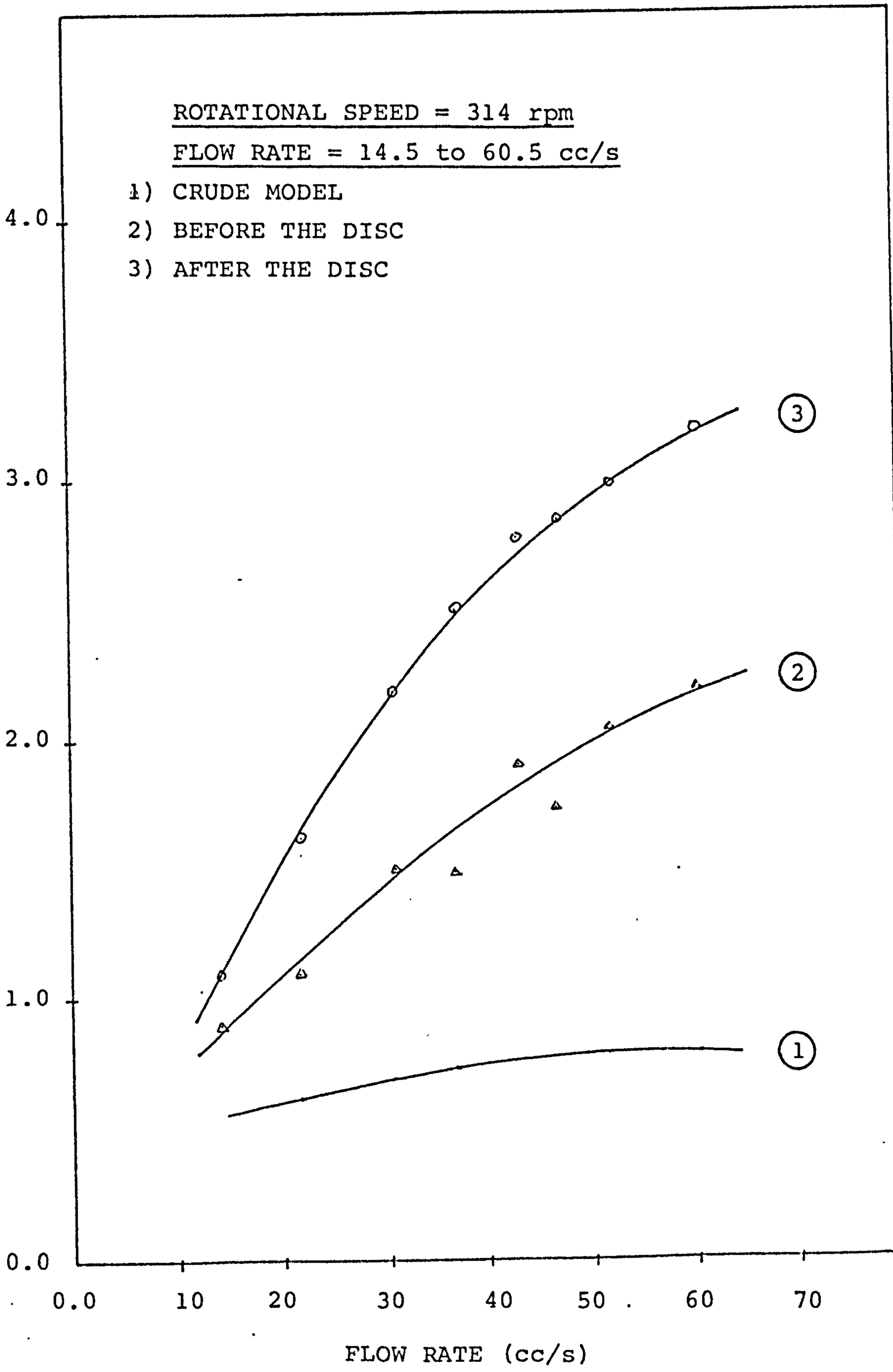

FIGURE 11.2 MASS TRANSFER RATE BEFORE AND AFTER THE DISC

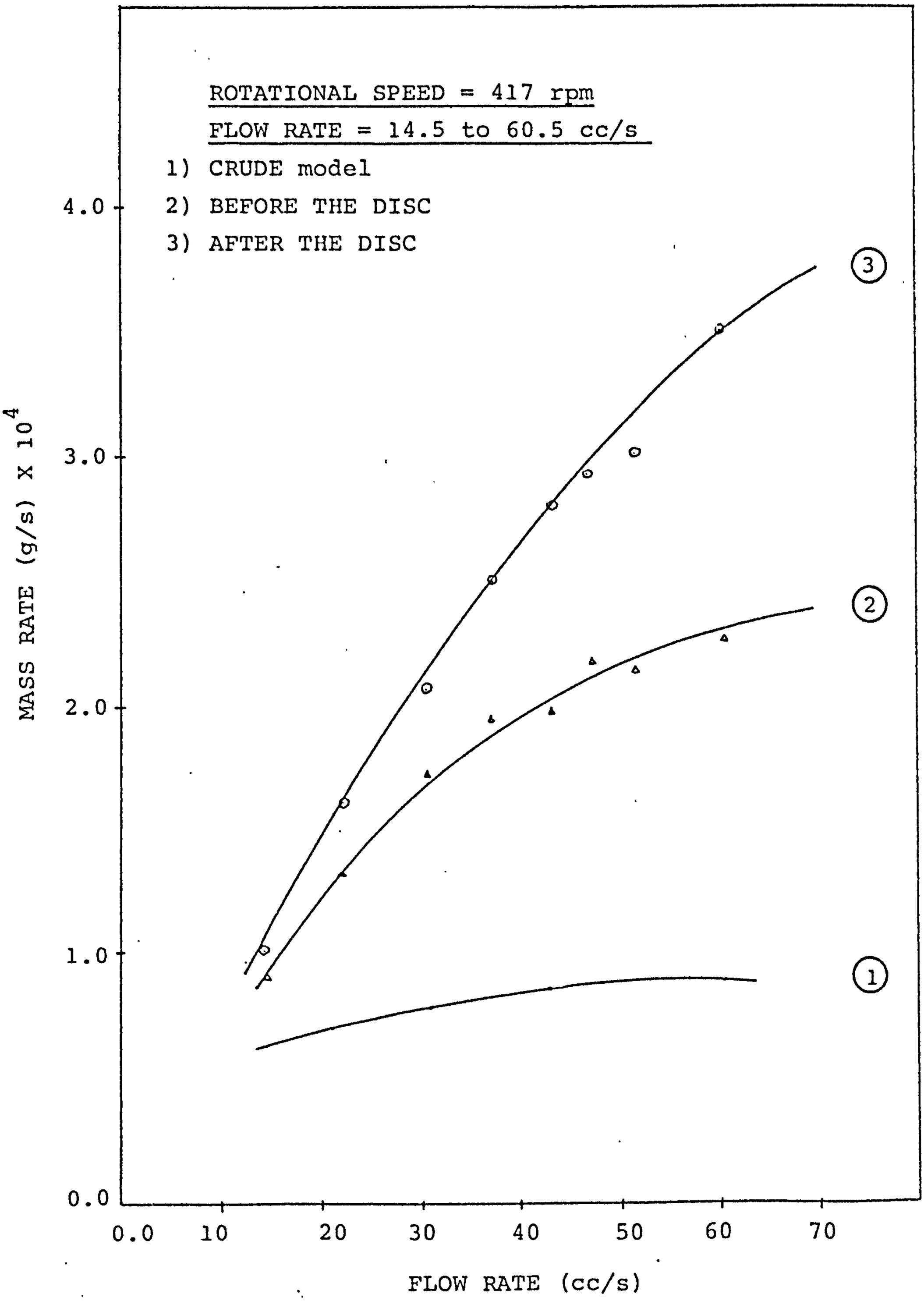

FIGURE 11.3 MASS TRANSFER RATE BEFORE AND AFTER THE DISC

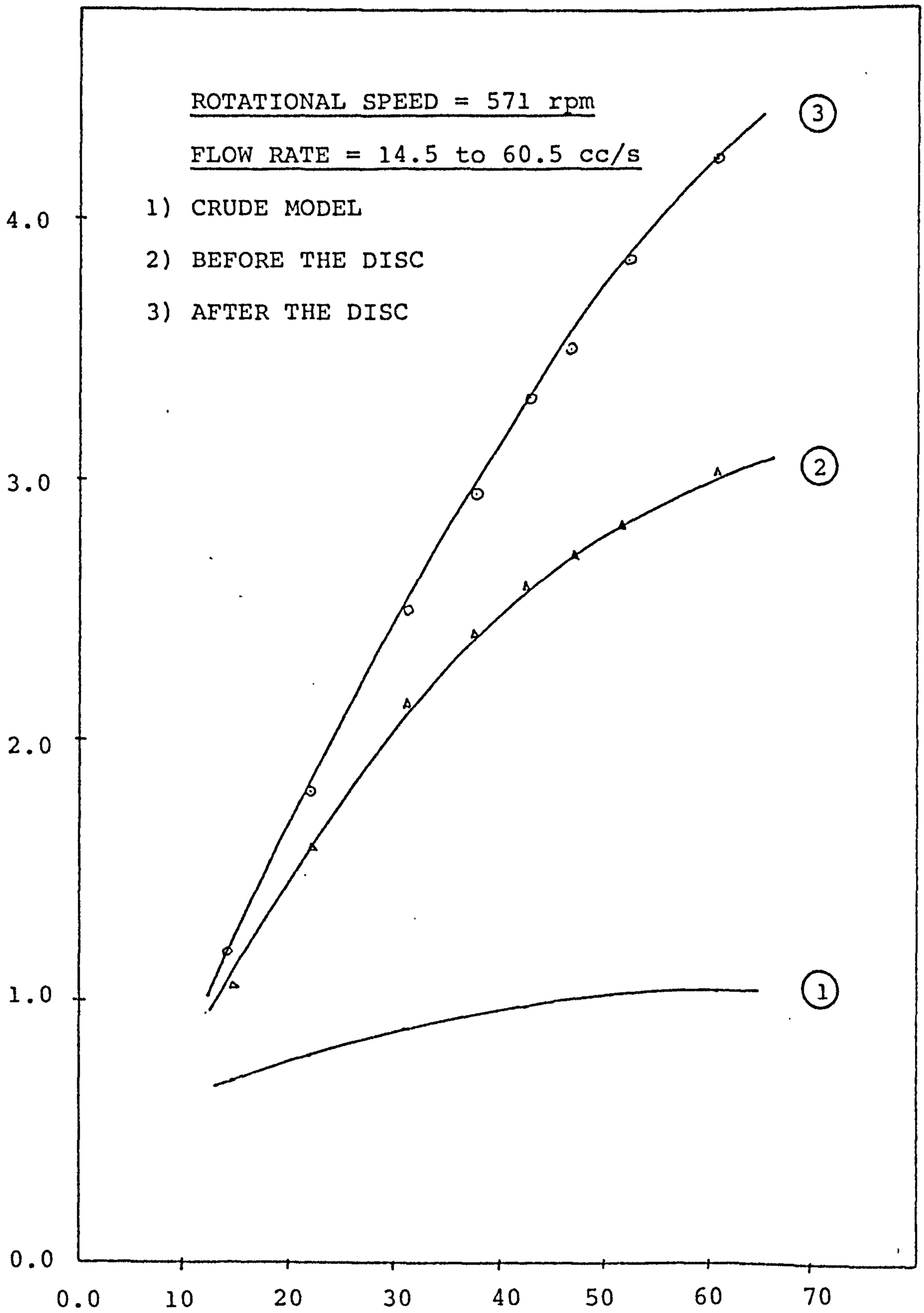

FIGURE 11.4 MASS TRANSFER RATE BEFORE AND AFTER THE DISC

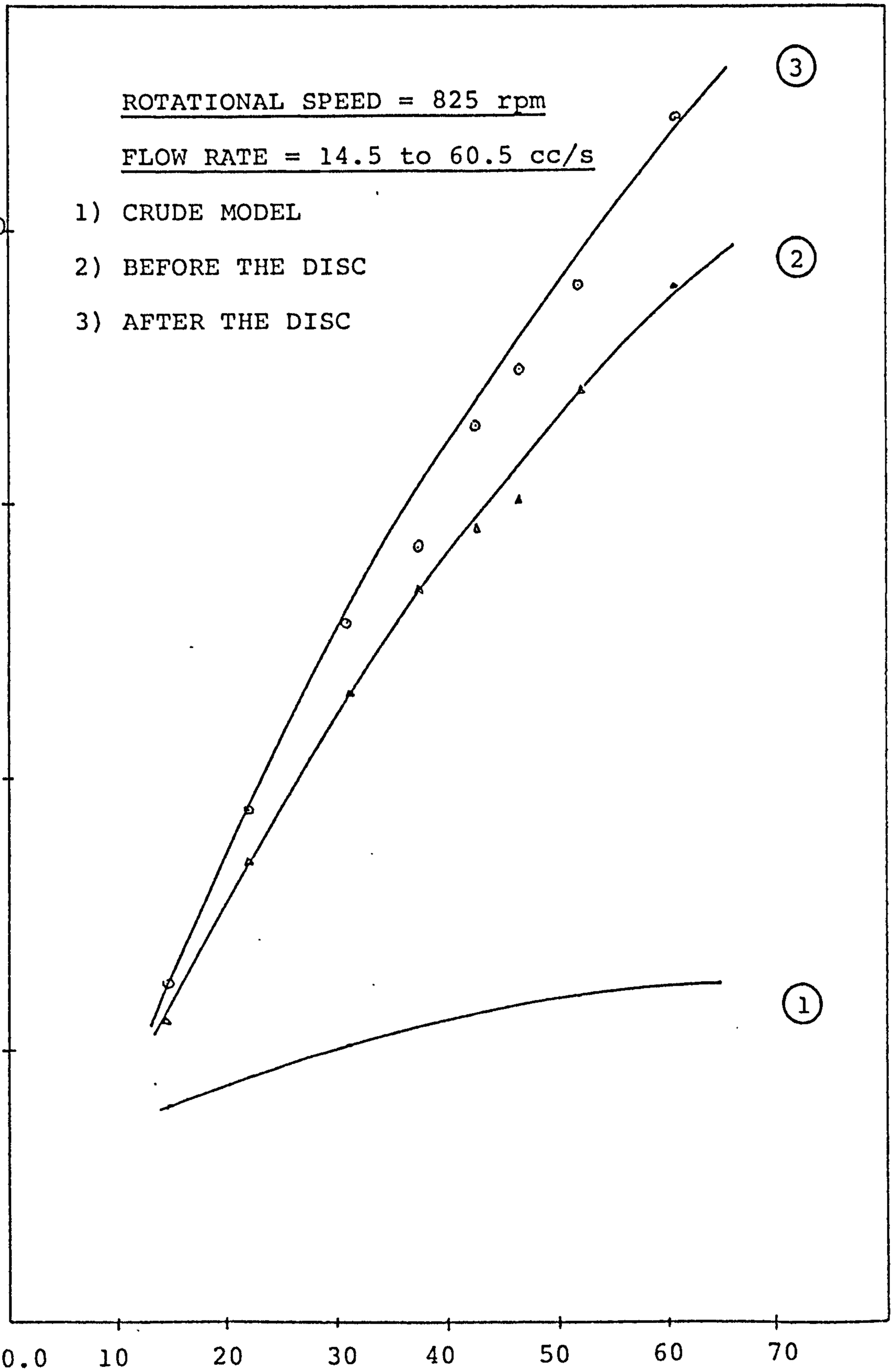

FIGURE 11.5 MASS TRANSFER RATE BEFORE AND AFTER THE DISC

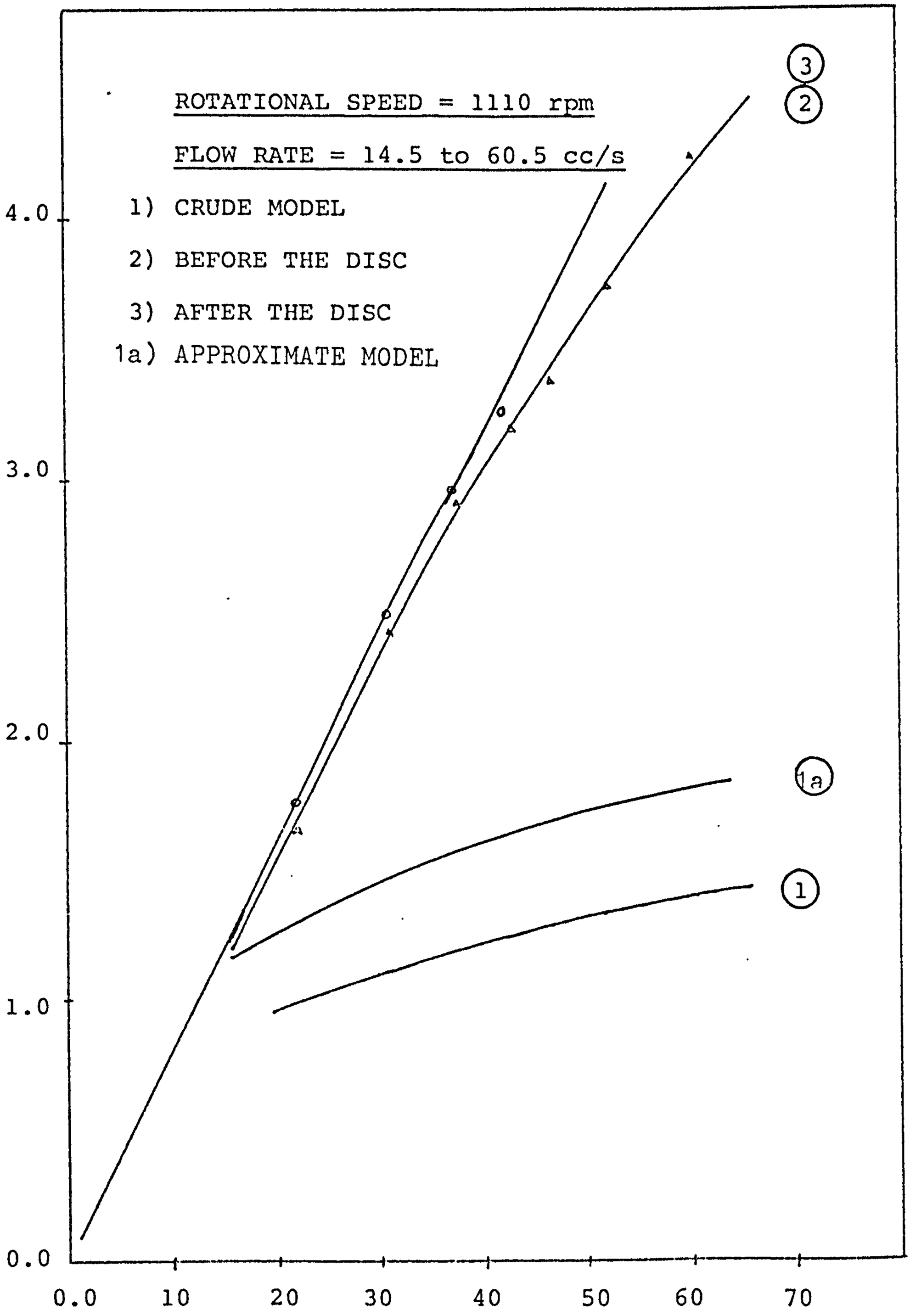

FIGURE 11.6 MASS TRANSFER RATE BEFORE AND AFTER THE DISC

reaches the edge of the disc for all flowrates less then about 40 cc/s. On this graph the complete line (3) has been drawn; this represents the saturated condition of the liquid.

In order to discuss the comparison between the theoretical models developed in section 9.6 and experimental data, Figure 11.6 will be used since the mass transfer characteristics on the disc, at 1110 rpm, with respect to liquid flowrate are typical of all other rotary speeds. On this figure, characteristics resulting from application of the 'crude' model (Equation 194) page 124, and the 'approximate' model (Equation 198) page 125, are shown as lines (1) and (1a) respectively. These models would certainly be expected to compare well with experimental results at low flowrates where the model conditions are satisfied, ie laminar flow within the film and a smooth interface. Since the surface of the films were distorted by waves, even at the lowest flowrates used in these studies, the experimental values for mass transfer were always higher than the predicted values. It can be concluded from the trends shown on these graphs (Figure 11.1 to 11.6)that for low flowrate (<10 cc/s) and low rotary speeds (<1000 rpm) the models would accurately predict mass transfer rates. However the use of such low flowrates is not appropriate to the practical application of these techniques. Furthermore at these low flowrates, there is a strong tendency for the film to break down into rivulets. As indicated above, at higher flowrates the surface of the films are distorted by waves at all disc speeds. This is reflected in the large differences in mass transfer over the whole range of flowrates investigated. For example with a flowrate of 50 cc/s the measured values of mass transfer rate are some 2.4 to 2.8 times higher than the predictions of the 'crude' model for disc speeds in the range 220 to 1110 rpm.

Figures 11.7 to 11.9 also show these effects are reflected in the variation of mass transfer coefficient with

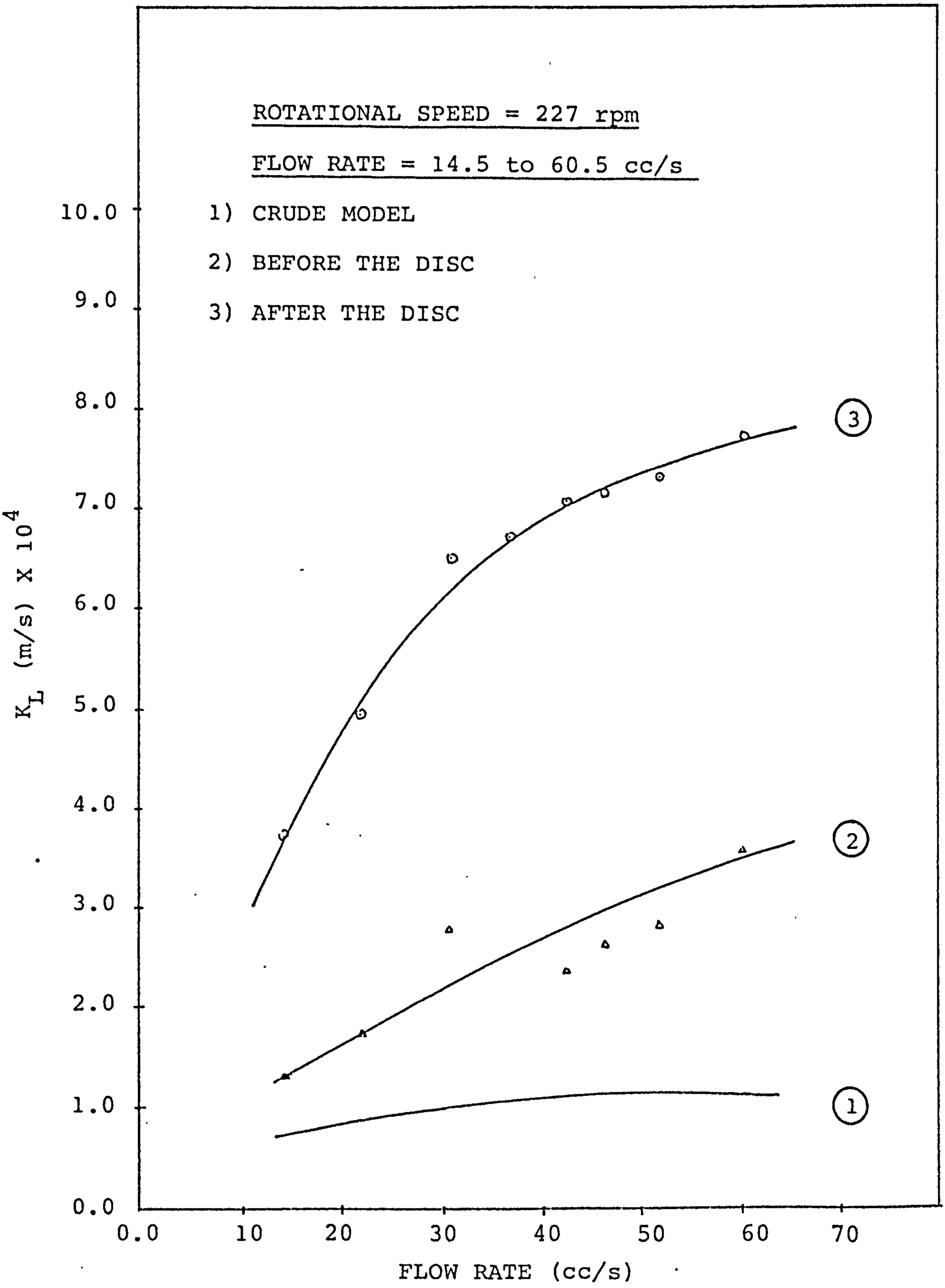

FIGURE 11.7 MASS TRANSFER COEFF. BEFORE AND AFTER THE DISC

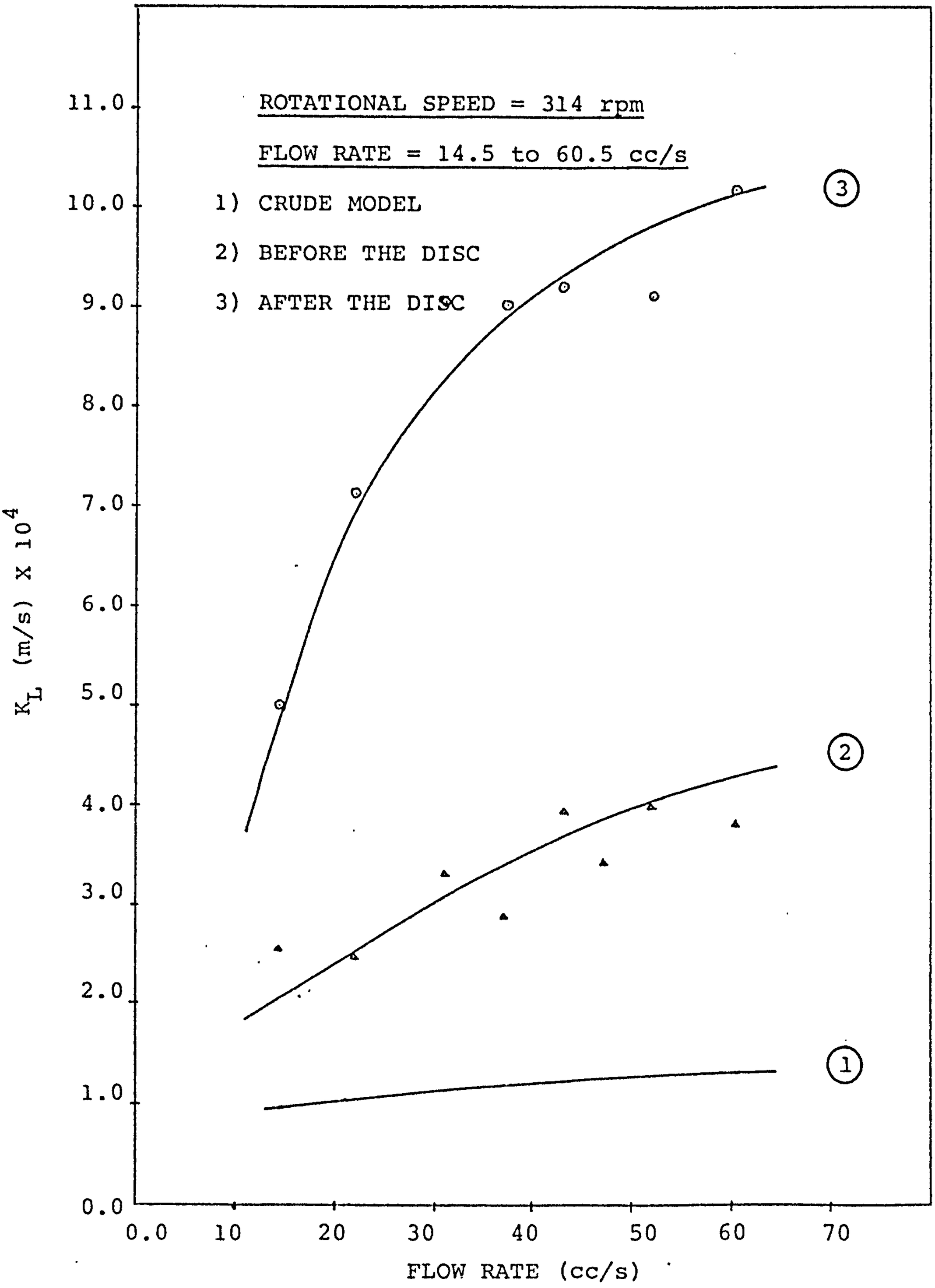

FIGURE 11.8 MASS TRANSFER COEFF. BEFORE AND AFTER THE DISC

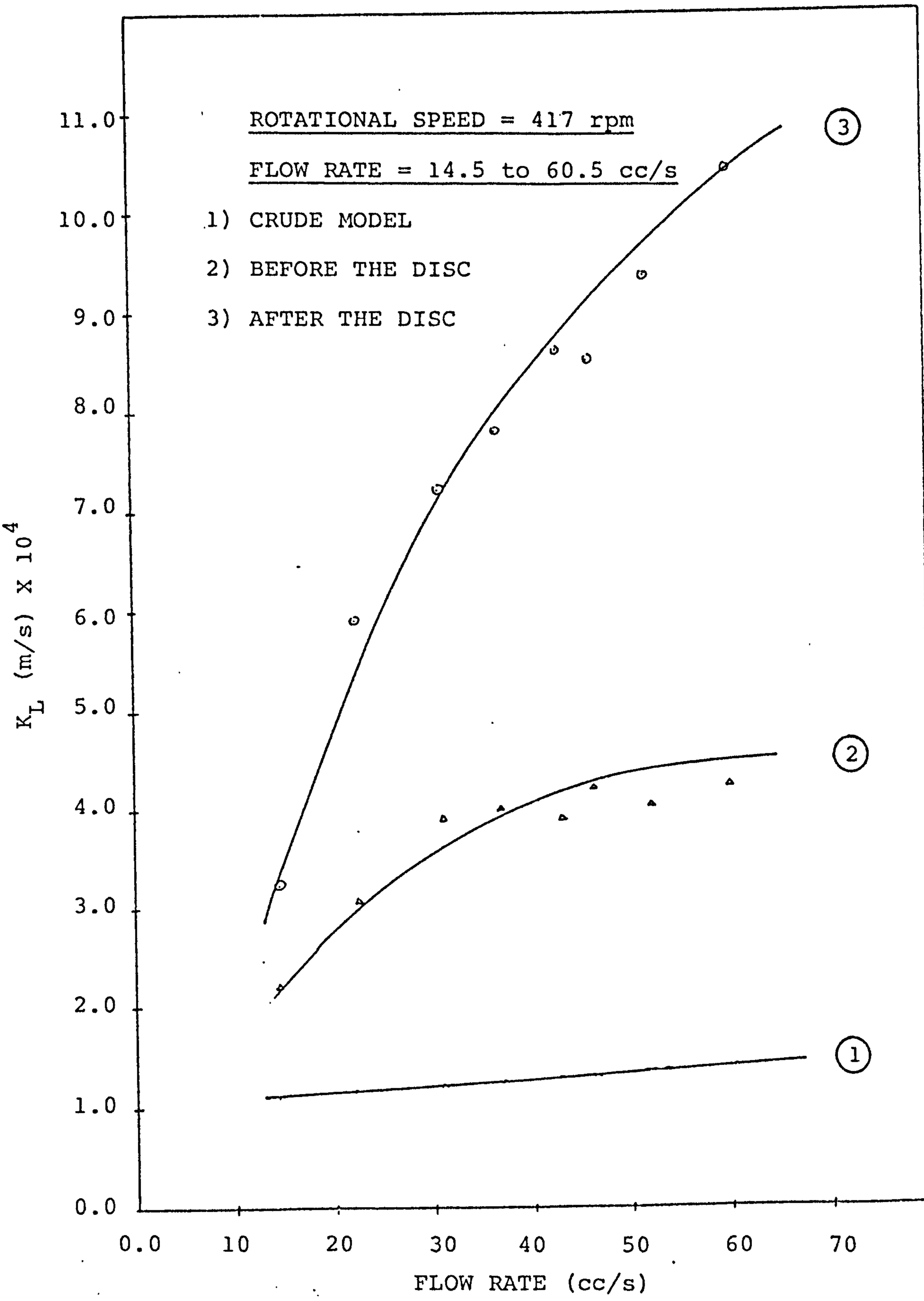

FIGURE 11. 9 MASS TRANSFER COEFF. BEFORE AND AFTER THE DISC

flowrate. Since the mass transfer in the spray region produces a near saturated condition in the liquid for disc speeds higher than those relevant to Figure 11.9 (417 rpm), mass transfer coefficients measured between the inlet nozzle and the collecting ring, which are based on the logarithmic mean concentration difference, become very large.

The preceeding discussion has been devoted to the total oxygen transfer, and the mass transfer coefficients averaged over the disc radius. In Figures 11.10 to 11.12 the variation of mass transfer with radial position on the disc is considered. Each figure shows the amount of oxygen absorbed in the liquid film as a function of radial position for a particular disc speed, with flowrate as a parameter. Since the figures represent disc behaviour at increasing speeds it can be seen that for a particular flowrate the mass transfer measured at a specified radial position increases with speed. For example to achieve a mass transfer rate of 3.0×10^{-4} gm/s with a flowrate of 60.5 cc/s and a disc speed of 571 rpm, a disc radius of 180 mm is required, whereas a disc with a radius of 120 mm can produce the same mass transfer at 60.5 cc/s provided the rotational speed is increased to 1110 rpm. Although the characteristics shown on Figure 11.10 (571 rpm) look different from those of Figure 11.12 (1110 rpm) the former should be regarded as the 'front end' of Figure 11.12. Again this figure shows that if the disc is considered as a whole, then rotation at 1110 rpm produces saturation of the liquid by the time it reaches the edge of the disc, provided the flowrate is less than about 40 cc/s.

Figures 11.13 to 11.19 show some of the mass transfer coefficient data plotted against flowrate for different radial points across the disc, with rotational speed as parameter. It can be seen that the effect of increasing

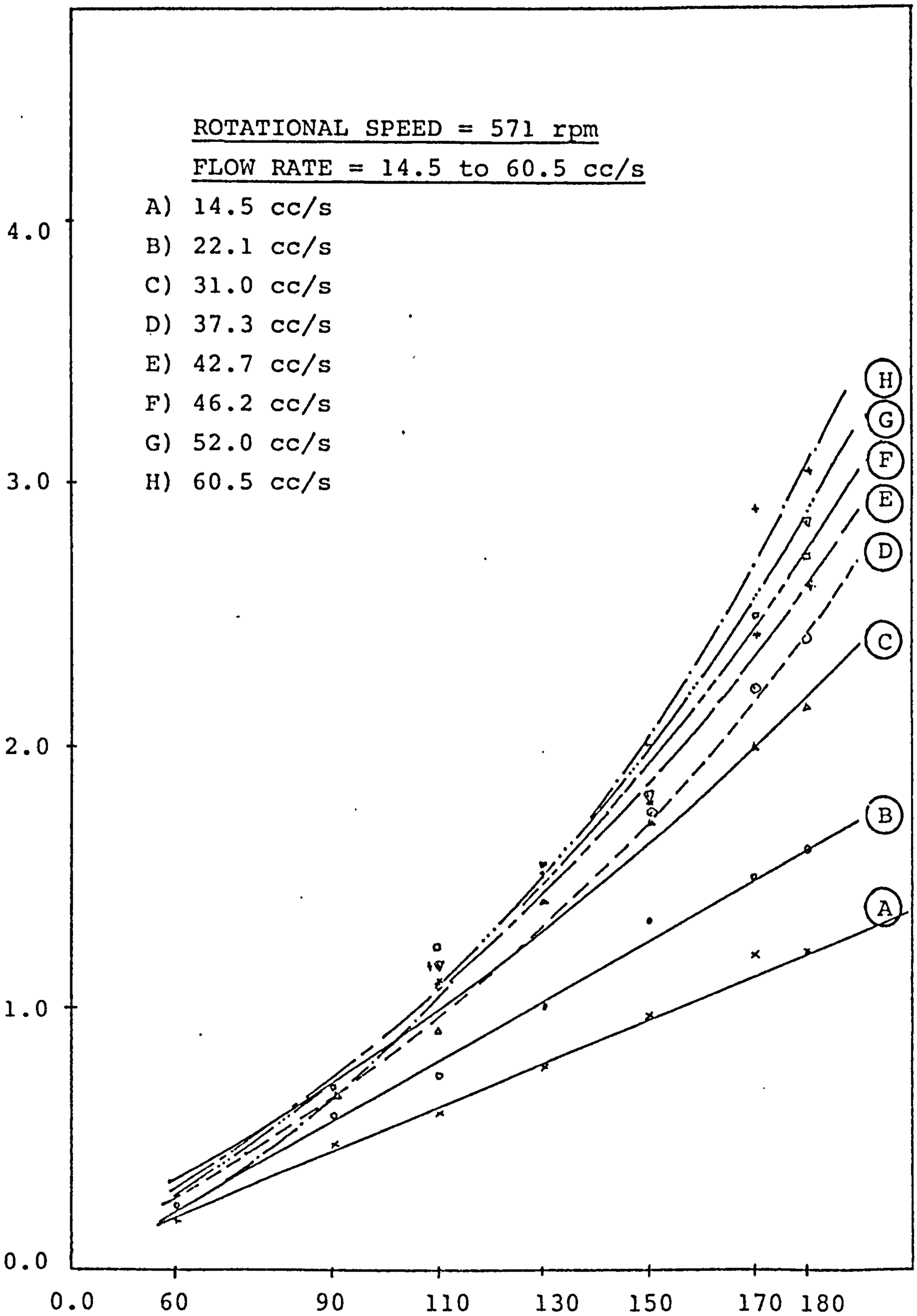

FIGURE 11.10 MASS TRANSFER RATE ACROSS THE DISC

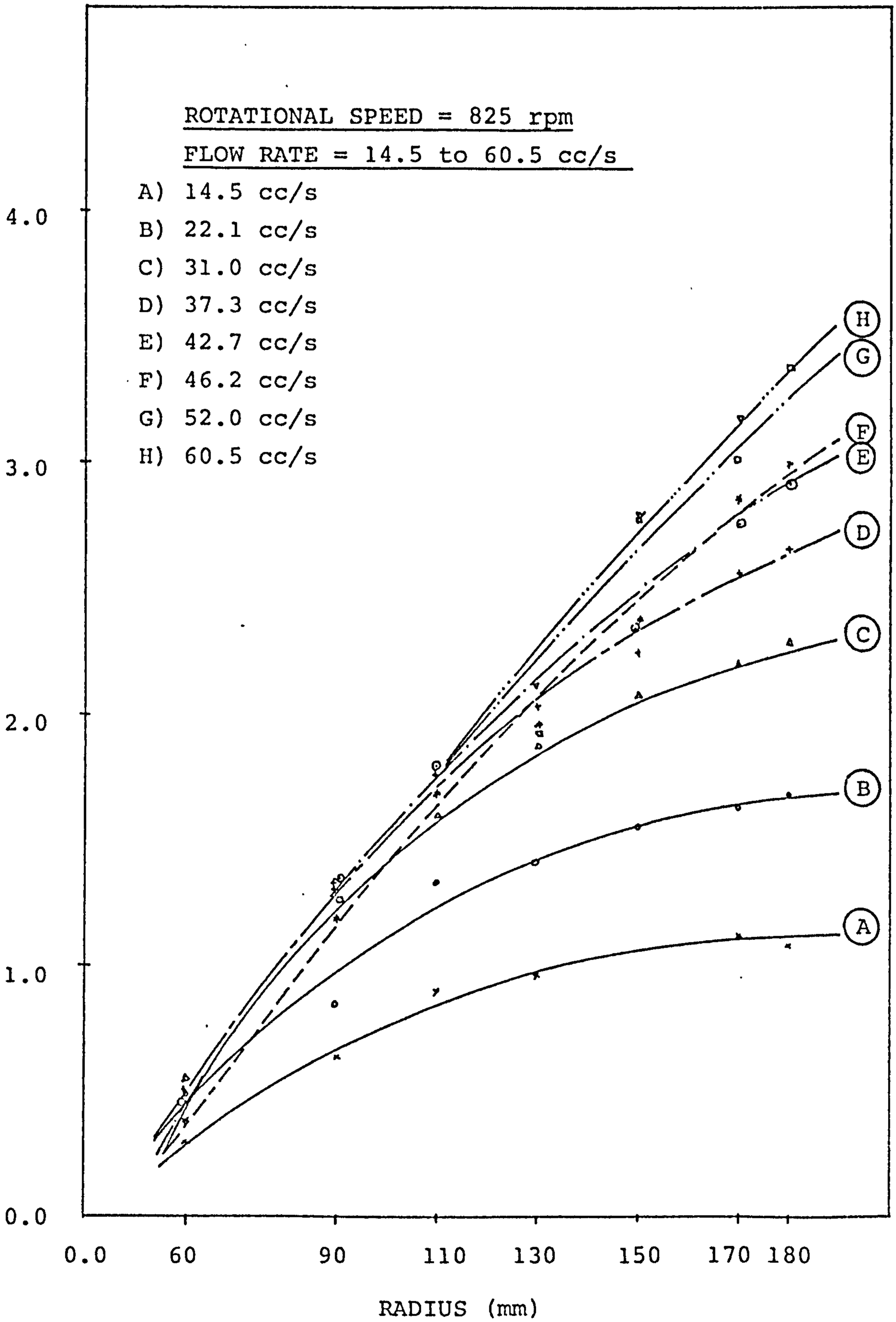

FIGURE 11.11 MASS TRANSFER RATE ACROSS THE DISC

ROTATIONAL SPEED = 1110 rpm

FLOW RATE = 14.5 to 60.5 cc/s

A) 14.5 cc/s
B) 22.1 cc/s
C) 31.0 cc/s
D) 37.3 cc/s
E) 42.7 cc/s
F) 46.2 cc/s
G) 52.0 cc/s
H) 60.5 cc/s

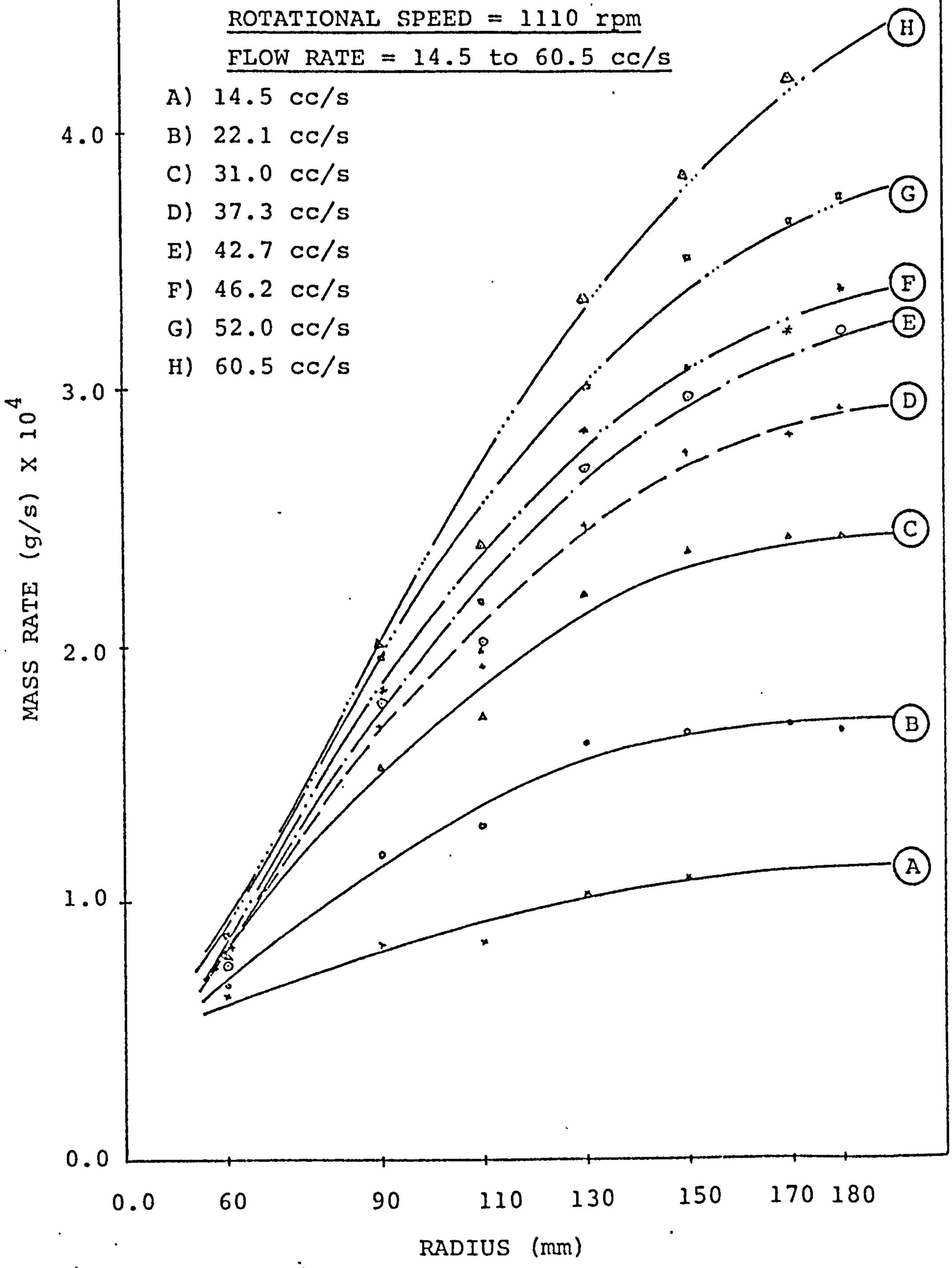

FIGURE 11.12 MASS TRANSFER RATE ACROSS THE DISC

flowrate is generally similar in all the figures with the mass transfer coefficient exhibiting a maximum value at flowrates in the range 30 to 40 cc/s. As the disc speed is increased this maximum occurs at higher flowrates. In order to explain these effects it is necessary to contruct at least a qualitative model for the processes occuring in the film. The most obvious mechanism capable of explaining both the high mass transfer rates and the above variation in mass transfer coefficient is mixing in the film, induced by the observed wave motion. It will be shown later that a simple model, based on the idea that during flow across the disc the liquid film is subjected to a series of alternate laminar flow conditions and mixing conditions induced by the waves, is capable of predicting the observed mass transfer rates. Furthermore the existence of a maximum value of the mass transfer coefficient can be explained as follows. Figure 11.14 shows values of mass transfer coefficient averaged over a radius of 90 mm. Referring for the moment to Figure 11.12 it can be seen that at a radius of 90 mm, even with a disc speed of 1110 rpm, the liquid does not approach the saturation condition at this radius provided flowrates are greater than 30 cc/s, the following comments can be made about the existence of the maximum value of the mass transfer coefficient. Considering with increasing flowrate can be explained by suggesting that as the film becomes thicker, with increasing flowrate, the waves are able to induce progressively more efficient mixing in the film. However as the film thickness (resulting from increasing flowrate) increases beyond some optimum value the waves are unable to exert the higher levels of mixing required to produce the higher mass transfer rates. This leads to a reduction in the mass transfer coefficient. It is known from the earlier study of waves that their characteristics vary with flowrate and rotary speed. However since sufficiently detailed experimental data on wave characteristics are not available at this time, precise correlation of wave behaviour with mass transfer rates is not possible

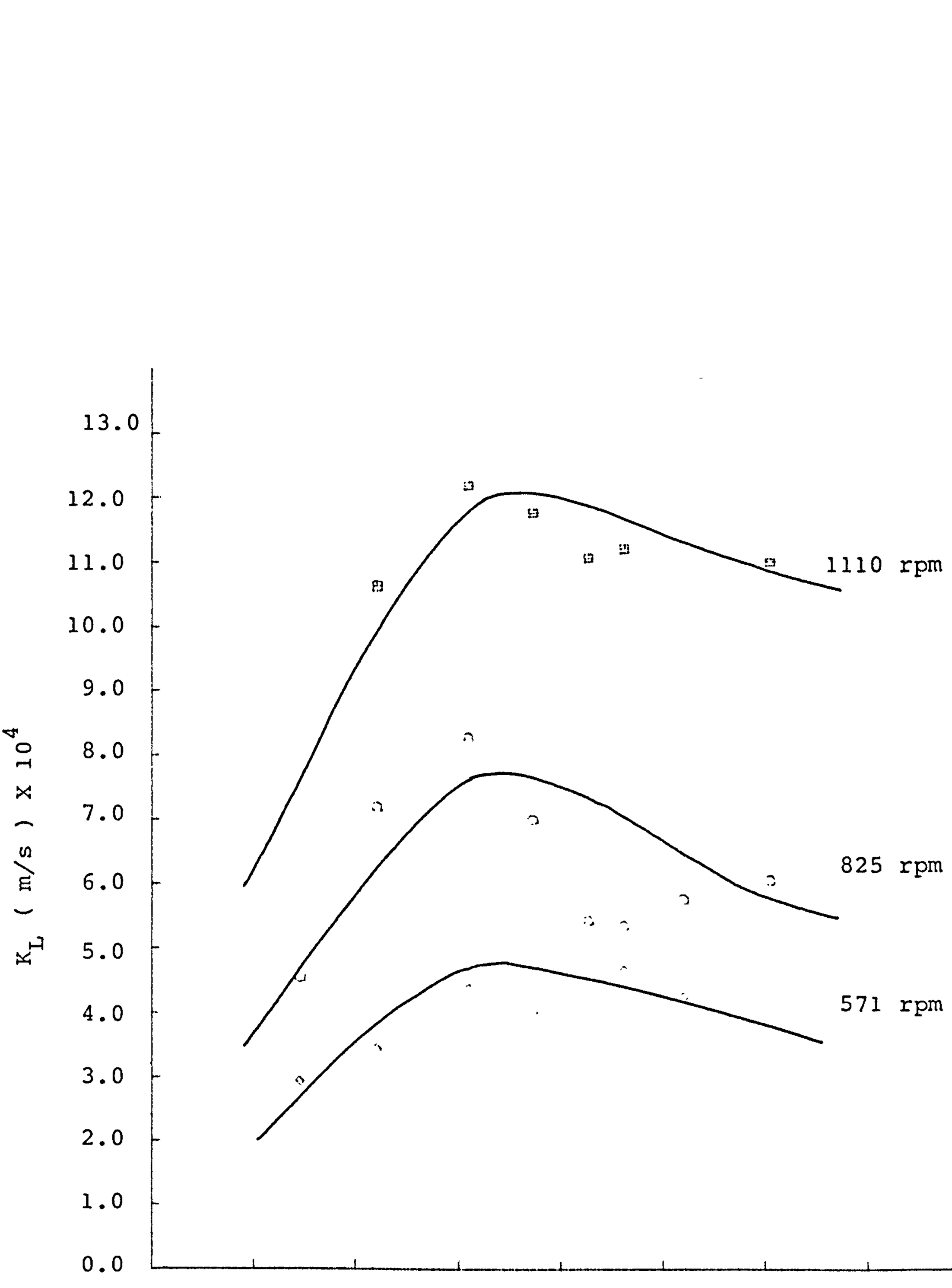

FIGURE 11.13 K_L AT RADIUS 60 mm WITH DIFFERENT SPEEDS

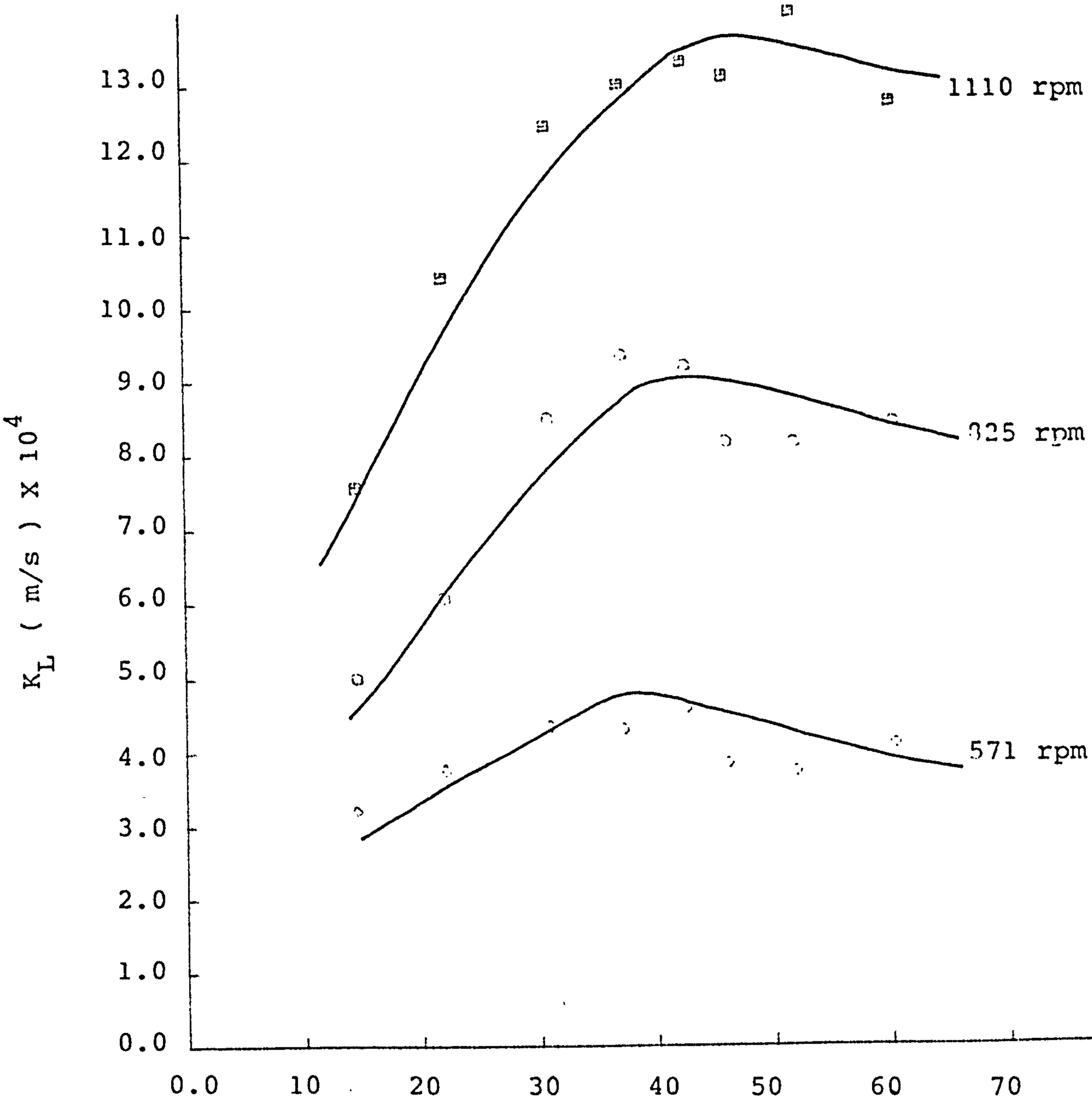

FIGURE 11.14 K_L AT RADIUS 90 mm WITH DIFFERENT SPEEDS

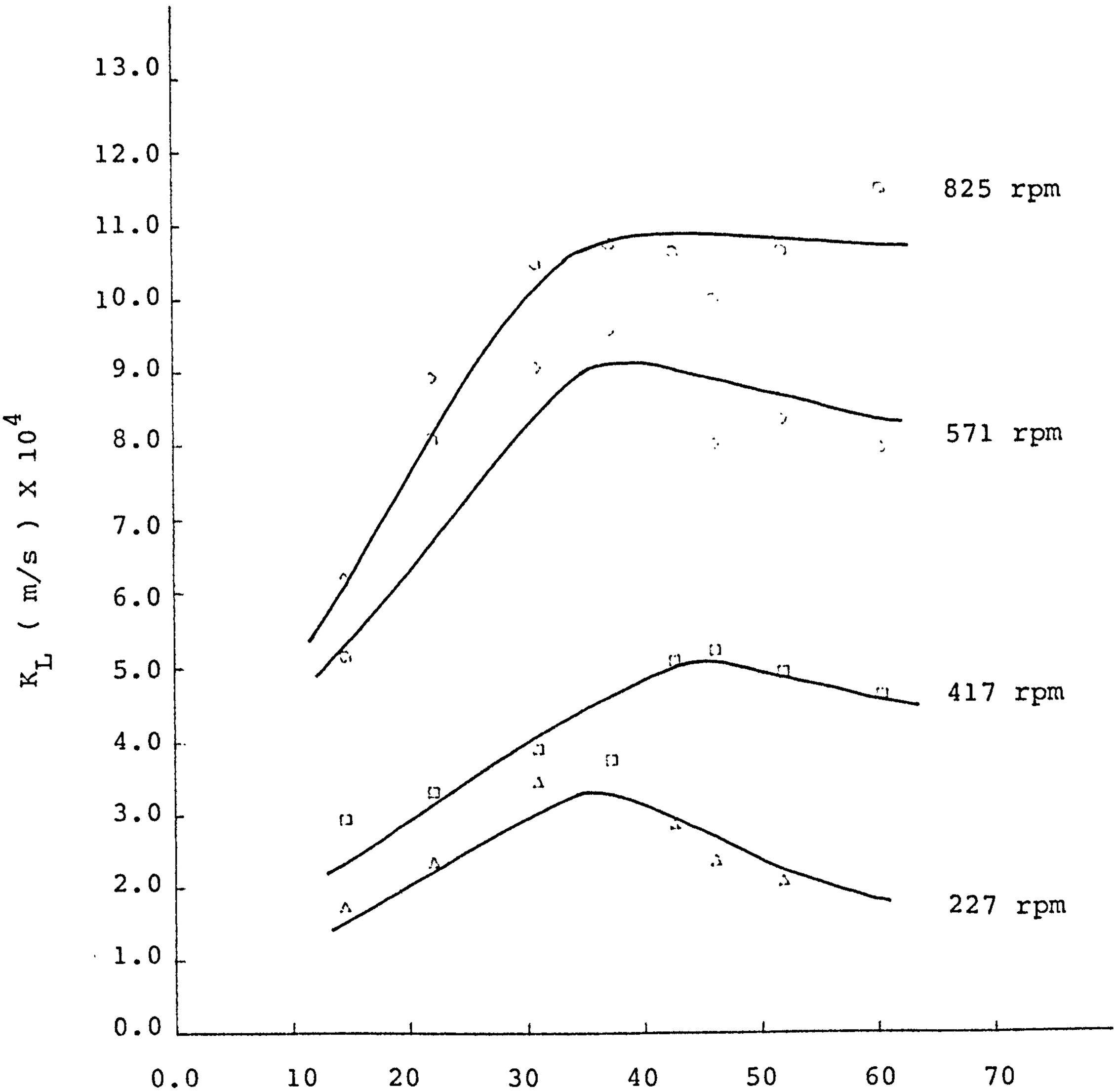

FIGURE 11.15 K_L AT RADIUS 110 mm WITH DIFFERENT SPEEDS

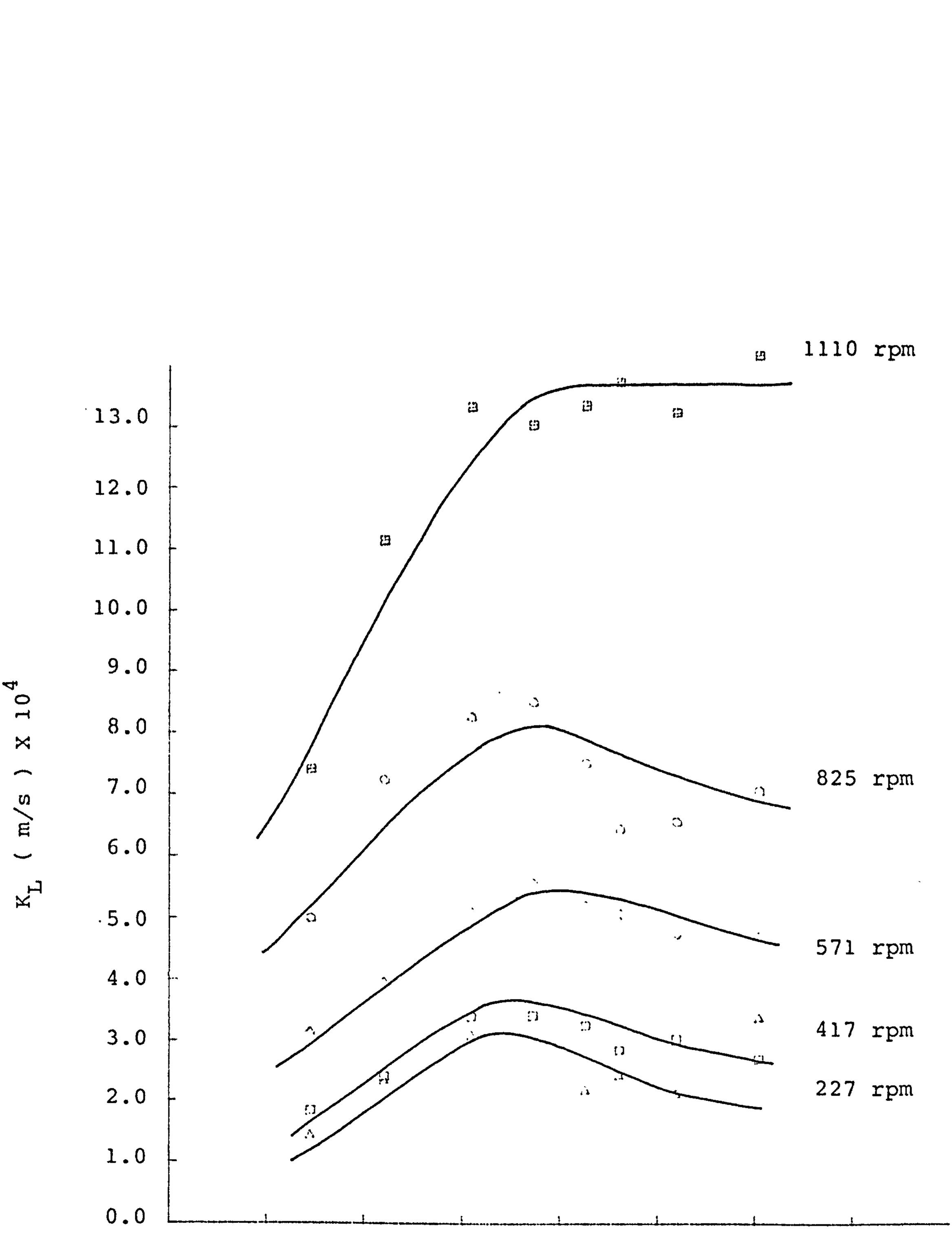

FIGURE 11.16 K_L AT RADIUS 130 mm WITH DIFFERENT SPEEDS

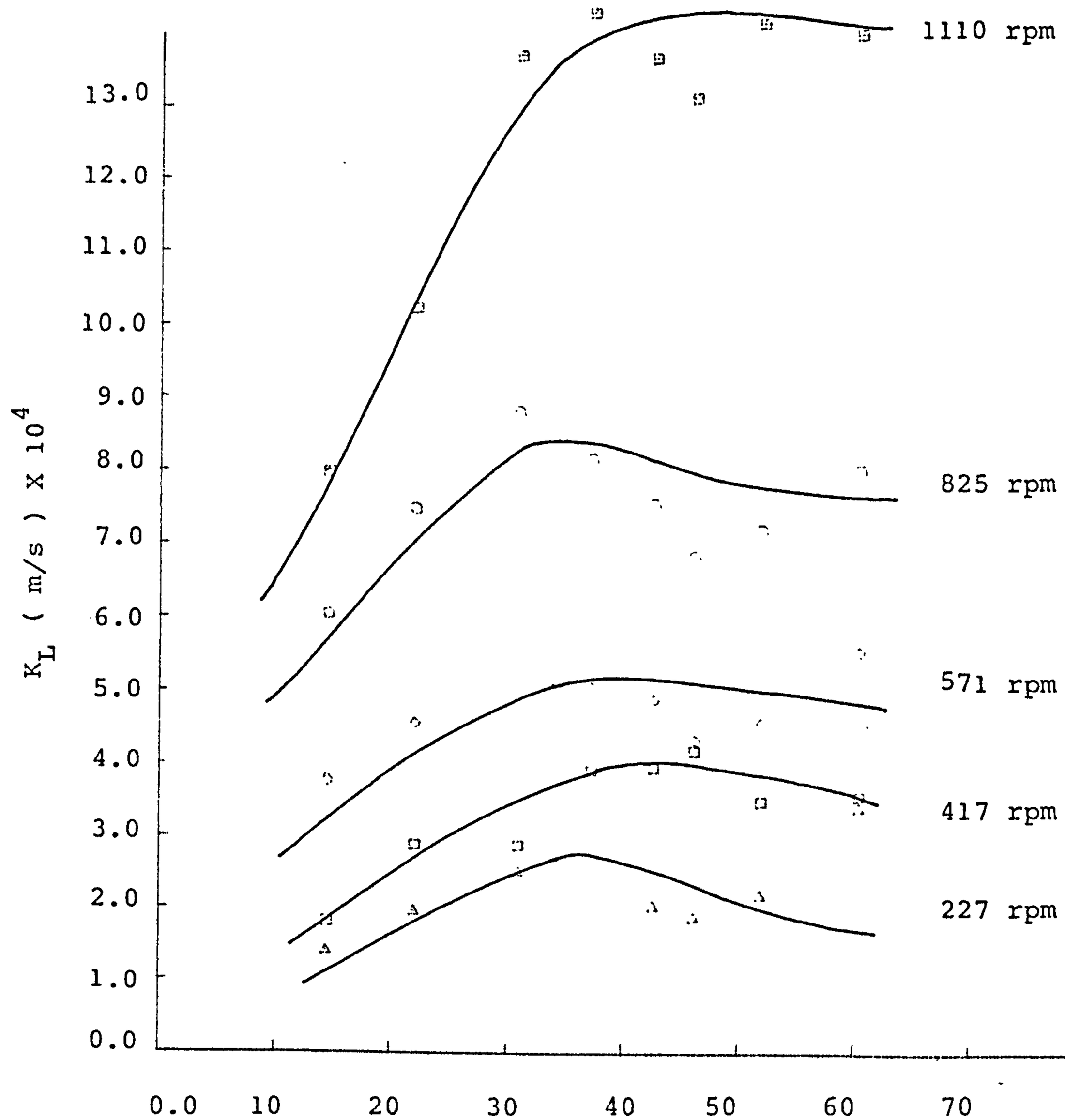

FIGURE 11.17 K_L AT RADIUS 150 mm WITH DIFFERENT SPEEDS

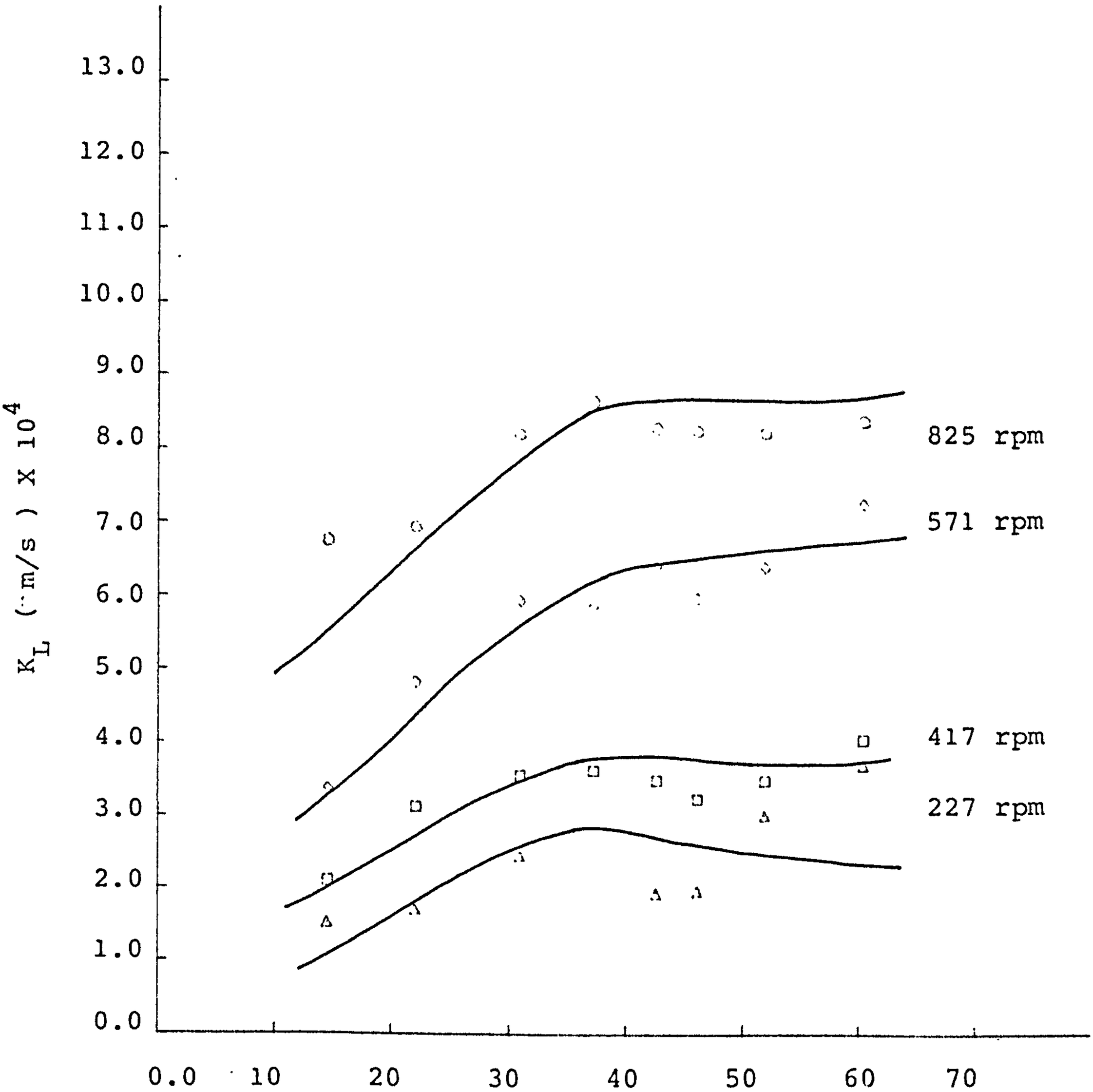

FIGURE 11.18 K_L AT RADIUS 170 mm WITH DIFFERENT SPEEDS

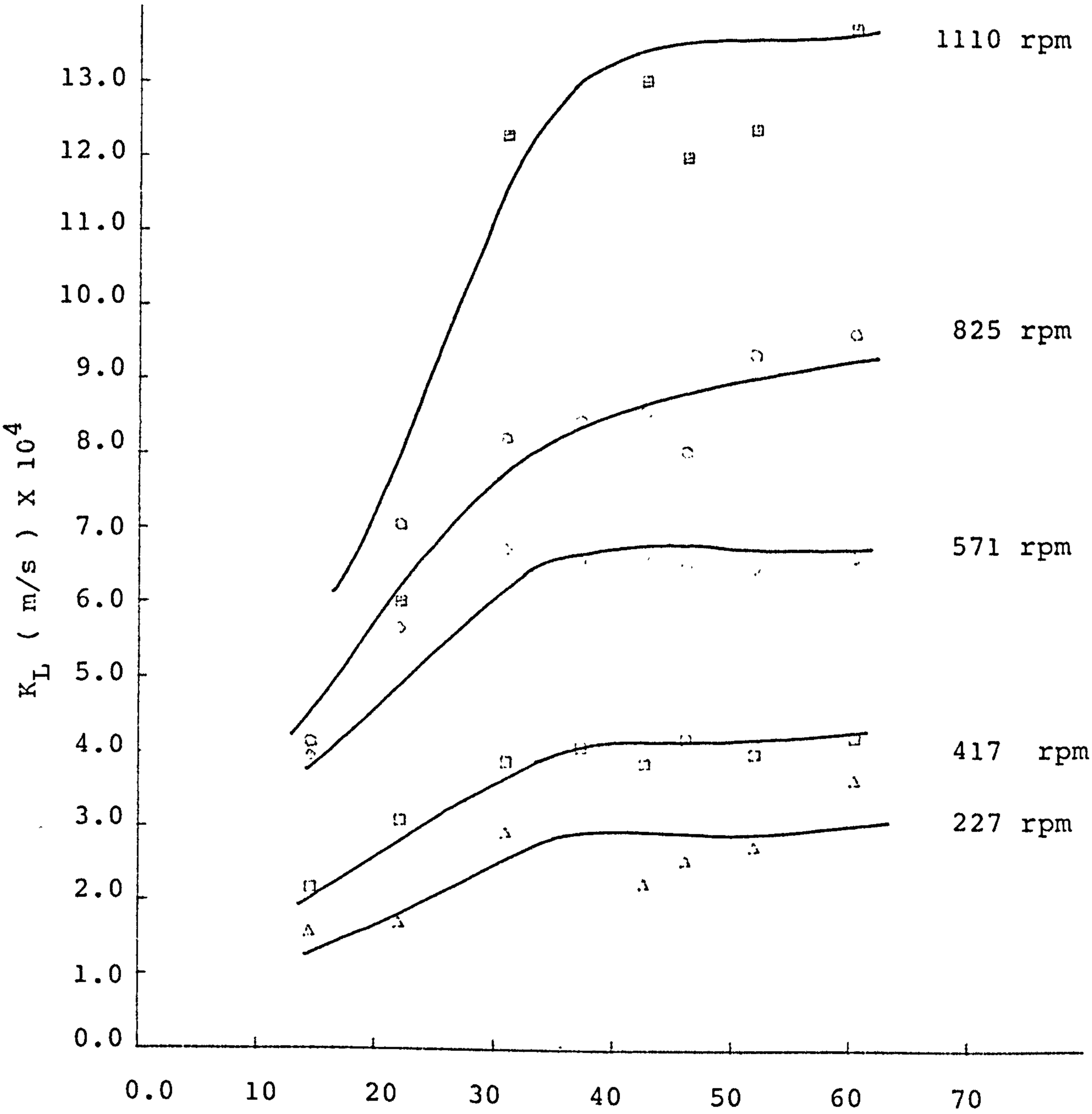

FIGURE 11.19 K_L AT RADIUS 180 mm WITH DIFFERENT SPEEDS

Nevertheless it is possible to extract some information from the data collected on wave behaviour in order to carry out some limited calculations with the proposed model, which can be compared with the experimental mass transfer data. As noted earlier the model assumes that the waves induce mixing in the film and that the film between the waves is in laminar flow and during this 'exposure' time mass transfer in this part of the film is diffusion conrtolled, as with the earlier models outlined in section 9.6. An estimate of the wavelength of the waves or ripples in the film can be made from the measurements reported in section 5.4. These wavelegths vary from 2 mm to 14 mm with the range of flowrates and disc speeds investigated in this study.

As an initial test of this type of model, the disc will be assumed to be divided into twenty concentric rings, each 7.9 mm wide. Between each ring boundary the flow in the film is assumed to be laminar, and fully developed, with a smooth surface, with thorough mixing occuring as the liquid crosses each ring boundary. Within the laminar flow region the 'Approximate' model (Equation 128) page 125 is assumed to control the diffusion process. This model has been compared with experimental data which are representative of the wide spectrum of conditions investigated. These are shown in the table below

	FLOWRATE (cc/s)	DISC SPEED (rpm)
Figure 11.20	14.5	227
Figure 11.21	14.5	1110
Figure 11.22	60.5	227
Figure 11.23	60.5	1110

on all these figures line ① is the initial 'Approximate' model of Equation 128, page 125. Line ② is the experimental data and line ③ represents the 'Modified Approximate' model outlined above.

Referring to Figure 11.20 which represents low flowrate and low disc speed it can be seen that whilst the 'Approximate' model underestimates the rate of mass transfer, the modified model substantially overestimates this parameter. This behaviour is expected since at this flowrate and disc speed the actual waves exhibited wavelegths much larger than that used for the model. At the higher disc speed Figure 11.21 the comparison between the model and the experimental data is quite good. Here the observed wavelength compares well with that used for the model.

Similar results are shown in Figure 11.22 and Figure 11.23 for the highest flowrate studied (60.5 cc/s). Again at the lower disc speed the new model overestimates the mixing effect of the waves, whilst good agreement is apparent at the highest disc speed.

It is obvious that any of the experimental data could be made to fit the modified model with the 'correct' choice of wavelength and that much more wave information is required before the behaviour proposed here can be verified. It will be necessary to produce data concerning the velocity of the waves relative to the mean velocity of the film. This will be required in order to confirm that the required number of mixing cycles can be achieved as a particular volume of liquid crosses the disc. In the above estimate the number of mixing cycles was twenty and this seems unreasonably large until other observations of the waves are considered. The most important of these is that the film thickness between the waves is probably much less than that which the simple hydrodynamic model (Equation 25.2), page 25, suggests; under these conditions the mean velocity in this film would be much less than that in a film of a mean thickness appropriate to the flowrate on the disc. This would lead to a high relative velocity between the waves and the films left in their wake.

The answer to questions such as this will require much

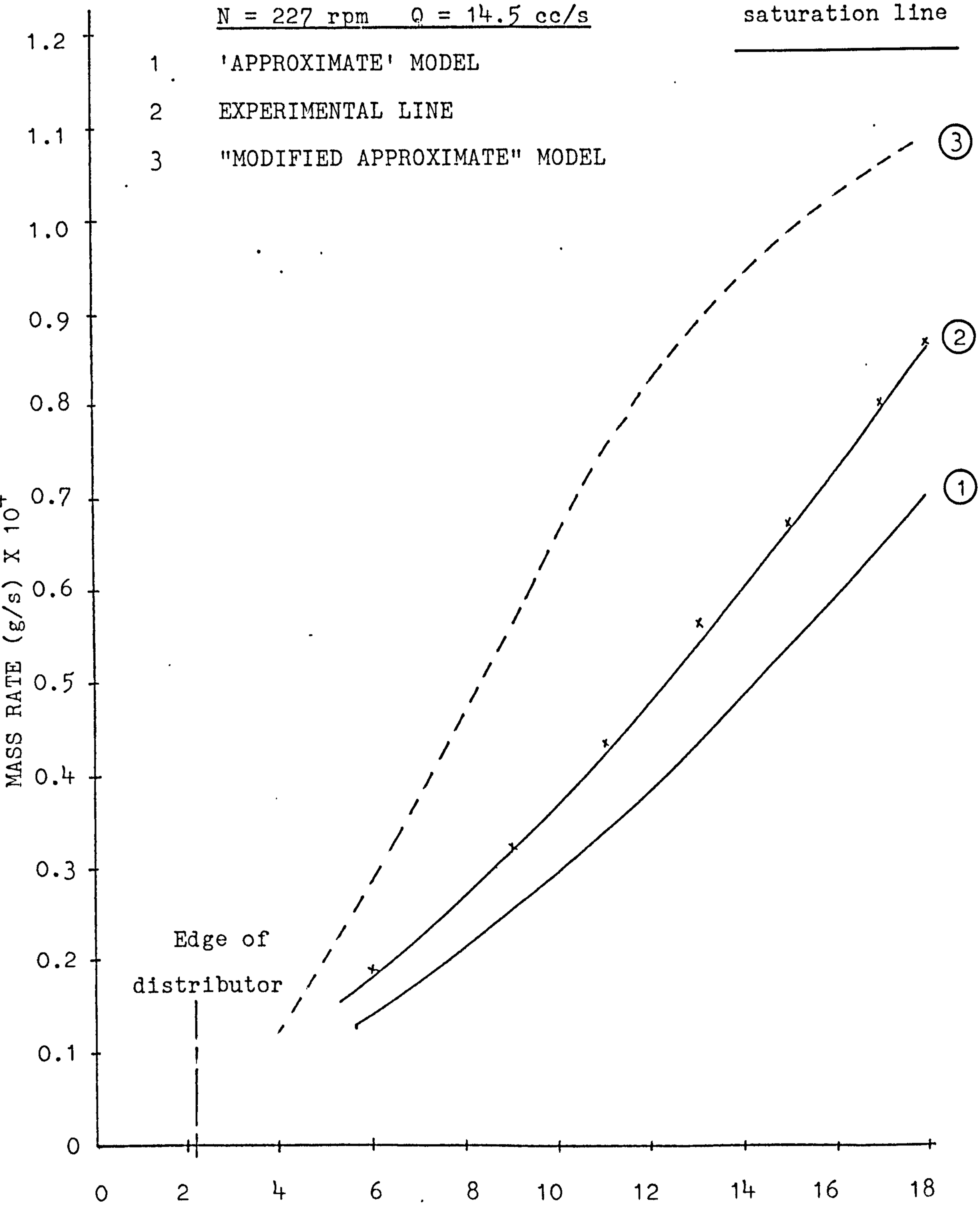

FIGURE 11.20 COMPARISON OF MASS TRANSFER RATE WITH EXPERIMENTAL AND THE MODIFIED MODEL ACROSS THE DISC

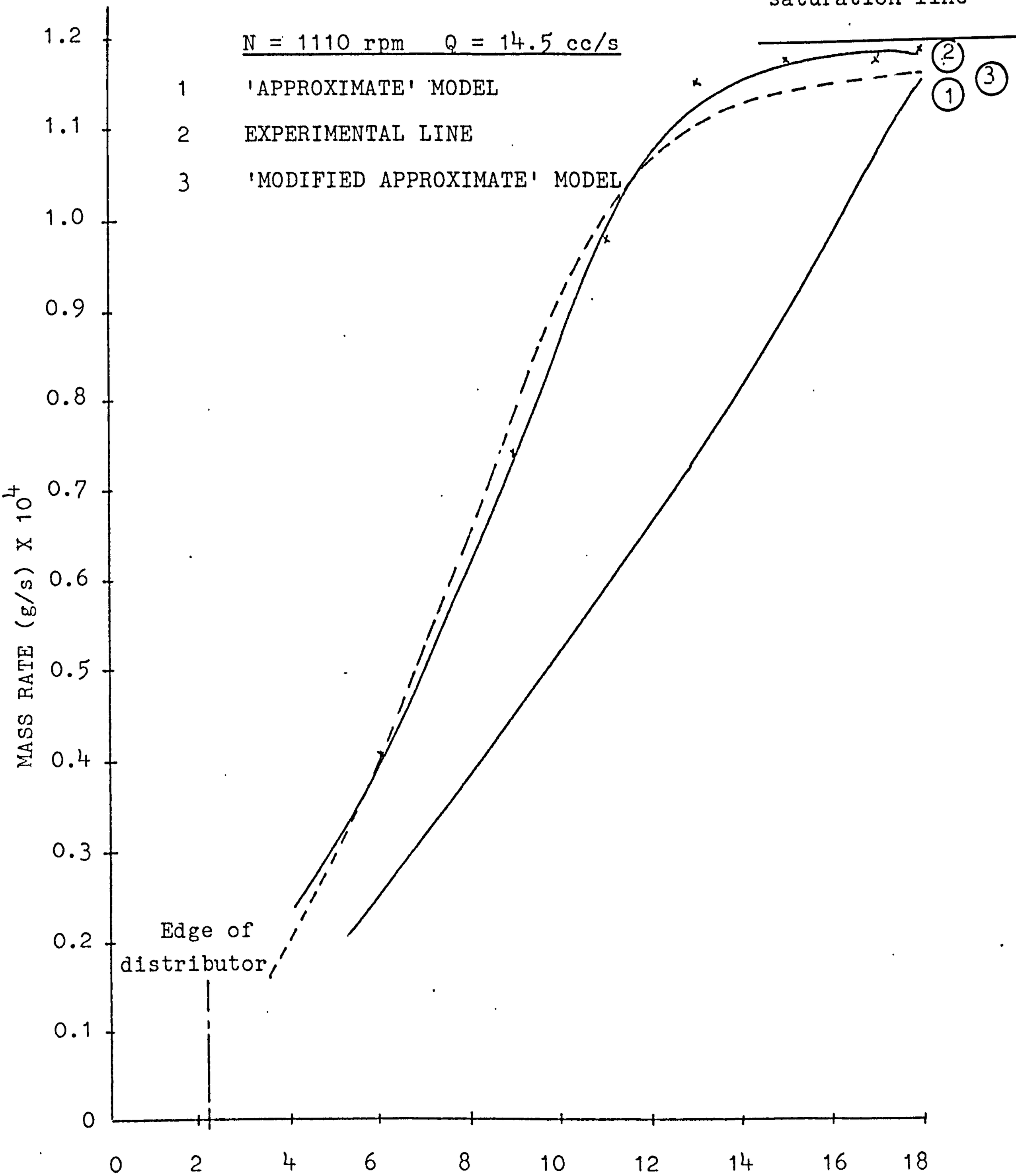

FIGURE 11.21 COMPARISON OF MASS TRANSFER RATE WITH EXPERIMENTAL AND THE MODIFIED MODEL ACROSS THE DISC

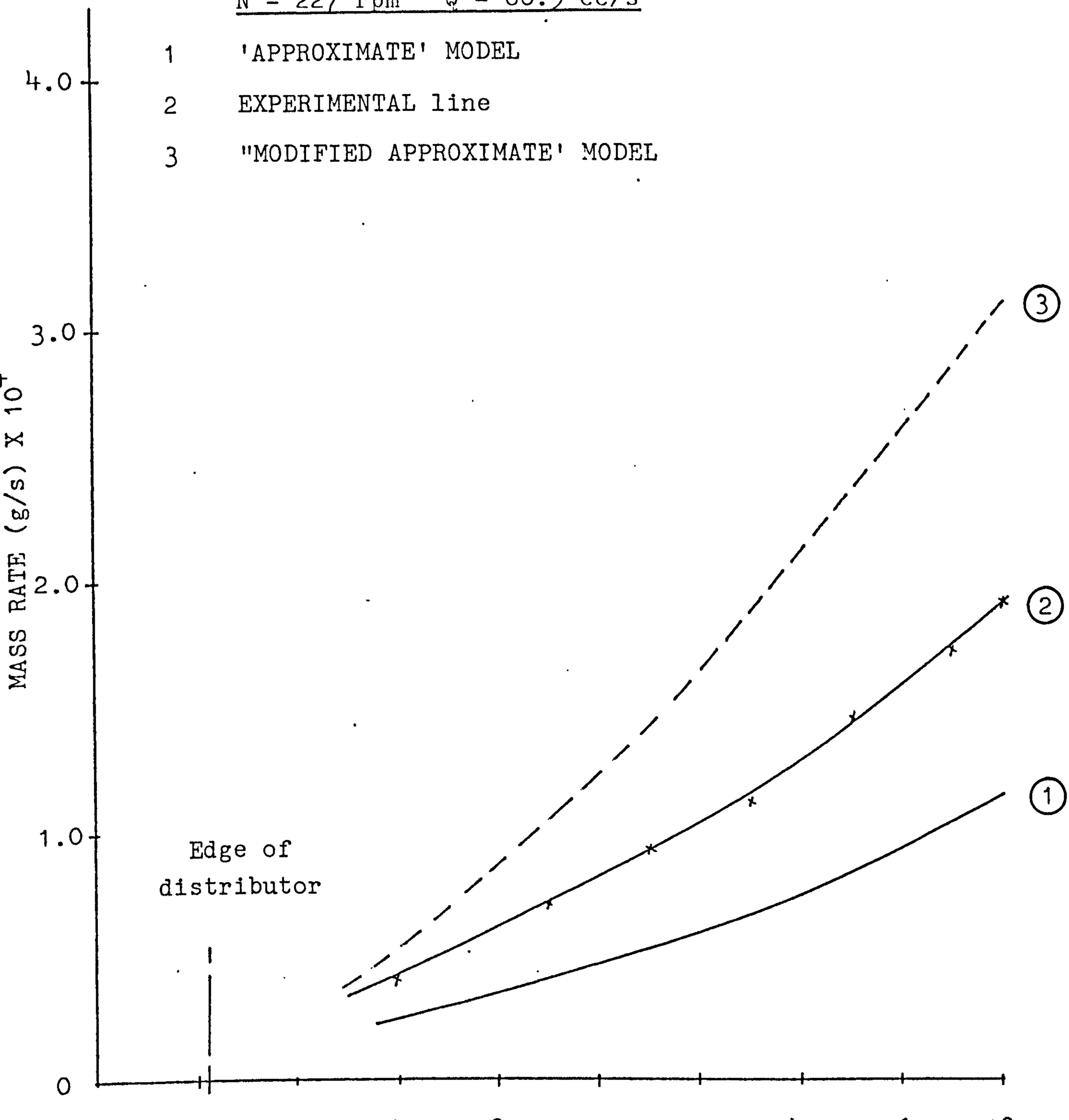

FIGURE 11.22 COMPARISON OF MASS TRANSFER RATE WITH EXPERIMENTAL AND THE MODIFIED MODEL ACROSS THE DISC

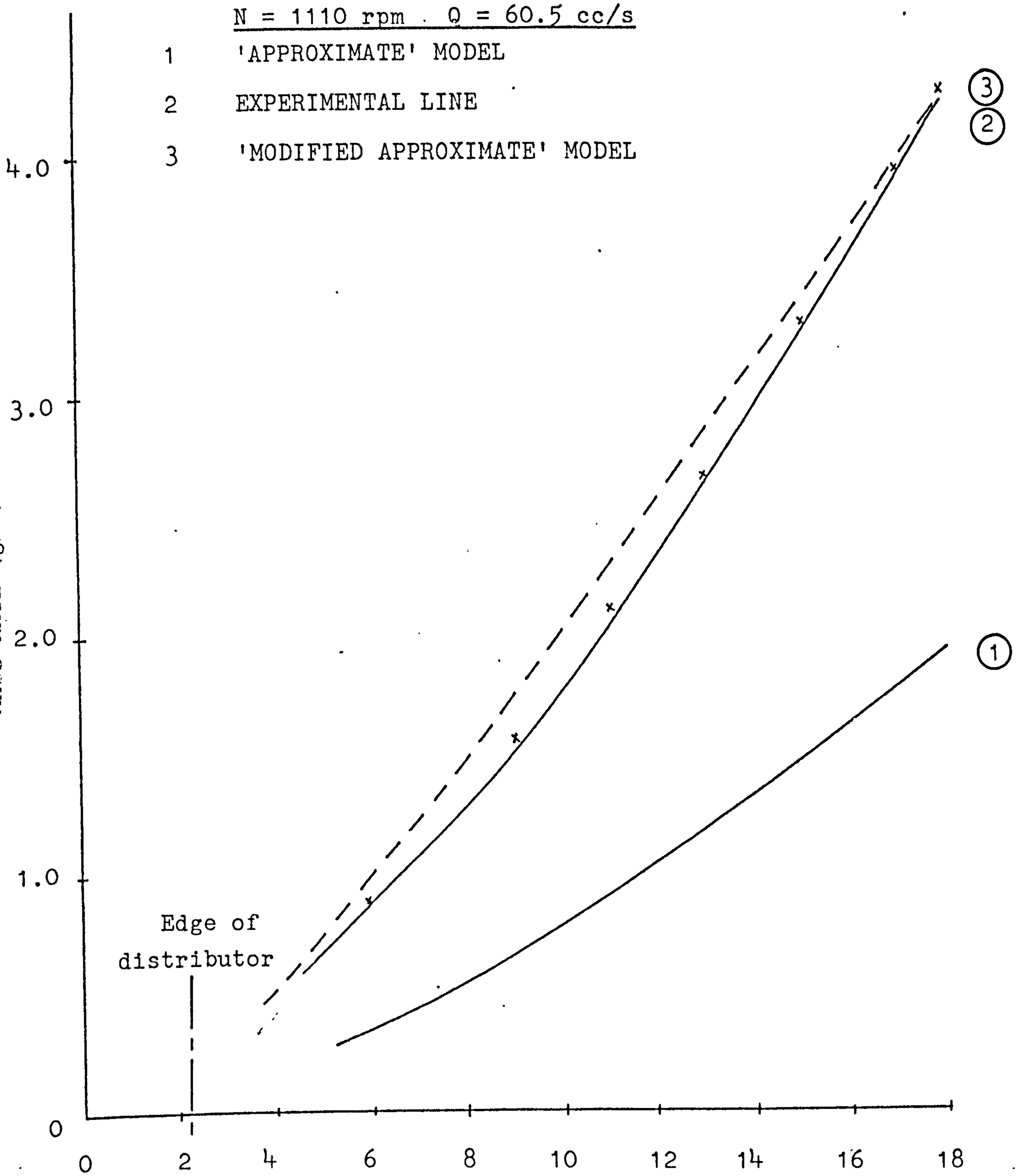

FIGURE 11.23 COMPARISON OF MASS TRANSFER RATE WITH EXPERIMENTAL AND THE MODIFIED MODEL ACROSS THE DISC

more detailed study of wave behaviour, involving residence time measurements. The measurement of residence time distributions on discs presents many problems and these will require solution before reliable information of this nature is available.

Since the effectiveness of wave induced mixing decreases with increasing flowrate at any disc speed it may be better to design the disc surface to induce this mixing artificially, rather than rely on the behaviour of the waves. If such discs can be made to 'perform' in accordance with the modified model discussed here, this will provide an effective mass transfer device which can be designed with confidence.

Whilst an accurate description of mass transfer on plain rotating discs will require further detailed studies, a simple design correlation was sought for the present experimental data. Two methods were chosen. One defines a function E_T as

$$E_T = \frac{C_{out} - C_{in}}{C^* - C_{in}}$$

(E_T has been called the fractional approach to equilibrium)

C_{out} = concentration at particular radius
C_{in} = inlet concentration
C^* = saturation concentration

This parameter has been correlated with other parameters which are known to describe some aspects of the hydrodynamic behaviour in the liquid films on a rotating disc ie,

$$E_T = \phi (Re.Ta.R^*) \qquad \text{where} \quad Re = \frac{\Omega}{r\nu}, \quad Ta = \frac{Wr^2}{\nu}, \quad R^* = \frac{r}{r_0}$$

Whilst the function ϕ should exhibit exponential behaviour (with a maximum value of $E_T = 1.0$), a simple power law fit was carried in the present case. A least squares fit of all the experimental data produced the following result

$$E_T = 6.17 \times 10^{-3} \; Re^{-0.46} \; Ta^{0.51} \; R^{*-0.05} \qquad (221)$$

The range of variables included in Equation 221 was as follow

$$80 < Re < 1030$$
$$8 \times 10^4 < Ta < 4 \times 10^6$$
$$2.67 < R^* < 8.0$$

The standard deviation was 12%

This correlation, together with all experimental data are shown on Figure 11.24, whilst Figure 11.25 shows selected data indicating their particular correspondence with the correlation line.

It should be noted that values of the parameter ($Re^{-0.46} Ta^{0.51} R^{*-0.05}$) greater than about 160 correspond to values of E_T greater than 0.95, which indicates that under the specified conditions the concentration of oxygen in the liquid approaches the saturation value.

Finally, the data have also been correlated using the traditional Sherwood number,

$$Sh = \frac{K_L \; \bar{\delta}}{D}$$

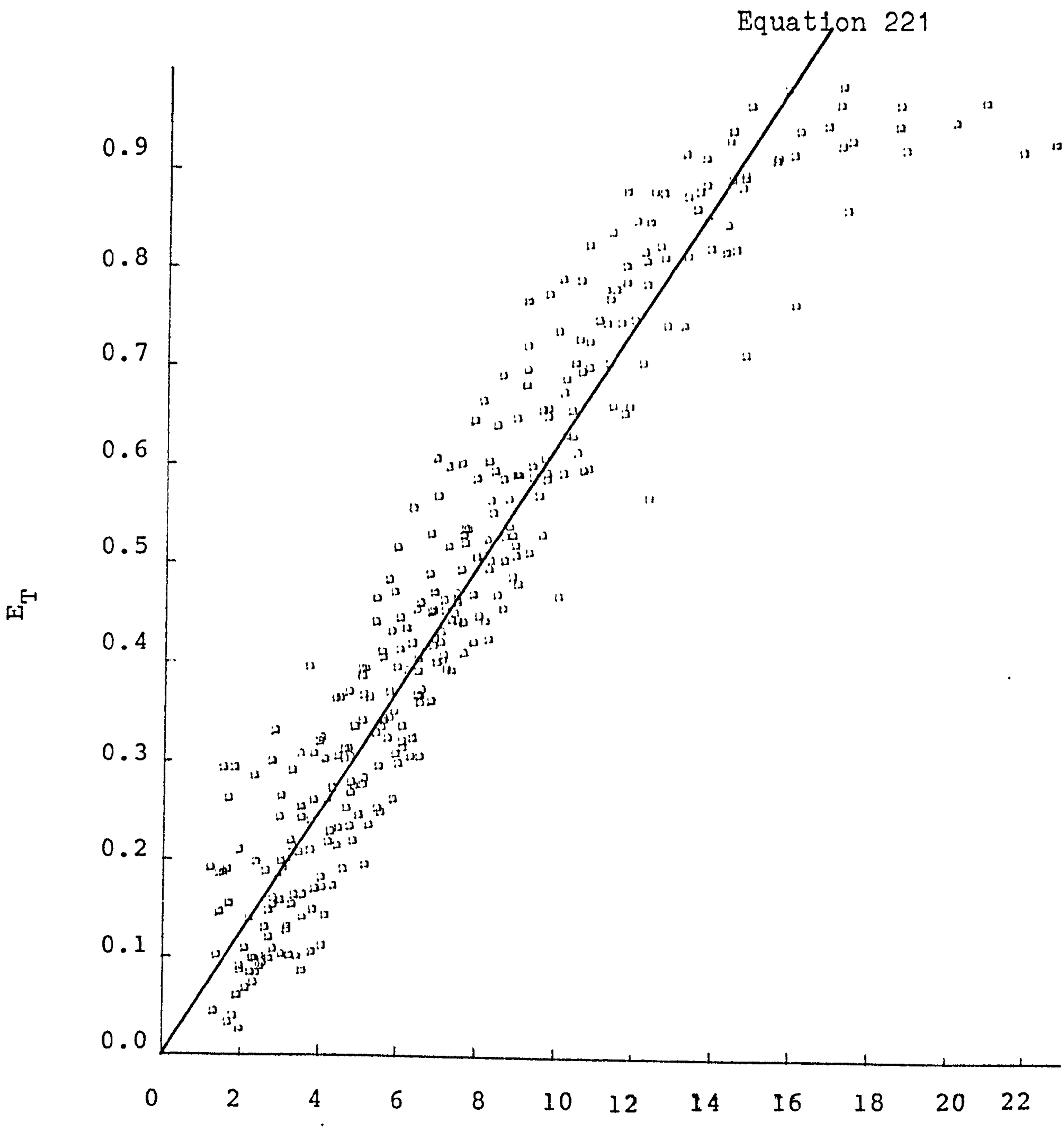

FIGURE 11.24 FRACTIONAL APPROACH TO EQUILIBRIUM CORRELATION

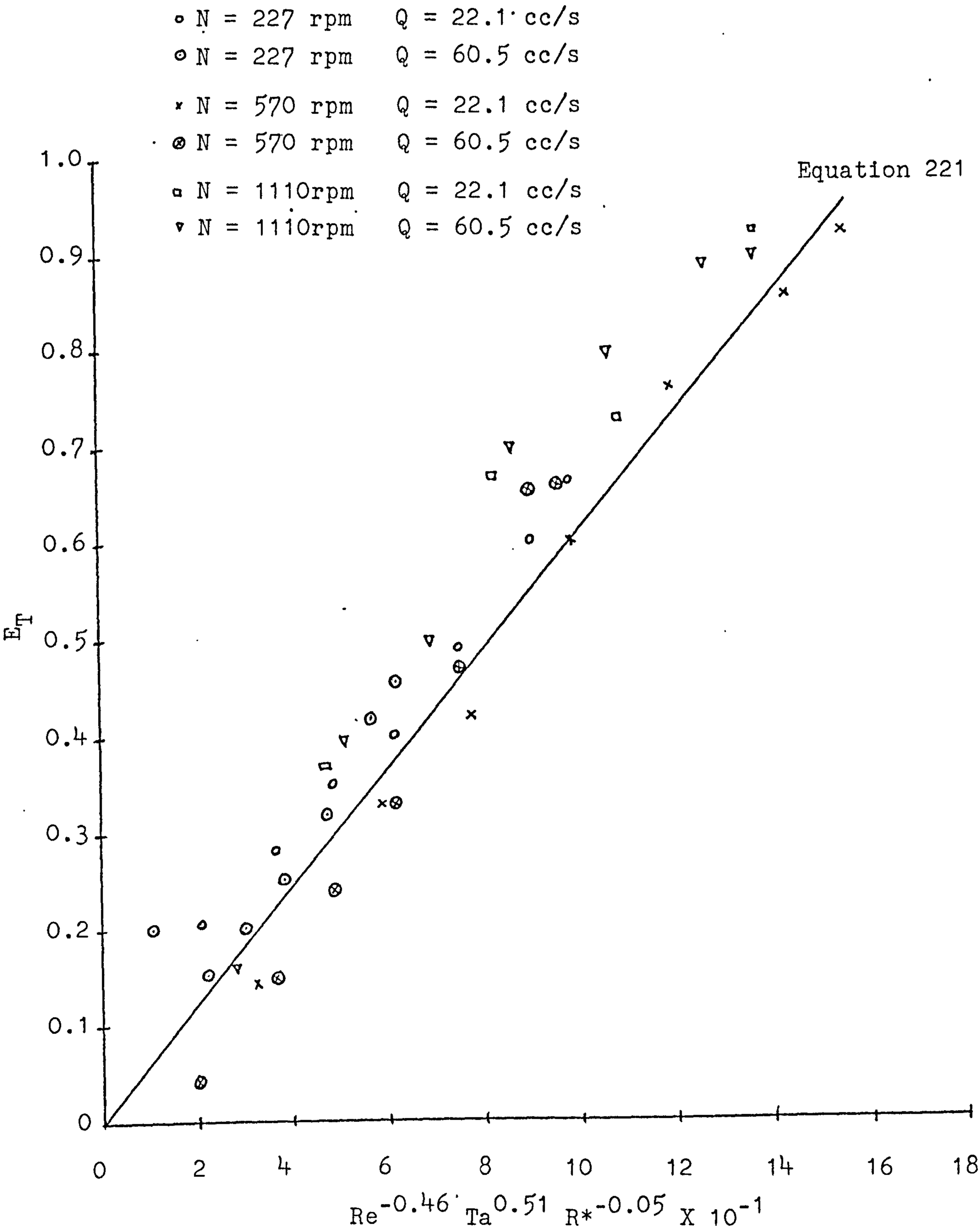

FIGURE 11.25 FRACTIONAL APPROACH TO EQUILIBRIUM CORRELATION WITH SOME SPECIFIED DATA

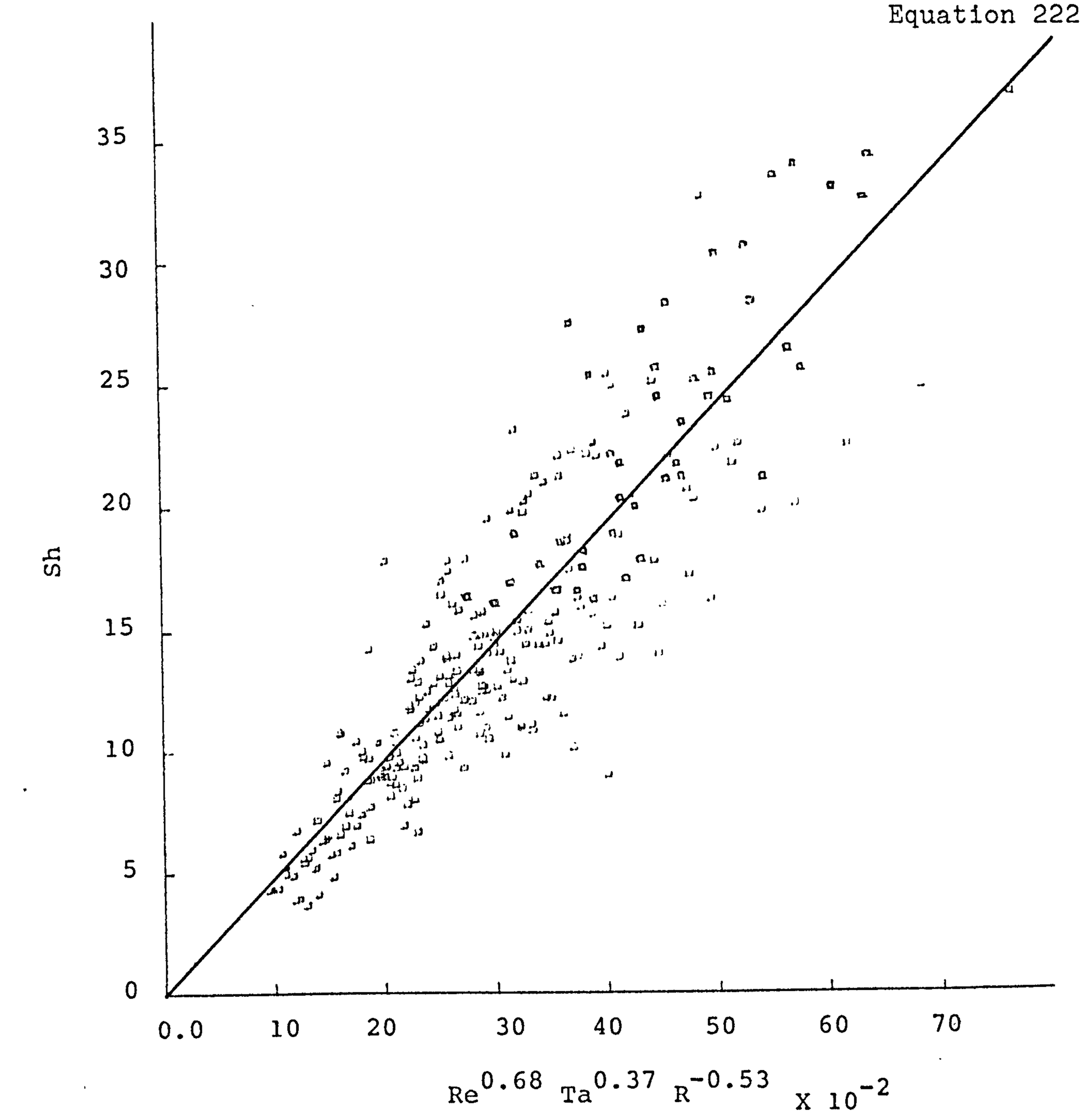

FIGURE 11.26 SHERWOOD NUMBER CORRELATION

together with the parameters Re,Ta and R*. In the Sherwood number the characteristic length $\bar{\delta}$, is the mean film thickness difined in Equation 25.2, page 25. Again using a least squares procedure, a simple power law correlation was determined as follows.

$$Sh = 4.76 \times 10^{-3} \; Re^{0.68} \; Ta^{0.37} \; R^{*-0.53} \qquad (222)$$

The standard deviation was 8.6%. It should be noted that the Sherwood number correlation contains only those data for which E_T was less than 95%.

12 CONCLUSIONS

The most important conclusion to be drawn from this section of the work is the dominant effect of wave motion on the mass transfer process in liquid films as they flow across the surface of a rotating disc.

Over the range of variables investigated in this study the measured mass transfer rates are always substantially higher than those predicted from the models which assume a smooth film in laminar flow. In some cases measured values are three times the predicted values emphasising the influence and importance of the waves.

Whilst such waves are present with all flowrates and disc speeds of practical interest, their absence at very low flowrate and disc speed provides a useful test of the simple mass transfer models which do not include the mixing effects induced by the waves.

A modified model has been introduced and is shown to be capable of predicting the rates of mass transfer which are determined experimentally. However the model relies on the specification of a wavelength or the equivalent exposure time,in order to make a prediction of mass transfer rate. At the present time these wavelengths have been estimated from rather limited data available from the earlier hydrodynamic studies. Whilst the model is capable of predicting rates of mass transfer which correspond accurately with measured values, this can always be achieved by suitable 'choice' of wavelength for use in the model. Futher detailed studies will be required to confirm the essential mixing/exposure features of the models, and to provide quantitative relationships between system parameters and wave characteristics which are appropriate to the proposed mass transfer model. The experimental techniques required to produce this information, notably direct wave statistics and residence

time distribution studies, present considerable practical difficulties when applied to rotating surfaces.

Since this information is not available at this time the data collected in this study have been correlated to provide simple equations by which the performance of a plain disc could be assessed. Whilst these equations, using either E_T, (Equation 221), or Sherwood number, Sh, (Equation 222), are concerned with the absorption of oxygen into water films, they could probably be used for any other physical absorption process.

One final, but extremely important observation on wave behaviour and its influence on mass transfer in the rotating disc system, is the tendency for the wave influence to decrease with increasing flowrate, at a particular disc speed. Since the practical application of this system may require operation with high flowrates (say 1.0×10^{-3} m^3/s disc) at the lower disc speeds (about 500 rpm), then the value of the mixing induced by the waves under these conditions may not make use of the smooth disc on economic proposition. However the predictions of the modified model indicate that attractive rates of mass transfer can be achieved with mixing/exposure behaviour which, whilst not provided by waves under conditions of high flowrate at low disc speed, might be achieved by a suitable design of disc surface.

This approach to the problem, from an engineering viewpoint, might be much more attractive than reliance on the rather arbitrary nature of wave behaviour.

13. RECOMMENDATIONS FOR FUTURE WORK

Mass Transfer Studies

(1) The initial experimental work on the concentration profile of oxygen across the disc should be extended with the effects of different mole fractions of surfactant (which have important implications in the commercial processing of industrial liquids).

(2) Roughened inclined plane has shown three fold increase in mass transfer rate compared with smooth surface inclined plane (154). This enhanced mass transfer effect should be extended on rotating disc.

(3) More sophisticated technique of oxygen concentration measurement should be developed, for example, embedded oxygen electrodes across the disc. This enables the concentration profile across the disc to be determined without disturbing the flow.

(4) The effect of shroud with and without induced air flow should be investigated. This enables the determination of the effect of drag on mass transfer rate at different shroud-disc clearance.

14. NOMENCLATURE

ROMAN		DIMENSIONS
Q', Γ, Q_l	volumetric flowrate per unit normal flow perimeter length	L^2T^{-1}
g	gravitational constant	LT^{-2}
Δs	interfacial area increase	L^2
u,v	velocity	L^2T^{-1}
r,R	in radial direction, also radius	L
y,Y	normal to flow direction	-
x,X	in flow direction	-
t	time	T
t_R	residence time	T
Q	total volumetric	L^3T^{-1}
K	consistency index for power law non-Newtonian liquids	$MT^{n-2}L^{-1}$
n	index for power law non-Newtonian liquids	-
A	aspect ratio (= G/r_i)	-
A	interfacial area	L^2
A	wave amplitude	L
G	distributor/flow surface gap	L
C	concentration	ML^{-3} (ppm)
D	diffusivity of solute in liquid	L^2T^{-1}
K_L	mass transfer coefficient	LT^{-1}
K_L	average mass transfer coeff.on disc	LT^{-1}
N	rotational speed	rpm
a	interfacial area per unit volume of liquid	L^{-1}
c	concentration of solute at any time in bulk liquid	moles/l
D_{turb}	turbulent diffusivity of solute in liquid	L^2T^{-1}
D_{mol}	molecular diffusivity of solute in liquid	L^2T^{-1}
a	proportionality constant in eddy diffusivity expression	$L^{2-n}T^{-1}$
m	mass of solute in liquid	ML^{-3}
w	angular velocity	T^{-1}

GREEK		DIMENSIONS
δ	film thickness	L
ν	kinematic viscosity($=\mu/\rho$)	L^2T^{-1}
μ,η	viscosity	$ML^{-1}T^{-1}$
ρ	density	ML^{-3}
α	surface tension contact angle	deg
σ, γ	surface tension	MT^{-2}
θ	angle of plane inclination	deg
τ	shear stress	$ML^{-1}T^{-2}$
ε	eddy viscosity	$ML^{-1}T^{-1}$
ε	energy dissipation rate per unit	$ML^{-1}T^{-3}$
ϕ	total mass transfer	MT^{-1}
ψ	contact time/δ^2	TL^{-2}
ε	eddy diffusivity	L^2T^{-1}

DIMENSIONLESS GROUP		
Re_l, Re^*	Reynolds number	$\frac{Q'}{\nu}$, $\frac{4Q'}{\nu}$
Re_i	critical Reynolds	$\frac{Q'}{\nu}$
N_σ	surface tension number	$\frac{\sigma}{\rho}\left(\frac{1}{\nu^4 g}\right)^{1/3}$
Re	Reynolds number	$Q/r\nu$
Ta	Taylor number	wr^2/ν
We	Weber number	$V_r/\left(\frac{\sigma}{\rho\delta}\right)^{1/2}$
Sc	Schmidt number	ν/D
N_{Gr}	Grasnof number	$g\rho^2\nu a^3\Delta z/\mu^2$
W^*	wavelength	λ/r_o
A^*	wave amplitude	amplitude/r_o

R_I^*	wave inception	inception length/r_c
R^*	radius	r/r_o
Sh	Sherwood number	$\frac{K_L \bar{\delta}}{D}$

SUB-SCRIPTS

C	CRITICAL
e	effective
i	at inlet
av	average
x,y,r,θ	in x,y,y,r,θ directions respectively
o	at the edge of the distributor
s	free surface
a	air
L	liquid
b	bulk
m	mean velocity
g	gas

SUPERSCRIPTS

-	average
+	non-dimensionalised
*	equilibrium

15. REFERENCES

1. EMMERT, R.E., PIGFORD, R.L.
   A study of gas absorption in falling liquid films
   Chem. Eng. Prog., 50, 87 (1954)

2. STIRBA, C., HURT, D.M.
   Turbulence in falling liquid film
   AIChE. J., 1, 178 (1955)

3. ALLEN, J.M.
   Some studies on falling liquid films
   Ph.D. thesis, Manchester Coll. Sci. and Technology (1962)

4. JACKSON, M.L.
   Liquid films in viscous flow
   AIChE. J., 1, 231 (1955)

5. PORTALSKI, S.
   The mechanism of flow in wetted wall columns
   Ph.D. thesis, Uni. London, England (1960)

6. DUCKLER, A.E., BERGELIN, O.P.
   Characteristics of flow in falling liquid films
   Chem. Eng. Prog., 48, 557 (1952)

7. BEEK, W.J., KRAMERS, H.
   Mass transfer during single drop formation
   Chem. Eng. Sci., 19, 357 (1964)

8. POPOVICH, A.T., JERVIS, R.E., TRASS, O.
   Mass transfer during single drop formation
   Chem. Eng. Sci., 19, 357 (1964)

9. BRAUER, H.
   Chem. - Ing. - Tech., 30, 75 (1958)

10. DAVIES, J.T., BRADLEY, P.J.
    Research Project
    Dept. Chem. Eng. Cambridge Uni. (1960)

11. DOWNING, A.L., TRUESDALE, G.A.
    Some factors affecting the rate of solution of oxygen in water
    J. Appl. Chem., 5, 570 (1955)

12. HOPf, L.
Turbulent bei einen flusse
Ann. Physik (4) 32, 777 (1910)

13. WARDEN, C.P.
M.Sc. thesis, Mass. Inst. Technol. Cambridge
Massachusetts (1930)

14. FALLAH, A., HUNTER, T.G., NASH, A.W.
J. Soc. Chem. Ind., 53, 3697 (1934)

15. BRAUER, H.
Stromung und warmeiibergang bei rieselfilmen
VDI - Forschungsheft, 457 (1956)

16. KAMEI, S. and OISHI, J.
Mass and heat transfer in a falling liquid film
up wetted wall tower
Mem. Fac. Eng. Kyoto Uni., 18, 1 (1956)

17. STAINTHORP, F.P., BATT, R.S.W.
The effect of co-current and counter-current air
flow on the wave properties of falling liquid films
Trans. Instn. Chem. Engrs., 45, 7372 (1967)

18. STAINTHORP, F.P., ALLEN. J.M.
The development of ripples on the surface of a
liquid film flowing inside a vertical tube
Trans. Instn. Chem. Engrs., 43, 785 (1965)

19. MUENZ, K., MARCHELLO. J.M.
Techniqud for measuring amplitudes of small surface
waves
The Review of Science Instruments, 35, No.8, 953 (1964)

20. SOLESIO, J.N.
Hydrodynamics of liquid films
Physicochemical Hydrodynamics (New Volume) by
Levich pp 711

21. TELLES, A.S., DUCKLER, A.E.
Statistical characteristics of thin, vertical, wavy
liquid films
Ind. Eng. Chem. Fundam., 9, No.3, 412 (1970)

22. NUSSELT, W.
Der warmeaustausch am berieselelungskiihler
Zeit. Vereines Deut. Ing., 67, 206, (1928)

23. CHWANG, C.T.
M.Sc. thesis, Mass. Inst. Technol. Cambridge,
Massachusetts (1928)

24. FULFORD, G.D.
The flow of liquid in thin film
Advances in Chem. Eng., 5, 151 (1969)

25. CLEGG, A.J., PORTALSKI, S.
An experimental study of wave inception on
falling liquid films
Chem. Eng. Sci., 27, 1257 (1972)

26. BELL, C.
The hydrodynamics and heat transfer characteristics
of liquid films on a rotating disc.
Ph.D. thesis, Univ. of Newcastle-u-Tyne (England 1975)

27. JAZAYERI, A.
Hydrodunamic of Newtonian and non-Newtonian liquids
across a rotating disc
Ph.D. thesis, Univ. of Newcastle-u-Tyne (England 1980)

28. KIRKBRIDE, C.G.
Heat transfer by condensing vapour on vertical tubes
Ind. Eng. Chem., 26, 425 (1934)

29. BINNIE, A.M.
Experiment on the onset of wave formation on a film
of water flowing down a vertical plane
J. Fluid Mech., 2, 551 (1957)

30. FRIEDMAN, S.L., MILLER, C.O.
Liquid films in the viscous flow region
Indus. Engng. Chem., 33, 885 (1941)

31. GRIMLEY, S.S.
Liquid flow conditions in packed towers
Trans. Inst. Chem. Engrs., 23, 228 (1945)

32. KAPITZA, P.L.
Wave flow of thin layers of a viscous fluid
Collected Works of Kapitza, P.L. Pergammon Press (London) 662 (1965)

33. YIH, C.S.
Stability of liquid flow down an inclined plane
Phys. Fluids, 6, 321 (1963)

34. GREENBERG, A.B.
The mechanics of film flow on a vertical surface
Ph.D. thesis, Univ. Purdue, Lafayette, Indiana (1956)

35. STAINTHORP, F.P., WILD, G.W.
Film flow - the simultaneous measurement of wave amplitude and the local mean concentration of a transferable component
Chem. Eng. Sci., 22, 701 (1967)

36. HEWITT, G.F., LOVEGROVE, P.C., NICHOLLS, B.
Atomic Energy Research Establishments - R4478

37. CLEGG, A.J.
Studies of film flow on wetted wall columns
Ph.D. thesis, Univ. of Surrey (1969)

38. BLACK, R.H.
Capacitance method of measuring water film thickness
Trans. Am. Soc. Civ. Eng., 126, pt.1, 88 (1961)

39. SHIROTSUKA, T., HONDA, N., OHATA, Y.
Chem. Eng. (Tokyo), 21, 702 (1957)

40. DUCKLER, A.E.
Fluid mechanics and heat transfer in vertical falling film systems
Amer. Inst. Chem. Engrs., 56, 1 (1960)

41. WILKES, J.O., NEDDERMAN, R.M.
The measurement of velocities in thin films of liquid
Chem. Eng. Sci, 17, 177 (1962)

42. TRACEY, H.J., LESTER, C.M.
Geological survey - water supply 1952 A
Washington : U.S. Department of the Interior (1961)

43. ATKINSON, B., CARUTHERS, P.A.
Velocity profile measurements in liquid films
Trans. Instn. Chem. Engrs., 43, T33 (1965)

44. POPOVICH, A.T., HUMMEL, R.L.
A new method for non-disturbing turbulent flow measurements very close to a wall
Chem. Eng. Sci., 22, 21 (1967)

45. JEPSEN, J.C., CROSSER, O.K., PERRY, R.H.
The effect of wave induced turbulence on the rate of absorption of gases in falling liquid films.
AIChE. J., 12, 186 (1966)

46. VOUYOUCALOS, S.
Effect of surface roughness and hydrolysis on mass transfer
M.Sc. thesis, Univ. Birmingham (England 1961)

47. WHITAKER, S.
Effect of surface active agents on the stability of falling liquid films
I.F.C. Fundamentals, 3, No.2, 132 (1964)

48. LEVICH, V.G.
Physicochemical hydrodynamics
Prentice-Hall (1962)

49. BENJAMIN, T.B.
Effects of surface contamination on wave formation in falling liquid films
Arch. Mech. Stes., 16, 615-626

50. HOLFMAN, M.A., POTTS, W.W.
Experimental behaviour of falling liquid films at high surface tension numbers.
Ind. Eng. Chem. Fundam., 18, No.1, 27 (1979)

51. BRAUER, H.
Stromung und warmeiibergang bei rieselfilmen
VDI - Forschungsheft, 457 (1956)

52. DAVIES. J.T.
University research in Chemical Engineering
Birmingham Univ. Chem. Eng., 12, 5 (1961)

53. HARTLEY, D.E., MURGATROYD, N.
Criteria for the break-up of thin liquid layers flowing isothermally over solid surfaces
Int. J. Heat and Mass Transfer, 7, 1003 (1964)

54. IIJIMA, T., KUZUOKA, T.
Kagaku Kogaku, 32, 52 (1968)

55. HOBLER, T., CZAJKA, J.
Chemia Stosowana Ser B, 5, 169 (1968)

56. BOND, J., DONALD, M.B.
The effect of absorption on the wetted area of absorption towers
Chem. Eng. Sci., 6, No.6, 237 (1957)

57. NORMAN, W.S., BINNS, D.T.
The effect of surface tension changes on the minimum wetting rates in a wetted rod distillation column
Trans. Instn. Chem. Engrs, 38, 20 (1960)

58. PONTER, A.B., BOYES, A.P.
The rupture of isothermal vertical liquid films.
J. Chem. Eng. Japan, 5, 80 (1972)

59. TYABIN, N.V., GLINKIN, A.D.
Movement of a stream of viscous liquid over the surface of a stationary plane disc
B.L.L. RTS 9301

60. WATSON, E.J.
The radial spread of a liquid jet over a horizontal plate
J. Fluid Mechanics, 20, 481 (1964)

61. VENKATARAMAN, R.S.
Mass transfer to an expanding interface
Ph.D. thesis, Leeds Univ. (England 1966)

62. WILSON, H., PAGE, G.A., CARTWRIGH V.S.
U.S. Bur. Mines, Repts. Investi., 3248 (1934)

63. WALTON, W.H., PREWETT, W.C.
The production of sprays and mists of uniform drop size by means of spinning disc type sprayers
Proc. Phys. Soc. London, 62B, 341 (1949)

64. HINZE, J.O., MILBORN, H.
Atomization of liquids by means of a rotating cup
J. Appl. Mechanics, 145 (1950)

65. VITER, A.V., ZAICHENKO, M., MARCHENKO, M. PLAUNIK, V.P.
Concentration of solution containing thermolabile and foaming substances
Khim. Farmat. Zhur., 12, 45 (1968)

66. HICKMAN, K.C.D.
High vacuum short path distillation
Chem. Reviews, 34, 51 (1944)

67. REES, E.L.
Flow and heat transfer on a rotating disc
M.Sc. thesis, Swansea Univ. (England 1962)

68. MANDAPURKAR, S.S., BEATTY, K.O.
Condensation on a horizontal rotating disc
Chem. Eng. Symposium Series, 56, 129 (1960)

69. SPARROW, E.M., GREGG, J.L.
Mass transfer, flow and heat transfer about a rotating disc
J. Heat Transfer (ASME Series C), 82, 294 (1960)

70. SPARROW, E.M., GREGG, J.L.
A theory of rotating condensation
J. Heat Transfer (ASME Series C), 81, 113 (1959)

71. SPARROW, E.M., GREGG, J.L.
The effect of vapour drag on rotating condensation
J. Heat Transfer (ASME Series), 82, 71 (1960)

72. ESPIG, H., HOYLE, R.
Waves in a thin liquid layer on a rotating disc
J. Fluid Mechanics, 22, 671 (1965)

73. DIXON, B.E., RUSSEL, A.A.W., SWALLOW, J.E.L.
Liquid films formed by means of rotating discs
British J. Appl. Phys., 3, 115 (1952)

74. EMSLIE, A.G., BONNER, F.T., PECK, L.G.
Flow of a viscous liquid on a rotating disc
J. Appl. Physic, 29, 858 (1958)

75. FRAIDENRAICH, N.
Flow of a liquid film over a rotating disc
Revista Mexicana de Fisica, 25, 69 (1976)

76. ACRIVOS, A., SHAH, M.J., PETERSEN, E.E.
On the flow of a non-Newtonian liquid on a rotating disc
J. Appl. Phys., 31, 963 (1960)

77. ZINNATULLIN, N.Kh., VACHAGIN, K.D., TYABIN, N.V.
The two dimensional flow of a non-Newtonian fluid over the open surface of a rapidly rotating flat disc
J. Eng. Physics, 15, 701 (1968)

78. ZINNATULLIN, N.Kh.
The flow of a non-Newtonian liquid on a rotating disc
B.L.L. RTS - 8933

79. TYABIN, N.V., SHKLYAR, L.A., MOSIKHIN, Ye.P., VINOGRADOV, G.V.
Rheologic investigation of a grease lubricant by the centrifugal method
Translation 14960 - U.S. Dept. Commerce, Office of Technical Services, Washington

80. UKLISTYI, A.E., TYABIN, N.V., RYABCHUK, G.V., LEPEKHIN, G.I.
Spreading of a non-Newtonian liquid over the surface of centrifugal atomisers
Khimicheskoe i Neftyaone Mashinostroenie, No.6, 19 (1976)

81. KOSTROMIN, V.P., KUZNETSOV, V.G., VACHAGIN, K.D.
Thin film flow of a quosiviscous fluid over the surface of a rotating nozzle
Inshenerno-Fizichenskii Shurnal, Vol.30, No.1, 88 (1976)

82. YURCHENKO, V.A., KOPTEV, A.A., ZAITSEN, A.I., ZHEBROVSKII, A.K.
Investigation of the hydrodynamics of two phase flow on the surface of a rotating disc
Theo. Foundations of Chem. Eng., 3, 341 (1969)

83. VACHAGIN, K.O, NIKOLAEV, V.S.
Flow of a viscous liquid over the surface of a rapidly rotating flat disc
B.L.L. RTS 8906

84. RAUSCHER, J.W., KELLEY, R.E., COLE, J.D.
An asymptotic solution for the laminar flow of a thin film on a rotating disc
J. Appl. Mechanics (ASME Series E) 40, 43 (1975)

85. MATSUMOTO, S., SAITO, K., TAKASHIMA, Y.
Flow of a viscous liquid on a rotating disc
Bull. Tokyo Inst. Tech., 109 (1972)

86. MATSUMOTO, S., SAITO, K., TAKASHIMA, Y.
Thickness of liquid film on a rotating disc
Bull. Tokyo Inst. Tech., 116 (1973)

87. MARSHALL, W.R. (Jr.), SELTZER, E.
Principles of spr ay drying
Chem. Eng. Prog., 46, 501 and 575 (1950)

87a. MARSHALL, W.R. (Jr.), ADLER, C.R.
Performance of spinning disc atomisers Part 1 and 2
Chem. Eng. Prog., Vol.47, No.10, 515 and 601 (1951)

88 CLARE
(See 90, 94)

89. WATTS, B.
The flow, heat and mass transfer characteristics of a rotating disc
Ph.D. thesis, Swansea Univ. (1971)

90. CLARE, H., JEFFS, R.A.
Some measurements of the thickness of a fluid film on a spinning disc
National Gas Turbine Establishment, Draft report 12.12.60

91. JONES, G.C.A.
Some mathematics relevant to the flow of a fluid film on a spinning disc
National Gas Turbine Establishment, Eng. report Note No.40, June 1962

92. SLEICHER, C.A.
Experimental velocity and temperature profiles for air in turbulent pipe flow
Trans. Amer. Soc. Mech. Engrs., 80, 693 (1958)

93. DAVIES, E.J.
An analysis of liquid film flow
Chem. Eng. Sci, 20, 265 (1965)

94. CLARE, H., ASHWOOD, P.F.
Measurement of the thickness of a liquid film on the surface of a rapidly rotating disc
Inst. Practice, 16, 70 (1962)

95. GAZLEY, C., CHARWAT, A.F.
The characteristics of a thin liquid film on a spinning disc
Third All-Union Conf. on Heat and Mass Transfer, Minsk., Hay 14-18, (1968)

96. CHARWAT, A.F., KELLEY, R.E., GAZLEY, C.
Flow and stability of thin liquid films on a rotating disc
J. Fluid Mechanics, 53, 227 (1972)

97. POVAROV, O.A., VASIL'CHENKO, E.G., PETROV, P.G.
Wave flows of thin fluid layers in a field of centrifugal forces
Izv-Akad Nauk SSSR. Energetika i Transport
Vol.16, No.1, 172 (1978)

98. KAMIYA, T., KAYANO, A.
Film type disintegration by rotating disc
J. Chem. Eng. Japan, 5, 174 (1972)

99. DE GRAAF, J.G.A.
The mechanism of spray drying liquids from a high speed rotating disc
High Speed Photography Editor R.B. Collings
Butterworths Scientific Publications 1957 (London)
p.385

100. BUTUZOV, A.I., RIFERT, V.G.
Experimental investigation of heat transfer to evaporating liquid film on a rotating disc
Izv. Vuz. Mashin., 2, 81 (1972) or B.L.L. RTS 9462

100a. ASBJORSEN, O.A.
The distribution of residence times in a falling water film
Chem. Eng. Sci., 4, 211 (1961)

100b. SCHLICHTING, H.
Boundary layer theory
McGraw-Hill (N.Y.) 4th Edition, p.87, 1960

100c. TAIBY, S., PORTALSKI, S.
The hydrodynamics of liquid films flowing on a vertical surface
Trans. Inst. Chem. Eng., 38, 324 (1960)

100d. THOMAS, W.J., PORTALSKI, S.
Countercurrent flow in wetted-wall columns
Ind. Engng, Chem., 50, 1081 (1958)

101. LEWIS, W.K., WHITMAN, W.G.
Two-film theory of gas absorption
Ind. Eng. Chemistry, 16, 1215 (1924)

102. WHITMAN, W.G.
The two-film theory of gas absorption
Chemical and Metallurfical Engineering, 29, 146 (1925)

103. HIGBIE, R.
The rate of absorption of a pure gas into a still liquid during short periods of exposure
AIChE Transactions, 31, 365 (1935)

104. DANCKWERTS, P.V.
Significance of liquid-film coefficient in gas absorption
Ind. Eng. Chemistry, 43, 1460 (1951)

105. TOOR, H.L., MARCHELLO, J.M.
Film-penetration model for mass and heat transfer
AIChE J., 4, 97 (1958)

106. BIRD, R.B., STEWART, W.E., LIGHTFOOT, E.N.
Transport phenomena
John Wiley and Sons, Inc., N.Y. (1966)

107. DAVIES, J.T.
Mass-transfer and interfacial phenomena
Advances in Chem. Engng., 4, 1 (1963)

108. DAVIES, J.T., RIDEAL, E.K.
Interfacial phenomena
2nd Ed., Academic Press, N.Y., (1963)

109. KISHINEVSKII, M.K., DAMILAV, A.V.
Zh. Prikl. Khim., 22, 1173 (1949)

110. HARRIOTT, P.
A random eddy modification of the penetration theory
Chem. Eng. Sci., 17, 149 (1962)

111. FURTESCUE, G.E., PEARSON, J.R.A.
On gas absorption into a turbulent liquid
Chem. Eng. Sci., 22, 1163 (1967)

112. RUCKENSTEIN, E.
Chem. Eng. Journal, 2, 1 (1971)

113. RITZEL, A.
Z. Phys. Chem., 60, 319 (1907)

114. ZIOKING, B.G., KAZARNOVSKII, Ya.S.
Zhurn, Fis. Khim., 4, 683 (1933)

115. UHLIG, H.H.
The solubilities of gases and surface tension
J. Phys. Chem. Vol.41, No.9, 1215 (1937)

116. LEVICH, V.G.
On the theory of surface phenomena
Izd. Sovotskaya Nauka (1941)

117. TERNOVSKAYA, A.N., BELOPOL'SKII, A.P.
The absorption of gases in the presence of surface active materials
Zhurnal Fizicheskoi Khimi, Vol.24, 43 (1950)

118. DAVIES, J.T., KILNER, A.A., RATCLIFF, G.A.
The effect of diffusivities and surface films on rates of gas absorption
Chem. Eng. Sci., Vol,19, 583 (1964)

119. WON, Y.S., MILLS, A.F., CHUNG, D.K.
The effect of surface tension on gas absorption into a freely falling turbulent liquid film
Levich, V.G. - Physicochemical Hydrodynamics (New Volume) pp 109

120. GAMENSON, A.L.H., TRUESDALE, G.A., VARLEY, R.A.
Water Sanit. Engr., 6, 52 (1956)

121. DOWNING, A.L., MELBOURNE, K.V., BRUCE, A.M.
The effect of contaminants on the rate of aeration of water
J. Appl. Chem., 7, 590 (1957)

122. LAMONT, J.C., SCOTT, D.C.
Mass transfer from bubbles in cocurrent flow
Can. J. Chem. Eng., 44, 201 (1966)

123. YOSHIDA, F., ARAKAWA, S.I.
Pressure dependence of liquid phase mass transfer coefficients
AIChE J., 14, No.6, 962 (1968)

124. PHILLIPS, K.L.
Proposed explanation for apparent dependence of liquid phase mass transfer coefficients on pressure
Can. J. Chem. Eng., 51, 371 (1973)

125. GOODRIDGE, F., GARTSIDE, G.
Mass transfer into near-horizontal liquid films
Trans. Instn. Chem. Engrs., Vol.43, T62 (1965)

126. LYNN, S., STRAATEMEIER, J.R., KRAMERS, H.
Absorption studies in the light of the penetration theory
Chem. Eng. Sci., 4, No.2, 49 (1955)

127. HATTA, S.
Soc. Chem. Ind. (Japan), 37, 375B (1934)

128. SHERWOOD, T.K., PIGFORD, R.L.
Absorption and extraction
2nd Ed., McGraw-Hill (1952)

129. VIVIAN, J.E., PEACEMAN, D.W.
Liquid-side resistance in gas absorption
AIChE J., 2, No.4, 437 (1956)

130. FULFORD, G.D.
The effect of thickness of flowing films on heat and mass transfer
Thesis Digest (Birm. Univ. Chem. Eng.)

131. OLIVER, D.R., ATHERINOS, T.E.
Mass transfer to liquid films on an inclined plane
Chem. Eng. Sci., 13, 525 (1968)

132. PIGFORD, R.L.
Ph.D. Thesis, University of Illinois (1941)

133. ROTEM, I., NEILSON, J.E.
Exact solution for diffusion to flow down an incline
Can. J. Chem. Eng., 47, 341 (1969)

134. MURTY, V.N., SARMA, P.K.
A theoretical analysis of mass transfer from a gas into accelerating thin falling liquid film flowing along an inclined surface
Int. Heat Transfer Conf. 6th, 2, 341 (1978)

135. MUENZ, K., MARCHELLO, J.M.
Surface motion and gas absorption
AIChE J., 12, No.2, 249 (1966)

136. BOYD, D.P., MARCHELLO, J.M.
Role of films and waves on gas absorption
Chem. Eng. Sci., 21, 769 (1966)

137. GOREN, S.L., MANI, R.V.
Mass transfer through horizontal liquid films in wavy motion.
AIChE J., 14, No.1, 57 (1968)

138. RICE, R.G.
A dynamic theory of mass transfer at a wavy interface
Can. J. Chem. Eng., 49, 241 (1971)

139. HOWARD, D.W., LIGHTFOOT, E.N.
Mass transfer to falling films
AIChE J., 14, No.3, 458 (1968)

140. RUCKENSTEIN, E., BERBENTE, C.
Mass transfer in wave flow
Chem. Eng. Sci., 20, 795 (1965)

141. JAVDANI, K.
Mass transfer in wavy liquid films
Chem. Eng. Sci., 29, 61 (1974)

142. RUCKENSTEIN, E., BERBENTE, C.
Mass transfer to falling liquid films at low Reynolds numbers
Int. J. Heat Mass Transfer, 11, 743 (1968)

143. BROTZ, W.
Chemie. Ing-Technik, 26, 470 (1954)

144. BRUMFIELD, L.K., HOUZE, R.W., THEOFANOUS, T.G.
Turbulent mass transfer at free, gas-liquid interfaces, with applications to film flows
Int. J. Heat Mass Transfer, 18, 1077 (1975)

145. BANERJEE, S., SCOTT, D., RHODES, E.
Mass transfer to falling wavy liquid films in turbulent flow
I and EC Fundamentals, 7, No,1, 22 (1968)

146. PHILLIPS, O.M.
J. Geophys. Res., 68, 2889 (1961)

147. LAMOURELLE, A.P., SANDALL, O.C.
Gas absorption into a turbulent liquid
Chem. Eng. Sci., 27, 1035 (1972)

148. DAVIES, J.T.
The effects of surface films in damping eddies at a free surface of a turbulent liquid
Proc. R. Soc. London, A290, 515 (1966)

149. ELROD, H.G.
Note on the turbulent shear stress near a wall
J. Aero. Sci., 24, 268 (1957)

150. Tien, G.L., WASAN, D.T.
Law of the wall in turbulent channel
Phys. of Fluids, 6, 144 (1963)

151. KING. C.J.
Turbulent liquid phase mass transfer at a free gas-liquid interface
I and EC Fundamentals, 5, No.1, 1 (1966)

152. BANERJEE, S., RHODES, E., SCOTT, D.S.
Mass transfer to falling wavy liquid films at low Reynolds numbers
Chem. Eng. Sci., 22, 43 (1967)

153. PRASHER, B.D., FRICKE, A.L.
Mass transfer at a free gas-liquid interface in turbulent thin films
Ind. Eng. Chem. Process Des. Develop, 13, No.4, 336 (1974)

154. DAVIES, J.T., WARNER, K.V.
The effect of large-scale roughness in promoting gas absorption
Chem. Eng. Sci., 24, 231 (1969)

155. DAVIES, J.T.
Turbulence phenomena at free surfaces
AIChE J., 18, No.1, 169 (1972)

156. HENSTOCK, W.H., HANRATTY, T.J.
Gas absorption by a liquid layer flowing on the wall of a pipe
AIChE J., 25, No.1, 122 (1979)

157. CHUNG, D.K., MILLS, A.F.
Experiemntal study of gas absorption into turbulent falling films of water and ethylene glycol-water mixture
Int. J. Heat Mass Transfer, 19, 51 (1976)

158. KOZIOL, K., BRONIAZ, L., NOWICKA, T.
Transfer process in film apparatus: Mass transfer during flow of a film of liquid down smooth pipes
Int. Chem. Eng., 20, No.1, 136 (1980)

159. RUCKENSTEIN, E.
The influence of the Marangoni effect on mass transfer in flowing films
Int. Chem. Eng., 5, No.1, 88 (1965)

160. SMIGELSCHI, O., SUCIU, D.G., RUCKENSTEIN, E.
Absorption under the action of artificially provoked Marangoni effect
Chem. Eng. Sci., 24, 1227 (1969)

161. KREITH, F., TAYLOR, J.H., CHONG, J.P.
Heat and mass transfer from a rotating disc
Trans. ASME, 95 (May 1959)

162. WAGNER, C.
Heat transfer from a rotating disc to ambient air
J. Appl. Phys., 19, 837 (1948)

163. KREITH, F., DOUGHMAN, E., KOZLOWSKI, H.
Mass and heat transfer from an enclosed rotating disc with and without source flow
Trans. of ASME, 153 (May 1963)

164. TIEN, C.L., CAMPBELL, D.T.
Heat and mass transfer from rotating cones
J. Fluid Mech., 17, 105 (1963)

165. FEDEROV, B.I., PLAVNIK, G.Z., ZHUKHOVITSKII, L.G.
Heat and mass transfer from a rotating disc
Vest. Akad. Narik. BSSR Ser. Fiz. Energy, Navuk

166. MISHRA, P., SINGH, P.C.
Mass transfer from spinning disc
Chem. Eng. Sci., 33, 1449 (1978)

167. MISHRA, P., SINGH, P.C.
Mass transfer from spinning disc
Chem. Eng. Sci., 33, 1463 (1978)

168. SHULMAN, Z.P., POKRYVAILO, N.A., KORDONSKY, O.I., NESTEROV, A.K.
Mass transfer peculiarities of a disc rotating in non-Newtonian fluid

169. HANSFORD, G.S., LITT, M.
Mass transfer from a rotating disc into poqer-law liquids
Chem. Eng. Sci., 23, 849 (1968)

170. SOVOVA, H., PROCHAZKA, J.
A new method of measurement of diffusivities of gases in liquids
Chem. Eng. Sci., 31, 1091 (1976)

171. MERSON, R.L., QUINN, J.A.
Diffusion and flow in a radially moving film
AIChE J., 10, No.6, 804 (1964)

172. POTTER, E.C.
The microdetermination of dissolved oxygen in water
J. Appl. Chem., 285 (1957)

173. WINKLER
10th Ed., Amer. Pub. Health Assn., N.Y. (1955)

174. OULMAN, C.S., BAUMANN, E.R.
A colorimetric method for determining dissolved oxygen
Sewage and Industrial Wastes, 28, No.12, 1461 (1956)

175. SNELL, F.D., SNELL, C.T.
3rd Ed., D. Van Nustrand Co. Inc., N.Y. (1953)

176. BRIGGS, K., KNOWLES, G., SCRAGG, L.J.
Analyst, 79, 744 (1954)

177. LAMBER-BEER LAW
Physical Chemistry p.750 by Walter J Moore
5th Edition

178. JANSSEN, C.
Analytica Chemica Acta, 2, 622 (1948)

179. MANCY, K.H., OKUN, D.A.
A galvanic cell oxygen analyser
Journal of Electroanalytical Chem., 4, 65 (1962)

180. WATANABE, H., LEONARD, J.E.
Beckman Instrument Co., Fullerton, Calif.,
Unpublished data, presented at Pittsburg,
Conference on Analytical Chemistry and Applied
Spectroscopy, March 1957

181. MULLER, O.H.
J. Am. Chem., 69, 2992 (1947)

182. DAVIDSON, J.F., CULLEN. E.J.
The determination of diffusion coefficients for
sparingly soluble gases in liquids
Trans. Instn. Chem. Engrs., 35, 51 (1957)

183. GAINER, J.C., METZNER, A.B.
Diffusion in liquids - theoretical analysis and
experimental verification
AIChE - Int. Chem. Eng. Symp. Series, 6, 74 (1965)

184. WILKE, C.R., CHANG, P.
Correlation of diffusion coefficients in dilute solution
AIChE J., 1. 264 (1955)

185. AKGERMAN, A.
Predicting gas-liquid diffusion coefficients
Ph.D. Thesis, Uni. of Virginia (1971)

186. AKGERMAN, A., GAINER, J.C.
Diffusion of gases in liquids
Ind. Eng. Chem. Fundam., 11, 373 (1972)

187. SRIDHAR, T., POTTER, O.E.
Predicting diffusion coefficients
AIChE J., 590 (1977)

188. HILDEBRAND, J.H.
Motions of molecules in liquids: viscosity and diffusivity
Science, 174, 490 (1971)

189. DULLIEN, F.A.L.
Predictive equation for self-diffusion in liquid: a different approach
AIChE J., 18, 62 (1972)

190. DUDA, J.L., VRENTAS, J.A.
Laminar liquid jet diffusion studies
AIChE J., 286 (1968)

191. CHIANG, S.H., TOOR, H.L.
Interfacial resistance in the absorption of oxygen by water
AIChE J., 5, 165 (1959)

192. BAIRD, M.H.I., DAVIDSON, J.F.
Annular jets - gas absorption
Chem. Eng. Sci., 17, 473 (1962)

193. WISE, D.L., HOUGHTON, G.
The diffusion coefficients of ten slightly gases in water at 10-60^{o}C
Chem. Eng. Sci., 21, 999 (1966)

194. KRIEGOR, I.M., MULHOLLAND, G.W., DICKEY, C.S.
Diffusion coefficients for gases in liquids from the rates of solution of small gas bubbles
J. Phys. Chem., 71, No.4, 1123 (1967)

195. FERRELL, R.T., HIMMELBLAU, D.M.
Diffusion coefficients of nitrogen and oxygen in water
J. Chemical and Engng. Data, 12, No.1, 111 (1967)

196. VIVIAN, J.E., KING, C.J.
Diffusivities of slightly soluble gases in water
AIChE J., 10, No.2, 220 (1964)

197. ONDA, K., OKAMOTO, T., YAMAJI, Y.
Chem. Engng. (Japan), 24, 918 (1960)

198. GORDON, A.R.
The diffusion constant of an electrolyte, and its relation to concentration
J. Chem. Phys., 5, 522 (1937)

199. GLASSTONE, S.K., LAIDLER, J., EYRING, H.
The theory of rate process
McGraw-Hill, N.Y. (1941) p.516

200. DARKEN. L.S.
Trans. Amer. Inst. Min. (Metall) Engrs., Metals Div., 175, 184 (1948)

201. HARTLEY, G.S., CRANK, J.
Some fundamental definitions and concepts in diffusion processes
Trans. Faraday Soc., 45, 801 (1949)

202. TANG, Y.P., HIMMELBLAU, D.M.
Effect of solute concentration on the diffusivity of carbon dioxide in water
Chem. Eng. Sci., 20, 7 (1965)

203. GUBBINS, K.E., BHATIA, K.K., WALKER, R.O.(Jnr.)
Diffusion of gases in electrolytic solutions
AIChE J., 12, No.3, 548 (1968)

204. LINEK, V., MAYRHOFEROVA, J., MOSNEROVA, J.
The influence of diffusivity on liquid phase mass transfer in solutions of electrolytes
Chem. Eng. Sci., 25, 1033 (1970)

205. IRAJ, Z., TURNER, C.D.
The absorption of oxygen by dilute polymeric solutions molecular diffusivity measurement
Chem. Eng. Sci., 25, 517 (1970)

206. GOFFI, J.N.
Rates of oxygen transfer from air through rippling surfaces of electrolytic solution
Microfilm (73, 32322) B.L.L. (1973)

207. McCALL, D.W., DOUGLASS, D.C.
The effect of ions on the self-diffusion of water
J. Phys. Chem., 69, 2001 (1965)

208. WANG. J.H.
Effect of ions on the self-diffusion and structure of water in aqueous electrolytic solutions
J. Phys. Chem., 58, 686 (1954)

209. DEVELL, L.
Acta Chemica Scandinavica, 16, 2177 (1962)

210. LONG. F.A., McDEVITT, W.F.
Chem. Rev., 51, 119 (1952)

211. BERNAL, J.D., FOWLER, R.H.
A theory of water and ionic solution, with particular reference to hydrogen and hydroxylions
J. Chem. Phys., 1, 515 (1933)

212. GURNEY, R.W.
Ionic process in solution
Dover Publications, Inc., N.Y. (1953)

213. LATIMER, W.M.
Single ion free energies and entropies of aqueous ions
J. Chem. Phys., 23, 90 (1955)

APPENDIX A

Laminar Flow under Gravitational Influence

The most general equations for laminar flow of a viscous incompressible fluid of constant density and dynamic viscosity are the Navier-Stokes equations. In terms of the rectangular co-ordinates x, y, z, these may be written as

$$U\frac{\partial u}{\partial x} + V\frac{\partial u}{\partial y} + W\frac{\partial u}{\partial z} + \frac{\partial u}{\partial t} = -\frac{\partial F}{\partial x} - \frac{1}{\rho}\frac{\partial p}{\partial x} + \nu\nabla^2 u \qquad A1$$

$$U\frac{\partial v}{\partial x} + V\frac{\partial v}{\partial y} + W\frac{\partial v}{\partial z} + \frac{\partial v}{\partial t} = -\frac{\partial F}{\partial y} - \frac{1}{\rho}\frac{\partial p}{\partial y} + \nu\nabla^2 v \qquad A2$$

$$U\frac{\partial w}{\partial x} + V\frac{\partial W}{\partial y} + W\frac{\partial w}{\partial z} + \frac{\partial w}{\partial t} = -\frac{\partial F}{\partial z} - \frac{1}{\rho}\frac{\partial p}{\partial z} + \nu\nabla^2 w \qquad A3$$

where u, v, w are the velocities in the x, y, z directions, t is the time, ρ and ν are the density and the kinematic viscosity, P is the pressure, F is the force potential of the field in which flow occurs, and ∇^2 is the laplacian operator. In addition, the continuity equation is

$$\frac{\partial u}{\partial x} + \frac{\partial v}{\partial y} + \frac{\partial w}{\partial z} = 0 \qquad A4$$

since only gravity fields will be considered here, the negative derivatives of F are merely equal to the components of g in the respective directions.

For flow on flat plates under gravitational influence the following co-ordinate will be used. The x-axis is directed along the plate surface in the direction of the greatest slope, the z-axis is directed across the plate, and the y-axis is taken perpendicular to the plate.

If the flow is steady, uniform and two dimensional (ie flow of a smooth film on an infinitely wide plate outside the acceleration zone), equation A1 to A3 reduce directly to the

very simple case originally obtained by Hopt and Nusselt ($_{22}$)

$$\frac{\partial^2 u}{\partial y^2} + \frac{g}{\nu} \sin\theta = 0 \qquad \text{A5}$$

$$\frac{\partial p}{\partial y} = \rho g \cos\theta \qquad \text{A6}$$

$$\frac{\partial p}{\partial z} = 0 \qquad \text{A7}$$

Where θ is the slope of the wall, the continuity equation is satisfied automatically with the boundary conditions

(no slip at all) $\quad u = o \quad$ at $\quad y = o$

(no drag at interface) $\quad \frac{du}{dy} = o \quad$ at $\quad y = \delta$

The velocity distribution is given by the semi-parobolic equation

$$u = \frac{g}{\nu} \sin(\delta y - \frac{y^2}{2}) \qquad \text{A8}$$

The surface velocity (at $y = \delta$) is therefore

$$u_s = \frac{g\delta^2}{2\nu} \sin\theta \qquad \text{A9}$$

By integrating (A8) over the film thickness, the mean velocity is found to be

$$u = \frac{g\delta^2}{3\nu} \sin\theta \qquad \text{A10}$$

Hence $$\frac{u_s}{u} = 1.5 \qquad \text{A11}$$

The volumetric flow rate per wetted perimeter is

$$Q_1 = \int_0^\delta u \, dy$$

substituting u from equation (A8) and $\theta = 90^o$ for a vertical wall

$$\delta = (\frac{3\nu Q_1}{g})^{1/3} \qquad \text{A12}$$

For $Re_1 = Q_1/\nu$, film thickness on a vertical wall could be

$$\delta = \left(\frac{3\nu^2}{g}\right)^{1/3} Re_1^{1/3} \qquad A13$$

In dimensionless form

$$\delta^+ = \delta\left(\frac{\theta}{\nu^2}\right)^{1/3}$$

$$= (3Re_1)^{1/3} \qquad A14$$

Equation (A14) has been obtained by Nusselt (22) and has been termed the Nusselt film thickness parameter for smooth and laminar film thickness under gravitational energy. Under wavy film flow, the prediction of Kapitza (24) dimensionless film thickness is

$$\delta^+ = (2.4Re_1)^{1/3} \qquad A15$$

<u>For Non-Newtonian Fluids</u>

The Nusselt model may be rederived for a non-Newtonian fluid described by a power law equation of the type

$$\tau = K\left(\frac{\partial u_x}{\partial y}\right)^n \qquad A16$$

results in the form

$$\frac{d}{dy}\left(\frac{du_x}{dy}\right)^n = -\left(\frac{\rho g \sin\theta}{K}\right) \qquad A17$$

and velocity distribution as

$$u_x = \left(\frac{\rho g \sin\theta}{K}\right)^{1/n}\left(\frac{n}{n+1}\right)\left(\delta^{\frac{n+1}{n}} - (\delta-Y)^{\frac{n+1}{n}}\right) \qquad A18$$

and integrating for the flow rate as

$$Q_1 = \int_0^{\delta} u_x\, dy = \left(\frac{\rho g \sin\theta}{K}\right)^{1/n}\left(\frac{n}{2n+1}\right)\delta^{\frac{2n+1}{n}} \qquad A19$$

and forming the ratio U_{sx}/U from equation A18 and A19

$$\frac{U_{sx}}{U} = \frac{2n+1}{n+1} \qquad A20$$

APPENDIX B

Duckler and Bergelin (25) in 1952 proposed a theory which attempted to give an experimental basis to the analysis. If the universal velocity profile (u.v.p.) concept developed by Prandtl (26) and fitted to the data of Nikuradse (26) for flow in tubes is assumed to be applicable to flow in thin film, then the velocity profile will be given as

for $0 < y^+ < 5$ $\quad v^+ = y^+$ B1

$5 < y^+ < 30$ $\quad v^+ = -3.05 + 5\ln y^+$ B2

$y^+ > 30$ $\quad v^+ = 5.5 + 2.5\ln y^+$ B3

where $y^+ = \frac{V^* y}{\nu}$; $v^+ = \frac{V_x}{V^*}$; $V^* = (\frac{\tau}{\rho})^{1/2}$ B4

Each of expression B1 to B3 can be integrated in turn with respect of y^+ to give the specific flow rate thus

$$Q_1 = \int_0^{\delta} V_x \, dy = \nu \int_0^{\delta} v^+ \, dy^+ \quad \text{B5}$$

so that $0 < y^+ < 5$ $\quad Re_1 = Q_1/\nu = \delta^{+2}/2$ B6

$5 < y^+ < 30$ $\quad Re_1 = 12.5 - 8.05\delta^+ + \delta^+ \ln \delta^+$ B7

$y^+ > 30$ $\quad Re_1 = -63.9 + 3\delta^+ + 2.5\delta^+ \ln \delta^+$ B8

When δ^+ is the dimensionless free surface defined similar to y^+ in equation B4

To a first approximation τ_o may be estimated from a simple force balance equating the wall shear stress to the fluid body force.

Whence $$\tau_o = g(\sin\theta)\delta\rho \quad \text{B9}$$

From equation B4 and for vertical film

$$\delta^+ = \frac{g^{1/2}\delta^{3/2}}{\nu} \qquad \text{B10}$$

Therefore from equation B6 to B8 the film thickness can be found (implicitly) for a given flow rate and fluid viscosity.

The distribution used above (u.v.p.) has two discontinuities within its operating range. Various 'smoothing' expressions have been proposed, for example, Churchill and Choi (26) recently proposed a continuous expression for $y^+ > 0.11$ (below which $v^+ = y^+$ may be used) as

$$v^+ = y^+\left(1 + \left(\frac{y^+}{(5.5 + 2.5\ln y^+)}\right)^2\right)^{1/2} \qquad \text{B11}$$

The original paper by Duckler and Bergelin contains an error, as pointed out by Portalski (5) in that although the three expressions for v^+ must be integrated separately over their respective ranges, Duckler and Bergelin claim that the final equation B8 (valid only for turbulent flow, $y^+ > 30$) is valid for all $y^+ > o$.

Later, Duckler (40) proposed another model in which the flow within the film is not stratified into distinct bands of laminar flow, transition flow and turbulent flow as in the u.v.p. model, but instead turbulent is allowed to exist at all values of y^+. Deissler's (26) expression for eddy viscosity in tube flow was used for $y^+ < 20$ and Von Karman's expression for $y^+ > 20$. Deissler's expression tends asymtotically to zero as $y^+ \rightarrow o$ giving a perfectly laminar layer strictly speaking only at the wall. The numerical constants used in the eddy viscosity equations were those obtained from analysis of full tube flow data. The result of Duckler's analysis was to obtain a numerical solution yielding δ as a function of (Re_1) with an additional parameter β where the numerical value of β was an indication of the intensity of shear within the film. β ranged from o (laminar) to 4000 (turbulent). When $\beta = o$, the results of the numerical study tended to agree to the simple model of Nusselt.

Portalski (5) from his film thickness measurements formed the dimensionless velocity distribution as follows:

For $0 < \delta^+ < 9$ $\quad V^+ = 8/9\ y^+ + 0.5$ B12

$9 < \delta^+ < 30$ $\quad V^+ = 1.7 + 3.1 \ln y^+$ B13

$\delta^+ > 30$ $\quad V^+ = 5.1 + 2.1 \ln y^+$ B14

and integrated specific flow rate equations are

$0 < \delta^+ < 9$ $\quad Re_1 = Q_1/\nu = 4/9\delta^{+2} + 0.5\delta^+$ B15

$9 < \delta^+ < 30$ $\quad Re_1 = 3.1\delta^+ \ln\delta^+ - 1.4\delta^+ - 8.2$ B16

$\delta^+ > 30$ $\quad Re_1 = 3.0\delta^+ + 2.1\delta^+ \ln\delta^+ - 38.17$ B17

APPENDIX C

Centrifugal Model

The Navier-Stokes equations in terms of cylindrical coordinates for the motion of liquid are fully defined by:

$$v_r\frac{\partial v_r}{\partial r} - \frac{v_\theta^2}{r} + v_y\frac{\partial v_r}{\partial y} = \frac{R_\rho}{\rho} - \frac{1}{\rho}\frac{\partial p}{\partial r} + \nu\frac{\partial^2 v_r}{\partial y^2} \qquad (c1)$$

$$v_r\frac{\partial v_\theta}{\partial r} + v_y\frac{\partial v_\theta}{\partial y} + \frac{v_\theta v_r}{r} = \frac{\Theta_\rho}{\rho} - \frac{1}{\rho}\frac{\partial P}{\partial \theta} + \nu\frac{\partial^2 v_\theta}{\partial y^2} \qquad (c2)$$

$$v_r\frac{\partial v_y}{\partial r} + v_y\frac{\partial v_y}{\partial y} = \frac{Y_\rho}{\rho} - \frac{1}{\rho}\frac{\partial p}{\partial y} + \nu\frac{\partial^2 v_y}{\partial y^2} \qquad (c3)$$

and from the continuity equation:

$$\frac{\partial v_r}{\partial r} + \frac{\partial v_y}{\partial y} + \frac{v_r}{r} = 0$$

Where v_r, v_θ, v_y are the axes of speed, ρ is the density , p is the pressure, ν is the kinematic viscosity and R_0 , Θ_0 , Y_0 are the body forces in radial , angular and vertical direction.

considering the assumptions:

1) The influence of the the force of gravity, surface tension and friction on the surrounding medium are insignificant.
2) The thickness of the liquid film δ is much less than the corresponding radius r, ie $\frac{\delta}{r} << 1$.
3) The flow of liquid on the disc is steady.
4) The angular rate of rotation of the liquid is equal to the rate of rotation of the disc throughout the liquid, $v_\theta = rw$

The equations of motion of the liquid can be defined by the Navier-Stokes equations and are simplified, assuming that:

A) v_r is small compared to v_θ ($v_r < rw$)

B) v_r changes in the 'r' direction are small compared to changes in the 'y' direction ($\frac{\partial v_r}{\partial r} < \frac{\partial v_r}{\partial y}$)

Therefore, equations c1,c2,c3 are represented in a simplified form as:

$$-\frac{1}{\rho}\frac{\partial p}{\partial r} + \frac{\partial^2 v_r}{\partial y^2} = -w^2 r \qquad \text{(c5)}$$

$$v_r \frac{\partial v_\theta}{\partial r} + \frac{v_\theta v_r}{r} = \nu \frac{\partial^2 v_\theta}{\partial y^2} \qquad \text{(c6)}$$

$$\frac{\partial p}{\partial y} = 0 \qquad \text{(c7)}$$

From equation c7 it appears that the pressure does not change with the thickness of the film. The pressure at the surface of the film is constant(atmospheric). From this it follows that $\partial p/\partial r = 0$, and

$$\nu \frac{\partial^2 v_r}{\partial y^2} = -w^2 r$$

APPENDIX D

Portalski Equation

This equation was derived assuming that the wave motion was two-dimensional and that the flow was laminar. Portalski applied the well known equation for the determination of the arc length of a curve in order to estimate the increase in interfacial area.

Length from point 1 to point 2 $= \int_1^2 (1 + (\frac{\partial y}{\partial x})^2)^{1/2} \, dx$

Using the steam function of Kapitza, $y = A_o \phi$

Where A_o is the amplitude and ϕ is expressed as a series (detail see Portalski (5)).

Therefore $\frac{\partial y}{\partial x} = A_o \frac{\partial \phi}{\partial x}$

The total surface area for the wavy film in the laminar region of flow is

$$s = \int_1^2 (1 + A_o (\frac{\partial \phi}{\partial x})^2)^{1/2} \, dx$$

Where s is the interfacial area, and the expression for the increase in interfacial area per unit area, Δs is given as

$$\Delta s = (\frac{A_o 1.444}{\lambda})^2 (1 + (\frac{0.91 \lambda^3}{A_o \delta})^2)$$

Clegg (37) shows that $(0.91 \lambda^3 / A_o \delta)^2$ is small in comparison to unity, thus

$$\Delta s = (1.444 A_o / \lambda)^2$$

The theoretical expression given for A_o by Portalski is $1.339 (\frac{\nu Q}{g})^{\frac{1}{3}}$ and that for λ is $7.5 (\frac{\nu \delta}{Qg})^{\frac{1}{2}}$.

APPENDIX E

Rotameters

Metric 14 $Q_1 = (-0.0249 + 0.825x - 0.06955x^2 + 0.003x^3) \times 10$

Metric 18E $Q_2 = (3.8380 + 0.2909x + 0.0216x^2) \times 10$

Metric 24p $Q_3 = (4.4887 + 1.0533x + 0.0154x^2) \times 10$

where Q in cc/s and x from rotameter scale unit

Sample Calculation

Input voltage = 15 volts

Rate output = 2.235 mv/volts input

Given rated load at 500 kg

ie 15 x 2.236 (v x mv/v) equivalent to 5×10^5 gm

OR 33.54 mv = 5×10^5 gm

water density = 1 gm/cc

ie 33.54 mv = 5×10^5 cc

$$1 \text{ mv} = \frac{5 \times 10^5}{33.54} \text{ cc}$$

From the Chart Recorder

Let variable = the change in (mv)

speed = the speed of the recorder (cm/min)

length = distance covered for the change in mv (cm)

$$\text{Flow rate} = \frac{\text{variable x speed}}{60 \text{ x length}}$$

$$= \frac{x}{60} \quad (\frac{\text{mv}}{\text{s}})$$

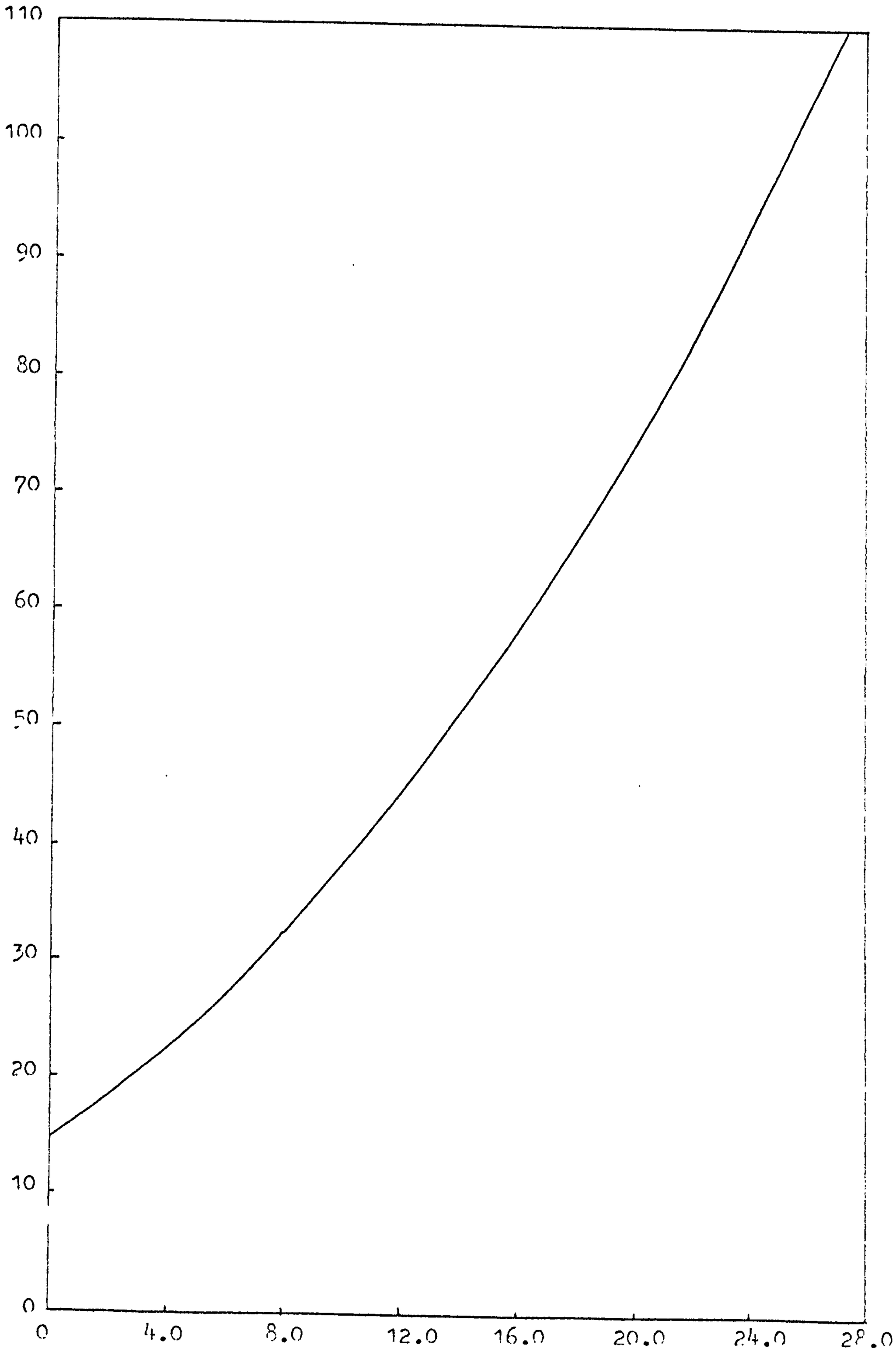

FIG.E1 CALIBRATION FOR ROTAMETER METRIC 14

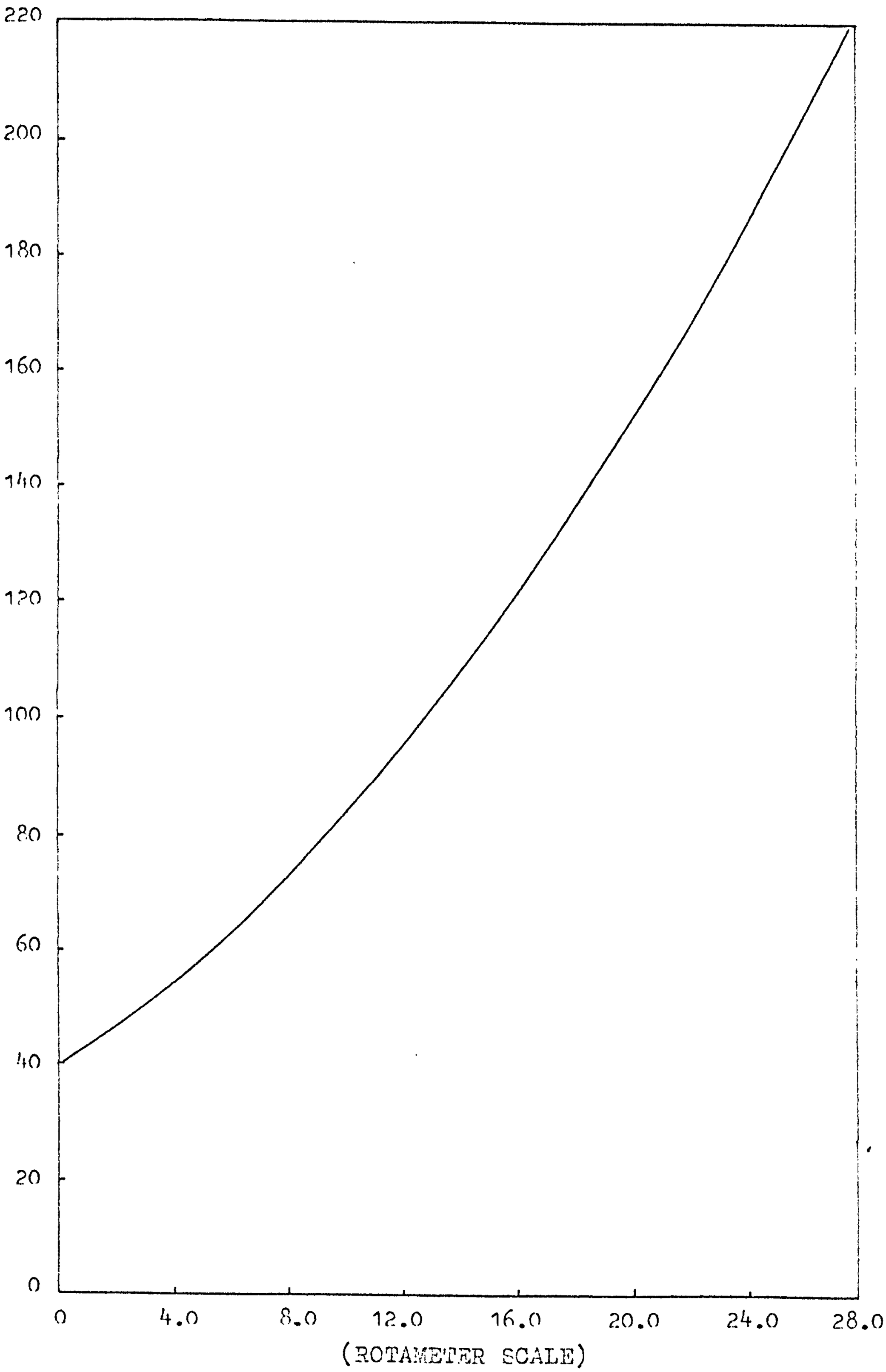

FIG. E2 CALIBRATION FOR ROTAMETER METRIC 18E

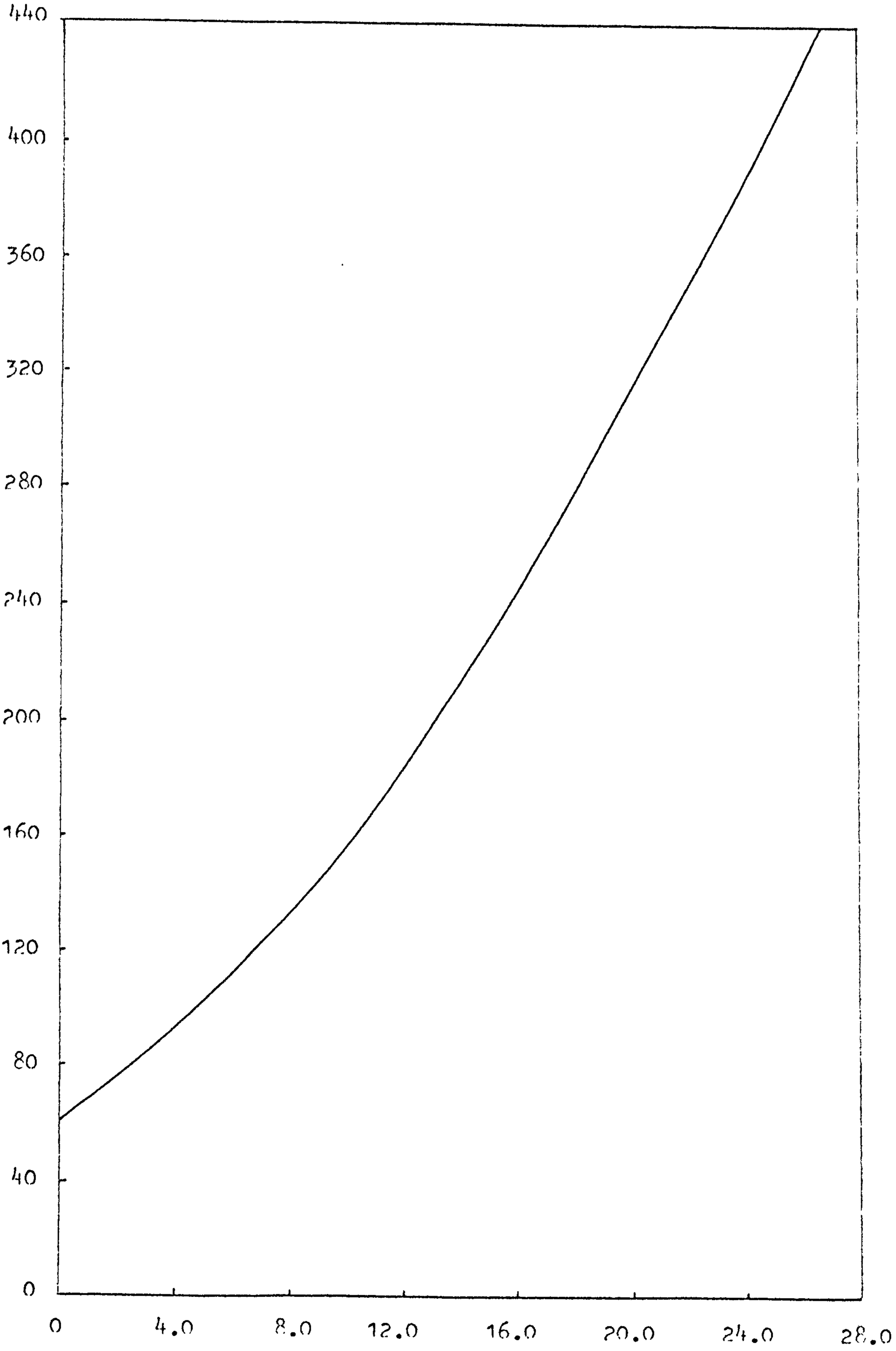

FIG.E3 CALIBRATION FOR ROTAMETER METRIC 24P

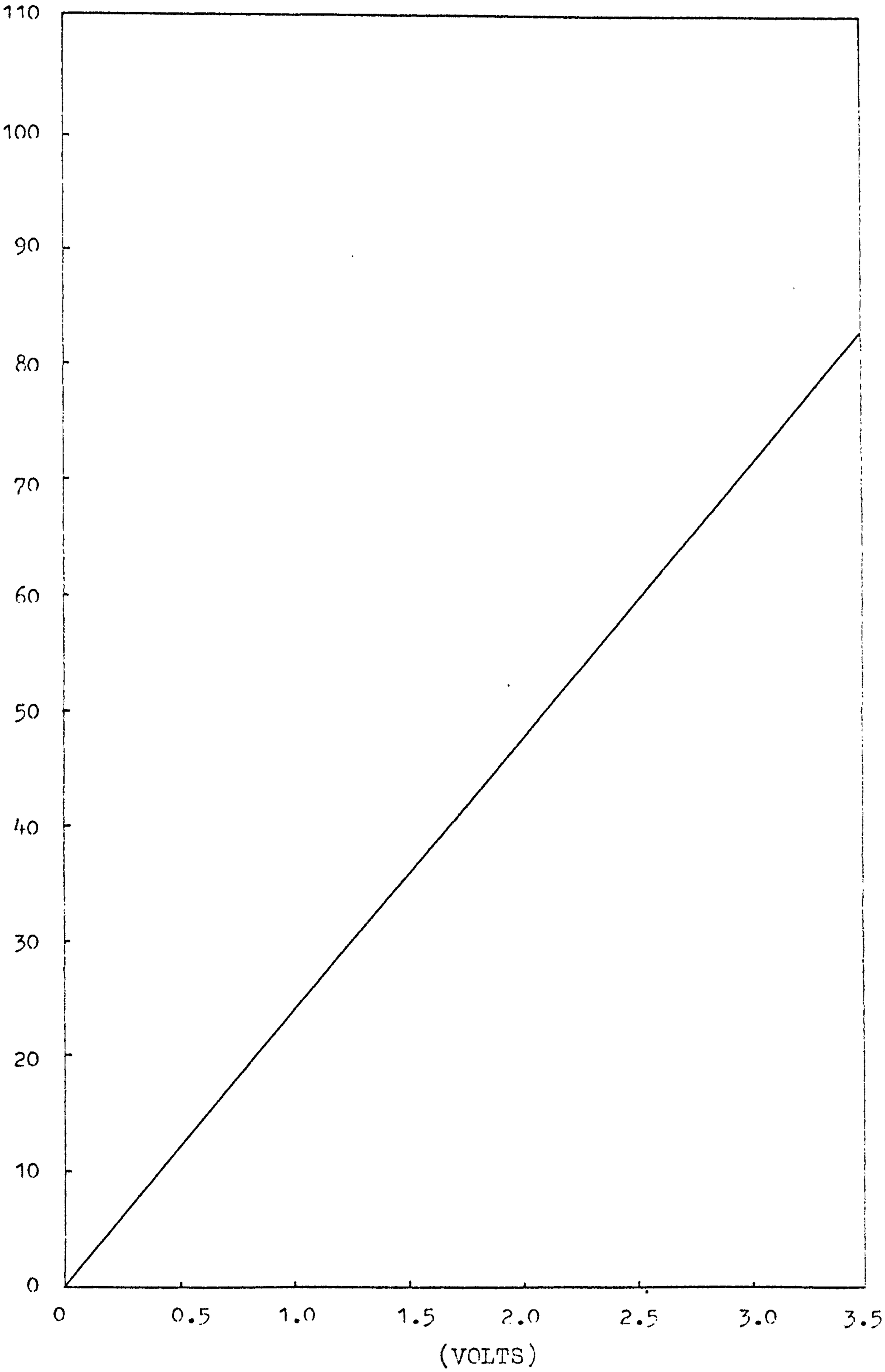

FIG.E4 CALIBRATION FOR THE CU/CON THERMOCOUPLE

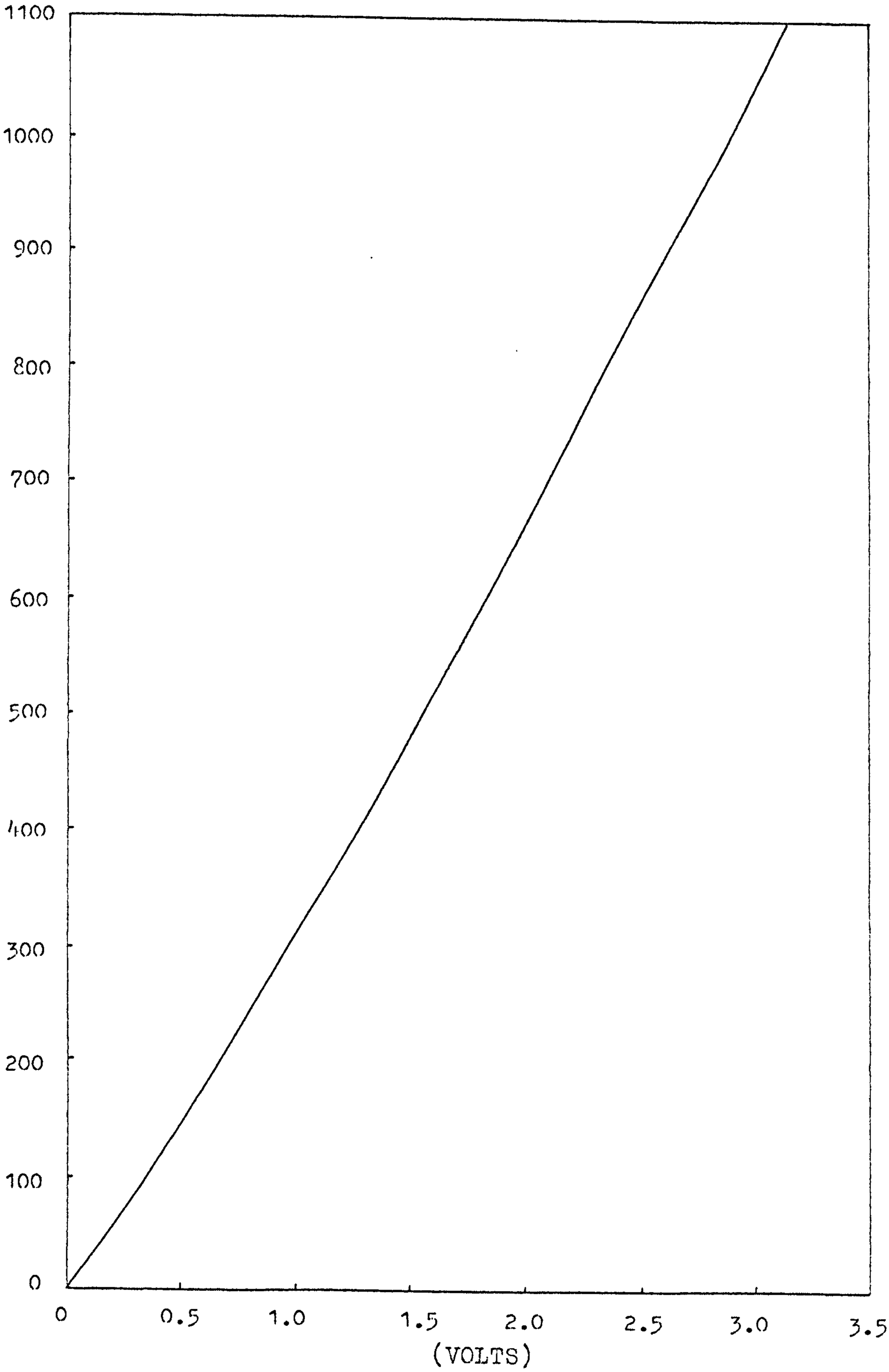

FIG. E5 CALIBRATION FOR THE TACHOGENETOR

From above $1\ mv = \frac{5 \times 10^5}{33.54}\ cc$

Flow rate $= \frac{x}{60} \times \frac{5 \times 10^5}{33.54}\ cc/s$

Thermocouple

$$T = 24.508 + 0.1537x - 0.1121x^2$$

where T in ^{o}C and x in mV

Tachogenerator

$$speed = 344.98x - 0.441$$

where speed in rpm and x in Volt

APPENDIX F

Determination of Effect Edge due to the Probe and obtain the Apparent D_L (125)

When a parabolic profile exists in the liquid, film equation

$$\frac{\partial c}{\partial \theta} = D\frac{\partial^2 c}{\partial x^2}$$

transforms as $$D\frac{\partial^2 c}{\partial x^2} = U_{max}\left(1-\frac{x^2}{B_F^2}\right)\frac{\partial c}{\partial x}$$

Pigford (132) presented the following solution

$$1 - E = 0.7857 \exp(-5.121p) + 0.1001 \exp(-39.21p) + 0.0360 \exp(-105.6p) + 0.0181 \exp(-204.7p) + \ldots$$

where $P = D\frac{\theta}{B_F^2}$, B_F is the depth of the liquid, θ is the time of contact between two phases and E is the fractional approach to Equilibrium

For short contact time the above equation becomes $E = 3\left(\frac{D\theta}{\pi B_F^2}\right)^{\frac{1}{2}}$

For long contact time, only the first term in the above equation is important.

On rotating disc system $\frac{\theta}{B_F^2} = \psi = \frac{3}{4}\frac{\nu}{w^2}\left(\frac{2\pi w^2}{3Q\nu}\right)^{4/3}\left(r_1^{\frac{8}{3}} - r_o^{\frac{8}{3}}\right)$

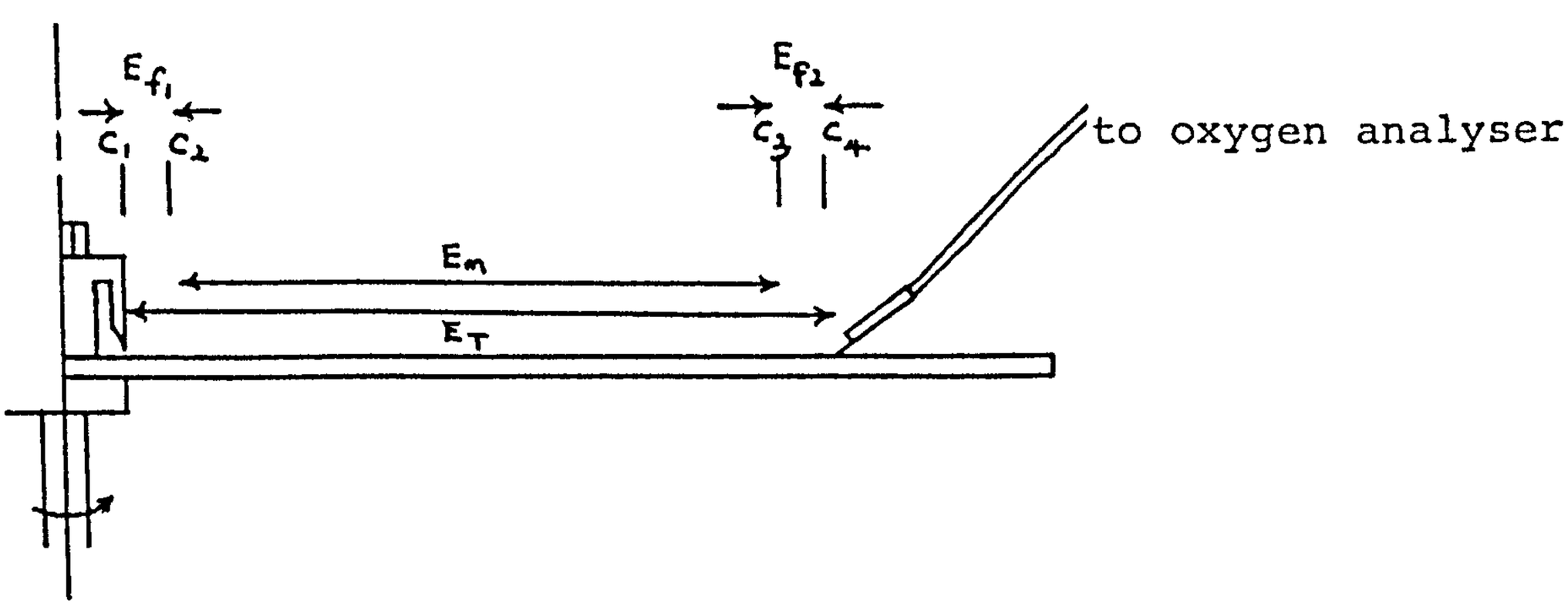

where inlet effect $E_{f1} = \frac{c_2 - c_1}{c^* - c_1} = A$

outlet effect $E_{f2} = \frac{c_4 - c_3}{c^* - c_3} = B$

Absorption sectiob $E_m = \frac{c_s - c_2}{c^* - c_2} = C$

overall absorption $E_T = \frac{c_4 - c_1}{c^* - c_1} = D$

$$E_m = \frac{c_3 - c_2}{c^* - c_2} = \frac{c_3 - c_2}{(c^* - c_1) - A(c^* - c_1)}$$

$$= \frac{(c_4 - c_1) - (c_4 - c_3) + (c_1 - c_2)}{(c^* - c_1)(1 - A)}$$

$$= \frac{D(c^* - c_1) - B(c^* - c_3) - A(c^* - c_1)}{(c^* - c_1)(1 - A)}$$

$$= \frac{D(c^* - c_1) - B(c^* - c_1) + B(c_3 - c_1) - A(c^* - c_1)}{(c^* - c_1)(1 - A)}$$

$$= \frac{(D - B - A)(c^* - c_1) + B(c_3 - c_2) + B(c_2 - c_1)}{(c^* - c_1)(1 - A)}$$

$$= \frac{(c^* - c_1)(D - B + BA + D - A + BC) - BC(c_2 - c_1)}{(c^* - c_1)(1 - A)}$$

$$= \frac{D - B + BA - A + BC - BCA}{(1 - A)}$$

$$= C$$

ie $C(1 - A) = D - B - A + BA + C(B - BA)$

ie $C = \frac{D - B - A + BA}{1 - A - B + BA}$

$$E_m = \frac{E_T - E_{f1} - E_{f2} + (E_{f1} \times E_{f2})}{1 - E_{f1} - E_{f2} + (E_{f1} \times E_{f2})}$$

Let $E_F = E_{f1} + E_{f2} - (E_{f1} \times E_{f2})$

we have $E_m = \frac{E_T - E_F}{1 - E_F}$

$$E_T = E_F + (1 - E_F) E_m$$

For short contact time $E_m = 3 \left(\frac{D\theta}{\pi B_F^2}\right)^{1/2}$

$$= 3\sqrt{\frac{D}{\pi}} \left(\frac{\theta}{B_F^2}\right)^{1/2}$$

For rotating disc $\frac{\theta}{B_F^2} = \psi = \frac{3}{4} \frac{\nu}{w^2} \left(\frac{2\pi w^2}{3Q\nu}\right)^{4/3} (r_1^{8/3} - r^{8/3})$

ie $E_T = E_F + (1 - E_F) \; 3\sqrt{\frac{D}{\pi}} \; \psi^{1/2}$

The intercept and the slope can be obtained using method of least square. Where the inception gives the edge effects and the slope of E_T Vs $\psi^{1/2}$ gives the apparent diffusion ($*\sqrt{\pi/3}$).

APPENDIX G

TABLE:G1 FILM THICKNESS MEASUREMENTS

ROTATIONAL SPEED = 24.24 RAD/S FLOW RATE = 14.5 CC/S

RADIUS (M)	TH/R X10^2	TH/R(RE)	TH/R(TA)$^{0.5}$	RE/TA$^{2.0}$ X10^7	RE$^{2.0}$/TA
0.06	0.259	0.662	0.748	0.369	0.782
0.09	0.152	0.284	0.597	0.786	0.227
0.10	0.0429	0.0648	0.209	0.0268	0.0960
0.12	0.0622	0.0774	0.368	0.0101	0.0441
0.14	0.0864	0.0933	0.589	0.0050	0.0251
0.16	0.0659	0.0618	0.618	0.0025	0.0142

ROTATIONAL SPEED = 24.24 RAD/S FLOW RATE = 22.1 CC/S

0.06	0.2536	0.9863	0.7317	0.5616	1.8167
0.08	0.1966	0.5611	0.7723	0.1198	0.5279
0.10	0.0636	0.1464	0.3100	0.0407	0.2229
0.12	0.05445	0.1032	0.3223	0.0154	0.1025
0.14	0.0728	0.1198	0.4958	0.0076	0.0584
0.16	0.0657	0.0938	0.5162	0.0037	0.0330

ROTATIONAL SPEED = 24.24 FLOW RATE = 31.0 CC/S

0.06	0.4191	2.2856	1.2089	0.7877	3.5748
0.09	0.2695	1.0792	1.0589	0.1680	1.0386
0.10	0.0976	0.3149	0.4755	0.0572	0.4386
0.12	0.0935	0.2487	0.5537	0.0217	0.2017
0.14	0.1152	0.2659	0.7847	0.0107	0.1148
0.16	0.0827	0.1656	0.6501	0.0053	0.0649

TABLE: G2 FILM THICKNESS MEASUREMENTS

ROTATIONAL SPEED = 24.24 RAD/S FLOW RATE = 37.3 CC/S

RADIUS (M)	TH/R $X10^2$	TH/R(RE)	$TH/R(TA)^{0.5}$	$RE/TA^{2.0}$ $X10^7$	$RE^{2.0}/TA$
0.06	0.5535	3.6323	1.5967	0.9478	5.1754
0.08	0.3607	1.7379	1.4172	0.2022	1.5037
0.10	0.1130	0.4388	0.5507	0.0688	0.6350
0.12	0.1146	0.3664	0.6780	0.0261	0.2921
0.14	0.0875	0.2429	0.5958	0.0129	0.1663
0.16	0.0946	0.2279	0.7434	0.0063	0.0940

ROTATIONAL SPEED = 24.24 RAD/S FLOW RATE = 42.7 CC/S

0.06	0.5984	4.4953	1.7261	1.0850	6.7824
0.08	0.4060	2.2393	1.5952	0.2315	1.9706
0.12	0.1064	0.3897	0.6299	0.0298	0.3827
0.14	0.1414	0.4495	0.9631	0.0148	0.2179
0.16	0.1150	0.3172	0.8037	0.0072	0.1232

ROTATIONAL SPEED = 24.24 RAD/S FLOW RATE = 46.2 CC/S

0.06	0.8053	6.5453	2.3229	1.1740	7.9398
0.08	0.4066	2.4264	1.5976	0.2504	2.3068
0.10	0.1562	0.7516	0.7615	0.0853	0.9741
0.12	0.1420	0.5626	0.8406	0.0323	0.4481
0.14	0.1648	0.5670	1.1227	0.0159	0.2551
0.16	0.1055	0.3146	0.8286	0.0078	0.1442

TABLE: G3 FILM THICKNESS MEASUREMENTS

ROTATIONAL SPEED = 24.24 RAD/S FLOW RATE = 52.0 CC/S

RADIUS (M)	TH/R $X10^2$	TH/R(RE)	$TH/R(TA)^{0.5}$	$RE/TA^{2.0}$ $X10^7$	$RE^{2.0}/TA$
0.06	1.0378	9.4940	2.9935	1.3213	10.0590
0.08	0.5196	3.4897	2.0414	0.2819	2.9224
0.10	0.1437	0.7778	0.7001	0.0959	1.2341
0.12	0.1035	0.4614	0.6124	0.0363	0.5676
0.14	0.1059	0.4093	0.7200	0.0180	0.3231
0.16	0.1282	0.4304	1.0072	0.0088	0.1827

ROTATIONAL SPEED = 24.24 RAD/S FLOW RATE = 60.5 CC/S

0.06	0.9594	10.2110	2.7674	1.5373	13.6160
0.08	0.4025	3.1452	1.9814	0.3279	3.9559
0.10	0.1498	0.9434	0.7299	0.1116	1.6705
0.12	0.0845	0.4384	0.5002	0.0423	0.7684
0.14	0.1018	0.4587	0.6936	0.0209	0.4374
0.16	0.1060	0.4140	0.8327	0.0102	0.2472

ROTATIONAL SPEED = 32.88 RAD/S FLOW RATE = 14.5 CC/S

0.06	0.2889	0.7370	0.9707	0.2003	0.5766
0.08	0.1689	0.3164	0.7729	0.0427	0.1675
0.10	0.0707	0.1068	0.4014	0.0145	0.0707
0.12	0.0578	0.0719	0.3985	0.0055	0.0325
0.14	0.0922	0.0999	0.7342	0.0027	0.0185
0.16	0.0858	0.0804	0.7855	0.0013	0.01047

TABLE:G4 FILM THICKNESS MEASUREMENTS

ROTATIONAL SPEED = 32.88 RAD/S FLOW RATE = 22.1 CC/S

RADIUS (M)	TH/R $X10^2$	TH/R(RE)	$TH/R(TA)^{0.5}$	$RE/TA^{2.0}$ $X10^7$	$RE^{2.0}/TA$
0.06	0.2423	0.9420	0.8139	0.3052	1.3394
0.10	0.0799	0.1839	0.4536	0.0222	0.1643
0.12	0.0668	0.1076	0.3914	0.0084	0.07559
0.14	0.0868	0.1428	0.6885	0.00415	0.0430
0.16	0.0662	0.0945	0.6059	0.0020	0.0243

ROTATIONAL SPEED = 32.88 RAD/S FLOW RATE = 31.0 CC/S

0.06	0.2915	1.5898	0.9793	0.4281	2.6354
0.08	0.2166	0.8672	0.9910	0.0913	0.7657
0.10	0.0916	0.2958	0.5201	0.0311	0.3233
0.12	0.0698	0.1855	0.4809	0.0118	0.1487
0.14	0.0908	0.2098	0.7209	0.0058	0.0847
0.16	0.0690	0.1382	0.6319	0.0029	0.0479

ROTATIONAL SPEED = 32.88 RAD/S FLOW RATE = 37.3 CC/S

0.06	0.3765	2.4705	1.2648	0.5151	3.8154
0.08	0.2719	1.3099	1.2441	0.1099	1.1085
0.10	0.0866	0.3364	0.4917	0.0374	0.4681
0.12	0.0737	0.2357	0.5080	0.01417	0.2153
0.14	0.0998	0.2774	0.7922	0.0070	0.1226
0.16	0.0765	0.1844	0.7004	0.00343	0.0693

TABLE: G5 FILM THICKNESS MEASUREMENTS

ROTATIONAL SPEED = 32.88 RAD/S FLOW RATE = 42.7 CC/S

RADIUS (M)	TH/R $X10^2$	TH/R(RE)	TH/R$(TA)^{0.5}$	RE/$TA^{2.0}$ $X10^7$	$RE^{2.0}/TA$
0.06	0.3785	2.8432	1.2715	0.5897	5.0002
0.08	0.2448	1.3502	1.1202	0.1258	1.4527
0.10	0.1021	0.4537	0.5793	0.0428	0.6135
0.12	0.0620	0.2269	0.4271	0.0162	0.2822
0.14	0.0847	0.2694	0.6722	0.0080	0.1606

ROTATIONAL SPEED = 32.88 RAD/S FLOW RATE = 46.2 CC/S

0.06	0.5136	4.1745	1.7255	0.6381	5.8535
0.08	0.2760	1.6470	1.2629	0.1361	1.7007
0.10	0.1066	0.5128	0.6051	0.0463	0.7182
0.12	0.0816	0.3232	0.5625	0.0176	0.3303
0.14	0.0976	0.3367	0.7765	0.0087	0.1880
0.16	0.0724	0.2160	0.6626	0.0043	0.1063

ROTATIONAL SPEED = 32.88 RAD/S FLOW RATE = 52.0 CC/S

0.06	0.5571	5.0967	1.8716	0.7182	7.4154
0.08	0.2301	1.5455	1.0529	0.1532	2.1545
0.10	0.0839	0.4547	0.4768	0.0521	0.9098
0.12	0.0789	0.3521	0.5443	0.0198	0.4185
0.14	0.0830	0.32137	0.6585	0.0098	0.2383
0.16	0.0626	0.2102	0.5728	0.0048	0.1347

TABLE:G6 FILM THICKNESS MEASUREMENTS

ROTATIONAL SPEED = 32.88 RAD/S FLOW RATE = 60.5 CC/S

RADIUS (M)	TH/R $X10^2$	TH/R(RE)	TH/R$(TA)^{0.5}$	RE/$TA^{2.0}$ $X10^7$	$RE^{2.0}/TA$
0.06	0.6432	6.8465	2.1610	0.8355	10.038
0.08	0.2995	2.3406	1.3706	0.1782	2.9164
0.10	0.1084	0.6829	0.6154	0.0607	1.2315
0.14	0.1041	0.4689	0.8258	0.0114	0.3225
0.12	0.0727	0.3769	0.5008	0.0229	0.5665
0.16	0.0745	0.2909	0.6815	0.0056	0.1823

ROTATIONAL SPEED = 43.67 RAD/S FLOW RATE = 14.5 CC/S

0.06	0.1641	0.4186	0.6353	0.1135	0.4341
0.08	0.0995	0.1863	0.5247	0.0242	0.1261
0.10	0.04725	0.0713	0.3091	0.0082	0.0533
0.12	0.0368	0.0458	0.2924	0.0031	0.0245
0.14	0.0566	0.0612	0.5180	0.0015	0.0139
0.16	0.0445	0.0417	0.4695	0.0008	0.0079

ROTATIONAL SPEED = 43.67 RAD/S FLOW RATE = 22.1 CC/S

0.06	0.1788	0.6950	0.6921	0.1730	1.0085
0.08	0.1071	0.3058	0.5650	0.0369	0.2930
0.10	0.0456	0.1050	0.2984	0.01256	0.1237
0.12	0.0401	0.0761	0.3186	0.0048	0.0569
0.14	0.0536	0.0883	0.4904	0.0024	0.0324

TABLE:G7 FILM THICKNESS MEASUREMENTS

ROTATIONAL SPEED = 43.67 RAD/S FLOW RATE = 31.0 CC/S

RADIUS (M)	TH/R $X10^3$	TH/R(RE)	TH/R$(TA)^{0.5}$	RE/$TA^{2.0}$ $X10^8$	$RE^{2.0}$/TA
0.06	2.0467	1.1162	0.7924	2.4270	1.9843
0.08	0.9537	0.3819	0.5029	0.5177	0.5765
0.10	0.4643	0.1499	0.3037	0.1762	0.2435
0.12	0.3782	0.1005	0.3005	0.0668	0.1120
0.14	0.6038	0.1394	0.5522	0.0330	0.0637
0.16	0.5071	0.1015	0.5349	0.0162	0.0360

ROTATIONAL SPEED = 43.67 RAD/S FLOW RATE = 37.3 CC/S

0.08	1.0007	0.4821	0.5276	0.6229	0.8347
0.10	0.4999	0.1942	0.3270	0.2121	0.3525
0.12	0.5859	0.1874	0.4654	0.0803	0.1621
0.14	0.5814	0.1615	0.5317	0.0397	0.0923

ROTATIONAL SPEED = 43.67 RAD/S FLOW RATE = 42.7 CC/S

0.06	2.1838	1.6405	0.8455	3.3430	3.7647
0.08	1.7244	0.9511	0.9094	0.7131	1.0938
0.10	0.5635	0.2505	0.3686	0.2428	0.4619
0.12	0.4777	0.1749	0.3795	0.0919	0.2125
0.14	0.6881	0.2188	0.6293	0.0455	0.1209
0.16	0.4555	0.1256	0.4804	0.0222	0.0684

TABLE: G8 FILM THICKNESS MEASUREMENTS

ROTATIONAL SPEED = 43.67 RAD/S FLOW RATE = 46.2 CC/S

RADIUS (M)	TH/R X10^3	TH/R(RE)	TH/R(TA)$^{0.5}$	RE/TA$^{2.0}$ X10^8	RE$^{2.0}$/TA
0.06	2.0220	1.6434	0.7828	3.6171	4.4072
0.08	1.2478	0.7446	0.6581	0.7716	1.2805
0.10	0.4019	0.1934	0.2629	0.2626	0.5407
0.12	0.3250	0.1288	0.2582	0.0995	0.2487
0.14	0.4050	0.1394	0.3703	0.0492	0.1416
0.16	0.3728	0.1113	0.3933	0.0241	0.0800

ROTATIONAL SPEED = 43.67 RAD/S FLOW RATE = 52.0 CC/S

0.06	3.5710	3.2669	1.3826	4.0711	5.5832
0.08	1.4361	0.9646	0.7574	0.8684	1.6221
0.10	0.4290	0.2323	0.2806	0.2956	0.6850
0.12	0.·352	0.1494	0.2662	0.1120	0.3151
0.14	0.4234	0.1675	0.3954	0.0554	0.1794
0.16	0.3057	0.1027	0.3224	0.0271	0.1014

ROTATIONAL SPEED = 43.67 RAD/S FLOW RATE = 60.5 CC/S

0.06	3.3538	3.7655	1.3697	4.7366	7.5576
0.08	1.1949	0.9338	0.6301	1.0104	2.1958
0.10	0.4210	0.2702	0.2806	0.3439	0.9273
0.12	0.3200	0.1660	0.2542	0.1303	0.4265
0.14	0.4246	0.1913	0.3883	0.0644	0.2428
0.16	0.3522	0.1376	0.3715	0.0316	0.1372

TABLE: G9 FILM THICKNESS MEASUREMENTS

ROTATIONAL SPEED = 59.53 RAD/S FLOW RATE = 14.5 CC/S

RADIUS (M)	TH/R $X10^3$	TH/R(RE)	$TH/R(TA)^{0.5}$	$RE/TA^{2.0}$ $X10^9$	$RE^{2.0}/TA$
0.06	0.7079	0.1806	0.3200	6.1091	0.3185
0.08	0.3124	0.0585	0.1923	1.3031	0.0925
0.10	0.1857	0.0280	0.1419	0.4436	0.0391
0.12	0.1373	0.0171	0.1274	0.1680	0.0180
0.14	0.2192	0.0237	0.2341	0.0831	0.0102
0.16	0.2076	0.0194	0.2556	0.0407	0.0058

ROTATIONAL SPEED = 59.53 RAD/S FLOW RATE = 22.1 CC/S

0.06	1.2908	0.50188	0.5835	9.3111	0.7398
0.08	0.6772	0.1933	0.4169	1.9861	0.2149
0.10	0.2167	0.0499	0.1656	0.6761	0.0907
0.12	0.1895	0.0359	0.1758	0.2561	0.0418
0.14	0.2686	0.4421	0.2868	0.1266	0.0238
0.16	0.2050	0.0293	0.2525	0.0621	0.0134

ROTATIONAL SPEED = 59.53 RAD/S FLOW RATE = 31.0 CC/S

0.06	1.2848	0.7007	0.5808	13.0610	1.4556
0.08	0.6007	0.2405	0.3698	2.7860	0.4229
0.10	0.2637	0.0851	0.2014	0.9484	0.1786
0.12	0.1920	0.0510	0.1781	0.3592	0.08214
0.14	0.3454	0.0798	0.3688	0.1776	0.0468
0.16	0.2437	0.0488	0.3002	0.0871	0.0264

TABLE:G10 FILM THICKNESS MEASUREMENTS

ROTATIONAL SPEED = 59.53 RAD/S FLOW RATE = 37.3 CC/S

RADIUS (M)	TH/R $X10^3$	TH/R(RE)	$TH/R(TA)^{0.5}$	$RE/TA^{2.0}$ $X10^9$	$RE^{2.0}/TA$
0.06	1.2729	0.8353	0.5754	15.7150	2.1074
0.08	0.6360	0.3064	0.3916	3.3522	0.6123
0.10	0.2663	0.1034	0.2034	1.1411	0.25855
0.12	0.18704	0.0598	0.1735	0.4322	0.1189
0.14	0.3173	0.0882	0.3388	0.2137	0.0677
0.16	0.2928	0.0705	0.3606	0.1048	0.03827

ROTATIONAL SPEED = 59.53 RAD/S FLOW RATE = 42.7 CC/S

0.06	1.2311	0.9248	0.5565	3.8375	0.8024
0.08	0.9007	0.4968	0.5546	3.8375	0.8024
0.10	0.2847	0.1266	0.2175	1.3063	0.3388
0.12	0.2320	0.0849	0.2152	0.4948	0.1559
0.14	0.3454	0.1099	0.3688	0.2447	0.0887
0.16	0.2902	0.0800	0.3574	0.1199	0.0501

ROTATIONAL SPEED = 59.53 RAD/S FLOW RATE = 46.2 CC/S

0.06	2.2339	1.8157	1.0098	19.4650	3.2530
0.08	0.8242	0.4919	0.5075	4.1520	0.9393
0.10	0.3297	0.1586	0.2518	1.4134	0.3967
0.12	0.2295	0.0909	0.2129	0.5354	0.1825
0.14	0.3454	0.1189	0.3688	0.2647	0.1039
0.16	0.2954	0.0881	0.3637	0.1298	0.0587

TABLE: G11 FILM THICKNESS MEASUREMENTS

ROTATIONAL SPEED = 59.53 RAD/S FLOW RATE = 52.0 CC/S

RADIUS (M)	TH/R X10^3	TH/R(RE)	TH/R(TA)$^{0.5}$	RE/TA$^{2.0}$ X10^9	RE$^{2.0}$/TA
0.06	1.5194	1.3900	0.6869	21.9080	4.0957
0.08	1.0243	0.6879	0.63066	4.6733	1.1900
0.10	0.3751	0.2031	0.2864	1.5908	0.5025
0.12	0.3023	0.1348	0.2804	0.6026	0.2311
0.14	0.4557	0.1765	0.4866	0.2980	0.1316
0.16	0.3574	0.1200	0.4401	0.1460	0.0774

ROTATIONAL SPEED = 59.53 RAD/S FLOW RATE = 60.5 CC/S

0.06	2.8120	2.9929	1.2711	25.4900	5.5441
0.08	1.5950	1.2464	0.9821	5.4372	1.6108
0.10	0.3617	0.2278	0.2762	1.8509	0.6802
0.12	0.2570	0.1336	0.2384	0.7011	0.3129
0.14	0.4050	0.1825	0.4324	0.3467	0.1781
0.16	0.3599	0.1406	0.4432	0.1699	0.1007

ROTATIONAL SPEED = 86.25 RAD/S FLOW RATE = 14.5 CC/S

0.06	0.9412	0.2401	0.5121	2.9102	0.2198
0.08	0.3830	0.0717	0.2838	0.6208	0.0639
0.10	0.2194	0.0331	0.2015	0.2113	0.0270
0.12	0.1771	0.0220	0.1977	0.0800	0.0124
0.14	0.2358	0.0255	0.3030	0.0396	0.0070
0.16	0.2334	0.0219	0.3460	0.0194	0.0039

TABLE:G12 FILM THICKNESS MEASUREMENTS

ROTATIONAL SPEED = 86.25 RAD/S FLOW RATE = 22.1 CC/S

RADIUS (M)	TH/R X10^3	TH/R(RE)	TH/R(TA)$^{0.5}$	RE/TA$^{2.0}$ X10^9	RE$^{2.0}$/TA
0.06	0.9882	0.3842	0.5377	4.4356	0.5106
0.08	0.4888	0.1396	0.3623	0.9462	0.1484
0.10	0.2350	0.0541	0.2160	0.3221	0.0626
0.12	0.1945	0.0369	0.2172	0.1220	0.0288
0.14	0.3654	0.0601	0.4696	0.0603	0.0164
0.16	0.3496	0.0499	0.5182	0.0296	0.0093

ROTATIONAL SPEED = 86.25 RAD/S FLOW RATE = 31.0 CC/S

0.06	1.1122	0.6066	0.6052	6.2219	1.0047
0.08	0.6477	0.2594	0.4801	1.3272	0.2919
0.10	0.2768	0.0894	0.2545	0.4518	0.1233
0.12	0.1970	0.05237	0.2199	0.1711	0.0567
0.14	0.3133	0.0723	0.4026	0.0846	0.0323
0.16	0.3057	0.0612	0.4531	0.0415	0.0182

ROTATIONAL SPEED = 86.25 RAD/S FLOW RATE = 37.3 CC/S

0.06	1.4650	0.9614	0.7972	7.4863	1.4545
0.08	0.9125	0.4396	0.6763	1.5970	0.4226
0.10	0.2874	0.1116	0.2642	0.5436	0.1785
0.12	0.1895	0.0606	0.2116	0.2059	0.0821
0.14	0.3374	0.0937	0.4337	0.1018	0.0467
0.16	0.2721	0.0656	0.4034	0.0499	0.0264

TABLE: G13 FILM THICKNESS MEASUREMENTS

ROTATIONAL SPEED = 86.25 RAD/S FLOW RATE = 42.7 CC/S

RADIUS (M)	TH/R X10^3	TH/R(RE)	TH/R(TA)$^{0.5}$	RE/TA$^{2.0}$ X10^9	RE$^{2.0}$/TA
0.06	1.6043	1.2052	0.8729	8.5702	1.9061
0.08	0.5771	0.3183	0.4277	1.8281	0.5538
0.10	0.2480	0.1103	0.2280	0.6223	0.2339
0.12	0.1821	0.0667	0.2032	0.2357	0.1076
0.14	0.3454	0.1098	0.4440	0.1166	0.0612
0.16	0.2747	0.0758	0.4072	0.0571	0.0346

ROTATIONAL SPEED = 86.25 RAD/S FLOW RATE = 46.2 CC/S

0.06	1.7629	1.4329	0.9593	9.2726	2.2314
0.08	0.7478	0.4462	0.55418	1.9779	0.6483
0.10	0.2900	0.1395	0.2666	0.6733	0.2738
0.12	0.2370	0.0939	0.2646	0.2550	0.1259
0.14	0.4089	0.1407	0.5255	0.1261	0.0717
0.16	0.3341	0.0997	0.4952	0.0618	0.0405

ROTATIONAL SPEED = 86.25 RAD/S FLOW RATE = 52.0 CC/S

0.06	2.2966	2.1011	1.2496	10.4370	2.8269
0.08	1.4597	0.9804	1.0818	2.2263	0.8213
0.10	0.5607	0.3036	0.5155	0.7578	0.3468
0.12	0.3884	0.1732	0.4336	0.2871	0.1595
0.14	0.4480	0.1735	0.5758	0.1419	0.0908
0.16	0.2928	0.0983	0.4340	0.0696	0.0513

TABLE:G14 FILM THICKNESS MEASUREMENTS

ROTATIONAL SPEED = 86.25 RAD/S FLOW RATE = 60.5 CC/S

RADIUS (M)	TH/R X10^3	TH/R(RE)	TH/R(TA)$^{0.5}$	RE/TA$^{2.0}$ X10^9	RE$^{2.0}$/TA
0.06	2.2527	2.3977	1.2257	12.1430	3.8266
0.08	1.3008	1.0165	0.9641	2.5902	1.1118
0.10	0.3456	0.2177	0.3178	0.8817	0.4695
0.12	0.2245	0.1165	0.2506	0.3340	0.2159
0.14	0.3773	0.1700	0.4849	0.1651	0.1229
0.16	0.3677	0.1437	0.5450	0.0081	0.0695

ROTATIONAL SPEED = 117.28 RAD/S FLOW RATE = 14.5 CC/S

0.06	0.7950	0.2028	0.5044	1.5740	0.1617
0.08	0.4653	0.0872	0.4022	0.3358	0.0469
0.10	0.2376	0.0359	0.2547	0.1143	0.0198
0.12	0.1945	0.0242	0.2532	0.0043	0.0091
0.14	0.2849	0.0308	0.4270	0.0021	0.0052
0.16	0.2747	0.0257	0.4749	0.0011	0.0029

ROTATIONAL SPEED = 117.28 RAD/S FLOW RATE = 22.1 CC/S

0.06	0.8826	0.3432	0.5600	2.3990	0.3755
0.08	0.3477	0.0992	0.3005	0.5117	0.1091
0.10	0.2142	0.0493	0.2296	0.1742	0.0461
0.12	0.1522	0.0288	0.1981	0.0066	0.0212
0.14	0.2604	0.0429	0.3903	0.0032	0.0121
0.16	0.2696	0.0385	0.4659	0.0016	0.0068

TABLE: G15 FILM THICKNESS MEASUREMENTS

ROTATIONAL SPEED = 117.28 RAD/S FLOW RATE = 31.0 CC/S

RADIUS (M)	TH/R $X10^3$	TH/R(RE)	$TH/R(TA)^{0.5}$	$RE/TA^{2.0}$ $X10^9$	$RE^{2.0}/TA$
0.06	0.9530	0.5197	0.6046	3.3651	0.7388
0.08	0.3359	0.1345	0.2903	0.7178	0.2147
0.10	0.1961	0.0633	0.2102	0.2444	0.0907
0.12	0.1373	0.0365	0.1788	0.0926	0.0417
0.14	0.2563	0.05918	0.3841	0.0457	0.0237
0.16	0.2153	0.04311	0.3722	0.0224	0.0134

ROTATIONAL SPEED = 117.28 RAD/S FLOW RATE = 37.3 CC/S

0.06	0.9177	0.6022	0.5823	4.0480	1.0697
0.08	0.4300	0.2072	0.3717	0.8637	0.3108
0.10	0.2142	0.0832	0.2296	0.2940	0.1312
0.12	0.1646	0.0527	0.2143	0.1114	0.0604
0.14	0.2971	0.0825	0.4452	0.0551	0.0344
0.16	0.2980	0.0718	0.5150	0.0269	0.0194

ROTATIONAL SPEED = 117.28 RAD/S FLOW RATE = 42.7 CC/S

0.06	1.1716	0.8801	0.7434	4.6351	1.4018
0.08	0.4948	0.2729	0.4276	0.9887	0.4072
0.10	0.1729	0.0769	0.1853	0.3366	0.1720
0.12	0.1497	0.0548	0.1949	0.1275	0.0791
0.14	0.2068	0.0657	0.3099	0.0630	0.0450
0.16	0.1947	0.0587	0.3365	0.0309	0.0255

TABLE:G16 FILM THICKNESS MEASUREMENTS

ROTATIONAL SPEED = 117.28 RAD/S FLOW RATE = 52.0 CC/S

RADIUS (M)	TH/R $X10^3$	TH/R(RE)	$TH/R(TA)^{0.5}$	$RE/TA^{2.0}$ $X10^9$	$RE^{2.0}/TA$
0.06	1.4228	1.3017	0.9028	5.6446	2.0789
0.08	0.5065	0.3402	0.4378	1.2041	0.6040
0.10	0.2979	0.1613	0.3194	0.4099	0.2551
0.12	0.1870	0.0834	0.2435	0.1553	0.1173
0.14	0.3254	0.1260	0.4876	0.0768	0.0668
0.16	0.2308	0.0775	0.3990	0.0376	0.0377

ROTATIONAL SPEED = 117.28 RAD/S FLOW RATE = 60.5 CC/S

0.06	1.0708	1.1398	0.6794	6.5673	2.8141
0.08	0.4183	0.3269	0.36148	1.4009	0.8176
0.10	0.2168	0.1366	0.2324	0.4769	0.3453
0.12	0.1696	0.0879	0.2208	0.1806	0.1588
0.14	0.2890	0.1302	0.4331	0.0893	0.0904
0.16	0.4891	0.0973	0.4302	0.0438	0.0511

TABLE:G17 WAVE INCEPTION MEASUREMENTS

SPEED=231 rpm (24.24 rad/s)

FLOWRATE	WAVE INCEPTION
14.5	4.48 cm
22.1	3.09 cm
31.0	4.23 cm
37.3	2.47 cm
42.7	3.09 cm
46.2	4.79 cm
52.0	4.63 cm
60.5	5.25 cm

SPEED=568 rpm (59.53 rad/s)

FLOWRATE	WAVE INCEPTION
14.5	1.54 cm
22.1	2.01 cm
31.0	2.32 cm
37.3	2.47 cm
42.7	3.09 cm
46.2	3.40 cm
52.0	2.16 cm
60.5	1.85 cm

SPEED=314 rpm (32.88 rad/s)

FLOWRATE	WAVE INCEPTION
14.5	3.09 cm
22.1	4.23 cm
31.0	4.01 cm
37.3	4.48 cm
42.7	5.25 cm
46.2	6.48 cm
52.0	4.79 cm
60.5	6.18 cm

SPEED=823 rpm (86.25 rad/s)

FLOWRATE	WAVE INCEPTION
14.5	1.54 cm
22.1	2.32 cm
31.0	1.85 cm
37.3	2.78 cm
42.7	2.78 cm
46.2	2.47 cm
52.0	1.54 cm
60.5	0.93 cm

SPEED=417 rpm (43.67 rad/s)

FLOERATE	WAVE INCEPTION
14.5	2.47 cm
22.1	2.93 cm
31.0	3.40 cm
37.3	2.01 cm
42.7	2.47 cm
46.2	4.32 cm
52.0	3.09 cm
60.5	2.47 cm

SPEED=1120 rpm (117.28 rad/s)

FLOWRATE	WAVE INCEPTION
14.5	1.43 cm
22.1	2.00 cm
31.0	1.72 cm
37.3	1.72 cm
42.7	1.58 cm
46.2	---
52.0	0.86 cm
60.5	0.29 cm

FLOWRATE IN CC/S

TABLE G18 WAVE AMPLITUDE DATA

SPEED (rad/s)	Q(m^3/s) x10^6	Radius(m) x10^2	Amplitude(m) x10^6
24.24	14.5	8.75	15.0
24.24	14.5	11.85	17.5
24.24	31.0	8.65	20.5
32.88	31.0	9.80	27.5
32.88	31.0	11.15	7.5
32.88	42.7	10.45	17.5
43.67	14.5	4.80	29.0
43.67	14.5	6.30	14.0
43.67	14.5	7.60	16.4
43.67	14.5	8.65	20.0
43.67	14.5	10.30	6.0
43.67	14.5	11.13	7.6
43.67	31.0	4.50	32.0
43.67	31.0	5.80	31.0
43.67	31.0	6.66	24.0
43.67	31.0	7.15	10.0
43.67	31.0	9.35	11.0
59.53	14.5	5.10	9.0
59.53	14.5	6.00	9.0
59.53	14.5	9.30	5.0
59.53	14.5	11.50	8.0
59.53	31.0	4.80	17.6
59.53	31.0	6.90	16.0
59.53	31.0	7.90	8.0
59.53	31.0	10.50	10.0
59.53	31.0	11.80	10.0
86.25	14.5	7.10	7.5
86.25	14.5	8.90	4.5
86.25	14.5	10.80	6.0
86.25	14.5	11.70	5.0
86.25	14.5	12.2	5.0

SPEED (rad/s)	Q(m^3/s) x10^6	Radius(m) x10^2	Amplitude(m) x10^6
86.25	31.0	4.60	15.0
86.25	31.0	5.65	13.0
86.25	31.0	6.60	8.5
86.25	31.0	8.20	7.5
86.25	31.0	10.30	5.5
86.25	31.0	11.60	7.5
117.28	14.5	3.90	10.0
117.28	14.5	7.35	4.0
117.28	14.5	9.50	3.5
117.28	14.5	10.60	6.0
117.28	14.5	12.20	6.0
117.28	31.0	3.75	20.0
117.28	31.0	5.35	11.5
117.28	31.0	5.65	9.5
117.28	31.0	6.20	6.5
117.28	31.0	7.65	5.0
117.28	31.0	9.20	6.5

TABLE G19 WAVELENGTH DATA

SPEED (rpm)	Q(cc/s)	WAVELENGTH(cm)
231	14.5	0.83
231	22.1	0.75
231	31.0	0.75
231	37.3	0.69
231	46.2	0.97
231	52.0	0.97
231	60.5	1.24
314	14.5	0.75
314	22.1	0.69
314	31.0	0.55
314	37.3	0.83
314	42.7	0.69
314	46.2	0.72
314	52.0	0.83
417	14.5	0.75
417	22.1	0.69
417	31.0	0.83
417	37.3	0.69
417	42.7	0.97
417	46.2	1.10
417	52.0	0.83
417	60.5	0.97
568	14.5	0.83
568	22.1	0.83
568	31.0	0.97
568	37.3	0.69
568	42.7	0.83
568	52.0	0.77

SPEED (rpm)	Q(cc/s)	WAVELENGTH(cm)
823	14.5	0.69
823	22.1	0.55
823	31.0	0.69
823	37.3	0.69
823	42.7	0.69
823	46.2	0.83
823	52.0	0.83
1120	14.5	0.55
1120	22.1	0.55
1120	31.0	0.41
1120	37.3	0.83
1120	42.7	0.83
1120	46.2	0.97
1120	52.0	0.97

TABLE:G19a SURFACE AREA INCREASE

INCREASE IN SURFACE AREA COMPARED WITH THE MEAN FILM THICKNESS

RATATIONAL SPEED	FLOW RATE	% INCREASE
RAD/S	CC/S	MM**2 X100
24.24	14.5	14.01
24.24	31.0	14.42
24.24	42.7	15.19
24.24	52.0	15.50
32.88	14.5	13.45
32.88	31.0	14.07
32.88	42.7	14.59
32.88	52.0	15.35
43.67	14.5	13.77
43.67	31.0	17.02
43.67	42.7	14.56
43.67	52.0	14.29
59.53	14.5	13.67
59.53	31.0	13.75
59.53	42.7	14.16
59.53	52.0	13.95

TABLE:G19b SURFACE AREA INCREASE

INCREASE IN SURFACE AREA COMPARED WITH THE MEAN FILM THICKNESS

ROTATIONAL SPEED RAD/S	FLOW RATE CC/S	% INCREASE MM**2 X100
86.25	14.5	13.82
86.25	31.0	16.35
86.25	42.7	14.07
86.25	52.0	14.10
117.28	14.5	13.62
117.28	31.0	16.76
117.28	42.7	14.32
117.28	52.0	14.34

TABLE: G20 E_T (FRACTIONAL APPROACH TO EQUILIBRIUM) WITH DIFFERENT FLOW RATE AND RADII AT ROTATIONAL SPEED OF 227 RPM

RADIUS	FLOW RATE	FLOW RATE	FLOW RATE	FLOW RATE
(MM)	14.5 CC/S	22.1 CC/S	31.0 CC/S	37.3 CC/S
60.0	0.207	0.219	0.272	0.302
90.0	0.284	0.252	0.275	0.310
110.0	0.354	0.323	0.334	0.405
130.0	0.402	0.423	0.403	0.380
150.0	0.490	0.460	0.429	0.441
170.0	0.608	0.497	0.504	0.578
180.0	0.665	0.540	0.614	0.612

RADIUS	FLOW RATE	FLOW RATE	FLOW RATE	FLOW RATE
(MM)	42.7 CC/S	46.2 CC/S	52.0 CC/S	60.5 CC/S
60.0	0.156	0.111	0.054	0.201
90.0	0.140	0.110	0.107	0.149
110.0	0.217	0.172	0.137	0.194
130.0	0.224	0.239	0.191	0.250
150.0	0.263	0.246	0.256	0.323
170.0	0.316	0.316	0.405	0.421
180.0	0.412	0.427	0.413	0.455

TABLE: G21 E_T (FRACTIONAL APPROACH TO EQUILIBRIUM) WITH DIFFERENT FLOW RATES AND RADII AT ROTATIONAL SPEED OF 314 RPM

RADIUS	FLOW RATE	FLOW RATE	FLOW RATE	FLOW RATE
(MM)	14.5 CC/S	22.1 CC/S	31.0 CC/S	37.3 CC/S
60.0	0.341	0.295	0.100	0.303
90.0	0.377	0.272	0.173	0.301
110.0	0.461	0.351	0.289	0.374
130.0	0.513	0.417	0.346	0.415
150.0	0.607	0.576	0.452	0.462
170.0	0.754	0.625	0.601	0.535
180.0	0.834	0.672	0.660	0.529

RADIUS	FLOW RATE	FLOW RATE	FLOW RATE	FLOW RATE
(MM)	42.7 CC/S	46.2 CC/S	52.0 CC/S	60.5 CC/S
60.0	0.164	0.199	0.196	0.195
90.0	0.201	0.253	0.170	0.197
110.0	0.312	0.331	0.219	0.318
130.0	0.375	0.351	0.279	0.316
150.0	0.463	0.402	0.360	0.306
170.0	0.545	0.481	0.441	0.382
180.0	0.604	0.518	0.531	0.473

TABLE: G22 E_T (FRACTIONAL APPROACH TO EQUILIBRIUM) WITH DIFFERENT FLOW RATES AND RADII AT ROTATIONAL SPEED OF 417 RPM

RADIUS (MM)	FLOW RATE 14.5 CC/S	FLOW RATE 22.1 CC/S	FLOW RATE 31.0 CC/S	FLOW RATE 37.3 CC/S
60.0	0.163	0.157	0.108	0.118
90.0	0.318	0.229	0.152	0.114
110.0	0.431	0.401	0.345	0.287
130.0	0.478	0.434	0.431	0.377
150.0	0.579	0.603	0.538	0.517
170.0	0.725	0.716	0.641	0.580
180.0	0.777	0.754	0.716	0.667

RADIUS (MM)	FLOW RATE 42.7 CC/S	FLOW RATE 46.2 CC/S	FLOW RATE 52.0 CC/S	FLOW RATE 60.5 CC/S
60.0	0.096	0.070	0.049	0.042
90.0	0.095	0.110	0.111	0.112
110.0	0.316	0.200	0.182	0.121
130.0	0.325	0.273	0.259	0.205
150.0	0.473	0.404	0.371	0.334
170.0	0.518	0.465	0.452	0.451
180.0	0.597	0.599	0.539	0.505

TABLE:G23 E_T (FRACTIONAL APPROACH TO EQUILIBRIUM) WITH DIFFERENT FLOW RATES AND RADII AT ROTATIONAL SPEED OF 571 RPM

RADIUS	FLOW RATE	FLOW RATE	FLOW RATE	FLOW RATE
(MM)	14.5 CC/S	22.1 CC/S	31.0 CC/S	37.3 CC/S
60.0	0.179	0.141	0.129	0.100
90.0	0.410	0.334	0.286	0.242
110.0	0.522	0.420	0.369	0.308
130.0	0.672	0.603	0.574	0.539
150.0	0.833	0.760	0.699	0.610
170.0	0.874	0.858	0.820	0.756
180.0	0.936	0.924	0.887	0.830

RADIUS	FLOW RATE	FLOW RATE	FLOW RATE	FLOW RATE
(MM)	42.7 CC/S	46.2 CC/S	52.0 CC/S	60.5 CC/S
60.0	0.082	0.094	0.077	0.036
90.0	0.227	0.181	0.158	0.150
110.0	0.353	0.339	0.294	0.244
130.0	0.462	0.434	0.376	0.331
150.0	0.548	0.479	0.457	0.471
170.0	0.739	0.685	0.667	0.658
180.0	0.791	0.758	0.715	0.668

TABLE: G24 E_T (FRACTIONAL APPROACH TO EQUILIBRIUM) WITH DIFFERENT FLOW RATES AND RADII AT ROTATIONAL SPEED OF 825 RPM

RADIUS	FLOW RATE	FLOW RATE	FLOW RATE	FLOW RATE
(MM)	14.5 CC/S	22.1 CC/S	31.0 CC/S	37.3 CC/S
60.0	0.263	0.271	0.229	0.167
90.0	0.562	0.481	0.481	0.451
110.0	0.790	0.777	0.656	0.608
130.0	0.831	0.815	0.747	0.692
150.0	0.944	0.904	0.860	0.781
170.0	0.984	0.939	0.906	0.874
180.0	0.943	0.959	0.930	0.897

RADIUS	FLOW RATE	FLOW RATE	FLOW RATE	FLOW RATE
(MM)	42.7 CC/S	46.2 CC/S	52.0 CC/S	60.5 CC/S
60.0	0.117	0.107	0.103	0.093
90.0	0.403	0.345	0.313	0.283
110.0	0.540	0.470	0.444	0.381
130.0	0.597	0.513	0.479	0.453
150.0	0.707	0.642	0.618	0.601
170.0	0.824	0.797	0.757	0.711
180.0	0.867	0.826	0.836	0.798

TABLE: G25 E_T (FRACTIONAL APPROACH TO EQUILIBRIUM) WITH DIFFERENT FLOW RATES AND RADII AT ROTATIONAL SPEED OF 1110 RPM

RADIUS	FLOW RATE	FLOW RATE	FLOW RATE	FLOW RATE
(MM)	14.5 CC/S	22.1 CC/S	31.0 CC/S	37.3 CC/S
60.0	-	0.374	0.318	0.264
90.0	-	0.675	0.617	0.566
110.0	-	0.737	0.708	0.651
130.0	-	0.926	0.891	0.836
150.0	-	0.959	0.953	0.930
170.0	-	0.964	1.000	0.997
180.0	-	0.935	0.981	0.981

RADIUS	FLOW RATE	FLOW RATE	FLOW RATE	FLOW RATE
(MM)	42.7 CC/S	46.2 CC/S	52.0 CC/S	60.5 CC/S
60.0	0.223	0.210	0.208	0.162
90.0	0.526	0.493	0.474	0.396
110.0	0.597	0.546	0.527	0.499
130.0	0.801	0.785	0.732	0.702
150.0	0.891	0.861	0.849	0.799
170.0	0.979	0.943	0.892	0.890
180.0	0.954	0.927	0.909	0.898

TABLE:G26 EDGE EFFECT AND APPARENT D_L

ROTATIONAL SPEED (RAD/S)	FLOW RATE (CC/S)	EDGE EFFECT (%)	APPARENT D_L (M*M/S) *E+09
23.74	14.5	5.48	2.46
23.74	22.1	11.06	2.35
23.74	31.0	13.45	3.51
23.74	37.3	17.33	4.13
23.74	42.7	4.83	2.90
23.74	46.2	-1.30	4.90
23.74	52.0	-8.86	9.32
23.74	60.5	3.86	7.53
32.90	14.5	14.38	2.38
32.90	22.1	9.95	3.17
32.90	31.0	-9.54	8.54
32.90	37.3	20.21	2.29
32.90	42.7	5.30	8.35
32.90	46.2	10.37	4.41
32.90	52.0	2.46	6.44
32.90	60.5	10.81	3.98
43.80	14.5	5.26	2.80
43.80	22.1	-4.77	5.46
43.80	31.0	-10.25	8.68
43.80	37.3	-10.69	9.70
43.80	42.7	-8.98	9.29
43.80	46.2	-12.83	10.13
43.80	52.0	-13.51	10.50
43.80	60.5	-14.24	12.19

TABLE:G27 EDGE EFFECT AND APPARENT D_L

ROTATIONAL SPEED (RAD/S)	FLOW RATE (CC/S)	EDGE EFFECT (%)	APPARENT D_L (M*M/S) *E+09
60.05	14.5	1.44	3.59
60.05	22.1	-7.79	7.08
60.05	31.0	-10.52	10.70
60.05	37.3	-13.08	12.77
60.05	42.7	-12.67	13.56
60.05	46.2	-12.19	13.16
60.05	52.0	-14.68	14.99
60.05	60.5	-18.38	19.07
86.27	14.5	21.57	2.19
86.27	22.1	18.40	3.94
86.27	31.0	12.73	6.37
86.27	37.3	7.03	8.42
86.27	42.7	0.38	10.33
86.27	46.2	-4.07	11.23
86.27	52.0	-6.41	13.24
86.27	60.5	-8.33	15.45
117.38	14.5	--	--
117.38	22.1	34.96	2.10
117.38	31.0	24.59	4.75
117.38	37.3	16.10	7.27
117.38	42.7	10.72	9.23
117.38	46.2	8.38	10.05
117.38	52.0	7.86	10.99
117.38	60.5	0.38	7.52

TABLE:G28 MASS TRANSFER RATE AT DIFFERENT SPEEDS AND FLOW RATE

ROTATIONAL SPEED = 227 RPM

FLOW RATE (CC/S)	CRUDE MODEL $(g/S)X10^4$	BEFORE THE DISC * $(g/S)X10^4$	AFTER THE DISC $(g/S)X10^4$
14.5	0.466	0.699	1.003
22.1	0.536	0.864	1.451
31.0	0.601	1.379	1.945
37.3	0.639	1.654	2.163
42.7	0.668	1.275	2.399
46.2	0.696	1.449	2.510
52.0	0.723	1.577	2.693
60.5	0.760	2.025	2.904
ROTATIONAL SPEED = 314 RPM			
14.5	0.527	0.889	1.108
22.1	0.607	1.091	1.628
31.0	0.680	1.503	2.213
37.3	0.743	1.488	2.530
42.7	0.766	1.921	2.781
46.2	0.765	1.736	2.846
52.0	0.817	2.058	2.988
60.5	0.889	2.202	3.214
ROTATIONAL SPEED = 417 RPM			
14.5	0.628	0.896	1.013
22.1	0.722	1.324	1.616
31.0	0.797	1.742	2.183
37.3	0.848	1.952	2.517
42.7	0.883	1.989	2.790

*AT RADIUS 180.0 MM FROM THE CENTRE OF THE DISC

ROTATIONAL SPEED = 417 RPM

FLOW RATE (CC/S)	CRUDE MODEL $(g/S)X10^4$	BEFORE THE DISC $(g/S)X10^4$	AFTER THE DISC $(g/S)X10^4$
46.2	0.918	2.185	2.937
52.0	0.924	2.144	3.059
60.5	0.941	2.260	3.505

ROTATIONAL SPEED = 571 RPM

14.5	0.683	1.058	1.171
22.1	0.786	1.593	1.796
31.0	0.881	2.145	2.498
37.3	0.930	2.400	2.950
42.7	0.974	2.617	3.337
46.2	0.999	2.715	3.519
52.0	1.026	2.843	3.855
60.5	1.064	3.052	4.247

ROTATIONAL SPEED = 825 RPM

14.5	0.787	1.087	1.229
22.1	0.904	1.686	1.872
31.0	1.013	2.292	2.552
37.3	1.077	2.660	2.933
42.7	1.120	2.925	3.285
46.2	1.115	3.016	3.486
52.0	1.200	3.435	3.807
60.5	1.264	3.815	4.418

ROTATIONAL SPEED = 1110 RPM

FLOW RATE (CC/S)	CRUDE MODEL $(g/S)X10^4$	BEFORE THE DISC $(g/S)X10^4$	AFTER THE DISC $(g/S)X10^4$
14.5	-	-	-
22.1	1.004	1.643	1.757
31.0	1.124	2.419	2.465
37.3	1.195	2.910	2.941
42.7	1.242	3.216	3.298
46.2	1.277	3.382	3.101
52.0	1.326	3.733	3.418
60.5	1.394	4.292	3.959

TABLE G29 MASS TRANSFER COEFFICENT AT DIFFERENT ROTATIONAL SPEEDS AND FLOW RATES BEFORE AND AFTER THE DISC

FLOW RATE (CC/S)	CRUDE MODEL $(M/S)X10^4$	BEFORE THE DISC* $(M/S)X10^4$	AFTER THE DISC $(M/S)X10^4$
14.5	0.848	1.583	3.700
22.1	0.900	1.710	4.939
31.0	0.962	2.943	6.501
37.3	1.004	-	6.691
42.7	1.037	2.262	7.043
46.2	1.057	2.566	7.138
52.0	1.089	2.762	7.318
60.5	1.133	3.669	7.726
ROTATIONAL SPEED = 227 RPM			
14.5	0.987	2.598	5.028
22.1	1.031	2.456	7.175
31.0	1.095	3.336	9.006
37.3	1.138	2.800	8.980
42.7	1.174	3.946	9.257
46.2	1.196	3.368	-
52.0	1.231	3.932	9.098
60.5	1.279	3.864	9.684
ROTATIONAL SPEED = 314 RPM			

* AT RADIUS 180.0 MM FROM THE CENTRE OF THE DISC

FLOW RATE (CC/S)	CRUDE MODEL $(M/S)X10^4$	BEFORE THE DISC $(M/S)X10^4$	AFTER THE DISC $(M/S)X10^4$
14.5	1.137	2.173	3.199
22.1	1.167	3.089	5.919
31.0	1.229	3.892	7.211
37.3	1.274	4.088	7.783
42.7	1.311	3.875	8.550
46.2	1.334	4.200	8.512
52.0	1.371	4.017	9.357
60.5	1.423	4.244	10.410

ROTATIONAL SPEED = 417 RPM

TABLE:G30 MASS TRANSFER RATE WITH DIFFERENT FLOW RATES AND RADII ACROSS THE DISC AT ROTATIONAL SPEED OF 227 RPM

RADIUS (MM)	FLOW RATE 14.5 CC/S (g/S)X10^4	FLOW RATE 22.1 CC/S (g/S)X10^4	FLOW RATE 31.0 CC/S (g/S)X10^4	FLOW RATE 37.3 CC/S (g/S)X10^4
60.0	0.229	0.371	0.646	0.862
90.0	0.315	0.426	0.652	0.884
110.0	0.393	0.545	0.793	1.157
130.0	0.441	0.706	0.944	1.069
150.0	0.529	0.758	0.992	1.225
170.0	0.648	0.807	1.149	1.580
180.0	0.699	0.864	1.379	1.654

RADIUS (MM)	FLOW RATE 42.7 CC/S (g/S)X10^4	FLOW RATE 46.2 CC/S (g/S)X10^4	FLOW RATE 52.0 CC/S (g/S)X10^4	FLOW RATE 60.5 CC/S (g/S)X10^4
60.0	0.508	0.394	0.216	0.195
90.0	0.457	0.390	0.425	0.690
110.0	0.710	0.606	0.544	0.898
130.0	0.763	0.845	0.759	1.158
150.0	0.922	0.859	0.996	1.475
170.0	1.079	1.088	1.567	1.895
180.0	1.275	1.449	1.577	2.025

TABLE:G31 MASS TRANSFER RATE WITH DIFFERENT FLOW RATES AND RADII ACROSS THE DISC AT ROTATIONAL SPEED OF 314 RPM

RADIUS	FLOW RATE	FLOW RATE	FLOW RATE	FLOW RATE
(MM)	14.5 CC/S	22.1 CC/S	31.0 CC/S	37.3 CC/S
	$(g/S)X10^4$	$(g/S)X10^4$	$(g/S)X10^4$	$(g/S)X10^4$
60.0	0.378	0.492	0.237	0.876
90.0	0.418	0.454	0.409	0.873
110.0	0.511	0.594	0.685	1.081
130.0	0.569	0.706	0.821	1.200
150.0	0.657	0.961	1.059	1.318
170.0	0.814	1.029	1.387	1.525
180.0	0.889	1.091	1.503	1.488

RADIUS	FLOW RATE	FLOW RATE	FLOW RATE	FLOW RATE
(MM)	42.7 CC/S	46.2 CC/S	52.0 CC/S	60.5 CC/S
	$(g/S)X10^4$	$(g/S)X10^4$	$(g/S)X10^4$	$(g/S)X10^4$
60.0	0.535	0.718	0.831	0.896
90.0	0.656	0.905	0.676	0.906
110.0	1.020	1.171	0.870	1.454
130.0	1.226	1.233	1.108	1.442
150.0	1.518	1.403	1.442	1.379
170.0	1.756	1.656	1.731	1.689
180.0	1.921	1.736	2.058	2.202

TABLE G32 MASS TRANSFER RATE WITH DIFFERENT FLOW RATES AND RADII ACROSS THE DISC AT ROTATIONAL SPEED OF 417 RPM

RADIUS	FLOW RATE	FLOW RATE	FLOW RATE	FLOW RATE
(MM)	14.5 CC/S	22.1 CC/S	31.0 CC/S	37.3 CC/S
	$(g/S)X10^4$	$(g/S)X10^4$	$(g/S)X10^4$	$(g/S)X10^4$
60.0	0.188	0.275	0.265	0.348
90.0	0.251	0.322	0.369	0.329
110.0	0.500	0.704	0.850	0.847
130.0	0.552	0.896	1.063	1.117
150.0	0.667	1.116	1.310	1.503
170.0	0.836	1.258	1.559	1.688
180.0	0.896	1.324	1.742	1.952

RADIUS	FLOW RATE	FLOW RATE	FLOW RATE	FLOW RATE
(MM)	42.7 CC/S	46.2 CC/S	52.0 CC/S	60.5 CC/S
	$(g/S)X10^4$	$(g/S)X10^4$	$(g/S)X10^4$	$(g/S)X10^4$
60.0	0.318	0.246	0.190	0.186
90.0	0.310	0.392	0.443	0.505
110.0	1.065	0.717	0.716	0.517
130.0	1.096	0.977	1.032	0.906
150.0	1.555	1.607	1.420	1.426
170.0	1.703	1.685	1.785	2.018
180.0	1.989	2.185	2.144	2.260

TABLE:G33 MASS TRANSFER RATE WITH DIFFERENT FLOW RATE AND RADII ACROSS THE DISC AT ROTATIONAL SPEED OF 571 RPM

RADIUS	FLOW RATE	FLOW RATE	FLOW RATE	FLOW RATE
(MM)	14.5 CC/S	22.1 CC/S	31.0 CC/S	37.3 CC/S
	$(g/S)X10^4$	$(g/S)X10^4$	$(g/S)X10^4$	$(g/S)X10^4$
60.0	0.205	0.246	0.311	0.286
90.0	0.470	0.579	0.686	0.664
110.0	0.602	0.739	0.908	0.913
130.0	0.774	1.060	1.414	1.568
150.0	0.961	1.336	1.721	1.785
170.0	1.002	1.498	2.008	2.229
180.0	1.058	1.593	2.145	2.400

RADIUS	FLOW RATE	FLOW RATE	FLOW RATE	FLOW RATE
(MM)	42.7 CC/S	46.2 CC/S	52.0 CC/S	60.5 CC/S
	$(g/S)X10^4$	$(g/S)X10^4$	$(g/S)X10^4$	$(g/S)X10^4$
60.0	0.262	0.331	0.294	0.151
90.0	0.694	0.660	0.649	0.715
110.0	1.192	1.230	1.168	1.099
130.0	1.540	1.554	1.496	1.513
150.0	1.815	1.725	1.795	2.022
170.0	2.445	2.502	2.689	2.986
180.0	2.617	2.715	2.843	3.052

TABLE: G34 MASS TRANSFER RATE WITH DIFFERENT FLOW RATE AND RADII ACROSS THE DISC AT ROTATIONAL SPEED OF 825 RPM

RADIUS	FLOW RATE	FLOW RATE	FLOW RATE	FLOW RATE
(MM)	14.5 CC/S	22.1 CC/S	31.0 CC/S	37.3 CC/S
	$(g/S)X10^4$	$(g/S)X10^4$	$(g/S)X10^4$	$(g/S)X10^4$
60.0	0.301	0.470	0.554	0.484
90.0	0.644	0.840	1.177	1.313
110.0	0.905	1.345	1.595	1.769
130.0	0.958	1.432	1.841	2.039
150.0	1.081	1.578	2.093	2.259
170.0	1.128	1.639	2.205	2.559
180.0	1.087	1.686	2.292	2.660

RADIUS	FLOW RATE	FLOW RATE	FLOW RATE	FLOW RATE
(MM)	42.7 CC/S	46.2 CC/S	52.0 CC/S	60.5 CC/S
	$(g/S)X10^4$	$(g/S)X10^4$	$(g/S)X10^4$	$(g/S)X10^4$
60.0	0.382	0.372	0.422	0.440
90.0	1.316	1.156	1.263	1.320
110.0	1.800	1.692	1.779	1.733
130.0	2.015	1.861	1.930	2.098
150.0	2.340	2.342	2.506	2.785
170.0	2.761	2.873	3.012	3.181
180.0	2.925	3.016	3.435	3.815

TABLE: G35 MASS TRANSFER RATE WITH DIFFERENT FLOW RATES AND RADII ACROSS THE DISC AT ROTATIONAL SPEED OF 1110 RPM

RADIUS (MM)	FLOW RATE 14.5 CC/S $(g/S)X10^4$	FLOW RATE 22.1 CC/S $(g/S)X10^4$	FLOW RATE 31.0 CC/S $(g/S)X10^4$	FLOW RATE 37.3 CC/S $(g/S)X10^4$
60.0	0.629	0.660	0.789	0.789
90.0	0.821	1.186	1.521	1.667
110.0	0.833	1.286	1.724	1.905
130.0	1.023	1.627	2.197	2.463
150.0	1.632	1.654	2.364	2.740
170.0	-	1.683	2.405	2.808
180.0	-	1.643	2.419	2.910

RADIUS (MM)	FLOW RATE 42.7 CC/S $(g/S)X10^4$	FLOW RATE 46.2 CC/S $(g/S)X10^4$	FLOW RATE 52.0 CC/S $(g/S)X10^4$	FLOW RATE 60.5 CC/S $(g/S)X10^4$
60.0	0.762	0.778	0.864	0.781
90.0	1.773	1.821	1.959	1.881
110.0	2.014	1.994	2.150	2.373
130.0	2.686	2.847	3.007	3.334
150.0	2.969	3.062	3.508	3.819
170.0	3.114	3.203	3.641	4.201
180.0	3.216	3.382	3.733	4.292

TABLE: G36 K_L^* AT RADIUS 60.0 MM WITH DIFFERENT FLOW RATES AND ROTATIONAL SPEEDS

FLOW RATE (CC/S)	ROTATIONAL SPEED 571 RPM	ROTATIONAL SPEED 825 RPM	ROTATIONAL SPEED 1110 RPM
14.5	2.943	4.553	-
22.1	3.455	7.192	10.634
31.0	4.392	8.294	12.204
37.3	4.049	7.026	11.784
42.7	4.476	5.460	11.086
46.2	4.703	5.392	11.229
52.0	4.282	5.795	-
60.5	-	6.086	11.030

TABLE: K_L^* AT RADIUS 90.0MM WITH DIFFERENT FLOWRATES AND ROTATIONAL SPEEDS

FLOW RATE (CC/S)	ROTATIONAL SPEED 571 RPM	ROTATIONAL SPEED 825 RPM	ROTATIONAL SPEED 1110 RPM
14.5	3.208	5.016	7.565
22.1	3.762	6.075	10.418
31.0	4.369	8.511	12.471
37.3	4.339	9.383	13.046
42.7	4.613	9.226	13.344
46.2	3.865	8.198	13.142
52.0	3.750	8.192	14.002
60.5	4.109	8.446	12.787

* K_L IN M/S X 10^4

TABLE:G37 K_L AT RADIUS 110.0 MM WITH DIFFERENT FLOW RATES AND ROTATIONAL SPEEDS

FLOW RATE (CC/S)	ROTATIONAL SPEED 227 RPM K_L (M/S) X 10^4	ROTATIONAL SPEED 417 RPM K_L (M/S) X 10^4	ROTATIONAL SPEED 571 RPM K_L (M/S) X 10^4
14.5	1.741	2.246	2.941
22.1	2.363	3.109	3.309
31.0	3.462	3.598	3.912
37.3	-	3.468	3.768
42.7	2.874	4.449	5.111
46.2	2.388	2.875	5.253
52.0	2.097	2.875	4.964
60.5	3.582	2.147	4.644

FLOW RATE (CC/S)	ROTATIONAL SPEED 825 RPM K_L (M/S) X 10^4	ROTATIONAL SPEED 1110 RPM K_L (M/S) X 10^4	ROTATIONAL SPEED
14.5	6.212	5.165	
22.1	8.930	8.094	
31.0	9.070	10.485	
37.3	9.590	10.766	
42.7	9.115	10.659	
46.2	8.042	10.026	
52.0	8.388	10.676	
60.5	7.991	11.505	

TABLE: G38 K_L AT RADIUS 130.0 MM WITH DIFFERENT FLOW RATES AND ROTATIONAL SPEEDS

FLOW RATE (CC/S)	ROTATIONAL SPEED 227 RPM K_L (M/S) X 10^4	ROTATIONAL SPEED 314 RPM K_L (M/S) X 10^4	ROTATIONAL SPEED 417 RPM K_L (M/S) X 10^4
14.5	1.449	2.025	1.832
22.1	2.360	2.318	2.412
31.0	3.107	2.557	3.398
37.3	-	3.883	3.424
42.7	2.206	3.900	3.258
46.2	2.451	3.880	2.858
52.0	2.139	3.298	3.031
60.5	3.383	4.420	2.698

FLOW RATE (CC/S)	ROTATIONAL SPEED 571 RPM K_L (M/S) X 10^4	ROTATIONAL SPEED 825 RPM K_L (M/S) X 10^4	ROTATIONAL SPEED 1110 RPM K_L (M/S) X 10^4
14.5	3.135	5.005	7.411
22.1	3.967	7.235	11.159
31.0	5.130	8.270	13.369
37.3	5.608	8.529	13.089
42.7	5.246	7.540	13.403
46.2	5.105	6.457	13.794
52.0	4.762	6.582	13.291
60.5	4.726	7.092	14.219

TABLE: G39 K_L AT RADIUS 150.0 MM WITH DIFFERENT FLOW RATES AND ROTATIONAL SPEEDS

FLOW RATE (CC/S)	ROTATIONAL SPEED 227 RPM K_L (M/S) X 10^4	ROTATIONAL SPEED 314 RPM K_L (M/S) X 10^4	ROTATIONAL SPEED 417 RPM K_L (M/S) X 10^4
14.5	1.413	1.958	1.814
22.1	1.973	2.745	2.874
31.0	2.520	2.702	2.874
37.3	-	3.344	3.924
42.7	2.048	3.838	3.958
46.2	1.890	3.441	4.204
52.0	2.203	3.361	3.495
60.5	3.415	3.198	3.562

FLOW RATE (CC/S)	ROTATIONAL SPEED 571 RPM K_L (M/S) X 10^4	ROTATIONAL SPEED 825 RPM K_L (M/S) X 10^4	ROTATIONAL SPEED 1110 RPM K_L (M/S) X 10^4
14.5	3.762	6.045	7.983
22.1	4.573	7.488	10.237
31.0	5.379	8.826	13.740
37.3	5.080	8.206	14.338
42.7	4.912	7.584	13.714
46.2	4.355	6.864	13.180
52.0	4.599	7.238	14.204
60.5	5.571	8.063	14.054

TABLE:G40 K_L AT RADIUS 170.0 MM WITH DIFFERENT FLOW RATES AND ROTATIONAL SPEEDS

FLOW RATE (CC/S)	ROTATIONAL SPEED 227 RPM K_L (M/S) X 10^4	ROTATIONAL SPEED 314 RPM K_L (M/S) X 10^4	ROTATIONAL SPEED 417 RPM K_L (M/S) X 10^4
14.5	1.527	2.276	2.099
22.1	1.700	2.431	3.118
31.0	2.439	3.190	3.556
37.3	-	3.197	3.628
42.7	1.945	3.765	3.494
46.2	1.968	3.398	3.236
52.0	3.021	3.390	3.503
60.5	3.700	3.268	4.064

FLOW RATE (CC/S)	ROTATIONAL SPEED 571 RPM K_L (M/S) X 10^4	ROTATIONAL SPEED 825 RPM K_L (M/S) X 10^4	ROTATIONAL SPEED 1110 RPM K_L (M/S) X 10^4
14.5	3.371	6.749	-
22.1	4.836	6.930	8.247
31.0	5.959	8.214	sat
37.3	5.904	8.665	sat
42.7	6.429	8.306	18.483
46.2	5.990	8.265	14.848
52.0	6.413	8.249	12.972
60.5	7.280	8.406	12.767

TABLE: G41 K_L AT RADIUS 180.0 MM WITH DIFFERENT FLOW RATES AND ROTATIONAL SPEEDS

FLOW RATE (CC/S)	ROTATIONAL SPEED 227 RPM K_L (M/S) X 10^4	ROTATIONAL SPEED 314 RPM K_L (M/S) X 10^4	ROTATIONAL SPEED 417 RPM K_L (M/S) X 10^4
14.5	1.583	2.598	2.173
22.1	1.710	2.456	3.089
31.0	2.943	3.336	3.892
37.3	-	2.800	4.088
42.7	2.262	3.946	3.875
46.2	2.566	3.368	4.200
52.0	2.762	3.932	4.017
60.5	3.669	3.864	4.244

FLOW RATE (CC/S)	ROTATIONAL SPEED 571 RPM K_L (M/S) X 10^4	ROTATIONAL SPEED 825 RPM K_L (M/S) X 10^4	ROTATIONAL SPEED 1110 RPM K_L (M/S) X 10^4
14.5	3.971	4.150	-
22.1	5.679	7.062	6.024
31.0	6.744	8.226	12.325
37.3	6.598	8.466	14.838
42.7	6.667	8.601	13.073
46.2	6.546	8.073	12.039
52.0	6.508	9.385	12.422
60.5	6.661	9.661	13.778

APPENDIX H COMPUTER PROGRAMS

PROGRAM A) TO READ EXPERIMENTAL DATA FROM COMPUTER TAPES ON FILM THICKNESS MEASUREMENTS

PROGRAM B) EXPERIMENTAL DATA PLOT OF δ/r Vs Re/Ta^2

PROGRAM C) EXPERIMENTAL DATA PLOT OF $\delta/r \times (Re)$ Vs Re^2/Ta

PROGRAM D) EXPERIMENTAL DATA PLOT OF $\delta/r \times (Ta)^{1/2}$ Vs Re^2/Ta

PROGRAM E,F) PROGRAM TO READ EXPERIMENTAL CONCENTRATION PROFILE ACROSS THE DISC AND CORRELATE INTO $E_T = ARe^aTa^bR^{*c}$ and $Sh = ARe^aTa^bR^{*c}$ RESPECTIVELY USING PROGRAM J FOR 3 VARIABLES AND 2 VARIABLES IN PROGRAM K.

PROGRAM J,K) LINEAR REGRESSION PROGRAMS

PROGRAM L) PROGRAM TO CALCULATE THE EDGE EFFECT (SEE APP.F)

PROGRAM M) READ OUT THE CALIBRATION VALUES OF OXYGENATED AND DEOXYGENATED WATER.

PROGRAM N) CALCULATE THE EXPERIMENTAL K_L AS WELL AS K_L FOR CRUDE AND APPROXIMATION MODELS.

PROGRAM A)

```
      DIMENSION VOLT(20)
      R1=0.058
      R2=0.079
      R3=0.098
      R4=0.119
      R5=0.137
      R6=0.158
      V=0.98E-06
      CALL OPEN(6,'THINFILMDAT',0)
C
C
      WRITE(5,2)
    2 FORMAT(' ENTER SPEED AND FLOW RATE '/)
      READ(5,3)W,Q
    3 FORMAT(2G12.5)
C
      DO 20 J=1,18
      READ(6,1)MAA,MBB,MDD,MCC
    1 FORMAT(I3,I7,I1,I2)
      VOLT(J)=FLOAT(MBB)*10.0**(-2.0)
      VOLT(J)=VOLT(J)+FLOAT(MDD)*10.0**(-3.0)
      VOLT(J)=ABS(VOLT(J))
   20 CONTINUE
C
C     FOR RADIUS 58MM
C
      C1=VOLT(1)+VOLT(2)+VOLT(3)
      D1=C1/3.0
      TH1=-0.035901+0.93153*(D1)+0.48548*(D1)*(D1)
      A1=(TH1/R1)*10.0**(-3.0)
      Q1=Q*10.0**(-6.0)
      RE=Q1/(R1*V)
      TA=(W*R1**2.0)/V
      CC1=(RE**2.0)/TA
      DD1=RE/(TA**2.0)
      A11=A1*RE
      A111=A1*SQRT(TA)
      WRITE(5,10)(VOLT(J),J=1,5)
   10 FORMAT(5G12.5)
      WRITE(5,11)R1,W,Q1,A1,DD1,A11,CC1,A111
   11 FORMAT(' RADIUS=',F6.2,' M',' SPEED=',F6.2,' FLOWRATE='
     £,G12.5,'CC/S'/' TH/R=',G12.5,' RE/TA2=',G12.5,/
     £' TH/R(RE)=',G12.5,' RE2/TA=',G12.5,' TH/R(SQRT(TA))='
     £,G12.5,///)
C
C      FOR RADIUS 79MM
C
      C2=VOLT(4)+VOLT(5)+VOLT(6)
      D2=C2/3.0
      TH2=-0.084551+1.3944*(D2)
      A2=(TH2/R2)*10.0**(-3.0)
      Q2=Q*10.0**(-6.0)
      RE2=Q2/(R2*V)
```

```
      TA2=(W*R2**2.0)/V
      CC2=((RE2)**2.0)/(TA2)
      DD2=(RE2)/((TA2)**2.0)
      A22=A2*(RE2)
      A222=A2*SQRT(TA2)
      WRITE(5,12)R2,W,Q2,A2,DD2,A22,CC2,A222
   12 FORMAT(' RADIUS=',F6.2,'M',' SPEED=',F6.2,' FLOWRATE=',
     £G12.5,'CC/S'/' TH/R=',G12.5,' RE/TA2=',G12.5,/
     £' TH/R(RE)=',G12.5,' RE2/TA=',
     £G12.5,' TH/R(SQRT(TA))=',G12.5,///)
C
C      FOR RADIUS 98MM
C
      C3=VOLT(7)+VOLT(8)+VOLT(9)
      D3=C3/3.0
      TH3=-0.023846+0.68388*(D3)+0.6335*(D3)*(D3)
      A3=(TH3/R3)*10.0**(-3.0)
      Q3=Q*10.0**(-6.0)
      RE3=Q3/(R3*V)
      TA3=(W*R3**2.0)/V
      CC3=((RE3)**2.0)/(TA3)
      DD3=(RE3)/((TA3)**2.0)
      A33=A3*(RE3)
      A333=A3*SQRT(TA3)
      WRITE(5,13)R3,W,Q3,A3,DD3,A33,CC3,A333
   13 FORMAT(' RADIUS=',F6.2,'M',' SPEED=',F6.2,' FLOWRATE=',G12.5,
     £/' TH/R=',G12.5,' RE/TA2=',G12.5,/' TH/R(RE)=',G12.5,' RE2
     £/TA=',G12.5,' TH/R(SQRT(TA))=',G12.5,///)
C
C      FOR RADIUS 119MM
C
      C4=VOLT(10)+VOLT(11)+VOLT(12)
      D4=C4/3.0
      TH4=-0.026829+0.85295*(D4)+0.32681*(D4)*(D4)
      A4=(TH4/R4)*10.0**(-3.0)
      Q4=Q*10.0**(-6.0)
      RE4=Q4/(R4*V)
      TA4=(W*R4**2.0)/V
      CC4=((RE4)**2.0)/(TA4)
      DD4=(RE4)/((TA4)**2.0)
      A44=A4*(RE4)
      A444=A4*SQRT(TA4)
      WRITE(5,14)R4,W,Q4,A4,DD4,A44,CC4,A444
   14 FORMAT(' RADIUS=',F6.2,'M',' SPEED=',F6.2,' FLOWRATE=',G
     £12.5,'CC/S'/' TH/R=',G12.5,' RE/TA2=',G12.5,/' TH/R(RE)
     £=',G12.5,' RE2/TA=',G12.5,' TH/R(SQRT(TA))=',G12.5,///)
C
C      FOR RADIUS 137MM
C
      C5=VOLT(13)+VOLT(14)+VOLT(15)
      D5=C5/3.0
      TH5=-0.05990+2.001*(D5)-3.292B*(D5)*(D5)+3.0744*(D5)**3.0
      A5=(TH5/R5)*10.0**(-3.0)
      Q5=Q*10.0**(-6.0)
      RE5=Q5/(R5*V)
      TA5=(W*R5**2.0)/V
      CC5=((RE5)**2.0)/(TA5)
      DD5=(RE5)/((TA5)**2.0)
```

```
      A55=A5*(RE5)
      A555=A5*SQRT(TA5)
      WRITE(5,15)R5,W,Q5,A5,DD5,A55,CC5,A555
   15 FORMAT(' RADIUS=',F6.2,'M',' SPZOLTEED=',F6.2,' FLOWRATE=',
     £G12.5,'CC/S'/' TH/R=',G12.5,' RE/TA2=',G12.5,/
     £' TH/R(RE)=',G12.5,' RE2/TA=',G12.5,' TH/R(SQRT(TA))=',G12.5,///)
C
C      FOR RADIUS 158MM
C
      C6=VOLT(16)+VOLT(17)+VOLT(18)
      D6=C6/3.0
      TH6=-0.03329+1.2239*(D6)
      A6=(TH6/R6)*10.0**(-3.0)
      Q6=Q*10.0**(-6.0)
      RE6=Q6/(R6*V)
      TA6=(W*R6**2.0)/V
      CC6=((RE6)**2.0)/(TA6)
      DD6=(RE6)/((TA6)**2.0)
      A66=A6*(RE6)
      A666=A6*SQRT(TA6)
      WRITE(5,16)R6,W,Q6,A6,DD6,A66,CC6,A666
   16 FORMAT(' RADIUS=',F6.2,'M',' SPEED=',F6.2,' FLOWRATE=',
     £G12.5,'CC/S'/' TH/R=',G12.5,' RE/TA2=',G12.5,/
     £' TH/R(RE)=',G12.5,' RE2/TA=',G12.5,' TH/R(SQRT(TA)=',
     £G12.5,///)
      STOP
      END
```

FILM THICKNESS MEASUREMENTS BY MICRODENSOMETRIC TECHNIQUE

PARAMETERS INVESTIGATED-ROTATIONAL SPEEDS,LIQUID FLOWRATES AND RADIAL POSITIONS ACROSS THE DISC.

ROTATIONAL SPEED= 231 RPM, 314 RPM, 417 RPM, 568 RPM, 823 RPM, and 1120 RPM.

FLOWRATE= 14.5 CC/S, 22.1 CC/S, 31.0 CC/S, 37.3 CC/S, 42.7 CC/S, 46.2 CC/S, 52.0 CC/S, 60.5 CC/S.

RADIUS= 58 MM, 79 MM, 98 MM, 119 MM, 137 MM, and 158 MM.

TOTAL EXPERIMENTAL POINTS ARE 280

CALIBRATION CURVES FOR 6 DIFFERENT POSITIONS ACROSS THE DISC

RADIUS= 58 MM STANDARD DEVIATION = 0.44454E-01

Y= -0.35901E-01+0.93153*X+0.48548*X*X

RADIUS= 79 MM STANDARD DEVIATION = 0.77699E-01

Y= -0.84551E-01+1.3944*X

RADIUS= 98 MM STANDARD DEVIATION = 0.15718E-01

Y= -0.23846E-01+0.68388*X+0.63350*X*X

RADIUS= 119 MM STANDARD DEVIATION = 0.13385E-01

Y= -0.26829E-01+0.85295*X+0.32681*X*X

RADIUS= 137 MM STANDARD DEVIATION = 0.43437E-01

Y= -0.59904E-01+2.001*X-3.2928*X*X+3.0744*X*X*X

RADIUS= 158 MM STANDARD DEVIATION = 0.48112E-01

Y= -0.33291E-01+1.2239*X

WHERE X IN MV AND Y IN MM THICKNESS.

21 MM ON THE NEGATIVE= 15.75 CM ON THE DISC

THEREFOR 1 MM = 15.75/21.0

= 0.75 CM ON THE DISC

1 REVOLUTION = 1/2 MM ONTHE NEGATIVE = 0.375 CM ON THE DISC

2 READINGS WERE TAKEN IN ONE REVOLUTION FOR FILM THICKNESS MENSUREMENTS (i.e. 1.875 MM ON THE DISC FOR EACH READING).

AVERAGE OVER 3 POINTS WERE TAKEN FOR EACH RADIUS (i.e. 5.625 MM).

PROGRAM B)

```
      CALL SCALEM(3.5,6.0,-0.5,-0.01)
      S=4.0
      T=1.0
      I=1
      DO 200 L=1,8
      DO 100 N=1,10
      P=N*I
      P=ALOG10(P)
      CALL EPLOT(1,P,T)
      CALL EPLOT(2,P,S)
  100 CONTINUE
      I=I*10
  200 CONTINUE
      S=8.0
      T=0.0
      J=1
      DO 300 L=1,3
      DO 400 N=1,10
      P=N*J
      P=ALOG10(P)+1.0
      CALL EPLOT(1,S,P)
      CALL EPLOT(2,T,P)
  400 CONTINUE
      J=J*10
  300 CONTINUE
      K=500
      DO 500 I=1,K
      READ(5,1,END=2)A,B,C,D,E
    1 FORMAT(5G12.5)
      B1=A*10000.0
      BA=ALOG10(B1)+1.0
      A1=B*1.0E+12
      AA=ALOG10(A1)
      CALL EPLOT(1,AA,BA)

      CALL CIRCLE(0.03)
  500 CONTINUE
    2 CONTINUE
      Y=1.0
      X=2.0
      Y=ALOG10(Y)+1.0
      X=ALOG10(X)
      CALL EPLOT(1,X,Y)
      Z=350.0
      W=1.0E+08
      Z=ALOG10(Z)+1.0
      W=ALOG10(W)
      CALL EPLOT(2,W,Z)
      LL=10
      DO 600 I=1,9
      P=FLOAT(I-1)-0.15
      CALL EPLOT(1,P,0.83)
      CALL PLTNUM(LL,'I2*',1.5,0.0)
      K=13-I
```

```
      P=FLOAT(I-1)+0.1
      CALL EPLOT(1,P,0.887)
      IF(K-10)10,20,20
   20 CALL PLTNUM(K,'"-",I2*',1.0,0.0)
      GOTO 600
   10 CALL PLTNUM(K,'"-",I1*',1.0,0.0)
      GOTO 600
  600 CONTINUE
      DO 700 I=1,4
      P=FLOAT(I)
      IF(I.EQ.4)P=P-0.133
      CALL EPLOT(1,-0.50,P)
      CALL PLTNUM(LL,'I2*',1.5,0.0)
      K=5-I
      P=FLOAT(I)+0.125
      CALL EPLOT(1,-0.35,P)
      IF(I-4)30,40,40
   30 CALL PLTNUM(K,'"-",I1*',1.0,0.0)
      GOTO 700
   40 P=FLOAT(I)
      CALL EPLOT(1,-0.35,P)
      CALL PLTNUM(K,'"-",I1*',1.0,0.0)
      GOTO 700
  700 CONTINUE
      CALL ENDPIC
      STOP
      END
```

PROGRAM C)

```
      CALL SCALEM(4.0,8.0,-0.5,-0.01)
      S=3.0
      T=1.0
      I=1
      DO 200 L=1,6
      DO 100 N=1,10
      P=N*I
      P=ALOG10(P)
      CALL EPLOT(1,P,T)
      CALL EPLOT(2,P,S)
  100 CONTINUE
      I=I*10
  200 CONTINUE
      S=6.0
      T=0.0
      J=1
      DO 300 L=1,2
      DO 400 N=1,10
      P=N*J
      P=ALOG10(P)+1.0
      CALL EPLOT(1,S,P)
      CALL EPLOT(2,T,P)
  400 CONTINUE
      J=J*10
  300 CONTINUE
      K=500
      DO 500 I=1,K
      READ(5,1,END=2)A,B,C,D,E
    1 FORMAT(5G12.5)
      D1=D*1000.0
      DA=ALOG10(D1)
      E1=E*10.0
      EA=ALOG10(E1)+1.0
      CALL EPLOT(1,DA,EA)
      CALL CIRCLE(0.03)
  500 CONTINUE
    2 CONTINUE
      Y=2.4
      X=1.0E-03*1000.0
      Y=ALOG10(Y)+1.0
      X=ALOG10(X)
      CALL EPLOT(1,X,Y)
      Z=23.5
      W=1000.0*1000.0
      Z=ALOG10(Z)+1.0
      W=ALOG10(W)
      CALL EPLOT(2,W,Z)
      LL=10
      JJ=1
      DO 600 I=1,7
      P=FLOAT(I-1)-0.15
      CALL EPLOT(1,P,0.875)
      IF(I.EQ.4)GOTO 10
      CALL PLTNUM(LL,'I2*',1.5,0.0)
```

```
      K=I-4
      P=FLOAT(I-1)+0.1
      CALL EPLOT(1,P,0.913)
      CALL PLTNUM(K,'I2*',1.0,0.0)
      GOTO 600
   10 P=P+0.15
      CALL EPLOT(1,P,0.875)
      CALL PLTNUM(JJ,'I1*',1.5,0.0)
  600 CONTINUE
      DO 700 I=1,3
      P=FLOAT(I)
      IF(I.EQ.3)P=P-0.125
      CALL EPLOT(1,-0.5,P)
      IF(I.EQ.2)GOTO 20
      CALL PLTNUM(LL,'I2*',1.5,0.0)
      K=I-2
      P=FLOAT(I)+0.1
      IF(I.EQ.3)P=P-0.15
      CALL EPLOT(1,-0.33,P)
      CALL PLTNUM(K,'I2*',1.0,0.0)
      GOTO 700
   20 CALL PLTNUM(JJ,'I1*',1.5,0.0)
  700 CONTINUE
      CALL ENDPIC
      STOP
      END
```

PROGRAM D)

```
      CALL SCALEM(4.0,3.0,-0.5,-0.5)
      S=7.0
      T=1.0
      I=1
      DO 200 L=1,6
      DO 100 N=1,10
      P=N*I
      P=ALOG10(P)
      CALL EPLOT(1,P,T)
      CALL EPLOT(2,P,S)
  100 CONTINUE
      I=I*10
  200 CONTINUE
      S=6.0
      T=0.0
      J=1
      DO 300 L=1,6
      DO 400 N=1,10
      P=N*J
      P=ALOG10(P)+1.0
      CALL EPLOT(1,S,P)
      CALL EPLOT(2,T,P)
  400 CONTINUE
      J=J*10
  300 CONTINUE
      K=500
      DO 500 I=1,K
      READ(5,1,END=2)A,B,C,D,E
    1 FORMAT(5G12.5)
      D1=D*1000.0
      DA=ALOG10(D1)
      C1=C*1000.0
      CA=ALOG10(C1)+1.0
      CALL EPLOT(1,DA,CA)
      CALL CIRCLE(0.03)
  500 CONTINUE
    2 CONTINUE
      Y=8.0E-03*1000.0
      X=1.0E-03*1000.0
      Y=ALOG10(Y)+1.0
      X=ALOG10(X)
      CALL EPLOT(1,X,Y)
      Z=79.0*1000.0
      W=1000.0*1000.0
      Z=ALOG10(Z)+1.0
      W=ALOG10(W)
      CALL EPLOT(2,W,Z)
      LL=10
      JJ=1
      DO 600 I=1,7
      P=FLOAT(I-1)-0.15
      CALL EPLOT(1,P,0.58)
      IF(I.EQ.4)GOTO 10
      CALL PLTNUM(LL,'I2*',1.5,0.0)
```

```
      K=I-4
      P=FLOAT(I-1)+0.1
      CALL EPLOT(1,P,0.7)
      CALL PLTNUM(K,'I2*',1.0,0.0)
      GOTO 600
   10 P=P+0.15
      CALL EPLOT(1,P,0.58)
      CALL PLTNUM(JJ,'I1*',1.5,0.0)
  600 CONTINUE
      DO 700 I=1,7
      P=FLOAT(I)
      IF(I.EQ.7)P=P-0.25
      CALL EPLOT(1,-0.50,P)
      IF(I.EQ.4)GOTO 20
      CALL PLTNUM(LL,'I2*',1.5,0.0)
      K=I-4
      P=FLOAT(I)+0.25
      IF(I.EQ.7)P=P-0.15
      CALL EPLOT(1,-0.33,P)
      CALL PLTNUM(K,'I2*',1.0,0.0)
      GOTO 700
   20 CALL PLTNUM(JJ,'I1*',1.5,0.0)
  700 CONTINUE
      CALL ENDPIC
      STOP
      END
```

PROGRAM E)

```
      DIMENSION VOLT(800)
      WRITE(6,1)
    1 FORMAT(' ENTER SPEED(RAD/S) AND FLOWRATE(CC/S) '/)
      READ(6,2)W,Q
    2 FORMAT(2G12.5)
      V=0.98E-06
      Q=Q*10.0**(-6.0)
C
C       READING THE EXPERIMENTAL DATA
C
      DO 10 J=1,627
      READ(5,3)MAA,MBB,MDD,MCC
    3 FORMAT(I3,I7,I1,I2)
      VOLT(J)=FLOAT(MBB)*10.0**(-2.0)
      VOLT(J)=VOLT(J)+FLOAT(MDD)*10.0**(-3.0)
      VOLT(J)=ABS(VOLT(J))
   10 CONTINUE
C
C       FIRST REGION WITH CALIBRATION AT PT 35.5 MM
C       FROM THE EDGE OF THE DISTRIBUTOR
C
      DO 30 I=30,195
      R=(FLOAT(I)*0.23437+22.5)/10.0
      TH=-0.033229+1.1443*VOLT(I)+0.62739*VOLT(I)*VOLT(I)
      WRITE(7,35)R,TH
   35 FORMAT(2G12.5)
   30 CONTINUE
C
C       2ND REGION WITH CALIBRATION AT PT 56.5 MM
C
      DO 40 I=196,281
      R=(FLOAT(I)*0.23437+22.5)/10.0
      TH=-0.010819+0.47934*VOLT(I)+1.7239*VOLT(I)*VOLT(I)
      WRITE(7,45)R,TH
   45 FORMAT(2G12.5)
   40 CONTINUE
C
C       3RD REGION WITH CALIBRATION AT PT 75.5 MM
C
      DO 50 I=282,366
      R=(FLOAT(I)*0.23437+22.5)/10.0
      TH=-0.018271+0.78861*VOLT(I)+0.99584*VOLT(I)*VOLT(I)
      WRITE(7,55)R,TH
   55 FORMAT(2G12.5)
   50 CONTINUE
C
C       4TH REGION WITH CALIBRATION AT PT 96.5 MM
C
      DO 60 I=367,437
      R=(FLOAT(I)*0.23437+22.5)/10.0
      TH=-0.046984+2.0616*VOLT(I)-3.9390*VOLT(I)*VOLT(I)+
     £4.6365*(VOLT(I)**3.0)
      WRITE(7,65)R,TH
   65 FORMAT(2G12.5)
```

```
60 CONTINUE
   DO 900 I=1,156
   R1=(22.5+FLOAT(I))*10.0**(-3.0)
   R2=(22.5+FLOAT(I+1))*10.0**(-3.0)
   RE1=Q/(R1*V)
   TA1=(W*R1**2.0)/V
   CONS=(3.0/(8.0*ATAN(1.0)))**(1.0/3.0)
   TH1=R1*CONS*(RE1/(TA1**2.0))**(1.0/3.0)*1000.0
   RE2=Q/(R2*V)
   TA2=(W*R2**2.0)/V
   TH2=R2*CONS*(RE2/(TA2**2.0))**(1.0/3.0)*1000.0
   RA=R1*100.0
   RB=R2*100.0
   WRITE(7,95)RA,TH1
   WRITE(7,95)RB,TH2
 95 FORMAT(2G12.5)
900 CONTINUE
C
      STOP
      END
```

PROGRAM F)

```
      DIMENSION A(1000),B(1000)
      SX=-5.0
      SY=-5.0
      CALL SETPEN(1)
      CALL SCALEM(1.0,1.0,SX,SY)
      CALL EGRID(0,0.0,0.0,1.0,20)
      CALL EGRID(1,0.0,0.0,1.0,10)
      DO 100 I=1,21
      Y=-0.5
      X=FLOAT(I-1)-0.5
      CALL EPLOT(1,X,Y)
      XA=FLOAT(I-1)
      CALL PLTNUM(XA,'WF2.1*',0.5,0.0)
  100 CONTINUE
      DO 200 J=1,11
      X=-1.0
      Y=FLOAT(J-1)
      CALL EPLOT(1,X,Y)
      YA=FLOAT(J-1)
      CALL PLTNUM(YA,'WF2.1*',0.5,0.0)
  200 CONTINUE
      DO 10 I=1,201,10
      X=FLOAT(I-1)/10
      CALL EPLOT(1,X,0.0)
      CALL EPLOT(2,X,10.0)
   10 CONTINUE
      DO 15 I=1,101,10
      Y=FLOAT(I-1)/10
      CALL EPLOT(1,0.0,Y)
      CALL EPLOT(2,20.0,Y)
   15 CONTINUE
      CALL EPLOT(1,8.0,-2.5)
      CALL PLTEXT('RADIUS IN CM',12,0.75,0.0)
      CALL EPLOT(1,-2.5,4.0)
      CALL PLTEXT('THICKNESS',10,0.75,-90.0)
      DO 300 K=1,1000
      READ(5,1,END=400)A(K),B(K)
    1 FORMAT(2G12.5)
  300 CONTINUE
  400 CONTINUE
      DO 500 K=1,407
      X=A(K)
      Y=B(K)*10.0
      CALL EPLOT(1,X,Y)
      XA=A(K+1)
      YA=B(K+1)*10.0
      CALL EPLOT(2,XA,YA)
  500 CONTINUE
      CALL EPLOT(1,XA,YA)
      DO 600 I=1,311
      X1=A(I+408)
      Y1=B(I+408)*10.0
      CALL EPLOT(1,X1,Y1)
      X2=A(I+409)
      Y2=B(I+409)*10.0
      CALL EPLOT(2,X2,Y2)
  600 CONTINUE
      CALL EPLOT(1,X2,Y2)
      CALL ENDPIC
      STOP
      END
```

PROGRAM G)

```
      DIMENSION VOLT(800),SUM(700),AREA(700)
      CALL OPEN(6,'SURFWAVEDAT',0)
      WRITE(5,2)
    2 FORMAT(' ENTER SPEED,FLOWRATE,MIN AND MAX PTS '/)
      READ(5,3)W,Q
    3 FORMAT(2G12.7)
C
C     READING THE EXPERIMENTAL DATA
C
      DO 20 J=1,627
      READ(6,1)MAA,MBB,MDD,MCC
    1 FORMAT(I3,I7,I1,I2)
      VOLT(J)=FLOAT(MBB)*10.0**(-2.0)
      VOLT(J)=VOLT(J)+FLOAT(MDD)*10.0**(-3.0)
      VOLT(J)=ABS(VOLT(J))
   20 CONTINUE
      WRITE(5,15)(VOLT(J),J=1,10)
   15 FORMAT(10G12.7)
C
C     SUM FOR THE FIRST REGION FROM 7.0 MM TO
C     46.0 MM WITH CALIBRATION AT PT 35.5 MM FROM
C     THE EDGE OF THE DISTRIBUTOR.
C
      DO 30 I=30,195
      R=FLOAT(I)*0.23437+22.5
      Y0=-0.033229+1.1443*VOLT(I)+0.62739*VOLT(I)*VOLT(I)
      Y1=-0.033229+1.1443*VOLT(I+1)+0.62739*VOLT(I+1)*VOLT(I+1)
      DY=ABS(Y1-Y0)
      DX=0.23437
      DR=SQRT(0.23437**2.0+DY**2.0)
      AREA(I+1)=(2.0*4.0*ATAN(1.0)*R*DR+4.0*ATAN(1.0)*DR**2.0)
      SUM(30)=0.0
      SUM(I+1)=SUM(I)+AREA(I+1)
   30 CONTINUE
      AREA1=SUM(196)
C
C
C

C     SUM FOR THE 2ND REGION FROM 46MM TO 66MM
C     WITH CALIBRATION AT PT 56.5MM FROM THE
C     EDGE OF THE DISTRIBUTOR.
C
      DO 40 I=196,281
      R=FLOAT(I)*0.23437+22.5
      Y0=-0.010819+0.47934*VOLT(I)+1.7239*VOLT(I)*VOLT(I)
      Y1=-0.010819+0.47934*VOLT(I+1)+1.7239*VOLT(I+1)*VOLT(I+1)
      DY=ABS(Y1-Y0)
      DX=0.23437
      DR=SQRT(0.23437**2.0+DY**2.0)
      AREA(I+1)=(8.0*ATAN(1.0)*R*DR+4.0*ATAN(1.0)*DR**2.0)
      SUM(196)=0.0
      SUM(I+1)=SUM(I)+AREA(I+1)
```

```
   40 CONTINUE
      AREA2=SUM(282)
C
C
C       SUM FOR THE 3RD REGION FROM 66MM 86MM
C       WITH CALIBRATION AT PT 75.5MM FROM THE
C       EDGE OF THE DISTRIBUTOR.
C
        DO 50 I=282,366
        R=FLOAT(I)*0.23437+22.5
        Y0=-0.018271+0.78861*VOLT(I)+0.99584*VOLT(I)*VOLT(I)
        Y1=-0.018271+0.78861*VOLT(I+1)+0.99584*VOLT(I+1)*VOLT(I+1)
        DY=ABS(Y1-Y0)
        DX=0.23437
        DR=SQRT(DY**2.0+DX**2.0)
        AREA(I+1)=(8.0*ATAN(1.0)*R*DR+4.0*ATAN(1.0)*DR**2.0)
        SUM(282)=0.0
        SUM(I+1)=SUM(I)+AREA(I+1)
   50 CONTINUE
      AREA3=SUM(367)
C
C
C       SUM FOR 4TH REGION FROM 86MM TO 105.5MM
C       WITH CALIBRATION AT PT 96.5MM FROM THE
C       EDGE OF THE DISTRIBUTOR.
C
        DO 60 I=367,449
        R=FLOAT(I)*0.23437+22.5
        Y0=-0.046984+2.0616*VOLT(I)-3.9390*(VOLT(I)**2.0)+
     £4.6365*(VOLT(I)**3.0)
        Y1=-0.046984+2.0616*VOLT(I+1)-3.9390*(VOLT(I+1)**2.0)
     £+4.6365*(VOLT(I+1)**3.0)
        DY=ABS(Y1-Y0)
        DX=0.23437
        DR=SQRT(DY**2.0+DX**2.0)
        AREA(I+1)=8.0*ATAN(1.0)*R*DR+4.0*ATAN(1.0)*DR**2.0
        SUM(367)=0.0
        SUM(I+1)=SUM(I)+AREA(I+1)
   60 CONTINUE
      AREA4=SUM(450)
C
C       SUM FOR 5TH REGION FROM 105.5 TO 125MM
C       WITH CALIBRATION AT PT 114.5MM FROM THE
C       EDGE OF THE DISTRIBUTOR.
C
        DO 70 I=450,532
        R=FLOAT(I)*0.23437+22.5
        Y0=-0.075122+3.3806*VOLT(I)-9.2343*(VOLT(I)**2.0)+
     £10.337*(VOLT(I)**3.0)
        Y1=-0.075122+3:3806*VOLT(I+1)-9.2343*(VOLT(I+1)**2.0)+
     £10.337*(VOLT(I+1)**3.0)
        DY=ABS(Y1-Y0)
        DX=0.23437
        DR=SQRT(DY**2.0+DX**2.0)
        AREA(I+1)=(8.0*ATAN(1.0)*R*DR+4.0*ATAN(1.0)*DR**2.0)
        SUM(450)=0.0
        SUM(I+1)=SUM(I)+AREA(I+1)
   70 CONTINUE
```

```
      AREA5=SUM(533)
C
C     SUM FOR THE 6TH REGION FROM 125MM TO 146.5MM
C     WITH CALIBRATION AT THE PT 135.5MM FROM THE
C     EDGE OF THE DISTRIBUTOR.
C
      DO 80 I=533,614
      R=FLOAT(I)*0.23437+22.5
      Y0=-0.11794+4.4883*VOLT(I)-13.389*(VOLT(I)**2.0)+
     £14.738*(VOLT(I)**3.0)
      Y1=-0.11794+4.4883*VOLT(I+1)-13.389*(VOLT(I+1)**2.0)+
     £14.738*(VOLT(I+1)**3.0)
      DY=ABS(Y1-Y0)
      DX=0.23437
      DR=SQRT(DY**2.0+DX**2.0)
      AREA(I+1)=(8.0*ATAN(1.0)*R*DR+4.0*ATAN(1.0)*DR**2.0)
      SUM(533)=0.0
      SUM(I+1)=SUM(I)+AREA(I+1)
   80 CONTINUE
      AREA6=SUM(615)
C
C

C     SUM OF EACH REGION
C
      WRITE(5,25)AREA1,AREA2,AREA3,AREA4,AREA5,AREA6
   25 FORMAT(' AREA1=',G12.7,' AREA2=',G12.7,' AREA3=',
     £G12.7,' AREA4=',G12.7,' AREA5=',G12.7,' AREA6=',
     £G12.7/)
C
C
C
C     SUM OF AREAS OF 6 REGIONS WITH WAVES
C
      SUMW=AREA1+AREA2+AREA3+AREA4+AREA5+AREA6
C
      WRITE(5,45)SUMW
   45 FORMAT(' TOTAL AREA WITH WAVES= ',G12.7)
C     CAICULATION OF SURFACE AREA WITHOUT WAVE
C     USING THE MODEL DELTA/R=CONT*(TA/RE**2)
C     FINAL FILM THICKNESS IS CONVERTED TO MM
C
      R0=29.531*10.0**(-3.0)
      R1=166.637*10.0**(-3.0)
      V=0.98E-06
      PI=4.0*ATAN(1.0)
      CON=(3.0/(2.0*PI))**(1.0/3.0)
      QA=Q*10.0**(-6.0)
      RE=QA/(R0*V)
      TA=W*R0**2.0/V
      RETA2=RE/(TA**2.0)
      DELTA=CON*(RETA2**(1.0/3.0))*R0*1000.0
      RE1=QA/(R1*V)
      TA1=W*R1**2.0/V
      RETA21=RE1/(TA1**2.0)
      DELTA1=CON*(RETA21**(1.0/3.0))*R1*1000.0
      DELX=166.637-29.531
      DELY=ABS(DELTA-DELTA1)
```

```
      DELR=SQRT(DELX**2.0+DELY**2.0)
      SUMN=PI*(2.0*29.531*DELR+DELR**2.0)
      WRITE(5,990)SUMN
  990 FORMAT(' AREA WITHOUT WAVE=',G12.7)
C
C     PERCENTAGE INCREASE IN SURFACE
C
      SUMP=((SUMW-SUMN)/SUMN)*100.0
      WRITE(5,991)SUMP
  991 FORMAT(' PERCENTAGE INCREASE IN AREA=',G12.7)
      STOP
      END
```

SURFACE WAVE MEASUREMENTS

CALIBRATION CURVES FOR 6 DIFFERENT POSITIONS ACROSS THE DISC

RADIUS= 58 MM STANDARD DEVIATION = 0.23284E-01

Y = -0.33229E-01+1.1443*X+0.62739*X*X

RADIUS= 79 MM STANDARD DEVIATION = 0.99020E-01

Y = -0.10819E-01+0.47934*X+1.7239*X*X

RADIUS= 98 MM STANDARD DEVIATION = 0.44402E-01

Y = -0.18271E-01+0.78861*X+0.99584*X*X

RADIUS= 119 MM STANDARD DEVIATION = 0.86040E-02

Y = -0.46984E-01+2.0616*X-3.9390*X*X+4.6365*X*X*X

RADIUS= 137 MM STANDARD DEVIATION = 0.16194E-02

Y = -0.75122E-01+3.3806*X-9.2343*X*X+10.337*X*X*X

RADIUS= 158 MM STANDARD DEVIATION = 0.50978E-02

Y = -0.11794+4.4883*X-13.389*X*X+14.738*X*X*X

WHERE X IN MV AND Y IN MM THICKNESS

21 MM ON THE NEGATIVE = 15.75 CM ON THE DISC

THEREFOR 1 MM = 15.75/21.0

= 0.75 CM ON THE DISC

1 REVOLUTION = 1/2 MM ON THE NEGATIVE = 0.375 CM ON THE DISC

16 READINGS WERE TAKEN IN ONE REVOLUTION FOR SURFACE WAVE MEASUREMENTS

(i.e. 0.23437 MM ON THE DISC FOR EACH READING)

REGION OF INTEREST FOR THE COMPARISION OF INCREASE IN SURFACE WAVE IS

FROM 29.531 MM TO 166.637 MM FROM THE CENTRE OF THE DISC.

PROGRAM H)

```
      DIMENSION Q(8),W(6),R(7),B(500),BA(500)
      DATA R/0.06,0.09,0.11,0.13,0.15,0.17,0.18/
      DATA Q/14.5E-06,22.1E-06,31.0E-06,37.3E-06,42.7E-06,4
     £52.0E-06,60.5E-06/
      DATA W/23.74,32.90,43.80,60.05,86.27,117.38/
C
      DO 99 N=1,500
      READ(5,1,END=22)B(N)
    1 FORMAT(G12.5)
      BA(N)=ALOG10(B(N))
   99 CONTINUE
   22 CONTINUE
      A=0.0225
      V=0.98E-06
      DO 100 K=1,6
      DO 200 J=1,8
      DO 300 I=1,7
      RE=ALOG10(Q(J)/(R(I)*V))
      TA=ALOG10((W(K)*(R(I)**2.0))/V)
      RA=ALOG10(R(I)/A)
      M=(J-1)*7+(K-1)*56+I
      ET=BA(M)
      WRITE(6,10)RE,TA,RA,ET
   10 FORMAT(4G12.5)
  300 CONTINUE
  200 CONTINUE
  100 CONTINUE
      STOP
      END
```

PROGRAM I)

```
      DIMENSION Q(8),W(6),R(7),B(500),BA(500)
      DATA R/0.06,0.09,0.11,0.13,0.15,0.17,0.18/
      DATA Q/14.5E-06,22.1E-06,31.0E-06,37.3E-06,42.7E-06
     £,46.2E-06,52.0E-06,60.5E-06/
      DATA W/23.74,32.90,43.80,60.05,86.27,117.38/
C
C
      DO 99 N=1,500
      READ(5,1,END=22)AA
    1 FORMAT(G12.5)
      B(N)=AA*10.0**(-4.0)
   99 CONTINUE
   22 CONTINUE
      A=0.0225
      V=0.98E-06
      D=2.45E-09
      CONS=(3.0/(8.0*ATAN(1.0)))**(1.0/3.0)
      DO 100 K=1,6
      DO 200 J=1,8
      DO 300 I=1,7
      RE=Q(J)/(R(I)*V)
      TA=(W(K)*(R(I)**2.0))/V
      BRE=ALOG10(RE)
      BTA=ALOG10(TA)
      BRA=ALOG10(R(I)/A)
      M=(J-1)*7+(K-1)*56+I
      CH=B(M)
      TH=CONS*R(I)*((RE/(TA**2.0))**(1.0/3.0))
      SH=(CH*TH)/D
      BSH=ALOG10(SH)
      WRITE(6,10)BRE,BTA,BRA,BSH
   10 FORMAT(4G12.5)
  300 CONTINUE
  200 CONTINUE
  100 CONTINUE
      STOP
      END
```

PROGRAM J)

```
C       EXAMPLE PROGRAM FOR G02BAF
        REAL*8 TITLE(7),A(800,8),XBAR(8),STD(8),SSP(8,8),CORR
     £ RESULT(13),COEFFT(8,8),RINV(8,8),C(8,8),W(8,8),CON(8
        INTEGER NIN,NOUT,I,M,N,J,IFAIL,NV,NI,NC
        DATA NIN /5/,NOUT /6/
        READ(NIN,999)M,N
        READ(NIN,99997)((A(I,J),J=1,M),I=1,N)
        WRITE(NOUT,99996)M,N,(J,J=1,M),(I,(A(I,J),J=1,M),I=1,
        IFAIL=1
        CALL G02BAF(N,M,A,800,XBAR,STD,SSP,8,CORR,8,IFAIL)
C
C
        WRITE(NOUT,99994)(I,XBAR(I),STD(I),I=1,M)
        WRITE(NOUT,99993)(I,I=1,M),(I,(SSP(I,J),J=1,M),I=1,M)
        WRITE(NOUT,99992)(I,I=1,M),(I,(CORR(I,J),J=1,M),I=1,M
C
C       EXAMPLE PROGRAM FO G02CGF
C
        NV=M
        NI=NV-1
        NC=N
        IFAIL=1
        CALL G02CGF(NC,NV,NI,XBAR,SSP,8,CORR,8,RESULT,
     £ COEFFT,8,CON,RINV,8,C,8,W,8,IFAIL)
C
C
        WRITE(NOUT,9994)(I,(COEFFT(I,J),J=1,3),I=1,NI)
        WRITE(NOUT,9993)(CON(I),I=1,3)
        WRITE(NOUT,9992)(RESULT(I),I=1,13)
        WRITE(NOUT,9991)(J,J=1,NI),(I,(RINV(I,J),J=1,NI),I=1,
        WRITE(NOUT,9990)(J,J=1,NI),(I,(C(I,J),J=1,NI),I=1,NI)
        STOP
99997 FORMAT(4G12.5)
99996 FORMAT('VARIABLES=',I4,'CASES=',I4,'DATA MATRIX IS :-
     £ //1H,4I12/(1H,I3,4G12.4))
99994 FORMAT(28HOVARIABLE   MEAN     ST. DEV./(1H,I5,2F11.4)
99993 FORMAT(49HOSUMS OF SQUARES AND CROSS-PRODUCTS OF DEVI
     £ 1H,4I12/(1H,I3,4F12.4))
99992 FORMAT(25HOCORRELATION COEFFICIENTS/1H,4I12/(1H,I3,
     £ 4F12.4))
 9994 FORMAT(43HOVBLE      COEFFT        STD ERR       T-VALUE
     £ I3,3F13.4/))
 9993 FORMAT(6HOCONST,F11.4,2F13.4/)
 9992 FORMAT(32HOANALYSIS OF REGRESSION TABLE :-//13H
     £ 55H          SUM OF SQUARES  D.F.     MEAN SQUARE      F
     £ 18H DUE TO REGRESSION,F14.4,F8.0,2F14.4/14H ABOUT  R
     £ 4HSION,F14.4,F8.0,F14.4/18H TOTAL                ,F14.4,
     £ F8.0///29H STANDARD ERROR OF ESTIMATE=,F8.4/11H MULT
     £ 18HORRELATION (R)    =,F8.4/29H DETERMINATION (R SQUA
     £ F8.4/29H CORRECTED R SQUARED          =,F8.4/)
 9991 FORMAT(50HOINVERSE OF CORRELATION MATRIX OF INDEPENDE
     £ 6HABLES:/1H,3I10/3(1H,I4,3F10.4/))
 9990 FORMAT(25HOMODIFIED INVERSE MATRIX:/1H,3I10/3(1H,I4,
     £ 3F10.4/))
  999 FORMAT(2I4)
      END
```

PROGRAM K)

```
C       EXAMPLE PROGRAM FOR G02BAF
        REAL*8 TITLE(7),A(800,8),XBAR(8),STD(8),SSP(8,8),CORR
     £ RESULT(13),COEFFT(8,8),RINV(8,8),C(8,8),W(8,8),CON(8
        INTEGER NIN,NOUT,I,M,N,J,IFAIL,NV,NI,NC
        DATA NIN /5/,NOUT /6/
        READ(NIN,999)M,N
        READ(NIN,99997)((A(I,J),J=1,M),I=1,N)
        WRITE(NOUT,99996)M,N,(J,J=1,M),(I,(A(I,J),J=1,M),I=1,
        IFAIL=1
        CALL G02BAF(N,M,A,800,XBAR,STD,SSP,8,CORR,8,IFAIL)
C
C
        WRITE(NOUT,99994)(I,XBAR(I),STD(I),I=1,M)
        WRITE(NOUT,99993)(I,I=1,M),(I,(SSP(I,J),J=1,M),I=1,M)
        WRITE(NOUT,99992)(I,I=1,M),(I,(CORR(I,J),J=1,M),I=1,M
C
C       EXAMPLE PROGRAM FO G02CGF
C
        NV=M
        NI=NV-1
        NC=N
        IFAIL=1
        CALL G02CGF(NC,NV,NI,XBAR,SSP,8,CORR,8,RESULT,
     £ COEFFT,8,CON,RINV,8,C,8,W,8,IFAIL)
C
C
        WRITE(NOUT,9994)(I,(COEFFT(I,J),J=1,3),I=1,NI)
        WRITE(NOUT,9993)(CON(I),I=1,3)
        WRITE(NOUT,9992)(RESULT(I),I=1,13)
        WRITE(NOUT,9991)(J,J=1,NI),(I,(RINV(I,J),J=1,NI),I=1,
        WRITE(NOUT,9990)(J,J=1,NI),(I,(C(I,J),J=1,NI),I=1,NI)
        STOP
99997 FORMAT(3G12.5)
99996 FORMAT('VARIABLES=',I4,'CASES=',I4,'DATA MATRIX IS :-
     £ //1H,3I12/(1H,I3,3G12.4))
99994 FORMAT(28HOVARIABLE   MEAN    ST. DEV./(1H,I5,2F11.4)
99993 FORMAT(49HOSUMS OF SQUARES AND CROSS-PRODUCTS OF DEVI
     £ 1H,3I12/(1H,I3,3F12.4))
99992 FORMAT(25HOCORRELATION COEFFICIENTS/1H,3I12/(1H,I3,
     £ 3F12.4))
 9994 FORMAT(43HOVBLE      COEFFT        STD ERR       T-VALUE
     £ I3,3F13.4/))
 9993 FORMAT(6HOCONST,F11.4,2F13.4/)
 9992 FORMAT(32HOANALYSIS OF REGRESSION TABLE :-//13H
     £ 55H          SUM OF SQUARES  D.F.     MEAN SQUARE      F
     £ 18H DUE TO REGRESSION,F14.4,F8.0,2F14.4/14H ABOUT  R
     £ 4HSION,F14.4,F8.0,F14.4/18H TOTAL                ,F14.4,
     £ F8.0///29H STANDARD ERROR OF ESTIMATE=,F8.4/11H MULT
     £ 18HORRELATION (R)   =,F8.4/29H DETERMINATION (R SQUA
     £ F8.4/29H CORRECTED R SQUARED         =,F8.4/)
 9991 FORMAT(50HOINVERSE OF CORRELATION MATRIX OF INDEPENDE
     £ 6HABLES:/1H,2I10/2(1H,I4,2F10.4/))
 9990 FORMAT(25HOMODIFIED INVERSE MATRIX:/1H,2I10/2(1H,I4,
     £ 2F10.4/))
  999 FORMAT(2I4)
      END
```

PROGRAM L)

```
      DIMENSION R(7),Y(7),EM(7),X(7)
      REAL N,N1
      DATA R/0.06,0.09,0.11,0.13,0.15,0.17,0.18/
      READ(5,3)W,Q
    3 FORMAT(2G12.5)
      Q=Q*10.0**(-6.0)
      R0=0.0225
      V=0.98E-06
      SUMX=0.0
      SUM2=0.0
      SUMXY=0.0
      CS=8.15
      N1=3.0
      N=7.0
      DO 10 I=1,7
      READ(5,4)CO,CI
    4 FORMAT(2G12.5)
      Y(I)=(CO-CI)/(CS-CI)
   10 CONTINUE
      SUMY=Y(1)+Y(2)+Y(3)+Y(4)+Y(5)+Y(6)+Y(7)
      SUMY1=Y(1)+Y(2)+Y(3)
      DO 20 I=1,7
      A=((2.0*4.0*ATAN(1.0)*W**2.0)/(3.0*Q*V))**(4.0/3.0)
      B=(R(I)**(8.0/3.0)-R0**(8.0/3.0))
      X(I)=SQRT(0.75*(V/(W**2.0))*A*B)
      SUMX=SUMX+X(I)
      XY=X(I)*Y(I)
      SUMXY=SUMXY+XY
      X2=X(I)**2.0
      SUMX2=SUMX2+X2
   20 CONTINUE
      SUMX1=X(1)+X(2)+X(3)
      SUMXY1=X(1)*Y(1)+X(2)*Y(2)+X(3)*Y(3)
      SUMX21=X(1)**2.0+X(2)**2.0+X(3)**2.0
      EF1=(SUMX1*SUMXY1-SUMY1*SUMX21)/(SUMX1**2.0-N1*
     £SUMX21)
      EF=(SUMX*SUMXY-SUMY*SUMX2)/(SUMX**2.0-N*SUMX2)
      WRITE(6,90)W,Q
   90 FORMAT(' SPEED=',G12.5,'     FLOWRATE=',G12.5/)
      WRITE(6,100)EF1
  100 FORMAT(' EF1=',G12.5///)
      WRITE(6,5)EF
    5 FORMAT(' EF=',G12.5/)
      DO 30 I=1,7
      EM(I)=Y(I)-EF
      WRITE(6,6)Y(I),EM(I),X(I)
    6 FORMAT(' ET=',G12.5,'    EM=',G12.5,'    X=',G12.5/)
   30 CONTINUE
      STOP
      END
```

PROGRAM M)

```
      DIMENSION MAA(5),MBB(5),MCC(5),MDD(5),PP(5),VOLT(5)
C
      CALL OPEN(6,'DATAAV1 DAT',0)
C
C     READ DATA FROM TAPE AND AVERAGE THEM
C
      WRITE(5,5)
    5 FORMAT(' ENTER NUMBER OF ROWS N ')
      READ(5,6)N
    6 FORMAT(I2)
      DO 15 J=1,4
   15 PP(J)=0.0
C
      DO 10 J=1,N
      READ(6,1)(MAA(K),MBB(K),MDD(K),MCC(K),K=1,4)
    1 FORMAT(I3,I7,I1,I2,3(I5,I7,I1,I2))
      DO 11 I=1,4
      VOLT(I)=FLOAT(MBB(I))*10.0**(-2.0-FLOAT(MCC(I)-1))
      VOLT(I)=VOLT(I)+FLOAT(MDD(I))*10.0**(-FLOAT(2+
     £(MCC(I))))
      VOLT(I)=ABS(VOLT(I))
      PP(I)=PP(I)+VOLT(I)
   11 CONTINUE
   10 CONTINUE
C
C     CONVERT TO AVERAGE VALUES
      DO 20 I=1,4
      PP(I)=PP(I)/FLOAT(N)
   20 CONTINUE
C
      WRITE(5,7)(PP(I),I=1,4)
    7 FORMAT(4G12.4)
      STOP
      END
```

A.

PROGRAM N)

```
      DIMENSION MAA(5),MBB(5),MCC(5),MDD(5),PP(5),VOLT(5)
      REAL KLMRAT,KLMCRU,KLMAPP
      RO=0.0225
      CI=8.15
      D=2.45E-09
      V=0.98E-06
C
      CALL OPEN(6,'DATAMAS DAT',0)
C
C     READ INLET,OUTLET CONTRATIONS AND ROTATIONAL
C     SPEED AND WATER TEMPERATURE IN VOLTAGES
C
      WRITE(5,2)
    2 FORMAT(' ENTER NUMBER OF ROWS N AND TITRATED INLET CONC'/)
      READ(5,3)N,CONIN
    3 FORMAT(I2,G12.5)
C
C
      DO 10 J=1,4
   10 PP(J)=0.0
      DO 20 J=1,N
      READ(6,1)(MAA(K),MBB(K),MDD(K),MCC(K),K=1,4)
    1 FORMAT(I3,I7,I1,I2,3(I5,I7,I1,I2))
      DO 30 I=1,4
      VOLT(I)=FLOAT(MBB(I))*10.0**(-2.0-FLOAT(MCC(I)-1))
      VOLT(I)=VOLT(I)+FLOAT(MDD(I))*10.0**(-FLOAT(2+
     £(MCC(I))))
      VOLT(I)=ABS(VOLT(I))
      PP(I)=PP(I)+VOLT(I)
   30 CONTINUE
   20 CONTINUE
C     CONVERT TO AVERAGE VALUES
C
      DO 40 I=1,4
      PP(I)=PP(I)/FLOAT(N)
   40 CONTINUE
C
      WRITE(5,7)(PP(I),I=1,2)
    7 FORMAT(' AV INLET CONC=',G12.5,'AV OUT CONC=',G12.5)
C
C     CONVERT PP(1) TO PP(4) TO SHORT FORM CHARACTERS
C     PP(1)=INLET CONC,PP(2)=OUTLET CONC,PP(3)=SPEED
C     PP(4)=WATER TEMPERATURE
C
      AA=PP(1)
      BB=PP(2)
      CC=PP(3)
      DD=PP(4)*1000.0
      ADE=0.5472E-02
      AOX=0.1540E-01
```

```
      BDE=0.2102E-03
      BOX=0.1173
C
C
C
C     TO CONVERT ACTUAL FPM ACROSS THE DISK
C
      A1=AA-ADE
      A2=AOX-ADE
      ACON=A1*8.15/A2
C
      B1=BB-BDE
      B2=BOX-BDE
      BCON=B1*8.15/B2
C
C      TO CONVERT VOLTAGES TO SPEED AND WATER TEMP
C
       SPEED=-0.44083E-02+344.9817*CC
       WTEMP=0.69744+24.450783*DD+0.1537252*DD**2.0
     £-0.1121066*DD**3.0
C
       WRITE(5,11)CONIN,BCON,SPEED,WTEMP
   11 FORMAT(' INLET CONC=',G10.5,'OUTLET CONC=',G10.5,
     £'SPEED=',F7.2,'WTEMP=',F6.2,'C')
C
C      TO CONVERT PPM FROM EXPTAL RUN TO MASS TRANSFER RATE IN
C      G/S AND COMPARE WITH THEORETICAL MODELS(CRUDE AND APP-
C      ROXIMATE MODELS
C
       WRITE(5,12)
   12 FORMAT(' ENTER RADIUS IN MM AND FLOWRATE IN CC/S ')
       READ(5,13)RR,FF
   13 FORMAT(2G12.5)
       R=RR*1.0E-03
       F=FF*1.0E-06
C
       ZMRATE=(BCON-CONIN)*F
C
       WW=SPEED*(4.0*ATAN(1.0)*2.0)/60.0
       B=0.306*WW**(2.0/3.0)*F**(2.0/3.0)/
     £(V**(1.0/3.0))
       AAA=SQRT(4.0*ATAN(1.0)*D*B/3.0)
       AAB=SQRT(4.0*ATAN(1.0)*D*B)
       AAC=((3.0/8.0)*(R**(8.0/3.0)-R0**(8.0/3.0)))**(1.0/2.0)
C
       SS=SQRT(R**(4.0/3.0)-R0**(4.0/3.0))
       AEE=R**(2.0/3.0)*SS/2.0+R0**(4.0/3.0)*ALOG
     £(R**(4.0/3.0)+SS)/2.0+8.0336E-03
C
       ZCRUDE=6.0*(CI-CONIN)*AAA*AEE
       ZAPP=4.0*(CI-CONIN)*AAB*AAC
C
       CCRUDE=ZCRUDE/F+CONIN
       CMAPP=ZAPP/F+CONIN
       CM1=(CI-CONIN)/(CI-BCON)
       CM2=(CI-CONIN)/(CI-CCRUDE)
       CM3=(CI-CONIN)/(CI-CMAPP)
       KLMRAT=F*ALOG(CM1)/(4.0*ATAN(1.0)*(R**2.0-R0**2.0))
       KLMCRU=F*ALOG(CM2)/(4.0*ATAN(1.0)*(R**2.0-R0**2.0))
```

```
    KLMAPP=F*ALOG(CM3)/(4.0*ATAN(1.0)*(R**2.0-R0**2.0))
    WRITE(5,14)R,F,WW,ZMRATE,ZCRUDE,ZAPP
14  FORMAT(' RADIUS=',F6.2,' M',' FLOWRATE=',G12.5,' CC/S',
   £' SPEED=',F6.2,'RAD/S'////'ZMRATE=',G12.5,' ZCRUDE=',
   £G12.5,' ZAPP=',G12.5,'G/S'///)
    WRITE(5,15)CCRUDE,CMAPP
15  FORMAT( 'THEORETICAL CRUDE CONC='G12.5,
   £'THEORETICAL APP CONC=',G12.5,'PPM'///)
    WRITE(5,16)KLMRAT,KLMCRU,KLMAPP
16  FORMAT(' KLRATE=',G12.5,' KLCRUDE=',G12.5,'KLMAPP=',G12.5,/)
    STOP
    END
```